Portofoliu de lucrări științifice

Șef lucr. Dr. Sonia Iurian

OPIS

Nr.	Articol	Pagina
1.	Casian T, **Iurian S***, Bogdan C, Rus L, Moldovan M, Tomuta I. QbD for pediatric oral lyophilisates development: risk assessment followed by screening and optimization. Drug Dev Ind Pharm. 2017;43(12):1932-1944. IF = 1,830	2
2.	Casian T, Bogdan C, Tarta D, Moldovan M, Tomuta I, **Iurian S**. Assessment of oral formulation-dependent characteristics of orodispersible tablets using texture profiles and multivariate data analysis. J Pharm Biomed Anal. 2018;152:47-56. doi: 10.1016/j.jpba.2018.01.040. IF = 2,983	16
3.	Gâvan A, **Iurian S***, Casian T, Porfire A, Porav S, Voina I, Oprea A, Tomuță I. Fluidised bed granulation of two APIs: QbD approach and development of a NIR in-line monitoring method. Asian J Pharm Sci. 2020;15(4):506-517. doi: 10.1016/j.ajps.2019.03.003. IF = 6,598	26
4.	Savencu I, **Iurian S***, Porfire A, Bogdan C, Tomuta I. Review of advances in polymeric wound dressing films. React Funct Polym. 2021;168:105059. IF = 4,96	38
5.	**Iurian S**, Bogdan C, Suciu Ș, Muntean DM, Rus L, Berindeie M, Bodi S, Ambrus R, Tomuță I. Milk Oral Lyophilizates with Loratadine: Screening for New Excipients for Pediatric Use. Pharmaceutics. 2022;14(7):1342. doi: 10.3390/pharmaceutics14071342. IF = 5,4	59
6.	Crișan AG, **Iurian S***, Porfire A, Rus LM, Bogdan C, Casian T, Ciceo Lucăcel R, Turza A, Porav S, Tomuță I. QbD guided development of immediate release FDM-3D printed tablets with customizable API doses. Int J Pharm. 2022;613:121411. doi: 10.1016/j.ijpharm.2021.121411. IF = 5,8	82
7.	Bogdan C, Hales D, Cornilă A, Casian T, Iovanov R, Tomuță I, **Iurian S**. Texture analysis - A versatile tool for pharmaceutical evaluation of solid oral dosage forms. Int J Pharm. 2023;638:122916. doi: 10.1016/j.ijpharm.2023.122916. IF = 5,3	102
8.	Iovanov R, Cornilă A, Bogdan C, Hales D, Tomuță I, Achim M, Tăut A, Iman N, Casian T, **Iurian S**. Testing the disintegration and texture-related palatability predictions for orodispersible tablets using an instrumental tool coupled with multivariate analysis: Focus on process variables and analysis settings. Eur J Pharm Sci. 2024;198:106801. IF = 4,3	132
9.	Hales D, Bogdan C, Tefas LR, Cornilă A, Chiver MA, Tomuță I, Casian T, Iovanov R, Katona G, Ambrus R, **Iurian S**. Exploring Vacuum Compression Molding as a Preparation Method for Flexible-Dose Pediatric Orodispersible Films. Pharmaceuticals (Basel). 2024;17(7):934. doi: 10.3390/ph17070934. IF = 4,3	145
10	Briciu C, Leucuța D, Popa A, Latiș A, Pop TL, Tomuță I, Man SC, Lazăr C, Voștinaru S, **Iurian S**. Acceptability of compounded preparations - A Romanian pediatric hospital perspective. Eur J Pharm Biopharm. 2024;202:114383. doi: 10.1016/j.ejpb.2024.114383. IF = 4,4	165

Drug Development and Industrial Pharmacy

ISSN: 0363-9045 (Print) 1520-5762 (Online) Journal homepage: http://www.tandfonline.com/loi/iddi20

QbD for pediatric oral lyophilisates development: risk assessment followed by screening and optimization

Tibor Casian, Sonia Iurian, Catalina Bogdan, Lucia Rus, Mirela Moldovan & Ioan Tomuta

To cite this article: Tibor Casian, Sonia Iurian, Catalina Bogdan, Lucia Rus, Mirela Moldovan & Ioan Tomuta (2017) QbD for pediatric oral lyophilisates development: risk assessment followed by screening and optimization, Drug Development and Industrial Pharmacy, 43:12, 1932-1944, DOI: 10.1080/03639045.2017.1350702

To link to this article: https://doi.org/10.1080/03639045.2017.1350702

Accepted author version posted online: 27 Jul 2017.
Published online: 16 Aug 2017.

DRUG DEVELOPMENT AND INDUSTRIAL PHARMACY, 2017
VOL. 43, NO. 12, 1932–1944
https://doi.org/10.1080/03639045.2017.1350702

Taylor & Francis
Taylor & Francis Group

RESEARCH ARTICLE

QbD for pediatric oral lyophilisates development: risk assessment followed by screening and optimization

Tibor Casian[a], Sonia Iurian[a], Catalina Bogdan[b], Lucia Rus[c], Mirela Moldovan[b] and Ioan Tomuta[a]

[a]Department of Pharmaceutical Technology and Biopharmacy, Iuliu Hatieganu University of Medicine and Pharmacy, Cluj-Napoca, Romania; [b]Department of Dermopharmacy and Cosmetics, Iuliu Hatieganu University of Medicine and Pharmacy, Cluj-Napoca, Romania; [c]Department of Drug Analysis, Iuliu Hatieganu University of Medicine and Pharmacy, Cluj-Napoca, Romania

ABSTRACT

Objective: This study proposed the development of oral lyophilisates with respect to pediatric medicine development guidelines, by applying risk management strategies and DoE as an integrated QbD approach.

Methods: Product critical quality attributes were overviewed by generating Ishikawa diagrams for risk assessment purposes, considering process, formulation and methodology related parameters. Failure Mode Effect Analysis was applied to highlight critical formulation and process parameters with an increased probability of occurrence and with a high impact on the product performance. To investigate the effect of qualitative and quantitative formulation variables D-optimal designs were used for screening and optimization purposes.

Results: Process parameters related to suspension preparation and lyophilization were classified as significant factors, and were controlled by implementing risk mitigation strategies. Both quantitative and qualitative formulation variables introduced in the experimental design influenced the product's disintegration time, mechanical resistance and dissolution properties selected as CQAs. The optimum formulation selected through Design Space presented ultra-fast disintegration time (5 seconds), a good dissolution rate (above 90%) combined with a high mechanical resistance (above 600 g load).

Conclusions: Combining FMEA and DoE allowed the science based development of a product with respect to the defined quality target profile by providing better insights on the relevant parameters throughout development process. The utility of risk management tools in pharmaceutical development was demonstrated.

ARTICLE HISTORY
Received 27 January 2017
Revised 11 April 2017
Accepted 18 June 2017

KEYWORDS
Orodispersible tablets; pediatric formulation; freeze drying; D-optimal design; failure mode effect analysis

Introduction

Formulating medicine for pediatric use faces many challenges, mainly related to the age appropriateness of the dosage forms, type of excipients, taste-masking technologies, and methods applied for taste assessment [1].

According to the recommendations of regulatory agencies, the desirable characteristics of pediatric dosage forms should include age appropriate, ready to use formulations with convenient administration that require a minimal manipulation by caregivers. Also for an increased acceptability, a palatable dosage form with minimum dosing frequency, formulated using the minimum non-toxic excipients is preferable [2,3].

A key step in product development after choosing an active pharmaceutical ingredient (API) is the selection of the pharmaceutical dosage form to be formulated considering the requirements of target patients. Tablets represent the most widely prescribed pharmaceutical dosage forms due to an increased patient compliance and ease of administration, however their use by pediatric or geriatric patients is often associated with the need of manipulation and compounding [4]. The difficulties in swallowing, mainly caused by tablet's dimensional (size, shape) or surface properties (texture), frequently lead to the splitting or the trituration of the dosage form, thus improper use. Such strategies menace clinical efficacy of the medicine and raise questions regarding the physical–chemical stability, bioavailability, or the occurrence of adverse effects [5].

The European Pharmacopoeia defines oral lyophilisates as a category of tablets prepared by freeze drying of a liquid or semi-solid preparation, intended either to be placed in the mouth for rapid disintegration or to be dispersed in water before administration [6]. This category of orally disintegrating dosage form overcomes issues related to swallowing difficulties associated with young children. As age appropriate products, orodispersible tablets are preferred over conventional tablets mainly due to a flexibility of administration [7]. Water-assisted administration is not required, the volume of the saliva being sufficient for a complete disintegration.

Several limitations of oral lyophilisates highlighted in literature refer to the low mechanical strength that raise difficulties in handling, issues regarding taste masking, and use of excipients with unknown safety profile [4].

In order to increase safety in drug administration, the entire quality concept was revised in the last years, having the quality defined by ICH Q8 as the suitability of the developed drug product for its intended use.

The new quality concept relies on making knowledge-based decisions both when selecting a dosage form for a certain population and during the product design and development stages.

CONTACT Sonia Iurian iuriansonia@yahoo.com Department of Pharmaceutical Technology and Biopharmacy, Faculty of Pharmacy, University of Medicine and Pharmacy "Iuliu Hatieganu", 41 Victor Babes, 400012 Cluj-Napoca, Romania

Supplemental data for this article can be accessed here.

This overall objective of pharmaceutical development can be fulfilled through the QbD approach by implementing quality risk management strategies since early development stages in association with multivariate experimental methods.

The highly recommended approach by the regulatory agencies involves the gain of relevant knowledge related to the product via systematic understanding of influential parameters that affect the product critical quality attributes (CQAs) by applying multivariate experiments instead of the mainly empirical, one factor at a time approach [8,9].

Applying design of experiments (DoE) as a quality by design (QbD) tool enables the evaluation of all potential factors in a systematic manner, highlighting their effects, and possible interactions. By means of DoE, the design space, or the multidimensional combination of variables that provide the assurance of quality, can be defined for both the formulation and process parameters [10].

To the best of our knowledge, there are no studies published in literature that describe the development of oral lyophilisates from a QbD point of view, combining Risk Management methods for risk identification with DoE for risk reduction and control.

Therefore, the objective of this study was to develop oral lyophilisates with loratadine (LOR) through QbD, using failure mode effect analysis (FMEA) as a risk management tool and DoE for systematic investigation of major influences of formulation factors that influence the product's CQAs. An initial screening experimental design (D-optimal Linear) was applied for the selection of the most suitable excipients, that were taken further to an optimization design (D-optimal Quadratic). Based on the obtained results, the Design Space was generated to specify the combination of factor levels where product quality target profile is ensured.

Materials and methods

Materials

As the developed product was meant for pediatric use, a minimum number of excipients were desired for formulation development. Matrix-forming agents (MFA) are polymers that are easily dispersed in water and form a tridimensional porous structure upon freeze drying that holds the lyophilisate together. Bulking agents (BA) are sugar alcohols that are initially dissolved in the gel system and after freeze drying they fill the polymeric matrix contributing to the product properties. All materials used in this study were selected to fulfill the previously mentioned properties.

The MFAs used in this study were: xanthan gum – Rhodigel 200 (Rhodia, Salindres, France), sodium alginate – Alginic acid sodium salt from brown algae (Sigma Aldrich, St. Louis, MO), methylcellulose – Methylcellulose 1500 (Serva, Heidelberg, Germany), HPMC K4M – Methocel K4M (Colorcon).

The BA used in this study were: mannitol – EMPROVE Parteck M200 (Merck, Darmstadt, Germany), lactose – Pharmatose 150 M (DFEPharma, Hardenberg, Germany), isomalt – galenIQ 721(Palatinit, Mannheim, Germany), trehalose – D(+) Trehalose dihydrate (Sigma Aldrich, St. Louis, MO), sucrose – D(+) Saccharose (Sigma Aldrich, St. Louis, MO). Loratadine, the API used in this study was purchased from Quimica Sintetica, Spain

Quality risk management through FMEA

First, the quality target profile of oral lyophilisates was defined, followed by the identification of CQAs. Product CQAs were overviewed by generating Ishikawa diagrams for risk assessment purposes, considering process, formulation, and methodology-related parameters. FMEA was applied as a risk management methodology for the evaluation and prioritization of parameters that are likely to affect product performance. For each critical parameter, a risk priority number (RPN) was calculated by multiplying score values related to the occurrence (O), severity (S), and detectability (D) of failure modes and effects. Occurrence is classified as: 5 for frequent, 4 for probable, 3 for occasional, 2 for remote, and 1 for improbable. The consequences of the failure mode, known as Severity can be 5 for catastrophic, 4 for critical, 3 for serious, 2 for minor, and 1 for negligible, whereas the detectability (D) of the failure mode can be 5 for hard to detect, 4 for low chance of detection, 3 for moderately detectable, 2 for highly detectable, and 1 for easy to detect [11,12]. For parameters with high RPN, control strategies were suggested and implemented.

Preparation of oral lyophilisates

The suspensions were prepared by dissolving the BA in distilled water followed by the formation of a gel by adding the MFA. After complete hydration of the polymer, LOR was homogenously dispersed into the gel system. Each tablet contained 2.5 mg of API.

About 0.2 ml of suspension was transferred in each blister socket followed by freeze drying, using a Virtis Advantage Plus equipment (SP Scientific, Gardiner, SUA). The freeze drying process included the following steps: freezing, annealing, primary drying, and secondary drying. The freeze-drying parameters were selected by considering the product's critical temperatures identified through thermal analysis.

Thermal analysis (DSC)

Thermal characterization of the formulations was done using a Differential Scanning Calorimeter (Mettler Toledo, Switzerland). The thermal cycle included the cooling of 25–30 mg sample inserted in perforated aluminum pans from 25 °C to –55 °C using a 10 °C/min cooling rate followed by reheating to 25 °C using a 5 °C/min heating rate. Temperature was calibrated using indium (melting point of 156.6 °C) as standard.

Experimental design

Principle steps in DOE include the selection of experimental objective, definition of factors, and responses relevant to the experimental goals, selection of the regression model and the generation of experimental design [13]. All DoE steps and calculations were done with Modde Pro 11 (MKS Data Analytics Solutions, Sweden) software. The objective was to develop a formulation that respected the defined quality target profile.

DoE was applied as a risk reduction strategy for formulation development, to evaluate the effect of both the type and concentration of MFA and BA, in a screening and optimization step. The quantitative variation level of the MFAs in the screening design ranged from 10 to 20 mg/ml for HPMC K4M, sodium alginate and methylcellulose, and from 2 to 5 mg/ml for xanthan gum. Lower ranges in case of xanthan gum are justified by the higher viscosity of its aqueous dispersion and on previous experience. Using coded values for quantitative factors allows to adapt their variation range to the properties of different qualitative variables.

The concentration domain for the BAs was chosen considering the aqueous solubility of the excipients, 120 mg/ml as the high level and 60 mg/ml as the low level.

For optimization, the experimental design was generated using one qualitative (MFA type: 2 levels) and two quantitative factors

Table 1. Qualitative and quantitative composition of each formulation from screening and optimization experimental designs.

	Screening design					Optimization design		
Exp name	X_{1S}	X_{2S}	X_{3S}	X_{4S}	Exp name	X_{1O}	X_{2O}	X_{3O}
N1.1	1	HPMC K4M	1	Mannitol	N2.1	Sodium alginate	–1	–1
N1.2	1	Xanthan gum	–1	Mannitol	N2.2	Sodium alginate	1	–1
N1.3	–1	Sodium alginate	1	Mannitol	N2.3	Sodium alginate	–1	1
N1.4	–1	Methylcellulose	–1	Mannitol	N2.4	Sodium alginate	1	1
N1.5	1	HPMC K4M	–1	Lactose	N2.5	Sodium alginate	–1	0.33
N1.6	–1	Xanthan gum	1	Lactose	N2.6	Sodium alginate	1	–0.33
N1.7	1	Sodium alginate	–1	Lactose	N2.7	Sodium alginate	–0.33	–1
N1.8	–1	Methylcellulose	1	Lactose	N2.8	Sodium alginate	0.33	1
N1.9	–1	HPMC K4M	1	Sucrose	N2.9	Sodium alginate	0	0
N1.10	1	Xanthan gum	1	Sucrose	N2.10	Xanthan gum	–1	–1
N1.11	1	Sodium alginate	–1	Sucrose	N2.11	Xanthan gum	1	–1
N1.12	–1	Methylcellulose	–1	Sucrose	N2.12	Xanthan gum	–1	1
N1.13	–1	HPMC K4M	–1	Isomalt	N2.13	Xanthan gum	1	1
N1.14	–1	Sodium alginate	1	Isomalt	N2.14	Xanthan gum	–1	–0.33
N1.15	1	Methylcellulose	1	Isomalt	N2.15	Xanthan gum	1	0.33
N1.16	–1	HPMC K4M	1	Trehalose	N2.16	Xanthan gum	0.33	–1
N1.17	–1	Xanthan gum	–1	Trehalose	N2.17	Xanthan gum	–0.33	1
N1.18	1	Methylcellulose	1	Trehalose	N2.18	Xanthan gum	0	0
N1.19	0	Sodium alginate	0	Mannitol	N2.19	Xanthan gum	0	0
N1.20	0	Sodium alginate	0	Mannitol	N2.20	Xanthan gum	0	0
N1.21	0	Sodium alginate	0	Mannitol				

X_{1S}: concentration of MFA; X_{2S}: type of MFA; X_{3S}: concentration of BA; X_{4S}: type of BA. X_{1O}: type of MFA; X_{2O}: concentration of MFA; X_{3O}: concentration of BA.

(MFA%: 5 levels; BA%: 5 levels), refined after the screening design (Table 1).

The evaluated responses included several pharmaceutical properties, both CQAs and additional characteristics: disintegration time, wetting time, water absorption ratio, mechanical resistance, and dissolution properties. For each response, a number of six samples per formulation were tested.

D-optimal experimental designs were generated for both screening and optimization purposes (Table 1). A D-optimal design represents the best subset of experiments chosen from a pool of theoretically possible experiments in a way that its runs cover the largest volume in the experimental region. The DoE software selects the best subset of runs through an automatic search algorithm. This design is selected in situations that cannot be handled using classical designs. These situations include the investigation of multi-level qualitative factors, irregular experimental regions and when a smaller number of runs is desired compared to a classical design. A drawback of D-optimal criterion is that it does not recognize the concept of lack of fit, but this is compensated by the software by adding three replicates at the overall center points [13,14].

The experimental design was selected based on its condition number and G-efficiency. The condition number shows the sphericity and symmetry of a design, and is defined as the ration of largest and smallest design diagonals. For a good screening design a condition number lower than 3 is needed whereas when our goal is optimization a condition number under 8 [13]. The design used for screening applications had a condition number of 2.9 and for the optimization design 5.4.

The second evaluation criteria, the G-efficiency is computed by considering the number of model terms, number of runs, and maximum relative prediction variance across the candidate set. For D-optimal designs, a G-efficiency above 60% is recommended [13]. This criteria had a value of 66% for the screening design and 86% for the optimization design.

For regression analysis the goodness of fit, capacity of prediction, model validity, and reproducibility were considered. The goodness of fit of a model is given by the value of R^2 and represents the variation of the response explained by the model. Q^2 represents the goodness of prediction and reveals how well the model can predict new experiments. R^2 and Q^2 are computed according to Equations (1) and (2).

$$R^2 = 1 - {SS_{res}}/{SS_{tot\ corr}}$$

Equation 1. Goodness of fit equation
SS_{res} – amount of variation that is not modeled
$SS_{tot\ corr}$ – total corrected variation in response

$$Q^2 = 1 - {SS_{press}}/{SS_{tot\ corr}}$$

Equation 2. Goodness of prediction equation
SS_{press}: prediction error sum of squares
$SS_{tot\ corr}$: total corrected variation in response

Model validity provides insights regarding the model error, and reproducibility (pure error) evaluates the variation of response under identical conditions compared to its total variation [13]. Model validity parameter relies on lack of fit test carried out in ANOVA, and for its calculation the p values is used. When there is no lack of fit ($p > .05$), the validity parameter will be above 0.25. Reproducibility is computed according to Equation (3).

$$Reproducibility = 1 - {MS_{pure\ \ error}}/{MS_{tot\ \ corr}}$$

Equation 3. Reproducibility calculation
MS variance

Pharmaceutical properties

The disintegration time (s) (Y1) was measured according to PhEur 8.0, by placing a lyophilized ODT in 200 ml of distilled water at a temperature of 20 ± 0.5 °C [6]. The time necessary for complete disintegration was recorded using a digital chronometer.

The wetting time (s) (Y2) was evaluated by recording the time necessary for complete water absorption of a tablet placed in a 4.5 cm diameter Petri dish with 4.5 ml 2% methylene blue aqueous solution on the surface of two pieces of filter paper. Each sample was weighed before (m1) and after (m2) the test, and by applying the *Y3 = 100*(m2 – m1)/m1* formula the water absorption ratio (%) (Y3) was determined [15].

Mechanical properties of lyophilized ODTs were evaluated using a Brookfield TexturePro CT1.5 analyzer (Brookfield Engineering, Lorch, Germany) equipped with an acrylic probe (TA10). A compression test was applied with a target value of 2 mm and a trigger load of 10 g. The speed of the probe was set to 0.1 mm/s. The mechanical resistance (g) (Y4) of the tablets represents the value of the load (g) at a penetration depth of 0.6 mm of the acrylic probe.

The *in vitro* dissolution studies were performed using a PharmaTest PTWS100 (PharmaTest, Germany) dissolution tester equipped with USP type 2 device (paddle). The dissolution study was carried out in 500 ml HCl 0.1 N at a stirring rate of 50 rpm. Sampling was done every 5 min for 30 min. Each redrawn sample was replaced with the equivalent volume of fresh dissolution media. The use of HCl 0.01 N as dissolution media for oral lyophilisates is justified considering the administration route and properties of this dosage form. After disintegration a dispersion is formed that is swallowed, therefore the dissolution of the API will take place mainly at the gastric level. Before reaching the gastric level, a part of the API may dissolve in the mouth, however considering the low solubility of LOR at pH 6.8 (pH of saliva) and the low volume of saliva, the main site of dissolution is the gastric fluid.

The responses used to evaluate the effect of variables on drug release were the percentage of API released at 5, 10, 15, 20, 25, and 30 min (Y5–Y10), respectively, the mean dissolution time (MDT) (Y11). The advantage for including the % of API released at each sampling point (Y5–Y10) in the response matrix is that it can highlight changes of factor effect through the dissolution process. Some factors may exert influence only in the initial phase of dissolution and others could have a consistent effect through the entire dissolution process. Using only a parameter that summarizes the dissolution process such as the MDT would not allow the identification of such effects, however it is kept as it provides an overview of the process.

The measured pharmaceutical parameters were included as responses into the two designs of experiments. Before model interpretation, ANOVA was used to test model significance and lack of fit. Effect of formulation variables on responses were evaluated by generating coefficient plots for linear design and surface contour plots for quadratic design.

Results and discussions

Quality risk management through FMEA

Development, manufacturing, and use of oral lyophilisates involve some degree of risk, mainly associated with the preparation process and the formulation robustness.

Therefore, the implementation of an effective quality risk management system should accompany the product's life cycle, since the development phase of the product, in order to ensure consistent high quality.

The quality target profile represents a prospective summary of quality attributes of a product designed to meet its intended use, considering the quality profile from both a safety and efficacy point of view [8]. Key product characteristics defined in the quality target product profile include: oral dosage form for pediatric use formulated using a minimum number of nontoxic excipients that will combine a good cake appearance with ultra fast disintegration time, a complete dissolution and an increased mechanical resistance.

Having a low disintegration time evaluated by *in vitro* method, suggests shorter *in vivo* times due to the mechanical forces exerted in the oral cavity, diminishing the risk for reduced therapeutic compliance caused by swallowing difficulties. Also for a fast onset of action a rapid dissolution is desired. Therefore, both disintegration and dissolution properties are relevant for the efficacy of the drug product. Considering the highly porous structure of freeze-dried cakes, they tend to be fragile and highly friable, therefore an appropriate mechanical resistance is needed for easy handling and administration.

All these properties were selected as CQA, for which specific ranges were defined to be within a specific domain to guarantee the desired product quality [8]. In order to meet its quality target profile, the drug product should disintegrate completely up to 10 s, along with a dissolution rate above 85% after 30 min, but still show a mechanical resistance above 300 g of load and a good cake appearance.

Figure 1 shows the Ishikawa diagram with process, formulation and analytical method related parameters that could exert an influence over disintegration time, hardness, and dissolution properties of oral lyophilisates selected as CQA's.

For each parameter, the RPN was calculated based on literature data and the experience of the researchers, considering their occurrence, severity of consequences, and detectability (Table 2). In the case of formulation and process-related parameters associated with RPN >30, risk-reduction strategies were suggested and implemented.

Process conditions were divided into suspension preparation phase and freeze-drying phase. Two critical aspects were identified in the suspension preparation step, one related to the hydration of the MFA and the second related to API's sedimentation. An incomplete hydration of the polymer in the volume of liquid could lead to differences in viscosity between batches or within the same batch, if an efficient distribution through the entire volume is not ensured. Viscosity differences, will affect especially the mechanical resistance, leading to heterogeneity into the dry cakes, and implicitly the disintegration time, dissolution properties and content uniformity of the final product. Viscosity differences were avoided by ensuring a complete over-night hydration of the MFA and by a homogenous distribution in the entire volume. To ensure the content uniformity of the API and avoid sedimentation, the suspension was transferred into blisters under continuous stirring and each filled blister was frozen immediately.

Out of the freeze drying parameters, the freezing rate and degree of supercooling will influence the ice crystal size leading to different internal porous structures and specific surface area of the cake [16]. However, the influence of this parameter was not investigated, as the lyophilization protocol included an annealing step for the complete crystallization of the BA. Annealing normalizes ice crystal size through Ostwald ripening, when larger ice crystals will grow at the expense of smaller ones, leading to a shift in particle size and particle size distribution [17].

Primary and secondary drying parameters such as shelf temperature, condenser temperature, and pressure can affect end product quality by influencing cake appearance and residual moisture. Working with lower than needed shelf temperatures in the primary drying phase would result a lengthy process and dramatically increase the cost of production, whereas a too high temperature could lead to batch loss due to product collapse and to a hard to handle product with low mechanical resistance [18]. The correct selection of process conditions was managed through preliminary thermal analysis applied as risk reduction strategy to identify the product's critical temperatures. Therefore, process related variables were not included as factors in the experimental design.

The physical properties of the API, type and concentration of both MFA and BA were identified as influential formulation factors.

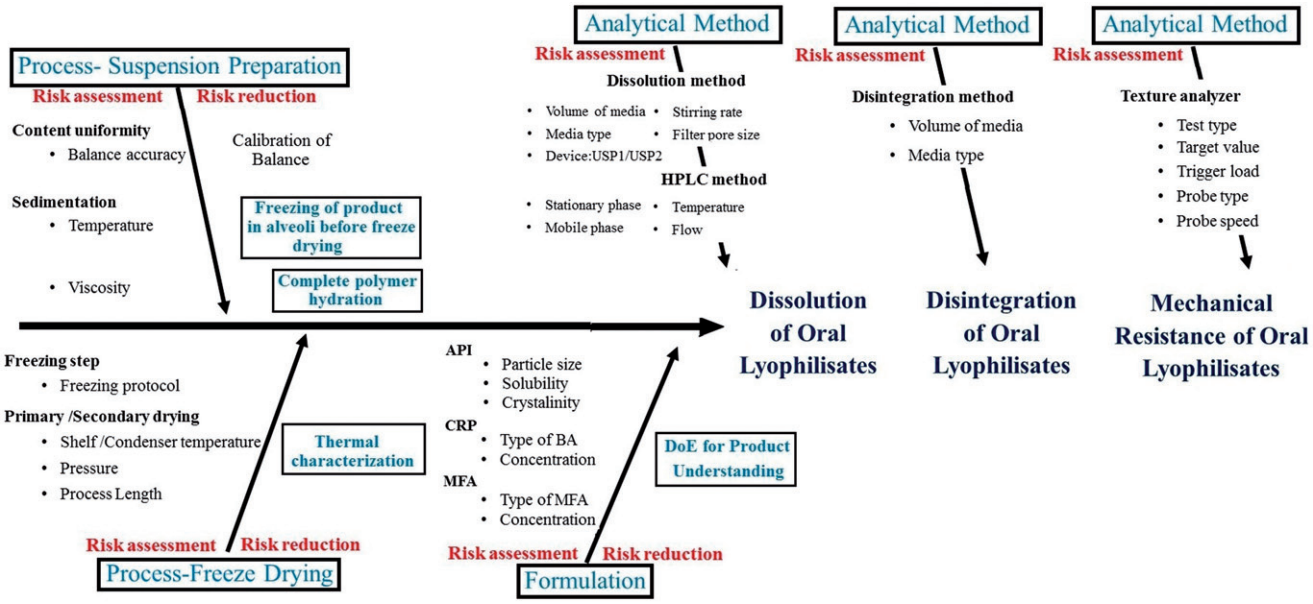

Figure 1. Ishikawa diagram illustrating factors with impact on CQA's of oral lyophilisates.

Table 2. FMEA Analysis for risk assessment.

Parameter	Failure mode	Failure effects	Potential causes	Control methods	O	S	D	RPN
Suspension preparation	Lack of content uniformity	Content uniformity	Non-calibrated balance	Calibrated balance	2	4	2	16
		Dissolution Disintegration	Incomplete hydration of polymer	Time for polymer hydration	3	4	3	36
		Mechanical resistance	Sedimentation	Quick freezing of product after dividing in blisters	4	4	3	48
Freeze drying	Cake structure: crystal and pore size	Dissolution Disintegration	Freezing rate	Thermal characterization	2	4	4	32
	Product collapse	Mechanical resistance	High-shelf temperature		3	4	3	36
	High residual moisture	API stability	Low drying time	Residual moisture determination	3	4	2	24
Formulation	API	Dissolution	Particle size, crystalinity	DoE for product understanding: design space development	3	3	3	27
	BA: type and concentration	Dissolution Disintegration	Unsuitable concentration, different excipients		5	5	3	75
	MFA: type and concentration	Mechanical resistance			5	5	3	75

D: the detectability; O: the occurrence; S: the severity.

Due to the low API content of each dosage unit and considering its high solubility in hydrochloric acid media (dissolution media), the physical properties of the API were not included in the experimental designs [19].The risk reduction strategy in this case would use relevant knowledge related to the effect of formulation variables by applying DoE to select a robust formulation from the generated Design Space.

Freeze drying cycle parameters selection

The optimization of the freeze-drying cycle should start with the assessment of the critical properties of the formulation, such as the product critical temperatures, drug stability and the characteristics of the excipients used [20].

DSC thermal analysis was used to gain insights over the type of physical structure that is formed during the freezing step and the associated critical temperatures that actually represent the maximum temperature the product can be exposed to without collapse or melting of the system.

Thermal analysis revealed the formation during the freezing process of a metastable glassy system for the formulations that contained mannitol, whereas formulations with other BA (lactose, sucrose, isomalt, trehalose) formed amorphous or partially amorphous systems. The thermograms of the amorphous systems showed only one endothermic thermal event, caused by the melting of the ice crystals surrounding the interstitial space.

The thermogram of the metastable glassy systems with mannitol, showed a glass transition temperature, followed by a crystallization exothermic event and the interstitial ice melt endotherm (Figure 2). The metastable glassy structure formed due to the incomplete crystallization of the BA.

As the sample (N1.2) was warmed up from –50 °C, the first thermal event captured in the thermogram was the glass transition temperature (Tg'), at –39.3 °C, where the system's viscosity reduced and increased its fluidity (Figure 2).

Above Tg' the mobility of the system is increased, a rearrangement takes place with the formation of stable crystalline structures due to crystallization events [21]. Compared to glass transitions, crystallization is a high energy event that is captured in the thermogram as an exothermic peak at –29.6 °C.

The potential of the system to form a metastable glassy structure and the temperature regions of the glass transition and

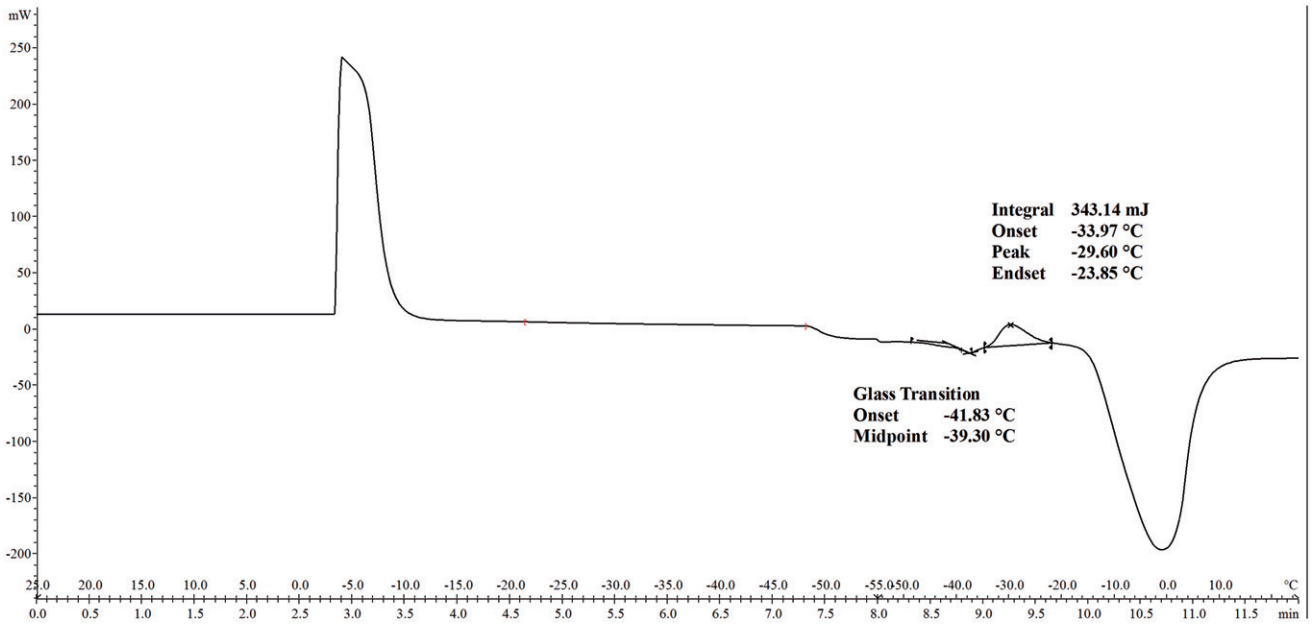

Figure 2. DSC thermogram of N1.2 screening formulation.

crystallization events provided by DSC were used for the implementation of an adequate annealing protocol in order to ensure the formation of the more stable crystalline form.

The recommended temperature for annealing should be taken above the glass transition and the crystallization exotherm, but not too far so that ice melt endotherm would not occur [21]. The formulations with mannitol manifested a crystallization endotherm peak from −27.55 °C to −29.6 °C with the ice melt endotherm onset at approximately −15 °C. According to these temperature regions, the annealing temperature should be set between −27.55 °C and −15 °C. Taking into consideration, the ice melting endotherm onset of non-mannitol formulations that manifested at lower temperatures (the lowest endothermic melt onset at −18.6 °C), and the presence of different effects (edge effect) that occur during the lyophilization process that contributes to the increase of the temperature in specific areas on the shelf, a safe, and appropriate annealing temperature of −25 °C was selected. This allowed the preparation of all experimental runs with one cycle without the risk of failure due to the collapse of cake.

As water desorption rate in the secondary drying phase is influenced mostly by temperature, a high shelf temperature (15 °C) was used to ensure an efficient water removal [20].

Screening step

CQAs are influenced by formulation variables, therefore a careful selection of the type of excipients and their quantitative level is necessary.

Fitting of experimental data

The screening experimental design (D-optimal Linear) was fitted using Projection to Latent Structures by Partial Least Square (PLS) model, being justified by the small amounts of missing data in the response matrix and the presence of several correlated responses. Other situations for PLS modeling are distorted designs with high condition number. Also the method assumes the presence of noise and can separate variability caused by changes in factor settings from the residuals [13].

The first PLS model developed for overview purposes included all responses. In the c1*c2 loadings (Figure 3), the relationship between the responses can be observed. The c vector is used in PLS to linearly combine the responses (Ys) to form the response score vector u, meaning that it represents the link between Ys and X score vector t [10].

The responses that are clustered together are correlated, having similar values of the influencing factors coefficients, therefore five different PLS models were generated based on the grouping patterns. There are two clusters of response, the first cluster includes disintegration (Y1) and wetting time (Y2), whereas the second cluster contains dissolution data (Y5–Y10). As expected, the mean dissolution time (Y11) is found in the opposite diagonal parts of the scatter plot compared to the dissolution data cluster (Y5–Y10), as they measure the same characteristic of the product in different ways. An increased dissolution of the active ingredient is associated with a low mean dissolution time. Water absorption ratio (Y3) and mechanical resistance (Y4) were modeled separately. The summary of fit for the responses evaluated in the screening step are presented in Table 3.

All PLS models presented good validity (>0.25) suggesting there is no lack of fit for each considered response. From the reproducibility values (>0.8) it can be deduced that the experimental setup was appropriate and by working under identical conditions similar responses were obtained within the replicates. The developed models take account of most of the response variation ($R^2 > 0.8$) and have good predictive capacity ($Q^2 > 0.5$).

Influence of factors over product quality attributes

Before interpreting a model, it is indicated to test the model significance and lack of fit applying ANOVA. In this regard, the total variation of a response is decomposed into a part that is captured by the regression model and into an un-modeled part, called residuals. The presence of replicated experiments allows further decomposition of the residuals into model error (model imperfections) and into replicate error. These types of variability are further compared by means of two *F*-tests [13].

The first test evaluates the model significance by comparing the variances of the modeled part with the residuals, and is

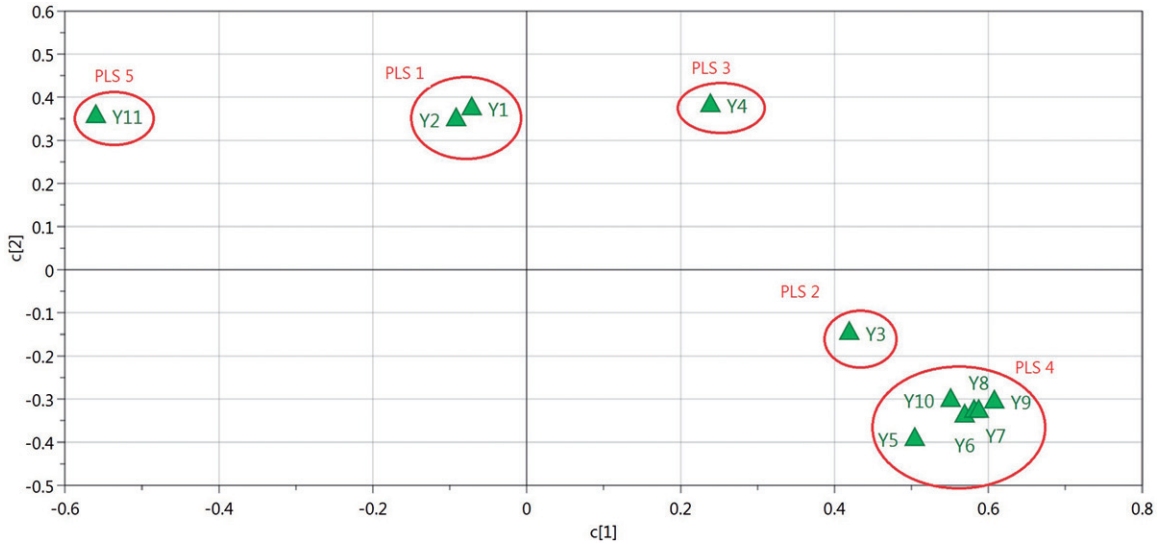

Figure 3. Loading plot c[2] versus c[1] of the initial PLS model generated for all responses. The five groups of correlated responses are marked with a red circle Y1-Disintegration time; Y2-Wetting time; Y3-%absorbed water; Y4-Mechanical resistance; Y5-% API released at 5 min; Y6-% API released at 10 min; Y7-% API released at 15 min; Y8-% API released at 20 min; Y9-% API released at 25 min ; Y10-% API released at 30 min; Y11-Mean dissolution time (TMD).

Table 3. Summary of fit for screening and optimization designs.

		Screening			
	Response	R2	Q2	Validity	Reproducibility
PLS model 1	Y1-disintegration time	0.905	0.710	0.586	0.926
	Y2-wetting time	0.802	0.517	0.628	0.826
PLS model 2	Y3-water absorption ratio	0.864	0.708	0.600	0.927
PLS model 3	Y4-mechanical resistance	0.956	0.749	0.857	0.909
PLS model 4	Y5-% API released at 5 min	0.896	0.613	0.492	0.928
	Y6-% API released at 10 min	0.955	0.724	0.766	0.926
	Y7-% API released at 15 min	0.965	0.734	0.775	0.941
	Y8-% API released at 20 min	0.969	0.731	0.785	0.946
	Y9-% API released at 25 min	0.952	0.648	0.696	0.937
	Y10-% API released at 30 min	0.948	0.647	0.853	0.882
PLS model 5	Y11-mean dissolution time	0.983	0.822	0.871	0.956
		Optimization			
MLR model	Y1-disintegration time	0.971	0.946	0.650	0.987
	Y2-wetting time	0.980	0.944	0.786	0.981
	Y3-water absorption ratio	0.915	0.755	0.723	0.938
	Y4-mechanical resistance	0.952	0.817	0.712	0.967
	Y5-% API released at 5 min	0.815	0.531	0.651	0.911
	Y6-% API released at 10 min	0.841	0.655	0.796	0.859
	Y7-% API released at 15 min	0.895	0.727	0.802	0.896
	Y8-% API released at 20 min	0.925	0.818	0.930	0.838
	Y9-% API released at 25 min	0.925	0.822	0.841	0.908
	Y10-% API released at 30 min	0.927	0.837	0.917	0.858
	Y11-mean dissolution time	0.862	0.704	0.680	0.930

satisfied when $p < .05$. The second f-test is also called lack of fit test and compares the model error with the replicate error. When the two variances are of comparable magnitude ($p > .05$) the test is satisfied and there is no lack of fit.

Considering the *F*-test results presented in Table 4 all models are significant and have no lack of fit.

Model interpretation can be done easily through coefficient plots that show the magnitude and direction of factor effect for each considered response (Figure 4). Coefficients are calculated by the software considering the design matrix and response matrix plots and are represented as bar charts with the corresponding 95% confidence interval superimposed. These error bars represent the uncertainty of each coefficient and if it includes 0 value, the term is insignificant [13].

According to the PhEur8.0 specifications regarding the disintegration time of orodispersible dosage forms, the maximum allowed time for complete disintegration is 3 min [6]. On the other hand, the FDA guidance recommends 30 s [22]. Disintegration ensures a complete dispersion of the product in saliva, allowing rapid drug release, and facilitates an easy administration.

The screening design formulations disintegrated between 2 and 160 s, except for the formulation with methylcellulose and trehalose, which did not disintegrate, leading to missing data in the response matrix.

The coefficient plot of Y1 revealed a marked influence from the type of the excipient used and not by the concentration of both BA and MFA (Figure 4). Lyophilisates with HPMC presented and increased disintegration time (40–160 s) followed by formulations with methylcellulose (9–61 s). The lowest values for this response were recorded for xanthan gum-based products (2–6 s) and for sodium alginate (8–22 s).

Table 4. ANOVA Test results for model significance and lack of fit (p values).

	Screening		Optimization	
Response	Model significance	Lack of fit test	Model significance	Lack of fit test
Y1-Disintegration time	4.92E−04	0.192	2.80E−10	0.248
Y2-Wetting time	1.39E−02	0.226	2.63E−10	0.427
Y3- water absorption ratio	1.22E−05	0.203	1.47E−05	0.332
Y4-Mechanical resistance	4.52E−05	0.566	4.94E−07	0.317
Y5-% API released at 5 min	3.23E−03	0.132	3.86E−04	0.248
Y6-% API released at 10 min	8.99E−05	0.394	3.65E−05	0.444
Y7-% API released at 15 min	3.02E−05	0.408	1.08E−05	0.454
Y8-% API released at 20 min	1.74E−05	0.424	1.35E−06	0.758
Y9-% API released at 25 min	1.26E−04	0.297	1.29E−06	0.531
Y10-% API released at 30 min	1.78E−04	0.556	1.05E−06	0.719
Y11-Mean dissolution time	6.46E−06	0.598	1.37E−05	0.279

The wetting of the tablet is a phenomenon that occurs before disintegration when the tablet gets in contact with the fluid, and water starts rapidly passing through its structure, considering the high porosity and hygroscopic nature of freeze dried products. The same effects characterize the wetting time (Y2) as it is correlated with Y1.

The percentage of absorbed water (Y3) was influenced by the concentration of BA and in the case of MFA by both concentration and excipient type. Higher MFA content increased the percentage of absorbed water, whereas the BA content exerted an opposite effect. Out of all MFA, the highest weight increase was obtained for sodium alginate based oral lyophilisates (Figure 4).

The mechanical resistance of the developed oral lyophilizates was influenced by the type of MFA used (Figure 4). Tablets with cellulose based MFAs showed the highest load at a penetration depth of 0.6 mm with values up to 2420 g for HPMC and 1805 g

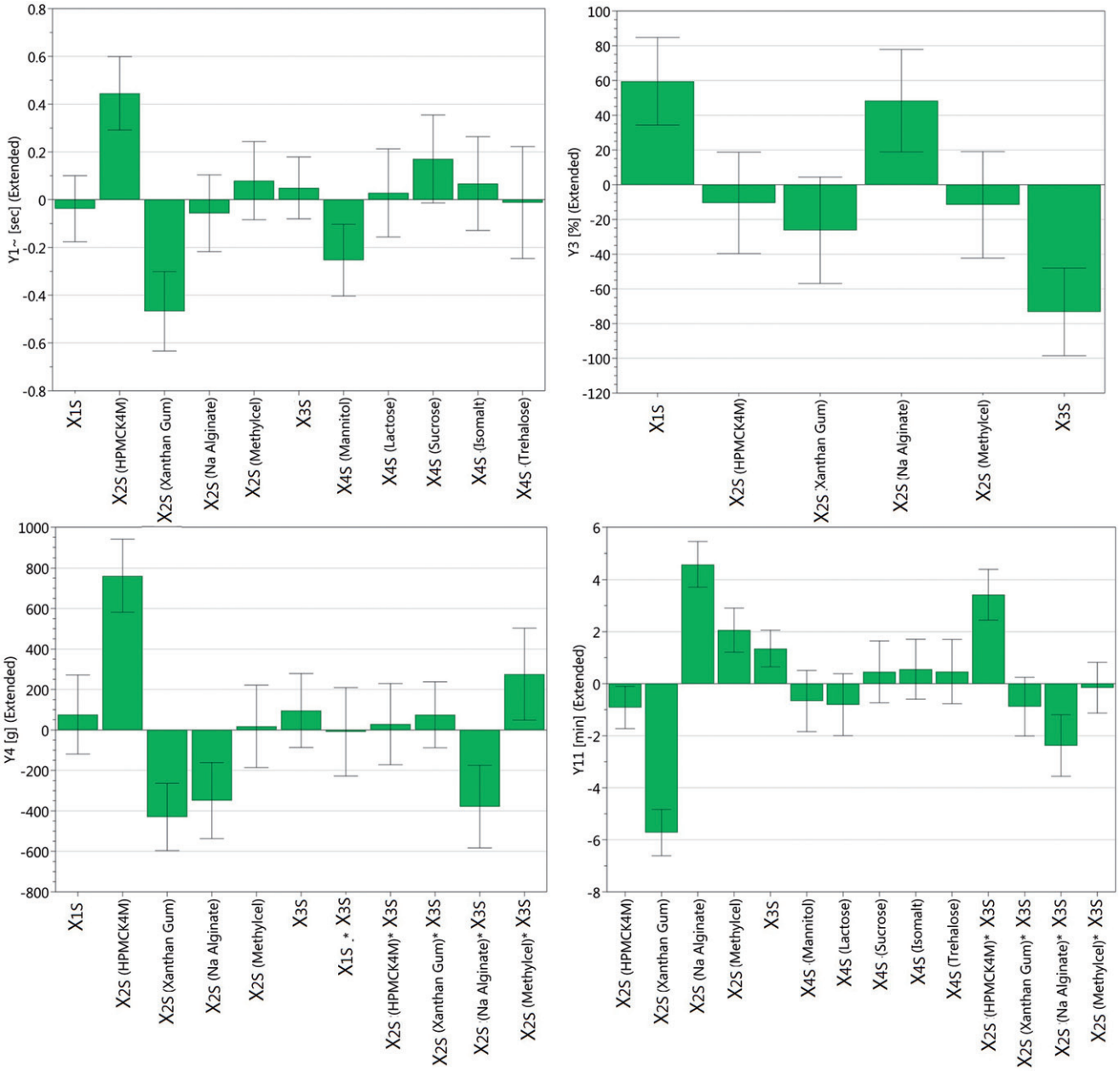

Figure 4. Coefficient plots showing the influence of formulation variables on the responses Y1, Y3, Y4, and Y11, revealed in the screening design Y1-Disintegration time; Y3-%absorbed water; Y4-Mechanical resistance; Y11-Mean dissolution time (TMD), X1S-Concentration of MFA, X2S-Type of MFA, X3S-Concentration of BA, X4S-Type of BA.

for methylcellulose. For sodium alginate load values ranged between 282–1215 g and for xanthan gum between 184 and 688 g.

The equation of the model developed for mechanical resistance included an interaction term between the type of MFA and the concentration of BA. Although such a behavior is not well-defined, the interaction term is kept in the model in order to maintain good model performance.

The mean dissolution time of the formulations varied between 3:40 and 22:33 min, being mainly influenced by the type of the MFA used. The release of the API from the pharmaceutical form was the fastest in tablets with xanthan gum (3:40–13:20 min), despite the type of BA used. Tablets with sodium alginate had the highest mean dissolution times (16:20–22:33 min), followed by methylcellulose formulations (14:23–19:14 min). The concentration of the BA exerted a positive effect, slightly increasing the time needed for complete release and this effect was independent of the BA qualitative levels (Figure 4). The same interaction term between the type of MFA and the concentration of BA is included in the model's equation. By increasing the concentration of BA it largely increases the mean dissolution time in the case of lyophilisates with HPMC, but it slightly reduces the dissolution time for lyophilisates with sodium alginate.

The most suitable MFAs considered for optimization studies were sodium alginate and xanthan gum, considering that formulations with these excipients presented the lowest disintegration time and sufficient mechanical resistance. Although xanthan gum and sodium alginate formulations showed lower than average resistance as suggested in the coefficient plot of Y4, it is possible to yield a mechanical resistance with these variables above the minimum admitted value considered to affect the product's ease of handling. Also sodium alginate lyophilisates favored higher water uptake compared to other MFA (Figure 4).

Frequently the development of a robust formulation involves making a compromise, especially if responses work against each other. Tablets with HPMC were associated with the highest mechanical resistance but also with an increased disintegration time, therefore it was not considered for further studies as a longer disintegration time could influence the product's ease of swallowing. Higher disintegration time was observed for methylcellulose formulations also.

Considering the dissolution properties the choice of xanthan gum is obvious as formulations with this MFA showed the lowest MDT. Polyelectrolytes such as xanthan gum exhibit more hydrophilic properties compared to non-charged polymers, like cellulose derivates, and allow fast hydration of the polymer chains [23]. Polymer hydration starts with the uptake of the primary-bound water by polymer's hydrophilic groups that leads to the swelling of the polymer and exposes hydrophobic groups for further hydration [24].

Longer MDT associated with sodium alginate based lyophilisates can be explained based on polymer properties and are not considered to occur under *in vivo* conditions as the tablet will be swallowed after disintegration. Sodium alginate is also an anionic polymer with hydrophilic properties due to the charges found on the monomeric units of α-D-mannuronate and sz-L-glucuronate [25]. The polymer is slowly soluble in water, but in aqueous solutions with pH below 3 becomes practically insoluble [26]. This solubility issue under acidic conditions prolongs the time needed for complete release of the API in the dissolution medium, when the dissolution testing is carried out on the tablet. However, by definition, this type of product after administration will form a dispersion in the oral cavity that is swallowed. The same sodium alginate formulations were subjected to disintegration in 5 ml of artificial saliva for 1 min, and the formed dispersion was transferred into the dissolution tester vessel. In this case, the complete dissolution of LOR was achieved in less than 7 min (data not shown). However, in order to ensure the discriminative power of the dissolution method, the test was carried out on tablets and not on dispersions formed by disintegration in artificial saliva.

Formulations with 10 mg/ml sodium alginate (ex. N1.3) had high mechanical resistance (586 g load), low disintegration time (5 s) with an API release after 30 min close to the specifications (84.16% released), therefore the −1 concentration level was decreased to 7 mg/ml. In the case of xanthan gum, its highest concentration range was increased up to 6 mg/ml considering observations from the experimental work. Oral lyophilisates with higher levels of xanthan gum and low levels of mannitol released slightly below 80% LOR after 30 min.

Out of all BAs, mannitol was selected due to its effect of reducing the disintegration time as suggested by the coefficient plot for this response and because of improved visual aspect of mannitol based cakes (Figure 4). Lower disintegration times linked to the use of mannitol as filler in orodispersible tablets were demonstrated in other studies, and are due to a higher hydrophilicity and porosity of the cake [27,28]. The concentration range of mannitol was kept constant (60–120 mg/ml).

Optimization step

The refined variables obtained from the screening experimental design were further investigated by adding higher variation levels to the quantitative factors, this way providing a better description of their effect. The presence of quadratic terms in the optimization experimental design allowed the modeling of curvature [13]. Using contour plots, non-linear effects can be visualized, while these are not pointed out in coefficient plots.

Fitting of experimental data

Before model interpretation ANOVA statistical test with 95% confidence interval was applied. The calculated p values suggest significant models with no lack of fit (Table 4). The fitting of experimental data was done using multi-linear regression, each model presented good predictive capacity ($Q^2 > 0.5$), high reproducibility and explained most of the response's variability ($R^2 > 0.8$) (Table 3).

Influence of factors over the CQA

All formulations from the optimization experimental design showed disintegration times under 1 min. The type of polymer used had an influence over this response, tablets with sodium alginate presented higher disintegration time, up to 54 s, whereas xanthan gum based lyophilisates were completely dispersed at maximum 6 s. The concentration of mannitol had no influence over the disintegration time, the response being mainly influenced by the concentration of the MFA (Figure 5).

A similar pattern was obtained for the surface contour plots for wetting time, in the case of both MFAs. Higher wetting times were obtained for tablets with sodium alginate. The response was influenced by the level of mannitol, as an increase in this variable lead to a structure with higher density, and water absorption was longer. The effect of mannitol concentration was not observed in the first response, suggesting that the disintegration time was limited only in the humectation phase, and then lost its

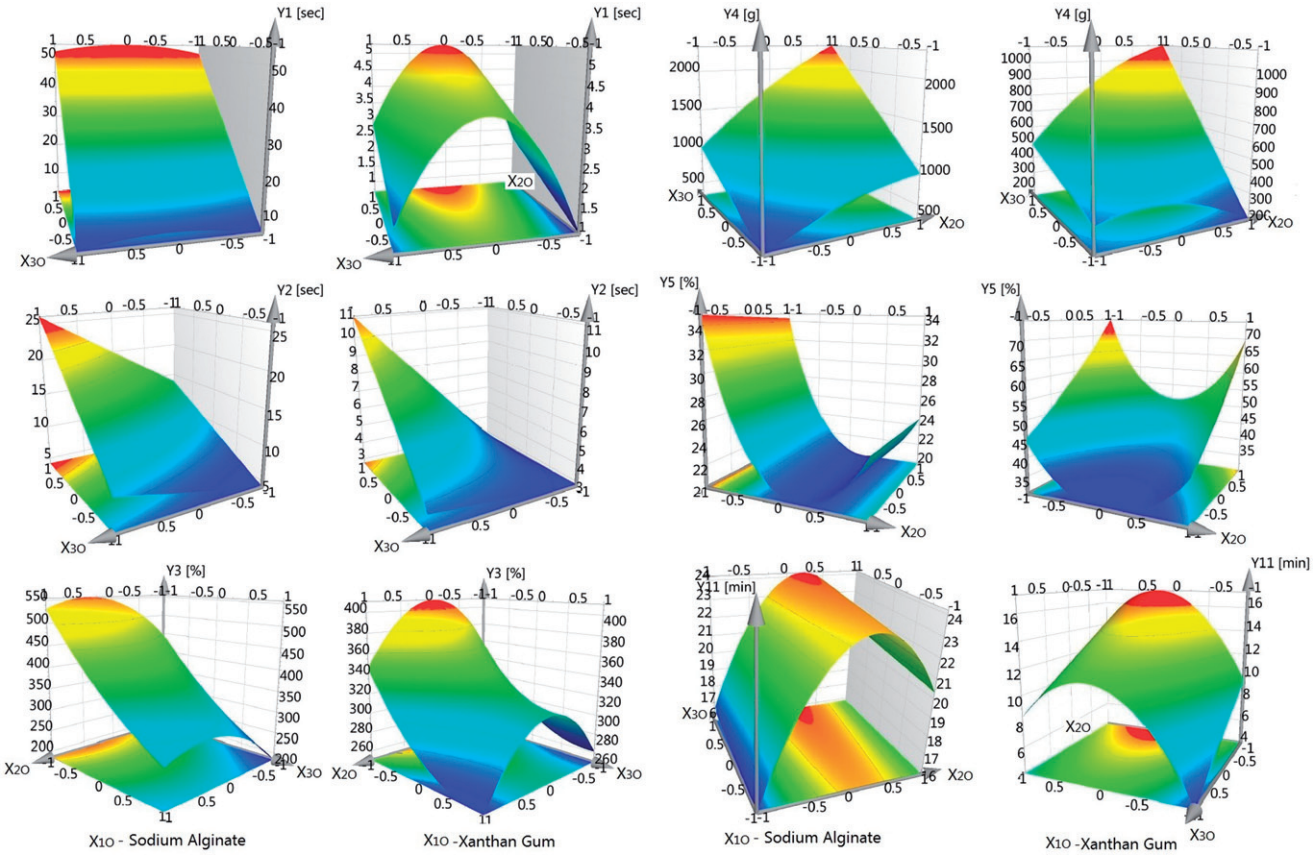

Figure 5. Response surface plots for Y1–Y5, Y11, derived from the optimization design Y1-disintegration time; Y2-wetting time; Y3-% absorbed water; Y4-mechanical resistance; Y5-% API released at 5 min; Y11-mean dissolution time; XO1-type of MFA; XO2-concetration of MFA; XO3-concentration of BA.

significance in front of the other quantitative factor, the concentration of MFA.

As water got absorbed into the tablet, the polymer hydrated and transformed into a gel. Depending on the quantity of the MFA in the formulation the viscosity of the gel increased, becoming a barrier for further penetration. The percentage of absorbed water can be maximized by using a low level of mannitol and an intermediate level of MFA. Both polymers led to a high percentage of water uptake, with slightly higher values in the case of sodium alginate. The concentration of mannitol had a negative influence, based on the consolidating effect on tablet structure. At low to intermediate concentration levels of MFA, the percentage of water absorbed is proportional to the quantity of polymer in the formulation, getting a higher mass increase proportionally to the quantity of gel formed. At high concentrations of MFA, the water uptake decreases, as the gel formed is more viscous and does not allow further water absorption. This effect is more predominant in case of lyophilisates with xanthan gum, and it's suggested by the more prominent curvature at middle concentrations of MFA in its surface contour plot (Figure 5).

The mechanical resistance of tablets was influenced by both the concentration of MFA and BA for both sodium alginate and xanthan gum formulations. The resistance of lyophilisates with sodium alginate reached load values up to 2579 g, approximately two times higher compared to maximum value for xanthan gum based products. A value of 300 g load was considered as the lowest value that was still suitable, allowing an easy handling.

According to other findings, an increase in binder concentration ensures longer disintegration times and higher mechanical strength [28]. An optimum mechanical strength and dissolution time is achievable by adding low concentrations of matrix former agents and appropriate concentrations of sugar alcohols as fillers in order to consolidate the porous structure [29].

Due to a lower mechanical resistance and lower disintegration times of xanthan gum tablets, the dissolution of the API was faster compared to sodium alginate tablets. The surface contour plots of the percentage of the API released at 5 min using the two polymers are presented in Figure 5.

In the case of sodium alginate tablets, only the concentration of the MFA exerted an influence over the release of the API, and the influence was constant through the entire dissolution.

The dissolution from xanthan gum tablets was influenced by both concentrations of MFA and BA. As dissolution advanced, the release of the API was influenced less by the level of mannitol, and this quantitative factor lost its significance in function of time. This effect can be observed in Figure 6, that represents simultaneously the surface contour plots of Y5–Y10 responses, where the sheets are becoming more horizontal along the X3 ax, as a function of time. The same effect over dissolution can be observed when using the mean dissolution time as a response (Figure 5). Coefficient values and statistical significance of model terms are given in Supplementary material.

Previous studies that investigated the effects of formulation variables and freeze drying parameters on the development of freeze dried oral lyophilisates with meloxicam and methylcellulose as MFA, concluded that mannitol exerts a positive influence over the dissolution rate and reduces the mechanical resistance of the product [15]. In this work, it was found that mannitol increased the mechanical resistance of both sodium alginate and xanthan gum tablets, and it was identified as a critical quantitative variable for the product quality attributes. These differences in effects of mannitol, suggests that its effect depended on the type of

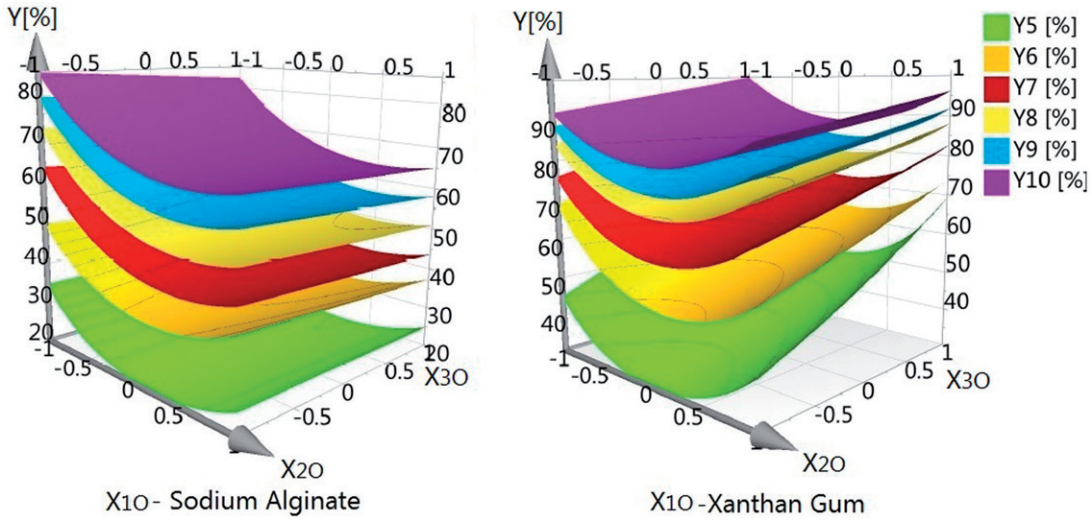

Figure 6. Response surface plots for Y5–Y10, derived from the optimization design; Y5-% API released at 5 min; Y6-% API released at 10 min; Y7-% API released at 15 min; Y8-% API released at 20 min; Y9-% API released at 25 min; Y10-% API released at 30 min; X1O-type of MFA; X2O-concentration of MFA; X3O-concentration of BA.

polymer used as MFA. Regarding the effect the BA over the dissolution rate, it did not influence the release rate from sodium alginate tablets, whereas it manifested a gradually decreasing influence in the case of xanthan gum based formulations.

Design space

Risk minimization and design space development for the product is a major objective of QbD. Design space plots are generated by superimposing several response contour plots and combining it with probability analysis. The probability to meet the product specifications in the design region were estimated using the models developed for CQAs and Monte Carlo simulations. Design space plot is a probability plot with color coded regions and contour lines that separate the design region according to the probability of failure expressed as percentage [13]. From the surface area of the color-coded window, regions with low probability of failure point out the variable combinations for which the quality target profile is fulfilled, with highest chance of meeting the desired properties.

As CQAs (Y1, Y4, Y10) are considered to be the most relevant parameters that reflect batch quality, they were selected as responses in the Optimizer software and were set to meet specific target values within an acceptable interval. Other associated responses (Y2, Y3, Y5–Y9, Y11) were used through the study to provide a better understanding of the product.

Because sodium alginate formulations from the optimization experimental design did not meet the requirements regarding the dissolution properties, design space was generated only for xanthan gum formulations.

For disintegration time, an interval of 1–30 s and a target value of 5 s, while for mechanical resistance, an interval of 300–930 g of load with a target value of 600 g was selected. The minimum load that enabled an easy handling of the product was considered to be at least 300 g at a penetration depth of 0.6 mm, so this value was set to be the low interval, whereas the maximum limit was set to 930 g, the highest value found among xanthan gum formulations. Considering the percentage of released API after 30 min, the minimum and maximum levels were set to 85% and 100%, and a target value of 95%. Based on these settings, the design space was generated for xanthan gum based formulations (Figure 7).

For the validation of the design space, formulations were prepared inside the 5% probability of failure (V1, V2), near the edge of 10% probability of failure (V3), near the edge of 20% probability of failure (V4), and above 50% probability of failure (V5). The recovery of the observed Y1, Y4, and Y10 responses of all the previously mentioned formulations outside and inside the low probability failure region was calculated against the values predicted by the model (Table 5).

For all the formulations the recovery of Y1, Y4, and Y10 was close to 100%. Although all the formulations presented low disintegration times, therefore meeting the first requirement, the difference between them was limited to the other two responses.

V1 and V2 combined a high mechanical resistance with dissolution properties and disintegration time, meeting the requirements of the previously defined quality target profile. Both formulations disintegrated in approximately 5 s and released above 90% API in 30 min, without compromising the mechanical resistance.

Formulations V3 and V4 had both good hardness values, but the released API was close to 85%, the minimum admitted limit. Formulation V5 failed the dissolution test, with only 84% released after 30 min, and also presented the minimum admitted resistance limit.

Optimization of medicinal products for pediatric use is a challenging task, considering the swallowing difficulties associated with tablet administration. Orodispersible tablets have been proposed and studied as alternative choice to conventional dosage forms throughout different studies. Chen et al. prepared oral dispersible tablets loaded with prednisolone nanoparticles by direct compression reaching a minimum disintegration time of 15 s through optimization of various formulation variables such as: superdisintegrant, microcrystalline cellulose and chitosan content and of process variables such as compression force [30]. Labib GS prepared highly palatable effervescent tablets with levocetirizine-hydroxypropyl-sz-cyclodextrine (HP-sz-CD) taste masked complexes by direct compression yielding *in vivo* disintegration times between 14 and 60 s [31].

Compared to other technologies applied for orodispersible dosage forms production for pediatric population, such as direct

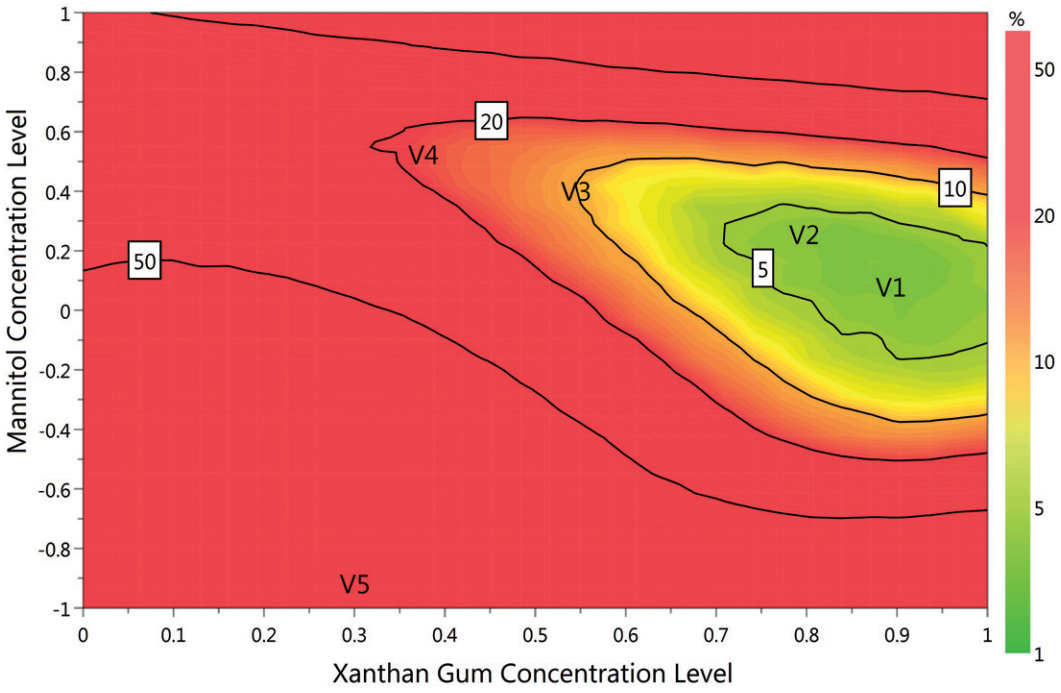

Figure 7. Design space plot represented by plotting the Mannitol concentration level against the MFA (Xanthan gum) concentration level. V1–V5 represents the five formulations prepared for design space validation.

Table 5. Design space validation results.

Formulation	V1	V2	V3	V4	V5
X_{10}	Xanthan gum				
X_{20}	0.9	0.8	0.55	0.4	0.33
X_{30}	0.1	0.3	0.4	0.5	−1
Predicted Y1	5.18	4.95	4.59	4.26	1.68
Observed Y1	5	5	5	4	2
Recovery	96.43	100.96	108.69	93.68	118.41
Predicted Y4	673.66	764.85	794.36	816.09	280.80
Observed Y4	699.4	821.3	806	812.25	300
Recovery	103.81	107.37	101.46	99.52	106.83
Predicted Y10	90.97	90.25	87.84	87.12	81.59
Observed Y10	93.47	93.86	86.64	86.04	84.67
Recovery	102.74	103.99	98.62	98.74	103.76

X_{10}: type of MFA; X_{20}: concentration of MFA: X_{30}: concentration of BA.

compression, freeze-drying allows the formulation of ultra-rapidly disintegrating drug products by ensuring a highly porous structure of the pharmaceutical system. Therefore the number of formulation components can be kept at minimum, excipients such as superdisintegrants and lubricants commonly found in compressed tablets are not needed [32].

Conclusions

This study proposed the development of orodispersible tablets by freeze-drying technology with respect to pediatric medicine development guidelines, by applying risk management strategies and DoE as an integrated QbD approach.

The development of an optimized formulation that respected the quality target profile was possible through the identification, systematic characterization, and control of influential process and formulation parameters.

Both quantitative and qualitative variables introduced in the experimental design influenced the product's disintegration time, mechanical resistance and dissolution properties selected as CQA. Therefore, the risk assessment results of FMEA were confirmed through DoE.

Disclosure statement

No potential conflict of interest was reported by the authors.

Funding

This research project was supported by Iuliu Hatieganu University of Medicine and Pharmacy through Doctoral Research Project number 7690/18/15.04.2016.

ORCID

Tibor Casian http://orcid.org/0000-0003-4984-8216
Sonia Iurian http://orcid.org/0000-0002-5009-9550
Catalina Bogdan http://orcid.org/0000-0003-3726-781X
Lucia Rus http://orcid.org/0000-0002-1718-1384
Ioan Tomuta http://orcid.org/0000-0002-5094-008X

References

[1] Salunke S, Hempenstall J, Kendall R, et al. European Paediatric Formulation Initiative's (EuPFI) 2nd conference commentary- Formulating better medicine for children. Int J Pharm. 2011;419:235–239.
[2] World Health Organization. Development of Paediatric Medicines: Points to Consider in Pharmaceutical Development. Working document QAS/08.257/Rev.3; 2011.
[3] EMA. Guideline on pharmaceutical development of medicines for paediatric use. 2013 [cited 2016 June 7]. Available from: http://www.ema.europa.eu/docs/en_GB/document_library/Scientific_guideline/2013/07/WC500147002.pdf

[4] Lopez FL, Ernest TB, Tuleu C, et al. Formulation approaches to pediatric oral drug delivery: benefits and limitations of current platforms. Expert Opin Drug Deliv. 2015;12:1727–1740.
[5] Fields J, Go JT, Schulze KS. Pill properties that cause dysphagia and treatment failure. Curr Ther Res Clin Exp. 2015;77:79–82.
[6] European Directorate for the Quality of Medicines (EDQM) European Pharmacopoeia. 8th ed. Strasbourg, France: Council of Europe; 2014.
[7] Sam T, Ernest TB, Walsh J, et al. A benefit/risk approach towards selecting appropriate pharmaceutical dosage forms-an application for paediatric dosage form selection. Int J Pharm. 2012;435:115–123.
[8] Guidance for Industry. Q8(R2) Pharmaceutical Development. 2009 [cited 2016 August 9]. Available from: http://www.fda.gov/downloads/Drugs/./Guidances/ucm073507.pdf
[9] Guidance for Industry Q9 Quality Risk Management. 2006 [cited 2016 October 18]. Available from: http://www.fda.gov/cder/guidance/index.htm.
[10] Eriksson L, Byrne T, Johansson E, et al. Multi- and megavariate data analysis: basic principles and applications. 3rd ed. Malmo: MKS Umetrics AB; 2013.
[11] Kaljevic O, Djuris J, Djuric Z, et al. Application of failure mode and effects analysis approach for formulation of carvedilol compression coated tablets. J Drug Deliv Sci Technol. 2016;32:56–63.
[12] Vora C, Patadia R, Mittal K, et al. Risk based approach for design and optimization of stomach specific delivery of rifampicin. Int J Pharm. 2013;455:169–181.
[13] Eriksson L, Johansson E, Kettaneh-Wold N, et al. Design of experiments principles and applications. 3rd ed. Sweden: Umetrics; 2008.
[14] Aguiar PF, Bourguigon B, Khots MS, et al. Tutorial D-optimal designs. Chem Int Lab Syst. 1995;30:199–210.
[15] Iurian S, Tomuta I, Bogdan C, et al. Defining the design space for freeze-dried orodispersible tablets with meloxicam. Drug Dev Ind Pharm. 2016;42:1977–1989.
[16] Geidobler R, Winter G. Controlled ice nucleation in the field of freeze-drying: Fundamentals and technology review. Eur J Pharm Biopharm. 2013;85:214–222.
[17] Searles JA, Carpenter JF, Randolph TW. Annealing to optimize the primary drying rate, reduce freezing-induced drying rate heterogeneity, and determine Tg′ in pharmaceutical lyophilization. J Pharm Sci. 2001;90:872–887.
[18] Pikal MJ, Shah S. The collapse temperature in freeze drying: Dependence on measurement methodology and rate of water removal from the glassy phase. Int J Pharm. 1990;62:165–186.
[19] Li H, Tan Y, Yang L, et al. Dissolution evaluation in vitro and bioavailability in vivo of self-microemulsifying drug delivery systems for pH-sensitive drug loratadine. J Microencapsul. 2015;32:175–180.
[20] Tang XC, Pikal MJ. Design of freeze-drying processes for pharmaceuticals: practical advices. Pharm Res. 2004;21:191–200.
[21] Schwegman J. Using differential scanning calorimetry (DSC) for Optimized Lyophilization Cycle Design, SP Sci. Techcnical Notes - LyoLearn Tech Briefs. 2011;1–6.
[22] U.S. Department of Health and Human Services Food and Drug Administration. Guidance for Industry Orally Disintegrating Tablets. [Online] 2008. Available from: http://www.fda.gov/downloads/Drugs/GuidanceComplianceRegulatoryInformation/Guidances/ucm070578.pdf
[23] Kocherbitov V, Ulvenlund S, Briggner LE, et al. Hydration of natural polyelectrolyte xanthan gum: comparison with non-ionic carbohydrates. Carbohydrate Polym. 2010;82:284–290.
[24] Bueno VB, Bentini R, Catalani LH, et al. Synthesis and swelling behavior of xanthan-based hydrogels. Carbohydr Polym. 2013;92:1091–1099.
[25] Tavassoli-Kafrani E, Shekarchizadeh H, Masodpour-Behabadi M. Development of edible films and coatings from alginates and carrageenans. Carbohydr Polym. 2016;137:360–374.
[26] Rowe R, Sheskey P, Quinn M. Handbook of Pharmaceutical Excipients. 6th ed. Chicago (IL): Pharmaceutical Press; 2009.
[27] Chandrasekhar R, Hassan Z, AlHusban F, et al. The role of formulation excipients in the development of lyophilised fast-disintegrating tablets. Eur J Pharm Biopharm. 2009;72:119–129.
[28] AlHusban F, Perrie Y, Mohammed AR. Preparation, optimization and characterization of lyophilised rapid disintegrating tablets based on gelatin and a saccharide. Cdd. 2010;7:119–129.
[29] Stange U, Fuhrling C, Gieseler H. Influence of non-water_-soluble placebo pellets of different sizes on the characteristics of orally disintegrating tablets manufactured by freeze drying. J Pharm Sci. 2013;102:1786–1799.
[30] Chen YD, Liang ZY, cen YY, et al. Development of oral dispersible tablets containing prednisolone nanoparticles for the management of pediatric asthma. Drug Des Devel Ther. 2015;9:5815–5825.
[31] Labib GS. Novel levocetirizine HCl tablets with enhanced palatability: synergistic effect of combining taste modifiers and effervescence technique. Drug Des Devel Ther. 2015;9:5135–5146.
[32] Iurian S, Tomuţă I, Leucuţa SE. Formulation of orodispersible tablets containing meloxicam and their in vitro and in vivo characterization. Farmacia. 2014;62:1097–1108.

Journal of Pharmaceutical and Biomedical Analysis 152 (2018) 47–56

Contents lists available at ScienceDirect

Journal of Pharmaceutical and Biomedical Analysis

journal homepage: www.elsevier.com/locate/jpba

Assessment of oral formulation-dependent characteristics of orodispersible tablets using texture profiles and multivariate data analysis

Tibor Casian[a], Cătălina Bogdan[b,*], Diana Tarta[a], Mirela Moldovan[b], Ioan Tomuta[a,1], Sonia Iurian[a,1]

[a] Department of Pharmaceutical Technology and Biopharmacy, Faculty of Pharmacy, University of Medicine and Pharmacy "Iuliu Haţieganu", V. Babeş nr. 41, Cluj-Napoca, 400012, Romania
[b] Department of Dermopharmacy and Cosmetics, Faculty of Pharmacy, University of Medicine and Pharmacy "Iuliu Haţieganu", I. Creanga nr. 12, Cluj-Napoca, 400010, Romania

ARTICLE INFO

Article history:
Received 20 December 2017
Received in revised form 16 January 2018
Accepted 18 January 2018

Keywords:
Texture analysis
Mouth feel
In vivo evaluation
Palatability
Multivariate calibration

ABSTRACT

Orodispersible tablets (ODTs) emerged as dosage forms recommended for special groups of patients like pediatrics or geriatrics, due to their multiple advantages. Among their critical quality attributes, palatability determines patient acceptance, with high impact on treatment efficacy. The aim of this study was to develop an instrumental method to assess *in vivo* disintegration time and palatability of ODTs.

The formulation factors that can influence palatability were refined through an experimental design. The most important ones were taken forward and a calibration set was prepared for multivariate calibration model development. The ODTs were tested for their pharmaceutical properties, texture profile, followed by *in vivo* disintegration and palatability characteristics assessed by a panel of 16 healthy volunteers.

Acceptability was correlated to high palatability scores, sweet taste and long disintegration time and negatively correlated to with the bitter taste and a voluminous residue. Results revealed the importance of choosing the right type of filler or filler ratio for the oral disintegration time and associated mouth feel. The calibration set included formulations with different ratios of mannitol and microcrystalline cellulose as fillers. Regression models were built by correlating the texture profiles to the *in vivo* evaluation parameters. The model performance was good on both external prediction set formulations and on marketed ODTs, with good predictive capacity ($Q^2 > 0.7$) for most of the subjective ODTs characteristics: *in vivo* disintegration time, residual volume and palatability.

1. Introduction

In the recent years a great emphasis was made on delivering easily accepted dosage forms, especially for the groups of patients who face the lack of therapeutic efficiency due to non-adherence [1,2,3,4]. As a result, orodispersible dosage forms (ODFs) were developed, that can be swallowed with no difficulty after prior disintegration in the oral cavity, without the need of water [1–6]. The wide patient acceptance determined the pharmaceutical industry to integrate the new technologies and products, often as replacements for classical dosage forms [7]. The orodispersible tablets (ODTs) emerged as class representatives. Their preparation was rapidly transferred to the production sites due to the simple and cost-effective technological process, to the conventional equipment, common excipients and packaging.

At the same time, the pharmaceutical industry faced another shift, within the FDA and EMA's Quality by Design initiative, which focuses on ensuring the quality of the drug products, starting from the design stage, by developing in-line methods to control manufacturing processes [8]. Among the fundamentals of this paradigm are establishing the quality target product profile (QTPP) and the critical quality attributes (CQA) of the developed medicines and consequently, a set of control methods associated to each CQA. The ICH Q8 guideline [8] enforces the need of a robust control strategy adapted for the product particularities, based on formulation and

* Corresponding author.
E-mail address: catalina.bogdan@umfcluj.ro (C. Bogdan).
[1] Joint last co-authorship.

https://doi.org/10.1016/j.jpba.2018.01.040
0731-7085/

process understanding. In what ODTs are concerned, none of these prerequisites is properly addressed [9].

The characteristic that defines ODTs is fast disintegration, therefore disintegration time is the CQA upon whose value one can decide whether a product is orodispersible or not. The United States Pharmacopoeia (USP) limits it at 30s, while the European Pharmacopoeia (EP) allows ODT disintegration in maximum 3 min [10,11]. The high differences between the two official requirements can lead to high product variability and difficulties in categorizing and comparing the ODTs. Moreover, the control method assigned for the disintegration time assessment is similar to the one applied for conventional tablets, even though the *in vivo* conditions, namely disintegration media composition, pH and volume, are poles apart. The poor *in vitro – in vivo* correlation that resides was repeatedly reported in the scientific literature and several research groups attempted to give better alternatives to the pharmacopoeia standard test.

The first shortcoming of the official disintegration test relates to the high volume of disintegration media, 900 ml compared to about 1 ml of saliva in the oral cavity conditions. Several wetting evaluation methods were proposed, that tried to simulate the *in vivo* conditions, by placing the tablet on moist tissue paper immersed in a small volume of water (2–10 ml, depending on the Petri dish diameter). The results showed good correspondence to the disintegration test; still, the method fails to reproduce the forces applied by the tongue during disintegration, which makes it difficult to correlate to *in vivo* performance [9]. On the contrary, the use of a texture analyzer as an operating structure for disintegration profile evaluation allowed exerting variable pressure on tablets during disintegration. The experimental setup reported by Abdelbary et al. [12] pictured the tablet on a mobile perforated grid that was immersed into the simulated saliva due to the force developed by the descending probe. The time-distance profiles accurately indicated both the start and the endpoint of disintegration process, with good correlation to the *in vivo* behavior. Moreover, a qualitative parameter associated to mouthfeel estimation was anticipated. Szakonyi and Zelkó [13] extended the texture approach to tablets with different disintegration mechanisms that target various groups of patients whose illnesses can modify the testing parameters. In addition to that, computational optimization was used to predict the formulation that yielded the best *in vivo* performance for patients with xerostomia.

Along with the disintegration time, palatability is another representative CQA for ODTs. It is defined as the overall appreciation of a medicinal product concerning its smell, taste, aftertaste, texture and mouthfeel [14] and it is usually marked by high variability due to the personal preferences of the volunteers, thus difficult to standardize. Progress has been made in the attempt to develop analytical methods for taste evaluation, e.g. the electronic tongue [15]. But up to date, to our knowledge, no one reported the development of an instrumental method that predicts palatability, although recent studies in children incriminated unpleasant texture and large volume medicines as reasons for medicines refusal, along with the unpleasant taste [16].

The aim of this study was to build a multivariate calibration model to predict several properties of orodispersible tablets by means of texture analysis, setting an instrumental method as an alternative for *in vivo* testing procedures.

In this respect, placebo tablets were prepared according to a 2^{6-2} screening experimental design and were analyzed in order to identify the most influential formulation factors that have an impact over pharmaceutical properties and *in vivo* characteristics. In order to reach high formulation diversity regarding disintegration time and mouthfeel, the independent variables included two superdisintegrants with different mechanisms, two fillers (one soluble and sweet, the other one insoluble in water), two sweeteners and granules prepared at two levels of the average size.

The classical pharmaceutical evaluation targeted the measurement of weight uniformity, mechanical strength, friability, disintegration time, wetting time and water absorption ratio. Texture analysis was performed using a previously reported experimental setup, modified towards a better simulation of oral conditions [13]. Moreover, 16 healthy volunteers assessed the *in vivo* disintegration time and oral tablet characteristics.

2. Materials and methods

2.1. Materials

The following excipients were used at the preparation of ODTs: sodium starch glycolate (SSG) (JRS Pharma, Germany), sodium croscarmellose (SCC) Ac-Di-Sol (FMC BioPolymer, Belgium), mannitol (Man) (Parteck M200, Merck, Germany), microcrystalline cellulose (MCC) (Avicel PH-101, Merck, Germany), polyvinylpyrrolidone (PVP) (Kollidon 25, BASF, Germany), aspartame (Ajinamoto, Japan), saccharine (Foodchem, China) and magnesium stearate (Merck, Germany). Aerius 5 mg orodispersible tablets (Merck Sharp & Dohme Ltd, United Kingdom) and Yasnal 10 mg orodispersible tablets (KRKA, Slovenia) were purchased from the local pharmacy.

2.2. ODTs preparation

The placebo ODTs were prepared by wet granulation, having the filler and the superdisintegrant within the granules and the sweetener and magnesium stearate mixed with the granules. 10% PVP in ethanol solution was used as binder solution. The filler, the superdisintegrant and the sweetener used for the preparation, are indicated in the experimental design matrix for each of the 19 formulations, together with the PVP ratio and the superdisintegrant ratio (Table 1). The sweetener ratio was kept constant, at 2% and the filler content was calculated and added as necessary, so that the total weight of a tablet would be 200 mg. Briefly, the filler and superdisintegrant were blended into a mixer (Erweka, Germany) for 2 min, at 50 rpm. The PVP solution was added, and the mixing continued for another 1 min, at 70 rpm. The wet mass was transferred into the oscillating calibrator (Erweka, Germany), equipped with a mesh of 400 μm or 800 μm, as specified in the experimental design matrix (Table 1). The granules were dried over night at room temperature and then calibrated again in the same equipment. Before compression, dried granules were blended with the sweetener and magnesium stearate using a planetary mixer, for 5 min, at 50 rpm. An eccentric tablet press (Korsch EK0, Germany) equipped with a 10 mm diameter flat punch set was used for tablet preparation, adjusted for an average weight of 200 mg/tablet.

2.3. ODTs pharmaceutical characterization

2.3.1. Disintegration time

The disintegration time was measured on six tablets, according to the European Pharmacopoeia method, in 800 ml distilled water kept at 37 °C (ZT 2 disintegration tester, Erweka, Germany). The times until complete disintegration, with no residue left on the sieves, were recorded. The results were expressed as mean disintegration times with the correspondent standard deviation.

2.3.2. Wetting time and water absorption ratio

For the wetting time measurement, two pieces of tissue paper were placed in a 4.5 cm diameter Petri dish, containing 4.5 ml distilled water, at room temperature. The tablet was placed on the tissue paper and the time until dissolution media reached the upper surface of the tablet was recorded. The tablets used in the wetting

Table 1
Experimental design matrix.

	The type of SD (X_1)	The type of filler (X_2)	The type of sweetener (X_3)	The average size of granules (X_4)	The binder ratio (X_5)	The SD ratio (X_6)	Crushing strength (N)	Disintegration time (s)	Wetting time (s)	Water absorption ratio (%)
N1	SSG	Man	Saccharine	353.22	1	6	38.6 ± 3.1	85.3 ± 10.5	116.3 ± 15.7	105.3 ± 26.5
N2	SCC	Man	Saccharine	309.01	4	6	29.1 ±2.5	89.5 ± 11.0	164.0 ± 19.5	50.0 ± 13.3
N3	SSG	MCC	Saccharine	233.52	4	12	28.6 ± 4.7	8.2 ± 1.5	3.0 ± 0	380.7 ± 9.9
N4	SCC	MCC	Saccharine	257.76	1	12	30.8 ± 2.8	8.1 ± 1.6	2.0 ± 0	353.2 ± 31.6
N5	SSG	Man	Aspartame	282.14	4	12	31.6 ± 2.9	74.0 ± 7.1	138.0 ± 27.6	100.8 ± 10.3
N6	SCC	Man	Aspartame	280.69	1	12	38.4 ± 3.6	41.3 ± 4.3	36.3 ± 9.6	110.2 ± 7.9
N7	SSG	MCC	Aspartame	254.14	1	6	31.9 ± 2.7	7.0 ± 1.1	2.7 ± 0.6	307.2 ± 25.0
N8	SCC	MCC	Aspartame	274.46	4	6	30.9 ± 2.1	10.2 ± 1.9	3.0 ± 0	250.0 ± 9.0
N9	SSG	Man	Saccharine	597.27	1	12	36.4 ± 2.6	106.2 ± 34.5	171.7 ± 17.4	129.6 ± 11.0
N10	SCC	Man	Saccharine	597.02	4	12	36.9 ± 3.5	66.5 ± 9.4	147.7 ± 9.7	64.9 ± 9.0
N11	SSG	MCC	Saccharine	698.09	4	6	34.0 ± 5.1	25.3 ± 6.9	14.0 ± 2.0	240.8 ± 14.0
N12	SCC	MCC	Saccharine	696.35	1	6	34.6 ± 4.8	10.6 ± 2.5	2.0 ± 0	368.6 ± 14.0
N13	SSG	Man	Aspartame	652.25	4	6	38.8 ± 2.9	147.8 ± 20.0	116.3 ± 10.7	104.0 ± 4.7
N14	SCC	Man	Aspartame	605.34	1	6	35.7 ± 5.3	54.6 ± 3.0	101.0 ± 1.0	81.1 ± 5.0
N15	SSG	MCC	Aspartame	674.62	1	12	34.3 ± 6.4	9.5 ± 0.5	3.3 ± 0.6	463.1 ± 5.7
N16	SCC	MCC	Aspartame	753.46	4	12	35.9 ± 5.8	29.6 ± 3.5	17.0 ± 2.6	296.5 ± 13.9
N17	SSG	Man	Saccharine	380.95	2.5	9	38.0 ± 4.5	108.6 ± 21.5	144.3 ± 5.1	82.7 ± 12.9
N18	SSG	Man	Saccharine	385.23	2.5	9	37.3 ± 4.2	106.2 ± 10.0	199.0 ± 1.0	99.7 ± 7.4
N19	SSG	Man	Saccharine	380.53	2.5	9	36.6 ± 4.1	84.3 ± 7.4	124.0 ± 15.6	73.2 ± 5.0

SD – superdisintegrant, SSG – sodium starch glycolate, SCC – sodium croscarmellose, Man – mannitol, MCC – microcrystalline cellulose.
* Results are reported as mean value ± standard deviation.

time test were weight before (w1) and after the test (w2) and the *water absorption ratio* (r) was calculated using the equation: r = 100 * (w2-w1)/w1. The measurements were done in triplicate and the standard deviation was calculated [17].

2.3.3. Crushing strength

Crushing strength was assessed using Dr. Schleuniger apparatus (Dr. Schleuniger, Germany) on ten tablets from each formulation. Mean crushing strength and standard deviation were calculated.

2.3.4. Friability

Friability was evaluated according to the European Pharmacopoeia method, on 20 tablets of each formulation, using TA 10 friabilator (Erweka, Germany). The lost weight after 5 min rotations with 20 rpm speed was quantified and expressed as a percentage of the initial weight.

2.4. Texture analysis

For the further evaluation of tablets, a CT3 texture analyzer (4500 g maximum load, Brookfield Engineering, USA) was used, following an experimental setup presented in Fig. 1.

The method was previously described by Szakonyi and Zelkó [13]. The tablet was attached to an acrylic probe (TA10, Brookfield Engineering, USA) using a thin film of glue. Underneath, a plastic plate containing 4.5 ml distilled water was placed, and covered with a stainless steel sieve (diameter, aperture), so that the distilled water would create a continuous liquid layer all over the surface of the sieve (Fig. 1) [13]. A compression test was applied at a constant speed of 0.01 mm/s. Measurements started when the probe with the attached tablet met a trigger load of 10 g and ended when the tablet was completely disintegrated and the surface of the sieve was reached, which resulted in an abrupt increase of load value. The disintegration profiles were recorded as load (g) versus time (s) curves using TexturePro CT 1.5 software (Brookfield Engineering, USA) for at least three tablets from each formulation and mean values ± standard deviation were reported.

2.5. In vivo *evaluation*

Nineteen placebo formulations were assessed on 16 volunteers (7 males and 9 females, aged between 22 and 57 years) after having signed the informed consent to participate to the study that was previously approved by the Ethics Committee from "Iuliu Haţieganu" University of Medicine and Pharmacy No. 315/21.07.2016. The inclusion criteria of the clinical study presumed healthy adult male and female volunteers without evidence of active or chronic disease and a normal taste sensitivity. The study was conducted in full accordance with the Declaration of Helsinki – Ethical Principles for Medical Research Involving Human Subjects.

The subjects were not allowed to eat for two hours before the test. First, they were asked to rinse their oral cavity with 50 ml of water, and then they placed a random ODT formulation on the tongue. They were allowed to make slight movements with the tongue, but were required not to apply high pressure on the tablets to accelerate disintegration and also to avoid chewing or swallowing them. The residue that formed upon disintegration was evacuated from the oral cavity and the mouth was rinsed with 50 ml of water. Disintegration time (Y_1) was recorded using a digital timer, up to the moment when no granules or large particles could be detected. The taste was evaluated on a visual analog scale with five scores, as it follows sweet taste (Y_2) (1–no sweet taste perceived, 5–very sweet), salty taste (Y_3) (1–no salty taste perceived, 5–very salty), sour taste (Y_4) (1–no sour taste perceived, 5–very sour) and bitter taste (Y_5) (1–no bitter taste perceived, 5–very bitter). The volume of residue (Y_6) was estimated on a VAS scale with

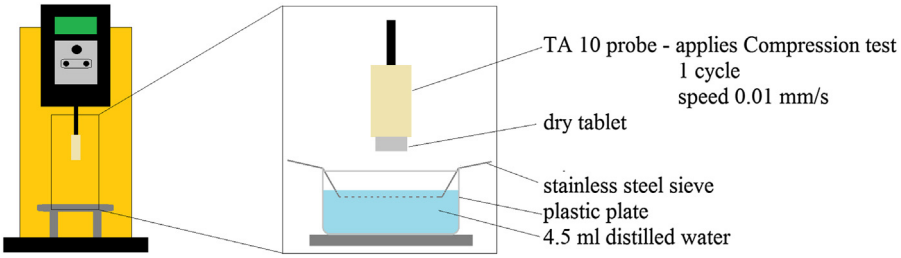

Fig. 1. Graphical procedure of the texture analysis performed on ODTs.

score values from 1, for no residue and complete dissolution, to 5, for a high amount of residue. The roughness (Y_7) was assessed on the same scale, the score 1 was attributed to a very soft texture and 5 to rough texture, made of big granules. The palatability was rated with 0 score for rejected tablets (low palatability) or 1 for accepted tablets (high palatability).

2.6. Experimental design

The ODT preparation was performed according to a fractional factorial experimental design with six independent variables and two variation levels developed using Modde 12.0 software (Sartorius Stedim, Sweden). 16 experimental trials were generated, and three replicate center points needed to calculate the degree of freedom, the reproducibility and the response curvature. The qualitative input variables were: the type of superdisintegrant (X_1) (SSG or SCC), the type of filler (X_2) (Man or MCC) and the type of sweetener (X_3) (saccharine or aspartame). The quantitative input variables were: the average size of granules (X_4) (300 μm or 650 μm) the binder, PVP, ratio (X_5) (1% or 4%) and the superdisintegrant ratio (X_6) (6% or 12%), as shown in the experimental design matrix (Table 1). The responses were selected to traditional pharmaceutical characterization of ODTs: the *in vitro* disintegration time (Y_1), the wetting time (Y_2), the water absorption ratio (Y_3), the mechanical strength (Y_4) and the fracturability (Y_5). The same software was used for data fitting and statistical parameters calculation. The influences of independent variables on the responses were assessed using Partial Least Squares (PLS) method.

2.7. Multivariate data analysis

2.7.1. PCA on in vivo evaluated parameters of experimental design formulations

Principal component analysis was used on *in vivo* data of the experimental design formulations to evaluate which variables contributed to the separation of the observations and how they relate to the palatability of the pharmaceutical product. All variables were scaled to unit variance.

PCA is a multivariate projection method that is applied to visualize the systematic variation in a data matrix. PCA works by representing each observation in a k multidimensional space, equal to the number of variables, followed by deriving a line that captures the largest direction of variability. This line represents the first principal component (t1). The second principle component (t2) is the line that captures the second largest variability in the k multidimensional space and that is orthogonal to t1. The first two principle components form a plane on which each observation will be projected, assigning them a new set of variables, called latent variables [18].

Applying PCA allowed the identification of possible outliers, grouping of observations and important variables that contribute to the separation of observation in the score plot.

Results were interpreted through graphical tools, such as score plots for observation overview and loading plots for variable understanding [19].

2.7.2. Multivariate calibration

To ensure representativeness, the calibration set formulations were built using the most important factors emerging from the screening design. The calibration set consisted of tablets prepared with five different cellulose: mannitol ratios (1:0; 3:1; 1:1; 1:3; 0:1). From each formulation 10 tablets were tested, both for texture profile and *in vivo* characteristics and further used for the regression development.

Projection to latent structures by means of PLS models were built to predict *in vivo* evaluated properties of orodispersible tablets (Y-dataset) from load versus time profiles. The X-dataset variables were centered, whereas *in vivo* evaluated properties were scaled to unit variance.

PLS models were interpreted by means of score and loading plots [20]. Model performance was evaluated by means of R^2, Q^2, RMSECV and the number of components used [21]. Multivariate data analysis was carried out using SIMCA 14 (Sartorius Stedim, Sweden).

2.7.3. Model validation

To validate the model, the formulations of the screening design were used as an external prediction set. Model predictive performance was evaluated by calculating the root mean square error of prediction (RMSEP) considering the predicted residuals of the observations from the prediction set.

2.7.4. Testing the model on marketed ODT formulations

In order to test the model on marketed ODT formulations, two products were considered. Aerius, containing desloratadine as active pharmaceutical ingredient and Yasnal containing donepezil. Both products were tested *in vivo* and through texture analysis using the previously described methodology.

3. Results and discussion

3.1. Pharmaceutical characterization of ODTs

One of the study's objectives was to simulate by means of an experimental design the formulation characteristics of the marketed ODTs. Therefore, our preliminary research (results not shown) focused on the analysis of the marketed ODTs' qualitative composition. Six classes of excipients were commonly identified: fillers, superdisintegrants, binders, sweeteners, flavors and lubricants. The most frequently used fillers which were also chosen for the experimental design were mannitol for its sweet taste, mouthfeel and negative heat of dissolution and microcrystalline cellulose due to its high disintegrating capacity [22]. As superdisintegrants, sodium starch glycolate, sodium croscarmellose, crosspovidone and low-substituted hydroxypropyl cellulose were mostly used in

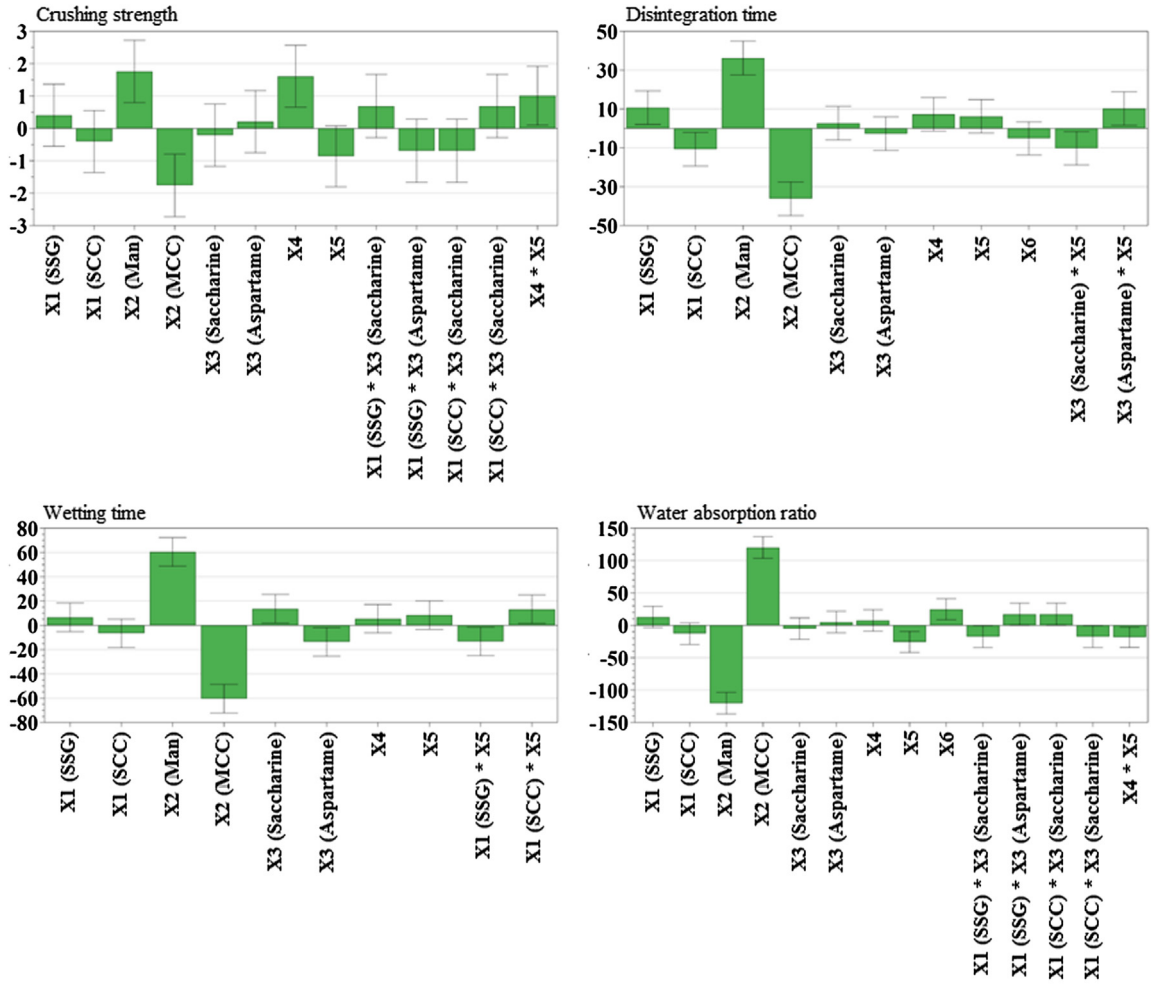

Fig. 2. Influence of formulation variables on ODT pharmaceutical characterization X_1- superdisintegrant type (SSG – sodium starch glycolate, SCC – sodium croscarmellose); X_2- filler type (Man – mannitol, MCC – microcrystalline cellulose); X_3- sweetener type; X_4- average size of granules; X_5- binder ratio; X_6- superdisintegrant ratio.

commercial drug products. Our experimental design included the first two, sodium starch glycolate and sodium croscarmellose, in order to ensure both wicking and swelling as disintegrating mechanisms. Polyvinylpyrrolidone was chosen as binder because it is typically used in wet granulated marketed ODT products. The most common sweeteners which were also included into the experimental design were saccharine and asparatam. Various flavors were found in the commercial preparations, but in this particular study their use was not considered necessary since placebo formulations were prepared and active ingredient taste masking was not needed.

The experimental design for ODT preparation was meant to yield formulations with a wide variety of pharmaceutical characteristics, in terms of disintegration, water absorption properties and hardness. The effects of the input variables on ODTs characteristics were assessed using Modde 12.0 software by generating the corresponding scaled and centered coefficient plots (Fig. 2). Coefficient plots reveal the magnitude and direction of effect exerted by each factor along with a 95% confidence interval (error bar) that estimates its uncertainty. The coefficient value of a factor is interpreted as the change in average response value induced by varying the factor settings from low to high level, while all other factors are at middle level [20].

The pharmaceutical analysis of the tablets (Table 1) showed disintegration times between 7.0 ± 1.1 s and 147.8 ± 20.0 s. The DoE analysis revealed the strong influence of the fillers, meaning although Man is a water-soluble polyol, its use led to longer disintegration as compared to tablets containing MCC. SCC led to quick disintegration, as well as saccharine in the presence of high PVP amounts. Wetting time was extended by the use of Man and saccharine and it ranged between 2.0 and 171.7 ± 17.4 s. Also, as expected, low ratios of binder and high amounts of superdisintegrant favored water absorption, with values between $50.0 \pm 13.3\%$ and $463.1 \pm 5.7\%$. The crushing strength of the samples ranged between 28.6 ± 4.7 N and 38.8 ± 2.9 N, values that were considered appropriate for further manipulation and packaging. It increased when Man was chosen as filler, at high granule sizes with simultaneous use of high PVP ratios. The friability was below 1%, which fulfills the requirements of the European Pharmacopoeia.

3.2. In vivo *evaluation of ODTs*

A panel of 16 volunteers evaluated the tablets and their disintegration times were between 34 s and 102.93 s (Table 2). The taste was rated as mostly sweet for all the ODTs. With respect to the other taste sensations (salty, sour or bitter), no significant variations among different formulations were identified for responses Y_3–Y_5. All scores ranged at a medium level, with changes that could not be correlated to formulation factors. The volume of residue (Y_6) was highly variable among the 19 tested formulations; three of them were rated at the maximum volume, while one led to complete disintegration with no sediment left. The roughness (Y_7) was a parameter enquired to give information about the texture of the moist tablet, whether it contains large, firm granules and heterogeneous structure or more like a smooth, velvety feeling during

Table 2
In vivo analysis results for experimental design formulations, calibration formulations and marketed pharmaceutical products.

	In vivo disintegration time (s) (Y_1)	Sweet taste (Y_2)	Salty taste (Y_3)	Sour taste (Y_4)	Bitter taste (Y_5)	Volume of residue (Y_6)	Roughness (Y_7)	Total palatability (Y_8)
N1	65.87 ± 22.18	54	22	22	20	18	30	16
N2	75.33 ± 24.72	50	20	22	29	27	35	15
N3	44.18 ± 12.43	32	25	25	30	62	40	3
N4	46.75 ± 16.27	30	23	22	34	64	36	2
N5	80.18 ± 32.12	55	22	21	21	25	32	16
N6	72.31 ± 25.49	51	18	17	19	27	27	14
N7	36.81 ± 15.31	29	23	20	26	56	34	5
N8	36.18 ± 12.18	33	22	20	27	58	33	5
N9	76.31 ± 19.13	45	25	25	22	26	31	15
N10	78.46 ± 18.09	53	21	17	26	23	32	13
N11	82.26 ± 13.25	31	25	20	31	46	41	3
N12	34.00 ±14.81	31	25	27	27	64	40	4
N13	102.93 ± 22.07	51	22	19	24	22	37	11
N14	67.75 ± 14.09	54	23	20	22	25	37	13
N15	30.93 ± 12.11	34	28	24	28	59	39	6
N16	56.25 ± 17.24	38	22	20	27	52	34	7
N17	72.93 ± 13.06	54	25	25	20	25	36	14
N18	70.06 ± 13.59	46	28	23	28	23	34	14
N19	70.50 ± 18.48	48	26	22	27	26	34	13
M:C 1:0	103.33 ± 17.87	62	18	18	15	22	34.5	15
M:C 3:1	57.93 ± 18.52	60	20	16	15	31	33	14
M:C 1:1	29.46 ± 20.19	57	18	14	17	44.5	32	11
M:C 1:3	23.53 ± 15.64	53	19	16	22	54	34.5	7
M:C 0:1	21.46 ±15.11	49	18	15	22	55	35.5	6
Aerius 5 mg	28.43 ± 7.39	61	18	32	36	51.5	42	6
Yasnal 10 mg	35.81 ± 4.34	25	39	22	52	59	25	1

M:C – mannitol: cellulose ratio. * *In vivo* disintegration time was calculates as mean ± standard deviation of the 16 values reported by the subjects, while the other parameters (Y_2–Y_8) were calculated as a sum of the reported values.

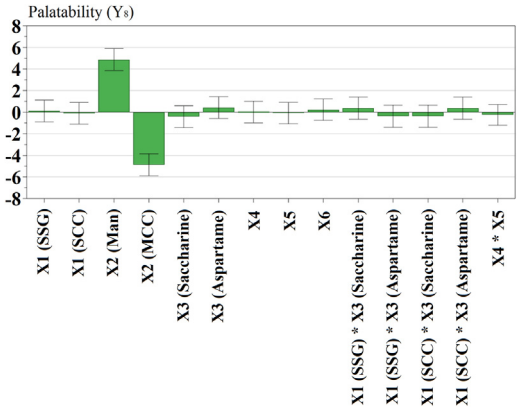

Fig. 3. Influence of formulation variables on *in vivo* evaluated palatability X_1- superdisintegrant type (SSG – sodium starch glycolate, SCC – sodium croscarmellose); X_2- filler type (Man – mannitol, MCC – microcrystalline cellulose); X_3- sweetener type; X_4- average size of granules; X_5- binder ratio; X_6- superdisintegrant ratio.

disintegration in the oral cavity. Although the ODTs were prepared by wet granulation and there was a high variability among the granules' average sizes, no significant changes were reported by the volunteers concerning the tablet roughness, probably due to the fast wetting and granule disintegration or granule crushing during compression.

The sum of all scores for total palatability (Y_8), meaning the overall acceptance of the tablet, seemed to be divided in two categories, low palatability with values below 7 and high palatability that exceeded 11 out of 16 points. As the coefficient plot (Fig. 3) shows, this parameter was mainly influenced by the type of filler: Man gave formulations with high palatability scores, while MCC led to a low level of acceptance.

3.3. Texture analysis

The texture measurement derived from moving a cylindrical probe with a constant speed into a wetted tablet and recording the load values as a function of distance or time. The shape and surface beneath the load vs. time curve were reported as good indicators of *in vivo* tablet softening and disintegration behavior [13].

Texture data for multivariate calibration was analyzed both as the whole load vs. time plot, but also as isolated parameters (T_1–T_7), shown in Table 3 and whose significance will be further explained. Using the entire curve in the modeling was expected to give better predictive precision in comparison with the analysis of individual parameters derived from it, but on the other hand, the individual parameters came to increase the understanding on the connection between the texture profiles and the disintegration-associated phenomena.

Apart from the area under the curve (AUC) (T_3) that was previously studied, we evaluated more parameters calculated from the texture data, in order to describe and predict not only the disintegration time, but also the mouthfeel and palatability. The ascending/upward part of the graph indicates water wicking into the tablet, caused by the capillary forces developed by superdisintegrants, followed by a peak load (T_4), which signals the beginning of disintegration. The structure and volume changes that occur during water absorption (swelling, drainage of the disintegrated particles, partial dissolution etc.), are perceived along oral disintegration as mouthfeel attributes and were assessed as rigidity values at1and 2 mm within the ODT (T_1 and T_2) and deformation at target values (T_5). The descending part of the graph indicates the continuous movement of the probe into the partially disintegrated ODT, up to the inflection point that shows complete disintegration. It was previously assigned as disintegration time and calculated as the difference between the time corresponding to the inflection point and the one corresponding to the peak load (T_6) [12]. Furthermore, the fractures on the curves that appear as sudden load drops, were evaluated as a measure of tablet smooth or rough texture (T_7). The

Table 3
Texture analysis results, load vs. time graph interpretation.

	Rigidity at 1 mm (g) (T_1)	Rigidity at 2 mm (g) (T_2)	Surface load = f(t) (T_3)	Maximum load (g) (T_4)	Deformation at target (mm) (T_5)	Time from peak load to inflection (s) (T_6)	Number of fractures (T_7)
N1	1378.5	2584.3	253905.7	2222.667	2.31	140.3	4.66
N2	2084.5	4157.5	176098	2555	1.69	153	2
N3	1.7	2.7	147.5	11.16	4.61	40.66	6.33
N4	5	13.2	341.08	37.41	4.34	23.66	2.33
N5	1271.8	2454.8	104694.2	1602.41	2.36	141.66	6
N6	1204.8	2900.7	227272.2	2714.66	2.36	192	2
N7	2.5	3.2	64.91	9.83	3.14	16	4.33
N8	1.7	3.3	20.16	8	4.76	10.66	2
N9	1789.2	3378.3	282878.8	3322	2.42	190	5.33
N10	1342.2	2691.5	177478.8	2148.83	2.32	170.66	4.33
N11	4.3	8.2	359.86	12.3	4.56	20	8
N12	2.5	8.7	467.91	11.3	4.22	27	19.3
N13	1456.6	2679.3	189349.5	2356.3	2.12	178.33	3
N14	1155.3	2350.8	138285.7	1957.5	2.39	152.66	3.66
N15	0.8	2.5	38.25	9	4.19	14	3.33
N16	197	16.5	16136	211	3.86	162	2
N17	197	16.6	190341.8	2590.33	3.86	168	6.66
N18	21.33	31.2	175819.3	2930.33	2.33	151.66	2.33
N19	21.086	27.318	226213.7	3616.33	2.06	160.66	3
M:C 1:0	3649.8	4179	449304.4	4257.25	11.14	184	3
M:C 3:1	857.27	1307.41	112872.6	1406.04	2.72	165.83	3.58
M:C 1:1	12.7	83.9	1694.45	54.91	2.76	41.33	9.83
M:C 1:3	14.6	85.2	925.16	58.87	2.94	29.5	10.58
M:C 0:1	7	21.5	652	69.53	2.84	20.69	10.76
Aerius 5 mg	2.4	20	632.1	17	3.28	59.6	12
Yasnal 10 mg	1.5	11.7	5102.25	116.8	3.52	80	2.2

M:C – mannitol: cellulose ratio

measurement ends when the probe reaches the sieve, which results in a sudden load increase.

3.4. *PCA on* in vivo *evaluated parameters of the Experimental Design Formulations*

As the objective of this study was to build multivariate regression models to predict *in vivo* estimated tablet quality parameters, the first step in data analysis was to identify which response variables caused separation/grouping of tablets. Therefore, a PCA-Y model was generated on the *in vivo* estimated parameters dataset.

PCA-Y model was fitted using 3 principle components, enough to capture 86.3% of total variability. The first principle component (t1) explained 56.3% of data variability caused by variables that contributed to the separation of observation into two groups, here considering the palatability. As this response is a computed variable (from the scores of other variables), the principle component that captures its variability also characterizes all other response variables that are important. To identify the variables that are responsible for the clustering of the tablets in the score plot, the corresponding loading plot was generated (Fig. 4).

Loadings are interpreted considering both groupings and graphical disposition of variables suggesting correlation and the distance to the origin of their projections. Palatability, sweet taste and disintegration time are clustered together, suggesting a positive correlation among them and a negative correlation with the bitter taste and the volume of residue as they are positioned in diagonally opposed quadrants. Tablets associated with high palatability, had higher scores for sweet taste and longer *in vivo* disintegration time and lower scores for bitter taste and small volume of residue. All these variables were the major source of variation in the response matrix that was captured by the first principal component. Our results are consistent with the study on pediatric population conducted by Venables et al. that showed that acceptability is highly dependent on palatability of the solid oral dosage form, further correlated to the taste of the drug product, the disintegration time, the texture and the residual volume [23]. These subjective parameters can be connected to the effects of formulation factors that were previously described to conclude that choosing the appropriate type of filler or fillers ratio is of paramount importance for the perception and acceptance of an ODT.

3.5. *Multivariate calibration model development*

Frequently the objective of multivariate calibration is to replace a reference method that tends to be laborious, expensive or time consuming. Compared to traditional calibration, where only one variable is used to predict the desired sample property, in multivariate calibration more variables are measured. The use of multiple variables stabilizes the calibration and makes it more robust, as variables are used in the form of latent variables [18].

The critical step in any calibration is to possess a sample set that represents the variation of interest, or the variation that is expected to occur in future prediction set samples [24]. To create a representative calibration set that produces the desired response variability, the correct selection of influential formulation variables is essential.

As the most important factor was the type of filler used, the initial factor was encoded as a quantitative variable by using the ratio of Man: MCC. Five different Man: MCC ratios were selected to represent the calibration set (1:0; 3:1; 1:1; 1:3; 0:1). From each formulation 10 tablets were tested, both for texture profile and *in vivo* characteristics (Fig. 5) and further used for the regression development.

Table 4 presents the PLS model characteristics obtained for different responses when load vs time profiles were used as X data.

There are several model performance indicating parameters that were considered, such as the percentage of variation in the X (R^2X) or Y (R^2Y) dataset explained by the model, the fraction of total variation that can be predicted by the model (Q^2) and the root mean square error of cross-validation (RMSECV). All responses excepting Y4-salty taste and Y7-roughness yielded models with good predictive capacity ($Q^2 > 0.7$) and low errors of prediction calculated through leave-one out cross validation method. Also, most

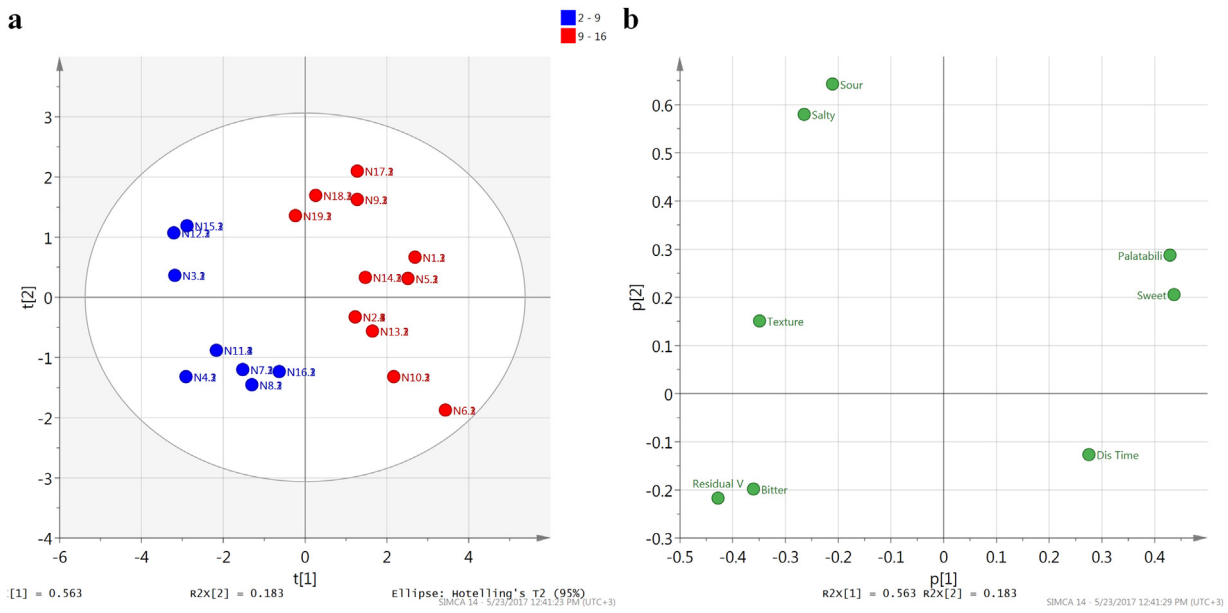

Fig. 4. PCA-Y score plot (a) and loading plot (b) t[1] – first principal component, t[2] – second principal component, p[1] – loading of t[1] vector, p[2] – loading of t[2] vector, R2X – fraction of captured variability by each component.

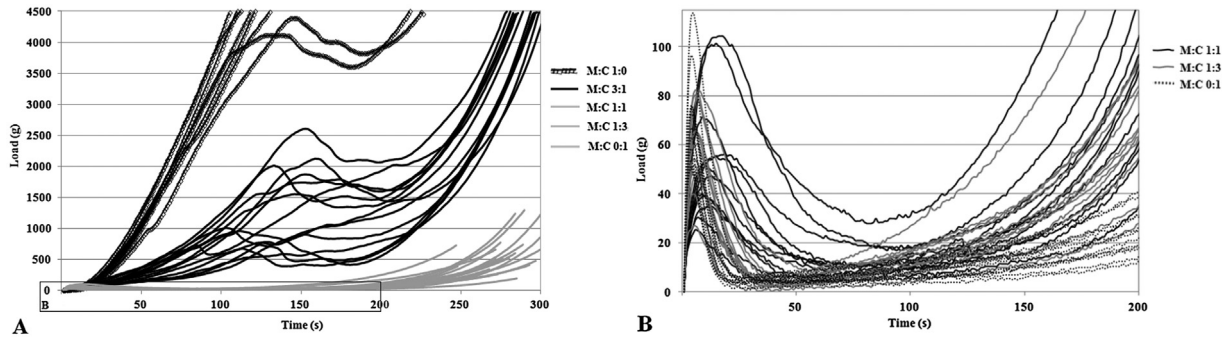

Fig. 5. Texture analysis, expressed as load vs. time plots for calibration formulations M:C – mannitol: cellulose ratio.

Table 4
PLS regression model characteristics and performance tested using external prediction set formulations.

Model Parameters	*In vivo* disintegration time (s) (Y_1)	Sweet taste (Y_2)	Salty taste (Y_3)	Sour taste (Y_4)	Bitter taste (Y_5)	Volume of residue (Y_6)	Roughness (Y_7)	Total palatability (Y_8)
Calibration model								
Load vs Time curve region	1–240	1–130	1–240	1–130	1–130	1–240	1–240	1–130
R2X	0.99	0.99	0.46	0.99	0.99	0.95	0.377	1
R2Y	0.936	0.953	0.21	0.712	0.863	0.773	0.052	0.914
Q2	0.932	0.913	0.074	0.71	0.808	0.756	0.0384	0.866
PLS components	2	8	1	1	5	2	1	5
RMSECV	7.6047	1.3963	0.796	0.6759	1.3126	6.2655	1.2290	1.2377
External prediction results								
RMSEP	Experimental design formulations							
	12.507	16.383	/	6.376	9.486	8.749	/	4.776
	Marketed orodispersible formulations							
	4.213	23.518	/	12.907	29.679	7.969	/	9.996

of the variation in the X and Y dataset was accounted by the number components used in the PLS modeling.

3.6. Validation of the calibration model

The predictive capacity of the calibration model was tested on the experimental design formulations. Fig. 6 describes the predicted *in vivo* parameters versus the ones that were measured by volunteers. The model showed good predictive performance on the experimental design formulations, with low RMSEP for oral disintegration time, volume of residue and palatability (Table 4). Thus the method was validated on the experimental design formulations with a good recovery, well within the limits of the established

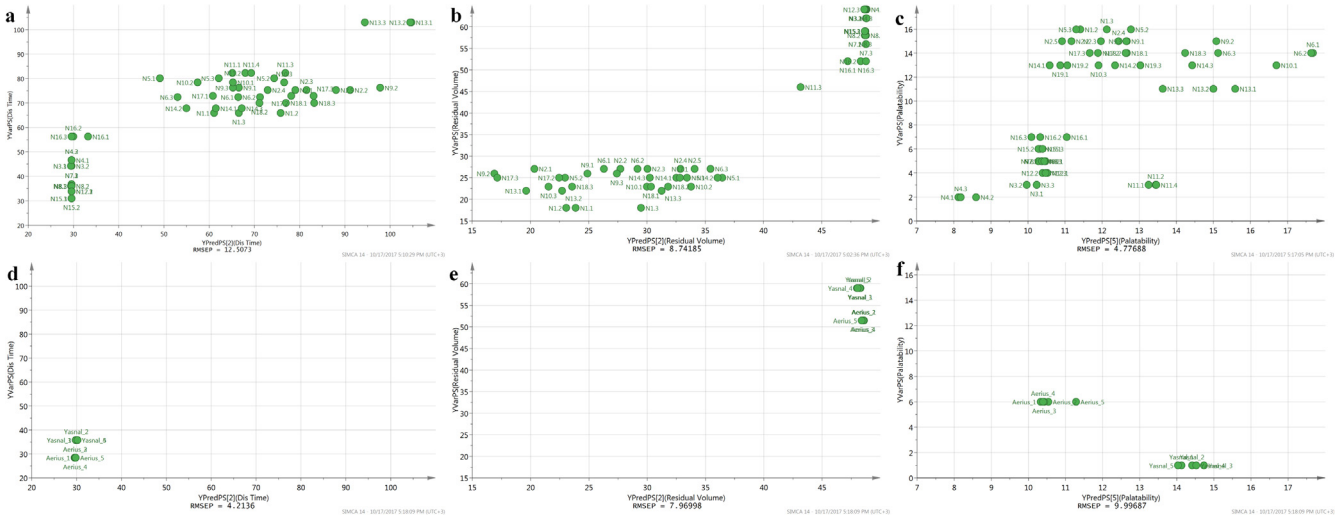

Fig. 6. Measured versus predicted values for the experimental design formulations: *in vivo* disintegration time (a), volume of residue (b), palatability (c) and marketed formulations: *in vivo* disintegration time (d), volume of residue (e), palatability (f), used for model validation.

acceptance interval of ±20% for the instrumental determination of the three characteristics: oral disintegration time, volume of residue and palatability.

3.7. Testing the model on marketed ODT formulations

In the case of marketed formulations, predictions were accurate for oral disintegration time and volume of residue, yet for palatability, the root mean square error of prediction RMSEP was higher than the one obtained for the experimental design batch. That could be explained by the fact that palatability is an overall appreciation parameter that includes the ease of disintegration, the mouthfeel and the taste. Thus the unpleasant taste of the active ingredient must have been responsible for the high palatability prediction errors.

Although the predictive capacity of the model ($Q^2 > 0.70$) was good also for the taste descriptors, sweet, sour and bitter, the prediction errors were significantly higher for these responses. As expected, the taste characteristics cannot be estimated on the basis of a texture profile especially when an active ingredient is present. On the other hand, the better prediction results for taste descriptors in case of placebo formulations can be related to the tablet composition. Dependent on the filler ratio the formulations were perceived as a sweet tasting (high mannitol content) or as a bitter tasting (high cellulose content) compositions. These changes in cellulose: mannitol ratios were easily detected by texture analysis.

3.8. Practical implications

Up to this stage, the study achieved the development of a model that predicts the *in vivo* characteristics of ODTs from an instrumental analysis. The well predicted features were *in vivo* disintegration time, volume of residue and total palatability. The disintegration time has well defined limits in the pharmacopoeias, although the evaluation methods are not meant to reproduce the oral conditions, but the volume of residue and palatability lack *in vitro* assessments. Apart from the unpleasant taste, these are the characteristics incriminated for the refusal of orodispersible dosage forms, especially in special groups of patients, like pediatrics and geriatrics [25]. The regulatory agencies emphasized the importance of developing palatable formulations for pediatric patients to prevent therapy refusal and low-adherence phenomena. In the research and development process, an important role is played by an accurate product characterization; *in vivo* evaluation on human volunteers is known to be subjective, with highly variable results, costly and time consuming, therefore the method this study proposes could be a viable alternative [26].

The taste can be assessed *in vitro* using the electronic sensing systems, the texture profiling coupled with MVDA could be used for disintegration time and mouthfeel properties, thus acting like complementary methods for a complete ODT characterization [15].

However, this study has some limitations: several variability factors were not included into the experimental design, as the different sizes and shapes of the tablets that could limit the contact of the tablet with water, the different crushing strengths or porosities. To surpass these shortages and extend the present model, these influences will be studied in a future research. In addition to that, our model was validated on placebo tablets, while the taste of the active ingredient, as it was previously shown, can lead to palatability score changes. This suggests that both texture analysis for formulation characteristics and taste sensing evaluation for active ingredient influence are necessary to predict the performance of the ODTs in the oral cavity.

4. Conclusions

The present study demonstrated that prediction of subjective characteristics of ODTs during oral disintegration is feasible by means of texture analysis and multivariate data analysis. Placebo ODTs were prepared according to an experimental design, following an investigation of marketed formulations. Fitting the experimental data obtained at the pharmaceutical evaluation lead to the identification of influential formulation factors that were taken into account for the development of a calibration set, that was further evaluated by volunteers and characterized through texture analysis.

Multivariate regression models were built by correlating texture analysis data (load vs time profiles) with *in vivo* tablet properties. Model performance was tested on both external prediction set formulations and marketed formulations and yielded good results for disintegration time, volume of residue and palatability. The quality of the predictions was promising, which calls for future studies to contribute to the refining and improving the models so that other identified variability factors are included.

References

[1] K. Wening, J. Breitkreutz, Oral drug delivery in personalized medicine: unmet needs and novel approaches, Int. J. Pharm. 404 (2011) 1–9.
[2] M. Slavkova, J. Breitkreutz, Orodispersible drug formulations for children and elderly, Eur. J. Pharm. Sci. 75 (2015) 2–9.
[3] S. Stegemann, M. Gosch, J. Breitkreutz, Swallowing dysfunction and dysphagia is an unrecognized challenge for oral drug therapy, Int. J. Pharm. 430 (2012) 197–206.
[4] S. Stegemann, F. Ecker, M. Maio, P. Kraahs, R. Wohlfart, J. Breitkreutz, A. Zimmer, D. Bar-Shalom, R. Hettrich, B. Broegmann, Geriatric drug therapy: neglecting the inevitable majority, Ageing Res. Rev. 9 (2010) 384–398.
[5] V. Navarro, Improving medication compliance in patients with depression: use of orodispersible tablets, Adv. Ther. 27 (11) (2010) 785–795.
[6] T.B. Ernest, J. Craig, A. Nunn, S. Salunke, C. Tuleu, J. Breitkreutz, R. Alex, J. Hempenstall, Preparation of medicines for children –a hierarchy of classification, Int. J. Pharm. 435 (2012) 124–130.
[7] F. Scaglione, S. Donde, T.A. Hassan, E.A. Jannini, Phosphodiesterase type 5 inhibitors for the treatment of erectile dysfunction: pharmacology and clinical impact of the sildenafil citrate orodispersible tablet formulation, Clin. Ther. 39 (2) (2017) 370–377.
[8] ICH Harmonised Tripartite Guideline: Pharmaceutical Development, 2018, Q8(R2) https://www.ich.org/fileadmin/Public_Web_Site/ICH_Products/Guidelines/Quality/Q8_R1/Step4/Q8_R2_Guideline.pdf.
[9] P. Hooper, J. Lasher, K.S. Alexander, G. Baki, A new modified wetting test and an alternative disintegration test for orally disintegrating tablets, J. Pharm. Biomed. Anal. 120 (2016) 391–396.
[10] ⟨701⟩ Disintegration in The USP Convention: United States Pharmacopeia, 34, United book Press Inc., Baltimore, Maryland, 2011, pp. 276–277.
[11] European Pharmacopoeia, 8th edition, 2018 (Accessed at http://online6.edqm.eu/ep802/).
[12] G. Abdelbary, C. Eouani, P. Prinderre, J. Joachim, Jp. Reynier, Ph. Piccerelle, Determination of the in vitro disintegration profile of rapidly disintegrating tablets and correlation with oral disintegration, Int. J. Pharm. 292 (2005) 29–41.
[13] G. Szakonyi, R. Zelko, Prediction of oral disintegration timeof fast disintegrating tablets using texture analyzer and computational optimization, Int. J. Pharm. 448 (2013) 346–353.
[14] H. Batchelor, R. Venables, J. Marriot, T. Mills, The application of tribology in assessing texture perception of oral liquid medicines, Int. J. Pharm. 479 (2015) 277–281.
[15] K. Woertz, C. Tissen, P. Kleinebudde, Jorg Breitkreutz Taste sensing systems (electronic tongues) for pharmaceutical applications, Int. J. Pharm. 417 (2011) 256–271.
[16] R.H. Venables, PhD Thesis: Determining the Prevalence and Nature of Oral Formulation-Related Barriers to Medicines Administration in Paediatric Patients Suffering from Chronic Conditions (Accessed 16 July 2017), University of Birmingham, 2014 http://etheses.bham.ac.uk/4799/.
[17] A. Gryczke, S. Schminke, M. Maniruzzaman, J. Beck, D. Douroumis, Development and evaluation of orally disintegrating tablets (ODTs) containing Ibuprofen Granules prepared by hot melt extrusion, Colloids Surf. B 86 (2011) 275–284.
[18] L. Eriksson, T. Byrne, E. Johansson, J. Trygg, C. Vikstrom, Multi- and Megavariate Data Analysis: Basic Principles and Applications, 3rd ed., MKS Umetrics, AB, Malmo, 2013.
[19] S. Wold, Principal component analysis, Chem. Int. Lab. Syst. 2 (1987) 37–52.
[20] L. Eriksson, E. Johansson, N. Kettaneh-Wold, C. Wikstrom, S. Wold, Design of Experiments Principles and Applications, 3rd edition, Umetrics, Sweden, 2008.
[21] T. Casian, A. Reznek, L. Vonica-Gligor, J. Van Renterghem, T. De Beer, I. Tomuta, Development, validation and comparison of near infrared and Raman spectroscopic methods for fast characterization of tablets with amlodipine and valsartan, Talanta 167 (2017) 333–343.
[22] R.C. Rowe, P.J. Sheskey, M.E. Quinn, Handbook of Pharmaceutical Excipients, sixth edition, Pharmaceutical Press, London, 2009.
[23] R. Venables, H. Batchelor, J. Hodson, H. Stirling, J. Mariott, Determination of formulation factors that affect oral medicines acceptability in a domiciliary paediatric population, Int. J. Pharm. 480 (2015) 55–62.
[24] S. Wold, M. Josefson, Multivariate Calibration of Analytical Data Encyclopedia of Analytical Chemistry, Wiley, 2006, http://dx.doi.org/10.1002/9780470027318.a5205.
[25] F.L. Lopez, A. Bowels, M. Orlu Gul, D. Clapham, T.B. Ernest, C. Tuleu, Effect of formulation variables on oral grittiness and preferences of multiparticulate formulations in adult volunteers, Eur. J. Pharm. Sci. 92 (2016) 156–162.
[26] European Medicines Agency Committee for Medicinal Products for Human Use, Guideline on Pharmaceutical Development of Medicines for Paediatric Use, 2013 (EMA/CHMP/QWP/805880/2012 Rev. 2).

Asian Journal of Pharmaceutical Sciences xxx (xxxx) xxx

Available online at www.sciencedirect.com

ScienceDirect

journal homepage: www.elsevier.com/locate/AJPS

Original Research Paper

Fluidised bed granulation of two APIs: QbD approach and development of a NIR in-line monitoring method

Alexandru Gavan[a], *Sonia Iurian*[a,*], *Tibor Casian*[a], *Alina Porfire*[a], *Sebastian Porav*[b], *Ioana Voina*[a], *Alexandru Oprea*[c], *Ioan Tomuta*[a]

[a] *Faculty of Pharmacy, Iuliu Hatieganu University of Medicine and Pharmacy, Cluj-Napoca 400012, Romania*
[b] *National Institute for Research and Development of Isotopic and Molecular Technologies, Cluj-Napoca 400293, Romania*
[c] *S.C. Laropharm SRL, Bragadiru 077025, Romania*

ARTICLE INFO

Article history:
Received 22 November 2018
Revised 28 January 2019
Accepted 18 March 2019
Available online xxx

Keywords:
Quality by design
Design space
Risk assessment
Process analytical technology
Fluid bed granulation
MicroNIR

ABSTRACT

The study focused on the fluid-bed granulation process of a product with two active pharmaceutical ingredients, intended for coated tablets preparation and further transfer to industrial scale. The work aimed to prove that an accurate control of the critical granulation parameters can level the input material variability and offer a user-friendly process control strategy. Moreover, an in-line Near-Infrared monitoring method was developed, which offered a real time overview of the moisture level along the granulation process, thus a reliable supervision and control process analytical technology (PAT) tool. The experimental design's results showed that the use of apparently interchangeable active pharmaceutical ingredients (APIs) and filler sorts that comply with pharmacopoeial specifications, lead to different end-product critical attributes. By adapting critical granulation parameters (i.e. binder spray rate and atomising pressure) as a function of material characteristics, led to granules with average sizes comprised in a narrow range of 280–320 µm and low non-granulated fraction of under 5%. Therefore, the accurate control of process parameters according to the formulation particularities achieved the maintenance of product within the design space and removed material related variability. To complete the Quality by design (QbD) strategy, despite its limited spectral domain, the microNIR spectrometer was successfully used as a robust PAT monitoring tool that offered a real time overview of the moisture level and allowed the supervision and control of the granulation process.

* Corresponding author. Faculty of Pharmacy, Iuliu Hatieganu University of Medicine and Pharmacy, 41 Victor Babes Street, Cluj-Napoca 400012, Romania. Tel.: +40 74 5629083.
E-mail address: iuriansonia@yahoo.com (S. Iurian).
Peer review under responsibility of Shenyang Pharmaceutical University.

https://doi.org/10.1016/j.ajps.2019.03.003

1. Introduction

Fluid bed granulation is frequently an indispensable step in solid oral dosage form manufacturing, which consists in obtaining granules by spraying a binder solution over a fluidised powder bed. The main purposes of granulation are to improve flow characteristics, blend uniformity, compression properties and to reduce the dust in the manufacturing areas [1]. Like in the case of all complex manufacturing processes, there are a series of critical key parameters that need to be monitored and controlled during the fluid bed granulation to ensure the delivery of constant quality products, such as inlet air flow rate, air temperature, air humidity, spray angle, flow rate, atomisation pressure [2]. The effects assessment of all mentioned variables requires high amounts of experimental work and data analysis. Moreover, materials used in pharmaceutical product preparation are also exposed to some variability. It is not uncommon for a pharmaceutical company to be forced to change the suppliers of active pharmaceutical ingredients (API) or excipients because of changes in the quality of the raw material, shortages of raw material, regulatory aspects or even natural disasters [3]. To overcome these issues, companies often initiate a dual-supply strategy for each API/excipient as backup for unanticipated interruptions. However, even if the substances seem to be equivalent and meet all the pharmacopoeial specifications, they are not necessarily inter-changeable: processability and critical quality attributes of the end-product may be affected [4,5].

Quality by design (QbD) approach endorsed by the drug regulatory authorities, offers a manner to identify and evaluate the sources of variability involved in a manufacturing process. After having established the quality target product profile (QTPP) and critical quality attributes (CQAs) of the desired product, Ishikawa diagrams and failure mode effects analysis (FMEA) can be used as risk assessment tools to rate the critical process parameters (CPPs) and critical material attributes (CMAs) [6,7]. Out of a plethora of factors that can influence the quality of the end-product, those associated to high risk scores can be further studied through design of experiments (DoE). This strategy was successfully applied for numerous dosage forms, including immediate release tablets, prolonged release drug delivery systems, oral lyophilisates and as a result it yielded design spaces that granted process flexibility and high product robustness [8,9]. Kushner et al. identified the changes caused by excipient variability in a QbD approach, however a proper mitigation strategy was not proposed to overcome the variability effects [10]. Working within the design space equalizes the effects of input material variability and leads to products that consistently meet the final requirements [4]. To confirm that the manufacturing process was carried out within the limits of design space and the quality of intermediate and final products, a real-time measurement of CQAs is necessary, with the possibility to perform immediate adjustment to correct the errors and prevent batch loss. This is why modern analytical technologies were developed and encouraged by regulatory authorities within the process analytical technology (PAT) initiative. PAT framework envisages the real-time information collection/gathering regarding all critical aspects of a manufacturing process, through process analysers as Raman and NIR spectrometers. PAT environment allows real-time process measurements by including the process analysers into the process stream or in its close proximity for at-line, on-line or in-line assessment [11–14].

In-line process monitoring is a promising solution that could enhance the understanding of a process and increase its reliability. But in order to be suitable for real time monitoring, an analytical method should have some distinct characteristics, such as high detection speed, the samples or the product should remain intact after the analysis, it should be process adaptable and with no interference in the processes. Near-infrared (NIR) spectroscopy holds all the mentioned characteristics, which is why it is being implemented for such purposes for a few years now [15]. Several authors have already developed real time NIR monitoring methods for the moisture content assessment during fluid-bed granulation and process end-point determination [2,16–19]. The moisture level reached along the binder spraying phase plays the most important role in the formation of granules, their growth, morphology and density. This parameter is also worth monitoring further, during the drying phase, to signal the end-point of the process; otherwise, unnecessary drying could lead to a decrease of granule size through erosion [1,15,20].

Lately, due to the widely known potential of NIR spectroscopy in pharmaceutical product quality and process monitoring, considerable attention has been given to the miniaturisation and portability of the spectroscopic devices [21]. The microNIR spectrometer is an ultra-compact, light weight device, suitable for integration in many process points in a non-invasive manner, but with limited spectral domain, 950–1650 nm. Its use was reported for the assessment of active principles in coffee beans and acerola fruits but to our knowledge its utility in in-line monitoring of fluid-bed granulation processes was not described yet [22].

This work focused on the fluid-bed granulation process of a product with two active pharmaceutical ingredients, intended for coated tablets preparation and further transfer to industrial scale. The experiment aimed to prove that an accurate control of the critical granulation parameters can level the input material variability and offer a user-friendly process control strategy. Risk assessment strategy was applied to rank the formulation and process variables as risk sources. Following an experimental design, design space was defined for granulation process. For CQAs' assessment, in-line monitoring of granules' moisture content was performed by NIR spectroscopy coupled with multivariate data analysis.

2. Materials and methods

2.1. Materials

Different sorts of the two APIs and intragranular filler were used in the formulation. The ingredient sorts were obtained from different suppliers or the same supplier, but presenting different characteristics. All samples were of commercial

Please cite this article as: Alexandru Gavan, Sonia Iurian and Tibor Casian et al., Fluidised bed granulation of two APIs: QbD approach and development of a NIR in-line monitoring method, Asian Journal of Pharmaceutical Sciences, https://doi.org/10.1016/j.ajps.2019.03.003

grade and complied with the European Pharmacopoeia specifications. For confidential reasons, samples were codded as: *Ibu A, B, C* for ibuprofen sorts; *Par A, B, C* for paracetamol sorts and *MCC A, B* for the two tested microcrystalline cellulose sorts.

The sodium starch glycolate used as disintegrant was Explosol from Blanver (Brazil) and the chosen binder was hydroxypropyl methylcellulose-Methocel E5LV kindly donated by Colorcon (UK).

During preformulation studies, in order to gain as much information as possible about the different sorts of APIs and excipients, X-ray powder diffraction and differential scanning calorimetry studies were performed (results not shown). Those studies did not reveal any polymorphism or behaviour differences between the different sorts. Besides this, all substances were stored in the same conditions, with the intention to minimize any differences in the materials' moisture content.

2.2. Scanning electron microscopy (SEM)

Active ingredients from different suppliers were evaluated for their morphology by SEM. Samples were sputter-coated with Pt/Pd in an Agar Automatic Sputter coater (Agar Scientific, USA), then images were captured at 15 kV with a Quanta 3D FEG electronic microscope (FEI, USA).

2.3. Granulation formulation and process parameters

The same formulation was used during all granulation runs, this consisted of a mixture of ibuprofen, paracetamol, microcrystalline cellulose, sodium starch glycolate and hydroxypropyl methylcellulose, resulting into a batch size of 200 g. The binder was sprayed over the fluidised powder bed as a 10% aqueous solution in order to granulate the dry components. The experimental runs were performed in a laboratory scale fluid bed granulator (Aeromatic Strea 1, GEA, Switzerland). During each run, the powder bed was fluidised with an air flow of 3–4.5 m^3/min, heated at an inlet temperature of 30 °C. At first, the powder mixture was preheated and homogenised for 10 min. After this first step, the binder solution was sprayed from the top of the granulation vessel, through a 0.8 mm nozzle, with variable pressures and the spraying rates according to the experimental design specifications (Section 3.2 and Table 3). After the binder spraying, the formed granules were dried in the same apparatus, over a period of 10 min.

2.4. Sampling and evaluation of granules

Along each run, samples of ~3 g were withdrawn from process, through a sampling valve placed on the side of the expansion vessel wall, at the height of the fluidised bed. A total of 6 samples were collected, 3 during the binder spraying and 3 during the drying, each time at one third, two thirds and at the end of each phase. The samples moisture content was analysed off-line for loss on drying (LOD), by keeping the samples in a Venticell 55 drying cabinet (MMM Medcenter Einrichtungen, Germany) for 48 h, at 50 °C.

The granulometry was measured for each end product by using a set of 8 sieves (Retsch, Germany) with sizes ranging between 100 and 800 µm. A quantity of ~130 g was analysed from each granulation batch. Mean size and distribution were calculated. An important purpose of the industrial granulation process is reducing the dust [1], for this reason, one more property of obtained granulates was analysed, namely the non-granulated fraction. The particles under 100 µm found in the collecting pan after the sieve analysis were considered non-granulated fraction and expressed as dust percentage from the total amount of analysed granules.

2.5. NIR process monitoring

All granulation runs were monitored using a MicroNIR PAT-U spectrometer (Viavi Solutions, USA), controlled with JDSU MicroNIR Pro software. The apparatus is equipped with Linear Variable Filter technology, which allows the reduction of the devices size and the direct attachment to the expansion vessel wall. The spectrometer was attached on the expansion vessel at the same height as the sampling valve, using a custom 3D printed support to ensure direct contact of the NIR detector with the fluidised powder bed and avoiding any interferences with process. Spectra were recorded continuously at 10 s intervals, in reflectance mode, over the whole range of the spectrometer, 950–1650 nm, with a resolution of 6 nm. Each spectra was the average of 200 scans, recorded with an integration time of 7 ms per scan, which resulted in a total of 1400 ms necessary for a full spectral acquisition. Until the next measurement, in the spare time of the 10 s interval the device entered automatically in stand by mode.

2.6. Analysis of the spectral data

By continuously collecting spectra during all performed runs, a large amount of spectral data was gathered, therefore requiring proper multivariate data analysis in order to obtain the desired information. For this purpose the data was imported and analysed using the SIMCA 14.0 software (Sartorius Stedim, Sweden). Principal Component Analysis (PCA) was performed in order to identify which spectral domain is specific for changes in the moisture content of the powder bed. This dimensionality reduction technique is designed to efficiently extract and describe systematic variation present in the NIR spectra, represented by the physico-chemical properties of the powder bed and to facilitate data interpretation [23,24]. By analysing the loading plots and comparing them with the pre-processed spectra, an appropriate spectral domain could be identified.

The multivariate prediction model was developed using orthogonal partial least squares (OPLS) method, which had the purpose to separate X-specific spectral systematic variation into predictive and orthogonal (uncorrelated) fractions. An optimal number of OPLS factors was chosen based on the highest fraction of X variation modelled in the component (R2X), fraction of Y variation predicted according to cross-validation, using the X model (Q2) and low root mean square error of cross-validation (RMSEcv), avoiding in the same time the overfitting of the model [24].

Please cite this article as: Alexandru Gavan, Sonia Iurian and Tibor Casian et al., Fluidised bed granulation of two APIs: QbD approach and development of a NIR in-line monitoring method, Asian Journal of Pharmaceutical Sciences, https://doi.org/10.1016/j.ajps.2019.03.003

Table 1 – Quality target product profile of granules containing paracetamol and ibuprofen.

QTPP element	Target	Observations
Route of administration	Intermediate product for oral solid dosage form preparation	The granules will be further used for coated tablet preparation
Dosage form	Granules	
Dosage form API content	32.68% (w/w) paracetamol 40.22% (w/w) ibuprofen	
Drug product quality attributes	Mean granule size	280–320 μm
	Granule size distribution	Gaussian distribution
	Granule polydispersity index	< 50%
	Moisture content	2%–4%
	Disintegration time	< 7.5 min
	Assay	90%–110% of the declared content of APIs

2.7. *Identification of granules' quality target product profile (QTPP), critical quality attributes (CQAs) and the risk analysis of CQAs*

According to the International Council of Harmonisation (ICH) Q8, QTPP is the basis of product development design. Thus, defining QTPP, as shown in Table 1, was the starting point of the present research study. Further, out of QTPP, CQAs were revealed as physical characteristics that should be in appropriate limits to ensure the desired product quality. The CQAs were evaluated by means of Ishikawa diagrams, in order to identify the potential variables that could have an impact on the CQAs [6,8].

2.8. *Risk assessment by failure mode effects analysis (FMEA)*

Further, failure mode and effect analysis (FMEA) was applied in order to identify and prioritize the failure modes that are most probable to lead to process failure and thus to an improper product [8]. The overall failure risk was assessed based on three criteria: occurrence frequency (O), effect severity (S) and detection difficulty (D), each of them ranked on a scale from 1, as the low level of the mentioned criteria to 5, as the high level of the criteria. The final score, the risk priority number (RPN) was obtained by the multiplication of the scores registered for each of the three criteria [25]. CPPs and Critical Material Characteristics (CMCs) that met the highest risk scores were studied in detail in DoE.

2.9. *Design of experiments*

Before the development of an appropriate experimental design which would allow the in depth study of the process, some preliminary experiments were performed in order to establish a stable and reliable granulation process (data not shown). This part aimed to define the granules composition, batch size and the basic process parameters. The MODDE 11.0 software (Sartorius Stedim, Sweden) was further used in order to develop a D-optimal DoE, which allowed the introduction of anticipated variability that could normally occur in an industrial scale manufacturing process and also the study of the effects of such variability. A D-optimal approach is based on the selection of experimental runs so that they span the largest possible volume of the variability matrix and for this reason, it is recommended when combinations of qualitative and quantitative multilevel factors are studied in the same experimental design [26].

3. Results and discussions

3.1. *QTPP, CQAs, CPPs and FMEA*

A team of researchers with in-depth knowledge on the fluid bed granulation process was brought together. During several discussion sessions, QTPP of the granules was established according to the type of dosage form and its intended use, for the preparation of coated tablets, as shown in Table 1. The selected CQAs that emerged from QTPP were those susceptible to variations during a large scale manufacturing process: granule average size, polydispersity index and humidity.

Further, risks associated with every step of process, from the raw materials properties to the final granules characteristics were identified, analysed and evaluated in detail [25]. The variables related to granule formulation, manufacturing process, analytical methods and equipment performance were summarised in an Ishikawa diagram (Fig. 1). CPPs and CMCs were further analysed using FMEA method for their associated risk, revealed as RPN (Table 2).

Once the qualitative and quantitative composition of a pharmaceutical product is established, few changes can occur with respect to formulation; however, variations in particle size, shape, polymorph of APIs or excipients could appear when switching suppliers. Such variability could influence the quality of granules, especially when the major components are concerned. Therefore, in our particular case, FMEA revealed that variations in the sort of APIs or filler could exert a higher risk (RPN = 60) than in the disintegrant agent or the binder (RPN = 24 and 16 respectively).

Among the process parameters, the mixing phase was considered less critical to the process, compared to the spraying and the drying phases. The inlet air temperature during mixing/heating of the powder blend was considered less important due to the fact that the binder solution is added only when the powder reaches an established temperature. The binder spray rate and atomising pressure were evaluated as the most hazardous, as their values could change because of

Please cite this article as: Alexandru Gavan, Sonia Iurian and Tibor Casian et al., Fluidised bed granulation of two APIs: QbD approach and development of a NIR in-line monitoring method, Asian Journal of Pharmaceutical Sciences, https://doi.org/10.1016/j.ajps.2019.03.003

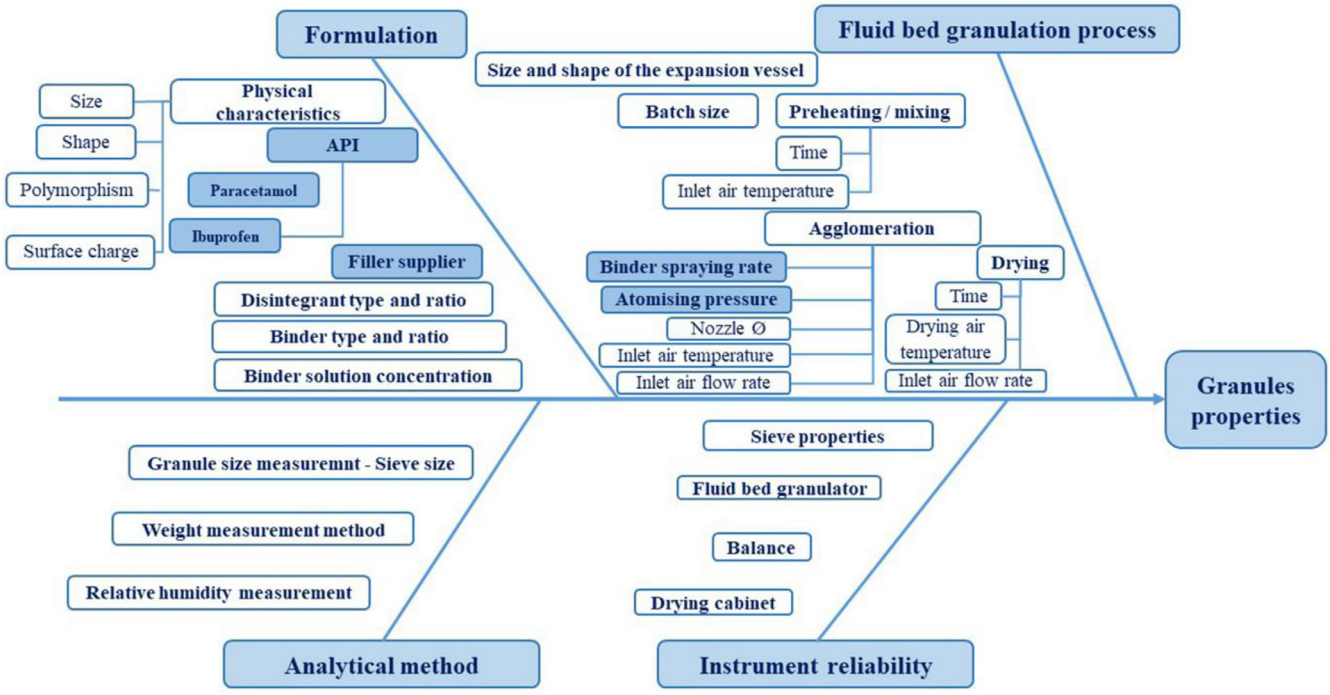

Fig. 1 – Ishikawa diagram highlighting parameters that could have an impact on the final product properties.

equipment malfunction or human error and they have a high impact on granule size and distribution. The drying parameters are also critical to the product quality: if the drying time is exceeded, granules could become friable and erode with impact on flow properties. These phenomena can be prevented by NIR monitoring, thus they were ranked lower than the granulation step, with RPN 48. An experimental design was developed based on the parameters that expose product quality to the highest risk, with RPN of 60: the APIs and filler sorts, binder spray rate and atomising pressure.

3.2. *Design of experiments*

When developing a D-optimal DoE, that includes quantitative as well as qualitative factors, the selection of experiments included in the design matrix is critical and needs to be decided based on scientific means. In this case, two evaluation criteria had to be considered: *condition number* and *G-efficiency*. The *condition number* assesses the sphericity and symmetry of the design, representing the ratio of the largest and smallest values of the variability matrix. Its ideal value is 1, representing an orthogonal design, the orthogonality of the design evolving inversely proportional with this parameter. In the case of an optimisation design with a mixture of quantitative and qualitative factors, the *condition number* value could increase substantially, hence a DoE with a condition number < 8 is still considered very good. The *G-efficiency* is a criteria that expresses the design performance by comparing it to the performance of a fractional factorial design, being expressed in perfectness. For a high quality, reliable D-optimal DoE, a *G-efficiency* above 60%–70% is recommended [26].

The risk analysis indicated that supplier changes can occur during the life span of a product, so most of the companies rely on a dual-supply strategy that comes with a variation in the physical characteristics of the materials. Three CMCs, namely the different sorts of APIs and filler were selected to be studied as qualitative variables of the DoE.

Based on the Ishikawa diagram and the conducted risk assessment, two quantitative variables represented by the binder spraying parameters were chosen for further investigation. Their control was meant to level the effects of the qualitative variables.

The DoE was developed based on the data presented in Table 3, consisting in a total amount of 39 experimental runs, including 4 centre points (Table S1).

The generated DoE registered a *G-efficiency* value of 70.21% and a *condition number* of 7.08. The studied responses were the moisture content levels of the samples withdrawn during each experimental run, the average size and the non-granulated fraction of the obtained granules (see Section 2.4). For the experimental design matrix and results, consult Table S1.

The registered response values were centralised, introduced into the design matrix and further, the fitting of the experimental data was accomplished by applying multiple linear regression (MLR) and was evaluated using the standard, most reliable statistical parameters, namely R^2 – *goodness of fit*, Q^2 – *goodness of prediction* and the response reproducibility. R^2 reflects the fraction of the response variation explained by the model, while Q^2 gives the model prediction capacities. The model reproducibility is calculated and represented strictly based on the replicates specified in the design matrix. A good fitting is represented by high values of the model performance indicators, as close to one as possible. Furthermore, for a valid model, the difference between R^2 and Q^2 should not exceed 0.2–0.3, and the reproducibility should be well over 0.5 [26].

Please cite this article as: Alexandru Gavan, Sonia Iurian and Tibor Casian et al., Fluidised bed granulation of two APIs: QbD approach and development of a NIR in-line monitoring method, Asian Journal of Pharmaceutical Sciences, https://doi.org/10.1016/j.ajps.2019.03.003

Table 2 – Failure mode effects analysis for risk assessment.

CPP/CMC	Failure mode	Failure effects	Potential causes	Control methods	O	S	D	RPN
Paracetamol	Changes in API particle size, shape, polymorphism	Variations of granule size, polydispersity index, humidity	Supplier change	Granule size, distribution and moisture content measurements, NIR spectra	4	5	3	60
Ibuprofen	Changes in API particle size, shape, polymorphism	Variations of granule size, polydispersity index, humidity	Supplier change	Granule size, distribution and moisture content measurements, NIR spectra	4	5	3	60
Filler	Changes in filler particle size, shape, polymorphism	Variations of granule size, polydispersity index, humidity	Supplier change	Granule size, distribution and moisture content measurements, NIR spectra	4	5	3	60
Disintegrant	Changes in disintegrant particle size, shape, polymorphism	Variations of granule size, polydispersity index, humidity, disintegration	Supplier change	Granule size, distribution and moisture content measurements, NIR spectra Disintegration test	4	3	2	24
Binder	Changes in binder particle size, shape, disintegration speed	Variations of granule size, polydispersity index, humidity, disintegration	Supplier change	Granule size, distribution and moisture content measurements, NIR spectra Disintegration test	4	2	2	16
Mixing / preheating time / temperature	Homogeneity issues Variations in the drying rate	Variations of granule size, polydispersity index, humidity	Human errors Equipment failure	Granule size, distribution and moisture content measurements, NIR spectra	4	4	3	48
Binder spray rate	Inhomogeneous moistening of the powder blend Variations in the drying rate	Variations of granule size, polydispersity index, humidity	Human errors Equipment failure	Granule size, distribution and moisture content measurements, NIR spectra	5	4	3	60
Atomising pressure	Inhomogeneous moistening of the powder blend Variations in the drying rate	Variations of granule size, polydispersity index, humidity	Human errors Equipment failure	Granule size, distribution and moisture content measurements, NIR spectra	5	4	3	60
Inlet air temperature	Variations in the drying rate	Variations of granule size, polydispersity index, humidity	Human errors Equipment failure	Granule size, distribution and moisture content measurements, NIR spectra	4	4	3	48
Drying time/temperature	Variations in the drying rate	Variations of granule size, polydispersity index, humidity	Human errors Equipment failure	Granule size, distribution and moisture content measurements, NIR spectra	4	4	3	48
Inlet air flow rate	Variations in the drying rate	Variations of granule size, polydispersity index, humidity	Human errors Equipment failure	Granule size, distribution and moisture content measurements, NIR spectra	4	4	1	16

Abbreviations: CPP – critical process parameter, CMC – critical material characteristic, O – occurrence, S – severity, D – detectability, RPN – risk priority number.

Please cite this article as: Alexandru Gavan, Sonia Iurian and Tibor Casian et al., Fluidised bed granulation of two APIs: QbD approach and development of a NIR in-line monitoring method, Asian Journal of Pharmaceutical Sciences, https://doi.org/10.1016/j.ajps.2019.03.003

Table 3 – Variables of the experimental design.

Quantitative independent variables	Levels of variation	Range of variation		
Binder spraying rate (g/min)	3	5–12.5–20		
Atomising pressure (atm)	2	0.5–0.75		
Qualitative independent variables		Sort of ingredient		
Paracetamol	3	*Par A*	*Par B*	*Par C*
Ibuprofen	3	*Ibu A*	*Ibu B*	*Ibu C*
Microcrystalline cellulose	2	*MCC A*		*MCC B*

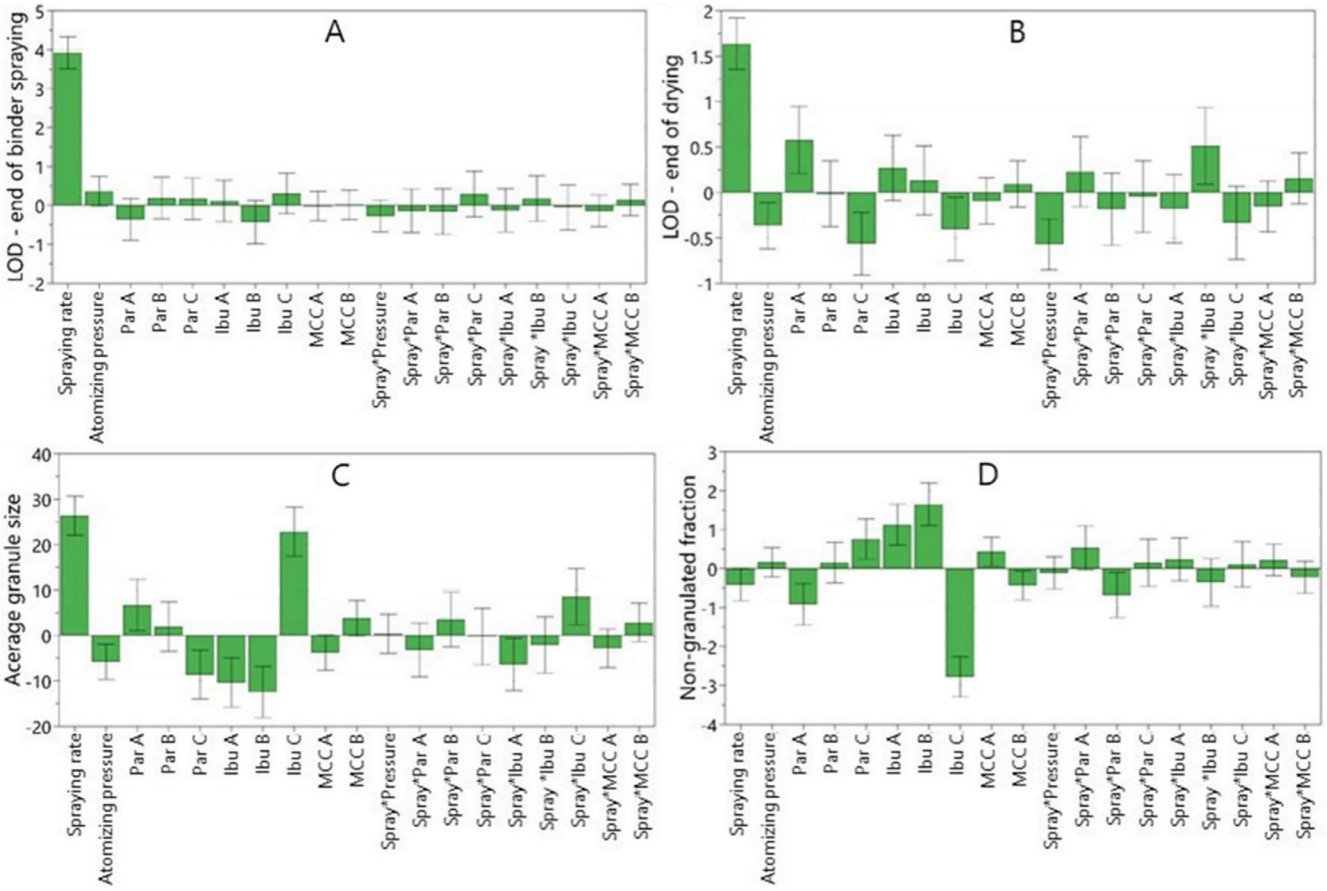

Fig. 2 – Scaled and centred coefficient plots – factor influence over the: (A) LOD% at the end of the binder spraying phase; (B) LOD% at the end of the drying process; (C) average size of the granules; (D) the non-granulated fraction.

The summary of fit and the statistical parameters were calculated based on the experimental design data. The chosen model presented excellent quality, with R^2 greater than 0.86 and Q^2 greater than 0.64 for all the eight studied responses. The model validity was also confirmed by a reliable reproducibility, with statistical values of over 0.84 for all studied responses/outputs (statistical values included in Table S2).

3.3. *Independent variables effects on the process and granules properties*

Based on the developed DoE model, regression coefficients were automatically calculated for the studied output variables. Fig. 2 presents the scaled and centred coefficient plots which describe the influence of the studied factors over the moisture levels registered at the end of the binder spraying phase and drying phase, i.e. end of the process, and over the average granule size and non-granulated fraction of each batch.

The first important observation is that the binder spraying rate had the highest effect over the average granule size and as expected, an increase of the spraying rate would also lead to an increase of granule size [20]. Naturally, a higher spraying rate will lead to higher moisture levels along the process, which promotes the granule forming and growth, especially when the formulation contains ingredients that are soluble in the spraying solvent, as it is the case.

Please cite this article as: Alexandru Gavan, Sonia Iurian and Tibor Casian et al., Fluidised bed granulation of two APIs: QbD approach and development of a NIR in-line monitoring method, Asian Journal of Pharmaceutical Sciences, https://doi.org/10.1016/j.ajps.2019.03.003

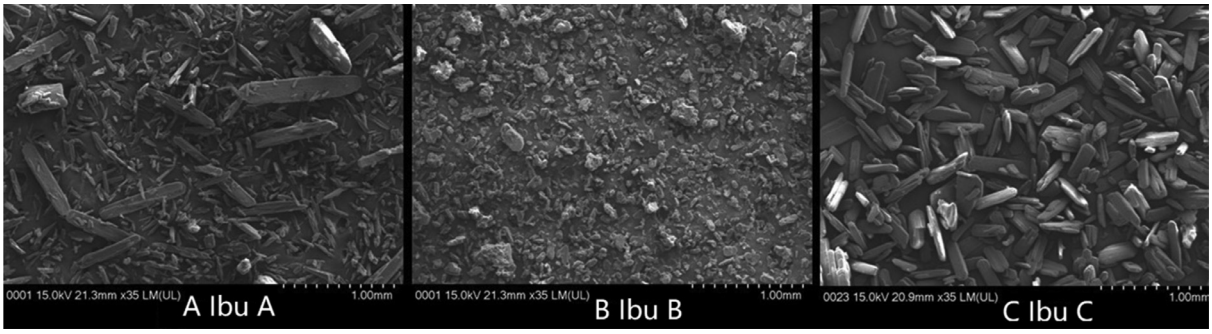

Fig. 3 – Scanning electron microscopy micrographs for the 3 studied ibuprofen sorts.

The influence of the second studied process parameter, the atomising air pressure used for the spraying of the binder solution, seemed to be minor, but still significant, representing that an increase of atomising pressure would reduce the average granule size. By increasing the atomising pressure, the size of the formed droplets decreases, favouring their evaporation before they actually get in contact with the fluid powder bed, thus limiting the binder effect [27].

Neither of the two studied process parameters seemed to have statistical significant influence over the non-granulated fraction size of each batch, which meant that only the formulation ingredients needed to be considered in this case.

Regarding the sort of paracetamol used in the formulation, it resulted that using *Par A* would lead to obtaining slightly larger granules, with a lower non-granulated fraction, while *Par C* presented opposite effects. The actual total granule size variation was about 10–20 µm. In the present model, this global effect is shared between all the three *Par* sorts, meaning that the sum of model coefficients equals zero, therefore the coefficients having opposite signs does not imply a substantial change in terms of particle size. However, this API sort presented a positive influence over the LOD% registered at the end of the process, which translates through a higher moisture content of the final product. On the other hand, *Par C* significantly decreased the final LOD%, due to its slightly lower bulk density (declared in the product's bulletin of analysis), favouring the final drying process, thus representing a viable alternative to a more reliable process.

The most influential qualitative factor was the sort of ibuprofen, the strongest effect in the coefficient plot appearing for *Ibu C*. This sort appeared to increase the granulometry, substantially reducing the dust fraction of the final product and, in the same time, favouring the drying process. The two other API sorts tested in the formulation had opposite effect compared to *Ibu C*, reducing the average granule size and increasing the dust fraction.

In order to identify the occurring phenomena causing those substantial differences, scanning electron microscopy was performed, the obtained images are shown in Fig. 3. It is well known that ibuprofen comes as acicular crystals, fact also observed in the figure for the first two sorts. The *Ibu C* had homogenous, large particles, with sizes averaging 500 µm; *Ibu A* however, presenting a much higher dispersity of particles size and shapes. In the case of *Ibu B*, which was a micronised sort, the particles were much finer and the acicular shapes can not be identified any more, most probable being broken through the micronisation process.

The larger particles size of *Ibu C* is the property which aids to dust reduction, the particles being already larger than the considered non-granulated fraction of under 100 µm. The granule growth phenomenon caused by *Ibu C* could be explained by the particle size and shape differences between it and the particles of all three studied paracetamol sorts (Fig. S1). It is probable that the larger, acicular ibuprofen crystals would act as cores, on whose surface adhere the much smaller, irregular paracetamol particles, thus forming granules.

The high influence of the ibuprofen sort over the studied responses suggests that this would be an important formulation factor that needs to be taken into consideration when adapting the CPPs. The influence of the MCC sort used in the granules composition did not seem to have statistically significant effects, nor had the factor interactions that can be observed in Fig. 2. Still, those factors aided the fitting of the experimental data, assuring the obtaining of a statistically valid model.

Up to this stage of the research, results showed that the use of apparently interchangeable APIs and filler sorts that comply with pharmacopoeial specifications, lead to different end-product critical attributes. Thus, in order to maintain the final product's desired characteristics, the critical process parameters and the Design Space should be adapted accordingly.

3.4. *NIR monitoring method development*

Parallel with the experimental design analysis, a noninvasive NIR method was developed for the in-line monitoring of the fluid bed granulation process by predicting the moisture content.

At first, all the acquired NIR spectral data was loaded into the SIMCA software and pre-processed by applying the first Savitzky–Golay derivative which removed the baseline shifts, reduced the additive effects and improved the overall spectral resolution [28].

The raw recorded reflectance spectra are illustrated in Fig. 4A, while Fig. 4B illustrates the spectral data pre-processed with the first Savitzky–Golay derivative. The highest spectral intensity variation can be noticed around the first –OH group overtone, around 1390–1450 nm. Especially in this specific region, the 1st derivative pre-processed spectral intensity increases with the increase of water content registered during

Please cite this article as: Alexandru Gavan, Sonia Iurian and Tibor Casian et al., Fluidised bed granulation of two APIs: QbD approach and development of a NIR in-line monitoring method, Asian Journal of Pharmaceutical Sciences, https://doi.org/10.1016/j.ajps.2019.03.003

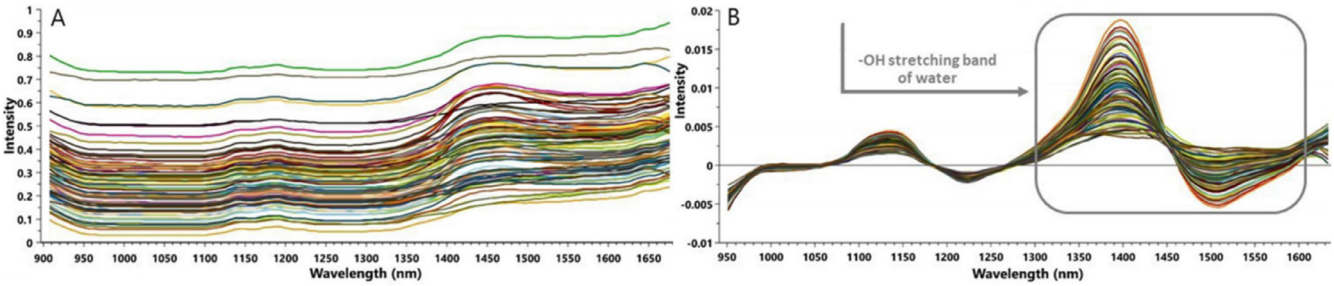

Fig. 4 – Raw (A) and pre-processed first derivative (B) spectra registered during the performed granulation runs.

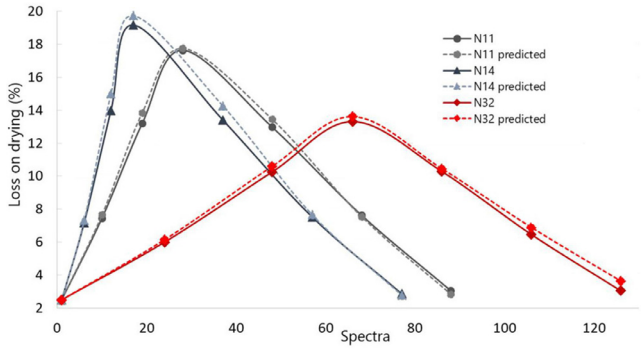

Fig. 5 – LOD% measured vs. NIR predicted values for 3 granulation runs performed with different binder spraying rate. Abbreviations: N11, N14, N32 – experimental runs performed in different conditions, according to the Design of Experiments.

the binder spraying and decreases when the water content reduces during the drying of the product [2].

A PCA model was developed including only the 1300–1600 nm spectral domain, situation where only one principal component (PC) was sufficient to explain 97% variability.

Further, for the moisture prediction model development, the 39 performed and recorded experimental runs were divided into two groups, chosen so that each of the two groups covered the entire studied variability. The first group contained 25 runs and was used for the multivariate calibration of the model, the second group contained the rest of 14 experiments and was used for validation. The calculated OPLS model included two factors, one for each fraction of the model. For the predictive fraction, high statistical parameters could be registered, with values of 0.937 for R2X and 0.906 for Q2. On the other hand, the orthogonal (uncorrelated) fraction registered only a low R2X value of 0.057 but which improved the overall model quality. The RMSEcv calculated for the model with 2 factors was 1.55. The second group, formed from the remaining 14 experimental runs, was used for the validation of the OPLS prediction model. The method was validated with a good prediction recovery, close to 100% and low relative bias.

The measured LOD% values were plotted against the NIR predicted values; Fig. 5 illustrates 3 of the monitored granulations, framed in the validation data set, preformed using different binder spraying rates. The correlation coefficient calculated between the measured LOD% and the NIR predicted values was greater than 0.98 for all 39 granulation runs, which shows good predictive capacities.

Even though the microNIR spectrometer has limited spectral domain compared to FT-NIR spectrometers, the development of accurate moisture content prediction method was possible, thus proving to be a powerful tool for pharmaceutical applications.

3.5. *Design space and process optimisation*

The DoE approach lead to an in depth understanding of the variables' influence over the process. Further, based on the initial investigation domain, the statistics software was used to generate a design space by introducing a set of constraints according to the QTTP [29,30]. The pre-set ingredients and the CQAs targets and variation intervals are presented in the upper part of Table 4. The intermediate LOD% limits were set based on the values obtained along the performed experimental runs with set process parameters inside the design space. The final LOD% and average granule size were set based on the QTPP specifications, and the non-granulated fraction was minimised. Depending on APIs and filler sort, each of them varied on 3, 3 and respectively 2 levels, 18 Design Spaces could be generated. As an example, three of them as a function of *Ibu* sort are shown in Fig. 6. *Ibu* was chosen for its high impact over all studied responses. The *Par C* sort was kept constant for its positive influence over the granule drying phase, while *MCC B*, due of its tendency to aid the granule growth, reducing the dust fraction (see Section 3.3).

Each of the three plots includes a different area where the specified constraints are fulfilled, highlighting that the same characteristics of granules can be obtained with different API sorts, by rigorously controlling the CPPs throughout the process. The different acceptable areas of the three Design Spaces plotted in Fig. 6 can be easily explained based on the influence of the different ibuprofen sorts described in Section 3.3 and depicted in Fig. 2. As it can be observed, the first two Design Spaces (Fig. 6A and B) present similar acceptable areas – by using a formulation with *Ibu A* or *Ibu B*, the granulation process needs to be performed with high spraying rate and low atomising pressure in order to ensure the required granulation conditions, leading to a final product which would comply with the QTPPs specifications. The high spray rate is needed to compensate the tendency of *Ibu A* and *Ibu B* to provide smaller granules and a higher dust fraction. Moreover, the acceptable area of the *Ibu B* formulation is slightly smaller than the one

Please cite this article as: Alexandru Gavan, Sonia Iurian and Tibor Casian et al., Fluidised bed granulation of two APIs: QbD approach and development of a NIR in-line monitoring method, Asian Journal of Pharmaceutical Sciences, https://doi.org/10.1016/j.ajps.2019.03.003

Table 4 – CQAs and results of the optimal granulation process.

Qualitative independent variables	Pre-set ingredient sort				
Paracetamol	*Par C*				
Ibuprofen	*Ibu C*				
Microcrystalline cellulose	*MCC B*				
Dependent variables (responses)	CQAs				
	Minimum		Target		Maximum
LOD (%) – 1/3 binder spraying	5.5		–		8.5
LOD (%) – 2/3 binder spraying	10.2		–		15.0
LOD (%) – end of binder spraying	13.3		–		19.9
LOD (%) – 1/3 drying	9.0		–		14.5
LOD (%) – 2/3 drying	4.5		–		9.0
LOD (%) – end of drying	2.0		3.0		4.0
Average granule size (μm)	280		300		320
Non-granulated fraction (%)	minimisation				
Dependent variables (responses)	Values				
	DoE		NIR		Experimental
	Predicted	Recovered (%)	Predicted	Recovered (%)	
LOD (%) – 1/3 binder spraying	6.75	90.0	8.0	106.6	7.5
LOD (%) – 2/3 binder spraying	12.1	88.9	14.2	104.4	13.6
LOD (%) – end of binder spraying	15.4	97.5	15.7	99.4	15.8
LOD (%) – 1/3 drying	10.7	98.2	11.1	101.8	10.9
LOD (%) – 2/3 drying	6.5	98.5	6.5	98.5	6.6
LOD (%) – end of drying	2.0	80.0	2.5	100	2.5
Average granule size (μm)	306	101.3	–		302
Non-granulated fraction (%)	4.5	104.6	–		4.3

Abbreviations: LOD – loss on drying; CQA – critical quality attributes; DoE – design of experiments; NIR – near-infrared.

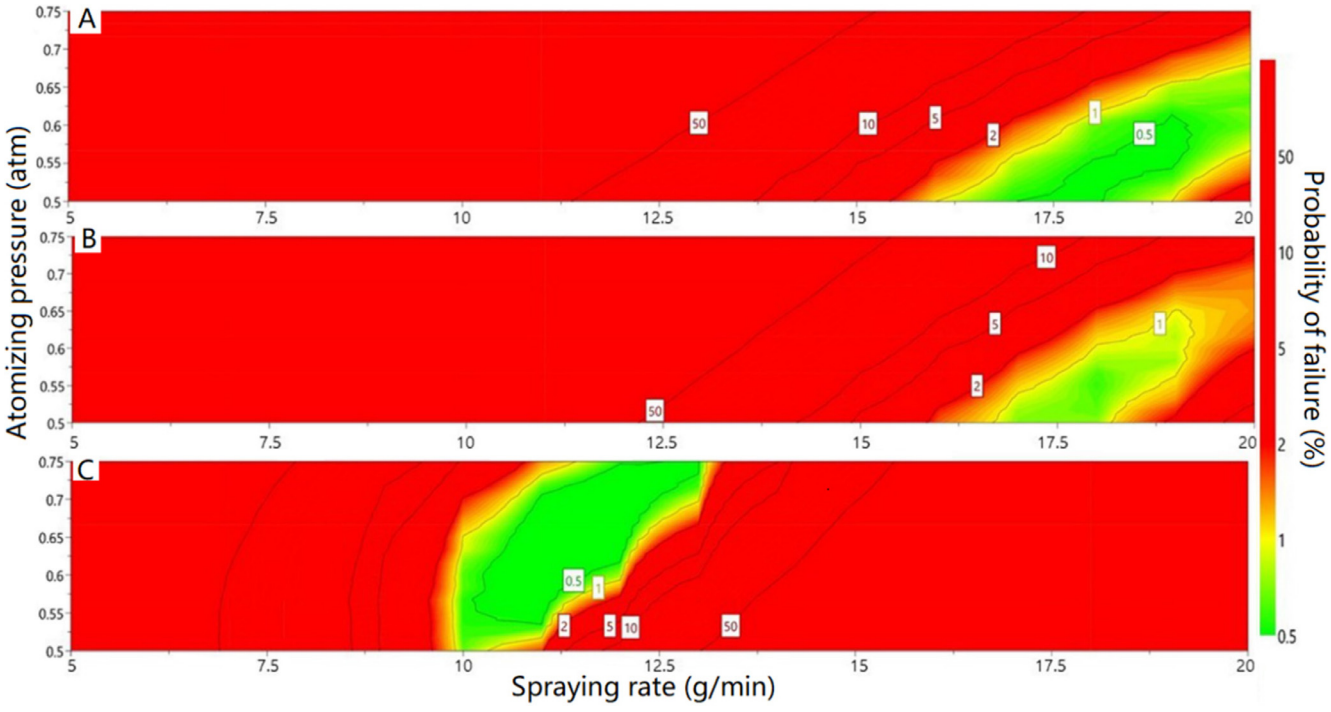

Fig. 6 – Design Spaces for granulation processes that provide optimal granules, adapted according to the sort of ibuprofen used in the formulation. (A): Ibuprofen A (Ibu A); Paracetamol (Par C); Microcrystalline cellulose (MCC B); (B): Ibuprofen B (Ibu B); Paracetamol (Par C); Microcrystalline cellulose (MCC B); (C): Ibuprofen C (Ibu C); Paracetamol (Par C); Microcrystalline cellulose (MCC B).

Please cite this article as: Alexandru Gavan, Sonia Iurian and Tibor Casian et al., Fluidised bed granulation of two APIs: QbD approach and development of a NIR in-line monitoring method, Asian Journal of Pharmaceutical Sciences, https://doi.org/10.1016/j.ajps.2019.03.003

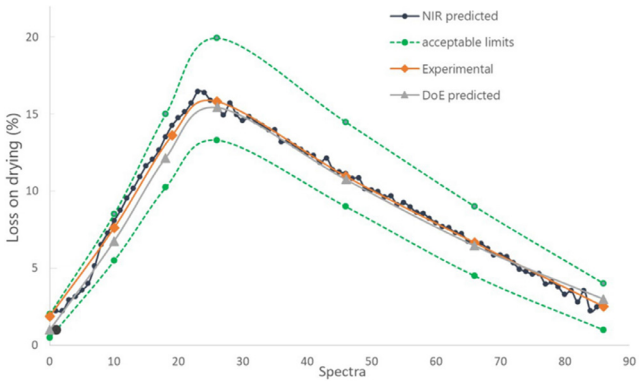

Fig. 7 – Moisture content measured and predicted along the optimal granulation process.

calculated for the *Ibu A* formulation, fact explained based on the *Ibu B* tendency to reduce the granule size and to increase the non-granulated fraction even more than Ibu A, thus lowering the probability of obtaining appropriate granules.

By using *Ibu C* in the granules' formulation, the process parameters acceptable variation range is completely different compared to the ones obtained for the previously two *Ibu* sorts. This sort substantially increases the particle size and reduces the dust fraction, favouring the drying process of the final product. The use of *Ibu C* in the formulation allows the performing of a successful granulation with average binder spraying rate, tolerating a variation of the atomising pressure over almost all the studied domain.

To confirm the robustness of the model and NIR monitoring method, the *design space explorer* function of the software generated the following process parameters: spraying rate of 11 g/min and atomising pressure of 0.6 atm for the qualitative formulation indicated in Table 4. The aforementioned granulation process was carried out and simultaneously monitored using the same NIR setup. The measured vs. predicted intermediate and end-product characteristics are listed in the lower part of Table 4. Fig. 7 pictures the LOD% evolution throughout the granulation process: NIR predicted LOD% values overlapped with the DoE predicted ones and were confirmed by the experimental measurements. All the outputs fell within the set intervals, hence the DoE could be considered valid for further use for the optimisation of process parameters according to the desired formulation factors. Moreover, as a non-invasive in-line method, the developed NIR spectroscopic technique yields LOD% values each 10 s of the process, compared with the classical measurements which allowed the analysis of a total of 6 samples per process.

4. Conclusion

The study demonstrated that the fluid bed granulation can be adapted through an accurate control of CPPs to eliminate the variability brought by possible API or excipient changes. Therefore, assuring a consistent end product quality and maintaining its characteristics within the QTPP is possible with a constant monitoring of the manufacturing process.

Practically, a multiple supplier strategy for all used substances prevents unexpected shortages in the manufacturing process. A simple QbD research provides enough information to handle ingredient variability in order to ensure constant product quality which falls into the limits of the Design Space. The developed model allows the easy and timely adaptation of CPPs as a function of the selected excipient, improving the process control. Process adjustment can be performed immediately, without the need of a process variation approval from the authorities.

However, if a new API or excipient sort, which has not been studied from beginning, needs to be introduced in the formulation, some additional experimental runs need to be performed. This does not mean repeating the entire study, sometimes the influence of a new substance sort over the end-product's critical attributes, may be similar to one that was already studied. This observation highlights how important it is for the manufacturer to choose reliable suppliers.

Moreover, the developed in-line microNIR monitoring method offers a real time overview of the moisture level and allows its maintenance in the desired intervals, thus a reliable PAT tool for the supervision and control of the granulation process.

Such an approach grants that the quality of the medicine gets not only to be tested, but built into the product.

Declaration of interest

The authors declare that there is no conflicts of interest.

Acknowledgements

The authors are thankful to S.C. Laropharm SRL (Bucharest, Romania) for kindly providing the APIs and excipients used in the study. Funding: This work was supported by the Romanian National Authority for Scientific Research and Innovation, CNCS-UEFISCDI [project number PN-III-P2-2.1-BG-2016-0201].

Supplementary materials

Supplementary material associated with this article can be found, in the online version, at doi:10.1016/j.ajps.2019.03.003.

REFERENCES

[1] Cantor S, Augsburger L, Hoag S, Gerhardt A. Granulation processes, mechanism, and the use of binders. Pharmaceutical dosage forms: tablets, I. 3rd ed. New York: Informa Healthcare; 2008.
[2] Kona R, Qu H, Mattes R, Jancsik B, Fahmy RM, Hoag SW. Application of in-line near infrared spectroscopy and multivariate batch modeling for process monitoring in fluid bed granulation. Int J Pharm 2013;452:63–72.
[3] Elder DP, Kuentz M, Holm R. Pharmaceutical excipients-quality, regulatory and biopharmaceutical considerations. Eur J Pharm Sci 2016;87:88–99.

[4] Zarmpi P, Flanagan T, Meehan E, Mann J, Fotaki N. Biopharmaceutical aspects and implications of excipient variability in drug product performance. Eur J Pharm Biopharm 2017;111:1–15.
[5] Flicker F, Eberle VA, Betz G. Variability in commercial carbamazepine samples - impact on drug release. Int J Pharm 2011;410:99–106.
[6] ICH Q8 (R2) Pharmaceutical Development 2009. www.ich.org%2Ffileadmin%2FPublic%0A_Web_Site%2FICH_Products%2FGuidelines%2FQuality%2FQ8_R1%2FStep4%2FQ8_R2_%0AGuideline.pdf. [accessed 12th June 2018].
[7] ICH Q9 Quality Risk Management 2006. www.ich.org%2Ffileadmin%2FPublic_Web_Site%2FICH_Products%2FGuidelines%2FQuality%2FQ9%2FStep4%2FQ9_Guideline.pdf. [accessed 12th June 2018].
[8] Iurian S, Turdean L, Tomuta I. Risk assessment and experimental design in the development of a prolonged release drug delivery system with paliperidone. Drug Des Devel Ther 2017;11:733–46.
[9] Casian T, Iurian S, Bogdan C, Rus L, Moldovan M, Tomuta I. QbD for pediatric oral lyophilisates development: risk assessment followed by screening and optimization. Drug Dev Ind Pharm 2017;43:1932–44.
[10] Kushner J IV, Langdon B, Hiller J, Carlson G. Examining the impact of excipient material property variation on drug product quality attributes: a quality-by-design study for a roller compacted, immediate release tablet. J Pharm Sci 2011;100:2222–39.
[11] Jamrógiewicz M. Application of the near-infrared spectroscopy in the pharmaceutical technology. J Pharm Biomed Anal 2012;66:1–10.
[12] Goodwin DJ, van den Ban S, Denham M, Barylski I. Real time release testing of tablet content and content uniformity. Int J Pharm 2018;537:183–92.
[13] De Beer T, Burggraeve A, Fonteyne M, Saerens L, Remon JP, Vervaet C. Near infrared and Raman spectroscopy for the in-process monitoring of pharmaceutical production processes. Int J Pharm 2011;417:32–47.
[14] Nagy B, Farkas A, Borbás E, Vass P, Nagy Z, Marosi G. Raman spectroscopy for process analytical technologies of pharmaceutical secondary manufacturing. AAPS PharmSciTech 2019;20:1–16.
[15] Fonteyne M, Arruabarrena J, de Beer J, Hellings M, Van Den Kerkhof T, Burggraeve A, et al. NIR spectroscopic method for the in-line moisture assessment during drying in a six-segmented fluid bed dryer of a continuous tablet production line: validation of quantifying abilities and uncertainty assessment. J Pharm Biomed Anal 2014;100:21–7.
[16] Findlay WP, Peck GR, Morris KR. Determination of fluidized bed granulation end point using near-infrared spectroscopy and phenomenological analysis. J Pharm Sci 2005;94:604–612.
[17] Frake P, Greenhalgh D, Grierson SM, Hempenstall JM, Rudd DR. Process control and end-point determination of a fluid bed granulation by application of near infra-red spectroscopy. Int J Pharm 1997;151:75–80.
[18] Rantanen J, Antikainen O, Mannermaa J. Use of the near-infrared reflectance method for measurement of moisture content during granulation. Pharm Dev Technol 2000;5:209–17.
[19] Alcala M, Blanco M, Bautista M, Gonzalez J. On-line monitoring of a granulation process by NIR spectroscopy. J Pharm Sci 2010;99:336–45.
[20] Parikh DM. Handbook of pharmaceutical granulation technology. 2nd ed. Boca Raton, FL, USA: Taylor & Francisc Group; 2005.
[21] Correia RM, Tosato F, Domingos E, Rodrigues RRT, Aquino LFM, Filgueiras PR, et al. Portable near infrared spectroscopy applied to quality control of Brazilian coffee. Talanta 2018;176:59–68.
[22] Malegori C, Nascimento Marques EJ, de Freitas ST, Pimentel MF, Pasquini C, Casiraghi E. Comparing the analytical performances of Micro-NIR and FT-NIR spectrometers in the evaluation of acerola fruit quality, using PLS and SVM regression algorithms. Talanta 2017;165:112–16.
[23] Sylvester B, Porfire A, Van Bockstal PJ, Porav S, Beer T, Tomuta I. Formulation optimisation of freeze-dried long-circulating liposomes and in-line monitoring of the freeze-drying process using an NIR spectroscopy tool. J Pharm Sci 2018;107(1):139–48.
[24] Eriksson L, Byrne T, Johansson E, Trygg J, Vikstrom C. Multi- and megavariate data analysis. Basic principles and applications. 3rd ed. Umea. Sweeden: MKS Umetrics AB; 2013.
[25] Lourenço V, Lochmann D, Reich G, Menezes JC, Herdling T, Schewitz J. A quality by design study applied to an industrial pharmaceutical fluid bed granulation. Eur J Pharm Biopharm 2012;81(2):438–47.
[26] Eriksson L, Johansson E, Kettaneh-Wold N, Wikstrom C, Wold S. Design of experiments, principles and applications. 3rd ed. Umea: Umetrics Academy; 2008.
[27] Vieira MMS, Martins RM, Freitas LAP. Characteristics of piroxicam granules prepared by fluidized bed hot melt granulation. Adv Powder Technol 2018:1–7.
[28] Rinnan A, Van Den Berg F, Engelsen SB. Review of the most common pre-processing techniques for near-infrared spectra. TrAC Trend Anal Chem 2009;28(10):1201–22.
[29] Gavan A, Porfire A, Marina C, Tomuta I. Formulation and pharmaceutical development of quetiapine fumarate sustained release matrix tablets using a QbD approach. Acta Pharm 2017;67:53–70.
[30] Iurian S, Tomuta I, Bogdan C, Rus L, Tokes T, Achim M, et al. Defining the design space for freeze-dried orodispersible tablets with meloxicam. Drug Dev Ind Pharm 2016;42(12):1977–89.

Please cite this article as: Alexandru Gavan, Sonia Iurian and Tibor Casian et al., Fluidised bed granulation of two APIs: QbD approach and development of a NIR in-line monitoring method, Asian Journal of Pharmaceutical Sciences, https://doi.org/10.1016/j.ajps.2019.03.003

Reactive and Functional Polymers 168 (2021) 105059

Contents lists available at ScienceDirect

Reactive and Functional Polymers

journal homepage: www.elsevier.com/locate/react

Review

Review of advances in polymeric wound dressing films

Ioana Savencu [a], Sonia Iurian [a,*], Alina Porfire [a], Cătălina Bogdan [b], Ioan Tomuță [a]

[a] Department of Pharmaceutical Technology and Biopharmacy, Faculty of Pharmacy, University of Medicine and Pharmacy "Iuliu Haţieganu", V. Babeş nr. 41, Cluj-Napoca 400012, Romania

[b] Department of Dermopharmacy and Cosmetics, Faculty of Pharmacy, University of Medicine and Pharmacy "Iuliu Haţieganu", I. Creangă nr. 12, Cluj-Napoca 400012, Romania

ARTICLE INFO

Keywords:
Polymeric film
Polymer
Nanosystem
Preparation methods
Characterization

ABSTRACT

Wound dressings represent the most common way to promote wound healing as they are non-invasive. They include films, hydrogels, hydrocolloids, hydroactives, foams, alginates and hydrofibers. Choosing one type over another depends on the wound depth and amount of exudate. Films are advantageous because they are flexible, easy to apply, allow some moisture evaporation, provide a barrier to external contamination, and endorse inspection of the wound bed without removing the dressing. This review article focuses on the topic of wound dressing films as drug delivery systems. It provides a summary of the preparation and characterization methods and highlights the most frequently used polymers for film fabrication. Moreover, it outlines and discusses recent developments regarding the active ingredients and nanosystems loaded into the wound dressing films with emphasis on the macromolecular structure. This work aims to guide researchers and developers into the selection of proper materials (polymers and active pharmaceutical ingredients), preparation processes, characterization techniques, and increase their understanding into how the desired product features can be reached.

1. Introduction

Wound healing is an essential process characterized by three classic phases: inflammation, proliferation, and remodeling. Their length is variable depending on the wound type and acuity [1]. Acute wounds follow all the above-mentioned phases and usually heal within 8–12 weeks [2]. On the other hand, chronic wounds are caused by deficient signals that prolong the time in the inflammatory phase. Thus, due to the delayed wound healing process which may take several months or years, chronic wounds are a major concern for clinicians [1,3].

There are different methods to promote wound healing, involving both surgical and non-surgical treatments. Wound dressings are the most used as they are non-invasive [4]. Since infection of a wound hinders the healing process, one approach is the development of wound dressings based on polymers with intrinsic antibacterial properties or incorporation of antibacterial ingredients into the polymeric matrix of the wound dressing. *Staphylococcus aureus, Staphylococcus epidermidis, Escherichia coli, Bacillus subtilis, Pseudomonas aeruginosa* are among the most frequently related to wound infections [5,6]. Therefore, antimicrobial activity of films is envisaged and tested against such microorganisms. Another way of promoting wound healing, especially of chronic wounds, is by simulating the extracellular matrix (ECM), the most abundant component of the dermal layer. ECM is composed of collagen and elastic fibers dispersed in glycosaminoglycans, proteoglycans and connective tissue glycoproteins. The most important elements of the ECM are proteins and polysaccharides, therefore polymers of such nature are highly desired in this kind of approach [7].

In recent decades, it has been well known that a moist environment promotes wound healing, due to a stimulation of keratinocytes' migration, which eventually leads to a fast healing of the wound bed [4]. An ideal wound dressing should be biocompatible, protect the wound bed, maintain wound hydration, allow gas exchange with the environment, remove excess exudate, and physically protect against microorganisms. It should also have specific mechanical properties such as flexibility and good resistance [8].

Wound dressings include films, hydrogels, hydrocolloids, hydroactives, foams, alginates and hydrofibers [1,9]. Choosing one type over another depends on the wound depth and amount of exudate [1]. Films are permeable to gas and impermeable to liquid and bacteria and they can be used for a direct drug delivery to the wound site. Films are advantageous due to their flexibility which enables an easy conformation to the patient's body even around difficult areas such as joints, they

* Corresponding author.
E-mail addresses: ioana.petrusan@umfcluj.ro (I. Savencu), sonia.iurian@umfcluj.ro (S. Iurian), aporfire@umfcluj.ro (A. Porfire), catalina.bogdan@umfcluj.ro (C. Bogdan), tomutaioan@umfcluj.ro (I. Tomuță).

https://doi.org/10.1016/j.reactfunctpolym.2021.105059
Received 20 July 2021; Received in revised form 23 September 2021; Accepted 30 September 2021
Available online 2 October 2021

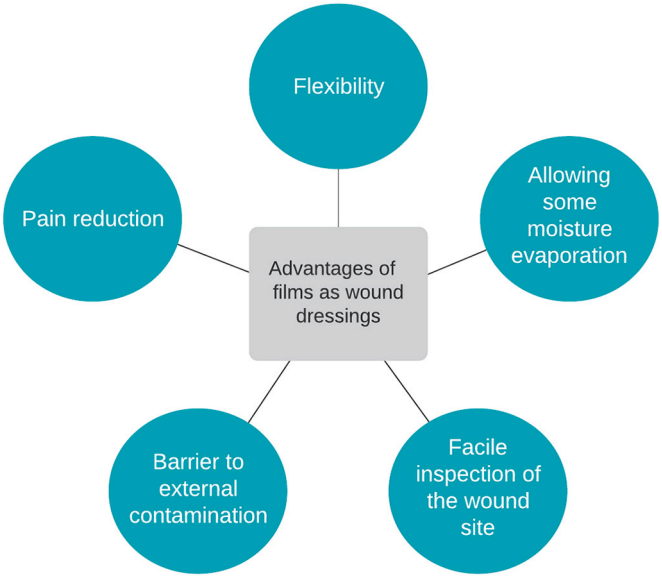

Fig. 1. Schematic representation of advantages of films as wound dressings.

allow some moisture evaporation, reduce pain, provide a barrier to external contamination, and endorse inspection of the wound bed without removing the dressing (Fig. 1). Their major disadvantages are their possible painful removal and their use only on non-highly exuding wounds [4,9].

So far, several reviews have been published regarding various aspects of wound dressings [9–12], but this one focuses on the topic of wound dressing films as drug delivery systems. It provides a brief summary of the preparation methods, highlighting the critical process parameters that may impact the quality and the latest improvements. Regarding the characterization methods, the state of art methods were explored and the acceptance criteria identified in the recent papers were mentioned. Further, the most frequently used polymers for film fabrication and the recent developments regarding the active ingredients and nanosystems loaded into the wound dressing films were presented with focus on the critical material attributes (Fig. 2). Films are emerging dosage forms with high clinical potential, so this paper aims to support the research and development scientists and the academia researchers in their quest for updated information and guide their way into the selection of proper materials and methods for their production and characterization.

2. Preparation methods

Wound dressing films should be easy to remove from the package, resistant to breakage, flexible, with good adhesion and remanence to the wound surface and a sufficient capacity to absorb exudates. Finally, they should have the ability to incorporate the active principles and to release them to the wound site. The preparation methods through the chosen process parameters and the materials are meant to ensure the aforementioned features, further related to the critical quality attributes of films.

Solvent casting is the most used method to prepare wound dressing polymeric films due to its facile manufacturing and low-cost processing [4,13,14]. It involves pouring a polymer dispersion into a mold, followed by solvent evaporation. Briefly, polymer dispersions are prepared in suitable solvents at defined temperatures (ranging from room temperature to 100–120 °C) with plasticizers (*e.g.* glycerin) if necessary, and specific extracts or drug solutions, under mechanical stirring until homogeneity. In this step, critical parameters which influence films' attributes are the temperature, the viscosity of the dispersion, stirring time and stirring speed. A constant volume of the homogeneous blend is poured into the molds (standardized Petri dishes or Teflon plates) and left to dry completely to obtain the films. After drying, films are carefully peeled off and are visually analyzed regarding their integrity, color, opacity. In the casting and drying steps, critical parameters include the drying temperature, humidity, the concentration of the plasticizer and the concentration of the polymer. The properties and stability of the films are determined by the materials used for their preparation [15], such as chitosan [13,14,16,17], hyaluronic acid (HA) [13], polyvinylpyrrolidone (PVP) [16], polyvinyl alcohol (PVA) [18,19], polyacrylic acid [8], starch [6,8], gellan gum [20], gum arabic [21], gelatin

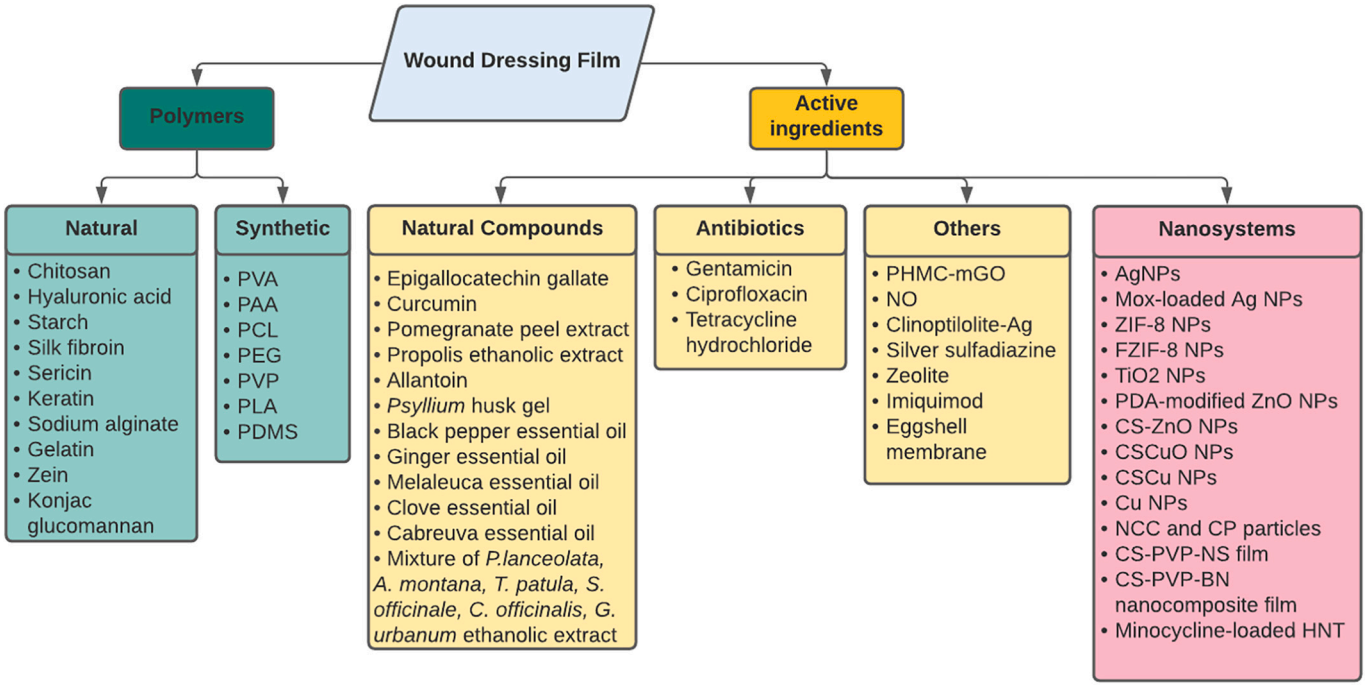

Fig. 2. Summary scheme of the components (reported in this review article) of a wound dressing film as drug delivery system.

[22], pluronic F127-gelatin-pectin [23], alginate-gelatin [24], agar [25], allantoin [26], silk sericin [18], silk fibroin [7], zein [27], keratin [28], hemicellulose [29]. Solvents used in solvent casting include acetic acid, lactic acid, formic acid, ethanol, and distilled water. Despite the length of the preparation process, solvent casting is a simple/accessible method that leads to robust films, suitable as bottom layer in multi-layered formulations such as the ones produced by Palo et al. [15]. Two-step casting conducted to bilayer films with improved mechanical properties when combining chitosan and konjac glucomannan [5].

An energy-saving and low-cost technique for obtaining highly porous films is *via* salt leaching. This procedure is possible due to the lack of solubility of inorganic salts in the typical organic solvents used to dissolve biodegradable polymers [30]. A large number of inorganic salts used as porophors has been reported in the literature and among them we mention sodium chloride, sodium bicarbonate, potassium bicarbonate, ammonium bicarbonate [31]. The typical procedure using a slurry implies the preparation of a polymer solution, adding a porophor and pouring the resulted slurry onto Petri dishes followed by washing with deionized water to leach out the salt crystals. The leached dressings are dried afterwards to generate porous dressings [32]. This procedure was reported for the preparation of symmetric and asymmetric chitosan-PVP films reinforced with nanostarch [33]. Another procedure involves pouring the polymer solution on the layer of the porophor, which is eluted with water after solidification. This approach was used to produce the porous medical dressings Medisorb® on an industrial scale, using butyric-acetic chitin *co*-polyesters containing 90% of butyryl and 10% of acetyl groups [31]. As critical parameters which may impact the films' characteristics are the type and ratio of porophor, the temperature, the viscosity of the dispersion, stirring time and stirring speed.

The spin coating process was developed for a low-cost deposition of uniform layers of polymer or inorganic solutions [34]. The homogenous dispersion containing the active ingredient, polymer and other necessary excipients is dispensed at the center of a rotating plate and spread due to centrifugal force in uniform thin layers of about 1–10 μm thickness. Rotation favors evaporation, while the thickness is influenced by the spinning speed, surface tension and viscosity of the dispersion [35,36]. Spin coating was used to produce clay-reinforced polycaprolactone/chitosan/curcumin composite films [37] and was recently reported for the preparation of bilayer membranes of gelatin and antibacterial cationic polyelectrolytes [38].

Microfluidic spinning was developed more than 15 years ago and is a useful approach to produce micro- and nanoscale materials [39]. Fibers with various shapes and sizes can be obtained without complicated devices or facilities [40]. It is of great interest due to the facile manipulation of fluids within channels, the ecological chemical processes and its controllability. Moreover, it is suitable for volatile compounds sensitive to high voltage and temperature (*e.g.* derivates of aromatic amines and phenols) [41]. Microfluidic spinning is based on the microscale fluid dynamics principle by which the core and sheath flows form a coaxial flow with the aid of a specially designed microchannel. The coaxially flowing polymer dispersion is solidified into microfibers *via* UV light, ionic or chemical crosslinking and solvent exchange [39]. To form films, microfibers are guided by a forward and reverse step process and an immobilization device is used to obtain a rapid prototyping of the film. Films are eventually obtained after immobilization for a defined period of time at a well-established temperature. This method allows the preparation of ultra-small scale batches and the quality of films depends on parameters such as pump speed, motor speed (which determine the diameter of the microfibers), concentration of spinning solution, core flow and sheath flow. The method was reported to produce films made of blends of konjac glucomannan, PVP and epigallocatechin gallate [41].

Three-dimensional (3D) printing is used as an alternative method to solvent casting for producing film scaffolds with a precise design and physical orientation. The method generally implies the printing of suitable polymer solutions and bioactive gels to produce biocompatible films. Compared to other fabrication methods, 3D printing has the advantage of producing more flexible matrices with pre-determined pore sizes in a reproducible manner. The microstructure of the printed films promotes cell attachment and migration, thus providing a fast tissue regeneration after injury [4]. 3D printers could be a great resource to develop personalized wound dressing films for the individual needs of patients [42] with the ability to control the size, the shape and the porosity of the product through fused deposition modeling, the most frequently used technology [43]. The product quality is influenced by the structure design, molten blend viscosity, printing temperature, print speed and layer height.

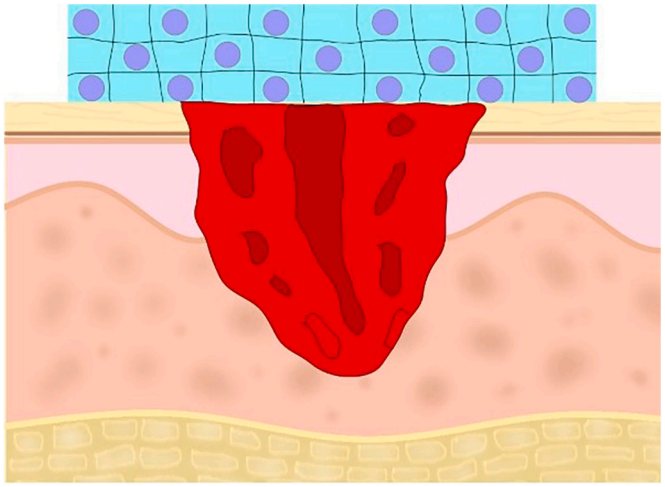

Fig. 3. Physical representation of the wound dressing film attached to the wound site, showing the active ingredient (purple) dispersed into the polymeric matrix (blue). (For interpretation of the references to color in this figure legend, the reader is referred to the web version of this article.)

Films obtained *via* 3D printing were reported by Hafezi et al. who prepared and characterized crosslinked chitosan-based bioadhesive films with potential healing properties of chronic wounds [4]. Palo et al. used either 3D printing, or electrospinning combined with solvent casting to obtain bi-layered polymer carriers from a mixture of polyvinyl alcohol and sodium alginate, however the electrospun nanofibers on solvent casted films were found to be more appropriate compared to the bi-layered carrier with patterned 3D printed layer [15].

3. Characterization of films

So far, there is not an official standard to characterize the wound dressing films. Their safety and efficacy have been evaluated based on different quality attributes by various research groups. The characterization consists in methods further related to the use and applicability of these products, such as measures of their strength, flexibility, physical appearance (Fig. 3), capacity to absorb fluids and release the drug candidates, of their stability and therapeutic efficacy. This section presents the most frequently reported methods for the evaluation of the quality attributes, followed by a summary in Table 1.

3.1. Film thickness

Film thickness represents the average of the random measurements and is generally expressed in millimeters (mm). Film thickness is influenced by the preparation method, amount of casting gel, and flatness of the drying surface [23].

3.2. Mechanical properties

The mechanical properties of a film vary depending on the polymer (structure and degree of polymerization), solvent, solution pH, presence

Table 1
Wound dressing film characterization.

Film quality attributes		Justification	Determination/ characterization methods/ instruments
Physicochemical attributes	Film thickness	To provide uniform mechanical properties and a homogeneous distribution of the drug [29]	Digital micrometer at multiple random positions (generally 5–10) on the film surface [6,8,65] Manual screw gauge [22] Caliper [22] SEM images [46]
	Mechanical properties	Proper values of the tensile strength (TS), percent elongation at break (%E) and Young's modulus are essential for the physical integrity of the films	Texture analyzer [4,27] Universal Testing Machine (UTM) [19,28,41], according to ASTM D882 [45]
	Solvent loss	To assess the amount of exudate that can be absorbed by the film before turning it into a free-flowing gel (washable from the wound surface)	Weighing the dried film and the casting mixture
	Swelling behavior (SI) and mass loss by solubilization (S)	Swelling is essential because this allows keeping a moist environment and releasing the incorporated drug on the wound bed Mass loss by solubilization defines the mass loss due to the solubilization of the polymer.	SI: Weighing the initial dry film and the swollen film/ measuring the expansion diameter of the film S: Weighing the initial dry film and the dried film after being swollen
	Wettability	A hydrophilic film is aimed (contact angles $<90^{\circ}$)	Contact angle measurement
	Water vapor transmission rate (WVTR) and Water vapor permeability (WVP)	To assess the absorption of the exudate, but also the moisture transfer	ASTM E96
	Crystallinity	To assess the physical form (crystalline or amorphous) of the films and pure starting materials	XRD
	Thermal behavior	To evaluate the weight loss of the materials and the thermal stability of films (TGA) To check the compatibility of the film components and the state of the drug molecules inside the film (DSC)	TGA, DSC
	Active substance-polymer interactions	To confirm the purity of the raw materials, identify change in the chemical structure of the composite films and/or determine the compatibility or interactions between the functional groups of the film components	FTIR
	Surface morphology	A smooth structure, free of voids and cracks is aimed	SEM
Active substance assay		To provide the content uniformity	HPLC, UV–Vis, FAAS
In vitro drug release		Essential for wound healing	*In vitro* dissolution study, FDC
In vitro cytotoxicity		To assess the toxicity of films	MTT assay
Antimicrobial activity		Essential to prevent wound contamination and promote efficient wound healing	Disc diffusion method, standard plate count method, optical density determination
Wound healing capacity		To assess the efficacy of the film dressing	*In vitro*: scratch assay, microenvironmental pH *In vivo*: wound closure rate of full thickness wounds on animal models

of plasticizer and mixing process [44]. The tensile strength (TS) and percent elongation at break (%E) can be measured using a texture analyzer [4,27] or a Universal Testing Machine (UTM) [19,28,41], according to the Active Standard Test Method (ASTM) D882 method [45].

The TS is a measure of the strength of the film as diametric tension or tearing force. It is calculated by dividing the force at which the film breaks by the transverse section area of the film [29,46]. %E defines the point at which the sample breaks after a sufficient increase in length. It generally increases with the plasticizer concentration.

In order to resist the natural deformations of the human skin, the TS of films should be in the range of 2.5–16 N/mm^2 (MPa), while the %E should be higher than 70% [29].

Young's modulus (elastic modulus) shows the stiffness of a film. It can be measured by the same methods as the TS. This parameter expresses the resistance to deformation and can be determined by plotting the stress-strain curve whose slope indicates the modulus. There is a direct proportionality relationship between the slope and the tensile modulus [29,46]. The Young's modulus for skin tissue ranges from 4.6 to 20 MPa [27].

3.3. Solvent loss

The solvent (water) loss during the film casting (drying) process equals the solvent needed to hydrate films to their original shape and relates to the amount of exudate that can be absorbed by the film before turning it into a free-flowing gel which can be washed from the wound surface. The water loss during the film casting can be calculated as a percentage of the lost weight during drying divided by the initial weight of the sample [23,29].

3.4. Swelling behavior and mass loss by solubilization

Swelling is one of the most important parameters of dressings because films absorb the wound fluid (exudate) and expand when applied on a wound, thus allowing the release of the incorporated drug. Various methods for determining the swelling index (SI) have been reported in the literature. Ahmad et al. (2020) reported the determination SI as the percentage increase in diameter of a circular sample kept in exudate environment (*e.g.* 4% gelatin solution) at predefined time intervals [29]. Other authors reported the immersion of previously dried pieces of films into deionized water [5,47] or Phosphate-buffered saline (PBS) solution [4,41,48]. PBS (pH = 7.4 at 37 °C) was the most frequently used swelling medium to mimic the wound exudate. After immersion, swollen films were collected at certain time points and the excess of water was gently removed from the surface. Weights were recorded until reaching the equilibrium state. SI was further calculated as the percentage increase in weight.

An ideal film should absorb the exudate formed by the wound without forming a free-flowing gel because of an excessive swelling. The values of the SI should be lower than the values found in the solvent loss

study, which define the solvent required to transform films into free-flowing gels [29].

Solubilization measurement requires the immersion of films into the solvent (*e.g.* deionized water, PBS solution) for a defined period and weighing them after a further drying step (*e.g.* in an incubator) and is calculated as the percentage loss of weight from the initial dry film [5,19,21]. To indicate good stability [21], it should not exceed 5% [5]. The term is often defined as "solubility" in research articles.

3.5. Wettability (hydrophilicity)

Wettability is directly related to the surface free energy and is determined by measuring the contact angle formed at the interface between deionized water and the sample surface [13,49].

Contact angles up to 90° signal hydrophilic surfaces, whereas contact angles larger than 90° indicate hydrophobic surfaces. A surface with a contact angle greater than 150° is classified as superhydrophobic [49]. A hydrophilic film is desired (with contact angles smaller than 90°), as this allows films to absorb the humidity in the wound area [50] and hydrophilic surfaces are also less likely to be contaminated by bacteria due to hydration effects [13] .

3.6. Water vapor transmission rate (WVTR) and water vapor permeability (WVP)

An efficient wound dressing should not only ensure good absorption of the exudate, but also transfer moisture to allow the gas exchange. Wound hydration is provided by an adequate WVTR, meaning that high WVTR rapidly dehydrates the wound causing scars, while low WVTR generates excessive exudate increasing the risk for infections [10]. The WVTR can be evaluated according to the ASTM E96 procedure, which provides two basic methods, the desiccant method and the water method. Choosing one method over another should be made taking into consideration which one approaches the conditions of use more closely [51].

Literature reports that the WVTR values for healthy and injured skin are 200–220 g/m^2/24 h [5] and 280–5100 g/m^2/24 h, respectively [29]. For commercially available wound dressings, the WVTR values generally range from 100 to 3300 g/m^2/24 h, while the ideal values lie between 2000 and 2500 g/m^2/24 h [29]. Water vapor permeability measures the capacity of adjusting water evaporation and hydration preservation to keep a balance on both sides of a biomedical film [28].

3.7. Crystallinity

The physical form (crystalline or amorphous) of the films and pure starting materials can be observed by X-Ray diffraction (XRD) analysis using an X-ray diffractometer [4,7,46]. XRD is based on Bragg's law and is a non-invasive method. The sample is hit by a monochromatic beam of X-rays which reflect [52] using a Cu Kα radiation source over a diffraction angle (2Θ) [46]. Amorphous regions of the sample generate broad peaks, while crystalline regions generate sharp peaks. The degree of crystallinity (X_c) can be calculated by determining the intensities of the crystalline (I_c) and amorphous (I_a) areas in the sample [52]. A crystalline state indicates a more stable, but less soluble compound while an amorphous state indicates a higher solubility, but a lower stability of the compound.

3.8. Active substance-polymer interactions

Fourier-transform infrared (FTIR) analysis can be used to confirm the purity of the raw materials, identify change in the chemical structure of the composite films and/or determine the compatibility or interactions between the functional groups of the film components [7,29]. Spectra are obtained at a fixed resolution (usually ranging from 2 to 4 cm^{-1}), generally in a range of 4000–400 cm^{-1} using a FTIR spectrophotometer [7,19] equipped with an attenuated total reflection unit (ATR-FTIR). There are specific regions of the spectrum from stretching and bending vibrations which reveal information about different types of bonds (*e.g.* hydroxyl bonds, single bonds, secondary bonds, ternary bonds).

3.9. Thermal behavior

Thermogravimetric analysis (TGA) can be used to evaluate the weight loss of the materials as well as the thermal stability of the prepared films. Thermal events which lead to mass variation include adsorption, desorption, evaporation, sublimation, oxidation, reduction and decomposition. The mass variation as a function of temperature is displayed on the thermogram. [5,7,29,41,46].

Differential scanning calorimetry (DSC) can be used to assess the compatibility of the film components and the state of the drug molecules inside the film [5,22,29,46]. Temperature-mediated physical modifications such as melting, crystallization, glass transition, cross-linking or decomposition/oxidation are observed and evaluated from the thermogram which records the variation of heat flow as a function of temperature.

3.10. Surface morphology

The surface morphology or texture, as well as the crystalline structure and drug distribution in the films can be investigated using the scanning electron microscopy (SEM). It is a non-invasive method which uses a focused beam of high-energy electrons [53] to evaluate the surface of a sputter coated sample [21,29,46,53]. Materials with widths ranging from approximately 1 cm to 5 μm can be imaged using conventional SEM techniques (magnification ranging from 20× to around 30,000×, spatial resolution of 50 to 100 nm) [53].

3.11. Active substance assay

The active substance assay is essential for providing the content uniformity of the formulation. It is usually performed *via* high-performance liquid chromatography (HPLC), after prior validation of the method. Aliquots randomly cut from the film are dissolved in a suitable solvent, diluted with the mobile phase, and analyzed. The active substance is eluted at a certain retention time and is quantified by the detector [17]. Quantification of the active substance can also be assessed by UV–Vis spectrophotometry. Film discs of small diameters are randomly taken from the original film and dissolved in a suitable solvent and the amount of active substance is determined at its maximum absorbance wavelength [54]. Flame atomic absorption spectroscopy (FAAS) was also reported to quantify the amount of silver ions in films, which was expressed as concentration (mg/100 g of film) [22].

3.12. In vitro drug release

The release of drug from films is essential for an efficient wound healing and is usually evaluated as the cumulative drug dissolved from a formulation over a certain period. No standard methods were issued for the investigation of the drug release from films, therefore different approaches have been chosen by research groups.

One way of determining drug release is the dissolution study in a small volume of release medium (*e.g.* 1–100 ml). Release media also vary among research groups and reported examples are PBS solution with pH = 7.4/6.8 [3,6,27], acetate buffer with pH = 5.5 [55], deionized water [24], a mixture of ethanol/PBS in different proportions [56], mixture of Dulbecco's modified eagle medium (DMEM)/ fetal bovine serum (FBS) [17], simulated exudate fluid (SEF) [22,57]. The most biomimetic and relevant medium is SEF, an isotonic solution of sodium and calcium ions in concentrations of 142 mM and 2.5 mM, respectively. It is similar to blood plasma and wound fluids. The temperature is generally established at 37 °C, but 32 °C has also been reported, so as to

mimic the skin temperature [17]. The amount of the released drug can be calculated based on the absorbance of samples determined by a UV–Vis spectrometer and using a predetermined calibration curve [24,27,56], by HPLC [6], FAAS [3,22,57] or by inductively coupled plasma atomic emission spectroscopy [58].

Another method to determine the drug release involves a Franz diffusion cell (FDC) which is normally used to evaluate the permeation of an active ingredient through the skin. The FDC consists of two chambers separated by a synthetic membrane. A constant temperature of 37 ± 1 °C is maintained during the experiment. The film to be tested is placed above the membrane in the upper chamber (donor compartment). At specific time intervals, a constant volume of sample is taken from the medium (*e.g.* PBS) that fills the bottom chamber (receptor compartment) and is replaced with the same volume of medium. The cumulative release of the drug is plotted as a function of time and, thus, the drug release mechanism can also be evaluated [23,29].

3.13. In vitro cytotoxicity (cell viability)

In vitro cytotoxicity of films can be examined by measuring their influence on cell viability. According to literature, examples of cell lines used for this purpose are murine fibroblasts (L929) [6,28,37,48], Balb/c 3 T3 [56], murine embryo fibroblasts (NIH/3 T3) [27,33,47,59], human dermal fibroblasts (GM07492) [55], human adult keratinocytes (HaCaT) [47,60], human embryonic kidney 293 (HEK293) [56], Chinese hamster ovary (CHO) [5], baby hamster kidney (BHK21) [29]. Cell viability, proliferation and cytotoxicity can be evaluated *via* 3-(4,5-dimethylthiazol-2-yl)-2,5-diphenyltetrazolium bromide (MTT) assay, which measures the cellular metabolic activity [7]. The method is based on the reduction of the yellow MTT to purple formazan crystals by metabolically active cells due to the NAD(*P*)H-dependent oxidoreductase enzymes present in viable cells. The insoluble formazan crystals are quantified spectrophotometrically at 500–600 nm. The darker the solution, the greater the number of viable, metabolically active cells [61]. The cell viability is calculated as a percentage and should be over 80% for non-cytotoxic films with potential medical applications [8].

3.14. Antimicrobial activity

Wounds can favor the growth of microorganisms, which may generate an infection that can delay the wound healing process. Therefore, the antimicrobial activity of films is often pursued, either using film-forming polymers with antimicrobial properties or loading bioactive compounds with antimicrobial effects. Their efficacy is tested on pathogen strains with potential to cause wound infections. Several bacteria, both Gram-positive and Gram-negative, associated with wound infection have been reported in the literature, while *Candida albicans* [5,57,62] is responsible for fungal infections. Among Gram-positive bacterial strains are *Staphylococcus aureus* [20,33,41], *Staphylococcus epidermidis* [3,6,13], *Streptococcus mutans* [16], *Bacillus subtilis* [16,33,41], *Bacillus cereus* [21,63], *Lysteria monocytogenes* [19] while Gram-negative bacterial strains include *Escherichia coli* [20,33,41], *Pseudomonas aeruginosa* [5,6,33], *Aeromonas hydrophila* [16], *Salmonella enterica* [41], *Salmonella typhimurium* [21], *Acinetobacter baumannii* [3,63].

3.15. Wound healing capacity

3.15.1. In vitro wound healing capacity

The *in vitro* wound healing capacity is performed on fibroblast cell lines (*e.g.* L929, 3 T3) *via* the scratch wound assay, which investigates the fibroblast migration after exposure to the active substance. After creating artificial wounds on the cell monolayer developed in a cell culture plate, they are divided into groups and treated with controls and films containing active substance. The plates are checked after different incubation times to evaluate the closure of the scratched area [8,20].

An indirect assay of the *in vitro* wound healing capacity of films is by determining the microenvironmental pH created by the films, after immersing them into normal saline solution for 24 h. The pH should be slightly acidic, similar to the one of the normal healthy skin (pH ranging from 4.0 and 6.8) [64]. This pH range promotes wound healing, compared to neutral or alkaline values of pH.

3.15.2. In vivo wound healing capacity

The *in vivo* wound healing capacity is tested on animal models (e.g rats, mice). Generally, full thickness wounds are created on a hairless part of the animals' skin, which are eventually divided into groups and treated with controls and the films to be tested. The size of the wound is measured and photographed on the day of wounding and in different days following the wounding. With the aid of an image software, the edges of each photographed wound are translated in terms of width and area for quantitative analysis. The wound closure rate is calculated as the closure area divided by the initial wound area [14,16,33,60].

4. Polymers used for wound dressing film preparation

The polymers used for wound dressing film preparation can have a natural or synthetic nature. Natural polymers include chitosan (CS), hyaluronic acid (HA), starch (St), silk fibroin (SF), sericin (Ser), keratin, sodium alginate (SA), gelatin (GE), zein, konjac glucomannan (KGM). Among synthetic polymers used for the preparation of wound dressing films, we mention polyvinyl alcohol (PVA), polyacrylic acid (PAA), polycaprolactone (PCL), polyethylene glycol (PEG), polyvinylpyrrolidone (PVP), polylactic acid (PLA). Natural polymers have desirable properties such as biocompatibility, biodegradability, easy resorption, and capacity to heal the injured tissue but can be easily contaminated by microorganisms. Synthetic polymers usually have better mechanical properties than natural ones, but their adherence, absorption and permeability is low. Combinations of synthetic and natural compounds were designed to improve the mechanical properties and extend the degradation time, while keeping the gas and water vapor permeability and biocompatibility of the product [12].

4.1. Natural polymers

Chitosan (CS) is a linear polysaccharide composed of *N*-acetyl-D-glucosamine and β (1 → 4)-D-glucosamine units. Obtained from deacetylation of chitin found in crustacean shells, it is a desired polymer for wound dressing preparation due to its nontoxicity, film-forming ability, low immunogenicity and outstanding antibacterial, antifungal, hemostatic and mucoadhesive properties [55,60,66]. Moreover, it is biocompatible, biodegradable and is efficient for controlling drug release [37]. One drawback is its high cost due to the laborious extraction process [19]. Due to the presence of amino and hydroxyl functional groups on its structure, CS can be crosslinked with various polymers and metallic particles. As a result of blending CS with other polymers, the rapid drug release in an aqueous medium may be prevented, while still retaining the swelling capacity of the composite [3]. Silvestro et al. produced HA-modified CS dressings with improved antibacterial effect and fibroblast adhesion [13]. Hafezi et al. developed 3D printed CS film scaffolds crosslinked with genipin (Gen) using either glycerol or polyethylene glycol as plasticizers [4].

Gelatin (GE) is a protein polymer of animal origin obtained by the hydrolysis of collagen. It is found in the skins, bones and connective tissues of mammals and marine animals. Due to its abundance, availability, and low cost, it can be successfully used for wound dressing production. Generally, gelatin-based films need the addition of a plasticizer to improve their properties. Glycerol is one of the most versatile plasticizers for film formation and combined with GE may generate an appropriate carrier of active ingredients [22].

Hyaluronic acid (HA) is a non-sulfated anionic glycosaminoglycan made of βD-glucuronic acid and *N*-acetyl-D-glucosamine units. It is one

of the main components of the ECM and has also been used in wound dressing preparation due to its biocompatibility and capacity to regulate biological processes [58]. Due to its biodegradability and hydrophilic character, HA has been used to produce various types of wound dressings such as films, sponges, hydrogels and electrospun membranes [67].

Keratin is the main structural fibrous protein found in hair, nails, wool, feathers and horns with a high concentration of cysteine (7–20% of the total amino acid residues) [68]. As an essential component of the human skin, it plays an important role in wound healing. Keratin proteins can be extracted from wool without hydrolyzing peptide bonds. They can eventually be purified and incorporated into dressings and topical creams, with therapeutic effect on chronic wounds [69]. Keratin-based materials have high strength and stability in *in vivo* conditions [70]. Mi et al. developed keratin films reinforced with submicron cysteine particles, as they are highly compatible with keratin and safe. Films with improved mechanical properties in the wet/hydrated state and good biocompatibility were obtained [28].

Silk fibroin (SF) is a fibrous protein composed of glycine, alanine, and serine in various proportions [71]. SF is derived from *Bombyx mori* (silkworms) cocoons, insects, and spiders. Along with sericin, it is one of the major components of silk fiber and has been reported as a good substrate for cell adhesion and proliferation. It possesses good mechanical properties, non-inflammatory effect [7,56] and can be completely degraded by naturally occurring proteolytic enzymes [72]. Previous reports show that SF was successfully combined with CS to form films (membranes), scaffolds, composites, micro/nanoparticles, nanofibers and hydrogels [71]. However, it does not possess antibacterial properties [73]. In a study performed by Hashimoto et al., SF-based films were reported to induce higher cell motility in human fibroblast (WI-38) cells as well as a higher expression of genes related to wound healing and skin reconstruction than collagen films [74]. SF has also been used combined with paramylon to produce biomimetic wound dressing films [7].

Sericin (Ser) is a hydrophilic polypeptide which wraps silk fibroin fibers. Although usually removed from fibroin by degumming process, Ser displayed antioxidant, antibacterial, anticoagulant, cell proliferative and wound healing properties, and non-toxic, biodegradable, biocompatible and bioadhesive character [3]. Its use in biomedical field is limited due to its fragile and amorphous nature. However, due to the amino, hydroxyl and carboxyl functional groups in its structure, it can be easily copolymerized, blended or crosslinked with other polymers with positive effects on its mechanical properties [3,47]. Wang et al. crosslinked silk sericin with dialdehyde carboxymethyl cellulose (DCMC) to improve its properties. Favorable results regarding the attributes of films were obtained [47].

Starch (St) is a highly available, inexpensive, biodegradable carbohydrate polymer composed of glucose units joined by alpha-(1,4) glycosidic bonds. It consists of two types of molecules: the linear amylose and the branched amylopectin, in different ratios depending on the botanic origin. Previous reports mentioned that the film-forming and mechanical properties of St depend on the amylose to amylopectin ratio. Generally, an increase in amylose content leads to improved aforementioned properties [6]. St displays both amorphous and crystalline states. The amorphous state leads to unfavorable mechanical properties; therefore, it is usually chemically modified by etherification, oxidation, hydrolysis and crosslinking. Although chemical modification somewhat improves its mechanical properties, the products were still not strong enough to be used in wound dressing applications and were often blended with other synthetic polymers to overcome this shortcoming [19]. It also has a low film-forming capacity, therefore blending with other polymers is necessary for wound dressing applications [8].

Konjac glucomannan (KGM) is a linear polysaccharide consisting of glucose and mannose at the molar ratio 1:1.5–1:1.7 and joined by beta-(1, 4) glycosidic bonds. This polymer is non-toxic, highly viscous in aqueous solutions and has specific slow-release performance. It also possesses outstanding biocompatibility, nutritional value, and stability. Due to the presence of acetyl and hydroxyl functional groups in its structure, KGM has high water affinity, which grants the KGM-based materials a high elasticity and a good absorption of wound exudate [5,41]. Bilayer films made of one inferior layer of CS and one top layer of KGM were prepared for a better preservation of the physicochemical properties of each polymer [5].

Zein is an amphiphilic protein found in the endosperm of corn. It consists of many nonpolar amino acids which form aggregates that can encapsulate drugs. Being water insoluble makes zein an excellent option for oral and dermal applications [27]. It is biocompatible, biodegradable and has good flexibility, high hardness and antioxidant properties [75].

Sodium alginate (SA) is a widely used hydrophilic, biodegradable and biocompatible polymer extracted from brown algae [15]. Its main advantage is the liquid-gel behavior in aqueous solutions. When monovalent sodium in SA is exchanged for calcium or other divalent ions (*via* crosslinking), the low viscosity solution is changed to a gel [76]. Alginate nanodevices have been intensely studied for controlled drug release purposes [77].

4.2. Synthetic polymers

Polyvinyl alcohol (PVA) is a widely used water-soluble polymer due to its smooth film forming capacity, straightforward processability and chemical stability [21]. It has a decent cost, good mechanical properties, a non-carcinogenic and biodegradable character. It is biocompatible and often combined with natural polymers (*e.g.* starch, silk fibroin) to improve their mechanical properties [18,19,73]. Covalent cross-linking can also be used in PVA-based formulations [15]. Water, glycerol or potassium sorbate can be used as plasticizers to increase the flexibility of PVA films [78]. PVA does not have intrinsic antibacterial properties [73]. Palo et al. investigated a combinational method for the fabrication of bi-layered carriers from a blend of PVA and SA. Solvent casting for the base layer and two surface modification techniques were used: electrospinning and 3D printing. They also performed an initial inkjet printing trial for the incorporation of the active substance for drug delivery purposes. Apparently the bi-layered carriers with electrospun nanofibers (bi-layered SC/NF carrier) were superior to the solvent casted films and to the bi-layered carriers with 3D printed layer (bi-layered SC/3D carrier) regarding their physical properties and bioadhesion [15]. Das et al. studied the feasibility of preparing composite films based on PVA, St, citric acid (CA) using glycerol (Gl) as plasticizer. The concentrations of CA and the crosslinking temperature were varied, while the drying time and the concentrations of PVA, St and Gl were kept constant [19]. Composite films of PVA, St, CA and Gl with improved properties were obtained one year later by the same research group using a response surface methodology (RSM) design. After varying the concentrations of the 4 constituents, appropriate film characteristics such as swelling index (SI), weight loss (WL%) for 27 days, tensile strength (TS) and percent elongation at break (%E) were obtained. The antibacterial activity and cytotoxicity of the optimized formulation was also assessed, revealing a great effectiveness against Gram-positive *Listeria monocytogenes* and Gram-negative *E. coli* as well as an improved cell growth due to the acidic medium generated by CA which reduced bacterial multiplication [65].

Polyacrylic acid (PAA) is a mucoadhesive polymer which can be used to improve the swelling and adhesion capacity of films [8]. The protonated form in acidic pH is responsible for mucoadhesion [79]. At neutral pH, it is soluble in aqueous media due to the ionization of the carboxyl side chains. Carbopols are polymers of acrylic acid crosslinked with polyalkanyl esters or divinyl glycol. They easily absorb water, hydrate and swell, making them suitable for controlled drug delivery systems [80].

Polycaprolactone (PCL) is a partially crystalline polyester with a low melting point (60 °C). It is obtained by ring opening of ε-caprolactone [81]. It is a stabilized, elastomeric and very flexible polymer; therefore, it is commonly used as a matrix for wound dressings [37]. Due to its

Table 2
Polymers used for wound dressing film preparation.

Polymers	Evaluated quality attributes	Biological study	Antimicrobial activity	Highlights	Ref.
SF 1% *w/v*	N/A	*In vitro* cell behavior on WI-38 cells	N/A	Fibroblasts were more mobile on the SF film than on collagen film or glass surface	[74]
Blends (1 *wt%*) of SF and paramylon at ratios of 100:0, 75:25, 50:50, 25:75, 0:100	Surface morphology, wettability, FTIR characteristics, crystallinity, stiffness, thermal behavior, water absorption capacity (swelling behavior), *in vitro* enzyme degradation	*In vitro* hemolytic activity *In vitro* cell viability *via* MTT assay	N/A	SF films have a high thermal stability, hydrophobicity, and stiffness Paramylon films show good water absorption capacity Both SF and paramylon films were non-hemolytic and non-toxic The ratio SF:paramylon = 75:25 was optimal	[7]
Keratin reinforced with 5 *wt* % L-cysteine	Tensile (mechanical) properties, crystallinity, WVP	*In vitro* biocompatibility on L929 cells	N/A	The reinforced films had a remarkable pliancy, good biocompatibility, and tensile properties under humid conditions Good interfacial properties and well packed secondary structures of polypeptides in keratin films revealed by dynamic mechanical analysis, WVP, Raman spectroscopy and XRD	[28]
Ser 3.75% *w/v* crosslinked with DCMC (6%, 12%, 18%, 24% *w/v*)	FTIR characteristics, surface morphology, mechanical properties, swelling behavior, wettability, water solubility	*In vitro* hemolytic activity *In vitro* cytocompatibility on NIH3T3 and HaCaT cells	N/A	Cross-linking truly improved the mechanical properties and stability of films DCMC/SS films had a great wettability, stability, blood compatibility, cytocompatibility and promotion of cell proliferation	[47]
Medium molecular weight CS 0.5% *w/v* and low molecular weight CS 1.2% *w/v* crosslinked with Gen 1% *w/v*	Mechanical properties, crystallinity, FTIR characteristics, surface morphology, mucoadhesion behavior, swelling behavior, *in vitro* drug dissolution	*In vitro* cell viability *via* MTT assay	N/A	CS-Gen-PEG600 3D printed films with the ratio polymer:plasticizer = 1:1 had the best flexibility High SI of plasticized films Non-toxic nature of the CS-Gen-PEG600 films with a cell viability >90% after 48 h	[4]
KGM and CS at (*w:w)* ratios of 100:0, 75:25, 50:50, 25:75, 0:100 (Blend films) CS and KGM at 30:70 *w/w* ratio (Bilayer films)	FTIR characteristics, surface morphology, crystallinity, thermal behavior, swelling behavior, solubility, WVTR, mechanical properties	*In vitro* cytotoxicity on CHO cells	Tested against *S. aureus, E. coli, P. aeruginosa, C. albicans*	XRD, FTIR and SEM analyses: the natural structure and physicochemical properties of each polymer were kept in the bilayer films *vs.* the blend films Thermal analysis: a good thermostability and miscibility for both polymers Highly biocompatible bilayer films with low cytotoxicity Appropriate mechanical properties, swelling degree and WVTR	[5]
CS 2% *w/v* and HA 0.5 *w/v* mixed to obtain HA concentrations of 1, 5 10, 15, 25 and 35%	Surface morphology, film transparency, water uptake capacity (SI), soluble fraction (mass loss by solubilization), WVTR, wettability, mechanical properties	*In vitro* adhesion of human dermal primary fibroblasts	Tested against *Staphylococcus epidermidis*	Incorporation of HA in the CS matrix decreased film transparency and homogeneity, but improved film water uptake and surface wettability WVTR reached its highest value (672 g/m^2/24 h) with a 5% HA content and decreased for higher HA contents HA generated more flexible matrices than pure CS Concentrations ≥5% HA inhibited *S. epidermidis* adhesion 5% HA: best fibroblast adhesion and proliferation	[13]
80:20 (*v:v)* ratio of PVA 12% and SA 2% (Solution A, for solvent casting and electrospinning) 80:20 (*v:v)* ratio of PVA 18% and SA 3% (Solution B, for 3D printing)	Thickness, FTIR characteristics, thermal behavior, stability study, swelling behavior, degradation degree (mass loss by solubilization), simulated bioadhesion study	*In vitro* cell viability on BHK-21 cells	N/A	Good stability and physical properties for the crosslinked bi-layered carriers with a SC base layer and an electrospun nanofibrous surface (SC/NF carrier) The bi-layered carriers presented as non-adherent dressings Both crosslinked and non-crosslinked carriers were safe and biocompatible with BHK-21 cells The bi-layered SC/NF carrier had a higher cell viability than the bi-layered SC/3D carrier A uniform liquid absorption profile was observed in the bi-layered SC/NF carrier during the inkjet printing trial	[15]
PVA/St/Gl (37.54 *wt%*)/CA (8.89, 17.79, 35.58 and 53.38 *wt%*)	Thickness, FTIR characteristics, swelling behavior, solubility, *in vitro*	N/A	Tested against *Listeria*	Optimal process conditions: a crosslinking temperature of 50 °C and a concentration of 35.58 *wt%* CA with a 12	[19]

(*continued on next page*)

Table 2 (*continued*)

Polymers	Evaluated quality attributes	Biological study	Antimicrobial activity	Highlights	Ref.
	degradation, gel fraction, mechanical properties, WVTR		*monocytogenes* and *E. coli*	h drying time Excellent swelling (260.5 ± 2.9%) and *in vitro* degradation (45.5 ± 1.8–59.8 ± 0.4% degradation for 14 days) Good antibacterial activity against tested bacteria	
PVA 5–10% *w/w*, St 5–10% *w/w*, CA 15–40% *w/w*, Gl 15–40% *w/w*	Thickness, FTIR characteristics, solubility, *in vitro* degradation, gel fraction, mechanical properties	*In vitro* cytotoxicity on HEK-293 cells	Tested against L. *monocytogenes* and *E. coli*	The optimal composition according to RSM design was 7.5 *w/w%* PVA, 7 *w/w%* St, 28.6 *wt%* CA and 18.4 *wt%* Gl Very good water absorption (300.5% SI) and flexibility (87.5%E) Acceptable *in vitro* degradation (51.4% WL) and TS (5 MPa) Efficient against tested bacteria Cell growth promotion of 145.5% after 48 h of incubation	[65]
Supramolecular PDMS elastomer with one EL and one AL (ratio not mentioned)	WVTR, adhesion, mechanical properties	-*In vitro* cytotoxicity on L929 cells *via* MTT assay, hemocompatibility *In vivo* wound healing capacity in Wistar rats	N/A	The BLF dressing was softer with a much lower modulus than Tegaderm®, which could enable an easy conformation on the skin The BLF dressing was highly biocompatible and had a favorable WVTR No significant difference between the BLF dressing and Tegaderm® regarding the wound healing capacity and the ability to create a moist wound healing environment	[87]

biodegradability, it can be used as an implantable biomaterial. PCL beads have also been used to encapsulate drugs for controlled drug release and targeted drug delivery. Combined with starch, it results in a low-cost biodegradable material [81].

Polyethylene glycol (PEG) or polyethylene oxide (PEO) is a versatile polyether available in various structures such as branched, star and *comb*-like polymers. In general, ethylene oxide polymers with molecular weights less than 20,000 g/mol are called PEG, whereas those with molecular weights above 20,000 g/mol are called PEO [82]. PEG is highly soluble in water, flexible, nontoxic and nonimmunogenic [83]. Its main drawback is its non-biodegradability [19].

Polyvinylpyrrolidone (PVP) is a hydrophilic polymer with good biocompatibility. Over the years it has been used as biomaterial or additive to drug compositions such as blood plasma expander, vitreous humor substitute [33], binder in oral dosage forms [84]. However, it has low mechanical strength and thermal stability [19].

Polylactic acid (PLA) is a biocompatible, biodegradable, non-toxic, absorbent, and cost-effective polymer. It is not flexible therefore it has to be blended with other polymers to overcome this shortcoming (*e.g.* PEG as a plasticizer) [83]. Its high polarity, high density and low thermal stability also limit its applications [85].

Polydimethylsiloxane (PDMS) is an outstanding polymer possessing desirable features such as flexibility, thermotolerance, resistance to oxidation, ease of fabrication, optical transparency. However, because of its hydrophobicity and poor biocompatibility, PDMS as such has limited biomedical applications and its surface properties need to be improved [86]. Wei et al. designed a supramolecular PDMS elastomer film with double layer structure. It consisted of an elastic layer (EL) and an adhesive layer (AL). The EL was a hydrogen-bond crosslinked elastomer based on linear amino-terminated polydimethylsiloxane while the

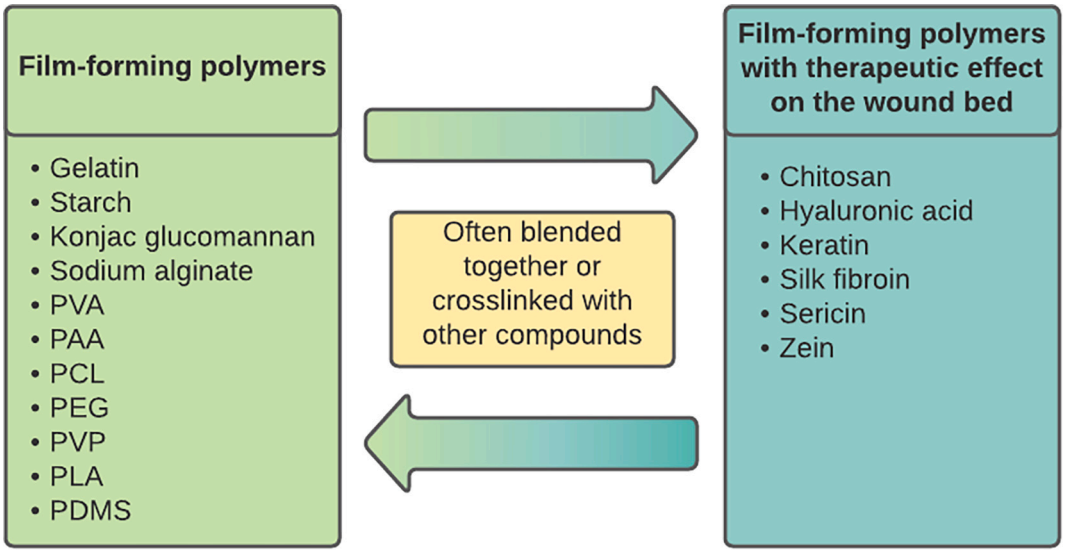

Fig. 4. Scheme of polymers classified according to their role in wound dressing film formulation.

Table 3
Natural compounds-loaded films, with therapeutic effect on the wound bed.

Natural compound	Film-forming polymer	Evaluated quality attributes	Biological study	Antimicrobial activity	Highlights	Ref.
Curcumin (Cur)	Hyaluronic acid-succinylated pullulan (HA-SPu) 6.66% *w/v*	Swelling behavior	*In vitro* cytotoxicity, antioxidant activity, hemolysis test, whole blood clotting time *In vivo* skin irritation test on mice, wound healing capacity on Wistar rats	Tested against *S. aureus, E. coli*	>90% cell viability of L929 cells The antimicrobial activity of Cur-HA-SPu was better on gram-positive bacteria than on gram-negative bacteria Cur-HA-SPu had higher antioxidant capacity than HA-SPu The hemolysis rate of Cur-HA-SPu was <5% No erythema and edema on the back of mice Conjugation of Cur with HA-SPu could efficiently improve the wound healing Cur-HA-SPu film had a higher swelling ratio than HA-SPu film	[48]
	PCL 14% *w/v*, CS 1.4% *w/v*, Montmorillonite (MMT) Clay (0.14, 0.28, 0.56 and 1.12% *w/v*)	Surface morphology, FTIR characteristics, crystallinity, thermal behavior, wettability	*In vitro* cytotoxicity on L929 cells	Tested against *S. aureus*	Clay-enhanced Cur-loading films had a porous sponge-like aspect with disconnected architecture Within 12 h, release of Cur *via* Non-Fickian diffusion After 12 h, release of Cur depended on Fickian diffusion Addition of clay increased the TS of PCL/CS/Cur from 1.94 to 11.81 MPa (PCL/CS/Cur/Clay-1) No cytotoxicity on L929 cells with or without clay	[38]
	SF 4% *w/v*	Water uptake study (swelling behavior), WVTR, wettability, surface morphology, FTIR characteristics, thermal behavior, Cur release from films	*In vitro* cytotoxicity on HEK293 cells	Tested against *S. aureus* and *E. coli*	The composite film had a good, sustained release of Cur Efficient inhibition of bacterial growth and penetration with a good WVTR Non-cytotoxic on HEK-293 cell lines	[56]
Epigallocatechin gallate (EGCG)	KGM 2 *wt%*, PVP 30 *wt%*	Surface morphology, FTIR characteristics, thermal behavior, crystallinity, mechanical properties, swelling behavior, *in vitro* degradation (mass loss by solubilization)	*In vivo* wound healing capacity on Sprague Dawley rats	Tested against *S. aureus, B. subtilis, E. coli* and *Salmonella enterica*	Thermally stable, orderly, transparent film with an average diameter of microfibers <1 μm Excellent antibacterial activity (> 97% against all tested bacteria) Good wound healing with neovascularization and hair follicle development	[41]
Pomegranate peel extract (PPE)	PVA 5% *w/v*, St 4% *w/v*, PAA 2.5% *w/v* at PVA:St:PAA (*v:v*) ratios of (75, 80, 85): (5, 10, 15):10	Thickness, swelling behavior, solubility, wettability, WVTR, permeability coefficient	*In vitro* hemolytic activity, cytotoxicity, healing activity on L929 cells	Tested against *Staphylococcus epidermidis*, MRSA and *E. coli via* disc diffusion method	The higher ratio of St (15% *v/v*) led to nonhemolytic, biocompatible, smooth, transparent, and domain-free films without phase separation Efficient against *S. epidermidis* and MRSA No toxicity on fibroblasts exposed to PPE Films containing 1.25% *w/v* PPE well reduced the scratch open area	[8]
Propolis ethanolic extract (EEP)	Cornstarch (CSt) 2 *wt %*, HA 1 *wt%*	FTIR characteristics, film opacity, surface morphology, mechanical properties, thickness, swelling behavior, degradation studies (mass loss by solubilization), EEP release	*In vitro* biocompatibility, viability on L929 cells *In vivo* wound healing capacity on Wistar rats	Tested against *S. aureus, E. coli S. epidermidis, P. aeruginosa*	None of the film dressings could inhibit the growth of *P. aeruginosa* but the CSt/HA/0.5%EEP film had the most appropriate properties: Higher antibacterial activity on *S. aureus, E. coli S. epidermidis* than the CSt, CSt/	[6]

(*continued on next page*)

Table 3 (*continued*)

Natural compound	Film-forming polymer	Evaluated quality attributes	Biological study	Antimicrobial activity	Highlights	Ref.
					HA and CSt/HA/0.25%EEP films No cytotoxicity on L929 cells Efficient acceleration of the wound healing process	
Allantoin (AT)	CS 1% *w/v* and GE 10% *w/v* at CS:GE ratios of 1:3, 1:1, 3:1	FTIR characteristics, surface morphology, crystallinity, water absorption capacity (swelling behavior), TS, stability studies	*In vitro* antioxidant activity, anti-inflammatory studies, blood compatibility studies, cytotoxicity on L929 cells, cell viability, cell adhesion study	Tested against *S. aureus, E. coli via* Agar well diffusion method	The smooth surface of CS/GE films changes to rough after adding AT Higher SI with higher CS ratio The higher ratio of CS increases the TS Amorphous nature of the biocomposite films (aids good hydrophilicity and cell activity) A higher CS ratio shows good stability Hemolysis values <2% (hemolysis up to 5% is considered safe) Reduced antibacterial activity against *S. aureus* than on *E. coli*	[26]
Psyllium husk gel	SA 0.75% *w/v* and Lauric acid-grafted alginate 0.25% *w/v*	Thickness, weight variation, folding endurance, %E, WVTR, swelling behavior, loss on drying, *in vitro* deformation studies, protein adsorption studies	N/A	Tested against *E. coli via* disc diffusion method	The glycolipid-containing composite film had better folding endurance, %E, swelling studies, *in vitro* deformation studies, WVTR, loss on drying The composite film had a lower protein adsorption Enhanced antimicrobial activity due to the lauroyl glycolipid derivative of alginate Films can be efficient on low suppurating wounds	[88]
Black pepper essential oil (BPEO) and ginger essential oil (GEO)	PVA 17% *w/v*, GA 50% *w/v* and CS 2% *w/v*	Swelling behavior, water solubility, volatile mass fraction, FTIR characteristics, crystallinity, surface morphology, thermal behavior thickness, TS, % E, BPEO and GEO retention and release study	N/A	Tested against 4 bacteria: *B. cereus, S. aureus, E. coli, Salmonella typhimurium*	BPEO- and GEO-incorporated PVA/GA/CS films were more resistant to breakage and flexible than PVA/GA/CS films. Incorporation of BPEO and GEO on films substantially decreased SI BPEO-PVA/GA/CS had better retention and release rate than GEO-PVA/GA/CS films Notable antibacterial activity of BPEO- and GEO-incorporated PVA/GA/CS films against the 4 bacteria	[21]
Melaleuca essential oil (MEO) and clove essential oil (CEO)	CS 1% *w/v*	Thickness, FTIR characteristics, swelling behavior, surface morphology, mechanical properties, wettability	N/A	Film-forming emulsions tested against *S. aureus, E. coli, C. albicans via* agar diffusion method	The CEO was the most efficient against the tested bacteria CS emulsions had modest antimicrobial activity compared to the essential oils (MEO and CEO) All essential oil-incorporated CS films showed good transparency, flexibility, mechanical resistance, smaller thickness than the dermis and higher wettability than CS films Incorporation of essential oils (1% and 3% *v/v*) increased the %E of films	[44]
Cabreuva essential oil (EO)	Crosslinked emulsions (CE): CS 0.75% *w/v*, PVA 0.75% *w/v* at 1:1 (*v:v*) ratio Composite dressings:	WVP, oxygen permeability, wettability, swelling behavior, mechanical properties, surface morphology, FTIR characteristics	*Ex vivo* diffusion and penetration assay on skin explants from healthy human volunteers *In vivo* percutaneous penetration *via* ATR-FTIR	Tested against *S. aureus* and *S. epidermidis*	The formulation containing CE:PVA in 1:1 (*v:v*) ratio had the best mechanical and barrier properties The composite dressing was efficient against the tested	[89]

(*continued on next page*)

Table 3 (*continued*)

Natural compound	Film-forming polymer	Evaluated quality attributes	Biological study	Antimicrobial activity	Highlights	Ref.
	CE and PVA 1% *w/v* at *(v:v)* ratios of 2:3, 1:1 and 3:2		on healthy volunteers Quantification of the penetration of EO in the explants by HPLC Diffusive analysis of cabreuva EO and optical sectioning by confocal scanning laser microscopy (CSLM) *In vitro* cytotoxicity on HaCaT cells *via* MTT assay *In vitro* cell regeneration assay on HaCaT cells *via* scratch assay		bacteria, showed no cytotoxicity on HaCaT cells and produced cell regeneration after 24 h of contact time The pure EO reached a similar penetration depth (after 1 h of contact time) with the composite dressing (after 8 h of contact time) *via* the *ex vivo* penetration of the EO in different layers of the explants	
An alcoholic extract of a mixture of *Plantago lanceolata, Arnica montana, Tagetes patula, Symphytum officinale, Calendula officinalis* and *Geum urbanum*	CS 2% *w/w* and PVA (ratio not mentioned)	Thickness, opacity, swelling behavior, solubility, texture and surface properties	*In vitro* antioxidant capacity *In vitro* cell viability on Hs 27 cells *In vivo* wound healing capacity on Wistar rats	Tested against *S. aureus, E. coli, P. aeruginosa via* disc diffusion method	The optimal formulation had a thickness of 0.09 mm, water solubility of 44.9% and a high swelling degree of 2157.4% Better antibacterial activity of the blank CS film (effective on *P. aeruginosa* and *E. coli*) *vs.* the bioactive-loaded film (effective only on *P. aeruginosa*) Good antioxidant activity and acceptable cell viability Significant wound healing acceleration compared to the reference (Betadine® ointment) and control (blank CS film)	[90,91]

AL was a dual-crosslinked elastomer based on linear carboxyl-terminated PDMS pre-polymer. The bilayer film (BLF) was characterized, and its clinical potential was assessed on both normal and diabetic rats and was compared to a commercial medical Tegaderm® film [87]. Table 2 provides an overview of recent studies that used different polymers for the preparation of wound dressing films.

5. Active ingredients with therapeutic effect on the wound bed

Film-forming polymers may have intrinsic beneficial properties for wound healing, such as antimicrobial (*e.g.* CS, Ser), restorative (*e.g.* HA, keratin, SF), antioxidant (*e.g.* zein, Ser) (Fig. 4). However, their number is limited, therefore bioactive ingredients often need to be loaded in film formulations, either to provide or enhance a certain desired effect on the wound bed. So far, scientists have reported the inclusion of a wide range of active ingredients into wound dressing films. The use of natural compounds, antibiotics and various ingredients and materials with antibacterial properties and wound healing potential was intensely studied. Table 3 summarizes findings of studies in which natural compounds were involved.

Curcumin (Cur) has drawn the attention of researchers all over the world. Duan et al. evaluated the wound healing properties of Cur-grafted hyaluronic acid modified pullulan (Cur-HA-SPu) films. The antibacterial and antioxidant properties were found to be promising for the healing process [48]. Controlled release of Cur from wound dressing films was studied by Huang et al., by adding nanoclay in the PCL/CS/Cur composite. Better controlled-release profiles were obtained with the addition of the clay compared to films without clay [37]. Zhang et al. produced composite films with sustained release of Cur by blending SF, Cur, glutaraldehyde, and glycerol. It was observed that the release of Cur was influenced by the percentage of ethanol in the release medium (ethanol/PBS solution) [56].

Ni et al. fabricated KGM-based films with PVP and epigallocatechin gallate (EGCG) at an ultra-small scale *via* microfluidic spinning. Films displayed an enhanced bactericidal and healing activity [41]. In the research done by Costa et al., pomegranate peel extract (PPE) promoted wound healing when incorporated in PVA/St/PAA films. It was initially observed that a lower concentration of PPE (1.25% *w/v*) displayed a similar, not statistically significant, antimicrobial activity against *Staphylococcus epidermidis* and *S. aureus* compared to a higher concentration of the extract (2.5% *w/v*). Therefore, the lower concentration (1.25% *w/v*) was used during the study [8]. Propolis ethanolic extract (EEP) was incorporated in a cornstarch (CSt)-based and HA-enriched wound dressing, generating films with promising antibacterial and wound healing properties. Incorporation of EEP into the CSt/HA film significantly decreased the swelling values and the degradation rates compared to the CSt and CSt/HA films [6]. In the study of Sakthiguru and Sithique, biocomposite films of chitosan/gelatin/allantoin (AT) were prepared and characterized. Films with higher CS ratio showed promising values for SI, TS, and good stability. Antioxidant, anti-inflammatory and antibacterial activities were also found to be promising for wound healing [26]. Fernandes et al. synthesized and characterized a hydrophobic glycolipid by grafting lauric acid on sodium alginate. The modified alginate was eventually incorporated into *Psyllium* husk gel-alginate composite films, and the resulting films showed improved physicochemical, mechanical and antibacterial properties [88]. Amalraj et al. incorporated black pepper essential oil and ginger essential oil on PVA/gum arabic (GA)/CS composites and obtained films with improved mechanical properties and antibacterial activity against gram-positive and gram-negative bacteria [21]. Melaleuca essential oil (MEO) and clove essential oil (CEO) of different concentrations (1%, 3% *v/v*) were used for the preparation of CS-based film-forming emulsions and films. Despite the modest *in vitro* antimicrobial activity of the CS-based emulsions compared to the pure MEO and CEO, the characterization of essential oil-incorporated CS films revealed that it is feasible to use MEO and CEO for wound healing purposes [44]. Lamarra et al. prepared composite films by assembling PVA with crosslinked CS-based emulsions functionalized with cabreuva essential oil (*Myrocarpus*

Table 4
Antibiotics loaded into films for wound healing.

Antibiotic	Film-forming polymer	Evaluated quality attributes	Biological study	Antimicrobial activity	Highlights	Ref.
Gentamicin (GM)	Hemicellulose (Arabinoxylan-AX) 2, 2.5 and 3% *w/v*	Thickness, solvent loss, mechanical properties, swelling behavior, WVTR, FTIR characteristics, thermal behavior, surface morphology, GM release profile	*In vitro* cytotoxicity on BHK21 cells *via* indirect contact method	Tested against *S. aureus, E. coli, P. aeruginosa via* Kirby-Bauer disc diffusion test	Thickness increased when increasing AX content Solvent loss decreased when increasing the amount of AX with a fixed amount of GM Higher AX contents led to stronger films (increased TS) Favorable SI values were 55%, 72% WVTR decreased when increasing AX content and adding GM The release times of GM from films containing 2.5% and 3% AX were 12 to 16 h The antibacterial activity of GM was kept after incorporation into films >90% cell viability after 24 h	[29]
	Zein 25% *w/v*	Surface morphology, mechanical properties, FTIR characteristics, wettability, swelling behavior, degradation, WVP, *in vitro* drug release	*In vitro* cytotoxicity, cell attachment, proliferation studies on NIH/3 T3 and HS2 (human keratinocyte) cells	Tested against *S. aureus* and *E. coli*	The sustained release of GM at the early stage was obtained with the bilayer structure Antimicrobial activity against tested bacteria Films were non-cytotoxic and NIH/3 T3 and HS2 cells were proliferated on each layer	[27]
Ciprofloxacin (Cip)	CS 2% *w/v* and BC (ratio not mentioned)	Surface morphology, roughness analysis, FTIR characteristics, crystallinity, thermal behavior, mechanical properties, WVTR	*In vitro* cytotoxicity studies on GM07492 cells *via* MTT assay	Tested against *S. aureus* and *P. aeruginosa*	Incorporation of CS (36.8 ± 3.2%) into BC matrix increased the normalized WVTR values from 0.7 to 3.2 g mm/m^2 h Addition of CS weakens the mechanical properties of BC films Cip loading onto the BC-CS film revealed a 30% decrease in antibiotic release due to CS A synergic effect of CS on Cip antimicrobial activity was observed BC-CS-Cip films were noncytotoxic on human fibroblasts	[55]
Tetracycline hydrochloride (TH)	SA 2% *w/w* and GE 2% *w/w* at (*w:w*) ratios of 40:60, 50:50 and 60:40; HyA 1, 2, 5, 10 and 20% *w/w*	Thickness, swelling behavior, solution degradation study (mass loss by solubilization), surface morphology, tensile properties, crystallinity, thermal behavior, *in vitro* TH release	N/A	Tested against *S. aureus* and *E. coli via* agar diffusion assay	SI and weight loss of films decreased when increasing the amounts of SA and HyA Increasing the amount of HyA generates a rougher surface of films Incorporation of HyA increased the thermal stability of films Less TH was released within 15 min as the amounts of SA and HyA increased TH containing films had a slightly higher antimicrobial activity against *S. aureus* than *E. coli*	[24]

fastigiatus) (CE-PVA). Its characterization revealed its potential to be used as wound dressing in superficial burns or minor wounds [89]. Colobatiu et al. prepared a CS film formulation loaded with an herbal extract of a mixture of *Plantago lanceolata, Arnica montana, Tagetes patula, Symphytum officinale, Calendula officinalis* and *Geum urbanum*, using a Quality by Design (QbD) approach. PVA was used to enhance the bioadhesivity of the films. The optimized formulation had good quality attributes and registered a good antimicrobial activity, as well as the placebo formulation [90]. Its potential as diabetic wound dressing material was also investigated, revealing promising results in terms of

Table 5
Other ingredients/materials incorporated in wound dressing films.

Active ingredient/ material	Film-forming polymer	Evaluated quality attributes	Biological study	Antimicrobial activity	Highlights	Ref.
PHMC-mGO	1:1 (*v:v*) ratio of PVA 5% *w:v* and CS 1% *w:v*	FTIR characteristics, crystallinity, thermal behavior, surface morphology, Zeta potential, mechanical properties, WVTR, swelling and deswelling behavior, gel fraction	*In vitro* cytotoxicity, cell viability on HaCaT cells *via* Cell Counting Kit-8 (CCK-8) *In vivo* wound healing assessment *via* murine infected full-thickness skin defect wound model and histological analysis	Tested against *S. aureus* and *E. coli via* plate counting assay	FTIR, XRD, TGA and Zeta potential analyses confirm the grafting of PHMG on GO The PVA/CS/mGO hybrid films had better mechanical properties, a proper WVTR, high SI and rapid exudate discharge capacity Good biocompatibility and efficiency against *S. aureus* and *E. coli* PVA/CS/0.5 *wt%* mGO had the fastest wound healing capacity *via* re-epithelialization	[60]
S-nitrosoglutathione (GSNO) as NO donor	CS 1% *w/v*	Thickness, surface morphology, mechanical properties, water absorption capacity (swelling behavior), thermal behavior, stability studies, *in vitro* NO release	*In vivo* wound healing efficacy in a rat model on full-thickness wounds; histopathological studies	Tested against *P. aeruginosa* and *S. aureus*	Good mechanical properties CS/NO film with 20 *wt%* GSNO had the highest antibacterial activity Promising wound healing effect of CS/NO films through wound size reduction and epithelialization NO release from films followed a Korsmeyer-Peppas model with Fickian diffusion	[14]
Clinoptilolite-Ag	GE 10% *w/v*	Thickness, moisture content, WVP, water vapor permeation flux, water absorption capacity (swelling behavior), mechanical properties, wettability, surface morphology, FTIR characteristics, thermal behavior, Ag quantification and Ag release *in vitro*	N/A	Qualitatively tested against *E. coli*, *S. aureus* and human skin natural microorganisms Quantitatively tested against *E. coli* and *S. aureus*	The formulation with 25% glycerol and 0.5% zeolite generated proper films Slow *in vitro* release of Ag^{+} Satisfactory bacterial growth reduction of *E. coli* and *S. aureus* Increasing glycerol concentration led to a faster antimicrobial action	[22]
Silver Sulfadiazine (Ag SD), Zeolite (Na—Y)	CS (ratio not mentioned)	Thickness, surface morphology, crystallinity, thermal behavior, FTIR characteristics, fluid handling capacity, mechanical properties, AgSD release test in SEF	*In vitro* indirect cytotoxicity on Balb/c 3 T3 cells	Tested against *E. coli, P. aeruginosa S. aureus, C. albicans*	Addition of AgSD-Y zeolite (0.2 g/100 g CS solution) into CS films modified the infra-red spectra, XRD diffractograms compared to AgSD-CS films (zeolite free) The use of zeolite promoted a sustained release of silver ions Some antimicrobial activity against *C. albicans* and a lower activity against bacterial strains was observed Cytotoxic at the tested conditions of 72 h of extraction (cell viability <70%)	[57]
Imiquimod	CS 1.5% *w/v*	Thickness, mechanical properties, swelling behavior, WVTR, thermal behavior, crystallinity, FTIR characteristics, *in vitro* imiquimod release, content uniformity of imiquimod	*In vitro* growth inhibition potential against A375P and B16-F10 cells *In vitro* skin penetration on human cadaver skin sample	N/A	Films were capable of releasing imiquimod for 7 days Bioactivity of imiquimod was not affected by its entrapment in CS matrix The film formulation had a much higher drug accumulation in the skin compared to Aldara®	[17]
Eggshell membrane (ESM)	CS 1% *w/v*	Thickness, transparency, mass uniformity, surface morphology, *in vitro* integrity and degradation	*In vitro* wound healing capacity (pH, wound fluid and BSA absorption capacity)	Tested against *E. coli* and *S. aureus*	The blend films had a higher stability than CS film after 95 h of incubation in solution The blend films provided an acidic pH for wound healing (pH = 5.86) *In vitro* wound healing capacity and antibacterial properties were enhanced when incorporating 0.01 g/ml ESM and 2% *v*/v glycerol into CS film	[64]

antioxidant activity, cell viability and wound healing [91].

Data regarding the use of antibiotics in wound dressing film preparation are displayed in Table 4. Ahmad et al. prepared and characterized hemicellulose (arabinoxylan)-based antibacterial films, both blank and gentamicin (GM)-loaded. Formulations with 2% to 3% arabinoxylan were found to be suitable regarding the target profile of a wound dressing film. The films were also cytocompatible and the antibacterial activity of GM-loaded films was similar to the standard gentamicin

solution [29]. Kimna et al. developed a bilayer GM-loaded zein-based membrane consisting of a fibrous layer and a film layer for a controlled antibiotic release for the treatment of acute skin infections. It was observed that the fibrous structure prolonged the release rate in the bilayer membrane when compared to the monolayer film which released more than 50% of the drug in 45 min. The bilayer GM-loaded membrane may be promising for wound healing applications also due to its good mechanical properties, non-toxic behavior and antimicrobial activity [27]. Cacicedo et al. produced bacterial cellulose (BC) films modified with low molecular weight chitosan for a controlled release of ciprofloxacin (Cip). The incorporation of Cip into BC-CS films led to a sustained release of the drug for more than 6 h, with a slower rate in the presence of CS than in the case of plain BC films [55]. Türe prepared hydroxyapatite (HyA)-containing alginate-gelatin films using calcium chloride as crosslinker to study to what extent HyA influences the attributes of the films. Tetracycline hydrochloride (TH) was used as a model drug and its release from the prepared films as well as the antimicrobial properties of the TH-loaded films were studied [24].

Table 5 includes recent studies that describe the development of wound dressing films loaded with a variety of ingredients or materials found active on the wound bed. In the work of Chen et al., modified graphene oxide (mGO) was obtained by grafting polyhexamethylene guanidine (PHMG) to the surface of graphene oxide through covalent bonding. mGO was incorporated into a PVA/CS matrix, resulting in wound dressing films with promising attributes [60]. Exploiting nitric oxide (NO) as therapeutic agent for wound healing was possible by producing films composed of S-nitrosoglutathione (GSNO) as NO donor and CS. The wound healing efficacy on non-infected full-thickness wounds was confirmed by the histopathological analyses revealing re-epithelialization and reconstruction of the wounded skin. Enhanced antibacterial activity of the CS/NO film compared to CS film was observed against non-antibiotic resistant bacteria [14]. Moreover, a later study demonstrated its wound healing capacity in methicillin-resistant *S. aureus* (MRSA) biofilm-infected wounds of diabetic mice. A faster biofilm dispersal, wound size reduction, collagen deposition and epithelialization rate were observed in the MRSA biofilm-infected wounds treated with the CS/NO film [92]. Hubner et al. produced gelatin-based films with glycerol as plasticizer (15, 20, 25% *v/v*) and adding different concentrations of clinoptilolite zeolite impregnated with silver ions (0.5, 1% *m/v*) for a controlled release of silver. A slow release of silver ions was obtained and a fast reduction of bacterial growth in the first hours was observed in the films assessed with *S. aureus versus E.coli*, on which films revealed a slower bactericidal activity [22]. Another research in which the controlled release of silver ions from films was aimed, is the study of Yassue-Cordeiro et al. who developed chitosan/silver sulfadiazine/zeolite films. Although the addition of the zeolite ensured a sustained release of silver ions, the films were found to be cytotoxic against the Balb/c 3 T3 cell lines [57]. Layek et al. developed imiquimod-loaded CS films to overcome the limitations of the commercially available cream Aldara® for the local treatment of basal cell carcinoma, such as dose variability, low bioavailability due to incomplete drug release and poor patient compliance. The film led to better results regarding drug accumulation in the skin when compared to the cream formulation [17]. An innovative way to use eggshell membrane (ESM) for medicinal purposes was the preparation of blend films of ESM (0.01, 0.02, 0.03 g/ml) and CS as potential dressings for wound care using glycerol as plasticizer (0, 1, 2% *v/v*). The swelling properties of ESM increased the bovine serum albumin (BSA) absorption capacity of the blend films, thus providing a better absorption of nutrients to stimulate the fibroblast migration and proliferation [64].

6. Nanosystems incorporated in wound dressing films

Nanotechnology can be used for wound healing in the form of drug delivery systems with controlled drug release in the wound environment or a direct delivery of the drug to the healing tissue or cells. The benefits are a better control over the drug dosage at the wound site, an improved stability of the drug and maintaining a constant drug concentration over a period of time [93].

Bardania et al. developed green synthesized silver nanoparticles (AgNPs) and incorporated them into PEG/PLA nanofilm. The innovative aspect of the study was that *Teucrium polium* extract was used as reducing agent for the nanoparticles' synthesis in a rapid, facile, cost-effective way. The AgNPs displayed promising antibacterial and antioxidant activity *in vitro* [83]. The antimicrobial potential of AgNPs was also investigated by blending AgNPs in a novel quaternized CS film, generating reinforced nanocomposite wound dressing films with promising antimicrobial properties. The quaternized CS film also displayed an intrinsic antimicrobial activity against all tested microorganisms, probably due to the imidazolium moiety in the film matrix [62]. Shah et al. prepared CS and Ser blends with moxifloxacin (Mox)-loaded and unloaded *in situ* AgNPs to obtain wound dressing films with sustained release of Mox and improved antibacterial properties. The composite films displayed a strong burn wound healing capacity with fibrosis, collagen reorganization, neovascularization and moderate epidermal regeneration with no silver ions detection in animal's blood after 7 days of treatment [3]. The same research group had previously developed *in situ* nanocomposites of CS, silver and Mox while also studying the influence of 3 different cross-linkers (*e.g.* sodium tripolyphosphate, γ-radiation and genipin) on drug release. Incorporation of cross-linkers was done to achieve an extended drug release, since CS has a hydrophilic nature which can lead to a rapid drug release from the polymeric composite in an aqueous medium. [94].

Mazloom-Jalali et al. prepared blended nanocomposite films of CS, PEG, cephalexin (CFX) and zeolitic imidazolate framework-8 (ZIF-8) NPs up to 5% to obtain a product with controlled drug release. The resulted films were characterized regarding mechanical properties, drug release profile, antibacterial activity, and cell viability. The drug release profile was best fitted to Korsmeyer-Peppas model [63]. To exploit the beneficial effect of HA in wound healing and improve its low mechanical strength and instability, functionalized ZIF-8 (FZIF-8) nanoparticles containing hydrophilic carboxylic acid groups were blended with HA-based wound dressing. It resulted in films with antibacterial properties and improved mechanical properties, which also promoted fibroblast migration and proliferation. Addition of FZIF-8 also enhanced the cell viability of fibroblasts, and the released zinc ions were maintained within a safe concentration range [58].

Titanium dioxide nanoparticles (TiO2 NPs) were incorporated by Ismail et al. into a gellan gum (GG) matrix, resulting in a promising wound dressing film (GG + TiO2 NPs film) with better antimicrobial and healing properties compared to pure GG film. The GG + TiO2 NPs film also displayed better mechanical properties and swelling capacity than the pure GG film [20]. Ai et al. prepared a composite film of Ser and PVA reinforced with modified zinc oxide nanoparticles (ZnO NPs) *via* polydopamine (PDA). Film characterization revealed outstanding performance of the nanocomposite product in terms of wettability, swellability, stability, mechanical properties and antibacterial activity against *S. aureus* and *E. coli*. [18]. PDA was also used by Liu et al. to coat the surface of a Ser-agar film and synthesize high density AgNPs on the surface of PDA-Ser-agar film. PDA is advantageous for the synthesis of AgNPs due to its structure (it has multiple sites to bind metal ions and phenolic hydroxyl groups to reduce silver ions to AgNPs). Composite films with excellent properties were obtained [50]. Aiming to use the synergic antibacterial activity of CS and ZnO NPs, hybrid CS-ZnO NPs were coated on SF-PVA films using a sonochemical process. That yielded reinforced nanocomposite films with outstanding antibacterial activity against Gram positive and Gram negative bacteria compared to uncoated SF-PVA and Sterizone® silver antimicrobial wound dressing [73]. Jayaramudu et al. prepared two new types of antibacterial composite films by incorporating CS with chitosan capped cooper oxide (CSCuO) and cooper (CSCu) NPs. Biopolymer-stabilized metal NPs are of high interest in the clinical field due to their significant antibacterial

Table 6
Types of nanosystems used in wound dressing films.

Nanosystem	Film-forming polymer	Evaluated quality attributes	Biological study	Antimicrobial activity	Highlights	Ref.
AgNPs using *Teucrium polium* extract	1:1 (*v:v*) ratio of PLA 1.25% *w/v* and PEG 1.25% *w/v*	Surface morphology, mechanical properties, thermal behavior	*In vitro* antioxidant capacity *In vitro* cytotoxicity on RAW264 cells	Tested against *S. aureus* and *P. aeruginosa via* Agar disc diffusion method and MTT assay of bacterial cells	Ratio of PLA:PEG = 1:1 and AgNPs concentrations were 5% and 10% The antioxidant activity of green synthesized AgNPs increased with AgNPs concentration Complete growth inhibition of *S. aureus* and *P. aeruginosa*	[83]
AgNPs	Quaternized CS 5% *w/v*	FTIR characteristics, crystallinity, surface morphology, elemental analysis, sample homogeneity, swelling behavior, blood clotting assay, hemolysis rate assay	*In vitro* cell viability on human fetal foreskin fibroblast (HFFF) cells *via* MTT assay *In vitro* cell attachment evaluation *via* DAPI staining	Tested against *E. coli, S. aureus*, *P. aeruginosa, C. albicans, MDR—P. aeruginosa via* disc diffusion method	High antimicrobial activity (even without AgNPs) on all tested microbial strains Cytocompatible films confirmed by DAPI staining and MTT assay	[62]
AgNPs	1:1 (*v:v*) ratio of Ser 2% *w/v* and agar 2% *w/v*	Surface morphology, FTIR characteristics, crystallinity, wettability, water absorption capacity (swelling behavior), mechanical properties	*In vitro* cytocompatibility on NIH/3 T3 cell lines	Tested against *S. aureus* and *E. coli*	The composite film had a great hydrophilicity and good mechanical properties Highly cytocompatible on the fibroblast NIH/3 T3 cells and efficient against tested bacteria	[50]
AgNPs with and without Mox	4, 6 and 8% *w/v* CS/Ser, at CS/Ser ratios of 1:1, 1:2 and 1:3	Thickness, weight, mechanical properties, swelling behavior, surface morphology, elemental analysis, FTIR characteristics, crystallinity, thermal behavior, content uniformity, *in vitro* Mox release, permeation analysis	*In vivo* wound healing capacity on burn-injured Sprague Dawley rats	Tested against 7 bacterial strains: *S. aureus, Staphylococcus epidermidis, MRSA, P. aeruginosa, Acinetobacter baumannii,* and 2 clinical isolates of MRSA.	Good swelling profile with a sustained *in vitro* Mox release and permeation profile Good antibacterial activity of films (especially the Mox-loaded) on all the tested strains; highest efficiency against MRSA Notable wound healing capacity after 7 days of treatment	[3]
Mox-loaded AgNPs	CS 1, 2 and 3% *w/v*	Thickness, weight, mechanical properties, swelling behavior, moisture content, disintegration in water (mass loss by solubilization), silver ions and Mox release, particle size and Zeta potential, drug content uniformity, surface morphology, elemental analysis, FTIR characteristics, crystallinity, thermal behavior	*Ex vivo* permeation of Mox across rat skin (*via* FDC)	Tested against *S. aureus, P. aeruginosa* and 2 clinical strains of MRSA	Higher swelling ratio, lower TS and higher %E than pure CS film All non-crosslinked Mox-loaded films had a sustained drug release of drug up to 12 h Crosslinked films had a prolonged drug release up to 36 h Maximum cumulative amount of permeated Mox among non-crosslinked and crosslinked films was 57.79% and 62.87%, respectively Excellent antibacterial activity against tested bacterial strains with highest antibacterial effect against *S. aureus*	[94]
ZIF-8 NPs	CS:PEG ratio of 70:30 *wt%*	FTIR characteristics, surface morphology, crystallinity, mechanical properties, swelling behavior, *in vitro* CFX release profile	*In vitro* cytotoxicity on L929 cells *via* MTT assay	Tested against 5 bacterial strains: *E. coli, P. aeruginosa, Acinetobacter, S. aureus, B. cereus*	$SI_{acidic\ medium} > SI_{neutral\ medium} > SI_{alkaline\ medium}$ TS and Young's modulus increased with ZIF-8 loading %E decreased with ZIF-8 loading CFX had an initial burst release followed by a sustained release in acidic, neutral, and alkaline media Notable antibacterial activity against *B. cereus, S. aureus, E. coli* High cell viability towards L929 cells	[63]
FZIF-8 NPs	HA 1% *w/v*	Surface morphology, crosslinking degree, mechanical properties, wettability, swelling behavior, Zn ion release, *in vitro* (hydrolytic and enzymatic) degradation	*In vitro* cell viability on L929 cells, cell adhesion behavior	Tested against*E. coli, S. aureus*	FZIF-8 blending of HA films increased Young's modulus (from 138 to 176 kPa) and hydrophilicity (water contact angle reduced from 37.4° to 27.7°) Better antibacterial properties	[58]

(*continued on next page*)

Table 6 (*continued*)

Nanosystem	Film-forming polymer	Evaluated quality attributes	Biological study	Antimicrobial activity	Highlights	Ref.
					and improved cell adhesion were obtained Proper cell viability was observed	
TiO_2 NPs	GG 1% *w/v*	Optical transparency, FTIR characteristics, crystallinity, surface morphology, mechanical properties, WVTR, swelling behavior	*In vitro* wound healing and cell proliferation on 3 T3 cells *In vivo* wound healing capacity *via* open wounds model on Sprague Dawley rats	Tested against *S. aureus* and *E. coli via* disc diffusion method	Higher mechanical strength and SI compared to pure GG film Good antimicrobial properties against tested bacteria Open wound healing on rats was accelerated by the GG + TiO2 NPs film *via* cell proliferation and cell migration Faster wound healing within 14 days when treated with GG + TiO2 NPs film *vs.* control and pure GG film Both GG and GG + TiO2 NPs films were not cytotoxic on mouse fibroblast cells	[20]
PDA-Modified ZnO NPs	Ser 4% *w/t* and PVA 5% *w/t*	Surface morphology, crystallinity, FTIR characteristics, wettability, swelling behavior, mechanical properties, mass loss analysis (mass loss by solubilization)	N/A	Tested against *E. coli* and *S. aureus*	Excellent wettability, swellability and stability of the composite films Improved TS and %E Antimicrobial activity against tested bacteria	[18]
CS-ZnO NPs	7% *w/v* SF/PVA, at a SF/PVA ratio of 1:2	crystallinity, surface morphology, FTIR characteristics, specific surface area, porosity, swelling behavior, mechanical properties	*In vitro* cell viability on L929 cells *via* MTT assay	Tested against *S. aureus, E. coli* and *P. mirabilis via* disc diffusion method	Excellent antibacterial activity of the composite films on tested bacteria Increasing the concentrations of CS-ZnO NPs (0.2, 0.5 and 1 wt%) on SF-PVA film led to a higher specific surface area, porosity, SI and enhanced mechanical properties Cytocompatible composite films	[73]
CSCuO NPs and CSCu NPs	CS 1.5% *w/v*	FTIR characteristics, crystallinity, thermal behavior, surface morphology, elemental analysis, swelling behavior	N/A	Tested against *E. coli* and *Bacillus* sp. *via* the inhibition zone method	Rod-like nanoflakes structure for CSCuO NPs and spherical shape for CSCu NPs with a size of ~7 ± 2 nm CSCu NPs had a higher thermal stability than the CSCuO NPs as revealed by TGA The percentage of CuO and Cu NPs in CSCuO and CSCu *via* TGA was found as 56.21% and 98.92%, respectively Excellent antibacterial activity against tested bacteria, CSCuO NPs and CSCuO-CS film being superior to the CSCu NPs and CSCu-CS film	[66]
Copper NPs (Cu NPs)	Agar 1.5% *w/v*	Surface morphology, crystallinity, Zeta potential	N/A	Tested against *E. coli*	The Cu NPs-modified agar film showed excellent antibacterial activity *vs.* bare agar film Cu NPs were stable at room temperature for at least 6 months	[25]
Nanocrystalline cellulose (NCC), Calcium peroxide (CP)	1:1 (*v:v*) ratio of CS 2% *w/v* and GE 4% *w/v*	FTIR characteristics, swelling behavior, mechanical properties, WVTR, oxygen release	*In vitro* cell viability on NIH 3 T3 cells *via* MTT assay	Tested against *E. coli* and *S. aureus via* disc diffusion method	NCC particles and CP reduced WVTR and swelling degree Mechanical properties were improved both for 0.3 and 1 wt % NCC concentrations Better mechanical properties were observed with 9 wt% CP *vs.* 13 wt% CP The antibacterial activity increased only against *E. coli* by adding CP to the film composition, while no effect on it of NCC particles was seen Almost no antibacterial activity was seen against *S. aureus,* but on *E. coli*	[59]

(*continued on next page*)

Table 6 (*continued*)

Nanosystem	Film-forming polymer	Evaluated quality attributes	Biological study	Antimicrobial activity	Highlights	Ref.
					The highest oxygen release for the CP containing films was on day 1, approaching a constant value for 10 days Compatibility with fibroblast cells	
Nanostarch (NS)	CS 1% *w/v* and PVP 1% *w/v* (± stearic acid-coated)	Nanostructural morphology, mechanical properties, WVTR, swelling behavior, surface morphology, porosity	*In vitro* cell viability on NIH 3 T3 cells *via* MTT assay *In vitro* hemolytic potential *In vivo* wound healing capacity on adult Albino rats; histological analysis	Tested against *S. aureus, B. subtilis, E. coli, P. aeruginosa*	Concentration of NS greatly influences the mechanical, barrier, swelling and hemolytic properties >80% cell viability of NS-reinforced dressings on NIH 3 T3 cells Promising antibacterial activity of stearic acid-coated films against *S. aureus* NS and stearic acid could effectively inhibit the bacterial adhesion	[33]
Nanocomposite film	BN, CS 3% *w/v* and PVP 1% *w/v*	FTIR characteristics, crystallinity, thermal behavior, surface morphology, mechanical properties, swelling behavior, WVTR, pH, porosity, degradation in Hank's solution (mass loss by solubilization), hydrolytic degradation	*In vitro* cytotoxicity on L929 and NIH3T3 cells *In vivo* wound healing capacity on mice; histological assessment	Tested against *B. subtilis, S. aureus, Streptococcus mutans, P. aeruginosa, E. coli, Aeromonas hydrophila via* agar disc and agar well diffusion method	Non-toxic nanocomposite film on fibroblast cells CS-PVP-BN2 film had a better *in vivo* wound healing *vs.* the other formulations CS-PVP-BN yielded less scar formation, thick granulation on the 11th day, a healing rate of 97%, epidermal regeneration on the 16th day, and increased deposition of collagen and fibroblast *vs.* controls	[16]
Halloysite nanotubes (HNT)-PVA nanocomposites loaded with minocycline	PVA 25% *w/v*	FTIR characteristics, crystallinity, Zeta potential, thermal behavior, surface morphology, elemental analyis, photostability, biodegradation, water absorption capacity (swelling behavior), minocycline *in vitro* release	N/A	Tested against *S. aureus* and *P. aeruginosa*	The photostability of minocycline was increased An absorbent and biodegradable wafer film was obtained Antibacterial activity on tested bacteria up to 7 days A controlled minocycline release was obtained (Korsmeyer-Peppas model)	[78]

properties, biocompatibility, and biodegradability. CSCuO and CSCu NPs were obtained from cooper sulfate by the reduction of Cu^{2+} ions using sodium hydroxide and ascorbic acid and their corresponding nanocomposite films (CSCuO-CS and CSCu-CS) were obtained *via* the solution casting method. A higher antimicrobial activity against *E. coli* and *Bacillus* was observed in the CSCuO NPs and its corresponding film compared to CSCuO NPs and its corresponding film [66]. Tang et al. prepared copper nanoparticles (Cu NPs) with improved oxidative stability and embedded them in an agar film, obtaining composite films with outstanding antibacterial properties against *E. coli.* To synthesize the Cu NPs, a modified corn starch was used as an ecological reducing agent and polyethyleneimine was used as stabilizer [25].

Nanocrystalline cellulose (NCC) and calcium peroxide (CP) particles were added to CS-GE-based films in order to improve their mechanical properties and the wound healing process. NCC is a type of cellulosic nanoparticles with potential to improve the mechanical properties of biopolymeric films with applications in medicine or food packaging industry. Additionally, CP is an oxygen generating biomaterial able to gradually release oxygen over a period of time, thus maintaining the cell viability under hypoxic conditions [59]. Poonguzhali et al. prepared CS-PVP films reinforced with nanostarch (NS) and coated with stearic acid on one side, which were found to have good antibacterial properties and wound healing properties. This was due to the hydrophobic surface of stearic acid which prevented bacterial adhesion and the hydrophilic surface of NS with bactericidal activity on the wound bed [33]. Shanmugapriya et al. prepared a nanocomposite film consisting of bentonite (BN), CS and PVP which showed encouraging results for wound care management [16]. Mohebali et al. developed a new nanocomposite wafer film based on halloysite nanotubes (HNT) and PVA loaded with minocycline for a controlled delivery of minocycline on burn wounds. Overall, the results were promising regarding the use of this type of dressing for wounds prone to infection such as burn wounds [78]. Table 6 is a synthesis of studies which used nanotechnology in the preparation of wound dressing films.

7. Concluding remarks

This paper is an overview on the topic of wound dressing films, starting with their preparation and characterization methods, highlighting the most used polymers and active ingredients incorporated in the form of a film dressing and ending with nanosystem-based films.

Although this literature review took into consideration recent research published between 2018 and 2020, it is not exhaustive. This paper focuses on the use of polymers in wound dressing film development and follows their processability in different types of production methods and their impact on the physicochemical profile as well as on the clinically related quality attributes. This work could guide researchers and developers into the selection of proper materials (polymers and active pharmaceutical ingredients), preparation processes, characterization techniques, and increase their understanding into how the desired product features can be reached.

Solvent casting is by far the most used method to produce thin films for cutaneous applications, but other methods have been reported as well: salt leaching, microfluidic spinning, spin coating and 3D printing.

Typical quality attributes investigated for their characterization are film thickness and morphology, mechanical properties, swelling behavior, wettability, water vapor permeation, crystallinity, thermal behavior, *in vitro* drug release. *In vitro* cytotoxicity has been investigated on various cell lines. Antimicrobial activity has been studied on pathogen strains most related to cutaneous wound infection while wound healing capacity has been assessed either *in vitro* or *in vivo*. Although data of the aforementioned studies may be promising, clinical efficacy on humans is lacking.

In recent years, numerous studies have been published, with active ingredients incorporated either as free form, or as nanosystems within the film. The latter approach is more and more explored and is chosen for enhancing drug penetration in the skin layers, for a better controlled drug release at the wound site or for a better stability of the active ingredient. Natural and synthetic polymers with high biocompatibility which enable a localized drug delivery are desirable in the development of modern formulations.

In the future, ongoing research to validate the efficacy of the films through clinical studies and thus demonstrating their applicability on a large scale would be welcome.

Declaration of Competing Interest

The authors of "Review of advances in polymeric wound dressing films", Ioana Savencu, Sonia Iurian, Alina Porfire, Cătălina Bogdan, Ioan Tomuță declare that they have no known competing financial interests or personal relationships that could have appeared to influence the work reported in this paper.

References

[1] K.C. Broussard, J.G. Powers, Wound dressings: selecting the Most appropriate type, Am. J. Clin. Dermatol. 14 (6) (2013) 449–459, https://doi.org/10.1007/s40257-013-0046-4.

[2] J. Koehler, F.P. Brandl, A.M. Goepferich, Hydrogel wound dressings for bioactive treatment of acute and chronic wounds, Eur. Polym. J. 100 (2018) 1–11, https://doi.org/10.1016/j.eurpolymj.2017.12.046.

[3] A. Shah, M. Ali Buabeid, E.-S.A. Arafa, I. Hussain, L. Li, G. Murtaza, The wound healing and antibacterial potential of triple-component nanocomposite (chitosan-silver-sericin) films loaded with moxifloxacin, Int. J. Pharm. 564 (2019) 22–38, https://doi.org/10.1016/j.ijpharm.2019.04.046.

[4] F. Hafezi, N. Scoutaris, D. Douroumis, J. Boateng, 3D printed chitosan dressing crosslinked with genipin for potential healing of chronic wounds, Int. J. Pharm. 560 (2019) 406–415, https://doi.org/10.1016/j.ijpharm.2019.02.020.

[5] R.J. Gomes Neto, G.M. Genevro, L.D.A. Paulo, P.S. Lopes, M.A. de Moraes, M. M. Beppu, Characterization and in vitro evaluation of chitosan/konjac glucomannan bilayer film as a wound dressing, Carbohyd. Polym. 212 (2019) 59–66, https://doi.org/10.1016/j.carbpol.2019.02.017.

[6] A. Eskandarinia, A. Kefayat, M. Rafienia, M. Agheb, S. Navid, K. Ebrahimpour, Cornstarch-based wound dressing incorporated with hyaluronic acid and propolis: in vitro and in vivo studies, Carbohyd. Polym. 216 (2019) 25–35, https://doi.org/10.1016/j.carbpol.2019.03.091.

[7] R. Arthe, D. Arivuoli, V. Ravi, Preparation and characterization of bioactive silk fibroin/paramylon blend films for chronic wound healing, Int. J. Biol. Macromol. 154 (2020) 1324–1331, https://doi.org/10.1016/j.ijbiomac.2019.11.010.

[8] N.N. Costa, L. de Faria Lopes, D.F. Ferreira, E.M.L. de Prado, J.A. Severi, J. A. Resende, F. de Paula Careta, M.C.P. Ferreira, L.G. Carreira, S.O.L. de Souza, M.A. P. Cotrim, T. Boeing, S.F. de Andrade, R.L. Oréfice, J.C.O. Villanova, Polymeric films containing pomegranate peel extract based on PVA/starch/PAA blends for use as wound dressing: in vitro analysis and physicochemical evaluation, Mat. Sci. Eng. C. 109 (2020) 110643, https://doi.org/10.1016/j.msec.2020.110643.

[9] C.D. Weller, V. Team, G. Sussman, First-line interactive wound dressing update: a comprehensive review of the evidence, Front. Pharmacol. 11 (2020) 155, https://doi.org/10.1007/s40257-013-0046-410.3389/fphar.2020.00155.

[10] M. Naseri-Nosar, Z.M. Ziora, Wound dressings from naturally-occurring polymers: a review on homopolysaccharide-based composites, Carbohyd. Polym. 189 (2018) 379–398, https://doi.org/10.1016/j.carbpol.2018.02.003.

[11] D. Simões, S.P. Miguel, M.P. Ribeiro, P. Coutinho, A.G. Mendonça, I.J. Correia, Recent advances on antimicrobial wound dressing: a review, Eur. J. Pharm. Biopharm. 127 (2018) 130–141, https://doi.org/10.1016/j.ejpb.2018.02.022.

[12] A. Gaspar-Pintiliescu, A.-M. Stanciuc, O. Craciunescu, Natural composite dressings based on collagen, gelatin and plant bioactive compounds for wound healing: a review, Int. J. Biol. Macromol. 138 (2019) 854–865, https://doi.org/10.1016/j.ijbiomac.2019.07.155.

[13] I. Silvestro, M. Lopreiato, A. Scotto d'Abusco, V. Di Lisio, A. Martinelli, A. Piozzi, I. Francolini, Hyaluronic acid reduces bacterial fouling and promotes Fibroblasts' adhesion onto chitosan 2D-wound dressings, Int. J. Mol. Sci. 21 (6) (2020) 2070, https://doi.org/10.1007/s40257-013-0046-410.3390/ijms21062070.

[14] J.O. Kim, J.-K. Noh, R.K. Thapa, N. Hasan, M. Choi, J.H. Kim, J.-H. Lee, S.K. Ku, J.-W. Yoo, Nitric oxide-releasing chitosan film for enhanced antibacterial and in vivo wound-healing efficacy, Int. J. Biol. Macromol. 79 (2015) 217–225, https://doi.org/10.1016/j.ijbiomac.2015.04.073.

[15] M. Palo, S. Rönkönharju, K. Tiirik, L. Viidik, N. Sandler, K. Kogermann, Bi-layered polymer carriers with surface modification by electrospinning for potential wound care applications, Pharmaceutics 11 (12, 2019) 678, https://doi.org/10.1007/s40257-013-0046-410.3390/pharmaceutics11120678.

[16] K. Shanmugapriya, H. Kim, P.S. Saravana, B.-S. Chun, H.W. Kang, Fabrication of multifunctional chitosan-based nanocomposite film with rapid healing and antibacterial effect for wound management, Int. J. Biol. Macromol. 118 (2018) 1713–1725, https://doi.org/10.1016/j.ijbiomac.2018.07.018.

[17] B. Layek, S.S. Rahman Nirzhor, S. Rathi, K.K. Kandimalla, T.S. Wiedmann, S. Prabha, Design, development, and characterization of Imiquimod-loaded chitosan films for topical delivery, AAPS PharmSciTech 20 (2) (2019) 58, https://doi.org/10.1208/s12249-018-1288-5.

[18] L. Ai, Y. Wang, G. Tao, P. Zhao, A. Umar, P. Wang, H. He, Polydopamine-based surface modification of ZnO nanoparticles on Sericin/polyvinyl alcohol composite film for antibacterial application, Molecules 24 (3) (2019) 503, https://doi.org/10.3390/molecules24030503.

[19] A. Das, R. Uppaluri, C. Das, Feasibility of poly-vinyl alcohol/starch/glycerol/citric acid composite films for wound dressing applications, Int. J. Biol. Macromol. 131 (2019) 998–1007, https://doi.org/10.1016/j.ijbiomac.2019.03.160.

[20] N.A. Ismail, K.A.M. Amin, F.A.A. Majid, M.H. Razali, Gellan gum incorporating titanium dioxide nanoparticles biofilm as wound dressing: physicochemical, mechanical, antibacterial properties and wound healing studies, Mat. Sci. Eng. C. 103 (2019) 109770, https://doi.org/10.1016/j.msec.2019.109770.

[21] A. Amalraj, J.T. Haponiuk, S. Thomas, S. Gopi, Preparation, characterization and antimicrobial activity of polyvinyl alcohol/gum arabic/chitosan composite films incorporated with black pepper essential oil and ginger essential oil, Int. J. Biol. Macromol. 151 (2020) 366–375, https://doi.org/10.1016/j.ijbiomac.2020.02.176.

[22] P. Hubner, N. Donati, L.K.D.M. Quines, I.C. Tessaro, N.R. Marcilio, Gelatin-based films containing clinoptilolite-Ag for application as wound dressing, Mat. Sci. Eng. C 107 (2020) 110215, https://doi.org/10.1016/j.msec.2019.110215.

[23] T. Alavi, M. Rezvanian, N. Ahmad, N. Mohamad, S.-F. Ng, Pluronic-F127 composite film loaded with erythromycin for wound application: formulation, physicomechanical and in vitro evaluations, Drug. Deliv. Transl. Re. 9 (2) (2019) 508–519, https://doi.org/10.1007/s13346-017-0450-z.

[24] H. Türe, Characterization of hydroxyapatite-containing alginate–gelatin composite films as a potential wound dressing, Int. J. Biol. Macromol. 123 (2019) 878–888, https://doi.org/10.1016/j.ijbiomac.2018.11.143.

[25] L. Tang, L. Zhu, F. Tang, C. Yao, J. Wang, L. Li, Mild synthesis of copper nanoparticles with enhanced oxidative stability and their application in antibacterial films, Langmuir 34 (48) (2018) 14570–14576, https://doi.org/10.1021/acs.langmuir.8b02470.

[26] N. Sakthiguru, M.A. Sithique, Fabrication of bioinspired chitosan/gelatin/allantoin biocomposite film for wound dressing application, Int. J. Biol. Macromol. 152 (2020) 873–883, https://doi.org/10.1016/j.ijbiomac.2020.02.289.

[27] C. Kimna, S. Tamburaci, F. Tihminlioglu, Novel zein-based multilayer wound dressing membranes with controlled release of gentamicin, J. Biomed. Mater. Res. B. 107 (6) (2019) 2057–2070, https://doi.org/10.1002/jbm.b.34298.

[28] X. Mi, H. Xu, Y. Yang, Submicron amino acid particles reinforced 100% keratin biomedical films with enhanced wet properties via interfacial strengthening, Colloid. Surface. B. 177 (2019) 33–40, https://doi.org/10.1016/j.colsurfb.2019.01.043.

[29] N. Ahmad, D. Tayyeb, I. Ali, N.K. Alruwaili, W. Ahmad, A. Ur Rehman, A.H. Khan, M.S. Iqbal, Development and characterization of hemicellulose-based films for antibacterial wound-dressing application, Polymers (Basel) 12 (3) (2020) 548, https://doi.org/10.3390/polym12030548.

[30] J. Tessmar, T. Holland, A. Mikos, Salt Leaching for Polymer Scaffolds, in: J.E.P. X. Ma (Ed.), Scaffolding In Tissue Engineering, CRC Press, 2005, pp. 111–124, https://doi.org/10.1201/9781420027563.pt2.

[31] Z. Draczynski, B. Kolesinska, I. Latanska, W. Sujka, Preparation method of porous dressing materials based on butyric-acetic chitin co-polyesters, Materials 11 (12) (2018), https://doi.org/10.3390/ma11122359.

[32] P. Aramwit, J. Ratanavaraporn, S. Ekgasit, D. Tongsakul, N. Bang, A green salt-leaching technique to produce sericin/PVA/glycerin scaffolds with distinguished characteristics for wound-dressing applications, J. Biomed. Mater. Res. B. 103 (4) (2015) 915–924, https://doi.org/10.1002/jbm.b.33264.

[33] R. Poonguzhali, S. Khaleel Basha, V. Sugantha Kumari, Fabrication of asymmetric nanostarch reinforced chitosan/PVP membrane and its evaluation as an antibacterial patch for in vivo wound healing application, Int. J. Biol. Macromol. 114 (2018) 204–213, https://doi.org/10.1016/j.ijbiomac.2018.03.092.

[34] J. Orava, T. Kohoutek, T. Wagner, 9 - deposition techniques for chalcogenide thin films, in: J.-L. Adam, X. Zhang (Eds.), Chalcogenide Glasses, Woodhead Publishing, Oxford, 2014, pp. 265–309, https://doi.org/10.1533/9780857093561.1.265.

[35] N.-T. Nguyen, Chapter 4 - fabrication technologies, in: N.-T. Nguyen (Ed.), Micromixers (Second Edition), William Andrew Publishing, Oxford, 2012, pp. 113–161, https://doi.org/10.1016/B978-1-4377-3520-8.00004-8.

[36] R. Smith, H. Inomata, C. Peters, Chapter 4 - historical background and applications, in: R. Smith, H. Inomata, C. Peters (Eds.), Supercritical Fluid Science and Technology, Elsevier, Oxford, 2013, pp. 175–273, https://doi.org/10.1016/B978-0-444-52215-3.00004-0.

[37] Y. Huang, N. Dan, W. Dan, W. Zhao, Reinforcement of Polycaprolactone/chitosan with Nanoclay and controlled release of Curcumin for wound dressing, ACS Omega 4 (27, 2019) 22292–22301, https://doi.org/10.1021/acsomega.9b02217.
[38] Y. Huang, N. Dan, W. Dan, W. Zhao, Z. Bai, Y. Chen, C. Yang, Facile fabrication of gelatin and polycaprolactone based bilayered membranes via spin coating method with antibacterial and cyto-compatible properties, Int. J. Biol. Macromol. 124 (2019) 699–707, https://doi.org/10.1016/j.ijbiomac.2018.11.262.
[39] J. Cheng, Y. Jun, J. Qin, S.-H. Lee, Electrospinning versus microfluidic spinning of functional fibers for biomedical applications, Biomaterials 114 (2017) 121–143, https://doi.org/10.1016/j.biomaterials.2016.10.040.
[40] Y. Jun, E. Kang, S. Chae, S.-H. Lee, Microfluidic spinning of micro- and nano-scale fibers for tissue engineering, Lab. Chip 14 (2014), https://doi.org/10.1039/c3lc51414e.
[41] Y. Ni, W. Lin, R. Mu, C. Wu, Z. Lin, S. Chen, J. Pang, Facile fabrication of novel konjac glucomannan films with antibacterial properties via microfluidic spinning strategy, Carbohyd. Polym. 208 (2019) 469–476, https://doi.org/10.1016/j.carbpol.2018.12.102.
[42] E.G. Andriotis, G.K. Eleftheriadis, C. Karavasili, D.G. Fatouros, Development of bioactive patches based on pectin for the treatment of ulcers and wounds using 3D-bioprinting technology, Pharmaceutics 12 (1) (2020), https://doi.org/10.3390/pharmaceutics12010056.
[43] Z. Muwaffak, A. Goyanes, V. Clark, A.W. Basit, S.T. Hilton, S. Gaisford, Patient-specific 3D scanned and 3D printed antimicrobial polycaprolactone wound dressings, Int. J. Pharm. 527 (1) (2017) 161–170, https://doi.org/10.1016/j.ijpharm.2017.04.077.
[44] E. Pereira Dos Santos, P.H.M. Nicácio, F. Coêlho Barbosa, H. Nunes da Silva, A.L. S. Andrade, M.V. Lia Fook, S.M. de Lima Silva, I. Farias Leite, Chitosan/essential oils formulations for potential use as wound dressing: physical and antimicrobial properties, Materials (Basel) 12 (14, 2019) 2223, https://doi.org/10.3390/ma12142223.
[45] ASTM D882– - 18, Standard Test Method for Tensile Properties of Thin Plastic Sheeting. https://www.astm.org/, 2018 (Accessed January, 20 2021).
[46] A.B. Nair, R. Kumria, S. Harsha, M. Attimarad, B.E. Al-Dhubiab, I.A. Alhaider, In vitro techniques to evaluate buccal films, J. Control. Release 166 (1) (2013) 10–21, https://doi.org/10.1016/j.jconrel.2012.11.019.
[47] P. Wang, H. He, R. Cai, G. Tao, M. Yang, H. Zuo, A. Umar, Y. Wang, Cross-linking of dialdehyde carboxymethyl cellulose with silk sericin to reinforce sericin film for potential biomedical application, Carbohyd. Polym. 212 (2019) 403–411, https://doi.org/10.1016/j.carbpol.2019.02.069.
[48] Y. Duan, K. Li, H. Wang, T. Wu, Y. Zhao, H. Li, H. Tang, W. Yang, Preparation and evaluation of curcumin grafted hyaluronic acid modified pullulan polymers as a functional wound dressing material, Carbohyd. Polym. 238 (2020) 116195, https://doi.org/10.1016/j.carbpol.2020.116195.
[49] C. Appendix, Contact angle goniometry, in: R. Förch, H. Schönherr, A.T.A. Jenkins (Eds.), Surface Design: Applications in Bioscience and Nanotechnology, 2009, pp. 471–473, https://doi.org/10.1002/9783527628599.app3.
[50] L. Liu, R. Cai, Y. Wang, G. Tao, L. Ai, P. Wang, M. Yang, H. Zuo, P. Zhao, H. He, Polydopamine-assisted silver nanoparticle self-assembly on Sericin/agar film for potential wound dressing application, Int. J. Mol. Sci. 19 (10, 2018) 2875, https://doi.org/10.3390/ijms19102875.
[51] ASTM E96 / E96M - 16, Standard Test Methods for Water Vapor Transmission of Materials. https://www.astm.org/, 2016 (Accessed January, 16 2021).
[52] J.P. Patel, P.H. Parsania, 3 - characterization, testing, and reinforcing materials of biodegradable composites, in: N.G. Shimpi (Ed.), Biodegradable and Biocompatible Polymer Composites, Woodhead Publishing, Oxford, 2018, pp. 55–79, https://doi.org/10.1016/B978-0-08-100970-3.00003-1.
[53] S. Swapp, Scanning Electron Microscopy (SEM). https://serc.carleton.edu/research_education/geochemsheets/techniques/SEM.html (Accessed December, 10 2020).
[54] M.C. García, A.A. Aldana, L.I. Tártara, F. Alovero, M.C. Strumia, R.H. Manzo, M. Martinelli, A.F. Jimenez-Kairuz, Bioadhesive and biocompatible films as wound dressing materials based on a novel dendronized chitosan loaded with ciprofloxacin, Carbohyd. Polym. 175 (2017) 75–86, https://doi.org/10.1016/j.carbpol.2017.07.053.
[55] M.L. Cacicedo, G. Pacheco, G.A. Islan, V.A. Alvarez, H.S. Barud, G.R. Castro, Chitosan-bacterial cellulose patch of ciprofloxacin for wound dressing: preparation and characterization studies, Int. J. Biol. Macromol. 147 (2020) 1136–1145, https://doi.org/10.1016/j.ijbiomac.2019.10.082.
[56] X. Zhang, Z. Chen, H. Bao, J. Liang, S. Xu, G. Cheng, Y. Zhu, Fabrication and characterization of silk fibroin/Curcumin sustained-release film, Materials 12 (20) (2019), https://doi.org/10.3390/ma12203340.
[57] P. Hissae Yassue-Cordeiro, C. Henrique Zandonai, B. Pereira Genesi, P. Santos Lopes, E. Sanchez-Lopez, M. Luisa Garcia, N. Regina Camargo Fernandes-Machado, P. Severino, E.B. Souto, C. Ferreira da Silva, Development of chitosan/silver sulfadiazine/zeolite composite films for wound dressing, Pharmaceutics 11 (10) (2019), https://doi.org/10.3390/pharmaceutics11100535.
[58] A. Abednejad, A. Ghaee, J. Nourmohammadi, A.A. Mehrizi, Hyaluronic acid/carboxylated Zeolitic Imidazolate framework film with improved mechanical and antibacterial properties, Carbohyd. Polym. 222 (2019) 115033, https://doi.org/10.1016/j.carbpol.2019.115033.
[59] N. Akhavan-Kharazian, H. Izadi-Vasafi, Preparation and characterization of chitosan/gelatin/nanocrystalline cellulose/calcium peroxide films for potential wound dressing applications, Int. J. Biol. Macromol. 133 (2019) 881–891, https://doi.org/10.1016/j.ijbiomac.2019.04.159.
[60] S. Chen, H. Wang, Z. Jian, G. Fei, W. Qian, G. Luo, Z. Wang, H. Xia, Novel poly (vinyl alcohol)/chitosan/modified Graphene oxide biocomposite for wound dressing application, Macromol. Biosci. 20 (3) (2020) 1900385, https://doi.org/10.1002/mabi.201900385.
[61] Merck, Protocol Guide: MTT Assay for Cell Viability and Proliferation. https://www.sigmaaldrich.com/technical-documents/protocols/biology/roche/cell-proliferation-kit-i-mtt.html, 2020 (Accessed December, 02 2020).
[62] M. Rahimi, R. Ahmadi, H. Samadi Kafil, V. Shafiei-Irannejad, A novel bioactive quaternized chitosan and its silver-containing nanocomposites as a potent antimicrobial wound dressing: structural and biological properties, Mat. Sci. Eng. C. 101 (2019) 360–369, https://doi.org/10.1016/j.msec.2019.03.092.
[63] A. Mazloom-Jalali, Z. Shariatinia, I.A. Tamai, S.-R. Pakzad, J. Malakootikhah, Fabrication of chitosan–polyethylene glycol nanocomposite films containing ZIF-8 nanoparticles for application as wound dressing materials, Int. J. Biol. Macromol. 153 (2020) 421–432, https://doi.org/10.1016/j.ijbiomac.2020.03.033.
[64] X. Li, M. Ma, D.U. Ahn, X. Huang, Preparation and characterization of novel eggshell membrane-chitosan blend films for potential wound-care dressing: from waste to medicinal products, Int. J. Biol. Macromol. 123 (2019) 477–484, https://doi.org/10.1016/j.ijbiomac.2018.10.215.
[65] A. Das, S. Bhattacharyya, R. Uppaluri, C. Das, Optimality of poly-vinyl alcohol/starch/glycerol/citric acid in wound dressing applicable composite films, Int. J. Biol. Macromol. 155 (2020) 260–272, https://doi.org/10.1016/j.ijbiomac.2020.03.185.
[66] T. Jayaramudu, K. Varaprasad, R.D. Pyarasani, K.K. Reddy, K.D. Kumar, A. Akbari-Fakhrabadi, R.V. Mangalaraja, J. Amalraj, Chitosan capped copper oxide/copper nanoparticles encapsulated microbial resistant nanocomposite films, Int. J. Biol. Macromol. 128 (2019) 499–508, https://doi.org/10.1016/j.ijbiomac.2019.01.145.
[67] M.F.P. Graça, S.P. Miguel, C.S.D. Cabral, I.J. Correia, Hyaluronic acid—based wound dressings: a review, Carbohyd. Polym. 241 (2020) 116364, https://doi.org/10.1016/j.carbpol.2020.116364.
[68] K. Numata, D.L. Kaplan, 20 - biologically derived scaffolds, in: D. Farrar (Ed.), Advanced Wound Repair Therapies, Woodhead Publishing, Oxford, 2011, pp. 524–551, https://doi.org/10.1533/9780857093301.4.524.
[69] K.R. Millington, J.A. Rippon, 14 - wool as a high-performance fiber, in: G. Bhat (Ed.), Structure and Properties of High-Performance Fibers, Woodhead Publishing, Oxford, 2017, pp. 367–408, https://doi.org/10.1016/B978-0-08-100550-7.00014-0.
[70] B. Kaczmarek, K. Nadolna, A. Owczarek, Chapter 6 - the physical and chemical properties of hydrogels based on natural polymers, in: Y. Chen (Ed.), Hydrogels Based on Natural Polymers, Elsevier, Oxford, 2020, pp. 151–172, https://doi.org/10.1016/B978-0-12-816421-1.00006-9.
[71] S.S. Silva, E.M. Fernandes, S. Pina, J. Silva-Correia, S. Vieira, J.M. Oliveira, R. L. Reis, 2.11 polymers of biological origin☆, in: P. Ducheyne (Ed.), Comprehensive Biomaterials II, Elsevier, Oxford, 2017, pp. 228–252, https://doi.org/10.1016/B978-0-12-803581-8.10134-1.
[72] Y. Zhang, A. Atala, Chapter 72 - regenerative medicine of the bladder, in: A. Atala, R. Lanza, A.G. Mikos, R. Nerem (Eds.), Principles of Regenerative Medicine (Third Edition), Academic Press, Boston, 2019, pp. 1263–1279, https://doi.org/10.1016/B978-0-12-809880-6.00072-2.
[73] P.P. Patil, R.A. Bohara, J.V. Meshram, S.G. Nanaware, S.H. Pawar, Hybrid chitosan-ZnO nanoparticles coated with a sonochemical technique on silk fibroin-PVA composite film: a synergistic antibacterial activity, Int. J. Biol. Macromol. 122 (2019) 1305–1312, https://doi.org/10.1016/j.ijbiomac.2018.09.090.
[74] T. Hashimoto, K. Kojima, Y. Tamada, Higher gene expression related to wound healing by fibroblasts on silk fibroin biomaterial than on collagen, Molecules 25 (8) (2020) 1939, https://doi.org/10.3390/molecules25081939.
[75] U. Dashdorj, M.K. Reyes, A.R. Unnithan, A.P. Tiwari, B. Tumurbaatar, C.H. Park, C. S. Kim, Fabrication and characterization of electrospun zein/Ag nanocomposite mats for wound dressing applications, Int. J. Biol. Macromol. 80 (2015) 1–7, https://doi.org/10.1016/j.ijbiomac.2015.06.026.
[76] L.A. Loureiro dos Santos, Natural Polymeric Biomaterials: Processing and Properties☆, Reference Module in Materials Science and Materials Engineering, Elsevier, Oxford, 2017, https://doi.org/10.1016/B978-0-12-803581-8.02253-0.
[77] S. Maiti, L. Kumari, 3 - smart Nanopolysaccharides for the delivery of bioactives, in: A.M. Holban, A.M. Grumezescu (Eds.), Nanoarchitectonics for Smart Delivery and Drug Targeting, William Andrew Publishing, Oxford, 2016, pp. 67–94, https://doi.org/10.1016/B978-0-323-47347-7.00003-3.
[78] A. Mohebali, M. Abdouss, F. Afshar Taromi, Fabrication of biocompatible antibacterial nanowafers based on HNT/PVA nanocomposites loaded with minocycline for burn wound dressing, Mat. Sci. Eng. C. 110 (2020) 110685, https://doi.org/10.1016/j.msec.2020.110685.
[79] V. Soni, V. Pandey, R. Tiwari, S. Asati, R.K. Tekade, Chapter 13 - design and evaluation of ophthalmic delivery formulations, in: R.K. Tekade (Ed.), Basic Fundamentals of Drug Delivery, Academic Press, Boston, 2019, pp. 473–538, https://doi.org/10.1016/B978-0-12-817909-3.00013-3.
[80] G.C. Ritthidej, Chapter 3 - nasal delivery of peptides and proteins with chitosan and related Mucoadhesive polymers, in: C. Van Der Walle (Ed.), Peptide and Protein Delivery, Academic Press, Boston, 2011, pp. 47–68, https://doi.org/10.1016/B978-0-12-384935-9.10003-3.
[81] L.W. McKeen, 13 - environmentally friendly polymers, in: L.W. McKeen (Ed.), Permeability Properties of Plastics and Elastomers (Third Edition), William Andrew Publishing, Oxford, 2012, pp. 287–304, https://doi.org/10.1016/B978-1-4377-3469-0.10013-X.
[82] Chapter 18 - Application of compatibilized polymer blends in biomedical fields, in: P. Zarrintaj, M.R. Saeb, S.H. Jafari, M. Mozafari, S. Thomas (Eds.), Compatibilization of Polymer Blends, Elsevier, Oxford, 2020, pp. 511–537, https://doi.org/10.1016/B978-0-12-816006-0.00018-9.

[83] H. Bardania, R. Mahmoudi, H. Bagheri, Z. Salehpour, M.H. Fouani, B. Darabian, S. S. Khoramrooz, A. Mousavizadeh, M. Kowsari, S.E. Moosavifard, G. Christiansen, D. Javeshghani, M. Alipour, M. Akrami, Facile preparation of a novel biogenic silver-loaded Nanofilm with intrinsic anti-bacterial and oxidant scavenging activities for wound healing, Sci. Rep-Uk. 10 (1) (2020) 6129, https://doi.org/10.1038/s41598-020-63032-5.

[84] M.Y. Kariduraganavar, A.A. Kittur, R.R. Kamble, Chapter 1 - polymer synthesis and processing, in: S.G. Kumbar, C.T. Laurencin, M. Deng (Eds.), Natural and Synthetic Biomedical Polymers, Elsevier, Oxford, 2014, pp. 1–31, https://doi.org/10.1016/B978-0-12-396983-5.00001-6.

[85] K. Deshmukh, M. Basheer Ahamed, R.R. Deshmukh, S.K. Khadheer Pasha, P. R. Bhagat, K. Chidambaram, 3 - biopolymer composites with high dielectric performance: Interface engineering, in: K.K. Sadasivuni, D. Ponnamma, J. Kim, J. J. Cabibihan, M.A. AlMaadeed (Eds.), Biopolymer Composites in Electronics, Elsevier, Oxford, 2017, pp. 27–128, https://doi.org/10.1016/B978-0-12-809261-3.00003-6.

[86] Chapter 15 - Plasma Modified Polymeric Materials for Biosensors/Biodevice Applications, in: L. Jothi, G. Nageswaran, S. Thomas, M. Mozetič, U. Cvelbar, P. Špatenka (Eds.), Non-Thermal Plasma Technology for Polymeric Materials, Elsevier, Oxford, 2019, pp. 409–437, https://doi.org/10.1016/B978-0-12-813152-7.00015-9.

[87] S. Wei, Y. You, Y. Ma, W. Huang, X. Liang, A. Zhang, Y. Lin, Bi-layer supramolecular polydimethylsiloxane elastomer film: synthesis, characterization, and application in wound dressing on normal and diabetic rat, React. Funct. Polym. 141 (2019) 21–32, https://doi.org/10.1016/j.reactfunctpolym.2019.05.002.

[88] C. Fernandes, P.C. Acharya, S. Bhatt, Preparation of Lauroyl grafted alginate-Psyllium husk gel composite film with enhanced physicochemical, mechanical and antimicrobial properties, Sci. Rep-Uk. 8 (1) (2018) 17213, https://doi.org/10.1038/s41598-018-35632-9.

[89] J. Lamarra, P. Bucci, L. Giannuzzi, J. Montanari, S. Rivero, A. Pinotti, Biomaterial-based dressings as vehicle for chitosan-encapsulated cabreuva essential oil: cytotoxicity and regenerative activity, React. Funct. Polym. 156 (2020) 104728, https://doi.org/10.1016/j.reactfunctpolym.2020.104728.

[90] L. Colobatiu, A. Gavan, A. Mocan, C. Bogdan, S. Mirel, I. Tomuta, Development of bioactive compounds-loaded chitosan films by using a QbD approach – a novel and potential wound dressing material, React. Funct. Polym. 138 (2019) 46–54, https://doi.org/10.1016/j.reactfunctpolym.2019.02.013.

[91] L. Colobatiu, A. Gavan, A.-V. Potarniche, V. Rus, Z. Diaconeasa, A. Mocan, I. Tomuta, S. Mirel, M. Mihaiu, Evaluation of bioactive compounds-loaded chitosan films as a novel and potential diabetic wound dressing material, React. Funct. Polym. 145 (2019) 104369, https://doi.org/10.1016/j.reactfunctpolym.2019.104369.

[92] M. Choi, N. Hasan, J. Cao, J. Lee, S.P. Hlaing, J.-W. Yoo, Chitosan-based nitric oxide-releasing dressing for anti-biofilm and in vivo healing activities in MRSA biofilm-infected wounds, Int. J. Biol. Macromol. 142 (2020) 680–692, https://doi.org/10.1016/j.ijbiomac.2019.10.009.

[93] S. Saghazadeh, C. Rinoldi, M. Schot, S.S. Kashaf, F. Sharifi, E. Jalilian, K. Nuutila, G. Giatsidis, P. Mostafalu, H. Derakhshandeh, K. Yue, W. Swieszkowski, A. Memic, A. Tamayol, A. Khademhosseini, Drug delivery systems and materials for wound healing applications, Adv. Drug. Deliver. Rev. 127 (2018) 138–166, https://doi.org/10.1016/j.addr.2018.04.008.

[94] A. Shah, M.A. Yameen, N. Fatima, G. Murtaza, Chemical synthesis of chitosan/silver nanocomposites films loaded with moxifloxacin: their characterization and potential antibacterial activity, Int. J. Pharm. 561 (2019) 19–34, https://doi.org/10.1016/j.ijpharm.2019.02.029.

pharmaceutics

MDPI

Article

Milk Oral Lyophilizates with Loratadine: Screening for New Excipients for Pediatric Use

Sonia Iurian [1], Cătălina Bogdan [2,*], Ștefana Suciu [1], Dana-Maria Muntean [1], Lucia Rus [3], Mihaela Berindeie [1], Szidonia Bodi [1], Rita Ambrus [4,†] and Ioan Tomuță [1,†]

[1] Department of Pharmaceutical Technology and Biopharmacy, Faculty of Pharmacy, "Iuliu Haţieganu" University of Medicine and Pharmacy, 41 V. Babes Street, 400012 Cluj-Napoca, Romania; sonia.iurian@umfcluj.ro (S.I.); suciu.stefana@umfcluj.ro (Ș.S.); dana.muntean@umfcluj.ro (D.-M.M.); mihaelaberindeie95@gmail.com (M.B.); bodi_szidonia@yahoo.com (S.B.); tomutaioan@umfcluj.ro (I.T.)

[2] Department of Dermopharmacy and Cosmetics, Faculty of Pharmacy, "Iuliu Haţieganu" University of Medicine and Pharmacy, 12 I. Creangă Street, 400010 Cluj-Napoca, Romania

[3] Department of Drug Analysis, Faculty of Pharmacy, "Iuliu Haţieganu" University of Medicine and Pharmacy, 6 Louis Pasteur Street, 400349 Cluj-Napoca, Romania; lucia.rus@umfcluj.ro

[4] Faculty of Pharmacy, Institute of Pharmaceutical Technology and Regulatory Affairs, University of Szeged, Eotvos u. 6, H-6720 Szeged, Hungary; ambrus.rita@szte.hu

* Correspondence: catalina.bogdan@umfcluj.ro

† These authors contributed equally to this work.

Abstract: The development of suitable formulations for the pediatric population remains a challenging field with great advances reported every year in terms of excipients and technology. When developing pediatric formulations, the acceptability of medicines represents a key element to consider. For this reason, milk can be a widely accepted excipient with taste-masking properties and supplementary advantages for drug solubility. In recent years, the orodispersible dosage forms have come onto the market as child-friendly formulations. The current study aimed to develop freeze-dried orodispersible dosage forms containing bovine milk or infant formulae as the main component. In the first stage, an exploratory study evaluated the mechanical properties of placebo milk formulations and the suitability of milk as a matrix-forming agent. As the appropriate mechanical strength to withstand manipulation was demonstrated, milk oral lyophilizates were loaded with a poorly soluble model API, loratadine. Hence, a D-optimal design was conducted to prepare milk lyophilizates with loratadine and to evaluate the effects of three factors (dose of loratadine, the lyophilizate size, and the type of milk) and their interactions. Finally, three formulations were prepared to confront the predictions of the DoE and further studied to thoroughly understand the observed effects. The experimental results showed the potential of milk in the development of oral lyophilizates loaded with different doses of suspended API.

Keywords: milk; freeze-dried orodispersible tablets; design of experiments; pediatric dosage form

Citation: Iurian, S.; Bogdan, C.; Suciu, Ș.; Muntean, D.M.; Rus, L.; Berindeie, M.; Bodi, S.; Ambrus, R.; Tomuță, I. Milk Oral Lyophilizates with Loratadine: Screening for New Excipients for Pediatric Use. *Pharmaceutics* **2022**, *14*, 1342. https://doi.org/10.3390/pharmaceutics14071342

Academic Editor: Nadia Passerini

Received: 23 May 2022
Accepted: 21 June 2022
Published: 24 June 2022

1. Introduction

In recent years, there has been an important effort toward developing optimal age-appropriate formulations. In the early 2000s, the high prevalence of off-label unauthorized drug product prescriptions in the pediatric population drew the attention of regulatory authorities. They noticed the scarcity of adequate medication tailored to the demands of each age group regarding the high diversity of this patient population, ranging from neonates to adolescents. Since then, global stakeholders, including academia, industry, and regulatory agencies, have worked together to fill the therapeutic gaps with the most adequate formulations based on the currently available technologies [1–3]. To facilitate the patient's compliance, it is important to consider those attributes affecting the accepta-

bility of the formulation, such as palatability, frequency of administration, or administration complexity[4]. The development of medicines for the pediatric population is particularly challenging. Emphasis is placed upon technologies and dosage forms intended to improve current formulations in terms of ease of administration, patient compliance, and safety profile [5,6]. In this context, orodispersible dosage forms have reached the pharmaceutical market due to their easy administration that overcomes swallowing difficulties and emerged as dosage forms that fit the needs of special groups of patients, such as the elderly and children [7]. They showed important benefits over the traditional dosage forms in terms of patient preference and acceptability [8]. Among those, the oral lyophilizates (OLs) obtained by freeze drying drug solutions or suspensions display light structures that disintegrate rapidly in the oral cavity, obtained with a small number of excipients but with high frailty that often impairs manipulation [9]. In the preparation of OLs, the two essential classes of excipients that determine the strength and stability of the structures are the fillers and the matrix-forming agents. Fillers, such as mannitol, glucose, trehalose, or lactose, were reported to give satisfactory results in terms of strength and disintegration [10], as well as polymeric matrix-forming agents, such as methylcellulose, xanthan gum, polyvinyl acetate [9,11,12], gelatin, and amino acids [13,14]. Furthermore, the suitable selection of the filler is correlated with the mouthfeel attributes [15]. When the pediatric population is targeted, a rigorous, benefit vs. risk approach is advised for the selection of excipients, and researchers have started looking for excipients with improved safety and acceptability profile [4]. Out of all the foods, milk is the most widely accepted by children, and its use as a liquid for drug administration has already been confirmed [16]. Rich in carbohydrates, proteins, and fats, stabilized in the form of a complex solution–emulsion–suspension system, it has been studied as an excipient, while its constituents (e.g., casein) as drug delivery systems. The increased tolerance and acceptability, the pleasant taste, the high availability, and the low associated costs recommend it as useful in the preparation of medicines. Milk from various sources has already been tested; bovine milk has been used as such in liquid formulations [17–19], freeze-dried [20], spray-dried milk [21,22], and infant formulae [5,20,23] for solid dosage forms, with important benefits for drug solubility. As manufacturing technologies, direct compression was used to transform powdered milk into tablets, dispersible tablets, or minitablets [5,20,23] and spray drying of API milk dispersions for the preparation of powders [21,22], with promising results, especially when associated with traditional excipients. A recent literature review focused on milk formulations highlighted how active substances can be incorporated into milk constituents and the further impact on solubility and bioavailability [24]. As far as the stability of such systems is concerned, freeze drying was reported to be the method that best preserves the properties of milk [25]. Lal and coworkers described the preparation of OLs loaded with two antiretrovirals containing 8.8% of dry milk in association with mannitol, carboxymethyl cellulose, and Tween 80 [2]. However, information on the contribution of milk to the formation of the porous structure, to the disintegration of the solid form, and to the dissolution of the active substances in OLs is limited. Up to this point, to the best of the authors' knowledge, no work has been published on the potential of milk as the main excipient in the preparation of OLs.

The main questions that this study aims to answer are whether lyophilized milk could be a sufficiently resistant matrix to handle and whether it could incorporate suspended insoluble active ingredients. Among the secondary objectives of the study were evaluating the influence of the type of milk on the critical quality characteristics of the dosage forms, the impact of the dose of active pharmaceutical (API) ingredient on the lyophilized structure, and that of the alveolae volume or the lyophilizate size on the previously mentioned characteristics. The choice of API was based on the increased frequency of allergic manifestations in children frequently treated with loratadine, as a representative of the anti-H1 antihistamines listed in the WHO List of Essential Medicines for Children [26]. Loratadine is efficient in low doses, requires age-related dose adjustment,

and has low aqueous solubility, which makes it a good candidate to test the performance of milk freeze-dried cakes.

The study is divided into three parts, the preliminary part of which was meant to evaluate the mechanical properties of placebo milk formulations. Subsequently, based on the favorable results of the mechanical tests, lyophilizates loaded with loratadine as a model substance were prepared, according to a design of experiments in which the effects of three factors (dose of loratadine, the volume of the alveolae, or lyophilizate size and the type of milk) were studied. Finally, three formulations were prepared to confront the predictions of the design of experiments and were characterized for an in-depth understanding of the observed effects.

2. Materials and Methods

2.1. Materials

The active pharmaceutical ingredient (API) loratadine was purchased from Quimica Sintetica (Madrid, Spain). The types of milk coded L1 (skimmed milk, 1.5% fat) and L2 (full-fat milk, 3.5%) were locally produced by Albalact (Bucharest, Romania), while L3 (NAN A.R.) and L4 (NAN 1 Optipro) were infant formulae purchased from Nestle (Bucharest, Romania).

2.2. Preliminary Study to Investigate the Mechanical Properties of the Freeze-Dried Milk

Four types of milk, coded L1, L2, L3, and L4, with the composition described in Table 1, were included in the preliminary study that aimed to test whether milk could yield freeze-dried structures with mechanical profiles that allow easy and safe handling. L1 and L2 were used as such, while L3 and L4 were reconstituted following the recommendations of the producer. All four samples were poured into 0.2, 0.5, and 1 mL blister alveolae using an automatic pipette, submitted to freeze drying (see Section 2.3), and then evaluated for the mechanical profile (see Section 2.6.2).

Table 1. Milk composition as declared by the producers.

	L1	L2	L3	L4
Proteins (g/100mL)	3.1	3	1.27	1.2
Fat (g/100mL)	1.5	3.5	3.4	3.6
- Saturated fatty acids (g/100mL)	1	2.4	0.96	0.8
- Monounsaturated fatty acids (g/100mL)	n.s.	n.s.	-	1.8
- Polyunsaturated fatty acids (g/100mL)	n.s.	n.s.	-	0.6
Carbohydrates (g/100mL)	4.5	4.5	5.13	7.4

n.s., not specified.

2.3. Freeze Drying

The samples were subjected to a freeze-drying process (VirTis Advantage Plus, SP Scientific, Gardiner, NY, USA) consisting of a 12 h freezing stage at −55 °C, followed by 24 h primary drying at −25 °C and 150 mTorr, and 10 h secondary drying at 20 °C and 300 mTorr.

2.4. Design of Experiments

The DoE methodology is a statistical tool that allows the rational planning of experiments to cover as wide a study domain as possible [27]. The study was performed using a D-optimal screening experimental design, with three independent variables and three variation levels, developed using Modde 13 software (Sartorius Stedim, Umeå, Sweden). According to the DoE, 16 runs and 3 replicated center points were generated, as shown in Table 2.

Table 2. Design of experiments matrix.

Experiment Name	Run Order	Loratadine Dose (X1)	Alveolae Volume (X2)	Milk Type (X3)
N1	4	0	0.2	L1
N2	16	10	0.2	L1
N3	19	0	1	L1
N4	15	10	1	L1
N5	14	0	0.2	L2
N6	11	10	0.2	L2
N7	8	0	1	L2
N8	18	10	1	L2
N9	10	0	0.2	L3
N10	13	10	0.2	L3
N11	9	0	1	L3
N12	6	10	1	L3
N13	7	0	0.2	L4
N14	5	10	0.2	L4
N15	3	0	1	L4
N16	2	10	1	L4
N17	12	5	0.5	L4
N18	1	5	0.5	L4
N19	17	5	0.5	L4

The loratadine content was chosen as a quantitative factor (X1) and varied on three levels: 0–5–10 mg per OL. The suspension volume poured into each blister pocket was the second quantitative factor (X2) and varied between 0.2, 0.5, and 1 mL. Four types of milk were used as a qualitative factor (X3), which were encoded as L1 (1.5% fat), L2 (3.5% fat), L3, and L4, with compositions described in Table 1.

The selected responses entailed attributes related to a pharmaceutical product's quality, efficacy, and safety. They consisted of: disintegration time (Y1), mechanical properties (Y2—hardness; Y3—rigidity at 1 mm depth; Y4—fracturability), dissolution profile (Y5—% of dissolved loratadine after 5 mi; Y6—% of dissolved loratadine after 10 min), and particle size analysis (Y7—average particle size; Y8—PDI).

The same software (Modde 13, Sartorius Stedim, Sweden) was employed to model DoE data. In this sense, data processing, fitting, and statistical parameters calculation were performed, and the effects of the variables on the selected responses were graphically represented as coefficient histograms and response surfaces. The ANOVA test (variance analysis) was applied for all the responses to evaluate the validity of the experimental design. The model interpretation was carried out based on the regression equation coefficients. Their signs indicate the type of influence (negative or positive) they exerted on the response, while the absolute value shows the magnitude of the effect.

2.5. OLs Preparation

Placebo OLs were obtained by pouring 0.2, 0.5, or 1 mL of milk into the blister pockets according to the data presented in Table 2. For the OLs containing API, loratadine was suspended into the selected type of milk up to an amount of 5 mg/volume unit or 10 mg/volume unit. For each formulation, 30 mL suspension was obtained, and the exact volumes of 0.2, 0.5, or 1 mL were poured into 30 blister alveolae (3 blisters × 10 alveolae for each formulation). Immediately after the transfer into the blister alveolae, the samples were frozen at −80 °C to prevent API sedimentation.

2.6. OLs Pharmaceutical Characterization

2.6.1. Disintegration Time

The disintegration time was measured according to the method described in the *European Pharmacopoeia* [28]. Six samples from each formulation were placed in 200 mL distilled water and kept at 20 ± 5 °C; the necessary time to fully disintegrate was recorded using a digital stopwatch. The mean disintegration time (Y1) and standard deviation were calculated for each formulation.

2.6.2. Mechanical Characterization

Texture analysis is a common method of evaluating lyophilized matrices due to its ability to record small variations in the force or load required to penetrate the freeze-dried cake up to a given distance [29]. The characterization of the OLs' mechanical properties was performed by using a CT3 texture analyzer (Brookfield Engineering, Middleborough, MA, USA). For this purpose, a simple compression test was carried out by applying a load of 10 g and a speed of 0.10 mm/s to press the freeze-dried material until deformation of 2 mm for 0.2 mL OLs or 3 mm for 0.5 mL and 1 mL OLs was reached. The OLs` texture parameters describing the resistance of the sample to the applied pressure and the load vs. distance graphical curves were acquired with TextureProCT V 1.9 software. For each formulation, three OLs were tested, and the average and standard deviation were considered for the following parameters: hardness (Y2), rigidity (Y3), and fracturability (Y4).

2.6.3. In Vitro Dissolution

The in vitro dissolution study was performed in compliance with the method described in the *European Pharmacopoeia* [28], using the dissolution tester equipped with rotating paddles (Pharma Test PT-DT 7, PTWS100, Hainburg, Germany). The dissolution study was carried out in 900 mL phosphate buffer, pH 6.8, at a stirring rate of 50 rpm at 37 °C. Sampling was performed after 5, 10, 15, 20, 30, and 35 min, each redrawn sample being replaced with the same volume of fresh dissolution media. The dissolved API was quantified with an HPLC method; chromatographic separation was achieved on a Phenomenex Luna C18 column (150 × 4.6 × 5 mm), maintained at 30 °C; the mobile phase was H_3PO_4 0,1N: acetonitrile 60:40 (*v*/*v*). The flow rate was 1.5 m/min, and the injection volume was 50 µL. UV detection was performed at 250 nm [30]. The detected ratios of dissolved loratadine after 5 min (Y5) and 10 min (Y6) were included in the DoE. The mean values of the loratadine ratio and standard deviation were calculated out of three measurements.

2.6.4. Particle Size Analysis of the Reconstituted Samples

The average hydrodynamic diameter (Z-average) (Y7) and polydispersity index (PDI)(Y8) were measured with the dynamic light scattering (DLS) technique using a Malvern Zetasizer Nano ZS90 (Malvern Instruments, Worcestershire, UK). The reported results are the mean of three determinations and the standard deviation.

2.7. Contact Angle Measurements (Wetting Properties)

The determination of the polarity was performed by using Dataphysics OCA 20 analyzer (Dataphysics Inc. GmbH, Filderstadt, Germany). Briefly, 0.10 g of each sample was compressed at 1-ton compression force with the hydraulic press (Perkin Elmer, Waltham, MA, USA). Three pastilles per sample were analyzed by dripping the surface of the sample with distilled water and diiodomethane. The change of the contact angle (Θ) in a time interval of 1–25 s was measured, and the values of the contact angle were determined according to the following calculation: surface free energy (γ_s) consisting of a polar (γ_s^d) and a dispersed part (γ_s^p), therefore, $(\gamma_s = \gamma_s^d + \gamma_s^p)$. It was obtained from the Wu-equation:

$$(1 + \cos\Theta)\gamma_l = \frac{4(\gamma_s^d \gamma_l^d)}{\gamma_s^d + \gamma_l^d} + \frac{4(\gamma_s^p \gamma_l^p)}{\gamma_s^p + \gamma_l^p}$$

where Θ = contact angle; γ = surface free energy; s = solid phase; l = liquid phase; d = dispersion component; p = polar component, based on the values of the surface tension of the applied liquids, ($\gamma_l = \gamma_l^d + \gamma_l^p$), reported in the literature: γ^p = 50.2 mN/m, γ^d = 22.6 mN/m for distilled water and γ^p = 1.8 mN/m, γ^d = 49 mN/m for diiodomethane [31].

2.8. Solid-State Analysis

2.8.1. X-ray Powder Diffraction Analysis (XRPD)

XRPD was used to investigate the physical state of the API in the different stages of the preparation process (for LOR and the OLs). XRPD spectra were collected with a BRUKER D8 Advance X-ray diffractometer (Bruker AXS GmbH, Karlsruhe, Germany) system with Cu Ká1 radiation (ë = 1.5406 Ĺ) over the interval 5–30°/2. The experimental setup was the following: target, Cu; filter, Ni; voltage, 40 kV; current, 40 mA; time constant, 0.1 s; angular step, 0.010. The total area of the characteristic three peaks with the largest intensity was examined for the determination of the degree of crystallinity, after smoothing and background removal.

2.8.2. Fourier-Transform Infrared Spectroscopy (FT-IR)

FT-IR spectra of the OLs were obtained by using Fourier-transform infrared spectroscopy (Thermo Nicolet AVATAR 330, Thermo Electron, Waltham, MA, USA) equipped with a deuterated triglycine sulfate detector. The samples were ground with 150 mg potassium bromide, and the mean values of 128 co-added scans at a resolution of 4 cm^{-1} over 4000–400 cm^{-1} wavenumber region were collected and interpreted using the GRAMS/AI Version 7.00 software.

2.8.3. Scanning Electron Microscopy (SEM)

Scanning electron microscopy micrographs of the samples were acquired with Hitachi S4700 equipment (Hitachi Scientific Ltd., Tokyo, Japan) at an electric potential of 10 kV. The samples were coated with a sputter coater (Bio-Rad SC 502, VG Microtech, Uckfield, UK), and the OL's microstructure was investigated.

3. Results and Discussion

Milk has long been explored as an excipient for pediatric dosage forms, either in a dry state for solids preparation or as such for liquid dispersions. However, to the best of the authors' knowledge, its use as a multiple-function excipient for OL preparation is yet to be understood.

As one of the key issues in ensuring proper OL quality is overcoming the high friability, this study first focused on the selection of appropriate types of milk, which would grant the mechanical properties required for product transport, manipulation, and ejection from blister sockets without risking material loss, thus API dose inaccuracy.

3.1. Investigation of the Mechanical Properties of the Freeze-Dried Milk

The study's first phase was testing the feasibility of using milk as a lyophilized matrix. Oral lyophilizates are known for their high porosity, leading to increased friability and low handling resistance. Because the strength of a lyophilized matrix depends on the formulation but also its size, lyophilized products were obtained from the four types of milk (L1, L2, L3, and L4) poured into blister sockets with different volumes, then extracted from alveolae and subjected to a compression test. The mechanical characteristics of the freeze-dried milk samples expressed as load vs. time curves are shown in Figure 1. The profiles below show the load encountered by the probe when descending at a constant speed into the sample due to the compaction of the solid material. The increase in the load

with time, respectively, with the distance covered in the freeze-dried material is evident for all tested samples (Figure 1a–c). The depth of descent of the probe (displacement) was different depending on the product thickness correlated to the volume of the alveolae. For the products obtained in 0.2 mL alveolae, the displacement was 2 mm, while for thicker products obtained in 0.5 mL, respectively, 1 mL alveolae, the displacement was set to 3 mm. This explains the different profile lengths shown in Figure 1a compared to those in Figure 1b,c. The profiles also show sudden drops of load due to the fractures of the pore walls, which can be regarded as indicators of the brittleness of the structure [29]. The total hardness of the sample is estimated to be the maximum load reached during a compression cycle, and the highest hardness was reached for lyophilizates with volumes of 0.5 mL and 1 mL.

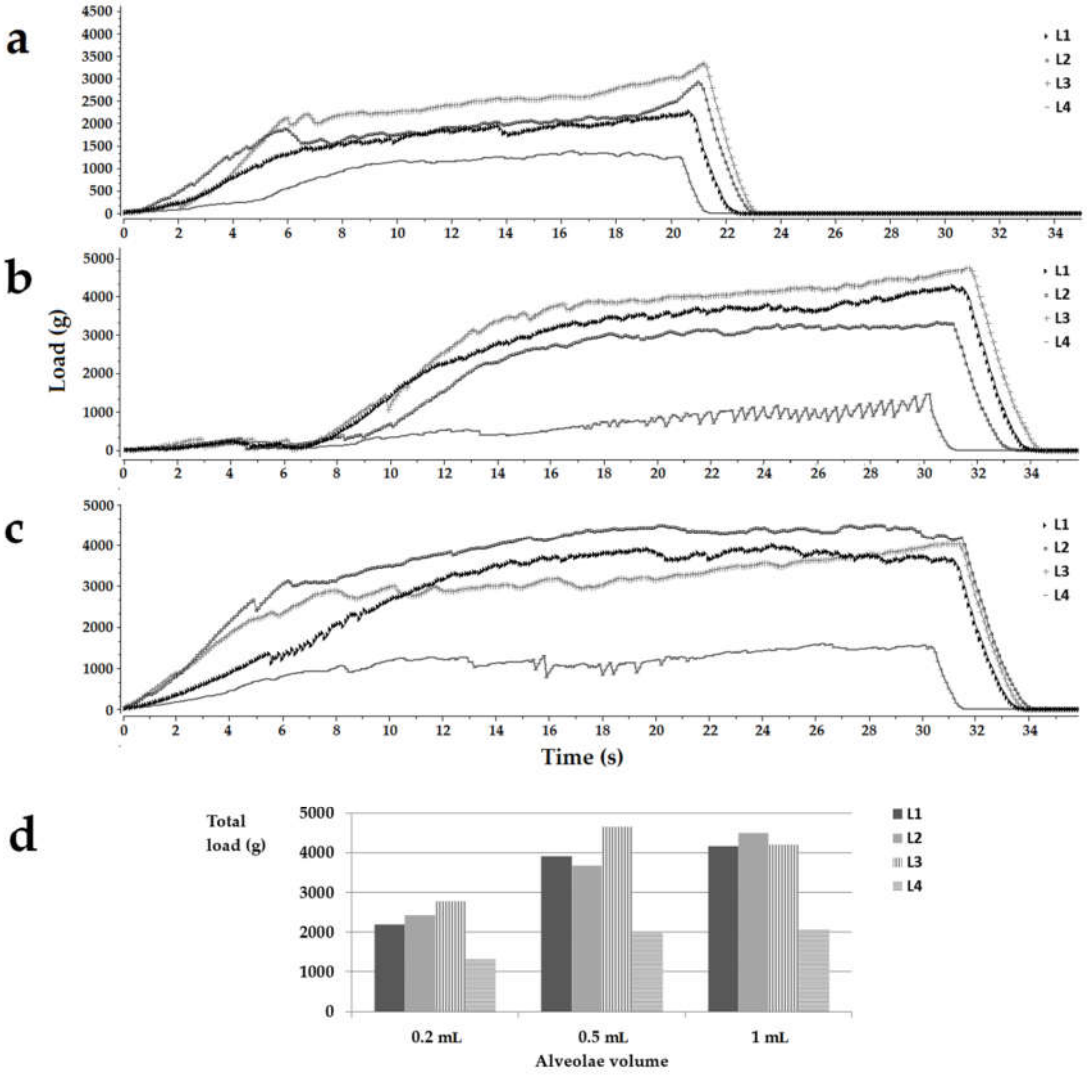

Figure 1. Load (g) vs. time(s) texture analysis representative profiles for the placebo OLs obtained in 0.2 mL (**a**), 0.5 mL (**b**), and 1 mL (**c**) alveolae and a histogram summarizing the total load of the samples (**d**). Legend: L1, L2, L3, L4, the type of milk.

In the case of samples poured into 0.2 mL alveolae, the hardness decreased in the following order L3> L2 > L1 > L4. For the 0.5 mL cakes, the highest hardness was obtained

for the L3 samples, followed by L1, L2, and L4. In the case of samples with a volume of 1 mL, L2 milk led to the most resistant structures, followed by L1, L3, and L4 (Figure 1d). As far as the authors know, no results have been reported on the texture analysis of lyophilized milk, so studies involving pharmaceutical excipients were used for comparison. Casian et al. reported a minimum value of 300 g load for the oral lyophilizates to withstand easy handling, while tests on commercial oral lyophilizates revealed loads of less than 200 g up to 1100–1200 g [30,32]. Considering the total load achieved by the tested samples, it falls above the acceptable values mentioned in the literature, regardless of the sizes or the types of milk. Although the values reported in the literature correspond to products containing the traditional OL composition, the drugs associated with matrix-forming agents and fillers meant to reinforce the structures, even the weakest samples in this study, obtained with L4 milk recorded load values of more than 1317.00 ± 209.40 g, well over the acceptable limits. These results support the attempt to load the freeze-dried milk structures with an active pharmaceutical ingredient.

Up to this point of evaluating the lyophilized milk structures, the only variation pattern observed was the increase in load depending on the alveolae volume or solid size, with no evident dependence on the type of milk, which leads to the premise of possible interactions between the studied factors. Therefore, the study was continued with the implementation of a design of experiments able to highlight the interactions between factors and to quantify the contribution of factors to the total effect.

3.2. Design of Experiments (DoE)

DoE is based on the choice of those independent variables that can influence the quality of a product, in this case, the quality of oral lyophilizates, and their levels of variation, which will be the starting point for drawing up the DoE matrix. The products prepared according to the DoE matrix are characterized as completely as possible by determining a set of dependent variables. The goal of the DoE is to determine the regression models, which correlate the dependent variables coded with Y_1 to Y_n with the independent variables coded with X_1 to X_n. Thus, equations such as $Y_n = f(X_1,...,X_n)$—reveals the influences of the independent variables and their interactions on the dependent variables. The models can be used for an in-depth understanding of the product and to further predict the characteristics of new products in the experimental domain.

As the characteristics of oral lyophilizates are multifactorial, and a sufficient resistance of the placebo structures does not guarantee the same behavior after loading an API, a DoE was developed to evaluate simultaneously the influences of the type of milk, the volume of the alveolae, and the API content, and their interactions. The dose of loratadine (X_1) was the first quantitative variable for which two levels were assigned, 0 mg and 10 mg, and further, the software chose an intermediate value of 5 mg for the three replicate center points. Finally, the design matrix included experiments with 0 mg, 5 mg, or 10 mg loratadine per unit. These values were chosen according to the dose tapering recommendations for children between 2 and 12 years of age: 5 mg for those below 30 kg of body weight and 10 mg for those over 30 kg [33]. The alveolae volume (X_2) was selected as the second quantitative factor, depending on the sizes that were easy to handle and that were considered acceptable for the administration to children. The aspect, sizes, and weights of OLs with different volumes were included in Table 3. The type of milk was set as qualitative variable X_3 and varied on four levels, L1, L2, L3, and L4. The dependence of disintegration time on the lipid content was revealed in the literature for conventional tablets, so L1 and L2 bovine milk were chosen for the differences in fat. Two infant formulae (L3 and L4) were added to the design due to their standardized compositions that could grant easier approval as excipients, while L3 was selected for its higher viscosity that could ensure suspension homogeneity before freezing.

Table 3. Appearance, weight, and sizes of OLs obtained in different alveolae.

Alveolae Volume	0.2 mL	0.5 mL	1 mL
Aspect			
Diameter (mm)	8.40 ± 0.35	11.82 ± 0.15	14.14 ± 0.85
Thickness (mm)	2.73 ± 0.19	4.02 ± 0.28	5.03 ± 0.24
Weight (g)	0.023 ± 0.002	0.056 ± 0.005	0.115 ± 0.010

3.2.1. Summary of Fit

Before interpreting the influence of independent variables on the responses based on the obtained mathematical models, the quality of the data fit was evaluated from statistical parameters, such as R2, Q2, validity, reproducibility, *p*-ANOVA, and lack of fit. The final mathematical models, whose performances are included in Table 4, were obtained following a fine-tunning stage of non-significant term elimination. For all responses, the variation in the data set was explained by the mathematical models (R2 > 0.671), and the prediction capacity of the models was good, with Q2 above 0.431 and close to R2. The chosen models were all valid (>0.25), and the data were recorded with high reproducibility, close to 1 for most of the responses.

Table 4. Model performance parameters for the DoE work set.

Response	R2	Q2	Validity	Reproducibility	ANOVA Regression	ANOVA Lack of Fit
Y1	0.993	0.982	0.756	0.992	0.000	0.378
Y2	0.927	0.899	0.501	0.983	0.000	0.136
Y3	0.871	0.779	0.640	0.944	0.000	0.237
Y4	0.798	0.555	0.720	0.862	0.001	0.326
Y5	0.671	0.431	0.300	0.966	0.007	0.061
Y6	0.780	0.618	0.435	0.960	0.001	0.105
Y7	0.822	0.574	0.642	0.922	0.000	0.240
Y8	0.888	0.621	0.972	0.568	0.001	0.895

Y1, disintegration time; Y2, hardness; Y3, rigidity; Y4, fracturability; Y5, % of dissolved loratadine after 5 min; Y6, % of dissolved loratadine after 10 min; Y7, particle size; Y8, PDI.

3.2.2. The Influence of Independent Variables on the Disintegration Time (Y1)

The disintegration time varied in a wide range, between 1.37 s and 265 s, and for some formulations even exceeded the 3 min acceptability limit of the *European Pharmacopoeia* for orodispersible tablets (Table S1). The disintegration time values were grouped at the two limits of the variation range; most of the values showed an ultra-fast disintegration in a matter of seconds, while others came close to 5 min. The floating tendency was also recorded for some of the formulations prior to wetting and disintegration. The mathematical model indicated that the most important effect came from the type of milk: bovine milk L1 and L2 led to slow disintegration, while L3 and L4, the infant formulae, determined fast disintegration, in less than 10 s. Within the four types of milk, the slowest disintegration was achieved by L2, the milk with 3.5% fat content, followed by L1, the milk with 1.5% fat content. As expected, the increase in fat content led to floating phenomena, longer wetting times, and slower disintegration. In contrast, infant formulae L3 and L4 led to ultra-fast disintegration, delayed in the L3 milk formulations by the viscosity agent found in the composition. Although the high-fat content of L2 milk was what caused the hydrophobicity of the matrices and a slower disintegration of L2 compared to L1, it

was not so important with respect to the disintegration of OLs containing infant formulae. Although L2, L3, and L4 types of milk had almost similar fat content, L3 and L4 OLs disintegrated much faster than L2 OLs. This effect could be related to the lower ratios of saturated fats (Table 1) found in infant formulae that aim to mimic the fat composition found in human milk [34]. Another argument to explain the differences is the complex composition of infant formulae that sometimes reaches hundreds of substances, which are intended for easy reconstitution. L3 contains potato starch used to increase the viscosity of the formula to prevent regurgitation phenomena in newborns but also maltodextrin, which was reported to reduce the crystallinity of lactose and improve dispersibility and solubility of infant formulae [35]. On the other hand, L4 contains soy lecithin, an amphiphilic molecule that has been shown to improve the wetting properties of milk powders [36]. Similar differences were reported between the effects of bovine milk and infant formulae by Binte Abu Bakar et al. (2019) in studies on compressed dispersible tablets [20].

The volume of the alveolae, and thus the size of the OL, had an important impact on disintegration, however, with a lower magnitude when compared to the type of milk (Figure 2a). Large OLs prepared out of high volumes of mixtures had high disintegration times. This effect was valid for placebo OLs. However, despite the increase in alveolar volume/OL size, the disintegration times were at their lowest for the OLs with 10 mg of loratadine.

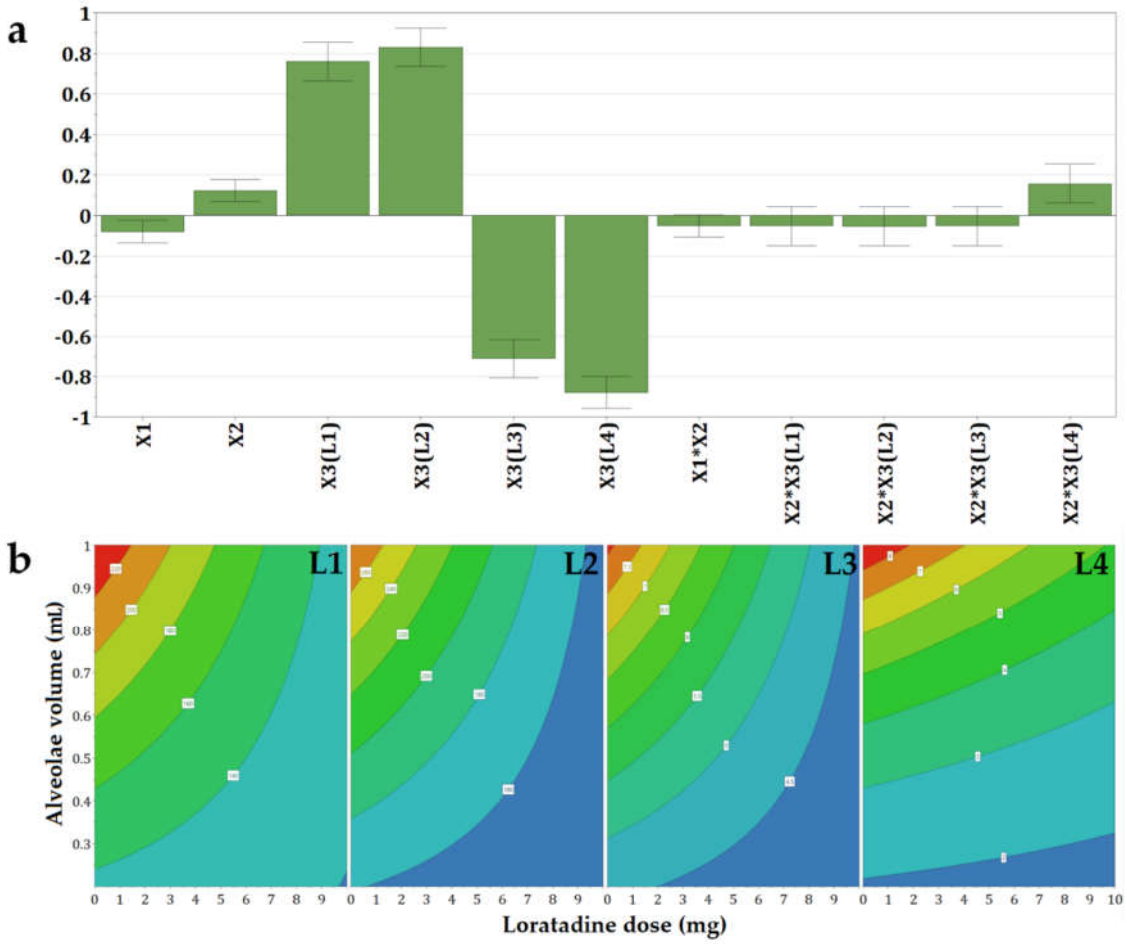

Figure 2. Coefficients of the regression equations displayed as (**a**) histograms and (**b**) representative contour plots for the disintegration time (Y1) as a function of the three independent variables.

Out of the four types of milk, the effect of loratadine content was barely noticed for L4, while the effect of the alveolae size was the most evident (Figure 2b). In contrast, the OLs containing L1, L2, and L3 milk showed a negative influence of the API dose. Thus, the increase in loratadine dose led to a faster disaggregation because insoluble loratadine was interposed between the constituents of the milk during drying, and in addition, an increase in loratadine content in the same volume of suspension was equivalent to a decrease in milk. The same effect of high milk content on disintegration was reported by Orubu and coworkers for compressed tablets [5] and by Pinto and coworkers for minitablets prepared with powdered milk and paracetamol [23].

3.2.3. The Influence of Independent Variables on the Mechanical Properties (Y2—Y4)

The mechanical attributes of the OLs containing loratadine prepared according to the DoE matrix were determined to evaluate whether the structures containing API provide adequate mechanical resistance to prevent breaking of the structures during transport or handling. The texture profiles as load vs. time were recorded, out of which three parameters were determined: Y2—hardness as the total load at the final displacement; Y3—rigidity at 1 mm depth, and Y4—fracturability as the load that produces the first fracture. Out of the tested factors, the API and the L4 type of milk had a negative influence on the calculated mechanical parameters (Figure 3).

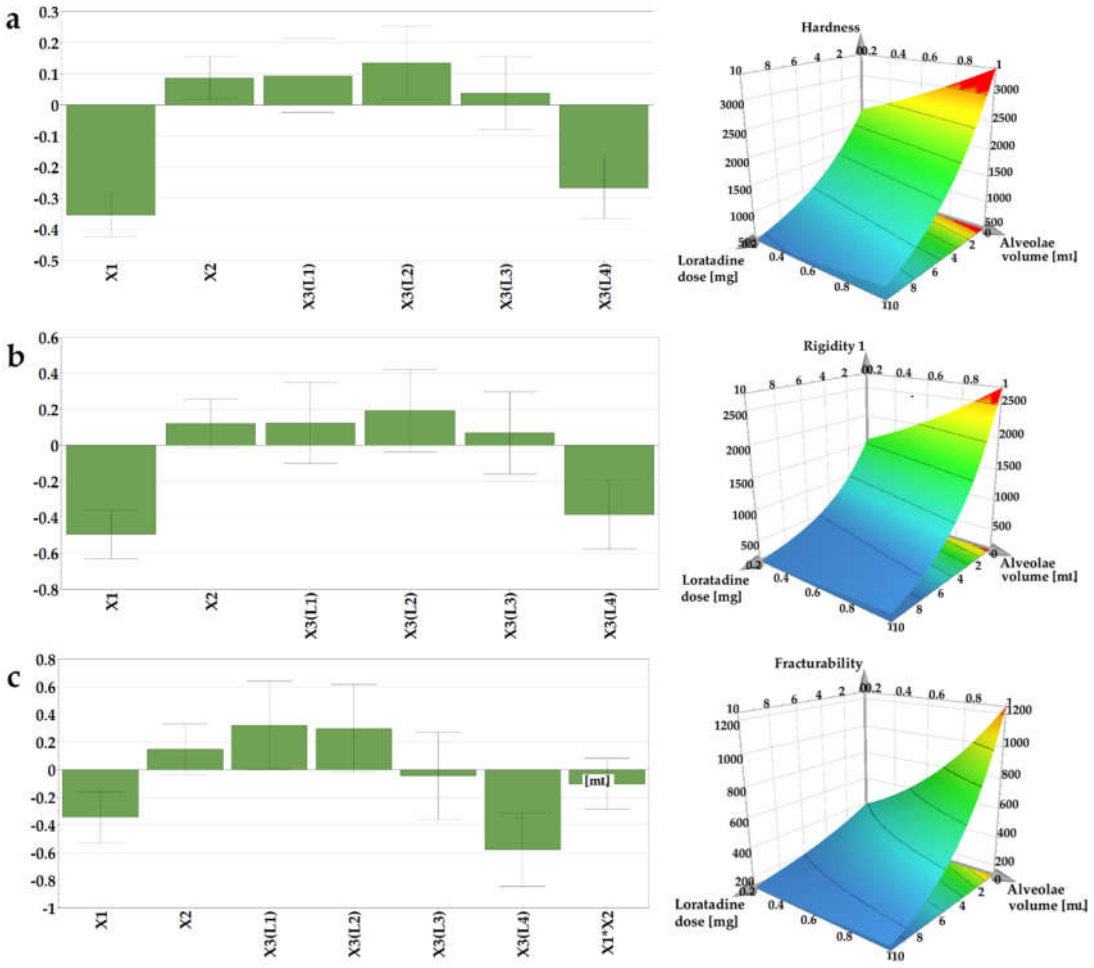

Figure 3. Coefficients of the regression equations displayed as histograms and representative response surfaces plotted for L1 milk for (**a**) hardness (Y2), (**b**) rigidity (Y3), and (**c**) fracturability (Y4).

The hardness of the sample is a result of the intermolecular bonding force and the contact points between the ingredients [37]. Within texture assessment, the hardness (Y2) of the samples was measured as the force necessary to attain the target deformation selected for the particular size of OL. The recorded values varied between 289, 8 g (N14), and 4486 g (N7). The lowest hardness was obtained in the case of the smallest OLs (0.2 mL sample volume) containing L4 and the highest ratio of API (10 mg), in contrast with the sample N7, prepared with L2 (1 mL sample volume and without API), where the highest hardness value was recorded. In comparison with the placebo OLs, the addition of the API had a significantly negative impact on the sample mechanical resistance, leading to weaker structures. However, these results are above the lowest values reported by Vanbillemont 2020 for some marketed OLs, where the minimum values reported were less than 200 g [32]. During the freeze-drying process, the ice is replaced by pores, resulting in a highly porous matrix [32]. The total porosity of the OL impacts the hardness of the samples; a decrease in the porosity leads to an increase in contact points within the matrix-forming agents, which stiffens the structure, resulting in an increase in hardness [37].

On the contrary, in our case, the addition of API led to the brittleness of the samples due to the interspersion of the API within the network, creating more friable structures. These results are in agreement with the disintegration data that revealed faster disintegration of samples with high doses of loratadine.

The rigidity values (Y3), measured as the hardness of the sample at a penetration depth of 1 mm, ranged between 82.2 and 3735 g. These measurements, recorded at the same depth, regardless of the size of the OL, indicate the same variation as the samples with the smallest size (0.2 mL volume) prepared with L4 type of milk, and the highest ratio of API (10 mg) displayed the lowest values for rigidity, while the samples with the highest volume (1 mL), prepared with L2 type of milk and without API, had the highest rigidity.

The internal ruptures and fractures of the samples were recorded as the probe progressed to the pre-established target deformation of 2 or 3 mm. The load value at the first fracture was recorded as the fracturability (Y4) of the samples. This parameter gives information on the sample`s resistance to fractures, a lower value indicating a more brittle product. Consistent with the previous results, the lowest value (42.2 g) for fracturability was obtained for N14, while the highest value, 3320 g, was obtained for N7, considered the most resistant to fractures.

When comparing the upper results with others reported in the literature for OLs prepared with traditional excipients, milk as a freeze-dried matrix yielded comparable results with those obtained by Casian et al. (2017) for OLs with xanthan gum and mannitol, or by AlHusban et al. (2010) for OLs with gelatin and various saccharides [13,30].

3.2.4. The Influence of Independent Variables on the Dissolved Loratadine after 5 and 10 min (Y5, Y6)

The dissolution behavior was assessed for 35 min, but out of the six sampling points, only two were included as responses in the experimental design, the % of dissolved loratadine after 5 and 10 min (Y5 and Y6), as after 10 min, the differences between the formulations flattened out, and no significant variations could be identified. The effect of the loratadine content was shown (Figure 4) with a significantly positive influence on the released percentages in the first part of the study. Its magnitude increased at the second time point, as dissolution unfolded. The increase in loratadine dose was shown to reduce the strength of the structures and the disintegration times. Moreover, higher doses of loratadine coincide with lower milk content per tablet, and in the case of bovine milk, this has an important impact on hydrophobicity and thus on API dissolution. Orubu also showed the negative effect of high ratios of milk on the dissolution rates of API [5].

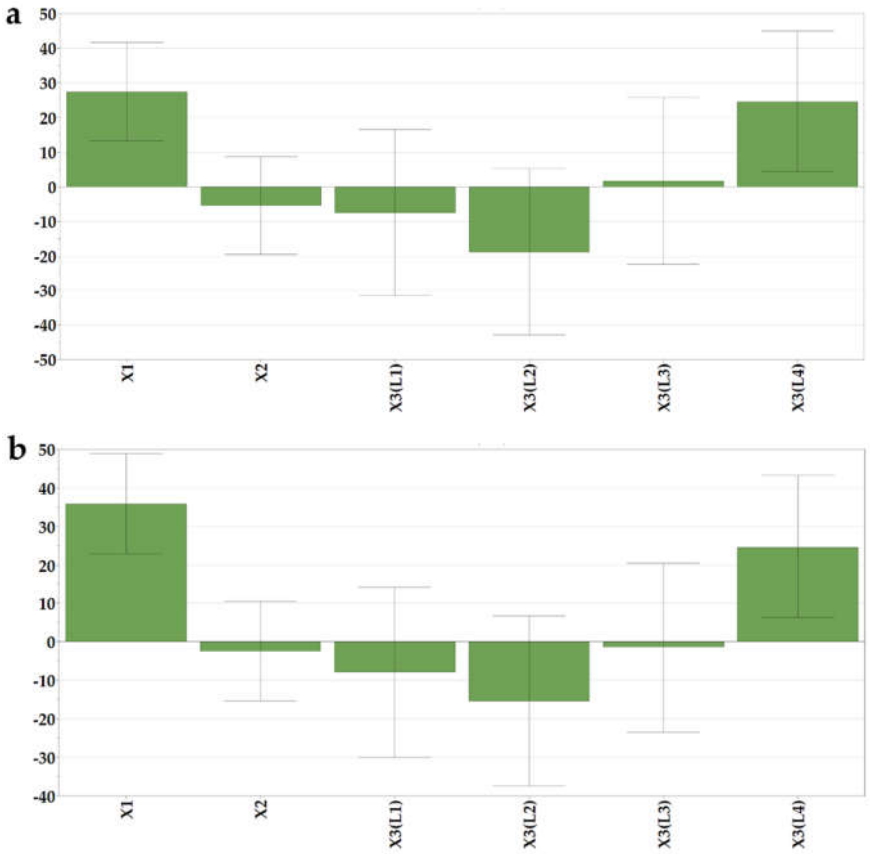

Figure 4. Coefficients of the regression equations displayed as histograms. (**a**) % of dissolved loratadine after 5 min (Y5) and (**b**) 10 min (Y6).

The type of milk also had a significant effect on the % of dissolved loratadine. L4 milk led to faster dissolution. L4 milk OLs were also those with the shortest disintegration times, which granted fast contact of the API with the media and subsequent dissolution. Additionally, the presence of soy lecithin as an emulsifier in the L4 infant formula could have determined the fast dissolution of loratadine from those formulations. Although L3 milk OLs also displayed fast disintegration times, in terms of seconds, the effect of L3 milk on dissolution was not significant.

3.2.5. The Influence of Independent Variables on Particle Size and Polydispersity Index (Y7, Y8)

The particle size determination was meant to give some hints regarding the aggregation phenomena that might have occurred during processing and the further palatability of the product. The average particle sizes of the reconstituted dispersions ranged between 292.97 ± 6.67 nm (N3) and 665.83 ± 34.90 nm (N9).

As shown in the histogram of the regression coefficients (Figure 5a), the highest particle sizes were obtained for formulations with high drug loading and associated with the L3 milk. On the contrary, the use of bovine milk L1 led to decreased particle sizes of the reconstituted samples.

As loratadine was incorporated into the initial suspensions as a micronized powder, with D50 of 3 μm and D90 of 7 μm, and milk constituents were also present in the recon-

stituted dispersions, the polydispersity index increased with the higher drug load. Additionally, an increase in polydispersity was obtained when L2 milk was used as a freeze-dried matrix-forming agent due to its higher lipid content.

No aggregation phenomena were recorded in milk constituents during freeze drying, as there were no significant differences between the average particle sizes of reconstituted placebo OLs and milk samples in their initial liquid state. This could be an argument in favor of freeze drying as a technique to obtain solid milk dosage forms, as the aggregation phenomena with an increase in particle size after redispersion were reported for compressed tablets [20]. The acceptability of dispersible solids is influenced by many criteria among which is the particle size after dispersion in the saliva. The acceptability limit for granule sizes within orodispersible tablets was 244 μm; therefore, all the OL formulations prepared in this study are well within this range [38].

The particle size distribution obtained for the reconstituted placebo formulations coincides with the DLS footprint reported by Kytariolos et al. Figure 6 displays the representative curves of particle size distribution for reconstituted freeze-dried L1 milk prepared in medium-sized alveolae compared to the same product loaded with increasing doses of loratadine of 5 mg and 10 mg, respectively. Bimodal distributions were obtained, with the first peak between 60 and 150 nm attributed to casein micelles and a second one between 200 and 800 nm corresponding to the fat globules [18].

The addition of loratadine led to the appearance of a third peak in the micrometer range that corresponds to the API. This correlates with the average size increase with the API dose revealed by the model coefficients and is in line with the variation of the polydispersity index. DoE analysis confirmed these observations; the PDI increased with the loratadine dose (Figure 5b) and L2 milk and decreased with the higher alveolae volumes, resulting in higher milk ratios and L4 milk. The narrow distribution obtained for L4 milk could be related to the excipients and other insoluble compounds found in the infant formula that display the same sizes as milk lipids, which led to low PDI correlated with particle sizes at the upper limits of the measured variation range.

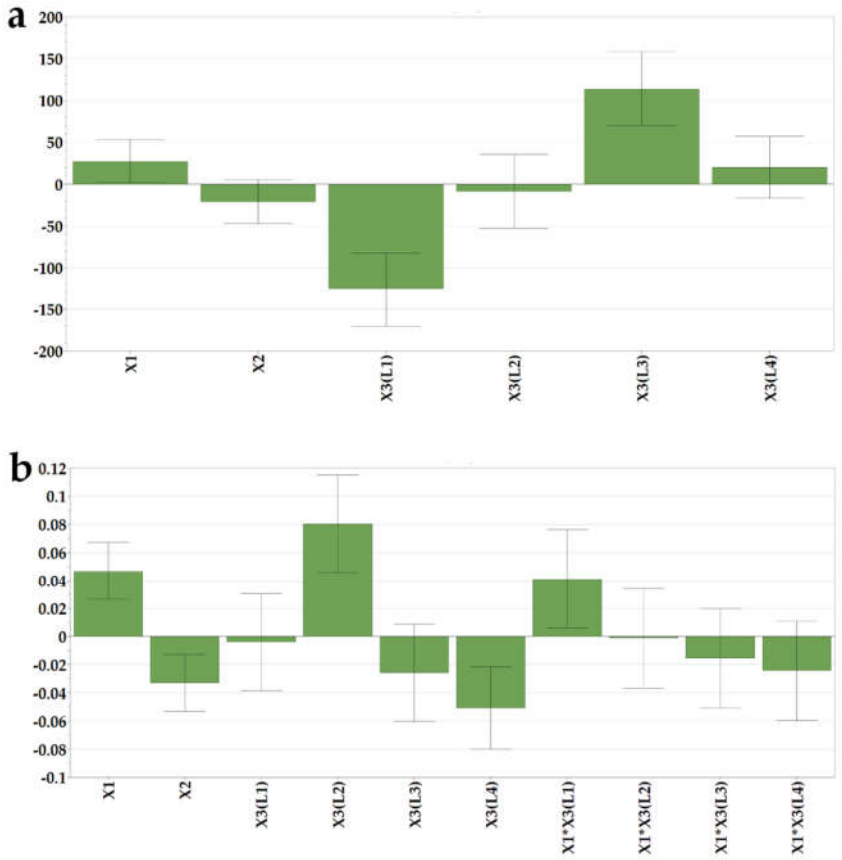

Figure 5. Coefficients of the regression equations are displayed as histograms and representative response surfaces for (**a**) particle size (Y7) and (**b**) polydispersity index (Y8).

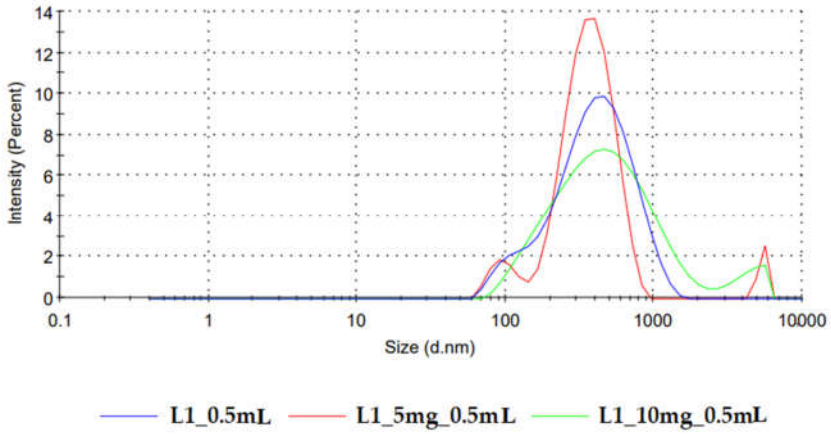

Figure 6. Particle size distribution of freeze-dried reconstituted samples of L1 milk and L1 milk loaded with increasing doses of loratadine.

3.3. DoE Conclusions

The DoE revealed the most important effects the three studied factors had on the OLs' pharmaceutical characteristics:

- bovine milk (L1 and L2) and large volumes of alveolae prolong disintegration, while infant formulae and high doses of API ensure rapid disintegration;

- the use of L2 milk and high-volume alveolae increase the resistance of oral lyophilizates, while high doses of loratadine and the use of L4 milk raise the structure friability;
- two types of milk simultaneously meet the criteria of fast disintegration and appropriate mechanical profile: bovine milk L1 and infant formula L3;
- high API doses and the use of L4 milk led to the highest amounts of dissolved loratadine.

Although all responses in the DoE showed acceptable predictability, three formulations were chosen from the experimental domain to test the predictions of the DoE. Based on the observed effects, in the third part of the study, we chose to use two types of milk, L1 and L3, with increasing doses of loratadine, prepared in medium-sized alveolae. Table 5 shows the three formulations, their codes, predicted values, experimental values, and the calculated residuals.

Table 5. Results of the DoE validation experiments.

Code		L1_5 mg_0.5 mL			L1_10 mg_0.5 mL			L13_10 mg_0.5 mL		
Formulation factors	X1	5			10			10		
	X2	0.5			0.5			0.5		
	X3	L1			L1			L3		
		Predicted	Actual	Residual	Predicted	Actual	Residual	Predicted	Actual	Residual
Responses	Y1	144.35	103.13 ± 22.57	−44.22	123.76	83.61 ± 16.28	−40.15	4.20	3.91 ± 0.45	−0.29
	Y2	1339.45	523.3 ± 160.20	−816.15	592.91	537.5 ± 100.03	−55.41	520.91	518.3 ± 20.70	−2.61
	Y3	700.70	122.2 ± 37.4	−578.5	223.70	118.3 ± 25.12	−105.4	196.99	127.00 ± 3.49	−69.99
	Y4	675.98	100 ± 38.4	−575.98	323.25	158.4 ± 50.17	−164.85	138.21	89.8 ± 5.84	−48.41
	Y5	28.05	31.40 ± 1.07	3.35	55.46	53.26 ± 7.08	−2.2	64.79	60.58 ± 4.11	−4.21
	Y6	34.68	47.79 ± 1.78	13.11	70.64	75.76 ± 11.36	5.12	77.12	89.09 ± 1.06	11.97
	Y7	359.14	355.07 ± 11.40	−4.07	386.79	390.90 ± 14.79	4.11	626.75	548.90 ± 3.48	−77.85
	Y8	0.375	0.370 ± 0.036	−0.005	0.463	0.453 ± 0.045	−0.01	0.385	0.327 ± 0.014	−0.058

Legend: L1_5 mg_0.5 ml—L1 type of milk, 0.5 mL sample volume, 5 mg loratadine; L1_10 mg_0.5 mL—L1 type of milk, 0.5 mL sample volume, 10 mg loratadine; L13_10 mg_0.5 mL—L3 type of milk, 0.5 mL sample volume, 10 mg loratadine.

The predictions were met for all parameters, except for the texture-analysis-derived parameters for the formulation L1_5 mg_0.5 mL due to the rather high variability between replicate samples or to the presence of nonlinear effects that were not accurately estimated by this type of DoE.

3.4. Supplementary Characterization of the OLs

The next step of the research was to submit those three formulations selected from the experimental domain to additional analyses for a thorough characterization and in-depth understanding of the observed effects.

3.4.1. Wetting and Dissolution

According to the biopharmaceutical classification system, loratadine is a class II drug with low solubility and high permeability. The bioavailability depends on its luminal dissolution, the limiting step of intestinal absorption. Loratadine is also known as an API with pH-dependent solubility. Its weak base character determines the higher solubility of the ionized form in acidic media when compared to its solubility in neutral media [39]. As the fast dissolution of raw loratadine and commercial immediate-release formulations in

acidic media were proved by several authors [40], an improved formulation would grant fast and reproducible dissolution at a higher pH. Therefore, the OL formulations were tested for in vitro dissolution at a pH of 6.8. Figure 7 depicts the dissolution profiles of three of the OL formulations prepared in medium-sized alveolae of 0.5 mL, two of them with L1 milk and increasing doses of API, of 5 mg (L1_5 mg_0.5 mL) and 10 mg (L1_10 mg_0.5 mL), and a formulation with L3 milk and a dose of 10 mg of loratadine (L13_10 mg_0.5 mL). As predicted by the DoE models, the increase in the API dose led to significantly higher dissolved API percentages, probably explained by the faster disintegration induced by the lower mechanical strength and by the lower milk content associated with the API dose increase. Out of the three formulations, the best dissolution profile was obtained for L13_10 mg_0.5 mL, with 80% of dissolved API in less than 10 min due to its good wettability and ultra-fast disintegration. The dissolution performance of the three formulations was sustained by their wetting behavior results (Table 6). When exposed to water, the L1 milk compressed samples showed a high contact angle, thus a low wetting capacity, as compared to the L3 milk samples, where the water spread immediately on their surface with a low contact angle and an improved surface free energy.

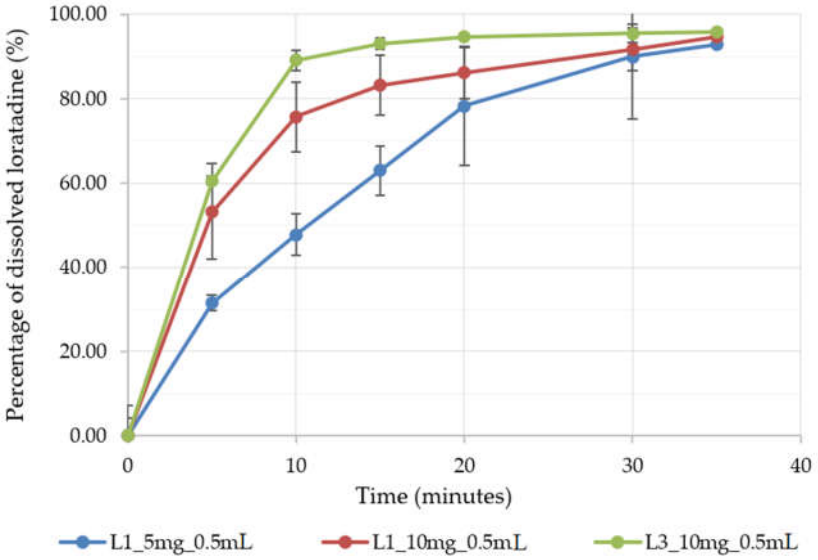

Figure 7. The dissolution profile of three selected OL formulations prepared in 0.5 mL alveolae.

3.4.2. Solid-State Analysis

As previous studies showed that loratadine dissolution behavior varied upon crystallinity [41], several determinations were made to assess the potential structural changes that may have occurred during OL preparation. Figure 8 displays the XRPD diffractograms and the FT-IR spectra of raw loratadine and selected formulations.

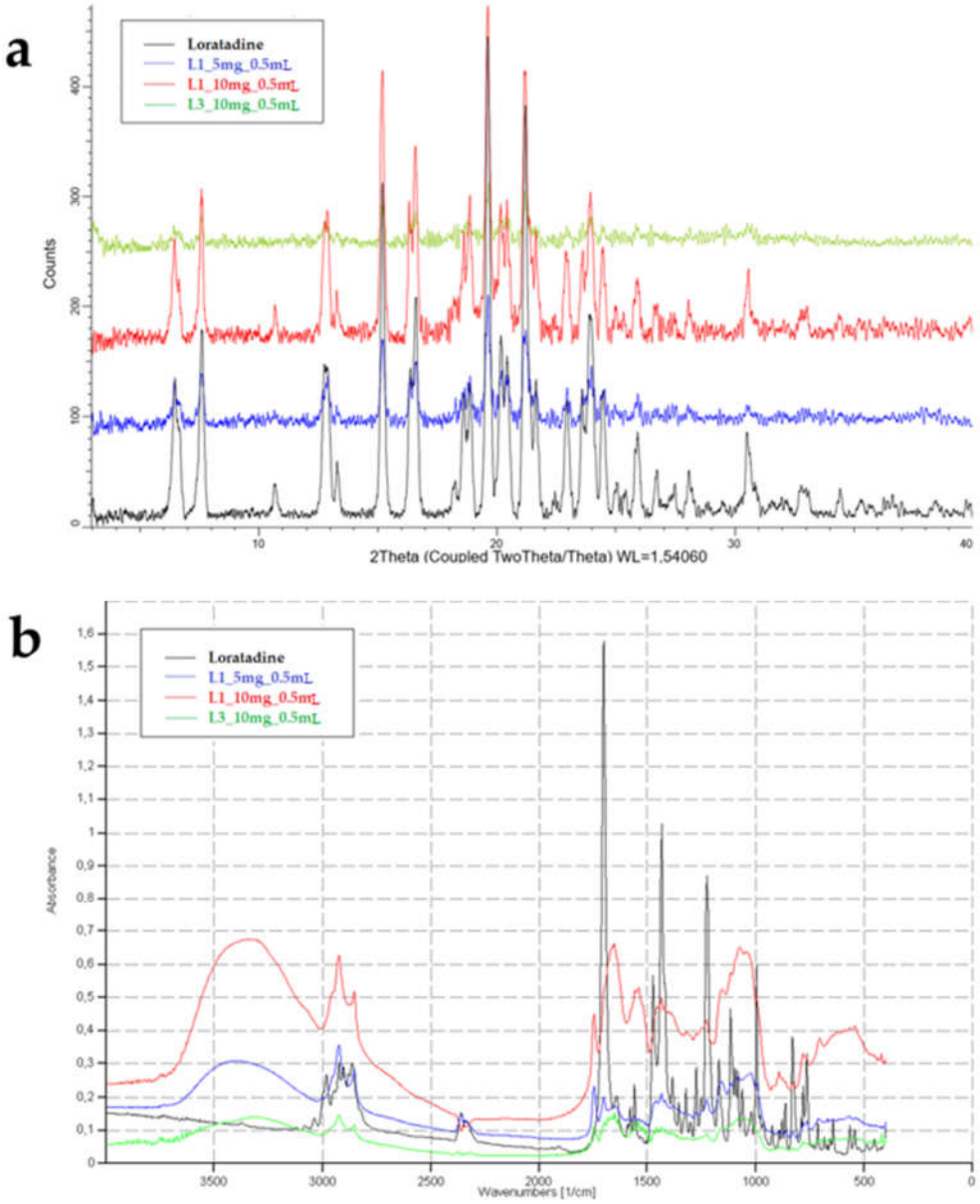

Figure 8. XRPD diffractograms (**a**) and FT-IR spectra (**b**) of raw loratadine and OL formulations.

Table 6. Wettability results.

	ΘWater [°]	ΘDiiodomethane [°]	γ [mN m^{-1}]	Polarity [%]
Loratadine	72.75	13.2	55.54	18.47
L1_5mg_0.5ml	71.46	1	57.14	18.62
L1_10 mg_0.5 mL	71.76	15	55.65	19.35
L13_10 mg_0.5 mL	1	10.2	82.22	45.16

Legend: L1_5 mg_0.5 mL—L1 type of milk, 0.5 mL sample volume, 5 mg loratadine; L1_10 mg_0.5 mL—L1 type of milk, 0.5 mL sample volume, 10 mg loratadine; L13_10 mg_0.5 mL—L3 type of milk, 0.5 mL sample volume, 10 mg loratadine.

The XRPD diffractogram of raw loratadine showed its crystalline nature through numerous sharp peaks between 3 and 33 degrees of the 2-θ scale, at 12.7, 15.1, 16.5, 19.7, 21.3, 23.9, 30.5, and 32.5 degrees [42]. The overlapped patterns highlight the characteristic peaks of loratadine in the OL formulations. A similar pattern was obtained for L1_10 mg_0.5 mL, and the peaks were visible but less intense for L1_5 mg_0.5 mL, where the loratadine content was lower in favor of the milk fraction. However, the characteristic peaks of loratadine significantly faded in the diffractogram of L13_10 mg_0.5 mL, which revealed a decrease in crystallinity in the OL prepared using infant formula. These results that indicate the partial amorphization of loratadine explain the good wettability and dissolution results displayed by the L13_10 mg_0.5 mL formulation.

FT-IR analysis aimed to highlight the compatibility and interactions between loratadine and milk as an excipient by evaluating the changes that appeared in its structure after OL preparation compared to the pure substance. The characteristic FT-IR bands of loratadine were found at 997 cm^{-1} for aryl C-Cl stretching and at 1227 cm^{-1} for -C-N stretching. C=O bonds of the amide or ester groups were represented by bands at 1550 and 1703 cm^{-1} and showed the regions where intermolecular interaction could occur. Bands from 3000 to 2850 cm^{-1} revealed the C–H bond stretching [39]. The OL samples containing freeze-dried milk showed a characteristic band from 3468 to 3300 cm^{-1}, which corresponded to O-H and N-H stretching in the protein structure, a single band at 1745 cm^{-1} for the C=O group stretching in the fatty esters, and the saccharide bands from 1200 to 900 cm^{-1} [21]. The increase in loratadine content that resulted in lower fractions of milk in the samples led to less intense signals of the milk constituents. All the characteristic peaks of loratadine were identified when included in the freeze-dried milk matrix, including the carbonyl band, but shifted to a lower wavenumber due to newly formed intermolecular hydrogen bonds [42]. As the FTIR results indicate the formation of new hydrogen bonding and no covalent bonds, the API shows good compatibility with the milk matrix [43].

Raw loratadine crystals, presented as polydispersed rod-shaped or oval-shaped crystals, are shown in Figure 9a. The images in Figure 9b–e correspond to the formulations L1_10 mg_0.5 mL and L3_10 mg_0.5 mL, and images captured on the outer surfaces of the freeze-dried products focusing on the loratadine particles and on their appearance were included in the structures. In all images, API particles seem completely included in the pore walls and surrounded by the solid milk matrix. An agglomeration tendency was observed for the formulations with L1 milk, probably caused by its lower viscosity when compared to the one with L3 milk. Moreover, a slight reduction in particle size was visible, partially hindered by the agglomerations. However, this was not sustained by the particle size determinations, which indicates that despite the appearance of solid structures, they will easily and completely redisperse in water. L3 milk formulation displayed thicker pore walls when compared to L1 formulation; visible particles embedded into the pore walls but with lower sizes and better distribution throughout the solid matrix, with a lower agglomeration tendency due to the higher viscosity of the infant formula.

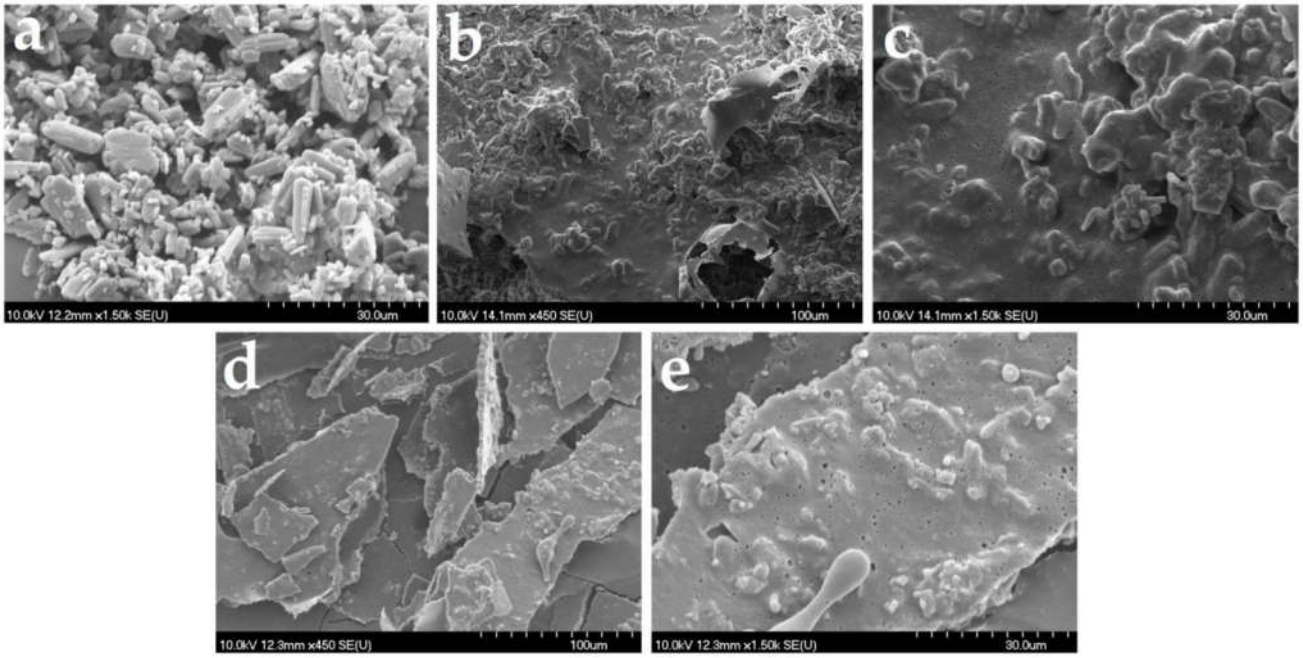

Figure 9. SEM images of raw loratadine (**a**) and OL formulations L1_10 mg_0.5 mL with 100 μm (**b**), 30 μm (**c**) magnitude, and L13_10 mg_0.5 mL with 100 μm (**d**), 30 μm (**e**) magnitude.

3.5. Practical Implications of the Study

A growing body of scientific literature is investigating the potential role of milk as a dispersing agent and drug carrier for poorly soluble drugs. Among liquid drug dispersions and compressed tablets, this study opens the way for the use of milk as an excipient for another dosage form: oral lyophilizate. However, even if the scientific evidence supports the performance and benefits of milk in drug development, certain aspects need to be considered. First, the regulatory hurdle, since milk is not registered as a pharmaceutical excipient. Its variability in the content of lipids and proteins is unlikely to lead to its approval as an excipient, as one of the main requirements is the consistency in composition and physical-chemical characteristics, sustained by the quality specification [24]. These drawbacks may be partially solved by using infant powdered formulae with a standardized composition [6], which, in the present study, gave the best results in terms of mechanical characteristics and API dissolution. Secondly, the potential allergic reactions should not be neglected, as bovine milk allergy represents the most common food allergy in infants and children [6,44], and furthermore, the potential unwanted interactions between milk compounds and drugs, such as the reaction of calcium ions with tetracycline [24]. In this respect, further studies are yet to be performed to obtain lactose-free formulations for lactose-intolerant patients [45] and to understand the features of the APIs that can be safely included into milk structures [24].

Of all the orodispersible forms studied using milk as an excipient, the products prepared in this study displayed a much faster disintegration in the context of adequate resistance. Therefore, lyophilization may be a viable option for the preparation of orodispersible milk-based products for substances that require ultra-fast release. Another key point of this study is the understanding of the influence of OL size and insoluble active substance loading on the characteristics of lyophilized structures. The obtained results could even be used to guide the development of oral lyophilizates with traditional excipients. Further studies could attempt to increase the strength of infant formula lyophilized matrices by adding small amounts of biocompatible polymers, investigate other infant formulae to understand how the properties of OLs are influenced by their composition,

or aim at the loading of APIs with different physical-chemical properties in freeze-dried milk structures.

4. Conclusions

This study aimed at the preparation of freeze-dried orodispersible dosage forms out of milk as a matrix-forming agent. Bovine milk and infant formulae were first tested for their mechanical properties in their freeze-dried state. As they proved sufficient mechanical strength to withstand manipulation, they were loaded with an insoluble model API, loratadine, at increasing doses, to obtain OLs of different sizes, according to a DoE. The pharmaceutical properties of the prepared products fulfilled the official quality requirements for oral lyophilizates. They displayed acceptable disintegration using bovine milk and ultra-rapid disintegration using infant formulae. The mechanical parameters confirm the obtention of lyophilizates with sufficient resistance to handling for the formulae with bovine milk but also for infant formula L3, even when loading different doses of suspended active pharmaceutical ingredient.

Supplementary Materials: The following supporting information can be downloaded at: www.mdpi.com/article/10.3390/pharmaceutics14071342/s1, Table S1. Response matrix.

Author Contributions: Conceptualization, S.I. and C.B.; methodology, S.I., C.B. and D.-M.M.; software, S.I. and C.B.; validation, R.A. and I.T.; formal analysis, S.I. and C.B.; investigation, Ș.S, D.-M.M., L.R., M.B. and S.B.; resources, S.I. and I.T.; data curation, M.B., S.B., S.I. and C.B..; writing—original draft preparation, S.I. and C.B.; writing—review and editing, R.A. and I.T.; visualization, L.R.; supervision, I.T.; project administration, S.I.; funding acquisition, S.I. All authors have read and agreed to the published version of the manuscript.

Funding: This work was supported by a grant of the Romanian Ministry of Education and Research, CNCS-UEFISCDI, project number PN-III-P1-1.1-PD-2019-0795, within PNCDI III. Project no. TKP2021-EGA-32 was implemented with the support provided by the Ministry of Innovation and Technology of Hungary from the National Research, Development and Innovation Fund, financed under the TKP2021-EGA funding scheme.

Institutional Review Board Statement: Not applicable.

Informed Consent Statement: Not applicable.

Data Availability Statement: Not applicable.

Conflicts of Interest: The authors declare no conflicts of interest. The funders had no role in the design of the study; in the collection, analyses, or interpretation of data; in the writing of the manuscript, or in the decision to publish the results.

References

1. Strickley, R.G. Pediatric Oral Formulations: An Updated Review of Commercially Available Pediatric Oral Formulations Since 2007. *J. Pharm. Sci.* **2019**, *108*, 1335–1365.
2. Lal, M.; Lai, M.; Estrada, M.; Zhu, C. Developing a Flexible Pediatric Dosage Form for Antiretroviral Therapy: A Fast-Dissolving Tablet. *J. Pharm. Sci.* **2017**, *106*, 2173–2177.
3. Montero-Padilla, S.; Velaga, S.; Morales, J.O. Buccal Dosage Forms: General Considerations for Pediatric Patients. *AAPS PharmSciTech* **2017**, *18*, 273–282.
4. Walsh, J.; Schaufelberger, D.; Iurian, S.; Klein, S.; Batchelor, H.; Turner, R.; Gizurarson, S.; Boltri, L.; Alessandrini, E.; Tuleu, C. Path towards efficient paediatric formulation development based on partnering with clinical pharmacologists and clinicians, a conect4children expert group white paper. *Br. J. Clin. Pharmacol.* **2021**. https://doi.org/10.1111/bcp.14989
5. Orubu, S.E.F.; Hobson, N.J.; Basit, A.W.; Tuleu, C. The Milky Way: Paediatric milk-based dispersible tablets prepared by direct compression-a proof-of-concept study. *J. Pharm. Pharmacol.* **2017**, *69*, 417–431.
6. Soulele, K.; Macheras, P. Milk as a medium for pediatric formulations: Experimental findings and regulatory aspects. *Int. J. Pharm.* **2015**, *492*, 344–345.
7. Slavkova, M.; Breitkreutz, J. Orodispersible drug formulations for children and elderly. *Eur. J. Pharm. Sci. Off. J. Eur. Fed. Pharm. Sci.* **2015**, *75*, 2–9.

8. Lottmann, H. Comparison of two sublingual types of desmopressin in 6-year-old and more children with primary nocturnal enuresis. About an international randomized cross-over study. *Prog. En Urol. J. L'association Fr. D'urologie La Soc. Fr. D'urologie* **2009**, *19*, 132–138.
9. Iurian, S.; Bogdan, C.; Tomuță, I.; Szabó-Révész, P.; Chvatal, A.; Leucuța, S.E.; Moldovan, M.; Ambrus, R. Development of oral lyophilisates containing meloxicam nanocrystals using QbD approach. *Eur. J. Pharm. Sci.* **2017**, *104*, 356–365.
10. Costa, J.S.R.; de Oliveira Cruvinel, K.; Oliveira-Nascimento, L. A mini-review on drug delivery through wafer technology: Formulation and manufacturing of buccal and oral lyophilizates. *J. Adv. Res.* **2019**, *20*, 33–41.
11. Iurian, S.; Tomuta, I.; Bogdan, C.; Rus, L.; Tokes, T.; Barbu-Tudoran, L.; Achim, M.; Moldovan, M.; Leucuta, S. Defining the design space for freeze-dried orodispersible tablets with meloxicam. *Drug Dev. Ind. Pharm.* **2016**, *42*, 1977–1989.
12. Vanbillemont, B.; De Beer, T. Application of polyvinyl acetate in an innovative formulation strategy for lyophilized orally disintegrating tablets. *Int. J. Pharm.* **2020**, *588*, 119717.
13. AlHusban, F.; Perrie, Y.; Mohammed, A.R. Formulation and characterisation of lyophilised rapid disintegrating tablets using amino acids as matrix forming agents. *Eur. J. Pharm. Biopharm. Off. J. Arb. Fur Pharm. Verfahr. E.V* **2010**, *75*, 254–262.
14. Hackl, E.; Ermolina, I. Application of Texture Analysis Technique in Formulation Development of Lyophilized Orally Disintegrating Tablets Containing Mannitol, Polyvinylpyrrolidone and Amino Acids. *AAPS PharmSciTech* **2019**, *20*, 71.
15. Casian, T.; Bogdan, C.; Tarta, D.; Moldovan, M.; Tomuta, I.; Iurian, S. Assessment of oral formulation-dependent characteristics of orodispersible tablets using texture profiles and multivariate data analysis. *J. Pharm. Biomed. Anal.* **2018**, *152*, 47–56.
16. Wollmer, E.; Neal, G.; Whitaker, M.J.; Margetson, D.; Klein, S. Biorelevant in vitro assessment of dissolution and compatibility properties of a novel paediatric hydrocortisone drug product following exposure of the drug product to child-appropriate administration fluids. *Eur. J. Pharm. Biopharm. Off. J. Arb. Fur Pharm. Verfahr. E.V* **2018**, *133*, 277–284.
17. Charkoftaki, G.; Kytariolos, J.; Macheras, P. Novel milk-based oral formulations: Proof of concept. *Int. J. Pharm.* **2010**, *390*, 150–159.
18. Kytariolos, J.; Charkoftaki, G.; Smith, J.R.; Voyiatzis, G.; Chrissanthopoulos, A.; Yannopoulos, S.N.; Fatouros, D.G.; Macheras, P. Stability and physicochemical characterization of novel milk-based oral formulations. *Int. J. Pharm.* **2013**, *444*, 128–138.
19. Boyd, B.J.; Salim, M.; Clulow, A.J.; Ramirez, G.; Pham, A.C.; Hawley, A. The impact of digestion is essential to the understanding of milk as a drug delivery system for poorly water soluble drugs. *J. Control. Release Off. J. Control. Release Soc.* **2018**, *292*, 13–17.
20. Binte Abu Bakar, S.Y.; Salim, M.; Clulow, A.J.; Hawley, A.; Boyd, B.J. Revisiting dispersible milk-drug tablets as a solid lipid formulation in the context of digestion. *Int. J. Pharm.* **2019**, *554*, 179–189.
21. Aguiar, J.P.; Fernandes, T.A.P.; Nese, C.; Fernandes, A.I.; Pinto, J.F. Production and characterization of spray-dried theophylline powders prepared from fresh milk for potential use in paediatrics. *J. Pharm. Pharmacol.* **2017**, *69*, 554–566.
22. Nese, C.; Palugan, L.; Cerea, M.; Pinto, J.F. Preparation and characterization of a powder manufactured by spray drying milk based formulations for the delivery of theophylline for pediatric use. *Int. J. Pharm.* **2020**, *580*, 119227.
23. Pinto, J.T.; Brachkova, M.I.; Fernandes, A.I.; Pinto, J.F. Evaluation of the ability of powdered milk to produce minitablets containing paracetamol for the paediatric population. *Chem. Eng. Res. Des.* **2016**, *110*, 171–182.
24. Salim, M.; Eason, T.; Boyd, B.J. Opportunities for milk and milk-related systems as 'new' low-cost excipient drug delivery materials. *Adv. Drug Deliv. Rev.* **2022**, *183*, 114139.
25. Aalaei, K.; Rayner, M.; Tareke, E.; Sjöholm, I. Application of a dye-binding method for the determination of available lysine in skim milk powders. *Food Chem.* **2016**, *196*, 815–820.
26. WHO Model List of Essential Medicines for Children-8th List. Available online: https://www.who.int/publications/i/item/WHO-MHP-HPS-EML-2021.03 (accessed on 14 June 2022).
27. Gavan, A.; Iurian, S.; Casian, T.; Porfire, A.; Porav, S.; Voina, I.; Oprea, A.; Tomuta, I. Fluidised bed granulation of two APIs: QbD approach and development of a NIR in-line monitoring method. *Asian J. Pharm. Sci.* **2020**, *15*, 506–517.
28. European Pharmacopoeia 10.7 Online Edition. Available online: https://pheur.edqm.eu/subhome/10-7 (accessed on 16 May 2022).
29. Hackl, E.V.; Ermolina, I. Using Texture Analysis Technique to Assess the Freeze-Dried Cakes in Vials. *J. Pharm. Sci.* **2016**, *105*, 2073–2085.
30. Casian, T.; Iurian, S.; Bogdan, C.; Rus, L.; Moldovan, M.; Tomuta, I. QbD for pediatric oral lyophilisates development: Risk assessment followed by screening and optimization. *Drug Dev. Ind. Pharm.* **2017**, *43*, 1932–1944.
31. Schuster, J.M.; Schvezov, C.E.; Rosenberger, M.R. Analysis of the Results of Surface Free Energy Measurement of Ti6Al4V by Different Methods. *Procedia Mater. Sci.* **2015**, *8*, 732–741.
32. Vanbillemont, B.; Everaert, H.; De Beer, T. New advances in the characterization of lyophilised orally disintegrating tablets. *Int. J. Pharm.* **2020**, *579*, 119153.
33. Loratadina-Rezumat Caracteristici Produs. Available online: https://www.anm.ro/_/_RCP/RCP_11020_12.10.18.pdf (accessed on 14 June 2022).
34. Wei, W.; Jin, Q.; Wang, X. Human milk fat substitutes: Past achievements and current trends. *Prog. Lipid Res.* **2019**, *74*, 69–86.
35. Masum, A.K.M.; Chandrapala, J.; Adhikari, B.; Huppertz, T.; Zisu, B. Effect of lactose-to-maltodextrin ratio on emulsion stability and physicochemical properties of spray-dried infant milk formula powders. *J. Food Eng.* **2019**, *254*, 34–41.
36. Hammes, M.V.; Englert, A.H.; Noreña, C.P.Z.; Cardozo, N.S.M. Study of the influence of soy lecithin addition on the wettability of buffalo milk powder obtained by spray drying. *Powder Technol.* **2015**, *277*, 237–243.

37. Gugulothu, D.; Desai, P.; Pandharipande, P.; Patravale, V. Freeze drying: Exploring potential in development of orodispersible tablets of sumatriptan succinate. *Drug Dev. Ind. Pharm.* **2015**, *41*, 398–405.
38. Mistry, P.; Batchelor, H. Evidence of acceptability of oral paediatric medicines: A review. *J. Pharm. Pharmacol.* **2017**, *69*, 361–376.
39. Frizon, F.; de Oliveira Eloy, J.; Donaduzzi, C.M.; Mitsui, M.L.; Marchetti, J.M. Dissolution rate enhancement of loratadine in polyvinylpyrrolidone K-30 solid dispersions by solvent methods. *Powder Technol.* **2013**, *235*, 532–539.
40. Li, H.; Tan, Y.; Yang, L.; Gao, L.; Wang, T.; Yang, X.; Quan, D. Dissolution evaluation in vitro and bioavailability in vivo of self-microemulsifying drug delivery systems for pH-sensitive drug loratadine. *J. Microencapsul.* **2015**, *32*, 175–180.
41. Kapote, D.N.; Wagner, K.G. Influence of shellac on the improvement of solubility and supersaturation of loratadine amorphous solid dispersion using a new grade of HPMC. *J. Drug Deliv. Sci. Technol.* **2021**, *61*, 102116.
42. Emami, M.S.; Haghshenasfard, M.; Zarghami, R.; Sadeghi, R.; Esfahany, M.N. Experimental study on the reduction of loratadine particle size through confined liquid impinging jets. *Int. J. Pharm.* **2020**, *587*, 119668.
43. Ambrus, R.; Alshweiat, A.; Csóka, I.; Ovari, G.; Esmail, A.; Radacsi, N. 3D-printed electrospinning setup for the preparation of loratadine nanofibers with enhanced physicochemical properties. *Int. J. Pharm.* **2019**, *567*, 118455.
44. Milk Allergy. Available online: https://www.foodallergy.org/living-food-allergies/food-allergy-essentials/common-allergens/milk (accessed on 24 April 2022).
45. Kamal, S.S.; Kaur, D.; Singh, S.; Sharma, A.; Katual, M.K.; Garg, A.K.; Kumar, R. An Investigative and Explanatory Review on Use of Milk as a Broad-Spectrum Drug Carrier for Improvement of Bioavailability and Patient Compliance. *J. Young Pharm.* **2016**, *8*, 72.

International Journal of Pharmaceutics 613 (2022) 121411

Contents lists available at ScienceDirect

International Journal of Pharmaceutics

journal homepage: www.elsevier.com/locate/ijpharm

QbD guided development of immediate release FDM-3D printed tablets with customizable API doses

Andrea Gabriela Crișan [a], Sonia Iurian [a,*], Alina Porfire [a], Lucia Maria Rus [b], Cătălina Bogdan [c], Tibor Casian [a], Raluca Ciceo Lucacel [d,e], Alexandru Turza [f], Sebastian Porav [f], Ioan Tomuță [a]

[a] Department of Pharmaceutical Technology and Biopharmacy, Faculty of Pharmacy, "Iuliu Haţieganu" University of Medicine and Pharmacy, 41 Victor Babeș Street, 400012 Cluj-Napoca, Romania
[b] Department of Drug Analysis, Faculty of Pharmacy, "Iuliu Haţieganu" University of Medicine and Pharmacy, 6 Louis Pasteur Street, 400349 Cluj-Napoca, Romania
[c] Department of Dermopharmacy and Cosmetics, "Iuliu Haţieganu" University of Medicine and Pharmacy, 12 I. Creangă Street, 400010 Cluj-Napoca, Romania
[d] Faculty of Physics, Babeș-Bolyai University, Cluj-Napoca, Romania
[e] Interdisciplinary Research Institute on Bio-Nano-Science, Babeș-Bolyai University, Cluj-Napoca, Romania
[f] National Institute for Research and Development of Isotopic and Molecular Technologies, 67-103 Donath Street, 400293 Cluj-Napoca, Romania

ARTICLE INFO

Keywords:
Quality by Design
Design space
Fused deposition modeling
3D Printing
Polyvinyl alcohol
Customization
Immediate release

ABSTRACT

The objective of this work was to develop a fused deposition modeling (FDM) 3D printed immediate release (IR) tablet with flexibility in adjusting the dose of the active pharmaceutical ingredient (API) by scaling the size of the dosage form and appropriate drug release profile steadiness to the variation of dimensions or thickness of the deposited layers throughout the printing process. Polyvinyl alcohol-based filaments with elevated API content (50% w/w) were prepared by hot melt extrusion (HME), through systematic screening of polymeric formulations with different drug loadings, and their printability was evaluated by means of mechanical characterization. For the tablet fabrication step by 3D printing (3DP), the Quality by Design (QbD) approach was implemented by employing risk management strategies and Design of Experiments (DoE). The effects of the tablet design, tablet size and the layer height settings on the drug release and the API content were investigated. Between the two proposed original tablet architectures, the honeycomb configuration was found to be a suitable candidate for the preparation of IR dosage forms with readily customizable API doses. Also, a predictive model was obtained, which assists the optimization of variables involved in the printing phase and thereby facilitates the tailoring process.

1. Introduction

Over the last few years, the tremendous progress that has been made in terms of digital technologies with applicability in the medical field urged the pharmaceutical sector to keep pace with the innovations. The demand for modern fabrication methodologies is increasing, as the concept of personalization of therapies is gaining more and more attention. The traditional pharmaceutical manufacturing processes are appropriate for the mass production of "one size fits all" dosage forms, but for the preparation of custom-made products adapted to the individual needs of each patient, flexible fabrication platforms are required. A promising alternative is three-dimensional printing (3DP), a technology that was successfully implemented in other areas such as aerospace, automotive, robotics or even medicine (Dumpa et al., 2021; Jamróz et al., 2020). The growing interest towards its applicability for pharmaceutical manufacturing purposes emerged following the

Abbreviations: FDM, Fused Deposition Modeling; IR, Immediate Release; API, Active Pharmaceutical Ingredient; HME, Hot Melt Extrusion; 3DP, Three-Dimensional Printing; QbD, Quality by Design; DoE, Design of Experiments; FDM-3DP, Fused Deposition Modeling Three-Dimensional Printing; PVA, Polyvinyl Alcohol; CQAs, Critical Quality Attributes; DCNa, Diclofenac Sodium; KTPGS, Kolliphor TPGS; QTPP, Quality Target Product Profile; TGA, Thermogravimetric analysis; DSC, Differential Scanning Calorimetry; FTIR, Fourier-Transform Infrared Spectroscopy; SEM, Scanning Electronic Microscopy.

* Corresponding author at: Department of Pharmaceutical Technology and Biopharmacy, Faculty of Pharmacy, "Iuliu Haţieganu" University of Medicine and Pharmacy, Mailing address: 41 Victor Babeș Street, 400012 Cluj-Napoca, Romania.

E-mail addresses: crisan.andrea@umfcluj.ro (A.G. Crișan), sonia.iurian@umfcluj.ro (S. Iurian), aporfire@umfcluj.ro (A. Porfire), lucia.rus@umfcluj.ro (L.M. Rus), catalina.bogdan@umfcluj.ro (C. Bogdan), casian.tibor@umfcluj.ro (T. Casian), raluca.lucacel@ubbcluj.ro (R.C. Lucacel), alexandru.turza@itim-cj.ro (A. Turza), poravsebastian@gmail.com (S. Porav), tomutaioan@umfcluj.ro (I. Tomuță).

https://doi.org/10.1016/j.ijpharm.2021.121411
Received 27 October 2021; Received in revised form 16 December 2021; Accepted 17 December 2021
Available online 23 December 2021

approval granted by the FDA for the first 3D printed medicine (Spritam®) (Okafor-Muo et al., 2020).

The "3DP" term includes a variety of techniques that are primarily based on three processes, namely powder consolidation, liquid solidification, and the extrusion-based methodology (Dumpa et al., 2021; Jamróz et al., 2020). Fused deposition modeling (FDM) belongs to the group of techniques premised on the latter mechanism, and it is the most explored 3DP technology for pharmaceutical applicability due to its simplicity, versatility, and cost-effectiveness. It relies on feedstock drug-loaded filaments that are pushed through a nozzle and liquefied by thermal treatment. The molten material is deposited in a layer-by-layer manner on a printing platform, in conformity with the pre-established digital design, up to the point where the desired object is finalized.

For the preparation of the drug-loaded filaments, two approaches are available. The first one is through passive diffusion, which implies immersion of commercially available filaments in a drug saturated solution. The drawback of this simple procedure is that only limited drug loading is achievable, as to our knowledge, the highest reported result in the literature was 4% (Ayyoubi et al., 2021). The second alternative is fabrication by hot melt extrusion (HME), which involves thermal processing of physical blends that consist of the active pharmaceutical ingredient (API) and excipients, followed by extrusion of the molten mass through a die and solidification into a filament shape by cooling. The major advantage of HME is the possibility to prepare high drug-loaded filaments, considering that products with up to 50–60% API content were already obtained (Ayyoubi et al., 2021; Macedo et al., 2020). However, besides the thermal stability of the drug, ensuring the proper mechanical and rheological properties in order to secure the printability of the feedstock filaments remains the main concern regarding the HME methodology (Elbadawi et al., 2020a, 2020b). A lately developed practical tool is M3DISEEN software, which was created to speed up the formulation development by employing artificial intelligence learning methodologies and generating predictions regarding the required processing parameters, the mechanical properties, and the printability of the filaments (Elbadawi et al., 2020b).

3DP holds a position of advantage over the traditional manufacturing methodologies due to its prospects the in fabrication of customized medications. Personalization of doses, release profiles or even incorporation of the patient's everyday treatment into a polypill are benefits particularly relevant for distinct categories such as pediatric or geriatric patients, but also for those suffering from chronic illnesses that require daily polymedication (Dumpa et al., 2021). Zheng et al. highlighted the superiority of on-demand fabrication by 3DP in assuring accurate doses of drugs compared to the conventional subdivision of tablets by splitting (Zheng et al., 2020). However, for the mass-production of fixed-dose drug products, the conventional drug manufacturing technologies remain the pillars, since by comparison, preparation by 3DP, but especially FDM-3DP, is considerably slower (Jamróz et al., 2020). Therefore, FDM-3DP is suitable for the small-scale fabrication of dosage forms in community or hospital pharmacies, where a limited number of units per batch are prepared, as each product is individualized to the needs of a single patient (Parulski et al., 2021). Thus, in the interest of moving forward to real-life applicability, the technology needs to be adapted for facile modulation of API doses or release profiles by using the same filament and simply adjusting printing-related parameters. However, the progress made through the widely employed trial-and-error strategy are slow and involve elevated costs. A more efficient approach appears to be the association of 3DP with machine learning, which is a form of artificial intelligence. Relying on de data available in the literature and by using mathematical models that identify connections between the input and the features of the end product, machine learning can be applied to accelerate product design and development, to predict the properties of the product, or to guide the selection of the most favorable working conditions based on the sought outcome (Elbadawi et al., 2021). Castro et al. collected literature data that implicated 968 formulations and employed machine learning algorithms to forecast important HME and FDM-3DP parameters, but also the dissolution behavior of the API and the main factors that had an impact on it. The work exemplifies the applicability and effectiveness of employing artificial intelligence to facilitate the transfer of 3DP into clinical settings. Still, additional data acquired from published works and further experiments would enhance the predictive performance of machine learning models (Muñiz Castro et al., 2021).

Polyvinyl alcohol (PVA) is a multifaceted polymer and one of the most investigated materials for pharmaceutical FDM-3DP purposes, as it is implicated in 35% of the currently available studies (Cailleaux et al., 2021). Although it is a water-soluble material, in the majority of cases, slow drug release was obtained from the PVA-based FDM-3DP tablets. For instance, the results reported by Goyanes et al. disclosed complete dissolution of the API from the PVA-based structures printed with 10% infill after 6 h, while in the same timeframe, only 70% of the drug was released from the tablets fabricated with 50% and 90% infill settings (Goyanes et al., 2014). Skowyra et al. obtained the dissolution of above 80% of the API after 12 h, from dosage forms prepared with 100% infill (Skowyra et al., 2015). More recent works explored the feasibility of preparing PVA-based FDM-3D printed products with rapid release. Tablets with different API loadings (10% and 20% w/w) and infill percentages (60% and 100%) exhibited complete drug release after 45 min for the more porous structures (60% infill), while the ones prepared with 100% infill assured over 90% drug dissolution in 120 min (Wei et al., 2020). The dosage forms fabricated by Macedo et al., with 100% infill and different paracetamol loadings (10%, 30%, and 50% w/w), presented complete drug release in 90 min for the 30% and 50% drug-loaded tablets, while the same results were obtained in 180 min for the 10% API loaded dosage forms (Macedo et al., 2020). Therefore, the importance of the polymer fraction in modulating the speed of the process was highlighted. Palekar et al. obtained minicaplets with dissolution performances that were highly influenced by the dimensions of the structures, since fast release was obtained for those with lower dimensions, but the dissolution rates decelerated by increasing the size of the dosage forms (Palekar et al., 2019). Moreover, the versatility of PVA was further evidenced by the preparation of tablets with different release patterns through variation of the shapes of the printed structures, as the dissolution behavior of the FDM-3D printed systems is susceptible to modulation by altering the surface area to volume ratio (Xu et al., 2019).

The Quality by Design (QbD) approach represents an effective instrument that supports the development of products with the desired quality attributes by assisting knowledge-gathering regarding the effects of variable factors on the output. The concept replaces the standard one factor at once method and enables the systematic acquisition of relevant information regarding the elements that affect the characteristics of the desired product by using multivariate investigations. The Design of Experiment (DoE) methodology is an effective QbD instrument that assists the analysis of the relevant independent variables in a structured way that provides insight into their effects and probable interactions (Gavan et al., 2020). Consequently, by connecting the relationships between the variables and the critical quality attributes (CQAs) of the desired product, the design space or the multidimensional association of factors that grant the best possible features is established. A limited number of published works have already applied the DoE approach to outline the 3DP related factors that determine the mass of the obtained tablet, the required printing time to create the object or the porosity of the obtained structure (Pires et al., 2020), but also to understand the interdependence between different printing variables and the drug release performance by examining structure–function connections by using QbD tools (Zhang et al., 2020). Another investigation aimed to develop IR tablets by focusing on the critical material attributes and conducting a systematical investigation of the influence of different compositions on the characteristics of the obtained products (Than and Titapiwatanakun, 2021).

Diclofenac is one of the most prescribed non-steroidal anti-

inflammatory drugs, primarily used for the management of pain and inflammation (Siozou et al., 2021). It is eligible to be included in drug products that enable dose adjustments since the lowest dose that still ensures clinical efficacy is recommended, particularly for specific patient categories such as the pediatric and geriatric population, or in the case of patients suffering from hepatic insufficiency. Moreover, it is an appropriate candidate to be incorporated in dosage forms prepared via the HME-FDM-3DP methodology on account of its good stability at the high processing temperatures required by the preparation techniques.

The aim of this work was to develop an immediate release (IR) FDM-3D printed tablet with flexibility in API dose adjustment by size scaling, and also good predictability and steadiness in terms of release profile to the variability of printing settings. The first step involved the preparation and optimization of PVA-based filaments, as our goal was to obtain the highest drug loading that still assured appropriate mechanical properties for FDM-3D printability. However, the novelty of the work mainly lies in the tablet development phase, for which a QbD approach was employed to investigate the effect of factors involved in the 3DP process on the characteristics of the dosage forms, and a model that enables the optimization of the printing parameters in order to obtain tablets with specific target doses and predictable dissolution behaviors was generated. As per the obtained findings, the proper association of variables guided by the QbD methodology, namely tablet architecture, tablet dimension, and thickness of the deposited layers throughout the 3DP step, secures the production of the desired product.

2. Materials and methods

2.1. Materials

The API, diclofenac sodium (DCNa, pharmaceutical grade), was kindly donated by Aarti Drugs Ltd (Mumbai, India). Polyvinyl alcohol Parteck® MXP (PVA, pharmaceutical grade) was kindly gifted by Millipore Sigma (Billerica, MA). Ph Eur and USP compliant D-alpha-tocopheryl polyethylene glycol succinate, Kolliphor® TPGS (KTPGS), was purchased from BASF (Ludwigshafen, Germany) and Aerosil® 200 (pharmaceutical grade colloidal silicon dioxide) was acquired from Evonik Industries AG (Essen, Germany). All other materials were of analytical grade and used as supplied.

2.2. Filament optimization

2.2.1. Filament preparation by HME

Hot melt extrusion technique was employed for the preparation of filaments by processing the physical mixtures with the compositions presented in Table 1. The blends were prepared by pre-weighing the constituents and mixing them in mortar with pestle. A single-screw equipment (Noztek Pro, Noztek, UK) with a screw speed of 65 rpm and one electrically heated compartment was employed for the fabrication of the drug-loaded filaments. The mixtures were fed into the apparatus at a 1–2 g/min rate, processed at 190 °C and extruded through a 1.75 mm die. The filaments were collected manually and stored at room temperature in sealed plastic bags to inhibit moisture absorption.

Table 1
HME blend compositions and the coding of the fabricated filaments.

Blend name	DCNa (%)	PVA (%)	KTPGS (%)	Aerosil (%)	Filament
PM-PVA	–	99	–	1	Fil-PVA
PM-PVA-P	–	90	9	1	Fil-PVA-P
PM-PVA-P-D10	10	80	9	1	Fil-PVA-P-D10
PM-PVA-P-D20	20	70	9	1	Fil-PVA-P-D20
PM-PVA-P-D30	30	60	9	1	Fil-PVA-P-D30
PM-PVA-P-D40	40	50	9	1	Fil-PVA-P-D40
PM-PVA-P-D50	50	40	9	1	Fil-PVA-P-D50
PM-PVA-P-D60	60	30	9	1	Fil-PVA-P-D60

2.2.2. Mechanical characterization and FDM printability of filaments

CT3 Texture Analyzer (Brookfield Engineering Laboratories, MA, USA) was used to assess the mechanical properties of the filaments. The registered data were analyzed by TexturePro CT V1.9 Software.

Brittleness and flexibility were evaluated by running the Rupture Test. Briefly, the filament samples were prepared by cutting 4 cm pieces and measuring their diameter by using a digital caliper. The employed accessories were the fixture base table and a custom-made removable insert with a 20 mm supporting gap as a sample holder, similar to the film support fixture, as shown in Fig. 1(a). The filament ends were immobilized between the two parts of the insert. A blunt blade of 3 mm thickness was set to move with a test speed of 1 mm/s, while the trigger load was set at 10 g. Measurements were carried out in triplicates.

For the evaluation of the filaments' stiffness, samples were cut into 5 mm pieces and placed on the sample holder, as shown in Fig. 1(b), in order to perform a texture profile analysis (TPA) test. A sharp blade was set to penetrate the sample with a deformation target value of 5%. Other test parameters were a trigger load of 10 g and 0.1 mm/s test speed. Five determinations were carried out for each formulation.

2.3. Solid state and morphological evaluations

2.3.1. Thermogravimetric analysis (TGA)

The TGA curves were obtained with a TGA SDTA 851e thermobalance (Mettler Toledo GmbH, Switzerland). The samples of API, excipients, physical mixture, API loaded filament and 3D printed tablet were weighed (approximately 5 mg) and placed in 70 μL open alumina pans. The measurements were carried out in the temperature range of 25–500 °C, with a heating rate of 10 °C/min, and by using N_2 as an inert purge gas (50 mL/min). The results were analyzed using Mettler Toledo STAR SW 12.10 software in order to assess the thermal decomposition of the samples.

2.3.2. Differential scanning calorimetry (DSC)

The DSC analysis was carried out using DSC 822 equipment (Mettler Toledo GmbH, Switzerland). Samples of API, excipients, physical mixture, API loaded filament and 3D printed tablet were accurately weighed (2–3 mg) to 40 μL aluminum pans and closed with pierced lids. Each sample was analyzed under a dynamic nitrogen atmosphere (50 mL/min), in the temperature range of 25–400 °C and a heating rate of 10 °C/min. Data was collected with Mettler Toledo STAR SW 12.10 software and assessed for the purpose of identifying physical state transformations occurring during the processing steps.

2.3.3. X-ray diffraction (XRD)

The XRD patterns of the samples (DCNa, excipients, physical blend, filament, and 3D printed tablet) were recorded on a Bruker D8 Advance powder diffractometer (Bruker AXS GmbH, Karlsruhe, Germany) with Cu Kα1 radiation and the X-ray tube operating at 40 kV and 40 mA. The diffractometer is equipped with a germanium monochromator which is used in order to obtain only the Cu-Kα1 radiation and a LINXEYE detector. All samples were scanned with DIFFRAC plus XRD Commander Software considering an angular range of 2° to 85° 2θ and a scan speed of 0.02 θ/s.

2.3.4. Fourier-Transform Infrared Spectroscopy (FTIR)

For the FTIR measurements, the powdered samples were mixed with KBr to obtain thin pellets with a weight ratio of sample:KBr of 1:100. The pellets thickness was about 1.5 mm. The spectra were recorded at room temperature in the 350–4000 cm^{-1} range on a 6100 Jasco spectrometer

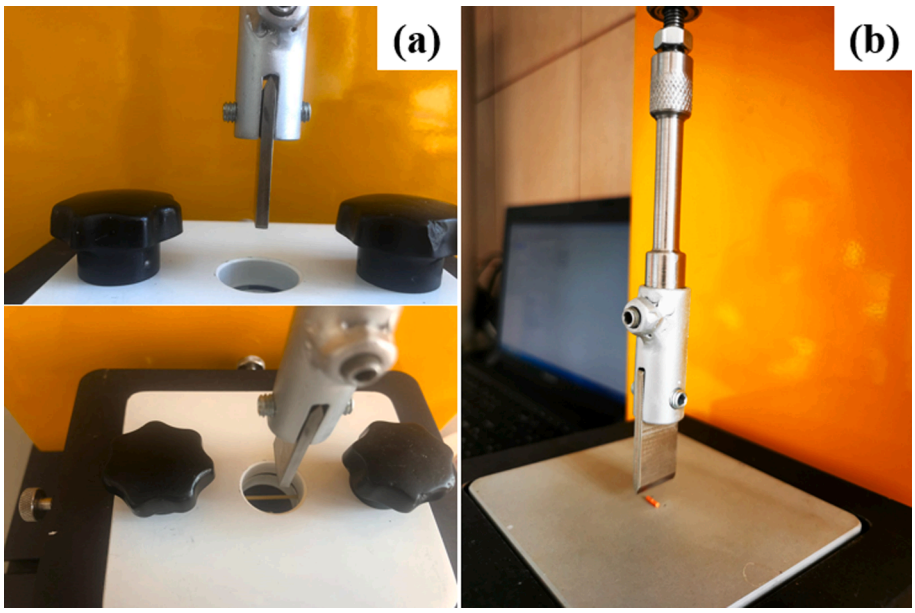

Fig. 1. Experimental set-up for (a) – flexibility and brittleness test and (b) – stiffness test.

with a resolution of 0.5 cm^{-1} and a signal/noise ratio 42.000:1.

2.3.5. Scanning electronic microscopy (SEM)

Samples provided for SEM analysis were prepared by the standard protocol. Briefly, the samples were mounted on carbon double adhesive tape, attached to brass stubs and coated with a 10 nm layer of gold. Image acquisition was conducted on a Hitachi SU8230 High Resolution Scanning Electron Microscope equipped with a cold field emission gun. The microscope was operated at 30 kV in both low and high magnification mode. Approximately 90% of each sample was scanned to give a realistic overview of its morphology, and only a few representative areas were captured.

2.4. FDM-3DP of tablets and evaluation of their physical characteristics

Two tablet models, depicted in Fig. 2(b), were designed using TinkerCad software (Autodesk® Inc, San Rafael, CA, USA). The dimensions of both tablets were the following: length = 18 mm, width = 8 mm, height = 5 mm. The surface area of each tablet was determined by employing MeshLab v2021.05 (Visual Computing Laboratory, CNR-ISTI, Italy) and was calculated to be 874.1 mm^2 for the concentric ellipses design and 978.2 mm^2 for the honeycomb design. The printing process was carried out using MakerBot Replicator 2X (MakerBot, Brooklyn, NY) fed with Fil-PVA-P-D50 filament. The custom-designed tablets were fabricated in different sizes, adjusted by uniform scaling (60%, 75%, and 85%), and the printing process was performed by deposition of layers of materials with distinct heights (0.1 mm, 0.2 mm, and 0.3 mm). Other working parameters included the printing temperature set at 185–190 °C, platform temperature 45 °C, first layer print speed 30 mm/s and infill print speed 90 mm/s.

The dimensions of three randomly selected tablets from each batch were manually measured using a digital caliper. For the evaluation of weight uniformity, five units of each tablet type were weighed using a digital balance (Ohaus® Analytical Plus balance), followed by calculation of the average mass and deviation from the average weight. The hardness of five tablets from each formulation was assessed by using a crushing strength tester (PTB 111 E, Pharma Test, Hainburg, Germany).

2.5. The development of FDM-3D printed tablets through the QbD approach

2.5.1. Risk analysis

The starting point of the project was the delineation of the Quality Target Product Profile (QTPP) in conformity with the main directions established in the ICH Q8 guideline. The QTPP is a forward-looking summary of the quality criteria that are desired to be attained for a

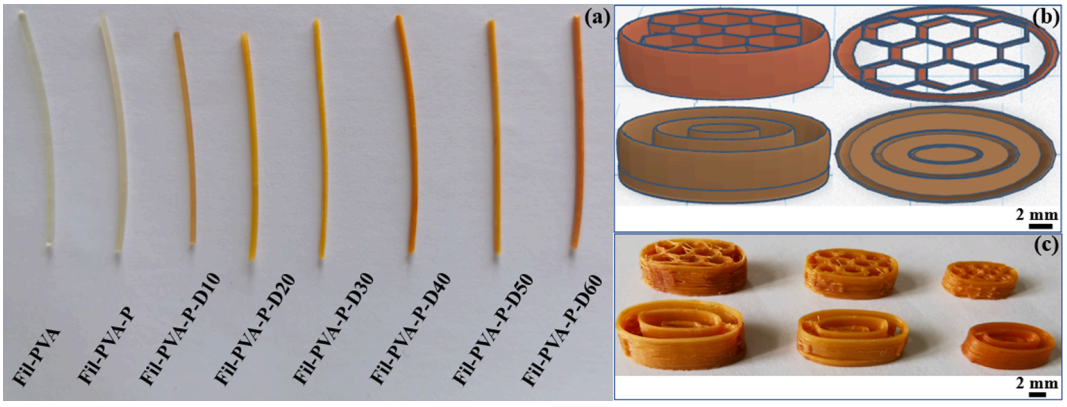

Fig. 2. (a) – Images of the filaments prepared by HME; (b) – tablet models considered for the preparation of DCNa-loaded dosage forms; (c) – images of the FDM-3D printed tablets.

pharmaceutical product (ICH Expert Working Group, 2009). In accordance with the QTPP, the CQAs of the tablets were established. The definition as per ICH Q8 establishes CQAs as physical, biological, or microbiological characteristics that are sought to be within restricted ranges, limits or distribution in order to assure the appropriate product quality (ICH Expert Working Group, 2009). The factors that were more likely to influence the quality of the target product were overviewed by Ishikawa diagrams (fish-bone diagrams) as risk analysis tools. Further, the variables with a high impact on the CQAs were evaluated through a DoE.

2.5.2. DoE

The DoE methodology, as a component of the QbD concept, was applied to investigate the effect of variables involved in the 3DP process on the quality of the final product, as the objective was the optimization of the printing phase. The Modde 12.1 software (Umetrics, Sweden) was employed for generating a D-Optimal experimental design, which is appropriate if the influence of combinations of qualitative and quantitative factors needs to be assessed. Governed by the risk analysis, three independent variables were selected for further evaluations: tablet design (X_1); tablet size by scaling (X_2); layer height (X_3). The examined responses (dependent variables) were the drug content (Y_1), the disintegration time (Y_2), the API percentages released in 5 min or D_{5min} (Y_3), and the API percentages released in 10 min or D_{10min} (Y_4). Table 2 summarizes the matrix of the experimental design consisting of 20 runs.

The results were fitted with a mathematical model, and the statistical parameters were generated in order to evaluate the quality of the chosen model. R^2 is an indicator that describes the goodness of fit, while Q^2 reveals the prediction capacity. The model validity provides an overview concerning the model error, while the differences between recorded results obtained under the same experimental conditions, evaluated against the total variation, are represented by the reproducibility parameter.

2.5.3. Evaluation of the responses

2.5.3.1. Drug content analysis. The API content in filaments and tablets was determined by placing fragments weighing approximately 37.5 mg in volumetric flasks (25 mL) containing a mixture of methanol and water (70:30). The samples were maintained in a thermostatic bath (37 ± 0.5 °C) and were intermittently subjected to shaking and ultrasonication (Transsonic T700, Elma, Germany) until complete dissolution. Aliquots (500 μL) were transferred to volumetric flasks (10 mL) and diluted with phosphate buffer at pH 6.8. The solutions were then filtered via 0.2 μm filters (Phenomenex, Torrance, CA, USA) and the DCNa contents were determined at 276 nm with a UV–VIS spectrophotometer (Specord®200 Plus, AnalytikJena, Germany).

Table 2
D-Optimal design matrix and results.

Exp. name	Run order	X_1	X_2	X_3	Y_1	Y_2	Y_3	Y_4
N1	1	A	60	0.1	29.62	240.0	57.7	83.4
N2	15	A	60	0.3	31.21	363.3	63.9	87.5
N3	12	A	85	0.1	54.11	355.0	64.6	84.4
N4	9	A	85	0.3	72.48	286.7	50.6	81.9
N5	6	A	75	0.1	46.32	260.0	83.4	96.1
N6	16	A	75	0.3	47.82	473.3	48.3	74.9
N7	17	A	60	0.2	38.52	466.7	33.0	58.0
N8	7	A	85	0.2	60.03	244.0	62.5	86.7
N9	5	B	60	0.1	36.58	365.0	53.6	86.4
N10	4	B	60	0.3	41.17	340.0	38.0	70.4
N11	10	B	85	0.1	71.43	411.0	45.5	62.2
N12	14	B	85	0.3	68.54	304.0	77.9	93.7
N13	2	B	75	0.1	54.11	270.0	73.1	92.8
N14	19	B	75	0.3	59.21	315.0	74.7	91.4
N15	8	B	60	0.2	34.42	228.3	44.1	78.5
N16	11	B	85	0.2	65.97	313.0	71.6	89.9
N17	13	B	75	0.2	51.96	297.0	69.1	94.6
N18	20	B	75	0.2	54.82	330.0	62.2	87.2
N19	18	B	75	0.2	66.18	308.0	36.2	74.1
N20	3	B	75	0.2	58.17	322.0	59.6	82.1

X_1 – tablet design (A – concentric ellipses, B – honeycomb); X_2 – tablet size by scaling (%); X_3 – layer height (mm); Y1 – drug content (mg); Y2 – disintegration time (s); Y3 – API percentages released in 5 min (%); Y4 – API percentages released in 10 min (%).

2.5.3.2. Disintegration test. The disintegration behavior of the 3D printed tablets was assessed in distilled water maintained at 37 ± 0.5 °C by using a QC-21 Hanson disintegration tester (Hanson Research, CA, USA). Each tablet subjected to evaluation was randomly chosen. The ultimate moment of disintegration was registered when no obvious tablet fragments were visible in the mesh of the basket rack assembly. All measurements were done in triplicates.

2.5.3.3. Dissolution tests. *In vitro* dissolution experiments were carried out using PT-DT70 apparatus (Pharma Test Apparatebau AG, Hainburg, Germany) with USP type II (paddle) configuration in 900 mL phosphate buffer at pH 6.8 maintained at 37 ± 0.5 °C and a stirring rate of 50 rpm. The dissolution process was monitored for 60 min. Samples were withdrawn at predefined time points (5 min, 10 min, 15 min, 30 min, 45 min, 60 min) and replaced with equal volumes of fresh medium. For the DCNa quantification, the collected aliquots were filtered and analyzed using a UV–VIS spectrophotometer (Specord®200 Plus, AnalytikJena, Germany) at 276 nm wavelength.

2.5.4. Design space determination

The "design space" is defined as "The multidimensional combination and interaction of input variables (e.g., material attributes) and process parameters that have been demonstrated to provide assurance of quality" (ICH Expert Working Group, 2009). In the present work, Modde 12.1 software was employed to assess the experimental results and to establish the design space where the QTPP stipulations are accomplished at a defined risk level. The determination of the design space relied on regression models and calculations of the probability of failure. Monte Carlo simulations were applied to merge the relevant probability statistics and risk analysis, enabling the determination of acceptable variations from the optimum factor settings that still result in the attainment of the predefined response criteria. The hazard of obtaining outputs that do not meet the response prerequisites was determined as probability of failure expressed as percentages.

3. Results and discussions

The fabrication methodology employed in the present work combines two techniques, specifically HME and FDM-3DP. In consequence, the first phase of the study focused on the preparation by HME and optimization of the drug-loaded filament, while the second one was oriented towards the optimization of the tablet preparation phase by FDM-3DP, following the QbD approach.

3.1. Filament optimization

3.1.1. Filament preparation

The aim of the HME step was to obtain high DCNa-loaded PVA-based filaments suitable for FDM-3DP. Generally, filaments with increased drug content are required to minimize the dimensions of the 3D printed dosage forms and assure patient compliance by preparing easy-to-swallow tablets. The matter is particularly important when the administration of high doses of the API is needed to obtain the desired therapeutic effect. Therefore, we systematically screened compositions by progressively increasing the API:polymer ratio, with the objective to determine the maximum drug loading that grants proper mechanical properties for the filaments intended to be further employed for the

printing process. Moreover, since the mechanical characteristics of the extrudates depend on the incorporated materials, in order to evaluate the effect of each component on these properties, a neat PVA filament (Fil-PVA) was prepared first, followed by the product based on the polymer and the plasticizer (Fil-PVA-P). Further, drug-loaded filaments with 10 to 60% w/w DCNa content (Fil-PVA-P-D10 to Fil-PVA-P-D60) were prepared, according to the qualitative and quantitative formulas of the physical mixtures subjected to HME presented in Table 1. Fragments of the obtained drug-loaded feedstock filaments are displayed in Fig. 2(a), and it is visible that the neat PVA filament (Fil-PVA), the plasticized PVA filament (Fil-PVA-P), and the filament loaded with 10% API (Fil-PVA-P-D10) are transparent and smooth products, while the filaments with higher API content are yellow. Also, it is perceivable that by increasing the DCNa content, the filaments become opaque, and the color intensity is accentuated.

3.1.2. Mechanical characterization of filaments

One of the technical challenges to overcome in pursuance of increasing the implementability of FDM-3DP as a pharmaceutical fabrication method is the assurance of proper mechanical properties of the drug-loaded filaments, which will ultimately determine their printability. Three main influencing factors were identified as determinants of filament processability by FDM-3DP, namely brittleness, flexibility, and stiffness (Xu et al., 2020). To withstand the forces applied by the feeding gears and avoid fractures, the filament must present a limited degree of brittleness. Brittle fractures appear when the involved materials break in the absence of considerable plastic deformation when exposed to stress (Gottschalk et al., 2021; Zhang et al., 2019). The flexibility of the filaments is relevant as excessive yielding impairs the process of passing forward towards the print head, and blockage might occur with printing failure, since the filament acts as a piston that pushes the molten material through the nozzle in order to enable its deposition (Aho et al., 2019; Nasereddin et al., 2018). Nonetheless, the feeding system of FDM-3D printers includes jagged gear teeth that augment grip, and therefore, the filament must be stiff to avoid surface scratching and damaging (Xu et al., 2020).

In our study, we considered two methodologies for the assessment of filament mechanical properties that are essential for FDM-3DP processability. The first one, with the experimental set-up shown in Fig. 1(a), is a variation of the three-point bending test adapted to the available equipment, which provides information regarding filament brittleness and flexibility. The second one, displayed in Fig. 1(b), is the stiffness test reported by Zhang et al., with adjusted working parameters (Zhang et al., 2019). The load-breaking distance curves obtained during the first test, represented in Fig. 3, revealed that the mechanical strength expressed by means of load decreased by elevating the API:polymer ratio. These findings were predictable since it is known that PVA has great mechanical properties (Shi et al., 2021) and by lowering the polymer content of the formulation, a decline of the resistance to deformation was to be expected. Also, the reduction of the polymer content foreseeably had an impact on the flexibility of the filaments. As a general consideration, a higher breaking distance indicates superior flexibility. Our results revealed that an increased PVA content, which corresponds to low API ratios, negatively influences the flexibility of the filaments reflected through the breaking distance (Fig. 3). The phenomenon is accountable to the constant amount of the KTPGS in each API containing filament that plasticizes different polymer quantities (i.e., 30% w/w PVA in Fil-PVA-P-D60, 80% w/w PVA in Fil-PVA-P-D10). Fig. 4(a) is a comparative overview of the fracturability of the hot melt extruded filaments, defined as the load value at break, which is an indirect indicator of the brittleness of the samples. It shows that by including the plasticizer and the drug in the formulations, the fracturability of the hot melt extruded filaments increases. Moreover, if the fracturability obtained for the Fil-PVA-P filament is compared to the results recorded for the API loaded filaments, it is noticeable that a significant increase of the brittleness caused by the presence of DCNa in the composition is encountered over drug contents of 40%, but it does not impair printing up to the 60% w/w DCNa load. Stiffness is a parameter that characterizes the mechanical features of the samples by measuring the necessary load that enables reaching a specified deformation (Zhang et al., 2019). Therefore, in terms of stiffness, the properties of the filaments were investigated by setting the blade to penetrate the sample with a deformation target value of 5%. The peak stress, which represents the ratio of the applied force to the cross-sectional domain, was selected as an indicator of the stiffness since the target deformation was kept constant. However, we were unable to perform the measurements on the filaments of neat PVA (Fil-PVA), PVA plasticized with KTPGS (Fil-PVA-P), or the ones that contained up to 40% w/w DCNa. The equipment failed to register data while these samples were subjected to analysis, as the elevated stiffness impaired the capacity of the apparatus to attain the specified target deformation. Therefore, the evaluation was successfully carried out only for the filaments loaded with 50% w/w and 60% w/w DCNa. The recorded values of the peak stress are represented in Fig. 4(b). The graphic shows that by increasing the API content and therefore diminishing the polymer:API ratio, the stiffness of the filaments is reduced.

The printability of the DCNa-loaded filaments was tested by using MakerBot Replicator 2X. Among the 6 formulations that were evaluated, the first 5 of them with drug loadings between 10% and 50% w/w presented good printability. Fil-PVA-P-D60, the filament with the highest drug content (60% w/w), was found to be unsuitable for the preparation of FDM-3D printed tablets. In case of Fil-PVA-P-D60, multiple trial printing processes were initiated and despite the fact that the deposition of the molten material was successfully initiated, the process was interrupted each time after a few layers. Therefore, in order to visualize and identify the possible causes behind the blockage of the printing process, the extrusion assembly of the printer was detached and disassembled. As shown in Fig. 4(c), the surface of the filament was practically grated by the jagged feed gear. This outcome is an indicator of the fact that the filament lacks enough stiffness. Presumably, Fil-PVA-P-D60 is appropriate for FDM-3DP in terms of brittleness and flexibility, as no filament breakage or curling was discovered. Therefore, according to the aforementioned considerations, the DCNa-loaded PVA-based filaments intended for the preparation of dosage forms by FDM-3DP require a minimum stiffness of 26.19 N/mm^2, which represents the value of the peak stress registered for Fil-PVA-P-D50.

Considering that the objective of the filament preparation and optimization phase was to obtain a product with the highest possible drug load and adequate mechanical properties to assure the FDM-3D printability, Fil-PVA-P-D50 was selected and included in the following tablet preparation phase by 3DP.

3.2. Solid state and morphological evaluations

Both HME and FDM-3DP are processes that involve thermal stress, and therefore, understanding the thermal properties of the API and the other components of the formulation (i.e., polymer, plasticizer) is a prerequisite. The heat-induced alterations in the materials were examined by means of TGA and DSC.

TGA is an analytical tool applied for the evaluation of the degradation profile of the samples. Therefore, it is employable for the determination of the maximum temperature limit for the HME and FDM-3DP phases, in order to avoid thermal decomposition of the API and the excipients. The obtained TGA thermograms, displayed in Fig. 5(a), demonstrated that the pure API and the other components are stable at the processing temperatures (HME 190 °C, FDM-3DP 185–190 °C). The thermograms of the PM-PVA-P-D50 physical mixture and Fil-PVA-P-D50 filament showed slight weight drops (~1.9% w/w and 2.5% w/w respectively) between 37 and 102 °C in case of the physical blend and 50–130 °C in case of the filament sample. These findings were caused by the progressive moisture loss from the hygroscopic polymer.

The DSC curves of DCNa, KTPGS, PVA, PM-PVA-P-D50, Fil-PVA-P-

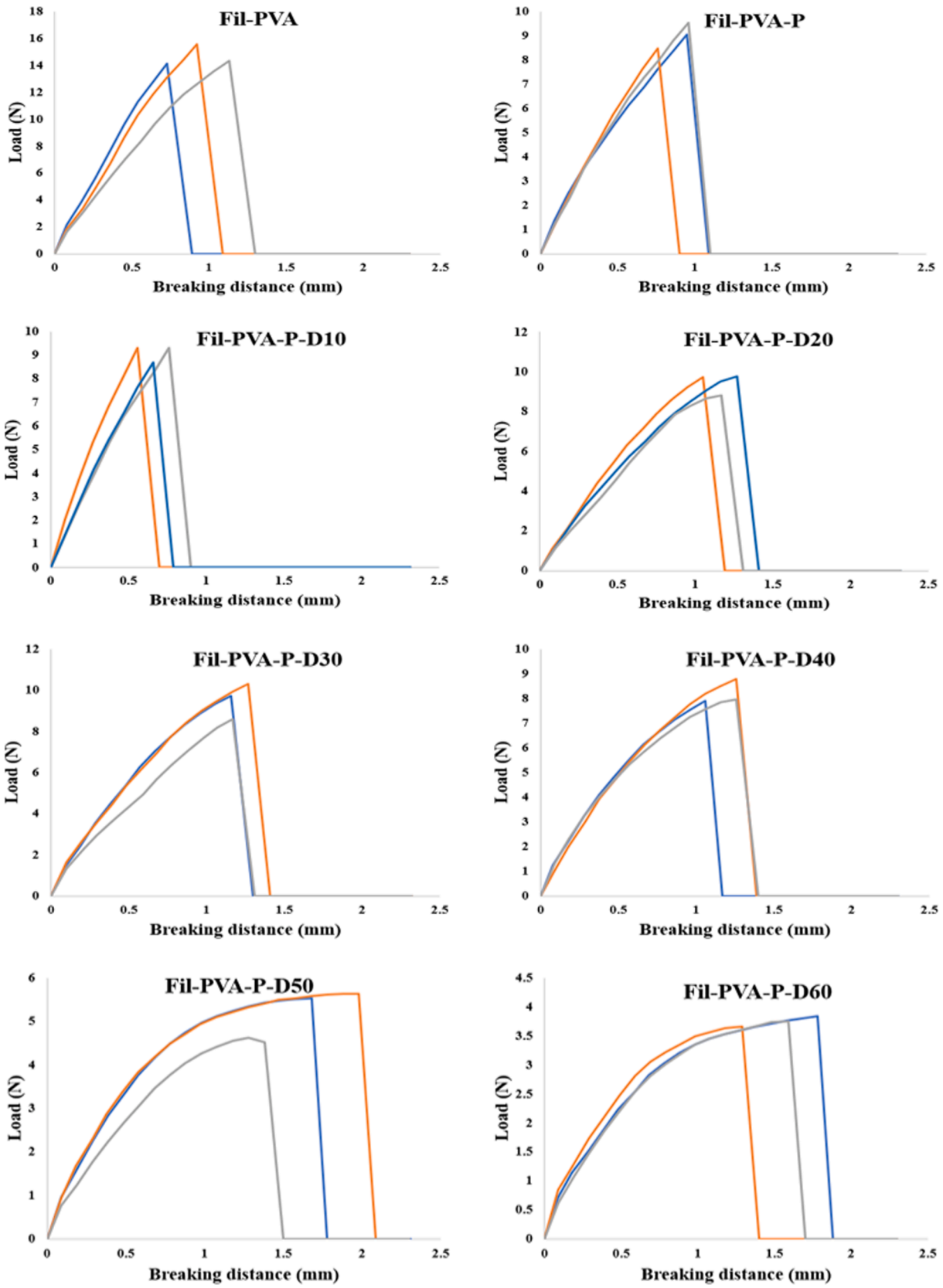

Fig. 3. Load-breaking distance curves of neat and DCNa-loaded PVA-based hot melt extruded filaments (curves of different colors represent measurements on three different samples of the same formulation).

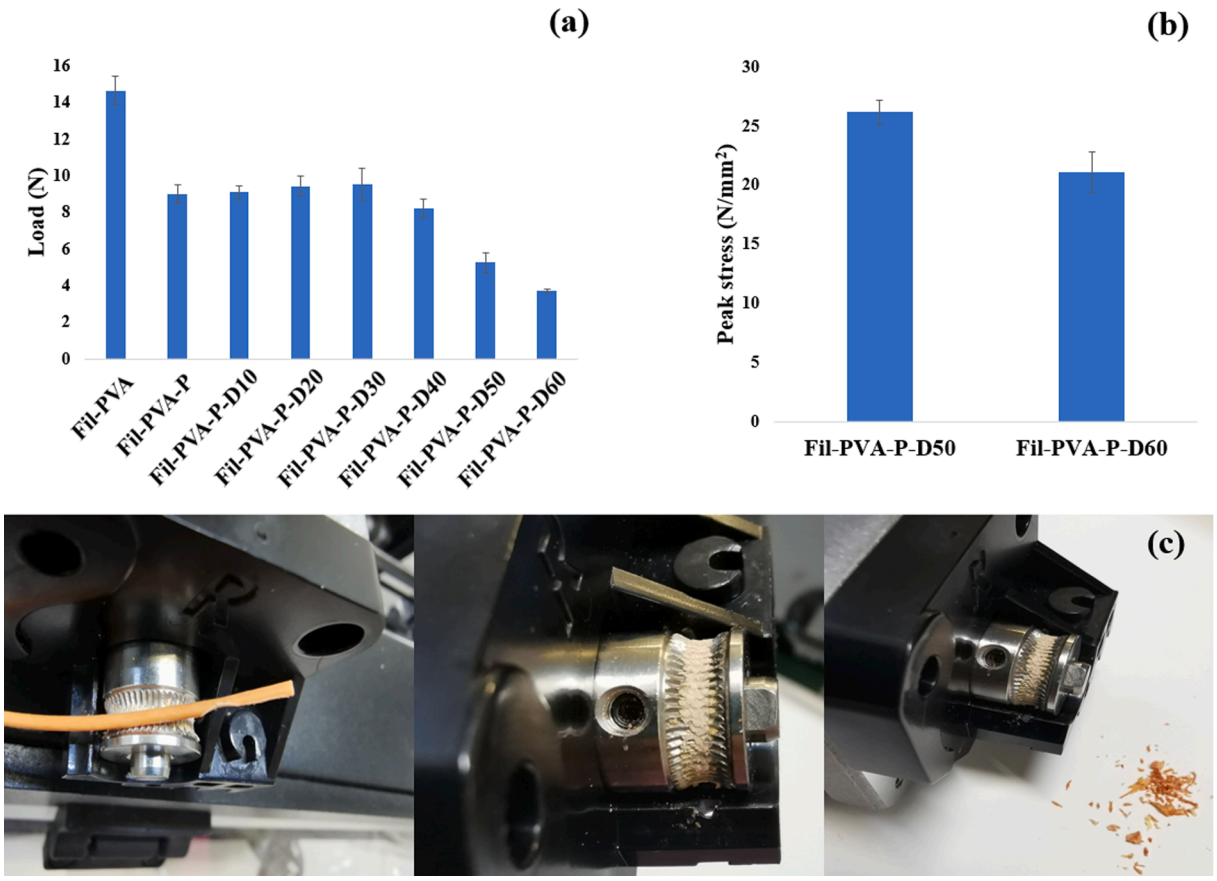

Fig. 4. (a) – Filament fracturability expressed as load at break; (b) – filament stiffness test results; (c) – detached and disassembled print head assembly following an interrupted printing process with Fil-PVA-P-D60.

D50, and 3D printed tablet are shown in Fig. 5(b). The thermogram corresponding to the pure DCNa presents a melting endotherm at approximately 287 °C, followed by an exotherm peak that corresponds to the decomposition of the API (Pasquali et al., 2007). The DSC curve of KTPGS reveals a melting endotherm at 40 °C, while in the DSC curve of PVA, the melting process is depicted at 191 °C. The results obtained in the case of the physical mixture, filament, and 3D printed tablet samples lack the melting endotherm of KTPGS and present a shift of the melting endotherm of DCNa to lower temperatures, along with a peak splitting phenomenon which presumably occurred due to an interaction between the API and KTPGS. Complementary investigations were carried out to understand the observed alterations. The absence of the KTPGS melting peak in the filament and tablet samples is also attributable to fulfilling its function as a plasticizer of the polymer, an advantage previously highlighted by Ilyés et al. (Ilyés et al., 2019), since the melting point of the polymer decreased to 180 °C.

The results of the XRD analysis of the raw materials, physical mixture, hot melt extruded filament, and the printed tablet are shown in Fig. 6(a). The diffraction pattern obtained for the pure DCNa presents multiple sharp peaks, evidencing the crystalline nature of the API. The characteristic crystalline peaks of DCNa (i.e., those with higher intensity at 6.63, 8.5 and 15.2° 2θ) are also visible in the diffractograms obtained for the filament and 3D printed tablet samples, suggesting that the API has remained crystalline following the two phases of thermal treatment. Presumably, the combination of the processing temperatures (190 °C for HME and 185–190 °C for FDM-3DP) that were below the melting point of DCNa and the high drug loading (50% w/w), that implied a reduced proportion of the matrix-forming polymer in the formulation (40% w/w), restricted the opportunity for solid state conversions to occur. The XRD findings are in accordance with the results obtained by DSC analysis, evidencing the crystallinity of the prepared drug-polymer systems.

In order to identify the possible interactions between the constituents before and after thermal processing, FTIR experiments were conducted. The FTIR spectra of the raw materials, PM-PVA-P-D50 physical mixture, Fil-PVA-P-D50 filament, and tablet samples are displayed in Fig. 6(b) and (c). The raw API exhibited representative bands for the symmetrical and asymmetrical stretching vibrations of the carboxylate groups at 1454 and 1580 cm^{-1}. The secondary amino group generated a vibration band at 3375 cm^{-1} (Barakh Ali et al., 2019; Yang et al., 2018), while the C–Cl stretching peak was exhibited at 747 cm^{-1} (Barzegar-Jalali et al., 2012). Additive spectrum was acquired for the physical mixture, and it presented the absorption bands of all the major components, showing that no chemical interactions occurred during the preparation of the blend. The spectra obtained for the filament and tablet samples followed the same pattern, except for the region where the vibration peak of the secondary amino group of DCNa was expected to be obtained. The lack of the mentioned characteristic peak following thermal treatment suggests that hydrogen bonds were established between DCNa and PVA, according to previous investigations that highlighted the occurrence of these types of interactions between PVA and other APIs presenting secondary amino groups (Wei et al., 2020). Thus, the recorded alterations involving the melting endotherm of DCNa (peak splitting and shifting) throughout the DSC analysis of the filament and tablet samples presumably occurred due to physical interactions between the API and the plasticizer.

Therefore, the solid state evaluations revealed that the raw materials are stable at the processing temperatures, and the thermal treatments applied within the HME and FDM-3DP phases do not induce a solid state conversion of the API, as DCNa remains in its stable crystalline form.

The surface morphology of the hot melt extruded DCNa-loaded filament (FIL-PVA-P-D50) is depicted in Fig. 7(a). The images expose a compact filament with a certain degree of surface roughness on account

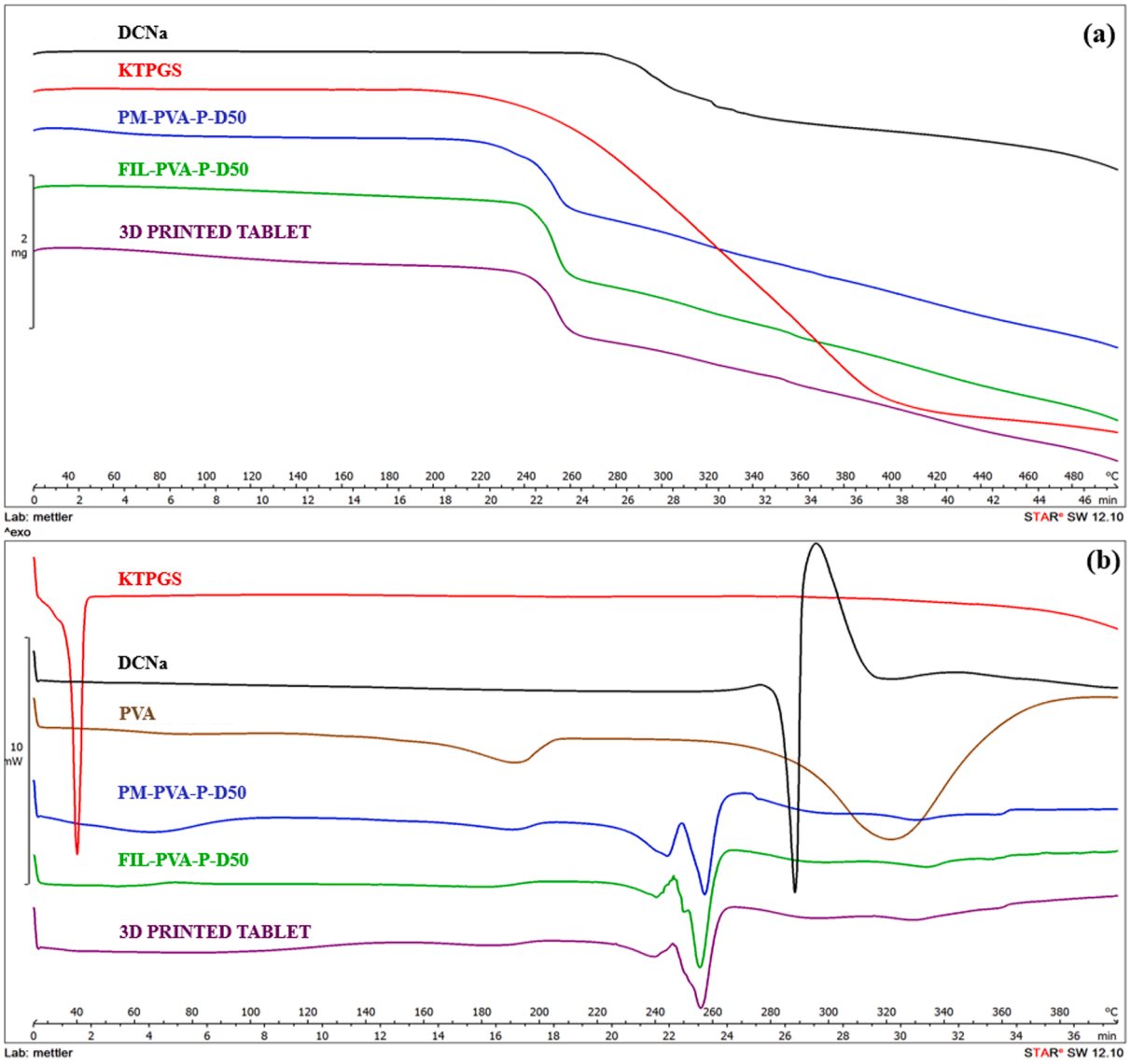

Fig. 5. Solid state evaluation (a) – TGA mass loss curves, (b) – DSC thermograms.

of the high DCNa content (50% w/w). The results were anticipated, as the API does not melt at the employed processing temperature, and therefore its crystals are dispersed in the polymeric matrix during the HME phase. In Fig. 7(b), the SEM images of the 3D printed tablets can be observed. By magnification, the API crystals disseminated within the system are visible since during the tablet preparation step, the feedstock filament was also subjected to thermal treatment at temperatures below the melting point of the drug. The observations emphasize the conclusion of the previously presented examinations, namely the absence of solid state conversions following thermal treatments.

3.3. Evaluation of the printing process and of the physical characteristics of the tablets

The PVA-based filament loaded with 50% w/w DCNa (Fil-PVA-P-D50, mean diameter of 1.38 ± 0.07 mm) was used for the preparation of the tablets, according to the experimental design matrix presented in Table 2. Images of the obtained products are displayed in Fig. 2(c). The dosage forms were prepared in three different sizes by scaling the dimensions to 85%, 75% and 60% directly through the MakerBot®Desktop Software settings. The surface areas and the volumes of the tablets with scaled dimensions were determined via MeshLab software (data not shown), and the calculations revealed that by decreasing the size of the dosage form, the surface area to volume ratio increases. Also, it was notable that the values of the surface area to volume ratio obtained for tablet B were superior to those determined for tablet A. The impact of the layer height was also studied, and three levels were investigated: 0.1 mm, 0.2 mm and 0.3 mm. It is also visible in Table 3 that the size of the tablet and the layer height settings both considerably influenced the printing time since the preparation time varied from 1 min to 8 min per unit. The differences are explicable as a larger object requires the deposition of more and wider layers, and therefore the printing time increases. On the other hand, by increasing the layer height, the desired model is realizable through the deposition of a lower number of layers (Pires et al., 2020). Therefore, although the optimization of the printing time to increase fabrication efficiency needs to be considered for the applicability of 3DP, the layer height should be carefully selected after a thorough evaluation of its potential influence on the characteristics of the final product.

Scaling the size of the digital design was applied as a strategy to modulate the drug content by modifying the average mass of the dosage forms. Table 3 shows the average weights of the prepared units, that ranged from 63.7 ± 2.0 mg to 148.24 ± 7.6 mg in case of the tablets with the concentric ellipses design (design A) and from 72.3 ± 1.1 mg to

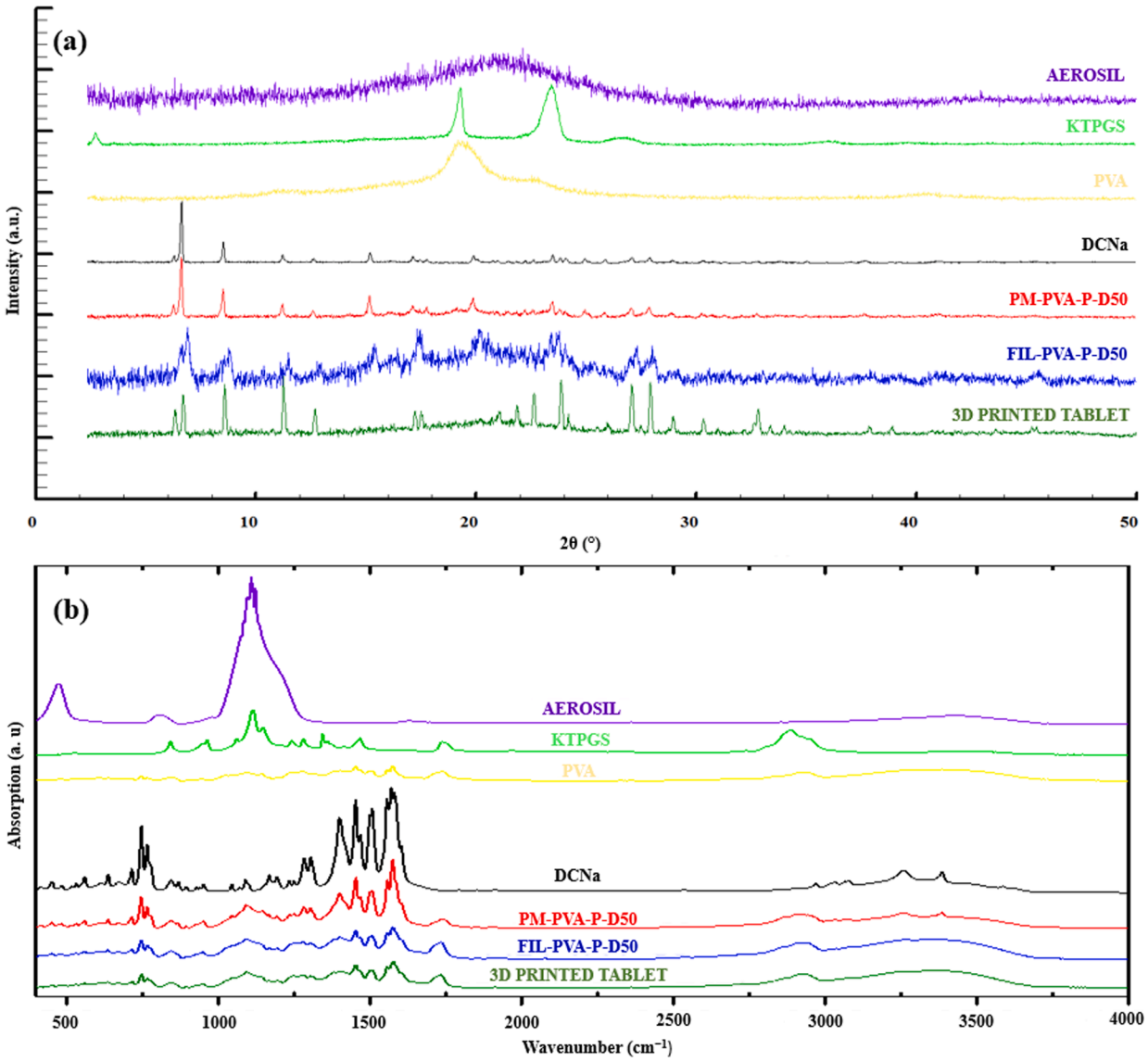

Fig. 6. Solid state examinations (a) – XRD patterns, (b) – FTIR spectra.

156.3 ± 4.9 mg for the tablets with the honeycomb pattern (design B). From the perspective of the requirements stated in the European Pharmacopoeia for the „uniformity of mass of single-dose preparations" (European Directorate for the Quality of Medicines & Healthcare, 2019a), the deviations from the average masses were below the specified limits, except for tablets N6, N17 and N18. The inconsistency in weight reproducibility in case of these formulations was most likely caused by fluctuations of the diameter of the filaments used for the printing process since the average diameter is an important parameter that is applied by the system to calculate the feed rate in the G-code. Therefore, increased attention regarding the uniformity of filament diameter is imperative to fabricate FDM-3D printed tablets with a specific API dose. In terms of hardness, the dosage forms could not be evaluated through the employed conventional methodology since the tablets solely deformed during testing, without visible breaking. Similar behavior of FDM-3D printed tablets was previously reported in the literature (Gültekin et al., 2019).

3.4. QbD guided development of FDM-3D printed tablets

The FDM-3DP technology enables the preparation of objects with various shapes and sizes. This versatility is particularly opportune in the pharmaceutical sector since more focus is directed towards developing fabrication methodologies that allow the customization of dosage forms according to the individual needs of each patient (Dumpa et al., 2021). However, it is known that within the FDM-3DP methodology, various process parameter settings are adjustable and affect the characteristics of the output. Therefore, a systematic and risk-based approach is appropriate for the development of 3D printed pharmaceutical products, that leads to knowledge-based decisions regarding the adaptable settings involved in the printing phase.

3.4.1. Risk analysis

The starting point in the development of a pharmaceutical product by applying the QbD approach, an effective tool that supports formulation and process design, is outlining the characteristics of the desired dosage form, or the QTPP. Our research was oriented towards the preparation of DCNa-loaded FDM-3D printed tablets with a predictable and reliable immediate release profile, that also grant facile dose adjustment by scaling the dimensions of the digital model. Accordingly, key product features delimited in the QTPP comprise: an appropriate geometry that enables fast disintegration of the polymeric structure and facilitates rapid and complete dissolution of the API, but also ensures a precise modulation of the drug content by modifying the size of the

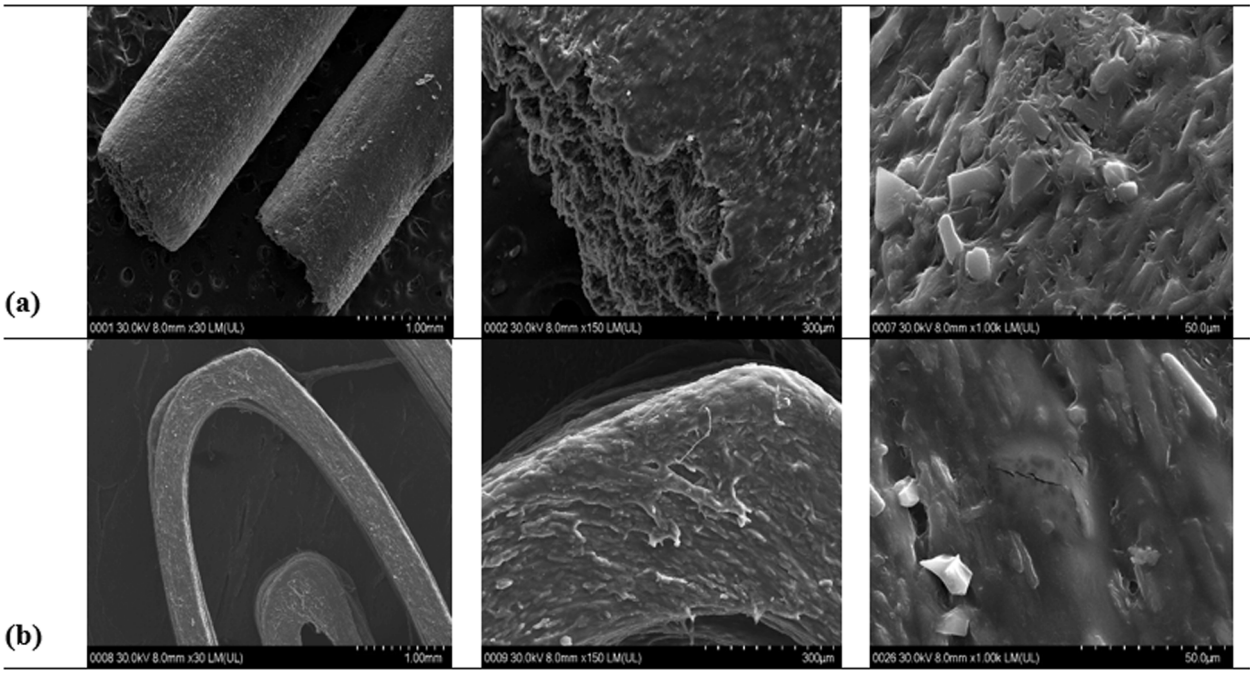

Fig. 7. SEM visualization of fragments of the (a) – hot melt extruded filaments and (b) – 3D printed tablets.

dosage form, without considerably impacting the API release profile. Therefore, in accordance with the QTPP, the drug content (Y_1), the disintegration time (Y_2) and the dissolution behavior (Y_3, Y_4) were established as CQAs.

The next step involved identifying and analyzing formulation and processing factors that might have an impact on the CQAs (ICH Expert Working Group, 2005). Thus, Ishikawa fishbone diagrams (Fig. 8) were employed as risk analysis tools to overview the material attributes and the process parameters with potential influence on the quality of the end product. Factors influencing the DCNa content of the tablets were divided into two categories, as displayed in Fig. 8(a), depending on their involvement in the HME or the FDM-3DP process. All the considered elements might alter the drug content either by affecting the stability of the API or by influencing the weight of the tablets. Factors affecting the disintegration and dissolution behavior were reviewed together (Fig. 8 (b)) since they are fundamentally the same, and were grouped in four categories: formulation, HME, 3DP and equipment variables.

No factors out of those involved in the HME process were selected to be further investigated since we considered that proper risk management is feasible by establishing the employable processing temperature that preserves the stability of the API through thermal characterization studies applied as pre-formulation tools and by good control over the powder feed rate and the screw speed which will ultimately affect the residence time of the materials in the barrel (Reitz et al., 2013). The residence time is an important process parameter that affects the properties of the filament, and consequently, the characteristics of the tablets. Prolonged exposure to shear and thermal stress could lead to degradation of the drug and other components of the formulation, but also to crosslinking between the polymer units that negatively impacts the release rate of the drug, a finding reported in our previous work (Crișan et al., 2021). On the other hand, insufficient residence time could result in deficient mixing. However, these risks are properly controllable, and the preparation of filaments with consistent attributes is achievable.

Although the formulation factors were identified as key determinants of the disintegration and dissolution behavior of the 3D printed tablets, these were not included in the experimental design. The good solubility of the API in the disintegration and dissolution media, distilled water and phosphate buffer at pH 6.8, respectively, allowed the drug-related factor to be excluded from the experimental design. Also, the polymer and plasticizer were chosen based on data available in the literature, on the experience of the researchers in the field, and on pre-formulation studies (Crișan et al., 2021; Ilyés et al., 2019; Wei et al., 2020). The factors with potential effects on the analytical methods were also reviewed and found to be adequately controlled.

Factors related to the printing phase were selected as focal points of the DoE since previous studies that explored the practicality of FDM-3DP for pharmaceutical manufacturing purposes revealed that by simply adjusting the geometry of the dosage form, its dimensions or the printing settings (i.e., infill pattern, infill density), modulation of the release profiles and the doses of the active ingredients could be feasible. Thus, the same API-loaded filament could be used for the preparation of dosage forms with customized drug content and release kinetics. Goyanes et al. were pioneers in identifying the effect of model geometry and surface area to volume ratio on the drug release patterns from 3D printed dosage forms (Goyanes et al., 2015), followed by other groups that explored channelled or multi-block unit designs to accelerate the dissolution process (Arafat et al., 2018; Crișan et al., 2021; Sadia et al., 2018). Therefore, in our study, we considered two custom-made tablet designs for developing PVA-based DCNa-loaded 3D printed dosage forms that ensure a rapid release of the API. The concept behind the designs shown in Fig. 2(b) settles on the premise that by considerably increasing the surface area/volume ratio, the API dissolution rate from the polymer abundant structure could be accelerated. Tablet design A is an original design consisting of concentric ellipses fixed on a base layer, while tablet design B is a honeycomb architecture that is similar to structures previously reported in the literature (Jamróz et al., 2020; Kyobula et al., 2017). The surface area and the volume of each tablet model with identical dimensions (length = 18 mm, width = 8 mm, height = 5 mm) were determined using MeshLab application, and the calculations revealed a surface area to volume ratio of 4.718 mm^{-1} for tablet model A and 12.128 mm^{-1} for tablet model B. As a reference, the surface area to volume ratio calculated for a conventional tablet design with the same dimensions is 0.775 mm^{-1}. Both geometries were included as qualitative factors in the DoE.

In addition to the dosage form design, the influence of the tablet dimensions was also chosen to be further studied by means of DoE. The preparation of tablets of different sizes was considered in order to

Table 3
Summary of printing time, tablet dimensions, average weight and deviation from the average weight.

Tablet	Printing time (min)	Dimensions			Average weight ± SD (mg), n = 5	Deviation from the average weight (%)
		L (mm)	W (mm)	H (mm)		
N1	3	10.46 ± 0.12	4.63 ± 0.09	2.83 ± 0.02	63.7 ± 2.0	+ 4.52 − 3.64
N2	1	10.56 ± 0.08	4.77 ± 0.04	2.8 ± 0.0	64.9 ± 2.6	+ 4.89 − 5.99
N3	5	15.01 ± 0.17	6.48 ± 0.14	4 ± 0.04	115.0 ± 2.8	+3.77 − 3.13
N4	2	15.07 ± 0.22	6.91 ± 0.35	3.89 ± 0.01	148.2 ± 7.6	+ 6.99 − 7.45
N5	4	13.04 ± 0.15	5.72 ± 0.18	3.42 ± 0.08	102.1 ± 3.4	+ 3.58 − 4.39
N6	2	13.38 ± 0.17	6.04 ± 0.10	3.34 ± 0.01	112.5 ± 12.3	+ 14.85 − 10.28
N7	2	10.59 ± 0.15	4.91 ± 0.07	2.99 ± 0.13	84.3 ± 4.0	+ 7.33 − 5.68
N8	3	14.98 ± 0.08	6.63 ± 0.25	3.96 ± 0.09	134.0 ± 8.2	+ 6.76 − 5.65
N9	4	10.25 ± 0.35	4.73 ± 0.13	2.79 ± 0.1	80.3 ± 3.6	+ 6.88 − 5.73
N10	2	10.21 ± 0.03	4.94 ± 0.11	2.83 ± 0.08	88.0 ± 2.7	+ 4.82 − 3.23
N11	8	14.73 ± 0.09	6.5 ± 0.05	4.13 ± 0.01	156.3 ± 4.9	+ 2.57 − 5.65
N12	3	14.87 ± 0.03	6.79 ± 0.01	3.96 ± 0.04	150.8 ± 8.5	+ 6.58 − 6.9
N13	6	12.83 ± 0.03	5.72 ± 0.07	3.52 ± 0.22	113.0 ± 5.8	+ 6.2 − 7.44
N14	5	13.02 ± 0.01	5.84 ± 0.04	3.69 ± 0.04	129.2 ± 5.8	+ 6.2 − 4.66
N15	2	10.24 ± 0.07	4.7 ± 0.01	2.7 ± 0.01	72.3 ± 1.1	+ 2.53 − 1.33
N16	4	14.73 ± 0.09	6.67 ± 0.05	3.88 ± 0.05	142.3 ± 7.3	+ 6.24 − 7.32
N17	3	12.96 ± 0.12	5.9 ± 0.05	3.52 ± 0.04	116.4 ± 5.6	+ 7.68 − 4.99
N18	3	13.18 ± 0.02	6.11 ± 0.07	3.68 ± 0.03	122.9 ± 10.5	+ 11.17 − 7.72
N19	3	13.10 ± 0.13	5.99 ± 0.07	3.72 ± 0.04	122.2 ± 2.0	+ 2.16 − 2.13
N20	3	12.96 ± 0.12	5.82 ± 0.13	3.57 ± 0.06	115.4 ± 1.4	+ 1.62 − 1.25

L = length, W = width, H = height.

explore the feasibility of modulating the API dose by scaling and achieving similar drug release performances since it was previously reported in the literature that the increased dimensions of the PVA-based 3D printed systems have a negative impact on the release rate of the drug (Palekar et al., 2019). Furthermore, since the effects of the layer height on the weight and the porosity of the fabricated dosage forms, as well as on the required time for the printing process, were previously investigated (Pires et al., 2020), we herein aimed to examine if the thickness of the deposited layers has an influence on the dissolution behavior of the tablets.

3.4.2. DoE

To gain a better understanding of the influence of factors involved in the printing phase on the quality of the final dosage form, a systematic investigation was conducted by employing the DoE methodology. DoE is a time and cost-efficient approach that provides a better insight into the studied process by disclosing the important factors that are involved in it, along with their main effects and the interactions between them. It allows obtaining complex information by performing a reduced number of experiments. The effects of three variables were chosen to be studied, namely: tablet design (X_1), tablet size scaling (X_2), and layer height (X_3). The levels set for the independent variables were founded on preliminary investigations. A D-Optimal experimental design (Table 2) was used to optimize the preparation process of the 3D printed tablets with the predefined QTPP by evaluating four responses (dependent variables): Y_1 – DCNa content, Y_2 – disintegration time, Y_3 – API percentages released in 5 min and Y_4 – API percentages released in 10 min.

3.4.2.1. Summary of fit. In attempt to fit the mathematical model to the results obtained for each dependent variable, which are presented in Table 2, the multiple linear regression approach was operated. Statistical validation was also carried out by analysis of variance (ANOVA, 95% confidence interval). The relevant findings are displayed in Table 4, which show that each response is properly fitted and predicted by the model since the calculations exposed high values for R^2 and Q^2 ($R^2 > 0.86$, $Q^2 > 0.59$) in each case. Moreover, the statistical significance of the models was evidenced by the ANOVA test that revealed p-values below 0.05 for each response.

3.4.2.2. Influence of factors over the drug content (Y_1). The evaluation of the drug content in filaments and 3D printed tablets serves as an indicator of the extrusion process efficiency, but also of the physical and chemical integrity of the drug following the thermal shock involving methodologies. Therefore, samples of Fil-PVA-P-D50 were firstly investigated, and a DCNa content of 48.10 ± 1.48% w/w was found for the filament with a theoretical API loading of 50% w/w. According to the literature, the lower drug content might be caused by the reaggregation and de-mixing resulting from melt viscosity discrepancies and intrinsic alterations in flow dynamics which are likely to occur when the process is carried out via a single-screw extruder (Ayyoubi et al., 2021). Other hypotheses under consideration include the adherence of the drug powder to the wall of the extruder barrel (Thanawuth et al., 2021) or the thermal decomposition of the API. However, the premise that no significant drug loss occurred during HME in our case is supported by the thermal investigations, which revealed that the drug is stable at the employed processing temperature. Secondly, the drug loading in the 3D printed dosage forms was assessed, and a mean amount of 47.87 ± 1.19% w/w DCNa content was obtained, confirming that no drug loss emerged throughout the printing process. Thus, the lower API content of the final dosage form compared to the theoretical value (50% w/w) is caused by the drug loss that occurs in the filament preparation step.

The DCNa doses in each tablet prepared according to the preset experimental design are presented in Table 2. The variation of the API content among the formulations is a result of the differences among the tablet masses. By overviewing the influence of the studied factors on the DCNa content (Y_1), predictably, the main element that determines the tablet weight is the dimension of the dosage form (X_2), as is revealed by the coefficient plot depicted in Fig. 9(a). The DCNa loading is also secondarily impacted by the layer height (X_3), considering that by carrying out the printing process through the deposition of thicker layers, higher drug contents were detected. The effect of the layer height on the

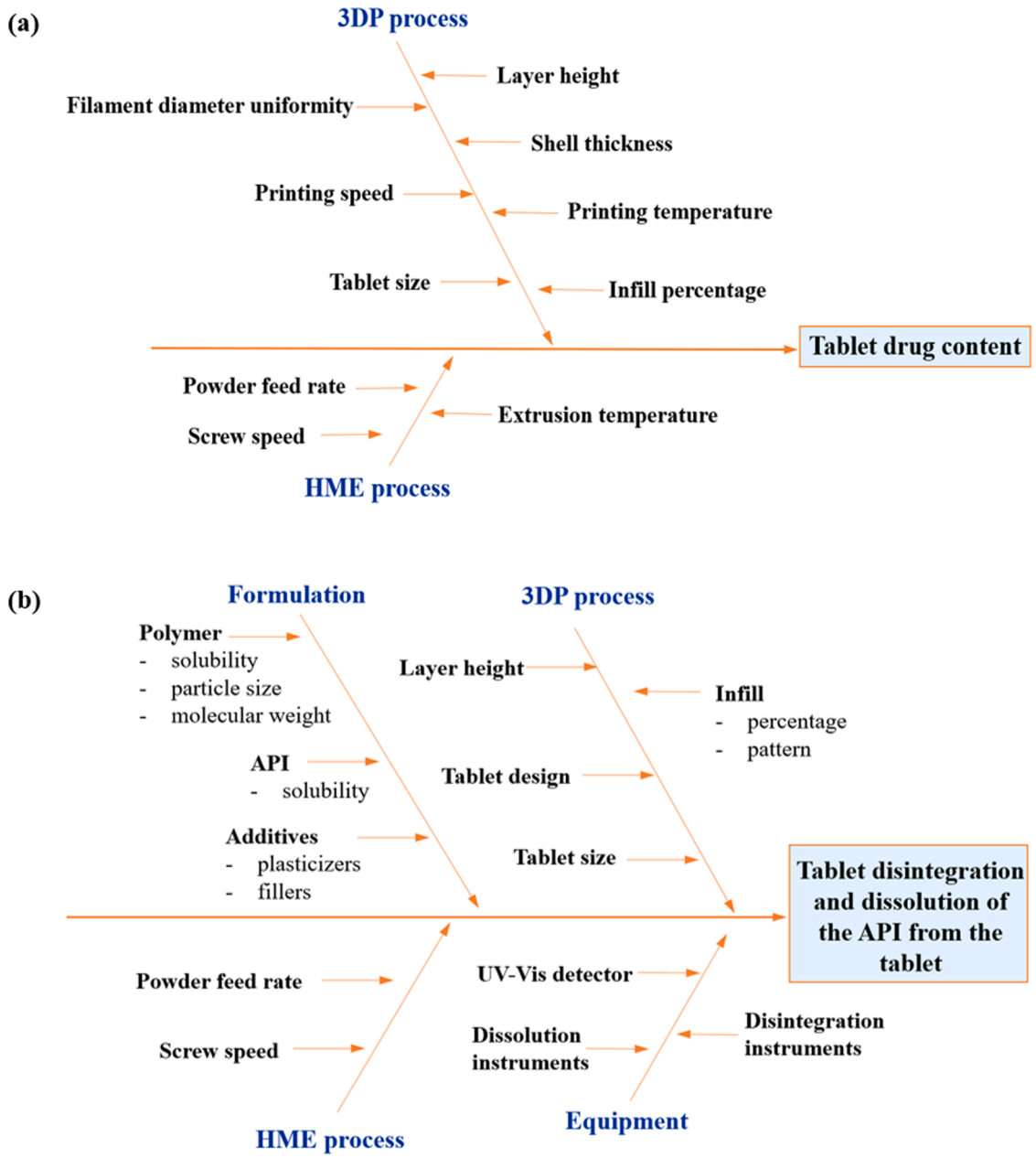

Fig. 8. Ishikawa diagrams depicting factors that may influence (a) – the DCNa content of the dosage forms, (b) – the tablet disintegration and the dissolution of the API from the 3D printed tablet.

drug content is more evident for the A design tablets, as it is noticeable in the contour plot displayed in Fig. 9(a).

3.4.2.3. Influence of factors over the disintegration (Y_2). In the case of the tablets fabricated through conventional methodologies, fragmentation into smaller pieces and particles is the characteristic behavior during the disintegration testing. In contrast, the polymer-rich dosage forms prepared by FDM-3DP are dissolved through surface erosion mechanisms (Gültekin et al., 2019; Nukala et al., 2019; Palekar et al., 2019; Patel et al., 2021). Therefore, the absence of visible tablet fragments in the mesh of the basket rack assembly was considered the endpoint of the disintegration process, and it occurred in less than 8 min for all the formulations, according to the results displayed in Fig. 10. As compared, Palekar et al. reported disintegration times from 20 min to 38 min for PVA-based FDM-3D printed minicaplets with smaller dimensions and diverse infill patterns and porosities modulated by variation of the infill percentages (Palekar et al., 2019). In our case, faster disintegration was presumably achieved for all the formulations as a result of the chosen tablet designs and the high drug loading, respectively. More specifically, the concentric ellipses and honeycomb patterns ensured a better interaction between the dosage forms and the media through the increased surface area, which promoted the erosion-mediated disintegration (Gültekin et al., 2019). On the other hand, the process was also facilitated by the high drug loading (50% w/w), which restrained the proportion of the polymer (40% w/w) in the formulation.

Although all the analyzed formulations disintegrated rapidly, the recorded results ranged from 228.3 s to 473.3 s, as attested by the data displayed in Table 2. The encountered variability reflects the effect of the independent variables chosen to be studied by means of DoE. According to the coefficient plot of Y_2 shown in Fig. 9(b), among the investigated factors, the layer height (X_3) had the greatest influence over the disintegration time, followed by the tablet design (X_1). Thus, lower disintegration times were recorded for the dosage forms fabricated through the deposition of thicker layers. The magnitude of the effect was

Table 4
Summary of fit.

Response	R^2	Q^2	P value	F value	Model validity	Reproducibility
Y1						
Regression	0.904	0.810	1.1690e-06	2.6381e + 01	0.947	0.792
Lack of fit			8.1114e-01	5.2759e-01		
Y2						
Regression	0.961	0.843	1.1351e-05	3.2228e + 01	0.707	0.958
Lack of fit			3.1086e-01	1.9558e + 00		
Y3						
Regression	0.879	0.682	1.7579e-04	1.3342e + 01	0.785	0.881
Lack of fit			4.2515e-01	1.6974e + 00		
Y4						
Regression	0.863	0.599	1.2735e-03	8.9672e + 00	0.926	0.661
Lack of fit			7.4555e-01	6.1277e-01		

Y_1 – drug content (mg); Y_2 – disintegration time (s); Y_3 – API percentages released in 5 min (%); Y_4 – API percentages release in 10 min (%); R^2 – the level of variation described by the model; Q^2 – measure of the predictive accuracy of the model; P value – statistical significance; Model validity – the degree of correspondence of the model to real measurements; Reproducibility – the variation of the response under the same conditions.

higher for those prepared according to tablet design A. Therefore, a more robust disintegration behavior to the alteration of layer thickness is representative for tablet design B. Also, an important interaction occurs between the tablet design (X_1) and the tablet size (X_2). The disintegration of tablets with concentric ellipses design is accelerated by increasing the size of the dosage form. Contrarily, the process is faster for honeycomb tablets with smaller dimensions. An interaction between the tablet size (X_2) and the layer height (X_3) was also identified. More specifically, the effect of the layer thickness is particularly important for the dosage forms with reduced sizes, as the disintegration process is faster if the tablets were constructed by depositing thin layers of the molten material. However, by increasing the dimensions, the effect of the layer height is diminished, and similar disintegration behaviors are attained.

3.4.2.4. Influence of factors over the in vitro release behavior (Y_3, Y_4). The dissolution profiles of the tablets with different designs, dimensions and prepared with various layer height settings are presented in Fig. 11. The results obtained for all the formulations are in agreement with the dissolution specifications of the European Pharmacopoeia for immediate release dosage forms (European Directorate for the Quality of Medicines & Healthcare, 2019b). Moreover, except for N7 and N11, all the tablets exhibited an API release of at least 85% in 15 min. The achievement is noteworthy since, in many cases, slow and incomplete API dissolution is characteristic for FDM-3D printed tablets. Therefore, considering that a rapid onset of the pharmacological effect is often required, identifying strategies for the development of immediate release FDM-3D printed tablets is important for the applicability of the technology for pharmaceutical fabrication purposes.

In the present work, the rapid release was facilitated by two major factors. The first one is the tablet geometry, which on account of the increased surface area to volume ratio, assured a greater contact between the dissolution media and both types of tablets with original 3D designs. The relationship between the surface area to volume ratio of FDM-3D printed tablets and their dissolution profiles was previously evidenced in the literature (Gorkem Buyukgoz et al., 2020). The second one is the reduced proportion of the polymer (40% w/w) in the formulation. Earlier works identified the limiting effect of the matrix-forming material on the dissolution rate of the API from FDM-3D printed structures, as the drug remains enclosed within the dosage form and is slowly released with the erosion of the polymer (Patel and Serajuddin, 2021). The influence of the PVA fraction on the release performance of 3D printed tablets was priorly emphasized, as complete drug dissolution was attained in 180 min for the dosage forms with 90% polymer content, while the process required 90 min for those that consisted of 50% PVA (Macedo et al., 2020). However, by coupling approaches that support dissolution rate enhancement, i.e., favorable tablet design and reduced polymer proportion, the dissolution process could be further accelerated, as attested by the release profiles observable in Fig. 11.

However, although the API was rapidly released from all the formulations, the variation of the tablet design, tablet size, and height of the deposited layers generated differences among the tablets regarding the speed of the process, mainly in the initial phase of the dissolution. Therefore, the responses that were selected to determine the influence of the studied factors on the release of the drug were the API percentages dissolved in 5 min (Y3) and 10 min (Y4), since the differences between the results obtained for the subsequent sampling points diminished with the passing of time. Thus, by knowledge-based modulation of the factors that exert an influence on the dissolution in the mentioned interval, the fastest possible release rate for different target API doses is achievable.

The data presented in Table 2 shows that the percentages of DCNa released after 5 min varied from 33.0% to 83.4% for different factor associations. The histogram displayed in Fig. 9(c) offers an insight into the type and the extent of each variable's effect on D_{5min}. A significant influence is revealed from the tablet size (X_2) and the layer height (X_3), respectively. Moreover, interactions between the tablet design (X_1) and the layer height (X_3), but also between the tablet size (X_2) and the layer height (X_3) are noticeable. The four-dimensional (4D) contour plots depicted in Fig. 9(c) facilitate the observation and interpretation of these effects. It is noticeable that the dissolution of the tablets prepared according to the A design (X_1-A) is significantly influenced by the chosen layer height (X_3) setting for the printing process. Therefore, a greater layer thickness has a negative impact on the percentages of DCNa released in 5 min, while the deposition of thinner stratums facilitates the dissolution process. On the other hand, the tablets with the honeycomb design (X_1-B) exhibit a more robust dissolution performance, regardless of the chosen layer height. The differences between the two types of tablets are most likely caused by the dissimilarities regarding the surface area to volume ratio, one of the factors established as determinative of the drug release rate by previous works (Gorkem Buyukgoz et al., 2020; Obeid et al., 2021). The surface area to volume ratios calculated based on the parameters determined for the two designs in the case of the tablets with unscaled dimensions were previously presented. Although the contact between the API-loaded polymeric matrix was significantly improved compared to a conventional tablet of the same dimensions by employing either of the two proposed original tablet designs, the higher surface area to volume ratio granted by the honeycomb pattern as compared to the concentric ellipses design, irrespective of the size of the dosage forms (data not shown), assures a steadier dissolution rate in case of layer height variations.

The interaction between the tablet size (X_2) and the layer height (X_3) is also perceivable in Fig. 9(c). More specifically, if the printing process is carried out by depositing thicker layers (0.3 mm), there is a considerable variation in the amount of the released drug in 5 min for tablets with different dimensions. In contrast, if the fabrication by FDM-3DP is done by choosing lower layer height settings (0.1 mm), reduced

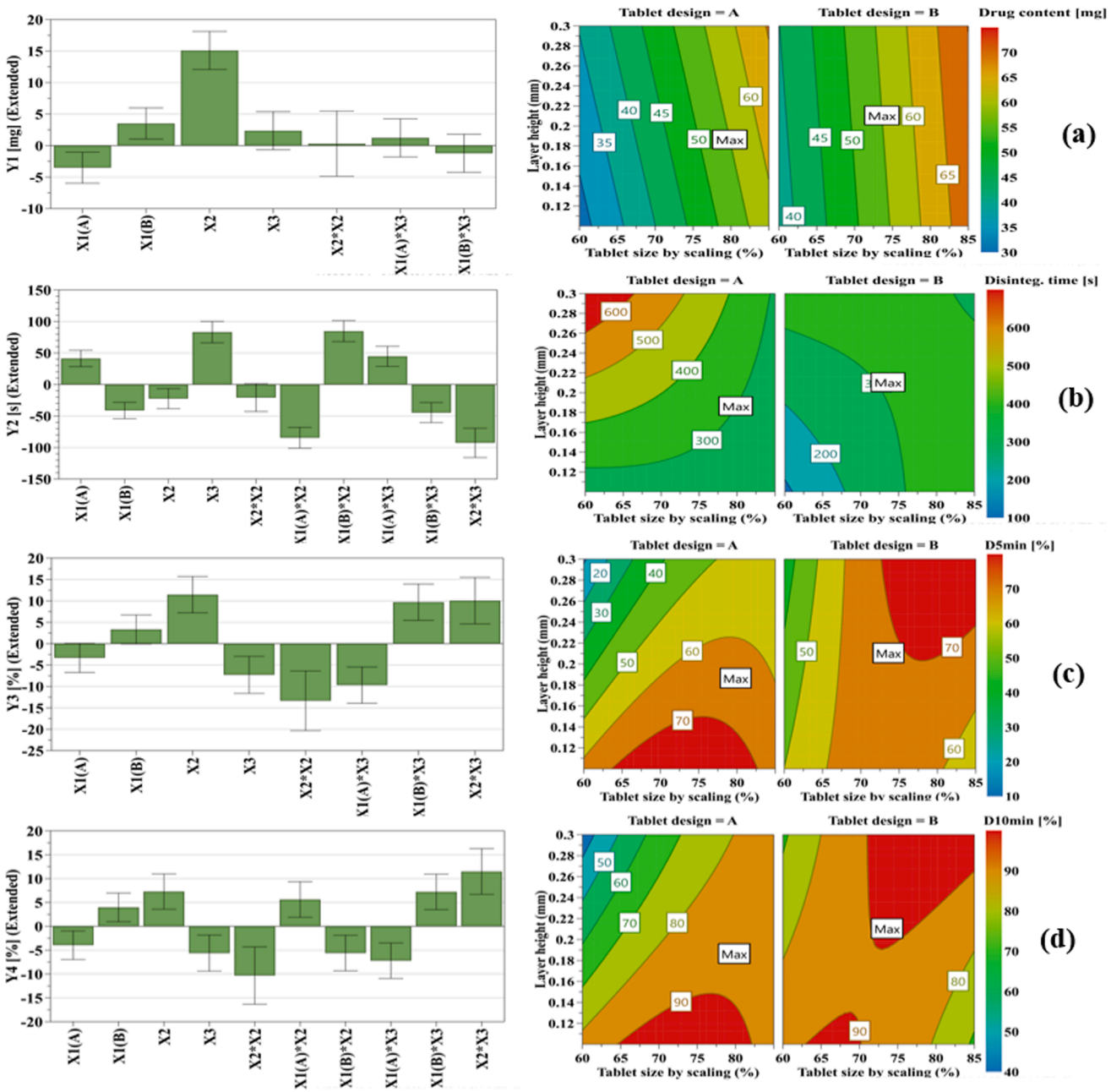

Fig. 9. Regression coefficients of the polynomial models and contour plots highlighting the effect of variables (X_1 – tablet design, X_2 – tablet size by scaling, X_3 – layer height) on the responses (Y_1 – drug content, Y_2 – disintegration time, Y_3 – D_{5min}, Y_4 – D_{10min}).

variability of the drug released in the first 5 min is encountered for tablet sizes scaled from 60% to 85%.

The API percentages released after 10 min (Y_4) varied from 58.0% to 96.1%, according to the results presented in Table 2. The main effects and the interactions between the factors with a significant impact on D_{10min} are observable in the coefficient plot displayed in Fig. 9(d), obtained by analyzing the correlations among the independent variables and D_{10min}. Therefore, the findings discussed in relation to Y_3 are also valid regarding the influence of the studied factors on D_{10min}. In addition, it is noticeable that the relevance of the tablet design (X_1) is amplified, and a new interaction is detected midst the tablet design (X_1) and the tablet size (X_2). Specifically, over time, the differences in tablet dissolution that occur due to the variation of the dosage form design become more evident. As per the contour plots shown in Fig. 9(d), the dimensions of the tablets have a limited impact on the drug ratios released in 10 min in the case of the tablets with honeycomb architecture. Contrastingly, the dissolution rate of the tablets with A design varies depending on the size of the dosage form, especially at high layer heights. Thus, the B tablet design is allegedly suitable for the fabrication of tablets with a more robust release profile and adjustable API doses by size scaling.

3.4.3. *Determination of the design space and validation of the model*

The rationale behind applying the DoE approach is to investigate the critical material attributes and the critical process parameters, the ultimate goal being the development of a design space that ensures risk minimization in obtaining the desired product with the predefined characteristics (Butreddy et al., 2021). The design space charts are created by overlapping multiple response contour plots and coupling probability analysis. The prospects of fulfilling the output requirements in the design area are calculated based on the models formulated for the CQAs and Monte Carlo simulations. The design space figure includes

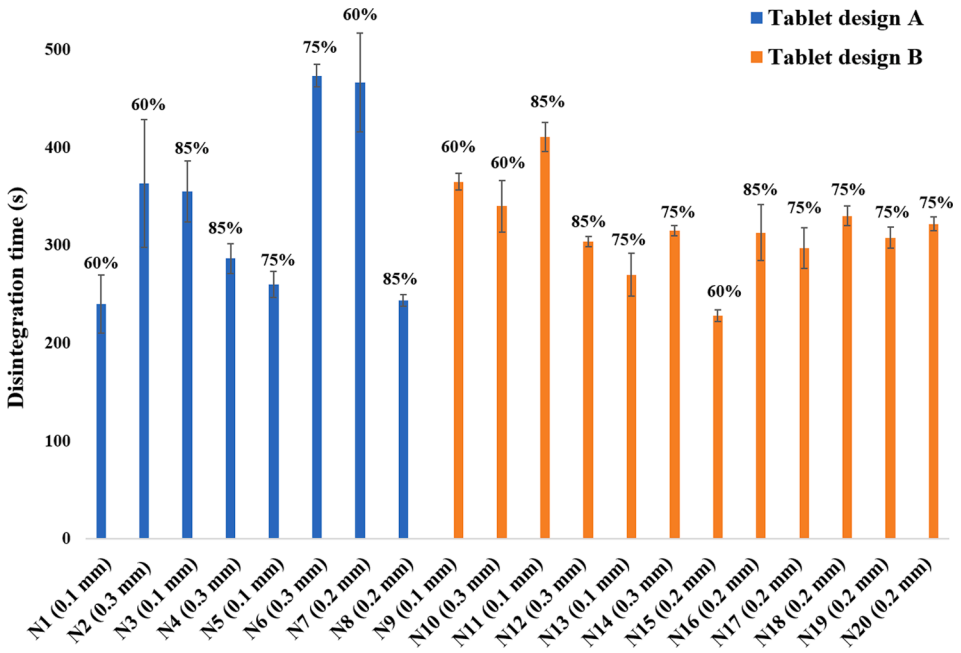

Fig. 10. Disintegration behavior of the tablets with different designs, sizes (indicated as the scaling by percentage of the original tablet dimensions) and prepared by the deposition of layers with distinct thicknesses (included in the x axis labels).

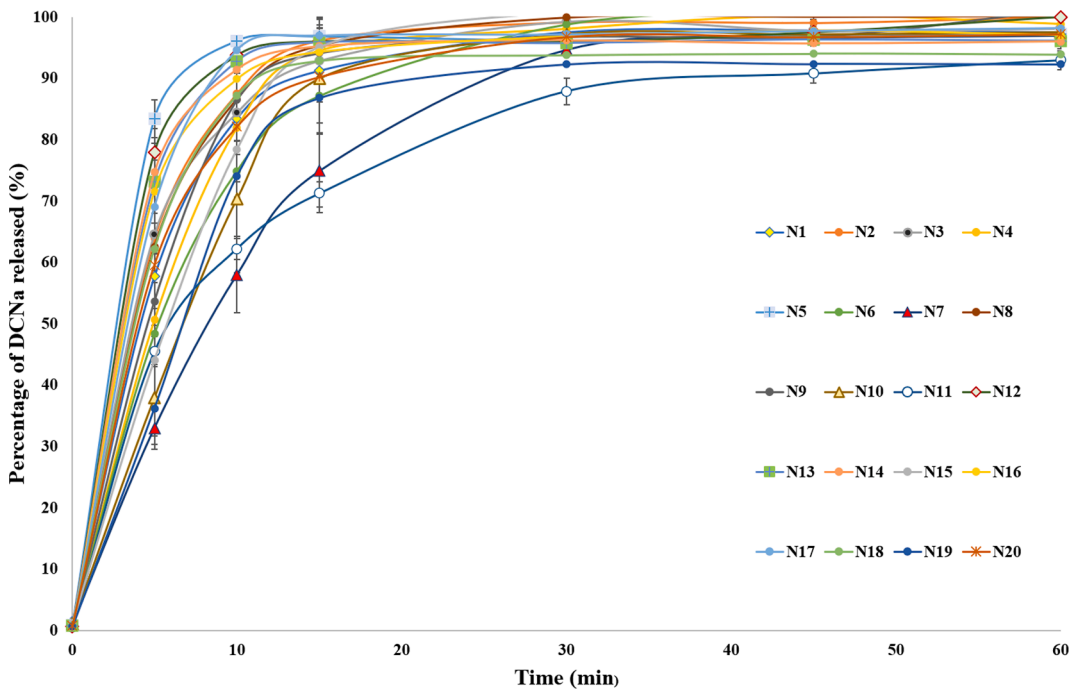

Fig. 11. *In vitro* release profiles of DCNa from the 3D printed tablets.

color-coded areas and edge lines that differentiate the design region as per the failure probability indicated as a percentage (Casian et al., 2017).

The examination of the obtained data disclosed that the drug release performance of the 3D printed dosage forms was influenced by the studied factors. Thus, customization of the drug dissolution behavior is achievable through the appropriate selection of the input variables. Our aim was to develop an IR 3D printed tablet with a predictable dissolution profile and adjustable API doses by scaling the dimensions of the dosage form. Thus, the drug content (Y1) and the percentages of API released within the initial phase of the dissolution process (Y3, Y4) were selected as pertinent criteria that define the quality of the product. For these quality attributes, specific target levels among admissible intervals were established in order to define the design space.

For the percentages of DCNa released after 5 min, a target value of 55% was set, with an acceptable variation between 40% and 70%, while for the DCNa released after 10 min, an interval between 75% and 95% was considered acceptable, with the objective to reach 85% API dissolution. Also, since we aimed to develop a 3D printed tablet with flexibility in adjusting the API dose by modifying the tablet dimensions without affecting the drug release performance, three target API contents were set: 40 mg, 50 mg, and 60 mg. These targets were considered

based on the currently applied dosing regimen for diclofenac containing IR formulations. Accordingly, diclofenac potassium is administered to adults in IR doses of 50 and 100 mg, but since the API is linked to dose-dependent adverse effects (gastrointestinal, cardiovascular, and renal), the dispensing of the lowest effective quantity is recommended (Altman et al., 2015) and therefore the flexibility of dose adjustment is indispensable. No setpoint values were established for the disintegration time, as a rapid process was encountered for all the analyzed formulations. The design spaces were created based on these settings for both types of tablets (design A and design B).

In Fig. 12, the probability plots showing the hazard of failure in meeting the desired DCNa content and API percentages released within 5 min and 10 min are depicted. The green regions represent the combination of factors that provide minimal risk for not fulfilling the QTPP, while increased hazard is encountered in the yellow and red areas. By inspecting the areas and the contour lines that delimit the design domains for the two tablet architectures, it is noticeable that the honeycomb design grants wider domains with lower failure probability compared to the dosage forms prepared according to the concentric ellipses structure. The observation is valid for different tablet dimensions. Accordingly, the B tablet type is revealed as the more secure and dependable alternative for any of the three target concentrations of DCNa. The design spaces resulting for the tablets with the concentric ellipses structure are lacking the areas with a very low probability of failure for target API doses of 40 mg, 50 mg, and 60 mg, as is visible in Fig. 12(a), Fig. 12(b) and Fig. 12(c). Thus, by choosing the A tablet design, there is a greater risk of not meeting the desired drug content and dissolution performance.

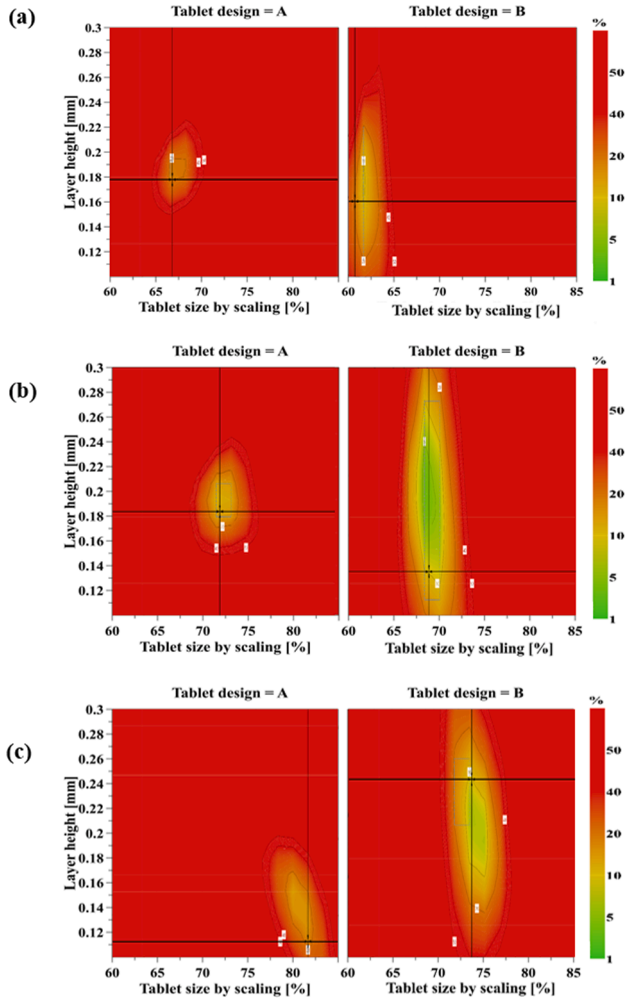

Fig. 12. Design space plots for the preparation of FDM-3D printed tablets containing (a) – 40 mg DCNa, (b) – 50 mg DCNa, (c) – 60 mg DCNa that meet the target of releasing 55% of the dose in a 5 min interval, and 85% of the dose in a 10 min timeframe.

Given that the main objective of this work was to develop a DCNa-loaded 3D printed tablet with easily adjustable API content that also presents a degree of robustness and predictability in terms of drug release performance, and based on the previously discussed findings, the honeycomb tablet design emerges as an appropriate candidate fulfilling the proposed objective. This design assures flexibility in customization of the included API dose by variation of the dosage form size and its dissolution performance is less affected by the variation of inputs in the studied limits.

For the validation of the developed model in terms of accuracy and robustness, supplementary tests were performed. Three formulations were prepared, with target doses of 40 mg, 50 mg, and 60 mg of DCNa, and were analyzed following the same methodologies as the previously presented formulations. The prediction sets and the average experimental values obtained for the evaluated responses are presented in Table 5. Each test was carried out in duplicate. The obtained results were close to the predicted ones, as indicated by the residuals, and therefore a good predictability of the model is indicated.

Through its simpleness and flexibility that allows the customization of the prepared products, FDM-3DP emerges as an appropriate methodology for the fabrication of on-demand tailored medications. However, the characteristics of the obtained dosage forms greatly depend on both formulation and process-related factors. Therefore, knowledge-based decisions guided by studies that systematically identify the influence of different variables on the quality of the output are required to successfully apply the technology as a tool that supports the implementation of personalized medicine. A limited number of studies reported the utilization of DoE approaches to elucidate structure–function relationships for FDM-3D printed dosage forms (Zhang et al., 2020) or to guide the selection of proper material compositions for the preparation of drug products with specific targets regarding the quality (Than and Titapiwatanakun, 2021). From a practical perspective, since the fabrication of patient-centered medications will presumably be performed by compounding pharmacies, a convenient alternative would be the use of one filament and technology able to customize the dose and the release profile of the API by modulation of factors involved in the printing process. Pires et al. developed a predictive model by means of DoE with the capacity of determining the appropriate printing configuration that enables the preparation of the desired product (Pires et al., 2020). The study was based on different types of commercially available filaments (ABS, HIPS, PLA), without further incorporation of APIs, and serves as a foundation for advanced investigations, as the results also revealed that the predictive equations vary depending on the involved materials. In contrast, our work comprised the preparation of a high drug-loaded (50% w/w) PVA-based filament, which was further used as feedstock material within the QbD guided study centered on the optimization of variables involved in the printing process, in accordance with the desired output. Subsequently, a predictive model was generated, which could be employed by the compounding pharmacies for the customization of the FDM-3D printed IR tablets in terms of API doses, but also for the anticipation or even modulation of the drug release in the initial phase of the dissolution process. By setting specific targets for the studied responses, the developed model allows the calculation of working parameters that assure the highest probability of achieving the desired characteristics for the fabricated product. Therefore, our study adds value to the previously discussed works available in the literature that also employed QbD tools by providing, to our knowledge, the first predictive model that allows the preparation of immediate release PVA-based tablets with customizable API doses and foreseeable drug release performance. Moreover, since PVA is a versatile polymer, suitable for the fabrication of both IR and modified release dosage forms via HME-FDM-3DP, using the same material for various formulations and

Table 5
Results of Design Space validation by analyzing optimized 3D printed tablet formulations with different API doses.

Independent variables		Dependent variables					
Factor	Value	Response	Criterion	Target	Predicted value	Experimental value	Residual
X_1	B	Y_1	Target	40	40.00	41.65 ± 0.07	1.65
X_2	60.22	Y_2	Predicted	–	165.49	172.3 ± 3.5	6.81
X_3	0.16	Y_3	Predicted	–	41.17	33.25 ± 4.88	−7.92
		Y_4	Predicted	–	77.06	64.78 ± 8.21	−12.28
X_1	B	Y_1	Target	50	49.99	47.67 ± 2.81	−2.32
X_2	69.04	Y_2	Predicted	–	200.01	214.3 ± 11.7	14.29
X_3	0.10	Y_3	Predicted	–	56.66	50.29 ± 0.29	−6.37
		Y_4	Predicted	–	84.84	83.75 ± 1.69	−1.09
X_1	B	Y_1	Target	60	60.00	60.14 ± 2.02	0.14
X_2	73.66	Y_2	Predicted	–	310.15	335.7 ± 8.0	25.55
X_3	0.25	Y_3	Predicted	–	65.20	74.82 ± 3.22	9.62
		Y_4	Predicted	–	86.24	90.20 ± 5.81	3.96

X_1 – tablet design (A/B); X_2 – tablet size by scaling (%); X_3 – layer height (mm); Y_1 – drug content (mg); Y_2 – disintegration time (s); Y_3 – API percentages released in 5 min (%); Y_4 – API percentages released in 10 min (%).

establishing specific QbD-driven predictive tools centered on PVA-based drug products could potentially boost the implementation of the technology in clinical settings. Tailoring the drug doses for different patients to obtain optimal therapeutic effects with minimal adverse events is a key point of personalized medicine. Therefore, since conventional tablet subdivision practices, including splitting or powdering, involve disadvantages such as imprecision of doses or limited patient compliance (Zheng et al., 2020), FDM-3DP of individualized drug products by employing a predictive model as the one developed in our study represents a promising direction for improving safety and efficacy of treatments.

Although 3DP encountered an accelerated development from a pharmaceutical standpoint, the road to its implementation as a tool for the preparation of medicines is paved with various challenges. One of the key constraints is the absence of regulatory guidance from health and drug agencies, as 3D printing does not fall under the framework of typical regulations for the manufacturing of drug products (Seoane-Viaño et al., 2021). It is also imperative to ensure that the fabrication is conducted in conformity with the latest GMP requirements (Awad et al., 2021). Consequently, pharmaceutical 3D printers which correspond to GMP and QC regulations are required. A recent step towards such fit-for-purpose equipment was done by FabRx Ltd. by creating the M3DIMAKER™, a GMP-compliant 3D printer purposely elaborated to be employed for the preparation of dosage forms (Seoane-Viaño et al., 2021). Another consideration to bear in mind is quality control, which for conventional dosage forms is performed on the end product. In contrast, for personalized 3D printed products prepared in limited quantities, a similar strategy is unrealistic since it would delay and escalate the expense of batch release. Thus, a reasonable approach could be the transition towards quality assurance of the manufactured batch through accurate quality assurance of the operations engaged in 3DP (Patel et al., 2021). Additional attention is directed towards the ability to scale-up 3DP since the throughput is considered a limitation of the technology. However, it is highly unlikely to witness a replacement of conventional pharmaceutical mass-production methods by 3DP (Cailleaux et al., 2021), which is more appropriate to be employed as a decentralized platform for the small-scale preparation of personalized drug products in community or hospital pharmacies. Therefore, a potential strategy to ensure appropriate productivity could include running multiple printers concurrently (Seoane-Viaño et al., 2021).

4. Conclusions

In this study, high drug-loaded (50% w/w) FDM-3D printable filaments based on polyvinyl alcohol as a thermoplastic material were fabricated by HME technology. The maximum DCNa content that still granted good processability of the filaments by 3DP was determined by systematic screening of physical mixtures with gradually increased API proportions. The mechanical characterization of the filaments revealed that a higher drug content (60% w/w) impaired printability mainly due to a lack of stiffness.

The fabrication of the DCNa-loaded tablets by FDM-3DP was addressed by applying the QbD approach, which involved risk assessment tools, DoE, and design space definition. The preparation of 20 batches of dosage forms was carried out according to a D-Optimal experimental design. The varied factors were the tablet architecture, the tablet dimensions (by scaling), and the chosen layer height for the printing process, all of which significantly influenced the quality of the prepared dosage forms, according to the systematic investigation of their effects and interactions. By appropriate formulation and tablet design strategies, rapid release of the API was attained. The D-Optimal design elucidated the impact of the studied factors on the accuracy of the drug content and the API release behavior, leading to the development of an accurate model that is employable for the optimization of the studied parameters in order to obtain a product with the desired characteristics. Moreover, the honeycomb tablet configuration has been established as a suitable choice for the personalization of the API dose, as it grants a steadier immediate release profile to the variation of the tablet dimensions and layer height settings. Therefore, this work consolidates the position of FDM-3DP as an appropriate drug manufacturing platform for the preparation of on-demand products adapted to the individual needs of the patients by providing an example of a flexible drug delivery system adequate for facile customization.

CRediT authorship contribution statement

Andrea Gabriela Crișan: Conceptualization, Methodology, Investigation, Data curation, Writing – original draft, Writing – review & editing. **Sonia Iurian:** Methodology, Investigation, Writing – review & editing. **Alina Porfire:** Conceptualization, Methodology, Validation, Visualization. **Lucia Maria Rus:** Methodology, Investigation. **Cătălina Bogdan:** Methodology, Investigation. **Tibor Casian:** Methodology, Formal analysis. **Raluca Ciceo Lucacel:** Methodology, Investigation. **Alexandru Turza:** Methodology, Investigation. **Sebastian Porav:** Methodology, Investigation. **Ioan Tomuță:** Conceptualization, Writing – review & editing, Resources, Supervision, Project administration.

Declaration of Competing Interest

The authors declare that they have no known competing financial interests or personal relationships that could have appeared to influence the work reported in this paper.

Acknowledgements

This project was supported by the "Iuliu Haţieganu" University of Medicine and Pharmacy through the internal doctoral research grant 1680/34/19.01.2018.

References

Aho, J., Bøtker, J.P., Genina, N., Edinger, M., Arnfast, L., Rantanen, J., 2019. Roadmap to 3D-Printed Oral Pharmaceutical Dosage Forms: Feedstock Filament Properties and Characterization for Fused Deposition Modeling. J. Pharm. Sci. 108 (1), 26–35. https://doi.org/10.1016/j.xphs.2018.11.012.

Altman, R., Bosch, B., Brune, K., Patrignani, P., Young, C., 2015. Advances in NSAID Development: Evolution of Diclofenac Products Using Pharmaceutical Technology. Drugs 75 (8), 859–877. https://doi.org/10.1007/S40265-015-0392-Z.

Arafat, B., Wojsz, M., Isreb, A., Forbes, R.T., Isreb, M., Ahmed, W., Arafat, T., Alhnan, M. A., 2018. Tablet fragmentation without a disintegrant: A novel design approach for accelerating disintegration and drug release from 3D printed cellulosic tablets. Eur. J. Pharm. Sci. 118, 191–199. https://doi.org/10.1016/j.ejps.2018.03.019.

Awad, A., Trenfield, S.J., Pollard, T.D., Ong, J.J., Elbadawi, M., McCoubrey, L.E., Goyanes, A., Gaisford, S., Basit, A.W., 2021. Connected healthcare: Improving patient care using digital health technologies. Adv. Drug Deliv. Rev. 178, 113958. https://doi.org/10.1016/j.addr.2021.113958.

Ayyoubi, S., Cerda, J.R., Fernández-García, R., Knief, P., Lalatsa, A., Healy, A.M., Serrano, D.R., 2021. 3D printed spherical mini-tablets: Geometry versus composition effects in controlling dissolution from personalised solid dosage forms. Int. J. Pharm. 597, 120336. https://doi.org/10.1016/j.ijpharm.2021.120336.

Barakh Ali, S.F., Mohamed, E.M., Ozkan, T., Kuttolamadom, M.A., Khan, M.A., Asadi, A., Rahman, Z., 2019. Understanding the effects of formulation and process variables on the printlets quality manufactured by selective laser sintering 3D printing. Int. J. Pharm. 570, 118651. https://doi.org/10.1016/j.ijpharm.2019.118651.

Barzegar-Jalali, M., Alaei-Beirami, M., Javadzadeh, Y., Mohammadi, G., Hamidi, A., Andalib, S., Adibkia, K., 2012. Comparison of physicochemical characteristics and drug release of diclofenac sodium-eudragit® RS100 nanoparticles and solid dispersions. Powder Technol. 219, 211–216. https://doi.org/10.1016/j.powtec.2011.12.046.

Butreddy, A., Bandari, S., Repka, M.A., 2021. Quality-by-design in hot melt extrusion based amorphous solid dispersions: An industrial perspective on product development. Eur. J. Pharm. Sci. 158, 105655. https://doi.org/10.1016/j.ejps.2020.105655.

Cailleaux, S., Sanchez-Ballester, N.M., Gueche, Y.A., Bataille, B., Soulairol, I., 2021. Fused Deposition Modeling (FDM), the new asset for the production of tailored medicines. J. Control. Release. 330, 821–841. https://doi.org/10.1016/j.jconrel.2020.10.056.

Casian, T., Iurian, S., Bogdan, C., Rus, L., Moldovan, M., Tomuta, I., 2017. QbD for pediatric oral lyophilisates development: risk assessment followed by screening and optimization. Drug Dev. Ind. Pharm. 43 (12), 1932–1944. https://doi.org/10.1080/03639045.2017.1350702.

Crișan, A.G., Porfire, A., Ambrus, R., Katona, G., Rus, L.M., Porav, A.S., Ilyés, K., Tomuță, I., 2021. Polyvinyl Alcohol-Based 3D Printed Tablets: Novel Insight into the Influence of Polymer Particle Size on Filament Preparation and Drug Release Performance. Pharmaceuticals 14, 418. https://doi.org/10.3390/ph14050418.

Dumpa, N., Butreddy, A., Wang, H., Komanduri, N., Bandari, S., Repka, M.A., 2021. 3D printing in personalized drug delivery: An overview of hot-melt extrusion-based fused deposition modeling. Int. J. Pharm. 600, 120501. https://doi.org/10.1016/j.ijpharm.2021.120501.

Elbadawi, M., Gustaffson, T., Gaisford, S., Basit, A.W., 2020a. 3D printing tablets: Predicting printability and drug dissolution from rheological data. Int. J. Pharm. 590, 119868. https://doi.org/10.1016/j.ijpharm.2020.119868.

Elbadawi, M., McCoubrey, L.E., Gavins, F.K.H., Ong, J.J., Goyanes, A., Gaisford, S., Basit, A.W., 2021. Disrupting 3D printing of medicines with machine learning. Trends Pharmacol. Sci. 42 (9), 745–757. https://doi.org/10.1016/J.TIPS.2021.06.002.

Elbadawi, M., Muñiz Castro, B., Gavins, F.K.H., Ong, J.J., Gaisford, S., Pérez, G., Basit, A. W., Cabalar, P., Goyanes, A., 2020b. M3DISEEN: A novel machine learning approach for predicting the 3D printability of medicines. Int. J. Pharm. 590, 119837. https://doi.org/10.1016/j.ijpharm.2020.119837.

European Directorate for the Quality of Medicines & Healthcare, 2019a. 2.9.5. Uniformity of mass of single-dose preparations, in: European Pharmacopoeia. pp. 335–336.

European Directorate for the Quality of Medicines & Healthcare, 2019b. 5.17.1. Recommendations on Dissolution Testing, in: European Pharmacopoeia. Council of Europe, Strasbourg, pp. 801–803.

Gavan, A., Iurian, S., Casian, T., Porfire, A., Porav, S., Voina, I., Oprea, A., Tomuta, I., 2020. Fluidised bed granulation of two APIs: QbD approach and development of a NIR in-line monitoring method. Asian J. Pharm. Sci. 15 (4), 506–517. https://doi.org/10.1016/j.ajps.2019.03.003.

Gorkem Buyukgoz, G., Soffer, D., Defendre, J., Pizzano, G.M., Davé, R.N., 2020. Exploring tablet design options for tailoring drug release and dose via fused deposition modeling (FDM) 3D printing. Int. J. Pharm. 591, 119987. https://doi.org/10.1016/j.ijpharm.2020.119987.

Gottschalk, N., Bogdahn, M., Harms, M., Quodbach, J., 2021. Brittle polymers in Fused Deposition Modeling: An improved feeding approach to enable the printing of highly drug loaded filament. Int. J. Pharm. 597, 120216. https://doi.org/10.1016/j.ijpharm.2021.120216.

Goyanes, A., Buanz, A.B.M., Basit, A.W., Gaisford, S., 2014. Fused-filament 3D printing (3DP) for fabrication of tablets. Int. J. Pharm. 476 (1-2), 88–92. https://doi.org/10.1016/j.ijpharm.2014.09.044.

Goyanes, A., Robles Martinez, P., Buanz, A., Basit, A.W., Gaisford, S., 2015. Effect of geometry on drug release from 3D printed tablets. Int. J. Pharm. 494 (2), 657–663. https://doi.org/10.1016/j.ijpharm.2015.04.069.

Gültekin, H.E., Tort, S., Acartürk, F., 2019. An Effective Technology for the Development of Immediate Release Solid Dosage Forms Containing Low-Dose Drug: Fused Deposition Modeling 3D Printing. Pharm. Res. 36, 1–13. https://doi.org/10.1007/s11095-019-2655-y.

ICH Expert Working Group, 2009. ICH Harmonised Tripartite Guideline. Pharmaceutical Development Q8(R2) [WWW Document]. URL https://database.ich.org/sites/default/files/Q8_R2_Guideline.pdf (accessed 2.24.21).

ICH Expert Working Group, 2005. ICH HARMONISED TRIPARTITE GUIDELINE. QUALITY RISK MANAGEMENT Q9 [WWW Document]. URL https://database.ich.org/sites/default/files/Q9 Guideline.pdf (accessed 6.5.21).

Ilyés, K., Balogh, A., Casian, T., Igricz, T., Borbás, E., Démuth, B., Vass, P., Menyhárt, L., Kovács, N.K., Marosi, G., Tomuță, I., Nagy, Z.K., 2019. 3D floating tablets: Appropriate 3D design from the perspective of different in vitro dissolution testing methodologies. Int. J. Pharm. 567, 118433. https://doi.org/10.1016/j.ijpharm.2019.06.024.

Jamróz, W., Kurek, M., Szafraniec-Szczęsny, J., Czech, A., Gawlak, K., Knapik-Kowalczuk, J., Leszczyński, B., Wróbel, A., Paluch, M., Jachowicz, R., 2020. Speed it up, slow it down…An issue of bicalutamide release from 3D printed tablets. Eur. J. Pharm. Sci. 143, 105169. https://doi.org/10.1016/j.ejps.2019.105169.

Kyobula, M., Adedeji, A., Alexander, M.R., Saleh, E., Wildman, R., Ashcroft, I., Gellert, P. R., Roberts, C.J., 2017. 3D inkjet printing of tablets exploiting bespoke complex geometries for controlled and tuneable drug release. J. Control. Release 261, 207–215. https://doi.org/10.1016/j.jconrel.2017.06.025.

Macedo, J., Samaro, A., Vanhoorne, V., Vervaet, C., Pinto, J.F., 2020. Processability of poly(vinyl alcohol) Based Filaments With Paracetamol Prepared by Hot-Melt Extrusion for Additive Manufacturing. J. Pharm. Sci. 109 (12), 3636–3644. https://doi.org/10.1016/j.xphs.2020.09.016.

Muñiz Castro, B., Elbadawi, M., Ong, J.J., Pollard, T., Song, Z., Gaisford, S., Pérez, G., Basit, A.W., Cabalar, P., Goyanes, A., 2021. Machine learning predicts 3D printing performance of over 900 drug delivery systems. J. Control. Release 337, 530–545. https://doi.org/10.1016/J.JCONREL.2021.07.046.

Nasereddin, J.M., Wellner, N., Alhijjaj, M., Belton, P., Qi, S., 2018. Development of a Simple Mechanical Screening Method for Predicting the Feedability of a Pharmaceutical FDM 3D Printing Filament. Pharm. Res. 35, 1–13. https://doi.org/10.1007/s11095-018-2432-3.

Nukala, P.K., Palekar, S., Solanki, N., Fu, Y., Patki, M., Shohatee, A.A., Trombetta, L., Patel, K., 2019. Investigating the application of FDM 3D printing pattern in preparation of patient-tailored dosage forms. J. 3D Print. Med. 3 (1), 23–37. https://doi.org/10.2217/3dp-2018-0028.

Obeid, S., Madžarević, M., Krkobabić, M., Ibrić, S., 2021. Predicting drug release from diazepam FDM printed tablets using deep learning approach: Influence of process parameters and tablet surface/volume ratio. Int. J. Pharm. 601, 120507. https://doi.org/10.1016/j.ijpharm.2021.120507.

Okafor-Muo, O.L., Hassanin, H., Kayyali, R., ElShaer, A., 2020. 3D Printing of Solid Oral Dosage Forms: Numerous Challenges With Unique Opportunities. J. Pharm. Sci. 109 (12), 3535–3550. https://doi.org/10.1016/j.xphs.2020.08.029.

Palekar, S., Nukala, P.K., Mishra, S.M., Kipping, T., Patel, K., 2019. Application of 3D printing technology and quality by design approach for development of age-appropriate pediatric formulation of baclofen. Int. J. Pharm. 556, 106–116. https://doi.org/10.1016/j.ijpharm.2018.11.062.

Parulski, C., Jennotte, O., Lechanteur, A., Evrard, B., 2021. Challenges of fused deposition modeling 3D printing in pharmaceutical applications: Where are we now? Adv. Drug Deliv. Rev. 175, 113810. https://doi.org/10.1016/j.addr.2021.05.020.

Pasquali, I., Bettini, R., Giordano, F., 2007. Thermal behaviour of diclofenac, diclofenac sodium and sodium bicarbonate compositions. J. Therm. Anal. Calorim. 90 (3), 903–907. https://doi.org/10.1007/s10973-006-8182-1.

Patel, N.G., Serajuddin, A.T.M., 2021. Development of FDM 3D-printed tablets with rapid drug release, high drug-polymer miscibility and reduced printing temperature by applying the acid-base supersolubilization (ABS) principle. Int. J. Pharm. 600, 120524. https://doi.org/10.1016/j.ijpharm.2021.120524.

Patel, S.K., Khoder, M., Peak, M., Alhnan, M.A., 2021. Controlling drug release with additive manufacturing-based solutions. Adv. Drug Deliv. Rev. 174, 369–386. https://doi.org/10.1016/j.addr.2021.04.020.

Pires, F.Q., Alves-Silva, I., Pinho, L.A.G., Chaker, J.A., Sa-Barreto, L.L., Gelfuso, G.M., Gratieri, T., Cunha-Filho, M., 2020. Predictive models of FDM 3D printing using experimental design based on pharmaceutical requirements for tablet production. Int. J. Pharm. 588, 119728. https://doi.org/10.1016/j.ijpharm.2020.119728.

Reitz, E., Podhaisky, H., Ely, D., Thommes, M., 2013. Residence time modeling of hot melt extrusion processes. Eur. J. Pharm. Biopharm. 85 (3), 1200–1205. https://doi.org/10.1016/j.ejpb.2013.07.019.

Sadia, M., Arafat, B., Ahmed, W., Forbes, R.T., Alhnan, M.A., 2018. Channelled tablets: An innovative approach to accelerating drug release from 3D printed tablets. J. Control. Release 269, 355–363. https://doi.org/10.1016/j.jconrel.2017.11.022.

Seoane-Viaño, I., Trenfield, S.J., Basit, A.W., Goyanes, A., 2021. Translating 3D printed pharmaceuticals: From hype to real-world clinical applications. Adv. Drug Deliv. Rev. 174, 553–575. https://doi.org/10.1016/j.addr.2021.05.003.

Shi, K., Salvage, J.P., Maniruzzaman, M., Nokhodchi, A., 2021. Role of release modifiers to modulate drug release from fused deposition modelling (FDM) 3D printed tablets. Int. J. Pharm. 597, 120315. https://doi.org/10.1016/j.ijpharm.2021.120315.

Siozou, E., Sakkas, V., Kourkoumelis, N., 2021. Quantification and Classification of Diclofenac Sodium Content in Dispersed Commercially Available Tablets by Attenuated Total Reflection Infrared Spectroscopy and Multivariate Data Analysis. Pharm 14 (5), 440. https://doi.org/10.3390/ph14050440.

Skowyra, J., Pietrzak, K., Alhnan, M.A., 2015. Fabrication of extended-release patient-tailored prednisolone tablets via fused deposition modelling (FDM) 3D printing. Eur. J. Pharm. Sci. 68, 11–17. https://doi.org/10.1016/J.EJPS.2014.11.009.

Than, Y.M., Titapiwatanakun, V., 2021. Tailoring immediate release FDM 3D printed tablets using a quality by design (QbD) approach. Int. J. Pharm. 599, 120402. https://doi.org/10.1016/j.ijpharm.2021.120402.

Thanawuth, K., Sutthapitaksakul, L., Konthong, S., Suttiruengwong, S., Huanbutta, K., Dass, C.R., Sriamornsak, P., 2021. Impact of Drug Loading Method on Drug Release from 3D-Printed Tablets Made from Filaments Fabricated by Hot-Melt Extrusion and Impregnation Processes. Pharm. 2021, Vol. 13, Page 1607 13, 1607. http://doi.org/10.3390/PHARMACEUTICS13101607.

Wei, C., Solanki, N.G., Vasoya, J.M., Shah, A.V., Serajuddin, A.T.M., 2020. Development of 3D Printed Tablets by Fused Deposition Modeling Using Polyvinyl Alcohol as Polymeric Matrix for Rapid Drug Release. J. Pharm. Sci. 109 (4), 1558–1572. https://doi.org/10.1016/j.xphs.2020.01.015.

Xu, P., Li, J., Meda, A., Osei-Yeboah, F., Peterson, M.L., Repka, M., Zhan, X.i., 2020. Development of a quantitative method to evaluate the printability of filaments for fused deposition modeling 3D printing. Int. J. Pharm. 588, 119760. https://doi.org/10.1016/j.ijpharm.2020.119760.

Xu, X., Zhao, J., Wang, M., Wang, L., Yang, J., 2019. 3D Printed Polyvinyl Alcohol Tablets with Multiple Release Profiles. Sci. Rep. 9, 1–8. https://doi.org/10.1038/s41598-019-48921-8.

Yang, Y.Y., Liu, Z.P., Yu, D.G., Wang, K., Liu, P., Chen, X., 2018. Colon-specific pulsatile drug release provided by electrospun shellac nanocoating on hydrophilic amorphous composites. Int. J. Nanomed. 13, 2395–2404. https://doi.org/10.2147/IJN.S154849.

Zhang, J., Thakkar, R., Zhang, Y.u., Maniruzzaman, M., 2020. Structure-function correlation and personalized 3D printed tablets using a quality by design (QbD) approach. Int. J. Pharm. 590, 119945. https://doi.org/10.1016/j.ijpharm.2020.119945.

Zhang, J., Xu, P., Vo, A.Q., Bandari, S., Yang, F., Durig, T., Repka, M.A., 2019. Development and evaluation of pharmaceutical 3D printability for hot melt extruded cellulose-based filaments. J. Drug Deliv. Sci. Technol. 52, 292–302. https://doi.org/10.1016/j.jddst.2019.04.043.

Zheng, Z., Lv, J., Yang, W., Pi, X., Lin, W., Lin, Z., Zhang, W., Pang, J., Zeng, Y., Lv, Z., Lao, H., Chen, Y., Yang, F., 2020. Preparation and application of subdivided tablets using 3D printing for precise hospital dispensing. Eur. J. Pharm. Sci. 149, 105293. https://doi.org/10.1016/j.ejps.2020.105293.

International Journal of Pharmaceutics 638 (2023) 122916

Contents lists available at ScienceDirect

International Journal of Pharmaceutics

journal homepage: www.elsevier.com/locate/ijpharm

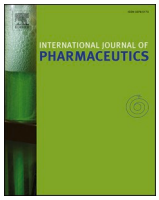

Review

Texture analysis – A versatile tool for pharmaceutical evaluation of solid oral dosage forms

Cătălina Bogdan [a], Dana Hales [b,*], Andreea Cornilă [b], Tibor Casian [b], Rareș Iovanov [b], Ioan Tomuță [b], Sonia Iurian [b]

[a] Department of Dermopharmacy and Cosmetics, Faculty of Pharmacy, "Iuliu Haţieganu" University of Medicine and Pharmacy, 12 I. Creangă Street, 400010 Cluj-Napoca, Romania
[b] Department of Pharmaceutical Technology and Biopharmacy, Faculty of Pharmacy, "Iuliu Haţieganu" University of Medicine and Pharmacy, 41 V. Babes Street, 400012 Cluj-Napoca, Romania

ARTICLE INFO

Keywords:
Texture analysis
Solid oral dosage forms
Mechanical characterization
Mucoadhesion characterization
Disintegration time
In vitro – in vivo correlation

ABSTRACT

In the past few decades, texture analysis (TA) has gained importance as a valuable method for the characterization of solid oral dosage forms. As a result, an increasing number of scientific publications describe the textural methods that evaluate the extremely diverse category of solid pharmaceutical products. Within the current work, the use of texture analysis in the characterization of solid oral dosage forms is summarised with a focus on the evaluation of intermediate and finished oral pharmaceutical products. Several texture methods are reviewed regarding the applications in mechanical characterization, and mucoadhesion testing, but also in estimating the disintegration time and *in vivo* specific features of oral dosage forms. As there are no pharmacopoeial standards for pharmaceutical products tested through texture analysis, and there are important differences between reported results due to different experimental conditions, the choice of testing protocol and parameters is challenging. Thereby, this work aims to guide the research scientists and quality assurance professionals involved in different stages of drug development into the selection of optimal texture methodologies depending on the product characteristics and quality control needs.

1. Introduction

The oral route is by far the most frequently used in pharmacotherapy, due to the easy administration and varied release profiles that can be achieved (Awad et al., 2021). In recent years, the number of solid pharmaceutical forms for oral use has increased significantly as a response to some newly recognized therapy problems: the need for personalized treatment, doses, or drug release profiles, for specific combinations of active substances, or the need for easier administration to special groups of patients (Khan et al., 2022; Tidau and Finke, 2022; Wening and Breitkreutz, 2010). Several new dosage forms have emerged, such as orodispersible tablets (ODTs), oral lyophilisates, thin films, buccal tablets, 3D printlets with different disintegration or dissolution characteristics, minitablets, orodispersible minitablets (ODMTs), multiple layer tablets or compression coated tablets.

The texture is an important component of the sensory evaluation of any orally administered product. ISO 2008 defines it as "the combination of rheological and structure (geometrical and surface) attributes of a food product perceptible by means of mechanical, tactile, and where appropriate, visual and auditory receptors" ("ISO - ISO 5492:2008 - Sensory analysis — Vocabulary," n.d.; Schreuders et al., 2021). Particularly, since the appearance of dosage forms that maintain prolonged

Abbreviations: CQA, critical quality attribute; ISO, International Organization for Standardization; TPA, Texture Profile Analysis; TBI, Tablet Brittleness Index; IT, indentation test; PT, puncture test; TT, tensile test; FT, flexural test; CPs, composite particles; TA, texture analysis; HPMC, hydroxypropylmethylcellulose; OL, oral lyophilizate; API, active pharmaceutical ingredient; PVP, polyvinylpyrrolidone; ASTM, American Society for Testing and Materials; AUC, area under the curve; PEG, polyethylene glycol; HME, hot melt extrusion; PVA, polyvinyl alcohol; PLA, polylactic acid; PETG, polyethylene terephthalate glycol-modified; ABS, acrylonitrile butadiene styrene; CDI, Chewing Difficulty Index; CT, compression test; UTS, universal testing system; CM, creep meter; PEO, poly(ethylene oxide); HEC, hydroxyethylcellulose; 3PBT, three-point bend test; ODT, orodispersible tablet; MCC, microcrystalline celluose; MAP, mucoadhesion properties; IVIVC, *in vivo/in vitro* correlation; BT, buckling test; PLS, partial least squares.

* Corresponding author.
E-mail address: dudas.dana@umfcluj.ro (D. Hales).

https://doi.org/10.1016/j.ijpharm.2023.122916
Received 14 February 2023; Received in revised form 25 March 2023; Accepted 29 March 2023
Available online 4 April 2023

contact with the oral mucosa, texture has become a defining quality parameter in pharmaceutical development.

Quality control is essential for pharmaceutical product development to enable the marketing of products that meet the required quality, efficacy, and safety standards. Derived from the Quality Target Product Profile, each pharmaceutical product has a set of critical quality attributes (CQAs) of finite dosage forms or intermediate products whose assessment relies on corresponding characterization methods. The testing of CQAs requires the use of accurate and reproducible methods. Many of the characterization methods are found in the European Pharmacopiea in the chapter"2.9. Pharmaceutical technical procedures" and include procedures for physical characterization of finite dosage forms such as disintegration, dissolution, friability, resistance to crushing, consistency, etc, or intermediate products such as powder flow, particle surface area, particle size, particle size distribution, porosity and pore-size distribution, bulk and tapped density of powders, wettability etc (2.9. Pharmaceutical technical, n.d.). But many other characterization methods are currently used, reported in the literature, but not included in the Pharmacopiea. In this regard, TA is a simple methodology that enables the evaluation of mechanical features such as hardness, fracturability, elongation, flexibility, but also mucoadhesion properties of various solid orally administered dosage forms and their intermediate products. Thus far, a high number of experimental setups and procedures were reported in the literature to discriminate small variations in composition that impact the features of a particular material or dosage form.

Over the past years, there has been a considerable increase in the number of original articles that include methods for testing oral solid forms through TA. Thus, a brief literature search on the Web of Science database showed an approximately two-fold increase every past decade since the nineties, in the number of original research studies using this method (Fig. 1). Although TA has been used for many years to test newly developed products, to the best of the authors' knowledge, there is currently no review that summarizes the applications of TA in the evaluation of solid oral dosage forms.

The current paper focuses on the most important applications of TA in the evaluation of intermediate and finished oral pharmaceutical products. The in-depth analysis of the texture methods allows a thorough selection of parameters and perfecting TA methods to grant the optimal features of the product under development but also to reduce the development time. In consequence, the addressability of this review paper envisages research scientists, academia, and quality assurance professionals involved in different stages from early formulation design to research and development activities, and routine quality control in the pharmaceutical industry. The first part provides a short summary of the principles of TA with a focus on the technical parameters of different texture analyzers. Further, the tests and the parameters for the assessment of mechanical and mucoadhesion properties are discussed together with several applications of TA in the characterization of oral dosage forms. Emerging applications of TA in estimating the disintegration time and *in vivo* specific features of oral dosage forms are also discussed.

2. General principles of TA

TA was first used in the food industry for quality assessment and comparison of food products, in a reproducible manner, following a standardized procedure and often replacing sensory evaluation on human volunteers (Chen and Opara, 2013; Foegeding and Drake, 2007). This was made possible by the large number of accessories developed specifically for the particularities of food products, intending to simulate the handling of the product by the end user.

The determination of textural features is a physical test mainly based on bulk destruction and shear deformation (Prakash et al., 2013). TA is a mechanical method that relies on compressing, shearing or pulling the sample. Most frequently used, compression tests involve the uniaxial penetration of the probe into a product, up to a stipulated force, distance or deformation. Single-cycle or double-cycle compression tests are available, the latter known as Texture Profile Analysis (TPA), which were designed to mimic the mastication movement in the oral cavity.

Texture analyzers are composed of a sample holder or fixture located on a base plate and a mobile arm that allows vertical movement at a controlled speed or load (Fig. 2). The mobile arm can accommodate various types of probes depending on the sample features and the required measurements, whereas the samples can be either placed on the fixture plane, in special sample holders or even attached to the probe. The arm is connected to a load cell that measures the force opposed by the sample to the descent or ascent of the probe. Alternatively, the load cell can be set to maintain a specific load and record the probe position changes. Through deformation or even complete failure, TA methods are usually destructive, which can be regarded as their major limitation (Schreuders et al., 2021). As a result, data is gathered into texture profiles, representing load/force as a function of the time or the distance travelled by the probe into the sample. Texture profiles can be analysed and compared as such, or various parameters can be calculated for the sample characterization.

The parameters that describe the characteristics of the equipment and their variation limits are summarized in Table 1, based on the data published by two of the most important equipment manufacturers. The parameters are often connected to each other, for example high load cell equipment usually display low load resolution, while small load cells are more sensitive and able to apply high resolution loads. The maximum test speed also varies for different load cell capacities (CT3 Texture Analyzer, Ametek Brookfield," n.d.; TA.XTplus , n.d.).

Texture analyzers can be operated in many different ways depending on the chosen test parameters. As texture applications evolve, accurate and detailed descriptions of the methodology become increasingly important, because different conditions lead to variable results. Table 1 includes the most important testing variables along with their

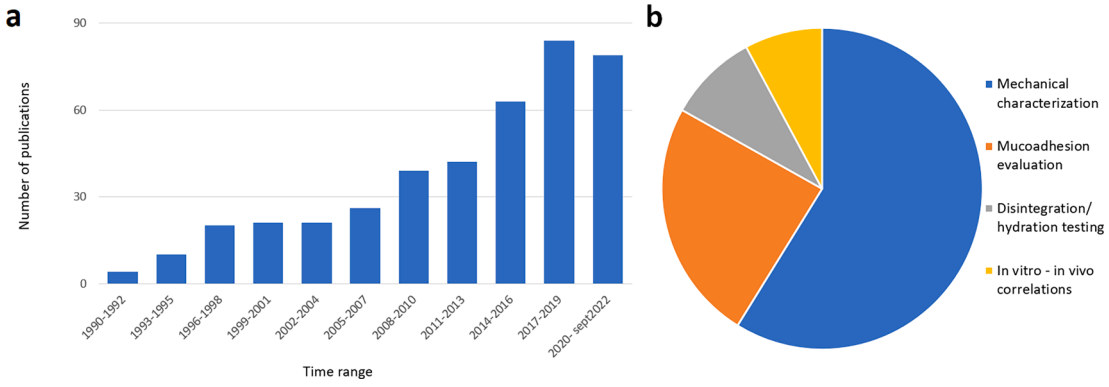

Fig. 1. Literature search results displayed as: a, number of publications per three years time range and b, TA applications.

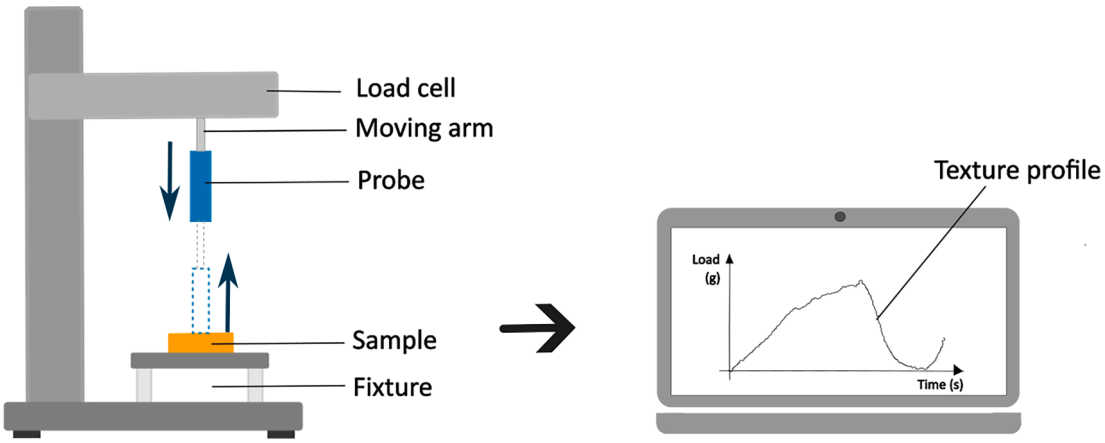

Fig. 2. Basic principle of texture analysis.

Table 1
Technical features of texture analyzers.

Equipment characteristics		Ref
Load cell capacity (kg.f)	0.1 – 750	("CT3 Texture Analyzer, Ametek Brookfield," n.d.; TA.XTplus , n.d.
Speed range (mm/s)	0.01 – 40	
Distance resolution (mm)	0.0005 – 0.001	
Data rate (pps)	500 – 2000	(TA.XTplus , n.d.)
Testing parameters		
The type of test	Compression/ Puncture/ Tensile/ Adhesion/ Fracture/ TPA	
The probe and fixture		
Test speed (mm/s)	The speed of the probe during the test	
Trigger load (g)	The load at which the test starts, meaning the instrument starts applying the set load or test speed and records the results	
Hold time (s)	Time length of contact between the probe and the sample	
Target load (g)	The load at which the test stops, and the probe returns to base	
Temperature (°C)	The temperature of the liquid media or the substrate that encounters the sample during the test	

definitions. When initiating a test, researchers must choose the test type and the accessories. The probes and fixtures that compose the experimental setups are actively developing in row with the numerous dosage forms and their needs. Further, the choice of testing parameters is not always straightforward, and strongly depends on the sample structure and on the desired outcome. For example, the test speed may not impact the results of a measurement that only targets the breaking force of a product but could be vital for a measurement on a hydrating or a disintegrating product. High values of the trigger load are acceptable for dense, hard structures, however, could lead to information loss when used with fragile, porous structures (Hackl and Ermolina, 2016). While most of the tests are performed at room temperature, when the tests aim *in vitro - in vivo* correlations, physiological temperature could be more appropriate.

3. TA in mechanical characterization

3.1. Tests and mechanical parameters

Mechanical characterization can be conducted through different types of tests such as compression, indentation, puncture, flexural or tensile tests, as described below. The mechanical parameters derived from the tests are listed in Table 2.

3.1.1. Compression tests (CT)

CT are the most common among those performed on pharmaceutical products and can be applied on a wide range of samples, from soft (Chachlioutaki et al., 2022) to hard (Oladeji et al., 2022) and from porous (Farias and Boateng, 2020) to dense materials (Fell and Newton, 1970). Flat cylindrical probes of different diameters compress the sample down to a certain distance, deformation or to complete structure failure (Fig. 3a).

For example, mechanical characterization of tablets frequently involves diametral CT, and their tensile strength is determined as described by Fell and Newton (Fell and Newton, 1970) or by using adapted formulas depending on the characteristics of the sample, as shown in Table 2. Variants of the diametral CT include the flattened Brazilian disc test (Mazel et al., 2016) and the diametral CT performed on tablets with perforated centers (Croquelois et al., 2017, 2020), which operate with certain adaptations of the aforementioned formula.

Out of the force/displacement curve certain parameters can be extrapolated, including the Tablet Brittleness Index (TBI) (Paul et al., 2021) used to determine the tabletability of an excipient mixture in tablet formulation development (de Backere et al., 2022; Dun et al., 2020; Gong and Sun, 2015; Paul and Sun, 2018).

Diametral CT also allow the determination of Young's modulus, calculated as the slope of the ascending portion of the stress/strain curve, and the elongation at the breakpoint, equal to the strain suffered by the material at the highest stress point (rupture stress) (Partheniadis et al., 2022). If the Poisson's ratio of the material is known, the Young's modulus can be extracted from the elastic deformation part of the curve (Flügel et al., 2020). Parameters such as the total load or hardness can easily be computed, as well as the total work and fracturability calculations that rely on the assessment of sudden load drops.

3.1.2. Indentation tests (IT)

IT assess the hardness of materials to deformation, by indenting the samples until an impression is formed at their contact area with the probe (Fig. 3b). They allow the determination of indentation hardness as well as of Young's modulus (Oliver and Pharr, 2004). Axial CT may complete the mechanical characterization as the force is applied on the surface of the tablets either with flat or with spherical indentation probes such as in the case of the Brinell Hardness test (Basim et al., 2019; Patel and Sun, 2016). IT can be used in the mechanical characterization of several dosage forms that are prone to deformation, however, they are rather specific to specimens in which the probe can reach a certain depth without passing through the sample.

3.1.3. Puncture tests (PT)

For thinner materials such as polymeric films, the PT has been developed as an adaptation of both mechanical and TT, aiming to

Table 2
Parameters derived from mechanical testing using TA.

	Equation	Parameter explanation	Observations	Reference
Diametral CT				
Tensile strength (σ)	$\sigma = \frac{2 \bullet P}{\pi \bullet D \bullet t}$	P – load applied to the tablet before it breaks D – diameter T – thickness	Described by Fell and Newton	(Fell and Newton, 1970)
	$\sigma = \frac{F_C \bullet D}{2 \bullet V_{eq}}$	Fc – diametrical breaking force Veq – the equivalent volume of the powder compact, calculated as a function of the tablet diameter and total thickness and the diameter and the volume of the cup in which the powder compact has been formed	For solid monolithic dosage forms without flat surfaces	(Mitra et al., 2015)
	$\sigma_{convex} = \frac{10 \bullet F}{\pi \bullet D^2}\left(\frac{2.84 \bullet H}{D} - \frac{0.126 \bullet H}{W} + \frac{3.15W}{D}\right)^{-1}$	D – diameter H – thickness of the entire tablet W – thickness of the flat-faced central segment	Convex-faced tablets with a specific width to diameter ratio	(Pitt et al., 1989)
Tablet Brittleness Index (TBI)	$TBI = \frac{1}{MES} = \frac{D}{MED}$	D – diameter MES – maximum elastic strain MED – maximum elastic deformation	Maximum elastic strain and deformation can be extrapolated from the force vs. displacement curve	(de Backere et al., 2022; Gong and Sun, 2015)
Young's modulus	$F_{el} = \frac{\pi hsE}{8(1-\nu^2)}$	F_{el} – force applied during the elastic deformation of the product h – specimen height s – displacement of the die during the elastic deformation process E – Young's modulus of the material ν – Poisson's ratio of the material	For materials with known Poisson's ratio	(Antonyuk et al., 2011; Flügel et al., 2020)
Indentation Tests (IT)				
Indentation hardness	$H = \frac{Pmax}{A}$	H – indentation hardness Pmax – maximum load A – projected contact area	Uses a wedge indenter	(Flügel et al., 2020; Oliver and Pharr, 2004)
Young's modulus	$S = \beta \bullet \frac{2}{\sqrt{\pi}} \bullet E_{eff} \bullet \sqrt{A}$	S – stiffness of the material β – dimensionless parameter specific to the type of indenter A – projected contact area E_{eff} – effective Young's modulus ν – Poisson's ratio of the sample E – Young's modulus of the sample νi – Poisson's ratio of the indenter Ei – Young's modulus of the indenter	Stiffness represents the slope of the initial segment of the unloading curve, β accounts for stiffness inconsistencies	(Flügel et al., 2020; Oliver and Pharr, 2004)
Tensile strength (σ)	$\sigma = \frac{F}{\pi r^2}$	F – maximum load applied to the tablet r – radius of the tablet	Axial CT	(Chang and Sun, 2019)
Hardness	$H = \frac{F}{A}$	F – the force applied to the surface of the tablet A – the projected area of the indent made into the tablet	Brinell hardness test Uses a spherical indentation probe	(Basim et al., 2019; Patel and Sun, 2016)
Puncture tests (PT)				
Puncture strength (PS)	$PS = \frac{F}{A_c} A_c = 2rh$	F – force needed to puncture the film sample A_c – cross-sectional area of the edge of the film located in the path of the cylindrical opening of the film holder r – radius of the hole h – mean thickness of the film	For film samples	(Kajthunyakarn et al., 2019; Peerapattana et al., 2015; Rongthong et al., 2013; Szabó et al., 2013)
Breaking factor (BF)	$BF = \frac{F_{max}}{h}$	F_{max} – puncture force h – film thickness		(Alaei et al., 2021)
Elongation at puncture (EAP, %)	$EAP\% = \frac{\sqrt{r^2 + D_T^2} - r}{r} \bullet 100$	D_T - displacement of the probe from the point of contact to the point of puncture r – radius of the hole		(Alaei et al., 2021; Kajthunyakarn et al., 2019; Peerapattana et al., 2015)
Energy to puncture (EP)	$EP = \frac{AUC}{SV}$	AUC – the area under the stress/strain or the force vs. displacement curve SV – sample volume		(Alaei et al., 2021; Preis et al., 2014b)
Young's modulus/ Elastic modulus (E)	$E = \frac{SL}{h \bullet CS}$	SL – slope of stress–strain curve in linear region h – thickness of the film CS – cross-head speed	Indicates the stiffness of a sample	(Alaei et al., 2021)
	$E = \frac{PS}{EAP\%}$	PS – puncture strength EAP – elongation at puncture		(Ciper and Bodmeier, 2005; Limmatvapirat et al., 2008; Peerapattana et al., 2015)
	$E = \frac{L_0}{A} \bullet S$	E – Young's modulus S – slope of force–deformation curve		(Baranauskaite et al., 2022)
Tensile tests (TT)				
Tensile strength (TS)	$TS = \frac{Fmax}{A}$	Fmax – maximum force A – cross-sectional area	The cross-sectional area is calculated from the characteristics of the filament or film	(Baranauskaite et al., 2022)

(*continued on next page*)

Table 2 (*continued*)

	Equation	Parameter explanation	Observations	Reference
Elongation at break (EAB, %)	$EAB\% = \frac{Lmax}{L_0} \bullet 100$	L_{max} – maximum length before breaking L_0 – initial length		(Baranauskaite et al., 2022)
Energy to break (EP)	$EP = \frac{AUC}{SV}$	AUC – the area under the force vs. displacement curve SV – sample volume		(Alaei et al., 2021; Preis et al., 2014b)
Flexural tests (FT)				
Flexural stress (σ_f)	$\sigma_f = \frac{F \bullet L}{\pi \bullet R^3}$	F – force needed to break the sample L – the size of the gap between the bending points R – radius of the analyzed specimen	Data from the 3PBT of filaments or other cylindrical samples	(Prasad et al., 2019; Samaro et al., 2021)
Flexural strain (ε_f)	$\varepsilon_f = \frac{600 \bullet s \bullet h}{L^2}$	s – deflection h – thickness of the analyzed specimen L – the size of the gap between the bending points		(Prasad et al., 2019; Samaro et al., 2021)
Flexural stress (σ_f)	$\sigma_f = \frac{3 \bullet F_f \bullet L}{2 \bullet D \bullet H}$	F_f – the force needed to break the tablet L – size of the gap between the bending points D – diameter of the tablet h – height of the tablet	Data from the 3PBT for tablets	(Rodríguez-Pombo et al., 2022)
	$\sigma_f = \frac{3 \bullet F_f \bullet L}{2 \bullet W \bullet H^2}$	F_f – the force needed to break the sample L – size of the gap between the bending points W – width of the specimen H – height of the specimen	Data from the 3PBT for rectangular specimens	(Chachlioutaki et al., 2022; Shumeyko et al., 2019)
Stiffness	$Stiffness = \frac{F}{\delta}$	F – applied force δ – deformation	Variant of the 3PBT	(Hu et al., 2022)

determine the force required to pierce the sample, thus its definitive and irreversible deformation. The setup for this test involves the use of a narrow cylindrical probe with a pointed or rounded contact area, along with a system that neatly fixes the specimen in horizontal position, while also allowing the needle probe to pass entirely through it (Fig. 3c) (Alaei et al., 2021; Kajthunyakarn et al., 2019; Peerapattana et al., 2015; Rongthong et al., 2013). Force-displacement profiles reveal parameters such as the maximum force used to calculate puncture strength. Further, elongation at puncture and energy to puncture can be determined, as well as the elastic modulus from the linear part of the stress–strain curve.

3.1.4. Tensile tests (TT)

TT measure the resistance of a product against a pulling force. The sample is usually placed vertically and attached on both sides with clamps or glued to the fixture and the probe (Fig. 3d). Such tests are frequently applied for products presenting certain flexibility, such as films or 3D printing filaments. Like PT, parameters such as tensile strength and elongation can be determined from the force–displacement or stress–strain curves, as well as the elastic modulus from the angular coefficient of the linear part of the profile. Although PT and TT lead to equivalent calculated parameters, some authors suggested that both should be applied as they complement each other in highlighting differences in the sample deformation mechanism (Radebaugh et al., 1988; Walicová et al., 2016).

3.1.5. Flexural tests (FT)

FT are meant for samples that display a certain flexibility, usually shaped as strips, bars or sticks. The 3-point bending test (3PBT) is a common method used in mechanics that involves a force applied perpendicularly to the middle of the sample placed horizontally on a fixture with two excentric arms (Fig. 3e). It became part of a battery of tests referred as Repka-Zhang methods for hot melt extruded (HME) filament characterization that included a first 3PBT in specified conditions, to determine flexibility. The buckling test (BT), also denoted as the resistance test (Xu et al., 2020) assumed the application of a force on the sample placed vertically into a cylindrical perforated sample holder (Fig. 3f). Most of the researchers reported parameters such as flexural strength, breaking distance or maximum stress, revealed by the texture profiles (Table 2). However, others defined parameters that better express the characteristics of the samples, such as brittleness, resistance, and toughness, calculated from the areas under the curves of the stress–strain profiles (Xu et al., 2020).

3.1.6. Texture profile analysis (TPA)

As TA was first designed to characterize foodstuff, the TPA is the most commonly used as a two-cycle CT. It is aimed to simulate mastication movements and forces (Chatzitaki et al., 2022) and is frequently used to evaluate chewable dosage forms. Samples are placed on a plane holder and compressed twice with a flat cylindrical probe whose diameter usually exceeds the size of the sample. Results are expressed as force–time profiles, out of which several parameters can be extracted, such as hardness which is linked to the force needed for the first bite. Cohesiveness, a measurement of how the material withstands the second compression cycle, considering the deformation already made in the first cycle, is related to a product's ability to withstand deformation when being chewed. Springiness is the ability of the material to go back to its original height between the two compression cycles and was reported to correlate to the elasticity of semi-solids, while adhesiveness (a measure of stickiness) and gumminess were accounted for the effort required for disintegration and breakage in the mouth (Chatzitaki et al., 2022). Chewiness is a parameter that could be associated with the difficulty to chew according to its mathematical definition, high values are obtained for hard, cohesive, and elastic materials (Texture Profile Analysis, n.d.).

3.2. Applications of TA in mechanical characterization

3.2.1. Raw materials

TA is known to be useful in the mechanical characterization of finished pharmaceutical products, but it was also reported in preformulation studies aimed at a better understanding of the properties of raw or processed material. For example, Flugel et al. aimed to study the effects of aging and structural relaxation on the mechanical properties of amorphous solid dispersions with a possible impact on compression behaviour. They applied both diametrical CT and IT to calculate and compare Young's modulus. The structural relaxation of amorphous material with ageing determined the increase of indentation hardness and Young's modulus derived from both tests, which translated into higher stiffness and resistance against elastic and plastic deformation. The results had a practical relevance as the tabletting performance

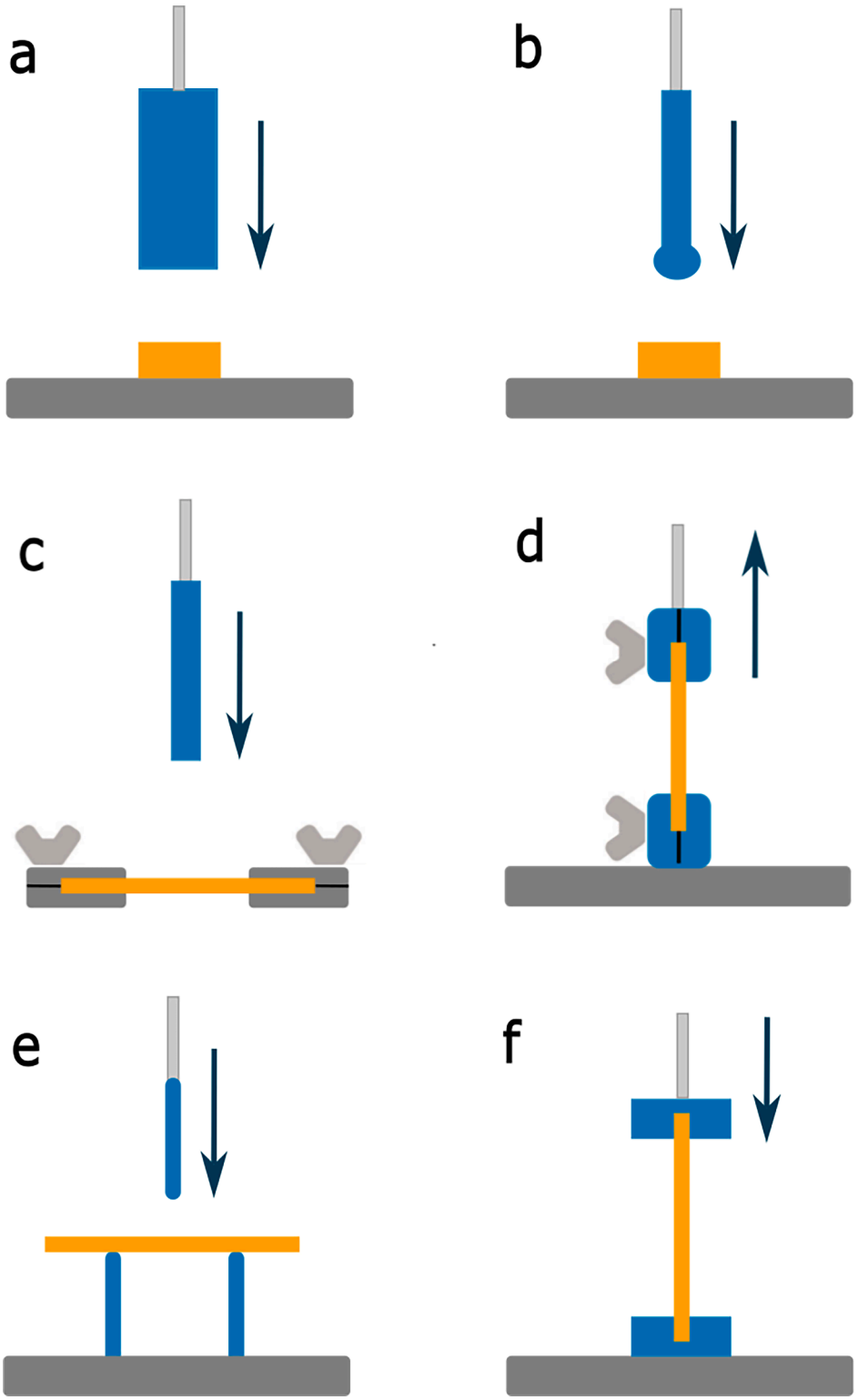

Fig. 3. Mechanical tests for different pharmaceutical products: principles and fixtures (a, compression test (CT); b, indentation test (IT); c, puncture test (PT); d, tensile tests (TT); e, 3-point bending test (3PBT); f, buckling test (BT); the sample is represented in orange). (For interpretation of the references to colour in this figure legend, the reader is referred to the web version of this article.)

of the materials worsened with time (Flügel et al., 2020). Zhou studied the impact of cocrystals of resveratrol with 4-aminobenzamide and isoniazid on the tabletability compared to their physical mixtures and to that of pure substances (Zhou et al., 2016).

In the attempt to optimize granulation, as it is known that both formulation and process parameters impact granules properties, Liu et al. measured granule‘s hardness on 30 granules per formulation for statistical reliability (Liu et al., 2022). Other researchers investigated the TPA characteristics of composite particles (CPs) of a natural extract and the stress–strain profiles of the resulting tablets and correlated them to the compactibility results to understand the functional properties of the CPs (Zhang et al., 2021). Electrospun nanofiber mats were tested for

Young's modulus, elongation at rupture and rupture stress, parameters which were further correlated to compaction measurements by means of Principal Component Analysis, and revealed good ability of TA to compare and distinguish between products (Partheniadis et al., 2022). Therefore, the particle behaviour studied through TA facilitated a better understanding of their subsequent processability aimed at obtaining solid dosage forms.

3.2.2. Tablets

One of the critical quality attributes of solid dosage forms is tensile strength. The diametrical force required for breaking is a standard test necessary as routine analysis for the determination of tensile strength of tablets, mini-tablets, and micro-tablets and can be measured using a texture analyzer equipped with a high-load cell (Basim et al., 2019; Bhatt et al., 2020; Chen et al., 2022, 2019; Croquelois et al., 2017; Dun et al., 2018; Hagen et al., 2016; Lura et al., 2021; Mazel et al., 2018; Meruva et al., 2021; Rai et al., 2012; Vreeman and Sun, 2022a). The test

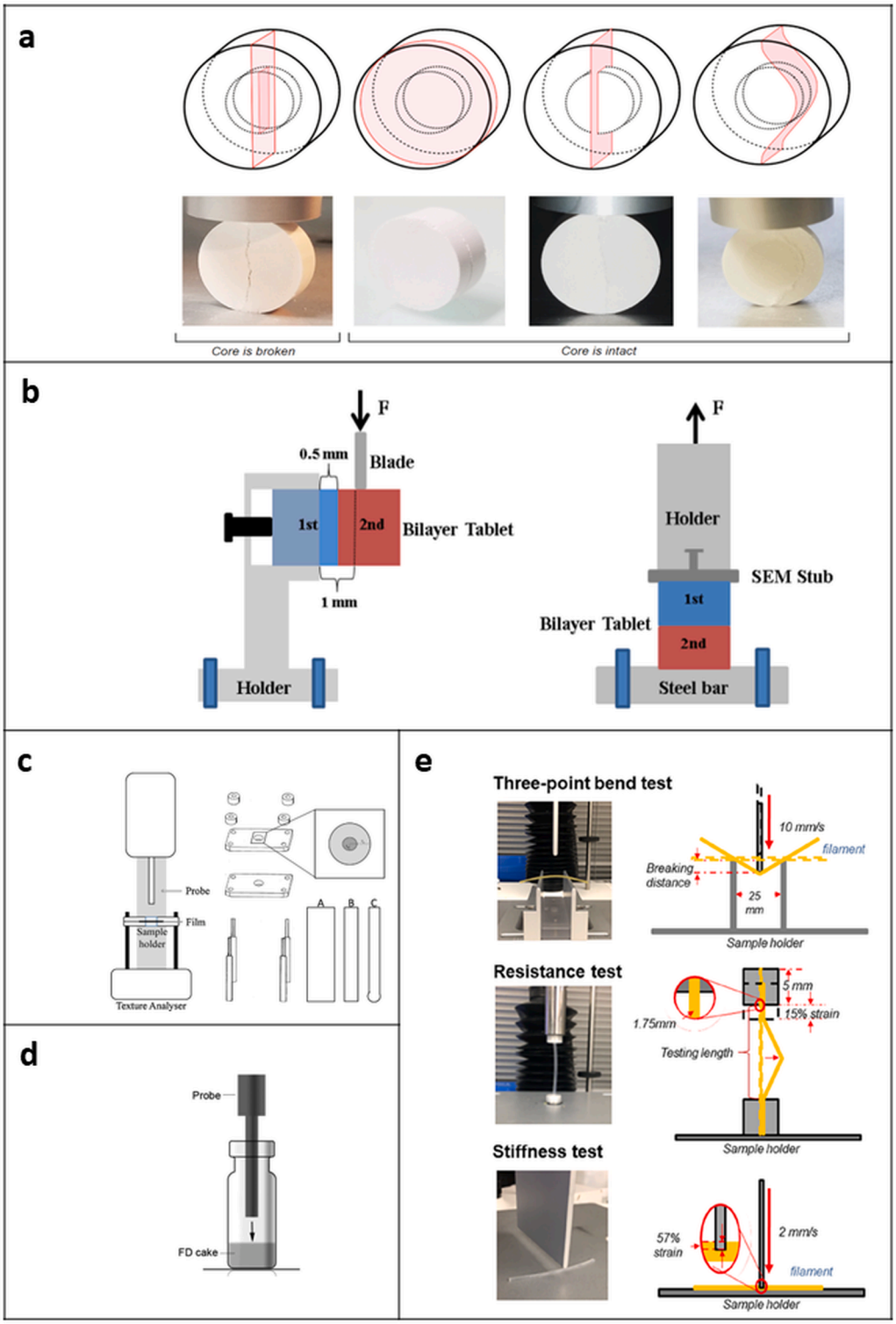

Fig. 4. Examples of experimental setups using texture analysers for the evaluation of: a, tablets through diametral compression tests (Reprinted with permission from Picart et al. (2022)); b, interfacial bonding strength of bilayer tablets (Reprinted with permission from Chang et al. (2017)); c, orodispersible films through puncture tests (Reprinted with permission from Preis et al. (2014b)); d, freeze-dried cakes in vials (Reprinted with permission from Hackl et al. (2016)); e, hot-melt extruded filaments through three different tests (Reprinted with permission from Xu et al. (2020)).

provides insight on the tablet behaviour through manufacturing stages, handling, packaging and transport, and tensile strength values comprised between 1.7 and 2 MPa are generally considered acceptable (Pitt and Heasley, 2013; Sabri et al., 2018). Many researchers plotted tensile strength versus compaction pressure to get insight on tabletability which contributes to preformulation knowledge and scale transfer (Lura et al., 2021, 2020; Perumalla and Sun, 2014; Vreeman and Sun, 2022a).

A more comprehensive material analysis can include plotting the force–displacement curve resulting from the diametrical fracture test that yields the maximum elastic deformation of a tablet with the further determination of TBI as friability indicator (de Backere et al., 2022; Gong and Sun, 2015; Paul and Sun, 2018). Gong and Sun applied two TA methods, a strain-based approach that led to the breakage of the tablet and an energy-based approach that avoided tablet breakage and allowed recovery measurements and came up with a total of 18 means to calculate TBI. Out of them, the best TBI as friability predictor was the reciprocal form of the elastic strain, which is convenient as it does not need additional experiments besides the diametrical breaking test (Gong and Sun, 2015). Further, Zhao et al. proposed an alternative parameter based on the previously demonstrated association between friability and diametrical deformation, as the ratio between the maximum strain and the maximum stress, called Strain/Stress Max (Zhao et al., 2022).

The gradient of the force–displacement curve can be assessed for the determination of Young's modulus, while the area under the curve can be associated to the tablet toughness defined as "the property of a tablet to absorb energy in the plastic region" (Sabri et al., 2018).

To investigate breakage phenomena in biconvex tablets and press-coated tablets, diametral CT were applied using systems equipped with cameras that captured the exact moment of tablet failure and contributed to the categorizing of the types of failures, as shown in Fig. 4a (Mazel et al., 2018; Picart et al., 2022).

Air entrapment during compression is one of the main reasons for tablet failure through lamination. To investigate the effect of deaeration through pre-compression on tablet quality, Vreeman et al. performed diametral crushing tests by TA, and measured the breaking forces instead of tensile strength for tablets that laminated with no diametrical breakage (Vreeman and Sun, 2022b).

Basim et al. used a spherical indentation probe to apply a 40 N force normal to the tablet plane and calculated the Brinell hardness, a material deformation-dependent parameter used to estimate tablet capping (Basim et al., 2019).

As solid material behavior under compression is a continuous concern of tablet formulation teams, Bonacucina et al. demonstrated that TA can be used to complement the information revealed by dynamic compression analysis fitted to Heckel equation. They performed two additional tests, for creep and stress vs. strain under static porosity conditions which enabled the determination of viscosity and elastic moduli and provided an optimal understanding of the material (Bonacucina et al., 2007). Zhang et al. performed TA on nano-silica modified plant extract powders as well as indentation and diametral CT on the resulting tablets and revealed that powder texture parameters are good indicators of tablet texture (Zhang et al., 2022c; Zhang et al., 2021).

As hardness testers only yield the force required for breakage, authors that needed more information on tablet failure performed TA to be able to distinguish between the compression and fragmentation phases. For instance, Rahman et al. compared force-distance curves of abuse deterrent Polyox tablet formulations to highlight the effects of polymer content and curing on the crushing resistance that could impact further manipulation (Rahman et al., 2017).

For mini-tablets, TA with diametrical CT seems to be the method of choice for the tensile strength evaluation, as the small sizes 1 – 3 mm hinder the use of conventional hardness testers (Hagen et al., 2016; Kottke et al., 2021; Kuck and Breitkreutz, 2022; Lura et al., 2021; Lura and Breitkreutz, 2022).

In what the mechanical characteristics of bilayer tablets are concerned, the achievement of sufficient interfacial bonding strength conditions their industrial production. In the attempt to develop standardized tests for the interfacial bonding strength evaluation, researchers tried to simulate the forces to which the tablets are subjected during handling and transport (Chang et al., 2017; Chang and Sun, 2019). Using a texture analyzer, a shear force parallel to the bilayer interface was applied for the shear method, on the tablet fixed vertically in a sample holder. The same authors applied a tensile method which involved a tensile force applied perpendicularly to the bilayer interface when tablets were placed horizontally on the fixture and glued on both sides to the fixture and the probe. Both setups are displayed in Fig. 4b. They showed that shear method results depend on tablet orientation and on the exact alignment of the sample holder at the interface, while the tensile method though time-consuming, does not depend on tablet orientation (Chang et al., 2017). Further, the developed tensile method allowed the understanding of the influence of particle size on the interfacial bonding strength in view of improving the mechanical characteristics of bilayer tablets (Chang and Sun, 2019).

Chewable gel tablets are usually evaluated applying TPA tests that are better correlated to mastication-related phenomena compared to other tests (Chatzitaki et al., 2022; Matulyte et al., 2021a, 2021b). Matulyte et al. determined the firmness, springiness, hardness, and stickiness of the products to assess the way formulation factors affect their quality after preparation and to investigate the changes occurred in one month (Matulyte et al., 2021a, 2021b).

3.2.3. Capsules

For capsules, equipment producers offer a special accessory to perform a TT and measure the force necessary to break a capsule. Machado et al. investigated the effects of lipid-based formulations with varying amounts of water on the integrity and mechanical properties of both gelatin and HPMC capsules to guide formulators in the development of robust liquid-filled capsules (Machado et al., 2016).

3.2.4. Oral lyophilisates (OLs)

TA is usually preferred for the evaluation of freeze-dried wafers because their porous structure and frailty makes conventional hardness testers use impractical (Vanbillemont et al., 2020) due to the high plastic deformation with no radial cracking. For OL mechanical testing, CT are usually applied to OLs down to a certain depth or deformation. Most of the authors chose to measure hardness and/or fracturability (Farias and Boateng, 2020) as they correlate them to the ease of handling and product integrity, or to simply compare load vs. distance profiles (Iurian et al., 2017a, 2017b). Hardness values between 3 and 6 N were considered appropriate (Boateng et al., 2010).

Additionally, other authors highlighted the importance of the relaxation phenomena that occur after removing the compressive force, depending on the penetration depth and quantified them as a compaction index (Boateng et al., 2010; Iftimi et al., 2019). Vanbillemont et al. applied an IT to determine the indentation hardness parameter that proved good discriminatory capacity between the commercial OLs. In addition to that, elastic recovery was also calculated and regarded as an indicator of behaviour upon unblistering (Vanbillemont et al., 2020). The same tests were further used in a study that aimed the development of OLs based on polyvinyl alcohol (PVA) loaded with a low-dose API (hydrochlorothiazide) and a high-dose active pharmaceutical ingredient (API) (paracetamol) through DoE methodology (Vanbillemont and de Beer, 2020).

To shorten the initial stages of OL development, Hackl et al. proposed a TA approach of testing freeze-dried cakes in vials for the quick determination of mechanical features as quality indicators for the final dosage forms or for lyophilization process performance (Hackl and Ermolina, 2016). They applied a CT with hold time to assess both stress and stress relaxation, using a setup shown in Fig. 4d. Results showed that TA profiles strongly depend on critical testing parameters. For instance, the recommended distance parameter should be below 55 – 60% of the

product's thickness to avoid structure densification. Furthermore, low testing speeds (0.01 – 0.05 mm/s) are preferable with porous and fragile matrices, for the high sensitivity to small load changes and the ability to differentiate brittle from soft materials out the appearance of the profile. As the proposed method caught the variability caused by material changes, preparation process and environmental factors, the authors further confirmed it with the development of polyvinyl pyrrolidone (PVP) and amino acids OLs (Hackl and Ermolina, 2019).

Besides CT that are appropriate for porous structures, Iftimi et al. also performed TT on several formulations of hydroxypropyl methylcellulose (HPMC)-based freeze-dried wafers (solid foams) intended for drug loading through inject printing. Comparing Young's modulus for flexibility, the ultimate tensile strength for overall substrate resistance, and the elongation at break for the capacity to deform without immediate failure, the authors were able to choose the optimal solid foam for injekt printing (Iftimi et al., 2019).

3.2.5. Films

The mechanical properties of films, either mucoadhesive, soluble or orodispersible are of paramount importance for the smooth running of the technological flow, packaging and handling by the patient when administered. They can be impacted by formulation factors, process parameters or storage conditions so they must be controlled throughout the development up to market release (Preis et al., 2014b). TA methods were described to characterize films obtained by solvent casting method (Speer et al., 2019), HME (Prodduturi et al., 2005, 2004) or electrostatic powder deposition (Prasad et al., 2015). Most researchers perform mechanical characterization by applying either TT (El-Malah and Nazzal, 2013; Owusu-Ware et al., 2019, 2016; Prodduturi et al., 2004), PT (Kajthunyakarn et al., 2019; Peerapattana et al., 2015) or sometimes both (Brniak et al., 2015). Strength and elongation at break are regularly considered to describe mechanical traits of films, either on dry (Alaei et al., 2021; Pongjanyakul and Khuathan, 2016; Preis et al., 2014b) or on wetted samples (Kajthunyakarn et al., 2019; Karrout et al., 2010; Khuathan and Pongjanyakul, 2014; Pongjanyakul and Khuathan, 2016).

For the evaluation of orodispersible films (ODFs), a strategy for the development of a PT (PT) was described, and revealed the selection of an appropriate probe that best distinguished between reference materials, and a sample holder that can accommodate small samples, usually down to 2 × 8 mm, as shown in Fig. 4c. A cylindrical flat surface probe was chosen, with a diameter of 4.8 mm. Besides strength and elongation, authors calculated the energy to puncture as the area under the force–displacement curve divided by the sample volume, which enabled the comparison of different thickness specimens (Preis et al., 2014b). The same parameter from PT was used to compare three-layer films of carrageenan: polyelectrolyte complex: chitosan with their single-layer correspondents (Volod'ko et al., 2021). However, Alaei, who evaluated films through PT, reported that out of all calculated parameters, the breaking factor was the only one that discriminated between commercial samples (Alaei et al., 2021).

Parameters derived from TA can be studied as responses in Design of Experiments (Kraisit et al., 2017; Peerapattana et al., 2015), as El-Malah et al. did with tensile strength and elastic modulus to estimate the effects of formulation factors (pullulan, HPMC, and PVP) on the strength and flexibility of films (El-Malah and Nazzal, 2013).

Brniak et al. investigated the effects of microparticles loaded into the films through TT and PT and showed the negative effect of microparticle inclusion on strength and flexibility. Also, they obtained high variability among Young's modulus results for films containing microparticles (Brniak et al., 2015). The mechanical properties of films can also be explained by the molecular mobility of polymers, as studies of Thermally Simulated Current demonstrated on hydroxyethyl cellulose (HEC) and plasticized hypromellose films (Owusu-Ware et al., 2016, 2019). Other authors highlighted the effects of moisture on hot-melt extruded films loaded with clotrimazole through TT performed on samples stored in different humidity conditions (Prodduturi et al., 2005, 2004). Tests were continued until film breakage, but results were considered valid only if films failed between the clamps and not at contact (Prodduturi et al., 2005, 2004).

On the other hand, films intended for microparticulate coating can be firstly solvent cast and evaluated for their mechanical properties (Khuathan and Pongjanyakul, 2014; Salawi et al., 2021). In this respect, Karrout et al. assessed the energy needed to break the films in their dry and wetted states to understand the way coatings could face mechanical stresses encountered in the gastrointestinal tract (Karrout et al., 2010).

Out of the applied tests, the puncture method was reported as less prone to set-up errors, less restrictive in terms of sample shape, and allows safe handling of fragile structures (Prasad et al., 2015).

The standard test method for tensile properties, ASTM D638 Type V requires dog bone shape samples which are not always appropriate for drug-containing films or for testing marketed formulations (Preis et al., 2014b).

3.2.6. Filaments

To assess filament mechanical properties and their printability most researchers apply FT such as the 3PBT (Alzahrani et al., 2022; Hu et al., 2022; Viidik et al., 2021; Zhang et al., 2017), BT (Xu et al., 2020) and stiffness tests (Crișan et al., 2022). Out of the mechanical parameters derived from this test, stiffness is the most frequently referred as a good printability indicator (Hu et al., 2022). Many authors reported the breaking forces, but when filaments with different diameters had to be compared Alzahrani et al. chose the breaking stress instead of the breaking force. Through a 3PBT, Alzahrani et al. fitted stress strain curves to Hooke's law to calculate k, the stiffness constant and demonstrated that high k values show better printability (Alzahrani et al., 2022).

Zhang et al. defined specific conditions to evaluate filaments for 3D printing through the so called Repka-Zhang methods. They include a first test to determine flexibility and brittleness/ toughness by means of a three-point bending test (3PBT) in specified conditions, and a second test that estimates filament stiffness by applying a force perpendicularly to the sample placed on a flat surface, which yields the peak stress as a stiffness indicator (Zhang et al., 2019). Flexibility was defined as "the tolerance of a filament to bending without breaking" and was measured by the breaking distance. The toughness or brittleness were described as "the breaking of a filament without significant plastic deformation" and stands for the breaking stress. Stiffness was equivaled to breaking stress in the second test, described as the load required to reach a certain deformation (Zhang et al., 2019). However, in other studies, the breaking distance was referred to as a measure of brittleness (Zhang et al., 2017, 2020).

The Repka-Zhang methods were taken over and sometimes adapted by other authors who aimed to optimize the mechanical properties of the filaments (Crișan et al., 2022; Than and Titapiwatanakun, 2021; Vo et al., 2020). An adapted version of the 3PBT with the edges of the filament fixed between clamps was used by Crișan et al. to estimate brittleness and flexibility of diclofenac sodium loaded filaments. The fracturability was obtained from the load value at break and was considered an indirect indicator of brittleness (Crișan et al., 2022).

In addition to the two tests described by Zhang, Xu added a third one, the resistance test, a BT to assess the softness of filaments, for which the testing parameters (sample length, speed and strain) were optimized through an experimental design to yield minimum result variability. The methodology of the three tests applied by Xu is briefly described in Fig. 4e. Comparing the results obtained with the three tests, the authors proposed stiffness test as the most appropriate for its accuracy, reliable results, ease of operation and low material investment. The toughness parameter calculated from the AUC of stress–strain profile of the stiffness test provided a comprehensive way to characterize filaments and predict printability (Xu et al., 2020). Samaro et al. reached the same conclusions regarding the relevance of toughness in printability prediction, however determined form a TT (Samaro et al., 2020).

Other authors also applied BT, referred to as dry spaghetti tests performed in food industry, and revealed filament flexibility as the breaking distance of the product (Gültekin et al., 2019, 2021).

TT were also reported for filaments although sometimes the fracture points do not show at the middle of the sample, in the measuring area, but at the contact with the grip which indicates a failure caused by the grip pressure rather than the applied tension. Zhang et al., who developed indomethacin/ Eudragit RL filaments reported an improvement after the addition of plasticizers in the mixture (Zhang et al., 2022a). Mirdamadian applied TT to check the effect of different loads of oxaliplatin alginate nanoparticles on the mechanical properties of Eudragit L100-55 filaments plasticized with PEG6000 and triethyl citrate (Mirdamadian et al., 2022). Tabriz et al. ranked a high number of polymers according to the results of TT (maximum tensile strength, Young's modulus and elongation at break) and matched the results with the actual printability through Principal Component Analysis. They revealed the importance of tensile stress in the accurate prediction of printability (Tabriz et al., 2021).

Applying three different mechanical testing methods (TT, 3PBT and BT), Samaro et al (2021) showed that printing with holt melt extrusion filaments could pose filament loading and printability issues that could be avoided with direct extrusion additive manufacturing technology (Samaro et al., 2021).

As shown above, most of the mechanical tests performed on filaments through TA aimed and achieved printability prediction. Still, the printing quality could not be accurately evaluated by such methods, so a 3D printed object retention rate was proposed for that (Zhang et al., 2022b). Regarding the acceptable values that some authors declare for certain filament formulations, these should not be considered as absolute values, but indicative and strictly correlated with the formulation in question and the test parameters. Even within the same group of authors, there were variations regarding the values of the mechanical parameters considered acceptable for printing (breaking distance $>$ 1 mm (Zhang et al., 2017), breaking distance $>$ 0.61 mm (Zhang et al., 2019)), which shows that printability is highly formulation dependent, and one parameter cannot be a sufficient descriptor of printing capacity. As there are no official regulations regarding the acceptable values for mechanical parameters of filaments, polyvinyl alcohol, polylactic acid (PLA) or acrylonitrile butadiene styrene (ABS) filaments are often used as a reference material in terms of mechanical properties (Samaro et al., 2020; Xu et al., 2020; Zhang et al., 2022b).

In the attempt to develop a new analytical tool to guide the selection of printing parameters, Gottschalk et al. used an experimental setup that included a texture analyzer to measure the feed forces needed to load a filament to a heated nozzle to print at a required speed. PLA, PVA and polyethylene terephthalate glycol-modified were used as testing materials, as well as a filament with PVA loaded with ketoconazole. Feed force limit assessment led to the prediction of printing parameters and the successful transfer to an actual printing process with final products within the 5% variation limit (Gottschalk et al., 2022).

3.2.7. 3D printlets

3D printed dosage forms are usually subjected to single or double CT under cylindrical probes (Cheng et al., 2020). Round-shaped chewable semi-solid dosage forms for paediatric use were 3D printed and subjected to a TPA test to simulate mastication. As there are no standard acceptability criteria, the calculated parameters such as hardness, cohesiveness, gumminess, chewiness, and adhesiveness were compared to the respective values obtained for well-accepted semi-solid foods such as peanut butter or banana (Chatzitaki et al., 2022). Other authors have considered printing and moulding different sizes and shapes of their products to get a better mechanical characterization through both CT and 3PBT. They linked their results obtained on chocolate samples to the sensory evaluation through the Chewing Difficulty Index (CDI), calculated using the breaking force value measured in the 3PBT (Chachlioutaki et al., 2022).

As shown in Table 3, many researchers combine texture characterization methods, using different fixtures, different test parameters or sample sizes to get an image as complete as possible on the mechanical profile of their samples. As different research groups describe different experimental setups, accessories and working conditions, their reported results are hardly comparable to one another. Sometimes results present high variability, therefore some authors chose to perform 10 (Mazel et al., 2016; Xu et al., 2020) or even 15 repetitions (Zhang et al., 2017, 2019).

4. TA in mucoadhesion

Mucoadhesion or bioadhesion represents one of the critical quality attributes of the mucoadhesive drug delivery systems which may influence the bioavailablity of the product. Briefly, the bioadhesion mechanism can be summarized in the following steps: 1) a good contact between the sample and the substrate that can be facilitated by the hydration of the bioadhesive surface; 2) the hydration favors the interpenetration of the polymer chain with the mucus to form semi-permanent bonds (Alaei and Omidian, 2021; Duchene et al., 2008).

The ability of a dosage form to adhere to a mucosa can be determined through TA by the measurement of the force and/or work needed to detach the dosage form from a mucosa or mucosa-like substrate (Hagesaether et al., 2009). During the CT, the force vs. time or force vs. distance curve can be plotted and the following parameters can be calculated: the detachment force (also reported as bioadhesion force or the force to detach the sample from the substrate) and the work of adhesion (also reported as adhesiveness or the work required to counteract the forces of attraction between the sample surface and the substrate when the probe withdraws), as depicted in Fig. 5. When the stress–strain plot is recorded, the value of maximum stress necessary to overcome the bond between the sample and substrate is a parameter of interest, as well as the adhesion energy which can be calculated as the area under the curve (Gennari et al., 2019). The adhesion energy value can be also calculated from the force of detachment and displacement at maximum load (Mizrahi et al., 2004). In addition, the post-peak area under the curve and the elongation at adhesive failure can be used to obtain information about the stringiness and the cohesiveness of the samples (Repka et al., 2006). In other studies, the cohesiveness was determined as the distance the samples moved before detaching from the substrate (Farias and Boateng, 2018).

Most of the TA studies report comparable experimental setups and procedures for the measurement of the adhesion; usually, the equipment used is a universal testing system or a texture analyzer (Carvalho et al., 2010). In most cases, the sample attached to the probe is lowered at a programmed speed until contact with the substrate, then a constant force is applied to the substrate for a defined time interval. After the hold time, the probe returns to the initial position (Fig. 6a) ("CT3 TEXTURE ANALYZER Operating Instructions," n.d.). In a second experimental setup, the substrate is fastened on the upper metal probe and the sample is fixed on the lower support of the device. The upper probe is moved downward until the contact with the sample and maintained for a predefined time, whereupon the probe returns to the starting position (Fig. 6b) (Nep and Conway, 2011; Tamburic and Craig, 1997).

In several research studies, the adhesion properties of the films were assessed by performing a mucin-interaction test where the 3 % mucin was evenly spread on two layers and, further attached to both the upper and the stationary part of the analyzer. The sample was placed in between, and the probe was lowered; a 200 g force was applied for 100 s and the probe was withdrawn while the displacement and force of detachment were recorded (Fig. 6c) (Alopaeus et al., 2020; Hagesaether et al., 2009).

Depending on the experimental setup, the technique can be optimized regarding the test parameters (test speed, contact time, or contact force) but also the pretreatment of the substrates (type and volume of the conditioning media, time to hydrate the substrate) to better

Table 3
Details on the methodology of mechanical tests using TA.

Experimental setup	Testing parameters	Sample details size	Parameters of interest (±acceptable values)	Reference
Tablets				
4 mm diameter cylindrical probe	TA (TA.XT2i), CT S: 1 mm/s	C: ibuprofen or acetaminophen, MCC at different ratios, magnesium stearate 1% Φ: 10 mm	Tensile strength	(Basim et al., 2019)
Flat surface probe	TA (TA.XT2i), CT S: 0.01 mm/s	C: acetaminophen and Copovidone solid dispersions Φ: 8 mm	Tensile strength	(Patel and Sun, 2016)
Flat surface probe	TA (TA.HDPlus), CT S: 0.1 mm/s	C: anhydrous calcium phosphate, magnesium stearate 2% Φ: 12 mm	Photographs of the failure modes	(Mazel et al., 2018)
	TA (TA.XT2i), CT S: 0.02 mm/s	C: MCC, HPC, povidone, lactose monohydrate, dibasic calcium phosphate, binary mixtures of diluents, magnesium stearate 0.5% Φ: 8 mm	TBI ($\langle 1\,5\,0 \rangle$)	(Gong and Sun, 2015)
	TA CT	C: lactose monohydrate, MCC at different ratios, magnesium stearate, sodium stearyl fumarate, stearic acid Φ: 9.5 mm	Tensile strength, TBI	(Paul et al., 2021)
Cylindrical probe 36 mm diameter	TA (TA.XTPlus), CT S: 0.1 mm/s D: 15%	C: MCC/ pre-gelatinized starch/ spray-dried monohydrate lactose/ dicalcium phosphate anhydrate, mannitol	Work of fracture, maximum stress, maximum strain, strain/stress max (<1 MPa^{-1} for friability $\ll$ 1%)	(Zhao et al., 2022)
	TA(TA.XTPlus), CT S: 1 mm/s	C: sotalol, Polyox™ 301 ± HPMC K100M or K4M/ monohydrate or anhydrous lactose/ MCC, magnesium stearate, butylated hydroxytoluene Φ: 8 mm	Hardness as force to fracture, fracture strain, gradient to fracture, work of fracture	(Rahman et al., 2017)
3.175 mm diameter indentation probe	TA (TA.XT2i) IT S: 0.05 mm/s F: 40 N	C: lactose monohydrate, MCC at different ratios, magnesium stearate, sodium stearyl fumarate, stearic acid Φ: 9.5 mm	Indentation hardness	(Paul et al., 2022)
3.18 mm diameter indentation probe	TA (TA.XT2i), IT S: 0.1 mm/s F: 40 N	C: ibuprofen or acetaminophen, MCC at different ratios, magnesium stearate 1% Φ: 10 mm	Brinell hardness	(Basim et al., 2019)
Mini-tablets				
4 mm diameter flat-faced probe	TA (TA.XTPlus), CT S: 0.1 mm/s	C: sodium salicylate and granulated or spray-dried mannitol Φ: 2 mm	Radial tensile strength	(Hagen et al., 2016)
5 mm punch	TA (TA.XTPlus), CT S: 0.1 mm/s	C: desmopressin acetate, povidone, and α-lactose monohydrate Φ: 2 mm	Tensile strength	(Kottke et al., 2021)
5 mm punch	TA (TA.XTPlus), CT S: 0.1 mm/s	C: Ludiflash®, Parteck® ODT, Prosolv® ODT, GalenIQ™ 721 or SuperTab® 50 ODT with different ratios of lubricants Φ: 2 mm	Tensile strength	(Kuck and Breitkreutz, 2022)
5 mm flat punch	TA (TA.XTPlus), CT S: 0.1 mm/s	C: Ludiflash®, GalenIQ™ 721, sodium stearyl fumarate Φ: 2 mm	Tensile strength (1 – 2 MPa), tabletability	(Lura et al., 2021)
Bilayer tablets				
Lateral sample holder	TA (TA.XT2i), CT S: 0.01 mm/s	C: binary mixtures of lactose and MCC of different grades Φ: 8 mm	Shear strength as interfacial bonding strength	(Chang and Sun, 2019)
Tablets attached on both sides to cylindrical probe	TA (TA.XT2i), TT S: 0.01 mm/s	C: binary mixtures of lactose and MCC of different grades Φ: 8 mm	Tensile strength as interfacial bonding strength	(Chang and Sun, 2019)
Chewable gel tablets				
–	TA (TA.XTPlus), TPA S: 1 mm/s D: 50% H: 60 s	C: gelatin, glycerol, water, Thyme syrup, preservatives Gummy bears	Firmness and springiness	(Matulyte et al., 2021b)
20 mm height probe	TA (TA.XTPlus), CT S: 2 mm/s D: 5 mm	C: gelatin, glycerol, water, Thyme syrup, Thyme extract, citric acid, nutmeg essential oil/ microcapsules Cylindrical tablets	Hardness, stickiness (adhesiveness)	(Matulyte et al., 2021a)
Capsules				
Capsule tensile rig	TA (TA.XT2i), 50 kg load cell TT S: 0.5 mm/s	C: gelatin and hypromellose capsules immersed in lipid-based formulations containing different amounts of water Capsules size 0	Elastic stiffness and elongation at break	(Machado et al., 2016)

(*continued on next page*)

Table 3 (*continued*)

Experimental setup	Testing parameters	Sample details size	Parameters of interest (±acceptable values)	Reference
Freeze-dried wafers				
Cylindrical probe 5 mm	TA (QTS- 25), CT S: 6 mm/min D: 2 mm	C: gelatin ± mannitol/sorbitol/sucrose ± Carbopol 974P-NF/Pluronic F217 Φ: 13.3 mm	Hardness at 1 mm depth (28 ± 3.3 N)	(Chandrasekhar et al., 2009)
Penetration probe	TA (QTS- 25), CT S: 6 mm/min D: 4 mm	C: gelatin ± mannitol/sorbitol/sucrose ± Carbopol 974P-NF/Pluronic F217 Φ: 13.3 mm	Fracturability at 3 mm depth	(Chandrasekhar et al., 2009)
Spherical indentation probe 1.5 mm diameter	TA (TA.XTPlus), 5 kg load cell IT S: 0.1 mm/s D: 0.65 mm	C: commercial OLs Samples of different diameters	Indentation hardness (12.45 – 322.74 kPa), elastic recovery (from dividing the area under the curve of the unloading plot with that of the loading plot)	(Vanbillemont et al., 2020)
Cylindrical probe 2 mm	TA (TA.HDPlus), 5 kg load cell CT	C: acetylsalicylic acid, Metolose®, kappa carrageenan/chitosan, and aspartame/sucralose Φ: 15.5 mm	Hardness	(Farias and Boateng, 2020)
Cylindrical probe with torsion area 20.27 mm^2	TA (TA.XTPlus), CT S: 0.01 mm/s D: 3 mm	C: povidone and mannitol and amino: acid L-alanine/ L-serine/ L-glycine/ L-proline 2 ml samples in 10 ml vials	Stress, stress relaxation, number of positive peaks, linear distance	(Hackl and Ermolina, 2019)
Conical penetration probe	TA (TA.XT2), CT S: 0.01 mm/s D: 1 mm	C: dextrin, β-limit dextrin or pre-gelatinised starch 18 mm diameter × 40 mm thickness	Force-distance profiles, strength	(Qi et al., 2012)
Cylindrical probe 5 mm, setup of two blank plates and a 1 cm diameter cylinder hole on the top plate	TA (TA.XT2), 5 kg load cell, CT S: 1 mm/s D: 2 mm TF: 5 g	C: sumatriptan succinate, gelatin, xanthan gum, disodium EDTA, magnesium stearate, ± Plasdone K90D, ± mannitol/ glycine/ sorbitol, ± camphor/ menthol, ± sucralose	Hardness (1.509 ± 0.131 kg)	(Gugulothu et al., 2015)
Tensile grips	TA (TA.XTPlus), 50 N load cell TT S: 5 mm/s D: 20 mm	C: hypromellose ± PEG 4000:Tween® 20: Glycerol (1:1:1) ± Poloxamer 188 20 × 70 mm samples	Young's modulus (12.2 mN/mm^2), ultimate tensile strength (218.9 mN/mm^2), elongation at break (23.5%)	(Iftimi et al., 2019)
Films				
Film fixture, semi-spherical probe head	TA (CT3-1000), PT S: 0.5 mm/s	Commercial oral film formulations of different sizes	Breaking factor (above 34.5 N/mm), elongation (below 5.55%)	(Alaei et al., 2021)
Film fixture	TA (TA.XT2), PT	C: casein sodium, glycerol ± halloysite 2 × 2 cm samples	Puncture strength and elongation on dry and wet films	(Kajthunyakarn et al., 2019)
Film fixture, 6 mm spherical probe	TA (TA.XT2), 50 kg load cell PT S: 0.1 mm/s	C: quaternary polymethacrylate ± sodium alginate 2 × 2 cm samples	Puncture strength and elongation on dry and wet films	(Khuathan and Pongjanyakul, 2014)
Film holder with mounting plates	TA (TA.XTPlus), 5 kg load cell PT S: 0.1 mm/s	C: hypromellose ± polycarbophil 3.5 × 0.6 cm samples	Puncture strength and elongation	(Kraisit et al., 2017)
Clamps fixture	TA (TA.XTPlus), 500 N load cell TT S: 0.5 mm/s	C: terbinafine HCl, povidone K30, Hypromellose and glycerol 3 × 1 cm samples	Tensile strength (>0.042 N/cm^2) and elongation at break (>36.15%)	(Arpa et al., 2021)
Clamps fixture	TA (Shimadzu EZ-SX) TT S: 10 mm/min	C: microparticles, hypromellose and glycerol/PEG 200 2 × 15 cm solvent cast film	Tensile strength (6.48 ± 0.37 MPa), Young's modulus (706.33 ± 96.89 MPa), % elongation (14.33 ± 1.8 %)	(Brniak et al., 2015)
Film fixture, 8 mm diameter spherical probe	TA (Shimadzu EZ-SX) PT S: 10 mm/min	C: microparticles, hypromellose and glycerol/PEG 200 2 × 15 cm samples	Maximum force (4.8 ± 1.6 N), displacement (1.16 ± 0.44 mm)	(Brniak et al., 2015)
Tensile grips setup	TA (TA.XTPlus), TT S: 5 mm/min	C: diclofenac sodium, pullulan, povidone, Hypromellose, glycerol, Tween 80 L: 40 mm solvent cast film	Tensile strength (11.21 MPa), elastic modulus (6.78 MPa%)	(El-Malah and Nazzal, 2013)
Tensile grips setup	TA (TA.Plus), TT S: 0.2 mm/s D: 300 mm	C: HEC films Dumb-bell shaped solvent cast samples	Tensile strength (10 ± 3 N/mm^2), elastic modulus (1150 ± 10 MPa), elongation at break (9%)	(Owusu-Ware et al., 2016)
Film fixture, 4.8 mm diameter flat probe	PT S: 5 mm/s	C: aripiprazole, HPC/povidone, citric acid, sucralose 22 × 22 × 0.1 mm 3D printed film	Puncture strength (>0.08 N/mm^2)	(Lee et al., 2022)
Film fixture, 4.8 mm diameter flat probe	TA (TA.XTPlus), 5 kg load cell PT S: 5 mm/s	C: commercial and newly developed ODFs with different compositions 20 × 30 mm solvent cast films	Puncture strength (>0.06 N/mm^2), elongation, energy to puncture	(Preis et al., 2014b)
TA, Tensile grips setup, grip distance 30 mm	TA (TA.XT2i), 5 kg load cell TT S: 2 mm/s	C: clotrimazole 10%, HPC of different grades 50 × 10 × 0.48 mm HME films	Tensile strength, elastic modulus, elongation at break	(Prodduturi et al., 2004)

(*continued on next page*)

Table 3 (*continued*)

Experimental setup	Testing parameters	Sample details size	Parameters of interest (±acceptable values)	Reference
Film fixture, cylindrical probe	TA (TA.XTPlus), PT S: 0.1 mm/s	C: metronidazole, polycaprolactone, HPMC, glyceryl monostearate 20 × 20 mm hot melt films	Puncture strength (11.58 ± 0.51 N/mm^2), elongation (33.51 ± 3.61%), Young's modulus (0.347 ± 0.021 N/mm^2)	(Peerapattana et al., 2015)
5 mm spherical puncture probe	TA (TA.XT2), load cell 500 N TT S: 0.1 mm/s	C: magnesium aluminium silicate, quaternary polymethacrylate 2 × 2 cm film	Puncture strength, elongation at break	(Rongthong et al., 2013)
Clamps fixture	TA (TA.XT2), load cell 500 N TT S: 15 mm/min	C: magnesium aluminium silicate, quaternary polymethacrylate 2 × 7 cm film	Tackiness	(Rongthong et al., 2013)
HME filaments				
3PBT rig 25 mm gap	TA (TA.XT2i), CT S: 10 mm/s D:15 mm	C: acetaminophen 30% ± different grades of polymers/ binary mixtures/ binary mixture + disintegrant 50 mm sample	Breaking stress (>2941 g/mm^2), breaking distance (>1 mm)	(Zhang et al., 2017)
3PBT rig 25 mm gap	TA (TA.XT2), CT S: 10 mm/s D:15 mm	C: acetaminophen 30% ± different grades of cellulose based polymers (HPC, HPMC, EC) 50 mm sample	Flexibility (breaking distance > 0.61 mm), toughness (breaking stress > 635.5 g/mm^2), stiffness (20758.3 g/mm^2)	(Zhang et al., 2019)
3PBT rig 20 mm gap	TA (TA.XT2), CT S: 5 mm/s D:15 mm	C: ibuprofen 20%, HPMCAS ± plasticizers 30 mm sample	Breaking force, breaking distance, gradient of the deflection curve	(Zhang et al., 2020)
3PBT rig 3 mm thick 25 mm gap	TA (TA.XTplus) CT S: 10 mm/s D:10 mm	C: different polymers ± ibuprofen 30% ± plasticizers 60 mm sample	The maximum force, fracture distance, the maximum stress and AUC of the stress–strain curve as brittleness	(Xu et al., 2020)
Cylinder rig with two sample holders for vertical placement of the sample	TA (TA.XTplus) CT S: 1 mm/s D: 5%	C: different polymers ± ibuprofen 30% ± plasticizers 40 mm sample	The maximum force, fracture distance, the maximum stress and AUC of the stress–strain curve as resistance	(Xu et al., 2020)
3PBT rig 3 mm thick (just the upper part) sample on a platform	TA (TA.XTplus) CT S: 2 mm/s D: 1 mm (57%)	C: different polymers ± ibuprofen 30% ± plasticizers 60 mm sample	The maximum force, fracture distance, the maximum stress and AUC of the stress–strain curve as toughness	(Xu et al., 2020)
3PBT rig	TA (TA.XT2i), CT S: 2 mm/s	C: ketoprofen 30%, HPMC K4M, HPMCAS HG ± HPC LF 50 mm sample	Breaking stress, breaking distance, stiffness (>63.46 ± 11.23 g/mm)	(Hu et al., 2022)
3PBT rig 25 mm gap	TA (TA.XT2), CT S: 10 mm/s D:1.5 mm	C: amlodipine besylate, polyvinyl alcohol, sorbitol; atorvastatin calcium, Kollidon® VA64 50 mm samples	Breaking stress (>330.6 ± 11.4 g/mm^2)	(Alzahrani et al., 2022)
Grip fixture	TT S: 20 mm/min	C: oxaliplatin nanoparticles loaded to filaments of Eudragit® L100-55, PEG6000, triethyl citrate 50 mm samples	Tensile strength (2.57 N/mm^2), Young's modulus (4.88 N/mm^2), elongation at break, stress–strain curves	(Mirdamadian et al., 2022)
Grip fixture	TA (TA.XT2), TT S: 5 mm/min	C: indomethacin, Eudragit RL, plasticizer	Yield strength (20.86 ± 1.31 Pa), fracture strength (27.96 ± 1.81 Pa)	(Zhang et al., 2022b)
TA, self-tightening roller grip system	TA (TA.XTPlus), load cell 50 kg TT S: 3 mm/s D: 140 mm	C: anhydrous theophylline (20% or 40%), Klucel™ HPC EF and LF/ Soluplus®/ Kollicoat® IR/ Affinisol™ 15cP and 4 M, Parteck® MXP/ Aquazol® 200 70 mm samples	Young's modulus, ultimate tensile strength, strain at breakage, toughness	(Samaro et al., 2020)
TA, self-tightening roller grip system	TA (TA. HDPlusC), load cell 30 kg TT S: 3 mm/s D: 140 mm	C: metoprolol tartrate 50%, different ethylene–vinyl acetate grades 70 mm samples	Elastic modulus calculated from the linear interpolation of 1% and 5% strain	(Samaro et al., 2021)
Mini 3 PB rig 8 mm gap	TA (TA. HDPlusC), load cell 30 kg CT S: 0.02 mm/s D: 20 mm	C: metoprolol tartrate 50%, different ethylene–vinyl acetate grades 20 mm samples	Flexural stress, flexural strain, flexural elastic modulus calculated from the linear interpolation of 1.5% and 5% strain	(Samaro et al., 2021)
BT gripper, cylinder rig with two sample holders for vertical placement of the sample	TA (TA. HDPlusC), load cell 30 kg CT S: 2 mm/s D: 15 mm	C: metoprolol tartrate 50%, different ethylene–vinyl acetate grades 60 mm samples	Buckling stress as the average maximum stress for each formulation	(Samaro et al., 2021)
Blade probe, plane fixture	TA (CT3-4500), CT S: 0.1 mm/s D: 5%	C: diclofenac sodium, polyvinyl alcohol, Kolliphor® TPGS, Aerosil® 200 5 mm sample	Peak stress (26.19 N/mm^2)	(Crișan et al., 2022)
Spaghetti flexure rig for vertical placement of the sample	TA (TA.XTPlus), TPA	C: Pramipexole monohydrate dihydrochloride, Polyox® N80 ± Eudragit® RSPO/RLPO ± Eudragit® RL100/RS100 50 mm sample	Flexibility	(Gültekin et al., 2021)

(*continued on next page*)

Table 3 (*continued*)

Experimental setup	Testing parameters	Sample details size	Parameters of interest (±acceptable values)	Reference
Spaghetti flexure rig for vertical placement of the sample	TA (TA.XTPlus), TPA	C: Pramipexole monohydrate dihydrochloride, Eudragit® EPO, Polyox™ WSRN10/WSRN80 50 mm sample	Flexibility	(Gültekin et al., 2019)
3D Printlets				
Cone penetrometer probe (30°)	TA (TA.XTPlus), CT S: 2 mm/s D: 10%	C: acetaminophen, Mycusini® 3D Choco Dark 15 × 15 × 10 mm sample	Hardness, fracturability	(Chachlioutaki et al., 2022)
3PBT set	TA (TA.XTPlus), CT S: 2 mm/s D: 20%	C: acetaminophen, Mycusini® 3D Choco Dark 60 × 15 × 10 mm sample	Flexural strength, CDI	(Chachlioutaki et al., 2022)
Cylindrical probe 50 mm	TA (TA.XTPlus), TPA S: 1 mm/s D: 40%	C: isoniazid, cornstarch 11.3 mm diameter × 6.5 mm height cylinders	Hardness, adhesiveness, cohesiveness, springiness, gumminess	(Chatzitaki et al., 2022)
Cylindrical probe 35 mm	TA (TA. XTPlusC), TPA S: 1 mm/s D: 50%	C: theophylline, HPMC K4M/E4M 20.37 × 8.35 × 6.6 mm samples	Hardness, adhesiveness, cohesiveness, springiness	(Cheng et al., 2020)

*Abbreviations: TA, texture analyzer; CT, compression test; TT, tensile test; 3PBT, 3-point bending test; TPA, TPA; S, probe speed; D, deformation; F, force; H, hydration time; C, composition; MCC, microcrystalline cellulose; HEC, hydroxyethylcellulose; HPC, hydroxypropylcellulose; HPMC, hydroxypropyl methylcellulose; EC, ethylcellulose; PEG, polyethylene glycol; TBI, Tablet Brittleness Index; CDI, Chewing Difficulty Index.
** Device model (Maximum load / Force resolution): CT3-1000 (1 kg/0.10 g), CT3-4500 (4.5 kg/0.50 g), TA.XTplus (50 kg/0.1 g), TA.HDplus (750 kg/0.10 g), TA. XTPlusC (50 kg/0.1 g), TA.HDplusC (30 kg/ 0.1 g), QTS- 2505 (5 kg/0.2 g), QTS- 2525 (25 kg/1 g), Shimadzu EZ-SX (500 N/2.5 N).

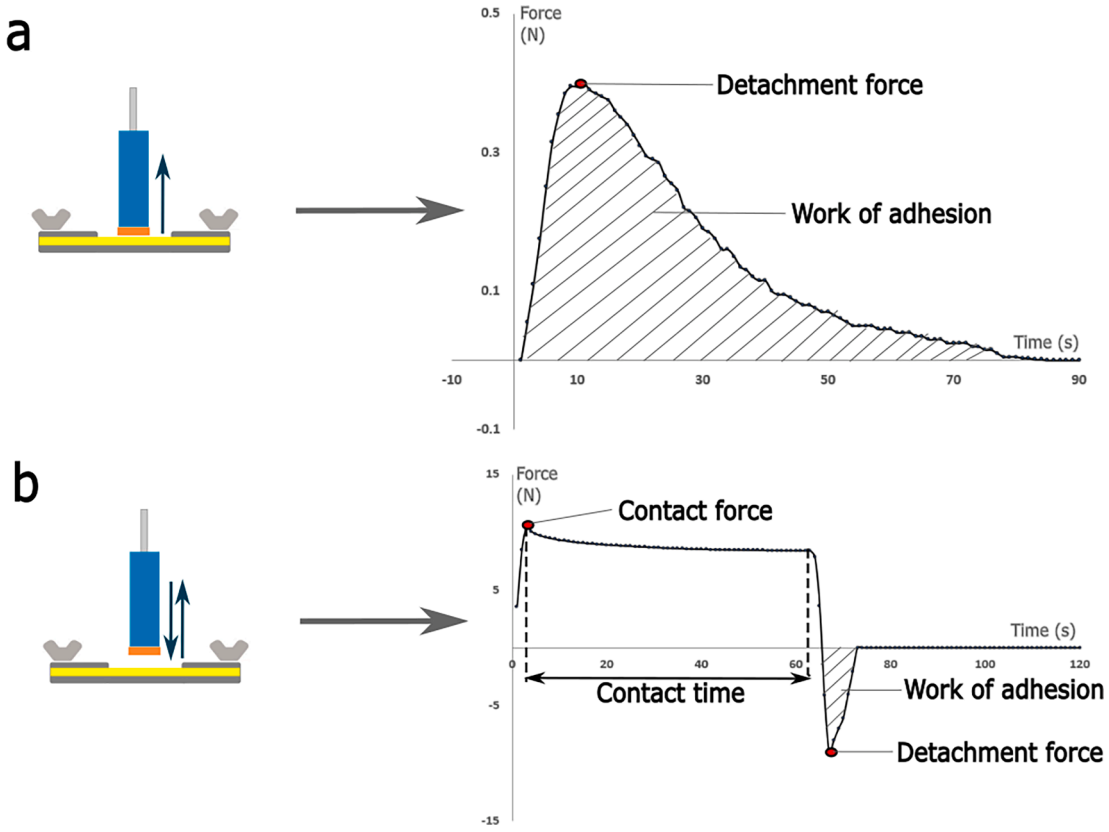

Fig. 5. Mucoadhesion parameters determined through TA when: a, recording starts after the contact between sample (orange) and substrate (yellow), and b, recording starts at the probe descent, before the contact between sample (orange) and substrate (yellow). (For interpretation of the references to colour in this figure legend, the reader is referred to the web version of this article.)

reproduce the *in vivo* conditions but also to discriminate small variations of mucoadhesive properties (Alaei et al., 2021; Shakweh et al., 2007).

According to the diffusion theory of mucoadhesion, the interpenetration of polymer chains with mucus chains creates semipermanent adhesive bonds, and the adhesive forces increase with the contact time (Chickering and Mathiowitz, 1999). The contact time or holding time is defined as the duration the sample is in contact with the surface of the tissue (Singh and Rana, 2014). For the evaluation of the mucoadhesive tablets, Mizrahi et al. investigated the influence of contact time on adherence to mucosal tissue. The experimental result revealed that the

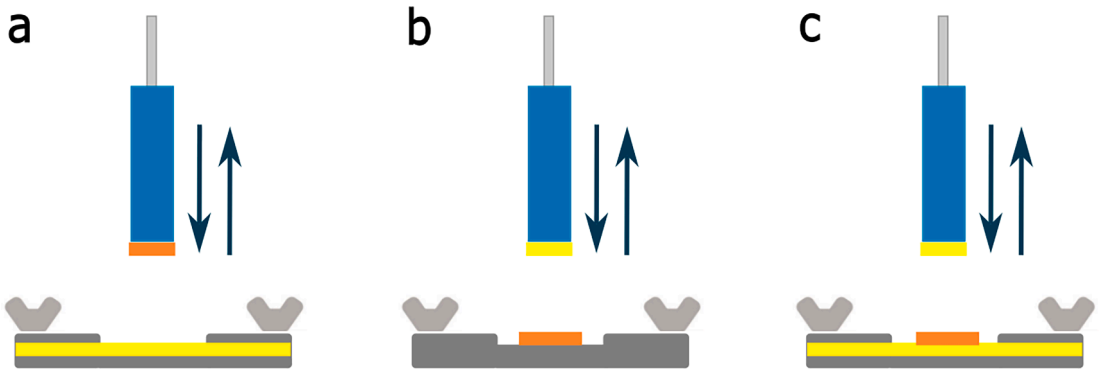

Fig. 6. Experimental setups for mucoadhesion testing with: a, the sample (orange) attached to the probe and substrate (yellow) on the fixture; b, the substrate (yellow) attached to the probe and the sample (orange) placed on the fixture; c, the substrate (yellow) placed on both the probe and the fixture and the sample (orange) between the two substrates. (For interpretation of the references to colour in this figure legend, the reader is referred to the web version of this article.)

detachment force and adhesion energy increased when the contact time varied between 10 and 600 s. In addition, patients' responses during the subsequent clinical trial confirmed that the mucoadhesive tablets exhibiting good mucoadhesion properties to the gums during the first minute of application ensure adequate mucoadhesion for the rest of the treatment (Mizrahi et al., 2004). Similar findings were reported for other types of mucoadhesive matrices (Singh and Rana, 2014; Thirawong et al., 2007). When extended-release tablets are characterized, the screening of bioadhesive behavior after a longer contact time is needed. Owens et al recorded the adhesion force and work of adhesion when the contact time varied between 30 s and 4 h. The optimal contact time to perform the experiments within an experimental design was selected as 300 s with a contact force of 20 g (Owens et al., 2005). In general, for most studies, a contact time between 60 and 300 s was considered a satisfactory value that helps to differentiate between small variations of adhesive features of the mucoadhesive tablets but also ensures the reproducibility of the test method (Table 4). In the case of conventional tablets, a shorter contact time is recommended. The study conducted by Shakwek et al. showed that a contact time higher than 2 min led to the disintegration of some formulations (Shakweh et al., 2007).

The adhesion bonds are efficient if the penetration and the entanglement of the polymer chains go up to 0.2–0.5 μm depth into the mucosal substrate; mucoadhesive strength is improved when the similarity of the sample and the mucosal tissue is higher (Chickering and Mathiowitz, 1999). Along with contact time, the contact force is another key factor in the bioadhesion mechanism. This parameter is defined as the adherence strength of the sample to the tissue's surface (Singh and Rana, 2014). Most *in vitro - ex vivo* methodologies report values for the contact force ranging from 0.05 to 5 N, most often values between 0.5 and 1 N which grants close contact of the dosage form with the substrate but also differentiates adhesive features of the samples. Singh et al. reported an optimal value of 1 N to be applied without the risk of destroying the tissue (Singh and Rana, 2014), while for gelatin-based substrates a lower value, of 0.1 N was found adequate (Göbel et al., 2021).

Other parameters related to the device settings that may impact the obtained results are the lowering speed and the return speed of the probe. These parameters can influence the sample-substrate interaction process and the formation of semi-permanent bonds between the polymer chains and the mucus glycoproteins. Intermediate values for contact force, contact speed, test speed, and return distance are recommended to obtain optimal values of mucoadhesion parameters (Singh and Rana, 2014). As regards the acceptable values, in the case of mucoadhesive tablets, a value of the detachment force above 100 g denotes good mucoadhesive properties of the product (Alam et al., 2015).

The tests measuring mucoadhesive strength are applied to investigate the mucoadhesion of dosage forms for different purposes, such as pharmaceutical development or quality control in the pharmaceutical industry (Alaei and Omidian, 2021). In most cases, TA is employed to evaluate the mucoadhesive properties of the developed products or commercial formulations, as a desired feature of the product. In other cases, mucoadhesivenes was evaluated as an undesirable characteristic of the product. Hence, the esophageal bioadhesive behavior of eight commercial formulations containing alendronate was determined to compare the risk of drug-esophageal bioadhesion, as a precondition of "pill-induced esophagitis". The differences in the bioadhesive behavior pointed out possible differences in the esophageal tolerance between the commercial formulations (Shakweh et al., 2007).

The methods of evaluating the mucoadhesiveness can be classified as *in vitro*, *ex vivo*, and *in vivo* depending on the substrates used to assess the mucoadhesion (Alaei and Omidian, 2021). Different *in vitro* substrates such as mucin, gelatin, agar, gellan gum, 2-hydroxyethyl methacrylate/N-acryloyl-D-glucosamine hydrogel were reported in the literature (Abdel-Haq et al., 2021; Alaei et al., 2021; Alopaeus et al., 2020; Chaud et al., 2013; Farias and Boateng, 2018; Gennari et al., 2019; Göbel et al., 2021; Hagesaether et al., 2009; Kawano et al., 2016; Kilicarslan et al., 2018; Kiniwa et al., 2019; Nep and Conway, 2011; Qi et al., 2012; Schmidt et al., 2022; Szekalska et al., 2015; Tamburic and Craig, 1997). The main advantages of artificial substrates are the reproducibility of the measurements and the ease of their purchasing. These are considered safer than *ex vivo* substrates since do not pose contamination issues. An adequate artificial substrate should have appropriate properties in terms of moisture content, flexibility, and permeability (Alaei et al., 2021).

Animal mucosal tissues are typically preferred as substrates for the evaluation of mucoadhesive properties. Depending on the animal model, the mucosal tissues have different characteristics as regards the composition, thickness, or mucus secretion (Alaei and Omidian, 2021; Woertz et al., 2013). The determinations using mucosal tissue may lead to a higher variability of the results (Woertz et al., 2013). According to the literature, the animal tissues employed in *ex vivo* studies on oral solid dosage forms include bovine mucosa (sublingual, gingival, esophageal, duodenal) (Accili et al., 2004; Mizrahi et al., 2004; Owens et al., 2005; Şenel et al., 1998), goat gastric mucosa (Alam et al., 2015; Karemore and Bali, 2021; Sankar and Jain, 2013), porcine mucosa (gastric, buccal, esophageal, intestinal) (do Couto et al., 2017; Eleftheriadis et al., 2020; Farias and Boateng, 2020; Göbel et al., 2021; Gurpreetarora et al., 2012; Hagesaether et al., 2009; Kraisit et al., 2017; LaFountaine et al., 2017; Pekoz et al., 2015; Pund et al., 2011; Sakloetsakun et al., 2016; Shakweh et al., 2007; Singh and Rana, 2014; Thirawong et al., 2007), rat gastric mucosa (Sharma et al., 2015), rabbit intestinal mucosa (Prodduturi et al., 2005; Repka et al., 2006) or chicken skin (Bodini et al., 2019). In the research conducted by La Fountaine et al, the quantitative *ex vivo* results were confirmed by the qualitative *in vivo* studies (LaFountaine et al., 2017).

To simulate the *in vivo* conditions, different wetting media

Table 4
Mucoadhesive properties assessment of solid oral dosage forms.

Experimental setup and testing parameters	Determined parameters	Substrate type	Sample details and recorded results regarding the mucoadhesive properties	Ref
Mucoadhesive tablets - *Setup in* Fig. 6a				
UTS (Instron 5543) F_{con} = 10 N, T_{con} = 5 min S_{det} = 5 mm/s	F_{det} W_{adh}	Sublingual, esophageal, duodenal bovine mucosa	Carbopol 974P tablets and Pharmacoat 606 tablets MAP depends on the type of mucosa and polymer type: Carbopol > Pharmacoat - sublingual mucosa, Carbopol ≈ Pharmacoat - oesophageal mucosa, Carbopol < Pharmacoat duodenal mucosa	(Accili et al., 2004)
UTS (Instron5965), load cell 50 N F_{con} = 1.3 N, T_{con} = 360 s S_{det} = 0.1 mm/s, T_{wet} = 5 min	σ_{max} W_{adh}	Mucin compacts (130 mg)	Mucoadhesive tablets for prolonged release of lysozyme obtained through freeze-drying The optimal ratio Na alginate/ HPMC E5 = 3/7 to obtain appropriate MAP W_{adh} = 4–5.7 mJ, σ_{max} = 35–58 kPa	(Gennari et al., 2019)
UTS (Instron 4301) F_{con} = 0.5 N, T_{con} = 10 min S_{det} = 5 mm/min	F_{det}	Bovine sublingual mucosa	Buccal bioadhesive tablets containing sodium glycodeoxycholate as penetration enhancer Addition of glycodeoxycholate → not significant impact on the MAP F_{det} = 9.52 ± 1.99 N	(Şenel et al., 1998)
UTS (Instron 4502) F_{con} = 0.5 N, S_{det} = 0.1 mm/s T_{con} = 10, 30, 120, 300, 600 s	F_{det} D_{max} E_{adh}	Bovine gingival tissue	Mucoadhesive tablet with hydroxypropyl cellulose, carbopol 934, citrus essential oil and magnesium salts ↗T_{con} →↗E_{adh} F_{det} = 0.3–2.07 N; D_{max} = 0.4–3.4 mm, E_{adh} = 1.5–6.2 mJ	(Mizrahi et al., 2004)
TA (TAX-TEE 32) S_{test} = 0.5 mm/s, F_{con} = 10 g T_{con} = 300 s	F_{det}	Goat gastric mucosa	Mucoadhesive osmotic pump tablets containing trimetazidine hydrochloride Linear increasing of AP with the increase of polymer amount; ↗ MAP when a combination of two polymers (ethyl cellulose and HPMC) was used F_{det} > 100 g	(Alam et al., 2015)
TA (TA.XT2i) F_{con} = 10–60 g, T_{con} = 30 s – 4 h	F_{det} W_{adh}	Bovine gingiva	Sodium fluoride bioadhesive tablets Various texture setups → selected conditions: F_{con} = 20 g, T_{con} = 300 s Positive effect of the F_{con} and T_{con} on the MAP F_{det} = 17.8–73.9 g; W_{adh} = 39 – 183.4 gs	(Owens et al., 2005)
TA (TA.XTPlus) Φ_{probe} = 6 mm S_{det} = 0.5 mm/s, F_{con} = 2 N, T_{con} = 60 s	W_{adh}	Porcine gastric mucosa	Mucoadhesive rifampicin tablets The optimal amount of Carbopol 71 G and MCC that maximizes the MAP and release properties - determined within DoE W_{ad} = 327.8–344 gs for the optimal formulation	(Pund et al., 2011)
TA (TA. XT Plus), S_{det} = 0.5 mm/s, F_{con} = 10 g T_{con} = 300 s, T_{wet} = 30 s	F_{det}	Goat gastric mucosa (2X2 cm)	Gastroretentive stained-release tablets containing acyclovir F_{det} ↘ when ↗ the ratio of polyethylene oxide An efficient water uptake of the sample → sufficient hydration of the polymer network, important in the mucoadhesion process F_{det} = 9.3 ± 4.7 g for the optimal formulation	(Sankar and Jain, 2013)
TA (QTS- 25), 5 kg load cell, S_{det} = 30 mm/s, D_{target} = 3 mm, T_{con} = 120 s	F_{det}	Rat stomach tissue	Gastroretentive tablets containing allopurinol The effect of the polymers on MAP was studied within a DoE: the polymers (CMCNa, polyoxyethylene oxide WSR 303) exhibited similar influence toward F_{det}; F_{det} ↗increased when the % of polymers ↗ F_{det} = 715.4–1097.6 mN	(Sharma et al., 2015)
TA (TA. XT Plus), Φ_{probe} = 10 mm S_{test} = 0.1, 0.3, 0.5, 1 mm/s F_{con} = 0.1, 0.2, 0.5, 1, 2 N T_{con} = 30, 60, 180, 300 s D_{return} = 10,15,20, 40 mm	F_{det} W_{adh}	Porcine stomach tissue	Polymeric tablets containing Eudragit-iron oxides conjugates Optimal value F_{con} = 1 N; optimal combination T_{con}↗ and ↘ S_{test} MAP ↗ F_{con} = 0.1 N −1N, MAP ↘ when F_{con} = 2.5 N MAP ↗ when T_{con}↗ F_{det} = 7.78–36.42 g	(Singh and Rana, 2014)
TA (TA. XT Plus), Φ_{probe} = 10 mm S_{test} = 0.5 mm/s, $F_{contact}$ = 1 N $T_{contact}$ = 60 s, D_{return} = 15 mm	F_{det}	Porcine stomach tissue	Mucoadhesive tablets containing 75 mg cinnarizine, Eudragit RLPO and iron oxide The effect of iron oxides on F_{det} studied within a DoE; Electrostatic interactions Eudragit RLPO-iron oxide polymer ↔ sialic acid → ↗MAP F_{det} = 5.7–42.8 g	(Singh and Rana, 2013)
TA (TA. XT Plus), 50 N load cell Φ_{probe} = 10 mm S_{det} = 0.1, 0.3, 0.5, 1.0 mm/s F_{con} = 0.05, 0.1, 0.2, 0.5 N T_{con} = 10, 30, 60, 180, 600 s T_{wet} = 0.5, 2, 5, 10, 20 min	F_{det} W_{adh}	Porcine buccal, stomach, small intestinal, large intestinal tissues (20x20 mm)	Pectin discs Selected optimal conditions: F_{con} = 0.05 N, T_{con} = 60 s The molecular weight and degree of esterification of pectin impact the MAP in the following rank order: CU201 > CU501 > CU020 > CU701 F_{det} = 55–85 mN	(Thirawong et al., 2007)
TA (CT3), Φ_{probe} = 12.7 mm S_{det} = 0.5 mm/s, F_{con} = 50 g, T_{con} = 5 min	F_{det}	Goat gastric mucosa 20 × 20 mm	Gastroretentive tablets containing cilnidipine DoE; F_{det} - Gellan gum > HPMC K4M F_{det} = 32.11–68.41 g	(Karemore and Bali, 2021)
Mucoadhesive tablets - *Setup in* Fig. 6b				
TA (TA. XTPlus), 5 kg load cell Φ_{probe} = 20 mm, T_{wet} = 1 min, F_{con} = 0.5 N, S_{det} = 10 mm/s, T_{con} = 60 s	F_{det} W_{adh}	30% mucin gel	Polymer compacts: Grewia polysaccharide gum, Carbopol 971P, HPMC, CMC and guar gum Comparable MAP of grewia polysaccharide gum to Carbopol 971P and HPMC W_{adh} = 1.23 ± 0.26 N.mm	(Nep and Conway, 2011)

(*continued on next page*)

Table 4 (*continued*)

Experimental setup and testing parameters	Determined parameters	Substrate type	Sample details and recorded results regarding the mucoadhesive properties	Ref
TA (TA. XT), 5 kg load cell F_{con} = 0.5 N, T_{con} = 60 s, S_{det} = 0.1 mm/s, T_{wet} = 1, 3, 5, 10, 20 min	F_{det}	30% mucin gel	Carbopol 974P, Carbopol 971P and Naveon AA-1 compacts MAP ↘ in the rank order: Carbopol 974P, Naveon AA-1, Carbopol 971P	(Tamburic and Craig, 1997)
Conventional tablets				
TA (TAXTT2), 50 N load cell T_{con} = 1, 2 min	F_{det} W_{adh}	Porcine esophageal mucosa	Eight commercial formulations containing alendronate Different mucoadhesive behaviors attributed to different excipients (HPC or sodium croscarmellose); T_{con} > 2 min → disintegration of some formulations F_{det} = 0.048–0.148 N; W_{adh} = 36.7–3461.5 x10^{-3} J	(Shakweh et al., 2007)
Minitablets				
TA (TA.XTPlus) Φ_{probe} = 7 mm, F_{con} = 0.1 N, T_{con} = 30 s	F_{det} W_{adh}	Porcine intestinal mucosa	Minitablets containing binary amorphous dispersion of itraconazole and Carbopol 71G *In vitro* MAP confirmed by *in vivo* results F_{det} = 100–200 mN; W_{adh} = 3.7–14 kPa s	(LaFountaine et al., 2017)
TA (TA.XTPlus), 5 kg load cell, Φ_{probe} = 10 mm, S_{test} = 1 mm/s, F_{con} = 500 g, T_{con} = 10 s, S_{det} = 0.5 mm/s	F_{det} W_{adh}	Porcine small intestine tissue	Chitosan–gum arabic polyelectrolyte complex films 600 kDA Chitosan: Arabic gum (1:0.75), 150 kDA Chitosan: Arabic gum (1:1) →↗MAP; Chitosan excess →↗MAP W_{adh} = 400–850 mJ	(Sakloetsakun et al., 2016)
TA (TA.XTPlus) F_{con} = 290 mN, T_{con} = 180 s, S_{det} = 0.1 mm/s	W_{adh}	Mucin disks	3D printed films containing triamcinolone acetonide in SBA-15 mesoporous silica ↗MAP of loaded films by comparison to unloaded films W_{adh} = 0.147–420 mN.mm	(Schmidt et al., 2022)
Mucoadhesive orally disintegrating tablets				
UTS (Force Tester MCT-2150) T_{con} = 20 s	W_{adh}	10% Mucin layer	Orally disintegrating tea tablets containing arabic gum, carrageenan, guar gum, tamarind gum and pectin The highest MAP for the samples prepared with tamarind gum	(Kiniwa et al., 2019)
TA (TA-XT2), Φ_{probe} = 37 mm, S_{test} = 0.1 mm/s, F_{con} = 0.25 N, T_{con} = 60 s, S_{det} = 1 mm/s	F_{det}	0.5% porcine mucin applied on nutrient agar	Wafers containing β-limit dextrin or pre-gelatinized starch β-limit dextrin wafers exhibited superior MAP F_{det} = 1.9–53.7 N	(Qi et al., 2012)
Freeze-dried wafers				
TA (HDPlus), 5 kg load cell F_{con} = 1 N, T_{con} = 60 s	F_{det} W_{adh} D_{cohes}	6.67 % gelatin gel	Composite wafers with acetylsalicylic acid Differences in the MAP when using pH 6.8 PBS and pH 6.8 simulated saliva → simulated saliva reproduces better the *in vivo* conditions F_{det} = 0.04–0.51 N; W_{adh} = 0.02–0.31 mPa; D_{cohes} = 0.73–1.37 mm	(Farias and Boateng, 2018)
TA (HDPlus), 5 kg load cell S_{test} = 0.5 mm/s, T_{con} = 60 s, S_{det} = 1 mm/s	F_{det} W_{adh} D_{cohes}	6.67 % gelatin gel, porcine buccal tissue	Wafers containing acetylsalicylic acid and taste-masking sweeteners MAP > when the porcine tissue was used *In vitro*: F_{det} = 0.03–0.21 N; W_{adh} = 0.01–0.12 mJ; D_{cohes} = 0.81–1.18 mm *Ex vivo:* F_{det} = 0.15–0.37 N; W_{adh} = 0.42–0.93 mJ; D_{cohes} = 5.14–11.53 mm	(Farias and Boateng, 2020)
Raw materials				
TA (TA.XTPlus), 5 kg load cell S_{test} = 0.1 mm/s, F_{con} = 1 N, T_{con} = 180 s, S_{det} = 0.1 mm/s	F_{det} W_{adh}	Gelatin, mucin, porcine stomach mucosa	Alginate microspheres containing ranitidine MAP - inversely correlated with the amount of the ranitidine F_{det} = 0.16–0.91 kg m s^{-2}; W_{adh} = 340.6–989.2 mJ	(Szekalska et al., 2015)
TA (TA.XTPlus), S_{test} = 0.5 mm/s, F_{con} = 2 mN, T_{con} = 10 min	F_{det} W_{adh}	Mucin disks	Solid dispersions with praziquantel and sodium starch glycolate The solid dispersion ↘ MAP of the glycolate F_{det} = 0.852 N; W_{adh} = 1058 μJ	(Chaud et al., 2013)
Mucoadhesive thin films - *Setup in* Fig. 6a				
TA (CT3-1000), 1 kg load cell Φ_{probe} = 12.7 mm, S_{det} = 0.01–0.5 mm/s, F_{con} = 0,49–1,96 N, T_{con} = 5–60 s	F_{det}	Agar, gellan gum, gelatine	Commercial films: Vitamin B12 Fast Dissolving strips, B12 Fast Dissolving Strips Listerine Breath Strips, Ziminta Mouth Freshener Films Different volumes of artificial saliva, different CT by varying target load, target speed and hold time → Unsatisfactory results for gelatine and agar substrates S_{det} = 0.1 mm/s, F_{con} = 0.98 N, T_{con} = 15 s, 4% w/v gellan gum and 2% w/v glycerine and 200 μl of artificial saliva → to discriminate the MAP F_{det} = 1.26–2.54 N	(Alaei et al., 2021)
TA (TA.XT Plus), 5 kg load cell S_{test} = 1 mm/s, F_{con} = 1 N, T_{con} = 30 s	W_{adh}	Porcine buccal mucosa	Dimenhydrinate buccal films prepared with xanthan gum or HEC Xanthan gum-based films exhibited better MAP W_{adh} = 1.994–3.055 mJ/cm^2	(Pekoz et al., 2015)
TA (TA.XT2i) F_{con} = 0.1 N, T_{con} = 60 s, S_{det} = 0.05 mm/s	F_{det} W_{adh}	Porcine cheeks esophagus, gelatin, HEMA/AGA hydrogel	Buccal films Among tested substrates 2-hydroxyethyl methacrylate (HEMA)/ N-acryloyl-D-glucosamine (AGA) hydrogel → similar results to tissue samples, variability ↘ than animal tissues	(Göbel et al., 2021)
TA (TA XTPlus) F_{con} = 0.5 N, T_{con} = 5 min, S_{det} = 1 mm/s	F_{det} W_{adh}	Porcine esophageal mucosa	Mucoadhesive films with prilocaine hydrochloride and lidocaine hydrochloride F_{det} and W_{adh} work were not significantly impacted when ↗ drug content F_{det} = 0.38–0.84 N, W_{adh} = 0.35–0.85 N/mm	(do Couto et al., 2017)

(*continued on next page*)

Table 4 (*continued*)

Experimental setup and testing parameters	Determined parameters	Substrate type	Sample details and recorded results regarding the mucoadhesive properties	Ref
TA (TA-XT), Φ_{probe} = 5 mm, S_{test} = 0.5 mm/s, F_{con} = 0.5 N, T_{con} = 120 s, S_{det} = 1 mm/s	F_{det} W_{adh}	Porcine buccal mucosa	3D printed mucoadhesive buccal films → films with chitosan ↗MAP Buccal films containing ketoprofen, lidocaine hydrochloride and l-menthol prepared through by combining fused deposition modeling and inkjet printing → ↗ adhesion values of the inkjet-printed films F_{det} = 8.1–9 N; W_{adh} = 14.2–18.3 N × m for the inkjet-printed films	(Eleftheriadis et al., 2019) (Eleftheriadis et al., 2020)
TA (TA.XTPlus), Φ_{probe} = 12 mm, S_{test} = 0.5 mm/s, D_{target} = 10 mm, T_{con} = 60 s, S_{det} = 0.5 mm/s	F_{det} W_{adh}	1 % mucin	Chitosan/alginate polyelectrolyte complex films containing clindamycin phosphate ↗ MAP when ↗ alginate ratio F_{det} = 0.080–2.601 N; W_{adh} = 0.007 – 0.187 N.mm	(Kilicarslan et al., 2018)
TA (TA.XTPlus), Φ_{probe} = 10 mm, S_{test} = 1 mm/s, F_{con} = 0.05 N, T_{con} = 60 s, S_{det} = 0.5 mm/s	F_{det} W_{adh}	Porcine buccal mucosa	HPMC/polycarbophil mucoadhesive films DoE to study the influence of the polymer on MAP F_{det} = 0.0191–0.0347 N; W_{adh} = 0.029–0.058 N.mm	(Kraisit et al., 2017)
TA (TA-XT2 *i*), Φ_{probe} = 7 mm, S_{test} = 0.1 mm/s, F_{con} = 3.5 N, T_{con} = 10, 20, 60 or 120 s, S_{det} = 0.5 mm/s	F_{det} W_{adh} D_{elong}	Rabbit intestinal mucosa	Hydroxypropylcellulose polymer matrices containing Δ^9-tetrahydrocannabidiol The addition of API in the matrix system ↘ W_{adh} W_{adh} ↗ when T_{con} ↗	(Repka et al., 2006)
TA (TA.XTPlus), S_{test} = 0.5 mm/s, F_{con} = 1 N, T_{con} = 60 s, S_{det} = 0.5 mm/s	F_{det}	Porcine gastric mucosa	Mucoadhesive matrix tablets of domperidone DoE to study the influence of HPMC K 15 M ratio on MAP F_{det} = 10.789–50.924 N	(Gurpreetarora et al., 2012)
Customized test-rig (Tribometer), dynamic adhesion measurements F_{con} = 1 N, T_{con} = 60 s	F_{det}	agar/mucin substrate	Poly(lactic-co-glycolic acid) films loaded with clotrimazole Adhesion ↗ when ↗ clotrimazole ratio	(Abdel-Haq et al., 2021)
CM (RHEONER II), F_{con} = 2 N, T_{con} = 30 s, S_{det} = 5 cm/min	F_{det}	10% mucin	Films containing xyloglucan and loperamide Adhesiveness of Xyloglucan films increased by adding HPMC	(Kawano et al., 2016)
Mucoadhesive thin films - *Setup in* Fig. 6b				
TA (TA.XT2i), 5 kg load cell Φ_{probe} = 7 mm, S_{det} = 0.5 mm/s, F_{con} = 3.5 N, T_{con} = 30 s, T_{wet} = 30 s	F_{det} W_{adh}	Rabbit intestinal mucosa	PEO films containing clotrimazole PEO N-750 had higher bioadhesion than PEO N-80 films due to the higher molecular weight of the polymer ↔ the long-chain molecules can form a stronger interpenetrating network with the mucus	(Prodduturi et al., 2005)
TA (TA.XT.Plus), Φ_{probe} = 20 mm S_{det} = 1 mm/s, F_{con} = 0.1 N, T_{con} = 30 s, T_{wet} = 20 s	F_{det}	Chicken skin	Orally disintegrating films based on HPMC and pre-gelatinized starch ↗ ratio of HPMC led to the ↘ MAP F_{det} = 0.4–1.9 N	(Bodini et al., 2019)
Mucoadhesive thin films - *Setup in* Fig. 6c				
TA (TA-XT2i) S_{det} = 0.01 mm/s, F_{con} = 200 g, T_{con} = 100 s	F_{det} W_{adh}	3 % porcine mucin	Mucoadhesive buccal films containing Soluplus, HPMC or Lycoat The films containing Soluplus and HPMC revealed favorable MAP	(Alopaeus et al., 2020)
TA (TA-XT2i) S_{det} = 0.01 mm/s, F_{con} = 200 g, T_{con} = 100 s	F_{det} W_{adh}	3 % porcine mucin	Pectin/chitosan films The peak force from *ex vivo* experiments was correlated to *in vitro* determinations; the friction test reproduces better the *in vivo* conditions	(Hagesaether et al., 2009)
Shear test: a 2x2 cm block on which the intestine was attached was displaced horizontally, S_{test} = 0.5 mm/s	F_{det} W_{adh}	Porcine small intestine	F_{det} = 6.8 = 27.5 g	

*Abbreviations: TA- texture analyzer; UTS- Universal Testing System; CM- Creep meter; Tcon- contact time; Twet- time of wetting the substrate or the sample; Sdet- detachment speed (speed of raising the upper probe); Stest- test speed of lowering the probe with the attached sample; Fcon- contact force; Dtarget- target distance; Dreturn- return distance; σmax - maximum stress necessary for detachment; Fdet - detachment force; Wadh - work of adhesion; Eadh - adhesion energy; Delong - elongation at adhesive failure; Dcohes – cohesiveness (the distance the samples moved before detaching from the substrate); Dmax displacement at maximal load; MAP- mucoadhesive properties; CMCNa, sodium carboxymethyl cellulose; HEC, hydroxyethylcellulose, HPMC, hydroxypropyl methylcellulose; PEO, Poly(Ethylene oxide); MCC, microcrystalline cellulose.

** Device model (Maximum load / Force resolution): CT3-1000 (1 kg/0.10 g), CT3-4500 (4.5 kg/0.50 g), TA.XTplus (50 kg/0.1 g), TA.HDplus (750 kg/0.10 g), QTS-2505 (5 kg/0.2 g), QTS-2525 (25 kg/1 g).

(phosphate buffer, artificial saliva, distilled water, etc.) were applied either to the substrate or to the sample, with a defined time interval before the determination. Farias et al. showed differences in the mucoadhesion profile when using different media such as phosphate buffer pH 6.8 or simulated saliva pH 6.8. More favorable results were obtained in the case of simulated saliva, which was considered to better mimic the *in vivo* conditions (Farias and Boateng, 2018). The research conducted by Alaei et al. analyzed the effect of artificial saliva volume on the measured adhesive properties of oral thin films. Different volumes between 50 and 300 μl were tested to hydrate but not to dissolve the films; finally, a volume of 200 μl was considered appropriate to differentiate the adhesive properties of the samples (Alaei et al., 2021).

A particular observation about the TA of the films regards the size of the samples analyzed and the type and size of the test probes. These features are reported only in a few studies even though the use of different dimensions probes and samples impact the obtained results. Thus, selected probes to perform the adhesion studies include 5-, 10-, 12.7-, and 20-mm cylindrical probes. (Alaei et al., 2021; Bodini et al., 2019; Eleftheriadis et al., 2020; Kraisit et al., 2017).

One of the current challenges of TA is represented by the difficulty of defining a set of standard parameters applicable to samples with substantially different characteristics. The adhesive behavior and implicitly the texture profile changes depend on factors such as the composition of the sample (type and ratio of polymer) (Accili et al., 2004; Alam et al.,

2015; Gennari et al., 2019; Karemore and Bali, 2021; Pekoz et al., 2015; Prodduturi et al., 2005; Sankar and Jain, 2013; Sharma et al., 2015; Tamburic and Craig, 1997; Thirawong et al., 2007) preparation method (Ikeuchi-Takahashi et al., 2013), type and ratio of API (Abdel-Haq et al., 2021; Repka et al., 2006; Schmidt et al., 2022; Szekalska et al., 2015). For an in-depth assessment of these influences, parameters derived from TA (adhesion force and work of adhesion) have been integrated as responses in Design of Experiments (Gurpreetarora et al., 2012; Karemore and Bali, 2021; Kraisit et al., 2017; Owens et al., 2005; Pund et al., 2011; Sharma et al., 2015; Singh and Rana, 2013). In the study conducted by Kraisit et al., the mucoadhesive properties of the films (work of adhesion and detachment force) were included as responses in a mixture design, and the effect of polymers and their interaction were analyzed to develop HPMC/polycarbophil films with higher mucoadhesion. (Kraisit et al., 2017). Different experimental design approaches were employed to obtain mucoadhesive tablets containing gum ghatti and HPMC K 15 M (Gurpreetarora et al., 2012), microcrystalline cellulose (MCC) and Carbopol 71G (Pund et al., 2011), sodium carboxymethyl cellulose (CMCNa) and polyoxyethylene oxide WSR 303 (Sharma et al., 2015), Eudragit RLPO and iron oxide (Singh and Rana, 2013) or gellan gum and HPMC K4M (Karemore and Bali, 2021) with optimal adhesive properties.

Based on the high number of published reports on this topic, it can be concluded that TA is a reliable method for the assessment of mucoadhesive properties; a rigorous choice of experimental setups, accessories, and testing conditions will guide the formulators in obtaining solid dosage forms with satisfactory mucoadhesive characteristics.

5. Disintegration and polymer hydration phenomena

Since the appearance of orodispersible dosage forms, new evaluation methods were proposed to resolve the drawbacks of compendial tests that usually fail to discriminate between their properties. First, Dor and Fix proposed a new disintegration method that involved the immersion with a constant force of a tablet attached to the probe in a small volume of media. The distance-time curves were regarded as disintegration profiles, as they allowed the detection of the onset and endpoint of disintegration (Dor and Fix, 2000). Further studies proposed maintaining the applied force for a predetermined time and placing the disintegration media, water, or simulated saliva, in a thermostated bath (Abdelbary et al., 2005; El-Arini and Clas, 2002). When investigating the media volume effect, it appeared that a volume increase from 1 to 3 ml determined faster disintegration onset and higher disintegration rate, but beyond 2 ml, no significant influence of the volume was shown. The applied force during testing did not impact disintegration-related parameters but could affect the measurement of dimensional changes produced by effervescence or burst effect, so a load of 50 g was considered appropriate (El-Arini and Clas, 2002). Abdelbary et al. implemented some changes to the previously reported operating structure to better mimic the oral conditions. Initially, they placed the tablet on a perforated grid, above the media layer, then a flat probe pushed the tablet into the media and maintained a constant load during disintegration. In contrast to prior methods, this allowed full contact between the tablet and the media and the continuous drainage of disintegrated particles during the process, just as it happens *in vivo*. As a result, disintegration times obtained with the instrumental method were close to those reported by volunteers and it was assumed that some parameters (such as penetration distance) could even be correlated to mouthfeel or residue (Abdelbary et al., 2005). Further, Szakonyi et al. modified the testing conditions by attaching the tablet to the probe and descending to a sieve covered with a thin layer of disintegration media. They showed the relevance of the pre-test speed, post-test speed and that of the disintegration media to the accuracy of results and optimized all these testing parameters through two experimental designs. Whereas previous papers reported time-distance curves as disintegration profiles, Szakonyi et al. used the load vs. distance curves and the area under the curve to estimate disintegration times (Szakonyi and Zelkó, 2013).

In a study that aimed at the development of paediatric dispersible tablets, Buck et al. compared the experimental setups reported by Dor and Fix (2000) and by Szakonyi (2013) to one where the tablet was attached vertically to the probe to improve the contact with the disintegration media on the flat sides of the tablet. The newly tested conditions provided the closest results to the disintegration in the beaker, which was used as a reference method, however, showed high variability for formulations with slow disintegration and high levels of viscosity enhancers (Buck et al., 2016). Fig. 7 depicts the most common ways results are recorded during TA disintegration tests of ODTs, depending on the established testing parameters.

Considering that TA techniques do not require visual observation of the beginning or the end point of disintegration, it was assumed that the evaluation of the behavior of ODTs in an opaque environment such as human milk would be feasible. Unlike previous methods, the tablets were placed vertically on the probe to increase the contact surface, then load and distance data were recorded versus time when the sample reached the sieve. This application could be used in the development of orodispersible forms intended to disintegrate in milk during administration, such as those given to newborns through nipple shields (Scheuerle et al., 2015).

While most of the developed methods evaluated disintegration during CT, Tomas et al. proposed a new method to investigate the early stages of tablet disintegration, based on the assessment of local stress relaxation that occurs in the product at the contact with the disintegration media. This involves applying an initial load on the tablet, allowing stress relaxation in the dry state under a particular hold time, then adding the disintegration media and recording the load changes. The proposed method can be exploited in the formulation development phases to better understand interparticulate bonding or in formulation troubleshooting (Tomas et al., 2018). Further, in the attempt to gain a better understanding of disintegration kinetics, TA was doubled by magnetic resonance imaging and particle size measurement of the disintegrating fragments which explained the way force relaxation curves can be used to measure disintegration rate (Dvořák et al., 2020).

Disintegration tests by TA became routine evaluation methods for researchers that aimed for the quick development of certain products to meet the compendial requirements and release on the market, and were also interested in the way certain process parameters such as compression force can impact disintegration (Wang et al., 2017a, 2017b).

Vanbillemont et al. investigated the different disintegration tests could be applied for commercial OLs. They compared the Pharmacopoeial tests with two TA-adapted tests reported in the literature and revealed that the texture approach was more appropriate for OL testing. First, they applied the El-Arini and Clas test developed for ODTs (El-Arini and Clas, 2002), which was unable to accurately evaluate the quick disintegration of OLs, and afterwards the Abdelbary test (Abdelbary et al., 2005), which was found suitable for OL testing and led to high result reproducibility (Vanbillemont et al., 2020).

Some authors prefer to complete the compendial disintegration tests by TA determinations, especially for less traditional dosage forms such as ODMTs, where the compendial methodology and acceptability limits do not necessarily apply (Hejduk et al., 2021).

For buccal film disintegration, a petri dish method was described in the literature as well as a method that records the time needed for a drop of water to penetrate through the film surface (Preis et al., 2014a). Still, as these methods do not subject the films to any mechanical force, TA methods were developed. Alopaeus et al. fixed the samples in a film holder and applied a force with a cylindrical punch onto the samples previously wetted with distilled water (Alopaeus et al., 2020). Due to the greater resistance of the unwetted film, the probe begins applying a larger force. The disintegration endpoint has been set as the moment when the probe returned to a force of 0.03 N, which was previously mentioned as the minimal force applied by tongue movement (Preis et al., 2014a). However, these conditions were unable to assess films

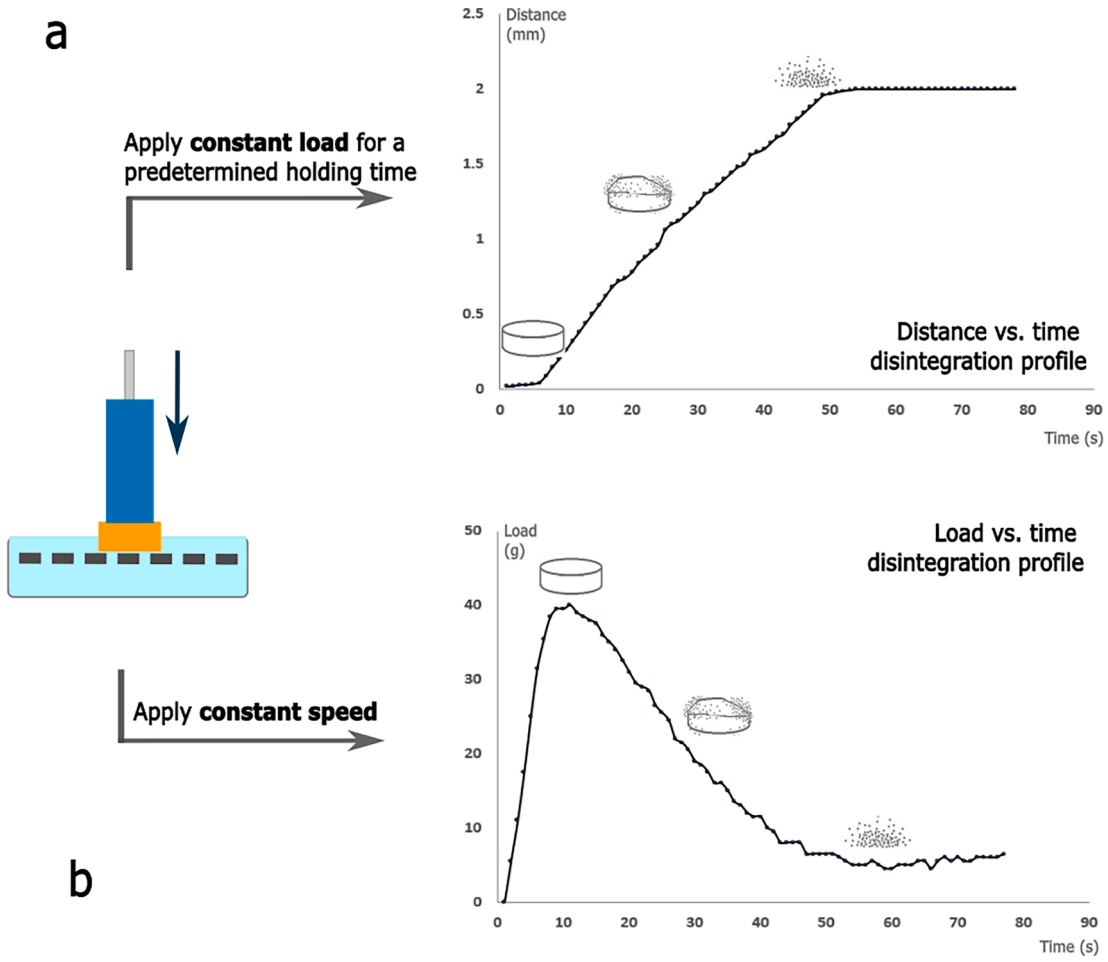

Fig. 7. Disintegration profiles for ODT disintegration testing when: a, a constant load is applied and distance vs. time profile is recorded, and b, when a constant speed is applied and the load vs. time profile is recorded (Fig. 7 b modified with permission from Szakonyi et al. (2013)).

with ultra fast disintegration or soft hydrogel formation (Alopaeus et al., 2020). More details regarding the experimental setups used in disintegration testing of different dosage forms are included in Table 5.

Modified-release dosage forms based on hydrophilic matrices also benefit from TA, not only from the point of view of their strength and hardness, but also from the results obtained in their hydrated states (Kulinowski et al., 2015). Hydrophilic matrix tablets can be evaluated for water content by interpreting force–displacement diagrams (Caccavo et al., 2015; Cascone et al., 2014; Li et al., 2014). When used as an alternative technique to the compendial dissolution tests to assess modified release matrix tablets, TA was able to detect differences in the internal structure properties of the products. While the compendial dissolution techniques revealed similar profiles for a developed formulation and the commercial reference, TA showed good discrimination capacity, which was further confirmed by biorelevant dissolution testing. In other words, TA (coupled with MRI or microCT techniques) included in matrix tablet R&D strategies could avoid bioequivalence pitfalls caused by the design based solely on compendial dissolution test results (Kulinowski et al., 2015).

Nazzal et al. developed a non-destructive TA probe that allows real-time measurements of swelling and erosion rates, as well as the size of the glassy core of tablets (Nazzal et al., 2007). The same experimental setup was later used to predict polymer (PVP, HPMC, Polyox) impact on drug dissolution for a compression coated pulsatile delivery system (El-Malah and Nazzal, 2010). As there is an established relationship between drug release and polymer hydration, TA was used to measure gel strength for dual-release bilayer tablets. The resulting profiles could be divided into three parts: erosion, gel, and dry core. The gel strength was estimated as the area under the curve of the gel region and contributed to the understanding of gelation mechanism as well as to the optimization of the two layers (Han et al., 2022). Li et al. applied TA to understand the swelling behavior of chitosan – anionic polymer drug delivery systems after a 12-hour dissolution study through load vs. time profiles comparison and the determination of the total work of penetration (Li et al., 2014).

6. *In vitro* – *In vivo* correlations derived from TA

There is a trend and a need for the use of characteristics determined *in vitro* to predict the *in vivo* behaviour and characteristics of dosage forms. The trend comes from the desire to simplify at most the characterization process during pharmaceutical drug development and therefore to reduce the costs involved. The need comes from the emergence of some situations in which it is difficult or impossible to test a certain pharmaceutical form on volunteers, for example in the case of the development of paediatric pharmaceutical forms. *In vitro - in vivo* correlations (IVIVC) have been reported to represent a powerful tool for predicting *in vivo* characteristics of oral dosage forms based on the *in vitro* assessments. As previously mentioned, among the benefits arising from IVIVC, the decrease of product development time and costs are of great importance (Patel et al., 2012).

TA is one of the *in vitro* methods used for estimating *in vivo* specific features of oral dosage forms, such as *in vivo* disintegration time, palatability, mouthfeel, transit time, ease of swallowing etc. (Asiri et al., 2021; Stokes et al., 2013). Mouthfeel, also referred to as oral sensory perception, and texture are mainly associated with foods and beverages,

Table 5
TA experimental setups reported for disintegration testing.

Experimental setup	Testing parameters	Sample composition, placement, size	Parameters of interest	Reference
ODTs				
0.5 in cylindrical acrylic flat-ended probe, 100 – 2000 μl water on a flat fixture	TA (TA-XT2i) CT PS: 5 mm/s S: 0.1 mm/s	C: Mannitol, maltose, 0.5 – 1% binder, 0.5 – 1% lubricant; samples attached to the probe Φ: NA	Extrapolation from the time-distance profile -identification of the start and the endpoint of disintegration Comparison with *in-vivo* data	(Dor and Fix, 2000)
Cylindrical stainless-steel flat-ended probe 1 cm^2, 1 – 6 ml water or simulated saliva in a thermostated bath	TA (TA-XT2i) CT L: 50 – 250 g HT: 60 s	C: commercial products representing the main ODT preparation technologies; samples attached to the probe Φ × h: 9.7 × 4 mm – 16 × 6.1 mm	Time-distance profile: disintegration onset, extrapolated disintegration time, total disintegration time, penetration distance	(El-Arini and Clas, 2002)
Cylindrical stainless-steel flat-ended probe 12 mm diameter; Perforated grid on top of a movable platform, immersed in a recipient with disintegration medium	TA (TA-XT2i) CT L: 50 – 250 g HT: 60 s	C: commercial products representing 3 of the main ODT preparation technologies, 2 wet granulated / emulsion granulated newly developed formulations; samples placed on the perforated grid Φ × h: 7.5 × 3.1 mm – 15.7 × 6.1 mm	Time-distance profile: disintegration onset, extrapolated disintegration time, total disintegration time, penetration distance Comparison with *in-vivo* data	(Abdelbary et al., 2005)
Acrylic cylindrical flat-ended probe 25.4 mm diameter; Stainless steel test sieve 38 mm diameter placed on an extruded polystyrene plate with 5.4 ml media	TA (CT3-4500) CT PS: 0.3 – 0.5 mm/s S: 0.04 – 0.05 mm/s	C: placebo ODT products composed of a directly compressible filler, superdisintegrant, sodium stearyl fumarate; samples attached to the probe Φ: 8 mm	Load-displacement curves	(Szakonyi and Zelkó, 2013)
14.23 mm diameter flat probe; Perforated horizontal platform immersed in 31 ml human/bovine milk	TA (TA.XTplus) CT L: 50 g HT: 60 s	C: commercial grade and in-house manufactured ODTs; samples attached vertically to the probe Φ: ~8 mm	Load vs. time and position vs. time profiles	(Scheuerle et al., 2015)
Needle probe 1 mm diameter; Crystallization dish where 80 ml disintegration medium was added to cover the tablet, after the hold time	TA (CT3) CT S: 0.1 mm/s F: 0.5; 1; 5; 10 N HT: 100 s	C: ibuprofen, lactose monohydrate, croscarmellose sodium; samples placed in the crystallization dish Φ: 8 mm	Wet relaxation expressed as the relative load (normalized by maximum force) vs. time Percentual structural change and wet relaxation rate were determined	(Tomas et al., 2018)
Spherical stainless-steel indenter 3.2 mm; 18.2 mm container; 2 ml simulated saliva added after the hold time with a syringe	TA (TA-XT2i) CT F: 3 N S: 0.1 mm/s HT: 30 s	C: metformin acesulfame salt, MCC, croscarmellose sodium, fumed silica, magnesium stearate; samples placed in the container then covered in 2 ml media Φ NA	Time-distance profile: disintegration time as the difference between the two plateau regions of the curve	(Wang et al., 2017a)
Spherical stainless-steel indenter 3.2 mm; 18.2 mm container; 2 ml simulated saliva added after the hold time with a syringe	TA (TA-XT2i) CT F: 3 N S: 0.01 mm/s HT: 30 s	C: diphenhydramine acesulfame salt, mannitol, croscarmellose sodium, fumed silica, magnesium stearate; samples placed in the container then covered in 2 ml media Φ NA	Time-distance profile: disintegration time as the difference between the two plateau regions of the curve	(Wang et al., 2017b)
Buccal films				
Flat-faced cylindrical probe of 7.03 mm diameter, fixture: plates with cylindrical hole of 38.82 mm^2 area; 200 μl of simulated saliva pipetted on the sample	TA (TA-XT2i) CT TD: 5 mm	C: furosemide, ± Soluplus®, ± HPMC and ± Lycoat®, glycerol; samples fixed between plates of the fixture 2 × 2 cm	Force vs. time profiles: disintegration endpoint was defined when the probe returned to a force of 0.03 N	(Alopaeus et al., 2020)

*Abreviation: S, test speed; PS, pretest speed; CT, compression test; HT, hold time; L, load; F, force; TD, target distance; C, composition; Φ, diameter; ODT, orodispersible tablet, MCC, microcrystalline cellulose.
* Device model (Maximum load / Force resolution): CT3-4500 (4.5 kg/0.50 g), TA.XTplus (50 kg/0.1 g).

in particular with their preference and acceptance (Guinard and Mazzucchelli, 1996). Lately, texture and mouthfeel were associated with pharmaceutical dosage forms, due to the need of assessing the acceptability of medicines (Asiri et al., 2021). Another discipline that contributes to the comprehension of texture and mouthfeel is tribology, which studies friction and lubrication between interacting surfaces in the mouth during the consumption of different products (Stokes et al., 2013). Tribological measurements are thus appreciated as one of the most adequate methods of evaluating oral textural phenomena associated with solid oral dosage forms and can be correlated with *in vivo* data (Hofmanová et al., 2021).

Although the value of IVIVC studies is indisputable and there are research groups that have studied the influence of the parameters obtained from TA with the data obtained *in vivo*, there is still a limited number of documents that can be found in this field. The articles included in this review meet the following criteria: they include TA; they correlate the parameters obtained from the TA with the data obtained *in vivo* and the tested product is a solid pharmaceutical form for oral administration (Table 6). There are many other publications that study IVIVC, but either they do not use TA as an *in vitro* characterization method, or the tested product belongs to another category of pharmaceutical forms, other than solid oral pharmaceutical forms (Baus et al., 2019; de Spiegeleer et al., 2001; Saab and Mehanna, 2019). Also, there are publications that predict the *in vivo* properties of dosage forms, without performing an *in vivo* study (Desai et al., 2022). As importantly, another category is the one in which the studies include TA and an *in vivo*

Table 6
In vitro - in vivo correlations for solid oral dosage forms.

Parameters of interest	*In vitro* experimental setup and testing parameters	*In vivo* experimental details	*In vitro - in vivo* correlations	Ref
ODTs				
In vitro: DT. Onset and end point of disintegration calculated by using the time-distance profiles obtained by the TA *In vivo*: oral DT	TA (TA-XT2i), CT, 2 kg load cell flat-ended acrylic cylindrical probe (Φ_{probe} = 0.5 in., H = 35 mm), $S_{pretest}$ = 5 mm/s, S_{test} = 0.1 mm/s	Recording the elapsed time between placing the tablet on the tongue and the moment of complete disintegration of the tablet	Force-displacement profiles generated by the TA software enabled accurate extrapolation of the start and end disintegration time by using a linear regression analysis between two variables An excellent correlation between the *in vivo* and *in vitro* disintegration times was found	(Dor and Fix, 2000)
In vitro: DT. Onset and end point of disintegration calculated by using the time-distance profiles obtained by the TA *In vivo*: oral DT	TA (TA-XT2i), CT,flat-bottomed cylindrical stainless steel probe (P/25, Φ_{probe} = 12 mm, H = 25 mm), perforated grid placed on the movable platform, F_{con} = 50 g, T_{con} = 60 s	Recording the elapsed time between placing the tablet on the tongue and the moment of complete disintegration of the tablet	An excellent correlation was observed for all tested tabletsThe new operating structure (the perforated grid on which the tablet is placed) appeared to be responsible for a better simulation of the *in vivo* conditions	(Abdelbary et al., 2005)
In vitro: DT *In vivo*: oral DT	TA (TA-XDPlus), CT, 5 kg load cell,flat-bottomed cylindrical stainless steel probe (P/25, Φprobe = 12 mm, H = 25 mm), F_{con} = 50 g, T_{con} = 60 s	Recording the elapsed time between placing the tablet on the tongue and the moment of complete disintegration of the tablet	There were no significant differences between texture analyzer and *in vivo* disintegration times. The TA method is an effective instrument for a precise and reproducible measurement of oral disintegration	(Gryczke et al., 2011)
In vitro: DT. Onset and end point of disintegration calculated by using the load–displacement profiles obtained by the TA. *In vivo*: oral DT	TA (CT3-4500), CT, 4.5 kg load cell,TA11/1000 (acrylic cylindrical) probe (Φ_{probe} = 25.4 mm),bottom: miniature stainless steel test sieve (Φ = 38 mm, aperture = 1.25 mm) placed on an extruded polystyrene plate	Recording the elapsed time between placing the tablet on the tongue and the moment of complete disintegration of the tablet	Sum of squared residuals function (SSR) used to compare *in vitro* and *in vivo* disintegration times. There was a good correlation between the *in vitro* results and the *in vivo* disintegration time Method optimization by mathematically predicting the method's efficiency using a theoretical patient group characterized by mild xerostomia Even if there were differences as against the original disintegration times, the method was able to predict the new *in vitro* values in this theoretical case	(Szakonyi and Zelkó, 2013)
In vitro: disintegration profile recorded as load vs. time curve. *In vivo*: oral DT, taste, volume of residue, roughness, palatability	TA (CT3-4500), CT, 4.5 kg load cell, TA10 probe, S_{test} = 0.01 mm/s	Recording the elapsed time between placing the tablet on the tongue and the moment of complete disintegration of the tabletTaste evaluation (sweet, salty, sour, bitter) using five scores VAS scales Volume of residue estimation using a five scores VAS scale. Roughness assessment using a five scores VAS scale.Palatability evaluation using a two scores scale (0 – rejected, 1 – accepted)	PLS was used in order to predict *in vivo* properties. Overall, the study managed to develop a model able to predict *in vivo* characteristics using instrumental analysis good prediction for *in vivo* disintegration time, volume of residue and total palatability Coupling of TA with multivariate data analysis enables the prediction of *in vivo* characteristics	(Casian et al., 2018)
Coated tablets				
In vitro: surface tribology *In vivo*: ease of swallowing, sensory attributes (roughness, adhesiveness, slipperiness)	Rheometer (DHR-2) with a tribo-rheology cell, top geometry: rotating, three tablets mounted on the flat top plate of the probe,bottom geometry: stationary, Transpore™ surgical tape (3 M™) attached to a clean steel cup (model for tongue asperity), F_{con} = 2 N, S_{test} = 0.001–1 rad/s	Ease of swallowing evaluation – swallowing tablet samples and assessing ease of swallowing on a 100 mm VASSensory attributes (roughness, adhesiveness, slipperiness) evaluation – maintaining the tablet in the mouth for minimum 10 s, then spit/swallow, then assess with 100 mm VAS	Pearson's correlation coefficient (r) and Spearman's correlation coefficient (rS) were used to assess the strength and direction of correlation between *in vitro* and *in vivo* variables Good IVIVC were obtained for ease of swallowing, slipperiness and stickiness Pearson's correlation coefficient was artificially increased when all tablet samples were included When only coated tablets were included, two significant linear correlations were obtained: high friction region at t = 30 s (COF_{30}) with slipperiness, and slip region at t = 10 s (COF_{10}) with stickiness The study demonstrated a relationship between tribological data and the oral sensory perception	(Hofmanová et al., 2021)
Buccal bioadhesive tablets				
In vitro: F_{det}, W_{adh}. *In vivo*: T_{adh}, AUC, C_{max}, T_{max}	TTing machine (L1000R), 20 N load cell	Measurement of the time after which the bioadhesive tablet was no longer visible under the lip by control at 30 min interval, following attachment to	The correlation studies showed an unclear correlation between the *in vitro* bioadhesive parameters (for which a difference was noticed between formulations) and *in vivo* adhesion time and biopharmaceutical	(Bouckaert et al., 1993)

(*continued on next page*)

Table 6 (*continued*)

Parameters of interest	*In vitro* experimental setup and testing parameters	*In vivo* experimental details	*In vitro - in vivo* correlations	Ref
		the gingiva Calculating the AUC, C_{max} and T_{max}	parameters (for which the difference between formulations was not significant) Therefore, differences observed *in vitro* are not necessarily transposed *in vivo*	
Soft chewable dosage forms				
In vitro: hardness, stickiness, water content, softening behaviour *In vivo*: chewing rate, number of chewing cycles to swallowing	TA (TA-XT2), CT, 5 kg load cell, cylindrical aluminum probe (Φ_{probe} = 5 mm), $S_{pretest}$ = 3.00 mm/s, S_{test} = 1.0 mm/s, $S_{posttest}$ = 1.00 mm/s	Counting the number of chewing cycles within 1 min and calculating the chewing rate Counting the number of chewing cycles needed for the oral breakdown of food to the point of swallowing	Multiple linear regression was used for predicting average chewing cycles for soft chewable dosage forms, based on hardness, fat content, water content, stickiness, softening behaviour New dissolution method developed based on *in vivo* chewing data – attaching the samples to a steel tooth coupled with a texture analyzer, in order to mimic both squeezing and grinding that occur during the mastication process The new method allows differentiating distinct soft chewable formulations which appear to be similar following the methods of the European Pharmacopoeia	(Stomberg et al., 2017)
Films				
In vitro: thin film tribology. Stribeck curves were obtained. *In vivo*: ease of swallowing, sensory attributes (roughness, adhesiveness, slipperiness)	Rheometer (DHR-2) with a tribo-rheology cell, top geometry: rotating, 3-balls-on a plate,bottom geometry: stationary, Tegaderm™ hydrocolloid thin dressing (3 M™) attached to the bottom surface, F_{con} = 1 N, S_{test} = 0.001–10 rad/s	Ease of swallowing evaluation – swallowing tablet samples and assessing ease of swallowing on a 100 mm VAS.Sensory attributes (roughness, adhesiveness, slipperiness) evaluation – maintaining the tablet in the mouth for minimum 10 s, then spit/swallow, then assess with 100 mm VAS.	Correlations between thin film tribology and sensory attributes were not significant However, it has the potential to help in mouthfeel comprehension	(Hofmanová et al., 2021)

*DT – disintegration/dispersion time; COF_{10} – coefficient of friction at 10 s; COF_{30} – coefficient of friction at 30 s; CT – compression test; IVIVC – *in vitro - in vivo* correlation; F_{con}- contact force; F_{det} - detachment force; $S_{pretest}$- pretest speed; $S_{posttest}$- posttest speed; S_{test}- test speed of lowering the probe with the attached sample; TA- texture analyzer; T_{adh} – time of adhesion; T_{con}- contact time; VAS - visual analogue scale; W_{adh} - work of adhesion

* Device model (Maximum load / Force resolution): CT3-1000 (1 kg/0.10 g), CT3-4500 (4.5 kg/0.50 g), TA.XTplus (50 kg/0.1 g), TA.HDplus (750 kg/0.10 g), DHR-2 (50 N/0.5 mN).

characterization of the solid oral pharmaceutical form, but no IVIVC is performed (Alopaeus et al., 2020; Cilurzo et al., 2003; Wang et al., 2021).

Therefore, despite the limited number of research documents that correlate *in vitro* and *in vivo* data in comparison with the ones that describe *in vitro* analysis of sensory properties, our review includes the description of this important tool which, as previously mentioned, provides a quality control method, reduces the costs of oral dosage forms evaluation by using data from TA and offers the possibility to understand how texture characteristics can estimate the behaviour of dosage forms after oral administration (Asiri et al., 2021).

The solid oral dosage forms evaluated in the studies that met all the criteria to be included in this subsection mainly belong to the category of tablets, in particular ODTs, but also to coated tablets, buccal mucoadhesive tablets, soft chewable dosage forms and films. It is clear that there is a strong connection between the category of the studied pharmaceutical form and the types of the determined or measured parameters. In the case of ODTs, IVIVC are generally performed between the *in vitro* disintegration time and oral disintegration time.

For example, Dor and Fix were among the first researchers to attempt developing a disintegration method that mimics *in vivo* conditions of the oral cavity by using a texture analyzer and determining the time for complete tablet disintegration versus distance. An important disadvantage of this method is the fact that in the oral cavity, the tablet would be completely moistened, while in the method developed by Dor and Fix the sample is only partially in contact with the disintegration medium, because one side of the tablet is taped to the probe (Dor and Fix, 2000).

Abdelbary *et al.* also assessed the possibility to link the *in vitro* disintegration profile of rapidly disintegrating tablets with oral disintegration time by determining time versus distance profiles. The researchers concluded that the use of a perforated grid during the TA minimised the operating errors and simulated well the *in vivo* conditions, thus gaining a successful, convenient, and precise method. The *in vitro* results obtained with the texture analyzer were very well correlated with the oral disintegration time for all the studied tablet types: a porous solid rapidly disintegrating tablet obtained by lyophilisation of an oil-in-water emulsion (Spasfon®), a rapidly disintegrating tablet which incorporated a disintegrating agent and a swelling agent (FlashTab®), a compression-moulding tablet (Wowtab®) and two rapidly disintegrating tablets formulations prepared with a powerful disintegrating agent, croscarmellose (Abdelbary et al., 2005).

In the study of Gryczke et al., the TA experimental setup used a perforated grid to better simulate the *in vivo* conditions and to ensure tablet wetting on all sides, like the method developed by Abdelbary et al. The results of the study showed no significant differences between the *in vitro* and *in vivo* disintegration times, hence the demonstrating the success of the IVIVC (Gryczke et al., 2011).

Another study that aimed at predicting the oral disintegration time by means of TA and mathematical optimization of the parameters of the method not only revealed a good correlation between the *in vitro* and *in vivo* data, but also calculated a new *in vivo* disintegration time for a theoretical patient group suffering from mild xerostomia (Szakonyi and Zelkó, 2013).

Casian et al. reported a complex study which followed the prediction of *in vivo* ODTs softening and disintegration behavior, volume of residue and total palatability, by using TA data. The research used, by partial least squares (PLS) and multivariate calibration, the entire curve load vs. time, but also individual parameters to perform the relationship evaluation between the texture profiles and disintegration. This study showed that the effects of formulation factors strongly influenced the perception and acceptance of ODTs (Casian et al., 2018).

Regarding the coated tablets and films, a different yet similar method with TA was used, namely a tribological method. Tribological measurements are relevant in the development of pharmaceutical

formulations due to their ability to predict mouthfeel and ease of swallowing. To assess the correlation capacity of *in vitro* tribological measurements (coefficient of friction) with oral sensory evaluation (slipperiness, stickiness, ease of swallowing, smoothness) for pharmaceutical coatings and coating tablets, Hofmanova *et al.* used Pearson's correlation coefficient and Spearman's correlation coefficient. The study reported surface and thin film tribological assessment of coated tablets and coating films, but the latter did not show a significant correlation and could not be used as a predictor of oral sensory characteristics. Regarding surface tribology, correlations were found between the static coefficient of friction and stickiness, as well as for the higher speed coefficient of friction and slipperiness. The explanation for the interconnection between stickiness at reduced speeds and slipperiness at more elevated speeds could be that adhesion is mostly linked to static friction, while slipperiness is associated with dynamic friction (Hofmanová et al., 2021).

One of the first attempts to perform an IVIVC in the field of mucoadhesive dosage forms was the study of Bouckaert *et al.*, on buccal bioadhesive tablets. The parameters which they assessed were the *in vitro* detachment force and work of adhesion, while the study in human volunteers determined bioadhesive properties of tablets. The apparatus used for determining *in vitro* properties was a TTing machine. One-way analysis of variance was used to statistically evaluate the *in vitro* results, while nonparametric statistics was used to evaluate the *in vivo* results. Even though there was a difference regarding the work of adhesion or the detachment force between formulations, the biopharmaceutical parameters and *in vivo* adhesion time did not reveal the same significant difference, which led to the conclusion that the study did not clarify if and which of the two parameters studied *in vitro* are important for the *in vivo* characteristics (Bouckaert et al., 1993).

Chewable dosage forms are another pharmaceutical product for which texture is essential for the compliance of patients, particularly in special patient populations. Multiple linear regression was used to predict the chewing cycles of different edibles according to the following independent variables determined by TA: hardness, stickiness, fat/water content, and softening behaviour (Stomberg et al., 2017). This statistical technique, used to analyse the relationship between independent and dependent variables, is successfully applied in the field of IVIVC.

Among the parameters of interest studied with the help of TA, it is observed that the disintegration time is predominant, being correlated with the oral disintegration time. The working methodology for determining the disintegration time is similar for all studies – the CT, even if there are small differences, such as the type of texture analyzer and probe, speed etc. Regarding the prediction method used, the disintegration profile was recorded either as load vs. time curve (Casian et al., 2018; Szakonyi and Zelkó, 2013) or as time vs. distance curve (Abdelbary et al., 2005; Dor and Fix, 2000).

Concerning the prediction method of the *in vivo* properties based on *in vitro* characteristics, it can be observed that good results are obtained using mathematical models, such as linear regression analysis, Pearson's correlation coefficient or Spearman's correlation coefficient (Dor and Fix, 2000; Hofmanová et al., 2021). Additionally, the multivariate data analysis is a powerful tool that has been recently used in a multitude of fields and situations. Casian et al. applied a PLS method and managed to predict subjective characteristics perceived during oral disintegration of ODTs based on TA data (Casian et al., 2018).

As mentioned earlier, there are other studies that, although they do not fully fit the criteria selected for this review, are worth mentioning. For example, the research conducted by Wang *et al.* used TA and dissolution testing to predict the time of dispersion in the oral cavity of levetiracetam from 3D printed instant-dissolving tablets, but without performing an actual *in vivo* study. The research also evaluated, with the ASTREE electronic tongue, the palatability of various formulations developed by optimizing the sucralose and spearmint flavour amounts through design of experiments. The oral dispersion time was predicted to be rapid based on TA results, which indicated a 30 s dispersion time of instant-dissolving tablets and a reduction of this dispersion time with tablet strength decrease, and also on the *in vitro* drug release test, which showed an almost complete release after 2.5 min (Wang et al., 2021). Another scientific article which did not perform an *in vivo* study but formulated hypotheses regarding sensory attributes (ease of swallowing) of the tested preparation based on the TPA is the study of Ito et al. (Ito et al., 2019). The research group focused on obtaining acetaminophen mini-tablets using various water-soluble polymers (eg. carrageenan, ι-carrageenan, HPMC, CMCNa, sodium alginate, pectin) to achieve rapid swelling and gelling, elasticity and low adhesiveness, therefore an easy deglutition. Their results showed that mini-tablets prepared with 20–30% carrageenan presented appropriate characteristics for a comfortable oral administration.

Overall, IVIVC is a valuable instrument for the prediction of the *in vivo* sensory attributes of pharmaceutical products based on TA data of solid oral dosage forms, which can be exploited to develop pharmaceutical forms based on texture studies, without including the stages of *in vivo* evaluations, which would lead to saving time, but also financial resources. However, the number of these studies is very small, which means that this topic can be successfully exploited in the future.

7. Insight into practical details derived from the review

In the past years, TA has become widely used in the pharmaceutical development, deemed as a very customizable method, with a wide range of easily available and affordable accessories. As shown in Fig. 8, mechanical characterization through TA was reported for most of the solid oral dosage forms, while the other TA methodologies address subgroups of dosage forms depending on product characteristics and quality control needs. Based on the summarised information in this work several practical implications emerge to guide future research.

Regarding mechanical characterization, for some types of products (e.g. tablets, films, filaments), formulations can be assessed through multiple different tests to obtain an overview of the mechanical profile. As up to date there are no official acceptance criteria for pharmaceutical products tested through TA, researchers often compare results with other published reports, which is problematic because of the differences in the experimental conditions and in the results. In this respect, prior testing of reference materials or commercially available products could be helpful as it allows to define standard values obtained in the same experimental settings. The reproducibility of results is variable, some studies were performed with as few as three replicates to 15–20 replicates for a formulation. In this context, a useful experimental approach to overcome the variability issue is the design of experiments, a methodology that discriminates the real effects of input variables from the experimental error.

In addition to the challenges met with mechanical testing, bioadhesion measurements bring extra variability. The diversity of the substrates, and implicitly of their characteristics significantly increase the inconsistency of the results. Apart from the substrate types, the pretreatment steps of the substrates and the experimental setups are sometimes difficult to compare between the reported studies. Consequently, the acceptance criteria based on such methods are not very reliable.

In contrast to the high number of studies describing the mechanical and mucoadhesive properties, the IVIVC data obtained through TA is modest. Therefore, the prediction of the *in vivo* properties based on *in vitro* characteristics represents an open topic that could be the focus of future studies, of particular interest in early formulation design for research and development scientists. However, the standardization of the test protocol for *in vitro - in vivo* analysis is required.

In conclusion, the main challenge of TA arises from the difficulty to define of a set of general tests which enables the assessment of samples varying from raw materials to a broad spectrum of oral dosage forms with distinct characteristics. The choice of the testing protocol and parameters depends entirely on the characteristics of the product that is

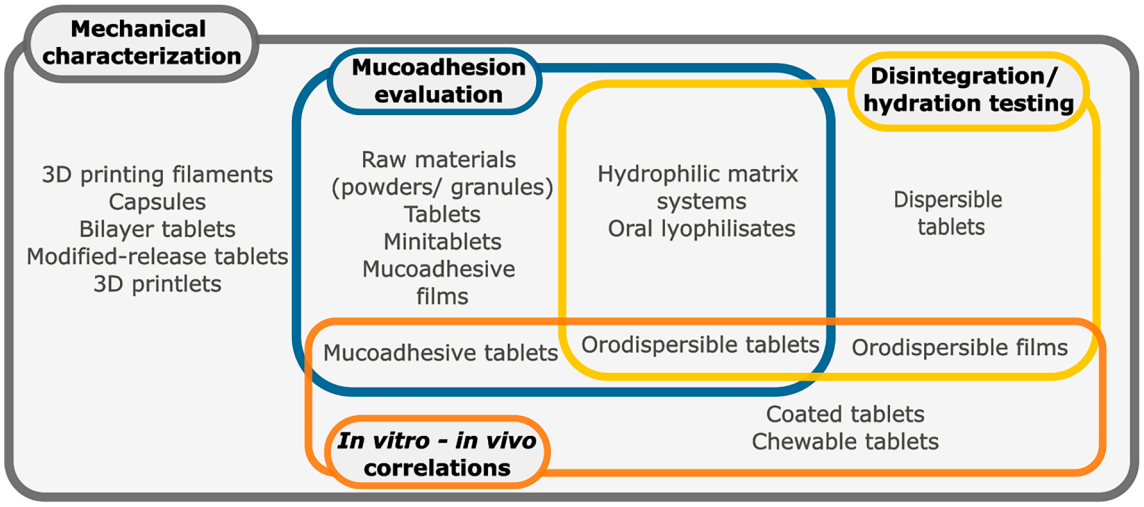

Fig. 8. Summary of texture analysis (TA) applications on solid oral dosage forms.

being tested and has a significant impact on the results. Therefore, a step ahead for researchers would be to standardize the tests and testing parameters as rigorously as possible, as well as the characteristics of the products that are being tested. Clear definitions of the texture attributes together with consistent terminology would enable the correspondence between studies and should be considered when developing texture methodologies.

As a versatile testing method, TA will evolve in accordance with the changes across the pharmaceutical industry, to fulfill the needs coming from emerging dosage forms, but also with the evolving regulatory requirements. The significant changes driven by the growing trend of enhanced drug products will require accurate testing methods. Thus, TA can provide multiple parameters describing the performance in improving dosage forms, such as through user friendly-dosage forms or 3D printed medicines.

8. Conclusion

Texture analysis is a testing method that constantly adapts, in order to meet the needs of the continous evolution and diversification of pharmaceutical dosage forms, trying to simulate the conditions in which a certain product is used. Several texture methods to characterize oral solid dosage forms have been published over the past decades. Among them, great emphasis is placed on mechanical testing; depending on the type and the characteristics of the samples various techniques such as compression, indentation, puncture, tensile, FT, and TPA were applied. Further, the parameters derived from mechanical testing were calculated to quantify the texture characteristics aiming to comprehensively describe the mechanical profile of the samples. In the current work, the applications of texture analysis in mechanical characterization are reviewed from the viewpoint of the suitability for various dosage forms, and comparability of experimental setups. Apart from mechanical characterization, different methods to evaluate the properties of mucoadhesive oral dosage forms have been summarized by discussing the test parameters but also the preliminary steps together with the interpretation of the experimental results for different sample types. In addition, reported studies to characterize the disintegration properties and the texture analysis experimental setups for disintegration testing are reviewed underlying the particularities of the methods and the advantages over traditional methods, but also the prediction of the *in vivo* sensory attributes of solid oral dosage forms based on texture analysis data.

CRediT authorship contribution statement

Cătălina Bogdan: Conceptualization, Writing – original draft. **Dana Hales:** Conceptualization, Writing – original draft. **Andreea Cornilă:** Conceptualization, Writing – original draft. **Tibor Casian:** Writing – review & editing. **Rareș Iovanov:** Writing – review & editing. **Ioan Tomuță:** Writing – review & editing. **Sonia Iurian:** Conceptualization, Writing – original draft, Writing – review & editing, Supervision, Project administration, Funding acquisition.

Declaration of Competing Interest

The authors declare that they have no known competing financial interests or personal relationships that could have appeared to influence the work reported in this paper.

Data availability

No data was used for the research described in the article.

Acknowledgements

This work was supported by a grant of the Romanian Ministry of Research, Innovation and Digitization, CCCDI - UEFISCDI, project number PN-III-P2-2.1-PED-2021-4198, within PNCDI III. The funding source had no involvement in the study design, in the collection, analysis and interpretation of data, in the writing of the report, or in the decision to submit the article for publication.

References

2.9. Pharmaceutical technical... - European Pharmacopoeia 11.0 [WWW Document], n.d. URL https://pheur.edqm.eu/app/11-0/content/11-0/20900E.htm (accessed 13.23).

Abdelbary, G., Eouani, C., Prinderre, P., Joachim, J., Reynier, J., Piccerelle, P., 2005. Determination of the in vitro disintegration profile of rapidly disintegrating tablets and correlation with oral disintegration. Int J Pharm 292, 29–41. https://doi.org/10.1016/J.IJPHARM.2004.08.019.

Abdel-Haq, M., Alyan, R., Abd-Rbo, K., Kasem, H., Aiman, A.A., 2021. Biomimetic clotrimazole-loaded PLGA films with enhanced adhesiveness for controlled drug release. Int J Pharm 601. https://doi.org/10.1016/j.ijpharm.2021.120578.

Accili, D., Menghi, G., Bonacucina, G., di Martino, P., Palmieri, G.F., 2004. Mucoadhesion dependence of pharmaceutical polymers on mucosa characteristics. European Journal of Pharmaceutical Sciences 22, 225–234. https://doi.org/10.1016/J.EJPS.2003.12.011.

Alaei, S., Omidi, Y., Omidian, H., 2021. In vitro evaluation of adhesion and mechanical properties of oral thin films. European Journal of Pharmaceutical Sciences 166, 105965. https://doi.org/10.1016/J.EJPS.2021.105965.

Alaei, S., Omidian, H., 2021. Mucoadhesion and Mechanical Assessment of Oral Films. European Journal of Pharmaceutical Sciences 159. https://doi.org/10.1016/j.ejps.2021.105727.

Alam, N., Beg, S., Rizwan, M., Ahmad, A., Ahmad, F.J., Ali, A., Aqil, M., 2015. Mucoadhesive elementary osmotic pump tablets of trimetazidine for controlled drug delivery and reduced variability in oral bioavailability. Drug Dev Ind Pharm 41, 692–702. https://doi.org/10.3109/03639045.2014.900076.

Alopaeus, J.F., Hellfritzsch, M., Gutowski, T., Scherließ, R., Almeida, A., Sarmento, B., Škalko-Basnet, N., Tho, I., 2020. Mucoadhesive buccal films based on a graft co-polymer – A mucin-retentive hydrogel scaffold. European Journal of Pharmaceutical Sciences 142. https://doi.org/10.1016/j.ejps.2019.105142.

Alzahrani, A., Narala, S., Adel Ali Youssef, A., Nyavanandi, D., Bandari, S., Mandati, P., Almotairy, A., Almutairi, M., Repka, M., 2022. Fabrication of a shell-core fixed-dose combination tablet using fused deposition modeling 3D printing. European Journal of Pharmaceutics and Biopharmaceutics 177, 211–223. 10.1016/j.ejpb.2022.07.003.

Antonyuk, S., Palis, S., Heinrich, S., 2011. Breakage behaviour of agglomerates and crystals by static loading and impact. Powder Technol 206, 88–98. https://doi.org/10.1016/J.POWTEC.2010.02.025.

Arpa, M.D., Ünükür, M.Z., Erim, Ü.C., 2021. Formulation, characterization and in vitro release studies of terbinafine hydrochloride loaded buccal films. Journal of Research in Pharmacy 25, 667–680. https://doi.org/10.29228/jrp.58.

Asiri, A., Hofmanová, J., Batchelor, H., 2021. A review of in vitro and in vivo methods and their correlations to assess mouthfeel of solid oral dosage forms. Drug Discov Today 26, 740–753. https://doi.org/10.1016/j.drudis.2020.12.015.

Awad, A., Trenfield, S.J., Basit, A.W., 2021. Solid oral dosage forms. Remington: The Science and Practice of Pharmacy 333–358. 10.1016/B978-0-12-820007-0.00019-2.

Baranauskaite, J., Ockun, M.A., Uner, B., Gungor, B., Duman, G., Tas, C., Yesilada, E., 2022. Development and In vitro characterization of pullulan fast dissolving films loaded with Panax ginseng extract, antioxidant properties and cytotoxic efficiency on lung and breast cancer cell lines. J Drug Deliv Sci Technol 76. https://doi.org/10.1016/j.jddst.2022.103701.

Basim, P., Haware, R. v., Dave, R.H., 2019. Tablet capping predictions of model materials using multivariate approach. Int J Pharm 569. 10.1016/j.ijpharm.2019.118548.

Baus, R.A., Haug, M.F., Leichner, C., Jelkmann, M., Bernkop-Schnürch, A., 2019. In Vitro-in Vivo Correlation of Mucoadhesion Studies on Buccal Mucosa. Mol Pharm 16, 2719–2727. https://doi.org/10.1021/acs.molpharmaceut.9b00254.

Bhatt, J.A., Bahl, D., Morris, K., Stevens, L.L., Haware, R. v., 2020. Structure-mechanics and improved tableting performance of the drug-drug cocrystal metformin:salicylic acid. European Journal of Pharmaceutics and Biopharmaceutics 153, 23–35. 10.1016/j.ejpb.2020.05.031.

Boateng, J.S., Auffret, A.D., Matthews, K.H., Humphrey, M.J., Stevens, H.N.E., Eccleston, G.M., 2010. Characterisation of freeze-dried wafers and solvent evaporated films as potential drug delivery systems to mucosal surfaces. Int J Pharm 389, 24–31. https://doi.org/10.1016/j.ijpharm.2010.01.008.

Bodini, R.B., Guimarães, J. das G.L., Monaco-Lourenço, C.A., Aparecida de Carvalho, R., 2019. Effect of starch and hydroxypropyl methylcellulose polymers on the properties of orally disintegrating films. J Drug Deliv Sci Technol 51, 403–410. 10.1016/j.jddst.2019.03.028.

Bonacucina, G., Cespi, M., Misici-Falzi, M., Palmieri, G.F., 2007. Mechanical characterization of pharmaceutical solids: A comparison between rheological tests performed under static and dynamic porosity conditions. European Journal of Pharmaceutics and Biopharmaceutics 67, 277–283. https://doi.org/10.1016/j.ejpb.2006.12.018.

Bouckaert, S., Lefebvre, R.A., Remon, J.P., 1993. In Vitro/in Vivo Correlation of the Bioadhesive Properties of a Buccal Bioadhesive Miconazole Slow-Release Tablet. Pharmaceutical Research: An Official Journal of the American Association of Pharmaceutical Scientists 10, 853–856. https://doi.org/10.1023/A:1018957126809/METRICS.

Brniak, W., Maślak, E., Jachowicz, R., 2015. Orodispersible films and tablets with prednisolone microparticles. European Journal of Pharmaceutical Sciences 75, 81–90. 10.1016/j.ejps.2015.04.006.

Buck, J., Huwyler, J., Kühl, P., Dischinger, A., 2016. Pediatric Dispersible Tablets: a Modular Approach for Rapid Prototyping. Pharm Res 33, 2043–2055. https://doi.org/10.1007/s11095-016-1946-9.

Caccavo, D., Cascone, S., Lamberti, G., Barba, A.A., 2015. Controlled drug release from hydrogel-based matrices: Experiments and modeling. Int J Pharm 486, 144–152. https://doi.org/10.1016/J.IJPHARM.2015.03.054.

Carvalho, F.C., Bruschi, M.L., Evangelista, R.C., Gremião, M.P.D., 2010. Mucoadhesive drug delivery systems. Brazilian Journal of Pharmaceutical Sciences 46, 1–17. https://doi.org/10.1590/S1984-82502010000100002.

Cascone, S., Lamberti, G., Titomanlio, G., D'Amore, M., Barba, A.A., 2014. Measurements of non-uniform water content in hydroxypropyl-methyl-cellulose based matrices via texture analysis. Carbohydr Polym 103, 348–354. https://doi.org/10.1016/J.CARBPOL.2013.12.060.

Casian, T., Bogdan, C., Tarta, D., Moldovan, M., Tomuta, I., Iurian, S., 2018. Assessment of oral formulation-dependent characteristics of orodispersible tablets using texture profiles and multivariate data analysis. J Pharm Biomed Anal 152, 47–56. https://doi.org/10.1016/j.jpba.2018.01.040.

Chachlioutaki, K., Karavasili, C., Mavrokefalou, E.E., Gioumouxouzis, C.I., Ritzoulis, C., Fatouros, D.G., 2022. Quality control evaluation of paediatric chocolate-based dosage forms: 3D printing vs mold-casting method. Int J Pharm 624. https://doi.org/10.1016/j.ijpharm.2022.121991.

Chandrasekhar, R., Hassan, Z., AlHusban, F., Smith, A.M., Mohammed, A.R., 2009. The role of formulation excipients in the development of lyophilised fast-disintegrating tablets. European Journal of Pharmaceutics and Biopharmaceutics 72, 119–129. https://doi.org/10.1016/j.ejpb.2008.11.011.

Chang, S., Li, J., Sun, C.C., 2017. Tensile and shear methods for measuring strength of bilayer tablets. Int J Pharm 523, 121–126. https://doi.org/10.1016/j.ijpharm.2017.03.010.

Chang, S.Y., Sun, C.C., 2019. Effect of particle size on interfacial bonding strength of bilayer tablets. Powder Technol 356, 97–101. https://doi.org/10.1016/j.powtec.2019.07.100.

Chatzitaki, A.T., Mystiridou, E., Bouropoulos, N., Ritzoulis, C., Karavasili, C., Fatouros, D.G., 2022. Semi-solid extrusion 3D printing of starch-based soft dosage forms for the treatment of paediatric latent tuberculosis infection. Journal of Pharmacy and Pharmacology 74, 1498–1506. https://doi.org/10.1093/JPP/RGAB121.

Chaud, M. v., Lima, A.C., Vila, M.M.D.C., Paganelli, M.O., Paula, F.C., Pedreiro, L.N., Gremião, M.P.D., 2013. Development and evaluation of praziquantel solid dispersions in sodium starch glycolate. Tropical Journal of Pharmaceutical Research 12, 163–168. 10.4314/tjpr.v12i2.5.

Chen, L., Opara, U.L., 2013. Texture measurement approaches in fresh and processed foods - A review. Food Research International 51, 823–835. https://doi.org/10.1016/j.foodres.2013.01.046.

Chen, L., He, Z., Kunnath, K.T., Fan, S., Wei, Y., Ding, X., Zheng, K., Davé, R.N., 2019. Surface engineered excipients: III. Facilitating direct compaction tableting of binary blends containing fine cohesive poorly-compactable APIs. Int J Pharm 557, 354–365. https://doi.org/10.1016/j.ijpharm.2018.12.055.

Chen, H., Zhang, J., Qiao, Q., Hu, E., Wei, Y., Pang, Z., Gao, Y., Qian, S., Zhang, J., Heng, W., 2022. A novel soluble lornoxicam-sodium chelate monohydrate with improved plasticity and tabletability. Int J Pharm 624. https://doi.org/10.1016/j.ijpharm.2022.122060.

Cheng, Y., Qin, H., Acevedo, N.C., Jiang, X., Shi, X., 2020. 3D printing of extended-release tablets of theophylline using hydroxypropyl methylcellulose (HPMC) hydrogels. Int J Pharm 591. https://doi.org/10.1016/j.ijpharm.2020.119983.

Chickering, D.E.I., Mathiowitz, E., 1999. Definitions, Mechanisms and Theories of Bioadhesion. In: Mathiowitz, E. (Ed.), Bioadhesive Drug Delivery Systems: Fundamentals, Novel Approaches, and Development. Marcel Dekker Inc, New York, pp. 1–10.

Cilurzo, F., Minghetti, P., Selmin, F., Casiraghi, A., Montanari, L., 2003. Polymethacrylate salts as new low-swellable mucoadhesive materials. Journal of Controlled Release 88, 43–53. https://doi.org/10.1016/S0168-3659(02)00459-5.

Ciper, M., Bodmeier, R., 2005. Preparation and characterization of novel fast disintegrating capsules (Fastcaps) for administration in the oral cavity. Int J Pharm 303, 62–71. https://doi.org/10.1016/J.IJPHARM.2005.07.004.

Crișan, A.G., Iurian, S., Porfire, A., Rus, L.M., Bogdan, C., Casian, T., Lucacel, R.C., Turza, A., Porav, S., Tomuță, I., 2022. QbD guided development of immediate release FDM-3D printed tablets with customizable API doses. Int J Pharm 613. https://doi.org/10.1016/j.ijpharm.2021.121411.

Croquelois, B., Girardot, J., Kopp, J.B., Cazautets, C., Tchoreloff, P., Mazel, V., 2017. Breaking pharmaceutical tablets with a hole: Reevaluation of the stress concentration factor and influence of the hole size. Powder Technol 317, 126–132. https://doi.org/10.1016/j.powtec.2017.04.033.

Croquelois, B., Girardot, J., Kopp, J.B., Tchoreloff, P., Mazel, V., 2020. Quantification of tablet sensitivity to a stress concentration: Generalization of Hiestand's approach and link with the microstructure. Powder Technol 369, 176–183. https://doi.org/10.1016/j.powtec.2020.05.002.

Texture Analyzer, Ametek Brookfield [WWW Document], n.d. URL https://www.scinteck.com/store/p1201/Brookfield.html (accessed 1.31.23).

CT3 TEXTURE ANALYZER Operating Instructions [WWW Document], n.d. URL https://www.brookfieldengineering.com/-/media/ametekbrookfield/manuals/texture/ct3%20manual%20m08-372-f1116.pdf (accessed 2.1.23).

de Backere, C., de Beer, T., Vervaet, C., Vanhoorne, V., 2022. Effect of feed frame on lubricant sensitivity during upscaling from a compaction simulator to a rotary tablet press. Int J Pharm 616. https://doi.org/10.1016/j.ijpharm.2022.121562.

de Spiegeleer, B., van Vooren, L., Voorspoels, J., Thoné, D., Rosier, J., 2001. Dissolution stability and IVIVC investigation of a buccal tablet. Anal Chim Acta 446, 343–349. https://doi.org/10.1016/S0003-2670(01)01074-1.

Desai, N., Masen, M., Cann, P., Hanson, B., Tuleu, C., Orlu, M., 2022. Modernising Orodispersible Film Characterisation to Improve Palatability and Acceptability Using a Toolbox of Techniques. Pharmaceutics 14. https://doi.org/10.3390/pharmaceutics14040732.

do Couto, R.O., Cubayachi, C., Calefi, P.L., Lopez, R.F.V., Pedrazzi, V., de Gaitani, C.M., de Freitas, O., 2017. Combining amino amide salts in mucoadhesive films enhances needle-free buccal anesthesia in adults. Journal of Controlled Release 266, 205–215. 10.1016/j.jconrel.2017.09.039.

Dor, P.J.M., Fix, J.A., 2000. In Vitro Determination of Disintegration Time of Quick-Dissolve Tablets Using a New Method. Pharm Dev Technol 5, 575–577. https://doi.org/10.1081/PDT-100102041.

Duchene, D., Touchard, F., Peppas, N.A., 2008. Pharmaceutical and Medical Aspects of Bioadhesive Systems for Drug Administration. Drug Dev Ind Pharm 14, 283–318. https://doi.org/10.3109/03639048809151972.

Dun, J., Osei-Yeboah, F., Boulas, P., Lin, Y., Sun, C.C., 2018. A systematic evaluation of dual functionality of sodium lauryl sulfate as a tablet lubricant and wetting enhancer. Int J Pharm 552, 139–147. https://doi.org/10.1016/j.ijpharm.2018.09.056.

Dun, J., Chen, H., Sun, C.C., 2020. Profound tabletability deterioration of microcrystalline cellulose by magnesium stearate. Int J Pharm 590. https://doi.org/10.1016/j.ijpharm.2020.119927.

Dvořák, J., Tomas, J., Lizoňová, D., Schöngut, M., Dammer, O., Pekárek, T., Beránek, J., Štěpánek, F., 2020. Investigation of tablet disintegration pathways by the combined

use of magnetic resonance imaging, texture analysis and static light scattering. Int J Pharm 587. https://doi.org/10.1016/j.ijpharm.2020.119719.
El-Arini, S.K., Clas, S.D., 2002. Evaluation of Disintegration Testing of Different Fast Dissolving Tablets Using the Texture Analyzer. Pharm Dev Technol 7, 361–371. https://doi.org/10.1081/PDT-120005732.
Eleftheriadis, G.K., Ritzoulis, C., Bouropoulos, N., Tzetzis, D., Andreadis, D.A., Boetker, J., Rantanen, J., Fatouros, D.G., 2019. Unidirectional drug release from 3D printed mucoadhesive buccal films using FDM technology: In vitro and ex vivo evaluation. European Journal of Pharmaceutics and Biopharmaceutics 144, 180–192. https://doi.org/10.1016/j.ejpb.2019.09.018.
Eleftheriadis, G.K., Monou, P.K., Bouropoulos, N., Boetker, J., Rantanen, J., Jacobsen, J., Vizirianakis, I.S., Fatouros, D.G., 2020. Fabrication of Mucoadhesive Buccal Films for Local Administration of Ketoprofen and Lidocaine Hydrochloride by Combining Fused Deposition Modeling and Inkjet Printing. J Pharm Sci 109, 2757–2766. https://doi.org/10.1016/j.xphs.2020.05.022.
El-Malah, Y., Nazzal, S., 2010. Preparation of delayed release tablet dosage forms by compression coating: Effect of coating material on theophylline release. Pharm Dev Technol 15, 305–310. https://doi.org/10.3109/10837450903188519.
El-Malah, Y., Nazzal, S., 2013. "Real-time" disintegration analysis and D-optimal experimental design for the optimization of diclofenac sodium fast-dissolving films. Pharmaceutical Development and Technology 18, 1355–1360. https://doi.org/10.3109/10837450.2012.700936.
Farias, S., Boateng, J.S., 2018. Development and functional characterization of composite freeze dried wafers for potential delivery of low dose aspirin for elderly people with dysphagia. Int J Pharm 553, 65–83. https://doi.org/10.1016/j.ijpharm.2018.10.025.
Farias, S., Boateng, J.S., 2020. In vitro, ex vivo and in vivo evaluation of taste masked low dose acetylsalicylic acid loaded composite wafers as platforms for buccal administration in geriatric patients with dysphagia. Int J Pharm 589. https://doi.org/10.1016/j.ijpharm.2020.119807.
Fell, J.T., Newton, J.M., 1970. Determination of Tablet Strength by the Diametral-Compression Test. J Pharm Sci 59, 688–691. https://doi.org/10.1002/jps.2600590523.
Flügel, K., Hennig, R., Thommes, M., 2020. Impact of structural relaxation on mechanical properties of amorphous polymers. European Journal of Pharmaceutics and Biopharmaceutics 154, 214–221. https://doi.org/10.1016/j.ejpb.2020.07.016.
Foegeding, E.A., Drake, M.A., 2007. Invited review: Sensory and mechanical properties of cheese texture. J Dairy Sci 90, 1611–1624. https://doi.org/10.3168/jds.2006-703.
Gennari, C.G.M., Sperandeo, P., Polissi, A., Minghetti, P., Cilurzo, F., 2019. Lysozyme Mucoadhesive Tablets Obtained by Freeze-Drying. J Pharm Sci 108, 3667–3674. https://doi.org/10.1016/j.xphs.2019.08.011.
Göbel, A., da Silva, J.B., Cook, M., Breitkreutz, J., 2021. Development of buccal film formulations and their mucoadhesive performance in biomimetic models. Int J Pharm 610. https://doi.org/10.1016/j.ijpharm.2021.121233.
Gong, X., Sun, C.C., 2015. A new tablet brittleness index. European Journal of Pharmaceutics and Biopharmaceutics 93, 260–266. https://doi.org/10.1016/j.ejpb.2015.04.007.
Gottschalk, N., Quodbach, J., Elia, A.G., Hess, F., Bogdahn, M., 2022. Determination of feed forces to improve process understanding of Fused Deposition Modeling 3D printing and to ensure mass conformity of printed solid oral dosage forms. Int J Pharm 614, 121416. https://doi.org/10.1016/J.IJPHARM.2021.121416.
Gryczke, A., Schminke, S., Maniruzzaman, M., Beck, J., Douroumis, D., 2011. Development and evaluation of orally disintegrating tablets (ODTs) containing Ibuprofen granules prepared by hot melt extrusion. Colloids Surf B Biointerfaces 86, 275–284. https://doi.org/10.1016/j.colsurfb.2011.04.007.
Gugulothu, D., Desai, P., Pandharipande, P., Patravale, V., 2015. Freeze drying: Exploring potential in development of orodispersible tablets of sumatriptan succinate. Drug Dev Ind Pharm 41, 398–405. https://doi.org/10.3109/03639045.2013.871551.
Guinard, J.-X., Mazzucchelli, R., 1996. The sensory perception of texture and mouthfeel. Trends Food Sci Technol 7, 213–219. https://doi.org/10.1016/0924-2244(96)10025-X.
Gültekin, H.E., Tort, S., Acartürk, F., 2019. An Effective Technology for the Development of Immediate Release Solid Dosage Forms Containing Low-Dose Drug: Fused Deposition Modeling 3D Printing. Pharm Res 36. https://doi.org/10.1007/s11095-019-2655-y.
Gültekin, H.E., Tort, S., Tuğcu-Demiröz, F., Acartürk, F., 2021. 3D printed extended release tablets for once daily use: An in vitro and in vivo evaluation study for a personalized solid dosage form. Int J Pharm 596. https://doi.org/10.1016/j.ijpharm.2021.120222.
Gurpreetarora, Malik, K., Rana, V., Singh, I., 2012. Gum ghatti - A pharmaceutical excipient: Development, evaluation and optimization of sustained release mucoadhesive matrix tablets of domperidone [WWW Document]. Acta Pol Pharm. URL https://www.researchgate.net/publication/230643748_Gum_ghatti_-_A_pharmaceutical_excipient_Development_evaluation_and_optimization_of_sustained_release_mucoadhesive_matrix_tablets_of_domperidone (accessed 2.2.23).
Hackl, E. v., Ermolina, I., 2016. Using Texture Analysis Technique to Assess the Freeze-Dried Cakes in Vials. J Pharm Sci 105, 2073–2085. 10.1016/j.xphs.2016.05.016.
Hackl, E., Ermolina, I., 2019. Application of Texture Analysis Technique in Formulation Development of Lyophilized Orally Disintegrating Tablets Containing Mannitol. Polyvinylpyrrolidone and Amino Acids. AAPS PharmSciTech 20. https://doi.org/10.1208/s12249-018-1269-8.
Hagen, E., Løding, F.S., Mattsson, S., Tho, I., 2016. Use of interactive mixtures to obtain mini-tablets with high dose homogeneity for paediatric drug delivery. J Drug Deliv Sci Technol 34, 51–59. https://doi.org/10.1016/j.jddst.2016.03.006.
Hagesaether, E., Hiorth, M., Sande, S.A., 2009. Mucoadhesion and drug permeability of free mixed films of pectin and chitosan: An in vitro and ex vivo study. European Journal of Pharmaceutics and Biopharmaceutics 71, 325–331. https://doi.org/10.1016/j.ejpb.2008.09.002.
Han, J.K., Kim, J.Y., Choi, D.H., Park, E.S., 2022. A formulation development strategy for dual-release bilayer tablets: An integrated approach of quality by design and a placebo layer. Int J Pharm 618. https://doi.org/10.1016/j.ijpharm.2022.121659.
Hejduk, A., Czajka, S., Lulek, J., 2021. Impact of co-processed excipient particles solidity and circularity on critical quality attributes of orodispersible minitablets. Powder Technol 387, 494–508. https://doi.org/10.1016/j.powtec.2021.03.063.
Hofmanová, J.K., Mason, J., Batchelor, H.K., 2021. Tribology provides an in vitro tool that correlated to in vivo sensory data on the mouthfeel of coated tablets. Int J Pharm 597. https://doi.org/10.1016/j.ijpharm.2021.120323.
Hu, Z., Xu, P., Zhang, J., Bandari, S., Repka, M.A., 2022. Development of controlled release oral dosages by density gradient modification via three-dimensional (3D) printing and hot-melt extrusion (HME) technology. J Drug Deliv Sci Technol 71, 103355. https://doi.org/10.1016/J.JDDST.2022.103355.
Iftimi, L.D., Edinger, M., Bar-Shalom, D., Rantanen, J., Genina, N., 2019. Edible solid foams as porous substrates for inkjet-printable pharmaceuticals. European Journal of Pharmaceutics and Biopharmaceutics 136, 38–47. https://doi.org/10.1016/j.ejpb.2019.01.004.
Ikeuchi-Takahashi, Y., Watanabe, N., Sasatsu, M., Onishi, H., 2013. Formulation and evaluation of matrix type mucoadhesive tablets aimed at treating oral aphtha. Drug Dev Ind Pharm 39, 1254–1261. https://doi.org/10.3109/03639045.2012.717297.
ISO - ISO 5492:2008 - Sensory analysis — Vocabulary [WWW Document], n.d. URL https://www.iso.org/standard/38051.html (accessed 1.31.23).
Ito, I., Ito, A., Unezaki, S., 2019. Preparation and evaluation of water-absorbing swollen mini-tablet aimed at improving ingestion. J Drug Deliv Sci Technol 50, 201–207. https://doi.org/10.1016/j.jddst.2019.01.009.
Iurian, S., Bogdan, C., Tomuță, I., Szabó-Révész, P., Chvatal, A., Leucuța, S.E., Moldovan, M., Ambrus, R., 2017a. Development of oral lyophilisates containing meloxicam nanocrystals using QbD approach. European Journal of Pharmaceutical Sciences 104, 356–365. https://doi.org/10.1016/j.ejps.2017.04.011.
Iurian, S., Dinte, E., Iuga, C., Bogdan, C., Spiridon, I., Barbu-Tudoran, L., Bodoki, A., Tomuță, I., Leucuța, S.E., 2017b. The pharmaceutical applications of a biopolymer isolated from Trigonella foenum-graecum seeds: Focus on the freeze-dried matrix forming capacity. Saudi Pharmaceutical Journal 25, 1217–1225. https://doi.org/10.1016/j.jsps.2017.09.006.
Kajthunyakarn, W., Khlibsuwan, R., Sakloetsakun, D., Pongjanyakul, T., 2019. Sodium caseinate films modified using halloysite: Physicochemical characterization and drug permeability studies. J Drug Deliv Sci Technol 54. https://doi.org/10.1016/j.jddst.2019.101235.
Karemore, M.N., Bali, N.R., 2021. Gellan gum based gastroretentive tablets for bioavailability enhancement of cilnidipine in human volunteers. Int J Biol Macromol 174, 424–439. https://doi.org/10.1016/J.IJBIOMAC.2021.01.199.
Karrout, Y., Neut, C., Wils, D., Siepmann, F., Deremaux, L., Flament, M., Dubreuil, L., Desreumaux, P., Siepmann, J., 2010. Enzymatically activated coated multiparticulates containing theophylline for colon targeting. J Drug Deliv Sci Technol 20, 193–199. https://doi.org/10.1016/S1773-2247(10)50029-7.
Kawano, Y., Sasatsu, M., Mizutani, A., Hirose, K., Hanawa, T., Onishi, H., 2016. Preparation and Evaluation of Stomatitis Film Using Xyloglucan Containing Loperamide. Chem. Pharm. Bull 564, 564–569. https://doi.org/10.1248/cpb.c15-00926.
Khan, D., Kirby, D., Bryson, S., Shah, M., Rahman Mohammed, A., 2022. Paediatric specific dosage forms: Patient and formulation considerations. Int J Pharm 616, 121501. https://doi.org/10.1016/J.IJPHARM.2022.121501.
Khuathan, N., Pongjanyakul, T., 2014. Modification of quaternary polymethacrylate films using sodium alginate: Film characterization and drug permeability. Int J Pharm 460, 63–72. https://doi.org/10.1016/j.ijpharm.2013.10.050.
Kilicarslan, M., Ilhan, M., Inal, O., Orhan, K., 2018. Preparation and evaluation of clindamycin phosphate loaded chitosan/alginate polyelectrolyte complex film as mucoadhesive drug delivery system for periodontal therapy. European Journal of Pharmaceutical Sciences 123, 441–451. https://doi.org/10.1016/j.ejps.2018.08.007.
Kiniwa, R., Miyake, M., Kimura, S. ichiro, Itai, S., Kondo, H., Iwao, Y., 2019. Development of muco-adhesive orally disintegrating tablets containing tamarind gum-coated tea powders for oral care. Int J Pharm X 1, 100012. 10.1016/J.IJPX.2019.100012.
Kottke, D., Burckhardt, B.B., Knaab, T.C., Breitkreutz, J., Fischer, B., 2021. Development and evaluation of a composite dosage form containing desmopressin acetate for buccal administration. Int J Pharm X 3. https://doi.org/10.1016/j.ijpx.2021.100082.
Kraisit, P., Limmatvapirat, S., Nunthanid, J., Sriamornsak, P., Luangtana-Anan, M., 2017. Preparation and characterization of hydroxypropyl methylcellulose/polycarbophil mucoadhesive blend films using a mixture design approach. Chem Pharm Bull (Tokyo) 65, 284–294. https://doi.org/10.1248/cpb.c16-00849.
Kuck, J., Breitkreutz, J., 2022. Impact of lubrication on key properties of orodispersible minitablets in comparison to conventionally sized orodispersible tablets. European Journal of Pharmaceutics and Biopharmaceutics 180, 71–80. https://doi.org/10.1016/j.ejpb.2022.08.023.
Kulinowski, P., Woyna-Orlewicz, K., Rappen, G.M., Haznar-Garbacz, D., Węglarz, W.P., Dorożyński, P.P., 2015. An understanding of modified release matrix tablets behavior during drug dissolution as the key for prediction of pharmaceutical product performance - Case study of multimodal characterization of quetiapine fumarate tablets. Int J Pharm 484, 235–245. https://doi.org/10.1016/j.ijpharm.2015.02.040.

LaFountaine, J.S., Prasad, L.K., Miller, D.A., McGinity, J.W., Williams, R.O., 2017. Mucoadhesive amorphous solid dispersions for sustained release of poorly water soluble drugs. European Journal of Pharmaceutics and Biopharmaceutics 113, 157–167. https://doi.org/10.1016/J.EJPB.2016.12.031.

Lee, J.H., Park, C., Song, I.O., Lee, B.J., Kang, C.Y., Park, J.B., 2022. Investigation of Patient-Centric 3D-Printed Orodispersible Films Containing Amorphous Aripiprazole. Pharmaceuticals 15. https://doi.org/10.3390/ph15070895.

Li, L., Wang, L., Li, J., Jiang, S., Wang, Y., Zhang, X., Ding, J., Yu, T., Mao, S., 2014. Insights into the mechanisms of chitosan-anionic polymers-based matrix tablets for extended drug release. Int J Pharm 476, 253–265. https://doi.org/10.1016/j.ijpharm.2014.09.057.

Limmatvapirat, S., Panchapornpon, D., Limmatvapirat, C., Nunthanid, J., Luangtana-Anan, M., Puttipipatkhachorn, S., 2008. Formation of shellac succinate having improved enteric film properties through dry media reaction. European Journal of Pharmaceutics and Biopharmaceutics 70, 335–344. https://doi.org/10.1016/J.EJPB.2008.03.002.

Liu, B., Wang, J., Zhou, Q., Zhao, L., Wang, Y., Shen, L., Feng, Y., Du, R., 2022. High shear wet granulation: Improved understanding of the effects of process variables on granule and tablet properties of a high-dose, high-hydrophobicity API based on quality by design and multivariate analysis approaches. Advanced Powder Technology 33. https://doi.org/10.1016/j.apt.2021.11.021.

Lura, A., Breitkreutz, J., 2022. Manufacturing of mini-tablets. Focus and impact of the tooling systems. J Drug Deliv Sci Technol 72. https://doi.org/10.1016/j.jddst.2022.103357.

Lura, A., Tardy, G., Kleinebudde, P., Breitkreutz, J., 2020. Tableting of mini-tablets in comparison with conventionally sized tablets: A comparison of tableting properties and tablet dimensions. Int J Pharm X 2. https://doi.org/10.1016/j.ijpx.2020.100061.

Lura, A., Elezaj, V., Kokott, M., Fischer, B., Breitkreutz, J., 2021. Transfer and scale-up of the manufacturing of orodispersible mini-tablets from a compaction simulator to an industrial rotary tablet press. Int J Pharm 602. https://doi.org/10.1016/j.ijpharm.2021.120636.

Machado, A.H.E., Kokubo, T., Dujovny, G., Jones, B., Scialdone, C., Bravo, R., Kuentz, M., 2016. A microstructural study of water effects in lipid-based pharmaceutical formulations for liquid filling of capsules. European Journal of Pharmaceutical Sciences 90, 64–75. https://doi.org/10.1016/j.ejps.2016.04.035.

Matulyte, I., Marksa, M., Bernatoniene, J., 2021a. Development of innovative chewable gel tablets containing nutmeg essential oil microcapsules and their physical properties evaluation. Pharmaceutics 13. https://doi.org/10.3390/pharmaceutics13060873.

Matulyte, I., Mataraite, A., Velziene, S., Bernatoniene, J., 2021b. The Effect of Myristica fragrans on Texture Properties and Shelf-Life of Innovative Chewable Gel Tablets. Pharmaceutics 13, 238. https://doi.org/10.3390/PHARMACEUTICS13020238.

Mazel, V., Guerard, S., Croquelois, B., Kopp, J.B., Girardot, J., Diarra, H., Busignies, V., Tchoreloff, P., 2016. Reevaluation of the diametral compression test for tablets using the flattened disc geometry. Int J Pharm 513, 669–677. https://doi.org/10.1016/j.ijpharm.2016.09.088.

Mazel, V., Diarra, H., Malvestio, J., Tchoreloff, P., 2018. Lamination of biconvex tablets: Numerical and experimental study. Int J Pharm 542, 66–71. https://doi.org/10.1016/j.ijpharm.2018.03.012.

Meruva, S., Thool, P., Gong, Y., Agrawal, A., Karki, S., Bowen, W., Mitra, B., Kumar, S., 2021. A Novel Use of Nanocrystalline Suspensions to Develop Sub-Microgram Dose Micro-Tablets. J Pharm Sci 110, 3276–3288. https://doi.org/10.1016/j.xphs.2021.05.025.

Mirdamadian, S.Z., Varshosaz, J., Minaiyan, M., Taheri, A., 2022. 3D printed tablets containing oxaliplatin loaded alginate nanoparticles for colon cancer targeted delivery. An in vitro/in vivo study. Int J Biol Macromol 205, 90–109. https://doi.org/10.1016/j.ijbiomac.2022.02.080.

Mitra, B., Hilden, J., Litster, J.D., 2015. Novel use of monodisperse granules to deconvolute impacts of granule size versus granule solid fraction on tablet tensile strength. Advanced Powder Technology 26, 553–562. https://doi.org/10.1016/J.APT.2015.01.004.

Mizrahi, B., Golenser, J., Wolnerman, J.S., Domb, A.J., 2004. Adhesive tablet effective for treating canker sores in humans. J Pharm Sci 93, 2927–2935. https://doi.org/10.1002/jps.20193.

Nazzal, S., Nazzal, M., El-Malah, Y., 2007. A novel texture-probe for the simultaneous and real-time measurement of swelling and erosion rates of matrix tablets. Int J Pharm 330, 195–198. https://doi.org/10.1016/j.ijpharm.2006.08.045.

Nep, E.I., Conway, B.R., 2011. Grewia gum 2: Mucoadhesive properties of compacts and gels. Tropical Journal of Pharmaceutical Research 10, 393–401. https://doi.org/10.4314/tjpr.v10i4.4.

Oladeji, S., Mohylyuk, V., Jones, D.S., Andrews, G.P., 2022. 3D printing of pharmaceutical oral solid dosage forms by fused deposition: The enhancement of printability using plasticised HPMCAS. Int J Pharm 616. https://doi.org/10.1016/j.ijpharm.2022.121553.

Oliver, W.C., Pharr, G.M., 2004. Measurement of hardness and elastic modulus by instrumented indentation: Advances in understanding and refinements to methodology. J Mater Res 19, 3–20. https://doi.org/10.1557/JMR.2004.19.1.3.

Owens, T.S., Dansereau, R.J., Sakr, A., 2005. Development and evaluation of extended release bioadhesive sodium fluoride tablets. Int J Pharm 288, 109–122. https://doi.org/10.1016/J.IJPHARM.2004.09.017.

Owusu-Ware, S.K., Boateng, J., Jordan, D., Portefaix, S., Tasseto, R., Ramano, C.D., Antonijević, M.D., 2016. Molecular mobility of hydroxyethyl cellulose (HEC) films characterised by thermally stimulated currents (TSC) spectroscopy. Int J Pharm 497, 222–227. https://doi.org/10.1016/j.ijpharm.2015.11.052.

Owusu-Ware, S.K., Boateng, J.S., Chowdhry, B.Z., Antonijevic, M.D., 2019. Glassy state molecular mobility and its relationship to the physico-mechanical properties of plasticized hydroxypropyl methylcellulose (HPMC) films. Int J Pharm X 1. https://doi.org/10.1016/j.ijpx.2019.100033.

Partheniadis, I., Athanasiou, K., Laidmäe, I., Heinämäki, J., Nikolakakis, I., 2022. Physicomechanical characterization and tablet compression of theophylline nanofibrous mats prepared by conventional and ultrasound enhanced electrospinning. Int J Pharm 616. https://doi.org/10.1016/j.ijpharm.2022.121558.

Patel, V.F., Liu, F., Brown, M.B., 2012. Modeling the oral cavity: In vitro and in vivo evaluations of buccal drug delivery systems. Journal of Controlled Release 161, 746–756. https://doi.org/10.1016/j.jconrel.2012.05.026.

Patel, S., Sun, C.C., 2016. Macroindentation hardness measurement—Modernization and applications. Int J Pharm 506, 262–267. https://doi.org/10.1016/J.IJPHARM.2016.04.068.

Paul, S., Baranwal, Y., Tseng, Y.C., 2021. An insight into predictive parameters of tablet capping by machine learning and multivariate tools. Int J Pharm 599. https://doi.org/10.1016/j.ijpharm.2021.120439.

Paul, S., Sun, C.C., 2018. Systematic evaluation of common lubricants for optimal use in tablet formulation. European Journal of Pharmaceutical Sciences 117, 118–127. https://doi.org/10.1016/j.ejps.2018.02.013.

Paul, S., Wang, C., Sun, C.C., 2022. An extended macroindentation method for determining the hardness of poorly compressible materials. Int J Pharm 624, 122054. https://doi.org/10.1016/J.IJPHARM.2022.122054.

Peerapattana, J., Ngamsupsiri, T., Cheucharoenvasuchai, N., Saikaew, C., 2015. Optimization of metronidazole sustained-release films using D-optimal design. Int J Pharm 484, 1–7. https://doi.org/10.1016/j.ijpharm.2015.02.019.

Pekoz, A.Y., Erdal, M.S., Okyar, A., Ocak, M., Tekeli, F., Kaptan, E., Sagirli, O., Araman, A., 2015. Preparation and in-vivo evaluation of dimenhydrinate buccal mucoadhesive films with enhanced bioavailability. Drug Dev Ind Pharm 42, 916–925. https://doi.org/10.3109/03639045.2015.1091470.

Perumalla, S.R., Sun, C.C., 2014. Enabling tablet product development of 5-fluorocytosine through integrated crystal and particle engineering. J Pharm Sci 103, 1126–1132. https://doi.org/10.1002/jps.23876.

Picart, L., Mazel, V., Moulin, A., Bourgeaux, V., Tchoreloff, P., 2022. Breaking patterns of press-coated tablets during the diametral compression test: Influence of the product, geometry and process parameters. Int J Pharm 612. https://doi.org/10.1016/j.ijpharm.2021.121371.

Pitt, K.G., Heasley, M.G., 2013. Determination of the tensile strength of elongated tablets. Powder Technol 238, 169–175. https://doi.org/10.1016/j.powtec.2011.12.060.

Pitt, K.G., Newton, J.M., Richardson, R., Stanley, P., 1989. The Material Tensile Strength of Convex-faced Aspirin Tablets. Journal of Pharmacy and Pharmacology 41, 289–292. https://doi.org/10.1111/J.2042-7158.1989.TB06458.X.

Pongjanyakul, T., Khuathan, N., 2016. Quaternary polymethacrylate-sodium alginate films: Effect of alginate block structures and use for sustained release tablets. Pharm Dev Technol 21, 487–498. https://doi.org/10.3109/10837450.2015.1022787.

Prakash, S., Tan, D.D.Y., Chen, J., 2013. Applications of tribology in studying food oral processing and texture perception. Food Research International 54, 1627–1635. https://doi.org/10.1016/j.foodres.2013.10.010.

Prasad, E., Islam, M.T., Goodwin, D.J., Megarry, A.J., Halbert, G.W., Florence, A.J., Robertson, J., 2019. Development of a hot-melt extrusion (HME) process to produce drug loaded Affinisol™ 15LV filaments for fused filament fabrication (FFF) 3D printing. Addit Manuf 29, 100776. https://doi.org/10.1016/J.ADDMA.2019.06.027.

Prasad, L.K., Keen, J.M., Lafountaine, J.S., Maincent, J., Williams, R.O., McGinity, J.W., 2015. Electrostatic powder deposition to prepare films for drug delivery. J Drug Deliv Sci Technol 30, 501–510. https://doi.org/10.1016/j.jddst.2015.08.011.

Preis, M., Gronkowsky, D., Grytzan, D., Breitkreutz, J., 2014a. Comparative study on novel test systems to determine disintegration time of orodispersible films. Journal of Pharmacy and Pharmacology 66, 1102–1111. https://doi.org/10.1111/jphp.12246.

Preis, M., Knop, K., Breitkreutz, J., 2014b. Mechanical strength test for orodispersible and buccal films. Int J Pharm 461, 22–29. https://doi.org/10.1016/j.ijpharm.2013.11.033.

Prodduturi, S., Manek, R. v., Kolling, W.M., Stodghill, S.P., Repka, M.A., 2004. Water vapor sorption of hot-melt extruded hydroxypropyl cellulose films: Effect on physico-mechanical properties, release characteristics, and stability. J Pharm Sci 93, 3047–3056. 10.1002/jps.20222.

Prodduturi, S., Manek, R. v., Kolling, W.M., Stodghill, S.P., Repka, M.A., 2005. Solid-state stability and characterization of hot-melt extruded poly(ethylene oxide) films. J Pharm Sci 94, 2232–2245. 10.1002/jps.20437.

Pund, S., Joshi, A., Vasu, K., Nivsarkar, M., Shishoo, C., 2011. Gastroretentive delivery of rifampicin: In vitro mucoadhesion and in vivo gamma scintigraphy. Int J Pharm 411, 106–112. https://doi.org/10.1016/j.ijpharm.2011.03.048.

Qi, X., Tester, R., Liu, Y., Mullin, M., 2012. Applications of β-limit Dextrin as a Matrix Forming Excipient for Fast Disintegrating Buccal Dosage Formats. Journal of Pharmacy & Pharmaceutical Sciences 15, 669–679. https://doi.org/10.18433/J3RC8M.

Radebaugh, G.W., Murtha, J.L., Julian, T.N., Bondi, J.N., 1988. Methods for evaluating the puncture and shear properties of pharmaceutical polymeric films. Int J Pharm 45, 39–46. https://doi.org/10.1016/0378-5173(88)90032-4.

Rahman, Z., Zidan, A.S., Korang-Yeboah, M., Yang, Y., Siddiqui, A., Shakleya, D., Khan, M.A., Cruz, C., Ashraf, M., 2017. Effects of excipients and curing process on the abuse deterrent properties of directly compressed tablets. Int J Pharm 517, 303–311. https://doi.org/10.1016/j.ijpharm.2016.12.015.

Rai, P.R., Tiwary, A.K., Rana, V., 2012. Optimization of an aqueous tablet-coating process containing carboxymethylated Cassia fistula gum. AAPS PharmSciTech 13, 431–440. https://doi.org/10.1208/s12249-012-9763-x.

Repka, M.A., Elsohly, M.A., Munjal, M., Ross, S.A., 2006. Temperature Stability and Bioadhesive Properties of Δ9-Tetrahydrocannabinol Incorporated Hydroxypropylcellulose Polymer Matrix Systems. Drug Dev Ind Pharm 32, 21–32. https://doi.org/10.1080/03639040500387914.

Rodríguez-Pombo, L., Awad, A., Basit, A.W., Alvarez-Lorenzo, C., Goyanes, A., 2022. Innovations in Chewable Formulations: The Novelty and Applications of 3D Printing in Drug Product Design. Pharmaceutics 14, 1732. https://doi.org/10.3390/PHARMACEUTICS14081732/S1.

Rongthong, T., Sungthongjeen, S., Siepmann, J., Pongjanyakul, T., 2013. Quaternary polymethacrylate–magnesium aluminum silicate films: Molecular interactions, mechanical properties and tackiness. Int J Pharm 458, 57–64. https://doi.org/10.1016/J.IJPHARM.2013.10.016.

Saab, M., Mehanna, M.M., 2019. Disintegration time of orally dissolving films: Various methodologies and in-vitro/in-vivo correlation. Pharmazie 74, 227–230. https://doi.org/10.1691/ph.2019.8231.

Sabri, A.H., Hallam, C.N., Baker, N.A., Murphy, D.S., Gabbott, I.P., 2018. Understanding tablet defects in commercial manufacture and transfer. J Drug Deliv Sci Technol 46, 1–6. https://doi.org/10.1016/j.jddst.2018.04.020.

Sakloetsakun, D., Preechagoon, D., Bernkop-Schnürch, A., Pongjanyakul, T., 2016. Chitosan–gum arabic polyelectrolyte complex films: physicochemical, mechanical and mucoadhesive properties. Pharm Dev Technol 21, 590–599. https://doi.org/10.3109/10837450.2015.1035727.

Salawi, A., Sonju, J.J., Kamal, M.M., Abu-Fayyad, A., al Hagbani, T., Nazzal, S., 2021. Preparation and characterization of aqueous vitamin E/Soluplus® dispersions for film coating applications. Drug Dev Ind Pharm 47, 1335–1341. 10.1080/03639045.2021.1991367.

Samaro, A., Janssens, P., Vanhoorne, V., van Renterghem, J., Eeckhout, M., Cardon, L., de Beer, T., Vervaet, C., 2020. Screening of pharmaceutical polymers for extrusion-Based Additive Manufacturing of patient-tailored tablets. Int J Pharm 586. https://doi.org/10.1016/j.ijpharm.2020.119591.

Samaro, A., Shaqour, B., Goudarzi, N.M., Ghijs, M., Cardon, L., Boone, M.N., Verleije, B., Beyers, K., Vanhoorne, V., Cos, P., Vervaet, C., 2021. Can filaments, pellets and powder be used as feedstock to produce highly drug-loaded ethylene-vinyl acetate 3D printed tablets using extrusion-based additive manufacturing? Int J Pharm 607. https://doi.org/10.1016/j.ijpharm.2021.120922.

Sankar, R., Jain, S.K., 2013. Development and characterization of gastroretentive sustained-release formulation by combination of swelling and mucoadhesive approach: A mechanistic study. Drug Des Devel Ther 7, 1455–1469. https://doi.org/10.2147/DDDT.S52890.

Scheuerle, R.L., Gerrard, S.E., Kendall, R.A., Tuleu, C., Slater, N.K.H., Mahbubani, K.T., 2015. Characterising the disintegration properties of tablets in opaque media using texture analysis. Int J Pharm 486, 136–143. https://doi.org/10.1016/j.ijpharm.2015.03.023.

Schmidt, L.M., dos Santos, J., de Oliveira, T.V., Funk, N.L., Petzhold, C.L., Benvenutti, E. V., Deon, M., Beck, R.C.R., 2022. Drug-loaded mesoporous silica on carboxymethyl cellulose hydrogel: Development of innovative 3D printed hydrophilic films. Int J Pharm 620. https://doi.org/10.1016/j.ijpharm.2022.121750.

Schreuders, F.K.G., Schlangen, M., Kyriakopoulou, K., Boom, R.M., van der Goot, A.J., 2021. Texture methods for evaluating meat and meat analogue structures: A review. Food Control 127. https://doi.org/10.1016/j.foodcont.2021.108103.

Şenel, S., Çapan, Y., Sargon, M.F., Giray, C.B., Hincal, A.A., 1998. Histological and bioadhesion studies on buccal bioadhesive tablets containing a penetration enhancer sodium glycodeoxycholate. Int J Pharm 170, 239–245. https://doi.org/10.1016/S0378-5173(98)00148-3.

Shakweh, M., Bravo-Osuna, I., Ponchel, G., 2007. Comparative in vitro study of oesophageal adhesiveness of different commercial formulations containing alendronate. European Journal of Pharmaceutical Sciences 31, 262–270. https://doi.org/10.1016/J.EJPS.2007.03.012.

Sharma, O.P., Shah, M. v., Parikh, D.C., Mehta, T.A., 2015. Formulation optimization of gastroretentive drug delivery system for allopurinol using experimental design. Expert Opin Drug Deliv 12, 513–524. 10.1517/17425247.2014.944861.

Shumeyko, C.M., Dunstan, M., Goins, P., Yin, D., Cline, J.E., Dunstan, M.K., Goins, P.E., Field, D.M., 2019. Snap, crackle and pop: breaking chocolate to understand composite design. Journal of Materials Education 41, 27–40.

Singh, I., Rana, V., 2013. Iron oxide induced enhancement of mucoadhesive potential of Eudragit RLPO: Formulation, evaluation and optimization of mucoadhesive drug delivery system. Expert Opin Drug Deliv 10, 1179–1191. https://doi.org/10.1517/17425247.2013.790361.

Singh, I., Rana, V., 2014. Exploiting the interaction of polymethacrylates with iron oxide for the enhancement of mucoadhesive strength. Pak J Pharm Sci 27, 343–350.

Speer, I., Lenhart, V., Preis, M., Breitkreutz, J., 2019. Prolonged release from orodispersible films by incorporation of diclofenac-loaded micropellets. Int J Pharm 554, 149–160. https://doi.org/10.1016/j.ijpharm.2018.11.013.

Stokes, J.R., Boehm, M.W., Baier, S.K., 2013. Oral processing, texture and mouthfeel: From rheology to tribology and beyond. Curr Opin Colloid Interface Sci 18, 349–359. https://doi.org/10.1016/j.cocis.2013.04.010.

Stomberg, C., Kanikanti, V.R., Hamann, H.J., Kleinebudde, P., 2017. Development of a New Dissolution Test Method for Soft Chewable Dosage Forms. AAPS PharmSciTech 18, 2446–2453. https://doi.org/10.1208/s12249-017-0729-x.

Szabó, B., Sebe, I., Kállai, N., Süvegh, K., Zelkó, R., 2013. Comparison of the micro- and macrostructural characteristics of biopolymer cast films. Eur Polym J 49, 2422–2425. https://doi.org/10.1016/J.EURPOLYMJ.2013.03.033.

Szakonyi, G., Zelkó, R., 2013. Prediction of oral disintegration time of fast disintegrating tablets using texture analyzer and computational optimization. Int J Pharm 448, 346–353. https://doi.org/10.1016/j.ijpharm.2013.03.047.

Szekalska, M., Amelian, A., Winnicka, K., 2015. Alginate microspheres obtained by the spray drying technique as mucoadhesive carriers of ranitidine. Acta Pharmaceutica 65, 15–27. https://doi.org/10.1515/acph-2015-0008.

TA.XTplus Texture Analyser | Stable Micro Systems Products [WWW Document], n.d. URL https://www.stablemicrosystems.com/TAXTplus.html (accessed 1.31.23).

Tabriz, A.G., Scoutaris, N., Gong, Y., Hui, H.W., Kumar, S., Douroumis, D., 2021. Investigation on hot melt extrusion and prediction on 3D printability of pharmaceutical grade polymers. Int J Pharm 604, 120755. https://doi.org/10.1016/J.IJPHARM.2021.120755.

Tamburic, S., Craig, D.Q.M., 1997. A comparison Research paper of different in vitro methods mucoadhesive performance for measuring. European Journal of Pharmaceutics and Biopharmaceutics 44, 159–167.

Texture Profile Analysis | Texture Technologies [WWW Document], n.d. URL https://texturetechnologies.com/resources/texture-profile-analysis#tpa-measurements (accessed 1.31.23).

Than, Y.M., Titapiwatanakun, V., 2021. Tailoring immediate release FDM 3D printed tablets using a quality by design (QbD) approach. Int J Pharm 599. https://doi.org/10.1016/j.ijpharm.2021.120402.

Thirawong, N., Nunthanid, J., Puttipipatkhachorn, S., Sriamornsak, P., 2007. Mucoadhesive properties of various pectins on gastrointestinal mucosa: An in vitro evaluation using texture analyzer. European Journal of Pharmaceutics and Biopharmaceutics 67, 132–140. https://doi.org/10.1016/j.ejpb.2007.01.010.

Tidau, M., Finke, J.H., 2022. Modified release kinetics in dual filament 3D printed individualized oral dosage forms. European Journal of Pharmaceutical Sciences 175, 106221. https://doi.org/10.1016/J.EJPS.2022.106221.

Tomas, J., Schöngut, M., Dammer, O., Beránek, J., Zadražil, A., Štěpánek, F., 2018. Probing the early stages of tablet disintegration by stress relaxation measurement. European Journal of Pharmaceutical Sciences 124, 145–152. https://doi.org/10.1016/j.ejps.2018.08.029.

Vanbillemont, B., de Beer, T., 2020. Application of polyvinyl acetate in an innovative formulation strategy for lyophilized orally disintegrating tablets. Int J Pharm 588. https://doi.org/10.1016/j.ijpharm.2020.119717.

Vanbillemont, B., Everaert, H., de Beer, T., 2020. New advances in the characterization of lyophilised orally disintegrating tablets. Int J Pharm 579. https://doi.org/10.1016/j.ijpharm.2020.119153.

Viidik, L., Vesala, J., Laitinen, R., Korhonen, O., Ketolainen, J., Aruväli, J., Kirsimäe, K., Kogermann, K., Heinämäki, J., Laidmäe, I., Ervasti, T., 2021. Preparation and characterization of hot-melt extruded polycaprolactone-based filaments intended for 3D-printing of tablets. European Journal of Pharmaceutical Sciences 158. https://doi.org/10.1016/j.ejps.2020.105619.

Vo, A.Q., Zhang, J., Nyavanandi, D., Bandari, S., Repka, M.A., 2020. Hot melt extrusion paired fused deposition modeling 3D printing to develop hydroxypropyl cellulose based floating tablets of cinnarizine. Carbohydr Polym 246. https://doi.org/10.1016/j.carbpol.2020.116519.

Volod'ko, A. v., Davydova, V.N., Petrova, V.A., Romanov, D.P., Pimenova, E.A., Yermak, I.M., 2021. Comparative Analysis of the Functional Properties of Films Based on Carrageenans, Chitosan, and Their Polyelectrolyte Complexes. Mar Drugs 19, 704. 10.3390/MD19120704.

Vreeman, G., Sun, C.C., 2022a. A powder tabletability equation. Powder Technol 408. https://doi.org/10.1016/j.powtec.2022.117709.

Vreeman, G., Sun, C.C., 2022b. Air entrapment during tablet compression – Diagnosis, impact on tableting performance, and mitigation strategies. Int J Pharm 615. https://doi.org/10.1016/j.ijpharm.2022.121514.

Walicová, V., Gajdziok, J., Pavloková, S., Vetchý, D., 2016. Design and evaluation of mucoadhesive oral films containing sodium hyaluronate using multivariate data analysis. Pharm Dev Technol 22, 229–236. https://doi.org/10.1080/10837450.2016.1194857.

Wang, C., Hu, S., Sun, C.C., 2017a. Expedited development of a high dose orally disintegrating metformin tablet enabled by sweet salt formation with acesulfame. Int J Pharm 532, 435–443. https://doi.org/10.1016/j.ijpharm.2017.08.100.

Wang, C., Hu, S., Sun, C.C., 2017b. Expedited Development of Diphenhydramine Orally Disintegrating Tablet through Integrated Crystal and Particle Engineering. Mol Pharm 14, 3399–3408. https://doi.org/10.1021/ACS.MOLPHARMACEUT.7B00423/SUPPL_FILE/MP7B00423_SI_001.PDF.

Wang, Z., Li, J., Hong, X., Han, X., Liu, B., Li, X., Zhang, H., Gao, J., Liu, N., Gao, X., Zheng, A., 2021. Taste Masking Study Based on an Electronic Tongue: the Formulation Design of 3D Printed Levetiracetam Instant-Dissolving Tablets. Pharm Res 38, 831–842. https://doi.org/10.1007/S11095-021-03041-9/FIGURES/12.

Wening, K., Breitkreutz, J., 2010. Novel delivery device for monolithical solid oral dosage forms for personalized medicine. Int J Pharm 395, 174–181. https://doi.org/10.1016/j.ijpharm.2010.05.036.

Woertz, C., Preis, M., Breitkreutz, J., Kleinebudde, P., 2013. Assessment of test methods evaluating mucoadhesive polymers and dosage forms: An overview. European Journal of Pharmaceutics and Biopharmaceutics 85, 843–853. https://doi.org/10.1016/J.EJPB.2013.06.023.

Xu, P., Li, J., Meda, A., Osei-Yeboah, F., Peterson, M.L., Repka, M., Zhan, X., 2020. Development of a quantitative method to evaluate the printability of filaments for fused deposition modeling 3D printing. Int J Pharm 588. https://doi.org/10.1016/j.ijpharm.2020.119760.

Zhang, J., Feng, X., Patil, H., Tiwari, R. v., Repka, M.A., 2017. Coupling 3D printing with hot-melt extrusion to produce controlled-release tablets. Int J Pharm 519, 186–197. 10.1016/J.IJPHARM.2016.12.049.

Zhang, Y., Li, Y.P., Wu, F., Hong, Y.L., Shen, L., Lin, X., Feng, Y., 2021. Texture and surface feature-mediated striking improvements on multiple direct compaction properties of Zingiberis Rhizoma extracted powder by coprocessing with nano-silica. Int J Pharm 603. https://doi.org/10.1016/j.ijpharm.2021.120703.

Zhang, Y., Li, J., Gao, Y., Wu, F., Hong, Y., Shen, L., Lin, X., 2022c. Improvements on multiple direct compaction properties of three powders prepared from Puerariae Lobatae Radix using surface and texture modification: Comparison of microcrystalline cellulose and two nano-silicas. Int J Pharm 622. https://doi.org/10.1016/j.ijpharm.2022.121837.

Zhang, B., Teoh, X.Y., Yan, J., Gleadall, A., Belton, P., Bibb, R., Qi, S., 2022a. Development of combi-pills using the coupling of semi-solid syringe extrusion 3D printing with fused deposition modelling. Int J Pharm 625. https://doi.org/10.1016/j.ijpharm.2022.122140.

Zhang, J., Xu, P., Vo, A.Q., Bandari, S., Yang, F., Durig, T., Repka, M.A., 2019. Development and evaluation of pharmaceutical 3D printability for hot melt extruded cellulose-based filaments. J Drug Deliv Sci Technol 52, 292–302. https://doi.org/10.1016/j.jddst.2019.04.043.

Zhang, J., Thakkar, R., Zhang, Y., Maniruzzaman, M., 2020. Structure-function correlation and personalized 3D printed tablets using a quality by design (QbD) approach. Int J Pharm 590. https://doi.org/10.1016/j.ijpharm.2020.119945.

Zhang, P., Xu, P., Chung, S., Bandari, S., Repka, M.A., 2022b. Fabrication of bilayer tablets using hot melt extrusion-based dual-nozzle fused deposition modeling 3D printing. Int J Pharm 624. https://doi.org/10.1016/j.ijpharm.2022.121972.

Zhao, H., Yu, Y., Ni, N., Zhao, L., Lin, X., Wang, Y., Du, R., Shen, L., 2022. A new parameter for characterization of tablet friability based on a systematical study of five excipients. Int J Pharm 611. https://doi.org/10.1016/j.ijpharm.2021.121339.

Zhou, Z., Li, W., Sun, W.J., Lu, T., Tong, H.H.Y., Sun, C.C., Zheng, Y., 2016. Resveratrol cocrystals with enhanced solubility and tabletability. Int J Pharm 509, 391–399. https://doi.org/10.1016/j.ijpharm.2016.06.006.

European Journal of Pharmaceutical Sciences 198 (2024) 106801

Contents lists available at ScienceDirect

European Journal of Pharmaceutical Sciences

journal homepage: www.elsevier.com/locate/ejps

Testing the disintegration and texture-related palatability predictions for orodispersible tablets using an instrumental tool coupled with multivariate analysis: Focus on process variables and analysis settings

Rareș Iovanov [a], Andreea Cornilă [a,*], Cătălina Bogdan [b], Dana Hales [a], Ioan Tomuță [a], Marcela Achim [a], Andrada Tăut [a], Nela Iman [a], Tibor Casian [a,1], Sonia Iurian [a,1]

[a] Department of Pharmaceutical Technology and Biopharmacy, Faculty of Pharmacy, "Iuliu Hațieganu" University of Medicine and Pharmacy, 41 Victor Babeș Street, Cluj-Napoca, Romania
[b] Department of Dermopharmacy and Cosmetics, Faculty of Pharmacy, "Iuliu Hațieganu" University of Medicine and Pharmacy, 12 Ion Creangă Street, Cluj-Napoca, Romania

ARTICLE INFO

Keywords:
Texture analysis
Prediction capacity
Texture profile
In vivo disintegration
Principal component analysis
acceptability

ABSTRACT

Orodispersible tablets (ODTs) represent a growing category of dosage forms intended to increase the treatment acceptability for special groups of patients. ODTs are designed to rapidly disintegrate in the oral cavity and to be administered without water. In addition, ODTs are easy to manufacture using standard excipients and pharmaceutical equipment.

This study adds to previously published research that developed an instrumental tool to predict oral disintegration and texture-related palatability of ODTs with different formulations. The current study aimed to challenge the predictive capacity of the models under variable process conditions. The studied process parameters with potential impact on the pharmaceutical properties, texture profiles, and palatability were the compression pressure, punch shape and diameter. Subsequently, for all the *placebo* and drug-loaded ODTs, the *in vivo* disintegration time and texture-related palatability were determined with healthy volunteers.

Previously developed regression models were applied to predict the formulation's disintegration time and texture-related palatability characteristics of ODTs obtained under different experimental conditions. The influence of process variables on the predictive performance of the models was estimated by calculating the residuals as the difference between the predicted and observed values for the investigated response. Increasing the speed of the analyser`s probe from 0.01 mm/s to 0.02 mm/s led to an improved differentiation of the texture profiles. The *in vivo* disintegration time and texture-related palatability scores were only influenced by the mechanical resistance and the tablet shape. Lower score was observed for the larger diameter tablets (10 mm). Overall, the prediction of the disintegration time at 0.02 mm/s was more accurate, except for stronger tablets. The best prediction of texture-related palatability was achieved for the 10 mm tablets, tested at 0.01 mm/s speed.

The same model achieved good predictions of the oral disintegration time for all API-loaded formulations, which confirmed the ability of the texture analysis to capture process-related variability. Drug loading decreased the predictive capacity of the texture-related palatability because of the taste effect.

1. Introduction

In recent years, the pharmaceutical industry shifted towards the manufacturing of easily acceptable dosage forms for those particular groups of patients dealing with therapeutic inefficacy due to poor treatment adherence, which led to the development of orodispersible dosage forms (ODFs). ODFs can be easily swallowed after disintegration in the oral cavity, without the need for additional water, resulting in increased patient acceptability (Bashir et al., 2023; Chauhan et al., 2018). Their production is simple, cost-effective, and uses common manufacturing equipment, common excipients, and packaging materials. Considering these advantages, the pharmaceutical industry

* Corresponding author.
E-mail address: ioana.an.cornila@elearn.umfcluj.ro (A. Cornilă).
[1] Last joint co-authors.

https://doi.org/10.1016/j.ejps.2024.106801
Received 16 June 2023; Received in revised form 18 March 2024; Accepted 14 May 2024
Available online 15 May 2024

responded with the development of ODFs as alternatives to conventional oral dosage forms (Casian et al., 2018a).

At the same time, Food and Drug Administration (FDA) and European Medicines Agency (EMA) proposed the Quality by Design (QbD) approach to drug development. This paradigm aims to ensure the quality of the drug product starting from the design to the pre-formulation step and throughout the manufacturing process, through in-line process monitoring. One of the crucial stages of this strategy is establishing a quality target product profile (QTPP) and the critical quality attributes (CQAs) of the developed drug product and then, a set of quality control methods for every CQA (Casian et al., 2018a; Suryawanshi et al., 2021).

Currently, orodispersible tablets (ODTs) are tempting to manufacturers due to their advantages over conventional tablets: first, they can be swallowed just as easily as liquid dosage forms in a few seconds after their contact with the saliva, which recommends them for patients like paediatrics or geriatrics. Furthermore, fast onset of action and bioavailability increase were reported for some active pharmaceutical ingredients (APIs), due to their absorption via the oral mucosa. (Abd Elbary et al., 2016; Ahmed, 2021; Haraguchi et al., 2016; Kokott et al., 2021; Kumar Gupta et al., 2020). Their main disadvantages are the poor mechanical properties and the requirement for dedicated packaging materials (Abay and Ugurlu, 2015; Chauhan et al., 2018; Kumar Gupta et al., 2020). Various processes, such as freeze-drying, phase transition, sublimation, and direct compression, can be used in the manufacturing of ODTs. Out of all of them, direct compression is the easiest, most accessible and cost-efficient method, as well as one of the most well-known and thoroughly understood by manufacturers (Abay and Ugurlu, 2015; Kumar Gupta et al., 2020). Direct compression follows two simple steps and uses various excipients: diluents, disintegrants, sweeteners, flavouring agents, and/or co-processed mixtures. To be suitable for direct compression, the excipients must meet certain criteria regarding powder granulometry, rheological properties and water solubility (Abay and Ugurlu, 2015; Augsburger and Zellhofer, 2007).

The defining characteristic of ODTs is their swift disintegration, because of which the disintegration time becomes the main CQA, as its value, among others, determines whether a dosage form is orodispersible or not. The limit for the disintegration time of ODTs established by the United States Pharmacopoeia (USP) is 30 s, while a limit of three minutes is mentioned by the European Pharmacopoeia (Ph. Eur.) (Abay and Ugurlu, 2015; Bashir et al., 2023; Rameesa and Drisya, 2015). Due to the difference between these requirements, the products can be subject to a large variability, leading to difficulties in their classification and comparison. Furthermore, the compendial assessment of the disintegration time of ODTs coincides with the one used for conventional tablets, even though the *in vivo* conditions are contrasting due to the very different disintegration conditions in terms of pH, composition, and volume of the disintegration media. The poor *in vitro-in vivo* correlation has been repeatedly reported in the literature, while many researchers tried to find a better alternative to the official pharmacopeial test (Casian et al., 2018a; Hooper et al., 2016). The main deficiency of the pharmacopeial disintegration test is the large volume of the disintegration media (900 ml for conventional tablets), which is an excessive amount compared to the low volume of saliva (approx. 1 ml) in the oral cavity (Hooper et al., 2016). To address this, wetting tests have been proposed to simulate *in vivo* conditions through the placement of the tablet on a piece of filter paper submerged in a small amount of water (2–10 ml). The results were comparable to the disintegration test, although an accurate *in vitro-in vivo* correlation cannot be established due to the lack of movement resembling the force applied by the tongue (Casian et al., 2018a).

Another testing strategy, used by Abd Elbary et al., involved the use of a texture analyser and different disintegration media and temperature conditions to simulate the pressure applied *in vivo* on the pharmaceutical product (Abd Elbary et al., 2005). The distance-time graphs precisely captured the beginning and end of the disintegration process, in a measurement that easily correlated to the *in vivo* data, proving that the system accurately simulated the *in vivo* conditions (Abd Elbary et al., 2012). Further, Szakonyi and Zelkó (Szakonyi and Zelkó, 2013) extended the texture analysis to ODTs with different disintegration mechanisms, addressing different groups of patients whose diseases can impact the oral disintegration of medicines and therefore, the testing parameters. In addition, by means of statistical tools, the formulation with the best performance in xerostomic patients was predicted (Casian et al., 2018a).

Another CQA of ODTs is their palatability, defined through an overall evaluation of the tablet, regarding its taste, texture, smell, and residue left after its disintegration. Because of the subjective nature of this parameter, it is heavily impacted by interindividual variability (Asiri et al., 2021). Our research group developed a texture analysis-based disintegration test that achieved the palatability prediction on *placebo* ODTs with variable compositions through multivariate correlations (Casian et al., 2018a). Predicting the palatability and *in vivo* disintegration time of ODTs using instrumental methods can be challenging, considering that various dosage form-related factors will influence the recorded instrumental data without changing the targeted responses. Thus, robust prediction tools should be developed to enable a correct estimation of the tablet's *in vivo* behaviour, even if the size and shape of the tablet are different. Moreover, depending on the size of the tablet, the optimal speed settings might change during the evaluation. For instance, at lower testing speeds, the disintegration profiles of mini-tablets/fast disintegrating formulations might not capture the associated phenomena or effects, as the product will lose its structural integrity faster than the probe can move.

Up to this point, several studies have evaluated the influence of formulation factors (such as fillers, disintegrants, binders etc.) on the pharmaceutical properties and *in vivo* disintegration of ODTs. However, to the best knowledge of the authors, no studies have investigated the effect of process variables, such as the compression pressure, punch shape and die diameter, on the performance of alternative disintegration methods. Therefore, the objective of the study was to investigate the influence of process variables and testing parameters of the texture analysis on the prediction accuracy of *in vivo* characteristics (disintegration time and texture-related palatability) using a previously validated method (Casian et al., 2018a). The study was carried out on both *placebo* and API-loaded ODTs, which were assessed by a group of healthy volunteers for disintegration time and texture-related palatability scores, subsequently correlated with the instrumental results obtained through texture analysis.

2. Materials and methods

2.1. Materials

For the manufacturing of the *placebo* ODTs, the following materials have been used: mannitol (Man) (Parteck M200, Merck, Germany), microcrystalline cellulose (MCC) (Avicel PH-101 Merck, Germany), croscarmellose sodium (CCS) (FMC Biopolymer, Belgium), ascorbic acid (Fagron, Spain), food grade turmeric powder (Niavis, Romania), aspartame (Ajinamoto, Japan), sodium saccharin (FoodChem, China), magnesium stearate (MgSt) (Merck, Germany).

2.2. Methods

2.2.1. ODT manufacturing

The flowability of *placebo* and API loaded formulations was assessed with the BEP2 powder flow tester (Copley Scientific, United Kingdom) and the SVM tapped density tester (Erweka GmbH, Germany). The angle of repose, Hausner ratio and compressibility index were calculated for all formulations.

The *placebo* ODTs used in this study were formulated according to a previous research study (Casian et al., 2018a) and manufactured through direct compression. A mass of 200 mg was selected for the ODT

manufacturing, considering the maximum weight recommended by the FDA, of 500 mg, and the fact that ODTs are usually small and loaded with small amounts of API (Guidance for Industry Orally Disintegrating Tablets, 2008). The qualitative and quantitative composition of the tablets is presented in Table 1.

The excipients were mixed in the double cone mixer DKM (Erweka, Germany) in the following manner: the first cycle involved the mixing for 5 min at 50 rpm of the fillers (Man, MCC), the superdisintegrant (CCS) and the sweeteners (aspartame, sodium saccharin), then MgSt was added, and mixed for 3 additional minutes. The final powder mixture was compressed in the eccentric tablet press EK0 (Korsch, Germany) with varying compression forces and using punches with different shapes and diameters, according to the data presented in Table 2.

Two levels of variation have been used for the compression pressure: corresponding to tablet hardness of approximately 30 N (F1) and above 50 N (F2), respectively. Both formulations (F1 and F2) were flat 9 mm tablets. The diameter of the die was the second studied parameter. For this purpose, different dies with 8, 9 and 10 mm diameters have been used to obtain three formulations: F1, F3 and F4. The third process variable whose influence was studied was the shape of the compression punch: 9 mm flat punch (F1) and a 9 mm biconvex punch (F5), both compressed to get a tablet hardness of 30 N.

Tablets with the same characteristics as the *placebo* formulations, obtained through the aforementioned process (Table 2) were loaded with two APIs, ascorbic acid and turmeric powder, at two different ratios of 10% and 20%. 20 API -loaded formulations resulted, as shown in Table S1 (Supplementary material) from the powder blends with the flow characteristics listed in Table S2 (Supplementary material). Ascorbic acid is a largely used food supplement that has a tart taste, resemblant of citrus fruits, usually formulated in chewable formulations, where its taste is tempered by the addition of sweetening agents. On the other side, turmeric, although used in multiple food supplements and known for the health benefits provided by the curcuminoids it contains (Nguyen et al., 2017), is more frequently used as a spice, having an easily recognizable umami taste.

2.2.2. Pharmaceutical evaluation of the placebo ODTs

2.2.2.1. Uniformity of mass. The uniformity of mass evaluation was done according to the Ph. Eur. (European Directorate for the Quality of Medicines, n.d.) and involves two weighing steps: first, 20 randomly chosen tablets are weighed together to calculate the average mass, then the tablets are weighed individually with the same scale. No more than two tablets should deviate from the average mass more than the allowed percentage and none of them ought to deviate more than twice the allowed percentage.

2.2.2.2. Hardness. The determination of tablet hardness has been performed on 10 tablets from each batch, using the Pharmatron 6D (Dr. Schleuniger, Germany) hardness tester. The obtained values were used to calculate the mean hardness and standard deviation.

2.2.2.3. Friability. For this measurement, 20 tablets were weighed before and after being tumbled for 5 min at 20 rpm in the TA 10 friability tester (Erweka, Germany), and the lost mass was quantified as a percent of the initial mass.

Table 1
The qualitative and quantitative composition of placebo ODTs.

Excipient	% of mixture mass
Mannitol	70.5
Microcrystalline cellulose	23.5
Croscarmellose sodium	3.0
Aspartame	1.0
Sodium saccharin	1.0
Magnesium stearate	1.0

Table 2
The process variables used for the ODT formulations.

Formulation	Compression force	Die diameter (mm)	Punch shape
F1	low	9	Flat
F2	high	9	Flat
F3	low	8	Flat
F4	low	10	Flat
F5	low	9	Biconvex

• Compression pressure corresponding to tablet hardness of approximately 30 N (low) and above 50 N (high),.

2.2.2.4. Disintegration time. For the *in vitro* assessment, 6 tablets from each batch were put into the basket of the ZT 2 disintegration tester (Erweka, Germany), using 900 ml of distilled water maintained at 37 ± 0.5 °C. The disintegration time was recorded only when the tablet had been completely disintegrated, without any remnants in the basket. The values were used to calculate the average disintegration time of every formulation.

2.2.3. Texture analysis

The *placebo* and API-loaded ODTs were evaluated with the CT3 Texture analyser (Brookfield Engineering, USA) with a 4500 g load cell, according to the method described in our previous study (Casian et al., 2018a). For the test to be as simple and reproducible as possible, water has been used instead of simulated salivary fluid, following protocols from other studies (Dor and Fix, 2000; El-Arini and Clas, 2002). Briefly, the ODT was attached to the acrylic probe (Brookfield TA10, 12.72 mm diameter) with a thin glue layer. Under the probe, a Petri dish (34.78 mm diameter) containing 4.5 ml of distilled water was placed, with a stainless steel mesh (26.8 mm diameter, 2.26 mm height and 1.5 mm aperture) inside, so that the water forms a continuous liquid layer at the surface of the mesh. Two different experimental settings were used, corresponding to two compression tests performed at different probe speeds. First, a probe speed of 0.02 mm/s was used, and secondly, a speed of 0.01 mm/s. When the probe with the attached sample reached a trigger load of 10 g, the measurement started; the test stopped when the tablet was completely disintegrated, and the probe touched the flat surface. For both tests, the plots of load (g) *versus* time (s) were recorded using TexturePro software (Brookfield Engineering, USA) for at least 3 tablets of each formulation. Fig. 1 shows the experimental setup for ODTs analysis.

2.2.4. In vivo ODT evaluation

The studies were conducted in conformity with the Helsinki Declaration regarding ethical principles for medical research involving human subjects and after obtaining the approval from the Ethics Committee of the "Iuliu Haţieganu" University of Medicine and Pharmacy in Cluj-Napoca, Romania. The study on *placebo* ODTs was approved under Approval no. 315/21.07.2016, while the one on API-loaded ODTs under Approval no. AVZ254/28.09.2023. The five formulations (F1-F5) of *placebo* ODTs were administered to 36 volunteers (8 males, 28 females) with ages between 14 and 58, while the API-loaded formulations were tested by 6 volunteers (2 males, 4 females) aged between 26 and 42. The subjects included in both studies were healthy volunteers, without any chronic or acute illnesses and with not impaired taste sensitivity. Before the study, all the subjects signed a consent form and received information regarding the rules they should follow for the study to run properly.

The subjects were asked not to consume any food for two hours before the evaluation. After rinsing their oral cavity with 50 ml of water, each subject placed one tablet on their tongue, in random order. They have been allowed to lightly move their tongues, being advised not to chew or crush the tablet, to avoid accelerating its disintegration. The time to complete disintegration was recorded using a digital stopwatch.

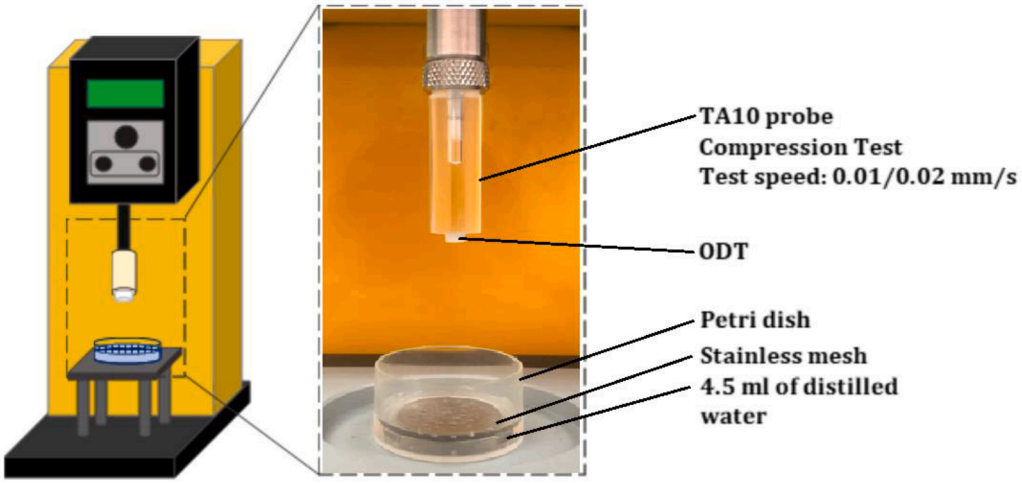

Fig. 1. Experimental setup for the assessment of ODTs.

For the texture-related palatability scores, the volunteers assigned a score of 0 to unpleasant tablets indicating low palatability and 1 to acceptable tablets showing high palatability. At the end of the test, the residue was evacuated, the oral cavity was rinsed with 50 ml of water, the procedure being repeated for all the formulations with 10 min of washout time.

2.2.5. Multivariate data analysis

Multivariate data analysis has been performed with SIMCA17 (Sartorius Stedim Data Analytics AB, Sweden). The prediction of the disintegration time and of the texture-related palatability score (Y variables) was evaluated using the previously developed PLS regression models. The calibration procedure used to develop these models was previously published by our research group (Casian et al., 2018a). The current prediction set was based on the formulations F1 – F5 described in Table 1. The quality of predictions was evaluated on two alternative models, considering a complete load *vs* time profile (not just the optimized domain) and a logarithmic variable transformation. To this respect, the X variables (time points) were centred, whereas the Y variables (were scaled to unit variance). Model performance was determined using the quality of fit (R^2), the predictive performance (Q^2) in relation to the number of principal components, and the root-mean-squared error of cross-validation (RMSECV) (Casian et al., 2018b).

To investigate the effect of probe speed and model type on the prediction errors for different formulations, PCA models were generated using as input variables the residuals of each observation. Residuals were calculated as the difference between the predicted and theoretical values. Biplots were generated by simultaneously representing the scores and loadings, enabling an easier visualization and interpretation of differences between observations in terms of variables.

3. Results and discussions

3.1. The influence of process parameters on the pharmaceutical properties of ODT formulations

Before ODT preparation, powder flow results showed that all powders had angles of repose below 30 ° This was expected since both diluents were grades for direct compression. The influence of ascorbic acid was negligible, while the turmeric powder increased the angle of repose; nevertheless, all the drug-loaded powders remained in the "excellent flow" category. The directly compressed *placebo* ODTs investigated in this study had the same qualitative and quantitative composition. However, the five formulations varied by one of the following process variables at a time: compression force, die diameter, and punch shape. The results of the pharmaceutical analysis are presented in Table 3.

Table 3
Results of the pharmaceutical analysis of the *placebo* ODTs.

Formulation	Uniformity of mass (mg)	Hardness (N)	Friability (%)
F1	209.8 ± 0.9	32.6 ± 3.1	0.23
F2	208.1 ± 0.6	80.9 ± 4.9	0.00
F3	169.8 ± 1.2	27.2 ± 6.5	0.57
F4	273.7 ± 0.8	38.2 ± 2.5	0.18
F5	187.5 ± 0.8	31.1 ± 2.9	0.26

* Results are expressed as mean ± standard deviation.

For the uniformity of mass evaluation, the average masses of the tablet batches varied between 169.8 ± 1.2 mg (F3) and 273.7 ± 0.8 mg (F4). When compared, the values showed that the compression load and the shape of the tooling had a lower impact on tablet mass uniformity, while the low die diameter lead to higher mass variability, however for all formulations the relative standard deviation was within 1 %. On the other hand, the crushing strength of the tablets was heavily impacted by the compression load, the results varying between 27.2 ± 6.5 N (F3) and 80.9 ± 4.9 N (F2). However, all batches exhibited a friability lower than 1% and met the compendial requirements.

As for the pharmacopeial disintegration test, the results varied between 18.4 ± 0.8 s (F5) and 59.9 ± 0.4 s (F2), all the process variables having an influence on this parameter.

From the five formulations developed in this study, F1 and F2 were differentiated through the compression force used in the manufacturing process. Both formulations were compressed with 9 mm flat punches, at two different compression force levels. Results showed that the hardness and disintegration time increased along with the compression force, while the friability decreased. As expected, due to the higher compression force, F2 displayed higher hardness and disintegration time and a lower friability.

The impact of die diameter was evaluated using the F3 (8 mm), F1 (9 mm), and F4 (10 mm) formulations, compressed at a low force with flat punches. Results highlighted a positive influence of die diameter on mass uniformity and hardness, also decreasing the friability and the *in vitro* disintegration time, as shown in Fig. 2. An increased surface area was responsible for the faster disintegration, as more liquid could penetrate the solid matrix of the tablet. Moreover, as other authors have previously stated, increasing diameters are related to lower pressures which result in higher porosity that enables quick liquid penetration and further disintegration (Lura et al., 2020).

The effect of punch shape was evaluated by comparing F1 (9 mm,

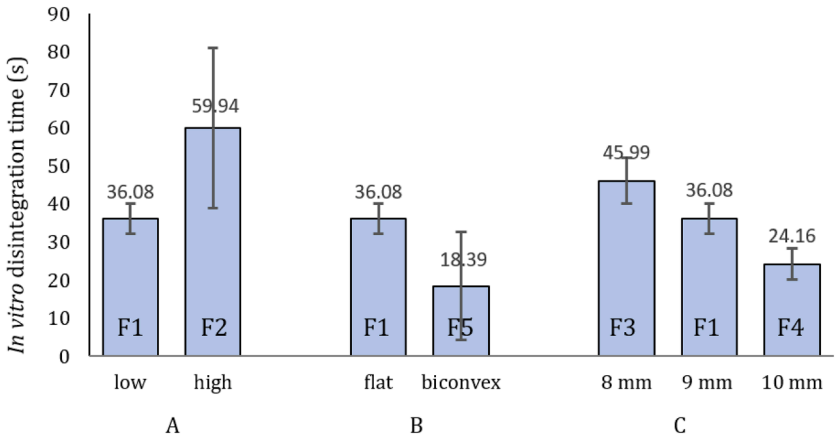

Fig. 2. Influence of process variables (A, compression force; B, punch shape; C, die diameter) on the *in vitro* disintegration time.

flat, low) and F5 (9 mm, biconvex, low) formulations. The differences between the average hardness were small and not statistically significant ($p > 0.05$). At the same time, the *in vitro* disintegration time decreased significantly ($p < 0.05$) from F1 to F5. The punch shape (flat shape *vs*. convex shape) influences the compression patterns inside the tablet. As stated by Eiliazadeh et al. and Laity et al., inside the flat-faced tablet (in cross-section), high-density regions will form in the upper part (at the top corners) and the middle bottom half of the tablet. Along the high-density regions, low-density regions appear, especially in the top centre part and the bottom corners of tablets. On the other hand, inside the convex-shaped tablets, the compression forces will create high-density regions at the site of the contact points of the compressed material with the die wall. Towards the tablet centre, the material density decreases, because in the highest part of the convex tablet, the compression forces aren't as high as in the corners, due to the punch shape. (Eiliazadeh et al., 2003; Laity et al., 2010). It is also known that the low-density regions indicate a more porous structure, regions that are prone to higher disintegration speed because the disintegration media penetrates faster through more porous regions, determining a higher disintegration rate for the convex shape due to rapid liquid uptake (Al-Sharabi et al., 2020). Pabari and Ramtoola published a study that highlighted the influence of process variables on the porosity and disintegration time of tablets prepared through direct compression. For this purpose, the study involved three variation levels for the compression load and die diameter. After manufacturing, the tablets were tested for various pharmaceutical characteristics, including uniformity of mass, hardness, and *in vitro* disintegration time. Examining the results, the authors demonstrated the influence of the compression load and die diameter on the evaluated quality attributes and were able to determine the critical parameters for the manufacturing of an optimal tablet (Pabari and Ramtoola, 2012). Our results are in line with those published by Pabari and Ramtoola, that showed a negative dependency between the disintegration time and the tablet diameter and correlated to the structure porosity that controlled water uptake (Pabari and Ramtoola, 2012).

3.2. The effects of ODT preparation process and texture analysis parameters on texture profile variability

Before testing the predictions of the previously developed models on this prediction set, the effect of the studied process variables on the texture profiles was assessed to investigate whether the texture analysis is able to capture the variability induced by the process parameter variations. Previous literature reports showed that the choice of texture analysis parameters could decide the quality of the results, as some settings reveal small variations in the structure and mechanical features of the products, while others hide structural changes (Hackl and Ermolina, 2016). As the speed of the probe is regarded as a critical testing parameter, two speed values were applied, of 0.01 mm/s and 0.02 mm/s, respectively. The average load *versus* time profiles were represented for the tested formulations considering the two speed settings (Fig. 3). The profiles show the moment when the tablet fixed onto the texture analyser probe comes into contact with the metallic mesh immersed in the medium and starts absorbing the liquid due to its porosity; thus, the disintegration process starts, and the load-time curves are recorded. The load increases due to the constant speed of the probe, which determines the disintegration of the tablet, the disintegrated particles being pushed through the mesh directly into the medium. After reaching the peak load, due to the softening of the tablet, the load decreases until the point where the tablet is transformed into a loose, paste-like material. After this point in the disintegration process, observed on the texture profile as an inflection point, the load shows a sudden increase as the probe reaches the sieve, which marks the end of the test (Szakonyi and Zelkó, 2013). Previous literature reports mention that the disintegration time could be calculated as the time span (s) between the maximum peak load and the inflection point (Casian et al., 2018a). Additionally, several individual parameters, *e.g.* hardness, deformation at hardness, hardness work, recoverable deformation, fracturability, and quantity of fractures, could be generated from the texture data. Because in the previous study (Casian et al., 2018a), investigating the entire curve yielded enhanced predictive accuracy compared to the analysis of the individual parameters extracted from it, in the current research the multivariate data analysis of the complete *in vitro* disintegration profiles was performed. This approach was considered convenient as no preliminary calculation steps would be necessary before the testing of the predictions.

As the PLS models developed for predicting *in vivo* disintegration time and palatability use individual profiles as input data, the average profiles were represented to highlight the variation induced by tablet properties and testing conditions. Thus, the use of a complete or specific region of the entire profile will also account for the variability referring to the time point where the maximum load in reached.

When working with a higher speed setting, a sample size increase from 8 mm to 9 mm did not influence the shape of the profiles, whereas a further increase in size (10 mm) offered higher load values and an additional peak at a lower time point. The larger amount of residue formed upon disintegration was considered responsible for the initial peak, whereas upon dispersion and drainage the load dropped and followed the trend of smaller tablets. An increased mechanical resistance (F2) led to higher initial load values and a faster appearance of the maximum load as the solid undisintegrated core of the tablet met the sieve. Changing the shape of the tablet from flat to biconvex (F5) led to a drop in the recorded load. Considering the previously identified influences on disintegration time, the texture profiles efficiently

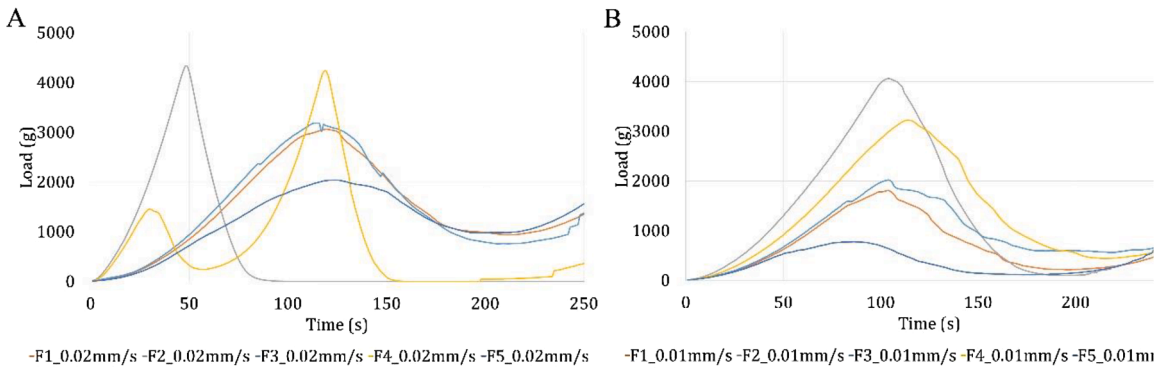

Fig. 3. Load *vs.* time texture profiles obtained for F1-F5 at 0.02 mm/s (A) and 0.01 mm/sec (B) testing speed.

discriminated formulations based on this criterion.

Decreasing the speed of the probe from 0.02 mm/s to 0.01 mm/s led to an improved differentiation of the profiles with respect to the peak load. The recorded load values under a 0.01 mm/s movement of the probe were smaller compared to the higher testing speed, as the tablet had more time to disintegrate and lose its structural integrity (Fig. 3B). The influence of probe speed on the recorded loads was more evident when a higher compression force was used (F2, Fig. 4B) and when higher diameter tablets were tested (F4, Fig. 4D). The slower disintegration of these samples offered a shift in peak position.

The same conclusion can be reached when comparing the peak loads attained using the two settings, listed in Table S3 (Supplementary Material): at a speed of 0.02 mm/s the values were comprised in a narrow range (Fig. 3A), while using the 0.01 mm/s, the range was significantly larger, between 997.6 ± 389.3 g and 4436.5 ± 188.2 g (Fig. 3B). Knowing the effects of variable TA working conditions on the quality of

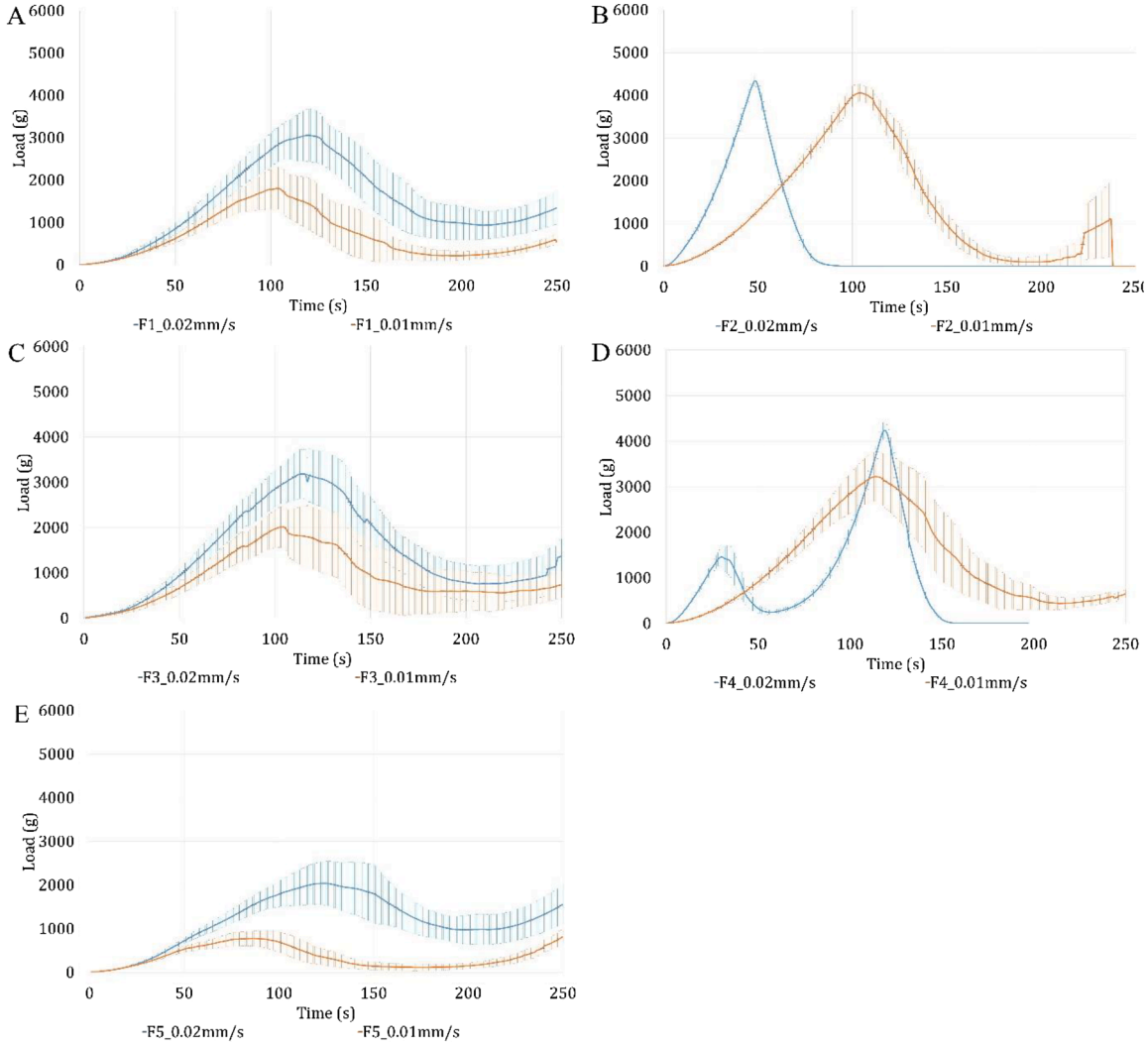

Fig. 4. The influence of probe speed on the recorded texture profiles. The blue and orange bars represent the 95 % confidence intervals of the 10 replicated results. Average values represented with a continuous line were calculated as means of load values at every time point.

the results allows the characterization of a wide range of ODT products: for very rapidly disintegrating products, a higher probe speed would be required to record the load *vs* time profiles, whereas a lower speed is needed for slowly disintegrating products to avoid overload.

3.3. The influence of process parameters on the in vivo disintegration time and texture-related palatability scores

It was previously reported that the subjective assessment performed by the volunteers is not always in line with the objective pharmaceutical evaluation. A study that aimed at developing directly compressed ODTs revealed that the optimal formulation according to pharmaceutical quality criteria was different from the one chosen by the volunteers as the most acceptable (Iurian et al., 2014). Therefore, the next stage investigated how the process parameters impact *in vivo* disintegration time and texture-related palatability characteristics. The *in vivo* evaluation yielded higher variability, the variation trend was the same, but the differences between formulations flattened. Out of the investigated factors, the compression force and tablet shape influenced the *in vivo* disintegration time, while the tablet diameter was not relevant. Tablets with higher hardness values had a prolonged disintegration, due to their lower porosity, which hindered the penetration of water. In agreement with the *in vitro* characterization, the biconvex shape of tablets compared to the flat-faced shape was beneficial for faster *in vivo* disintegration (Fig. 5A). In contrast with the instrumental pharmacopoeial method, the tablet diameter change for the *in vivo* disintegration led to a non-significant decrease in the disintegration time, which shows that the oral conditions levelled the size-related variability.

Despite the difference in the disintegration time, the texture-related palatability scores did not differ between F1, F2, F3 and F5. The lowest texture-related palatability scores were obtained for F4 ODTs, the formulation displaying the highest diameter, associated with lower acceptability (Fig. 5B). The only significant difference ($p < 0.05$) in terms of texture-related palatability score was obtained between F4 and F2, which cannot be attributed to a sole process parameter variation. Overall, the product's *in vivo* disintegration time was not correlated with its palatability, the two responses being influenced by different formulation factors. Previous results indicate that process-related variability in the studied domains does not necessarily have important *in vivo* consequences (Mistry and Batchelor, 2017).

3.4. Testing the predictions on placebo ODTs

Multivariate calibration procedures have been frequently applied for the development of surrogate characterization tools that could replace destructive, expensive, or time-consuming reference testing methods. In these procedures, several variables recorded through the proposed testing method are linked to the quality attributes of the product, through the use of appropriate calibration sets (Casian et al., 2021, 2018b). Our previous study demonstrated that texture profiles (load *vs.* time) could efficiently predict subjective characteristics of ODTs (*in vivo* disintegration, the volume of residue, and the palatability) based on a

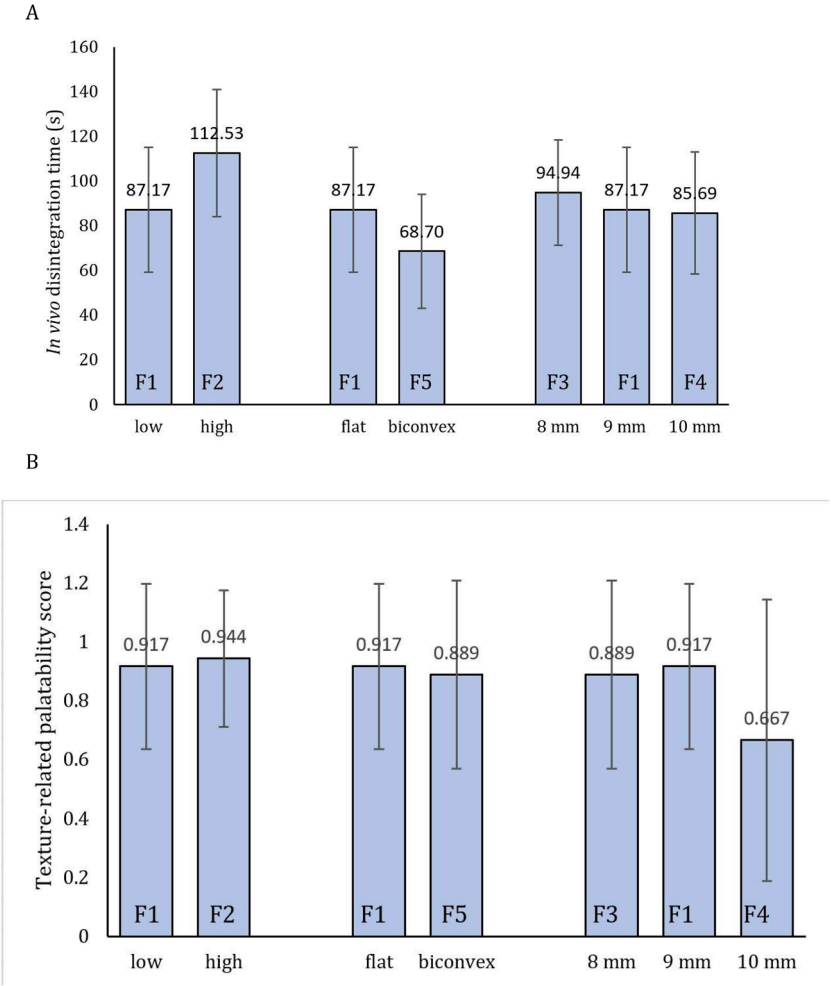

Fig. 5. The variation of *in vivo* disintegration time (with statistically significant differences between F2 and F5, when compared to F1-3-4) (A) and average texture-related palatability score (with significant differences between F2 and F4) (B) as an effect of process parameters variation, for *placebo* ODTs ($p \leq 0.05$).

representative calibration set. Moreover, the model performance was successfully tested on marketed formulations (Casian et al., 2018a).

The applicability of this method stands in the development process of palatable formulations, along with taste-sensing systems, both having been designed to replace *in vivo* testing by human volunteers. The calibration set of the previous model only included formulation-related variability. However, considering the diversity amongst the physical characteristics of ODTs, the current study aimed to evaluate the robustness of the previously developed model with respect to variations in tablet size, shape, and hardness. Furthermore, by evaluating the predictive performance through different modelling options (applying data processing methods to increase model predictability), an optimal strategy to increase the robustness of the methods could be identified.

The quality of predictions was tested on 3 different PLS models: a model built using all the variables (PLS-M1), a model presenting a selected domain of input variables (PLS-M2), and an identical reduced model, but with log-transformed variables (PLS-M3). The characteristics of the PLS models are presented in Table 4.

Texture analysis using small volumes of dissolution medium (water or artificial saliva), coupled with multivariate calibration, can be used to predict the *in vivo* disintegration time, because of its capability to mimic the forces applied by the tongue on the solid pharmaceutical product. Because the results may vary a lot depending on the test parameters, the two previously mentioned testing speeds were used. On the one hand, the testing method can influence the variability of the results or how close the replicates are, but it can also enhance or restrict the disintegration process, and it is possible that for formulations with different characteristics, different testing conditions will be needed.

The biplot developed for disintegration time displayed simultaneously the observations and the prediction errors of different models as variables, revealing several grouping tendencies (Fig. 6). The positioning of variables suggests that the probe speed and the model type had an impact on the prediction errors. The impact of probe speed was highlighted only for PLS-M1 and M2, whereas variable transformation reduced the differences between the residuals for different speed settings. Moreover, the variable selection procedure had a limited effect on predictions, as PLS-M1 and PLS-M2 variables for different speed settings were placed in similar regions.

Formulations F1, F3, F4 and F5 have average prediction errors, as they are placed closer to the origin, the effects of testing speed and model type on these samples being similar. The plot representing the residuals highlighted an under-prediction of disintegration time when the entire load *vs*. time profile or the reduced domain recorded at a lower speed was used as input in the PLS model (Fig. 7A, C). A testing procedure with a 0.02 mm/s probe speed produced smaller prediction errors (Fig. 7B, D), while further logarithmic transformation reduced the differences between the observed and predicted values of disintegration time (Fig 7E, F). Thus, for samples prepared using a lower compression force (30 N) the tablet shape and diameter were not relevant in the diameter range of 8 – 10 mm. Therefore, for low mechanical strength ODTs, regardless of the shape or size, the prediction performance of the *in vivo* disintegration time is kept, no matter the chosen model. The effect of changing the probe speed and model type is similar in this range of properties.

Observations of ODTs with higher mechanical resistance (F2) are separated from other samples in the biplot. The positioning with respect to the variables suggests that the largest residuals were obtained when a higher probe speed was applied. In this case, variable selection and transformation led to similar results, slightly underestimating the disintegration time. For these samples, a probe speed of 0.01 mm/s improved the prediction quality, as shown in Fig. 7.

The biplot generated for palatability revealed that the palatability of 10 mm ODTs (F4) is predicted variably depending on the testing speed and model type (Fig. 8). The score contribution plot highlighted a negative effect for the variable selection procedure (PLS-M2), whereas applying the second transformation step (PLS-M3) reduced the prediction errors. (Fig. 9). Palatability errors decreased especially at larger speed settings, except for the case of using the reduced texture profile.

The effect of tablet shape, hardness, and diameter on the predictions of the palatability was not highlighted in the 8–9 mm diameter range. At the same time, the effect of data transformation on prediction accuracy was similar for these samples.

The disintegration time of ODTs was predicted more accurately using the higher speed setting (0.02 mm/s) or by implementing a data transformation step. Meanwhile, in the case of samples with increased crushing strength, the lower test speed is advised. The obtained results indicate poor robustness of the method with respect to varying hardness for disintegration time prediction and towards larger diameter tablets (10 mm) for texture-related palatability scores. Thus, a robust method capable of predicting these attributes should efficiently handle such variations in ODTs characteristics. To some extent, these prediction errors were handled by correctly adjusting the probe speed during texture analysis and the characteristics of the prediction model.

3.5. Testing of predictions on API-loaded ODTs

The previous chapters demonstrated that texture analysis is able to capture the variability determined by process parameters variation, on *placebo* tablets. As in manufacturing sites, the texture profiles and the quality of predictions could be influenced by the impact of adding APIs, API-loaded ODTs were prepared and tested following the same procedure.

Two model APIs were selected to load the five *placebo* ODT formulations: ascorbic acid and turmeric powder, at variable ratios of 10% and 20%. For ethical reasons, their selection was based on their lack of toxicity issues and no risks to reaching maximum doses during the evaluation. Moreover, knowledge on both of them could be of use for both medicines and food supplement producers. Ascorbic acid displays a highly hydrophilic character (Zarmpi et al., 2017), while turmeric powder is known to contain hydrophobic compounds (Nguyen et al., 2017).

For the medicated tablets, the texture analysis and the *in vivo* disintegration tests were performed. The texture profiles had the same shapes as described before and captured the disintegration phenomena. For the placebo tablets the peak loads were reported, therefore those of medicated tablets were also added for comparison. The peak load values ranged from 15.6 ± 3.2 g to 3736.5 ± 692.1 g when tablets were tested at a speed of 0.01 mm/s, and from 18.7 ± 2.0 g to 4499 ± 11.7 g for tablets tested at a speed of 0.02 mm/s. The loads met during the disintegration of medicated tablets were well below their corresponding placebo formulations, which is an indicator of quicker disintegration, further confirmed in the *in vivo* disintegration studies. The same trend observed on the *placebo* tablets was visible, of reaching higher peak loads at higher speed settings (Table S4), due to the lower time allowed for disintegration which determines the probe to meet higher resistance from the disintegrated/partially disintegrated material. The texture profiles had the same shapes as described before and captured the disintegration phenomena.

Table 4
Properties of PLS models used to predict *in vivo* disintegration time and palatability.

Model	X variables	Data Transformation	R^2	Q^2	A	RMSECV
Disintegration time						
PLS-M1	1–378	–	0.951	0.972	3	8.617
PLS-M2	1–240	–	0.985	0.931	2	8.287
PLS-M3	1–240	log	0.982	0.899	2	9.642
Palatability						
PLS-M1	1–378	–	0.959	0.788	3	4.677
PLS-M2	1–130	–	0.991	0.876	5	2.845
PLS-M3	1–130	log	0.994	0.963	3	1.550

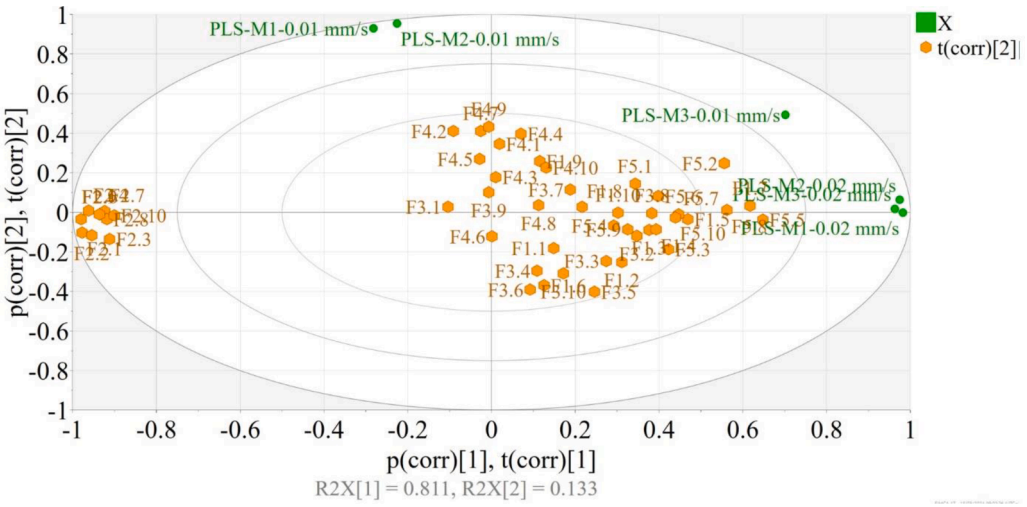

Fig. 6. Biplot of the PCA model developed for disintegration time (green – variables, orange – observations).

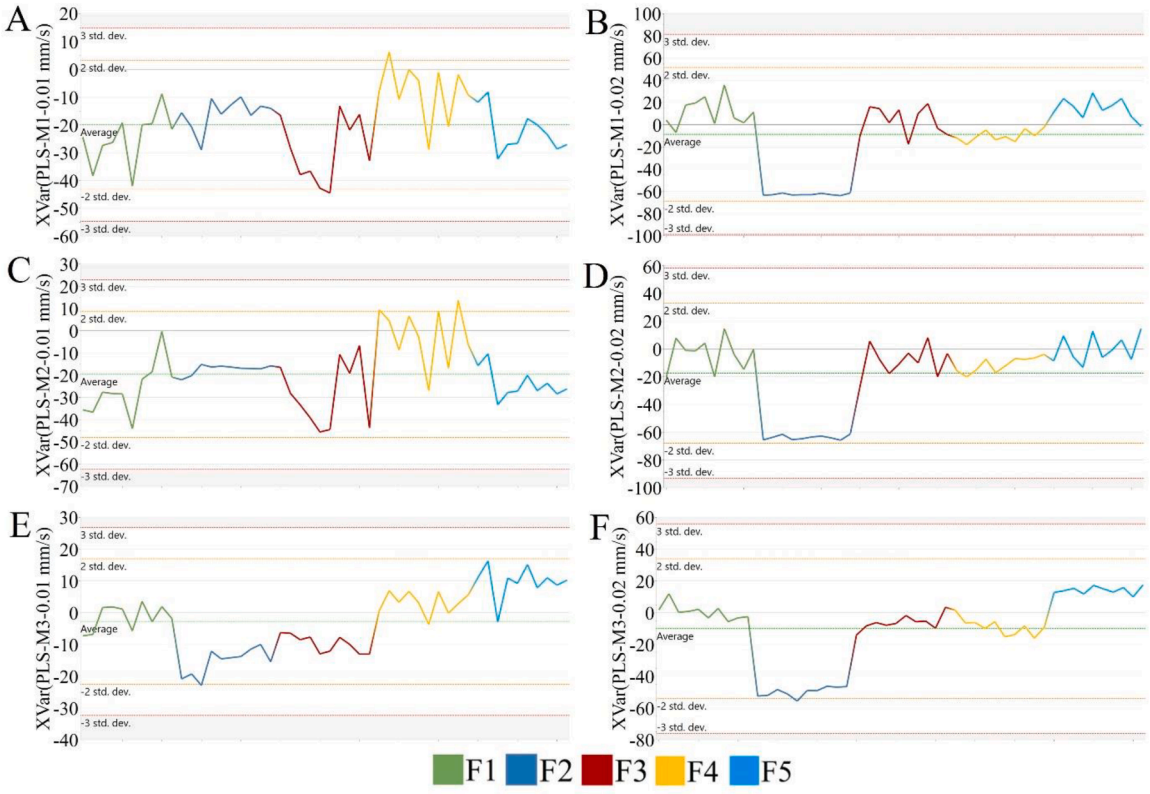

Fig. 7. Observed *versus* predicted differences in disintegration time obtained under different probe speed settings and model types.
A - PLS M1, 0.01 mm/s; B - PLS M1, 0.02 mm/s; C - PLS M2, 0.01 mm/s; D - PLS M2, 0.02 mm/s; E - PLS M3, 0.01 mm/s; F - PLS M3, 0.02 mm/s;
PLS M1- all variables; PLS M2 – var select; PLS M3 – variable select and transformation.

The *in vivo* evaluation of API-loaded ODTs was in agreement with the texture results, indicating a significant decrease of the oral disintegration times when compared to the *placebos* for all formulations except for F2, where no significant differences were obtained. Soluble ingredients like ascorbic acid are known to favour wicking and disintegration, while insoluble powders with good hydrophilic and wetting properties also display a high disintegration capacity. However, high compression pressures, which result in stronger interparticle bonds, prevent water uptake and delay swelling and disintegration, which explains that the active ingredients had no effects on F2, the formulation obtained at high compression pressure (Berardi et al., 2021).

As described for the *placebo* tablets, several models were generated that applied different data processing methods. For the *in vivo* disintegration time, the model that considered as input variables only a selected domain of the texture profiles (1 to 240 s) gave the best quality of predictions. Fig. 10A shows the experimental *in vivo* disintegration times along with the predicted disintegration times for the API-loaded formulations, at the two testing speeds. The predicted values were close to those reported by the volunteers, regardless of the analysis conditions, i.e. speed, API type or API content. The only formulation where the disintegration time was underpredicted was F2, with the highest hardness, which was also the formulation that displayed the

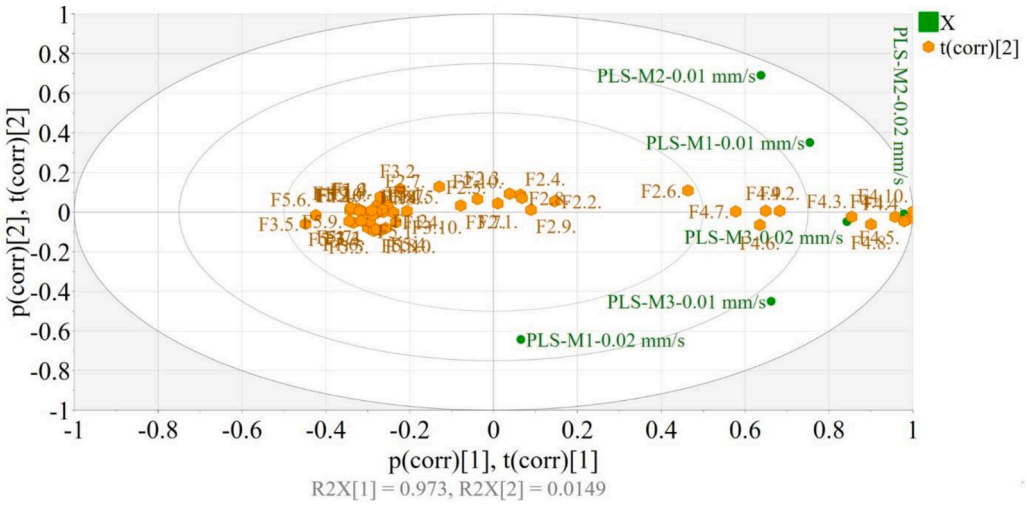

Fig. 8. Bi-plot of the PCA model developed for palatability (green – variables, orange – observations).

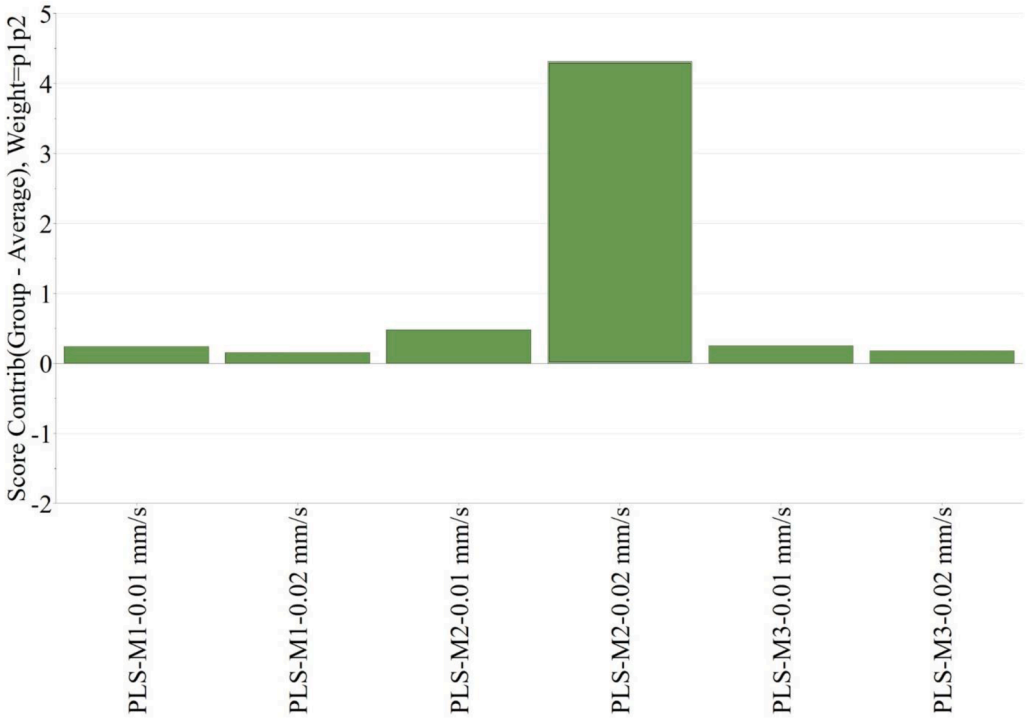

Fig. 9. Score contribution plot generated for the samples of formulation F4.

most important variability.

For the texture-related palatability characteristics, the highest prediction quality was met by the reduced model on logarithmic transformed input variables. However, the prediction capacity was lower than for *placebo* tablets. An important component of palatability, if not the most important, is the taste. The taste did not influence the initial assessment on *placebo* tablets, as the tablets had the same composition and a rather neutral taste given by the excipients. Therefore, the palatability score was based only on tablet characteristics such as roughness, texture, mouthfeel, volume of residue etc., features related to the mechanical structure and behaviour in liquid media. On the contrary, when adding the two APIs, the palatability score was composed of more characteristics, including taste and smell that cannot be assessed through texture analysis, leading to a lower prediction quality for tablets containing APIs compared to *placebo* tablets.

Texture analysis is a method already applied in the routine control of the mechanical properties (Basim et al., 2019; Lura and Breitkreutz, 2022; Mazel et al., 2018) of solid oral dosage forms, as well as of their disintegration properties (Wang et al., 2017; Wang and Sun, 2020). It is known that it has the ability to simulate the conditions of the oral cavity better than the conventional disintegration test. This study, unlike the others published up to this point (Casian et al., 2018a), emphasizes the ability of this method to capture the variability given by the process parameters and the physical characteristics of the tablets.

The quality of the raw results, as well as of the predictions, depends on the test parameters, and this study showed that a rational selection of the working conditions in relation to the properties of the tablets leads to reproducible raw results and satisfactory predictions. One of the main objectives of pharmaceutical development is to obtain an as specified acceptable product. Out of the current study a low compression force

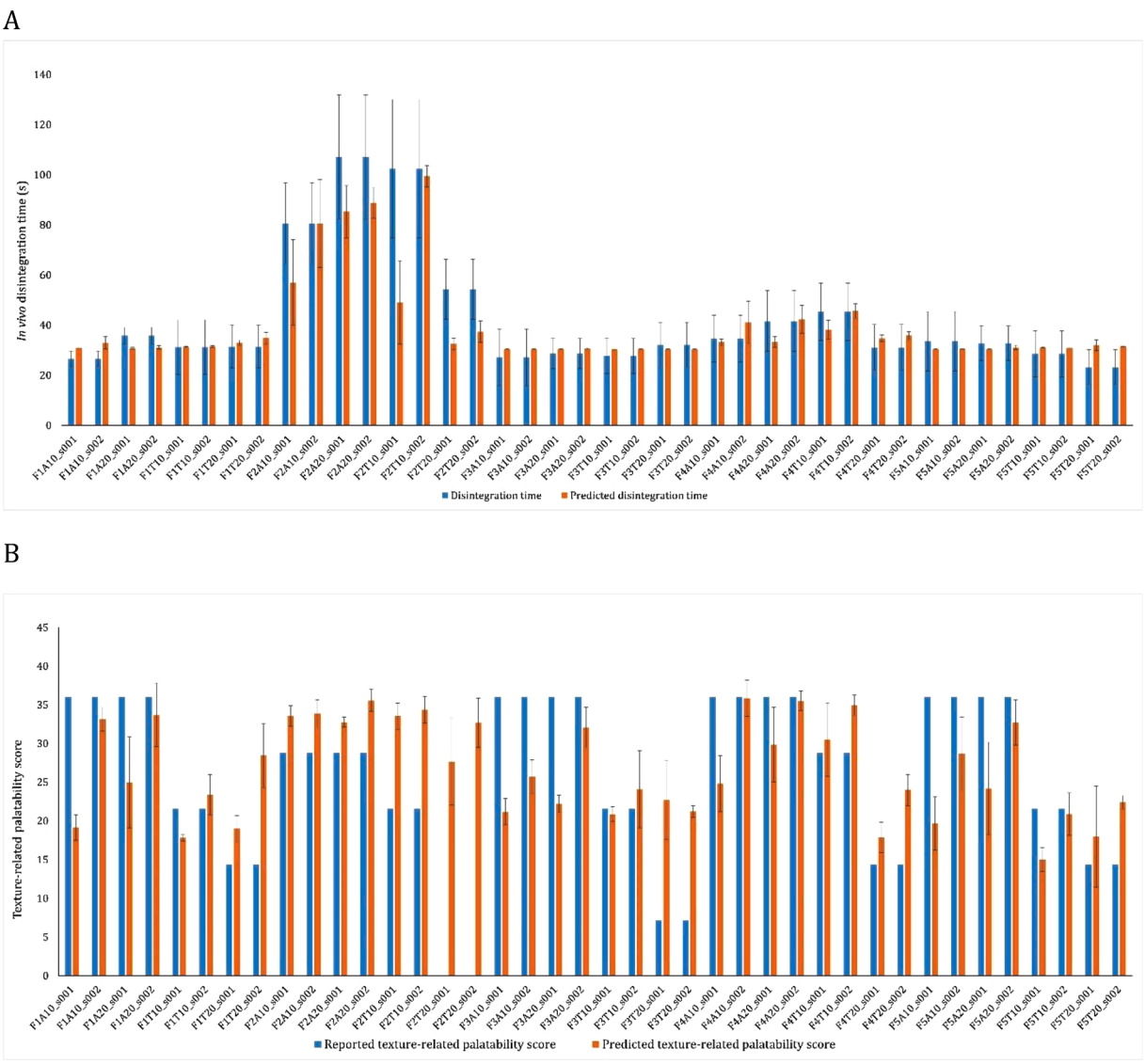

Fig. 10. Experimental *versus* predicted values of *in vivo* disintegration time (A) and texture-related palatability score (B) for the API-loaded ODTs.

associated to 8–9 mm diameter and a biconvex shape fulfil not only the compendial requirements, but also ensure the robustness of the texture-based sensory assessment.

The induced variability in the physical properties of ODTs was not always perceived by the volunteers. The *in vivo* disintegration times were concentrated in a narrower range than those obtained by the pharmacopoeial method, still maintaining the variation patterns. Texture analysis, however, captured the physical changes in the ODTs, enabling the correct prediction of the disintegration. Adding the API in the tested ratios did not seem to influence the disintegration predictions, so the method seems robust regardless of the flexibility in terms of formulation or preparation method.

The texture-related palatability scores proved a reduced ability of the method to discriminate between formulations with different physical characteristics. A limitation in this regard could be the binary evaluation scale chosen for this attribute, which is too restrictive for a correct evaluation of a complex characteristic such as palatability. However, on the *placebo* formulations, good predictions were obtained for texture-related palatability. As taste is known to have the most significant influence on acceptability and palatability scores, when the APIs were added, the prediction errors increased, showing that mechanical data needs complementary taste assessment, such as electronic tongues, to describe palatability in a more complete manner (Mistry and Batchelor, 2017).

4. Conclusions

The ability of TA to simulate the conditions in the oral cavity during disintegration is widely recognized. Previous work demonstrated that MVDA models based on TA profiles discriminate between ODT formulations and can predict oral disintegration time and palatability-related characteristics such as the volume of residue. As in industrial sites, multiple ODT products can be developed with diverse physical characteristics, this study aimed to test the MVDA models on products obtained in variable process conditions.

The results highlighted some differences regarding the impact of the studied process variables on the *in vitro/in vivo* disintegration time and product texture-related palatability scores. While the *in vitro* disintegration time was influenced by the applied load during compression, tablet diameter, and punch shape, the *in vivo* evaluation only highlighted the influence of the applied load and tablet shape. Regarding the product palatability-related characteristics, the volunteers identified the tablet diameter as the only variable affecting this attribute.

The differences in tablet hardness, diameter and shape were better

captured in the recorded texture profiles. Changing the speed settings amplified the differences between formulations. The utility of working with different analysis settings stands in the ability to characterize ODTs with a wide range of properties. Moreover, the right choice of testing parameters, associated with data selection or transformation during MVDA led to models with low prediction errors for all the formulations, *placebo* and drug-loaded alike. The texture-related palatability characteristics were well predicted on *placebo* formulations and less on the API-containing products, as when taste and smell are not in question, TA is efficient in capturing the mechanical changes correlated to pleasant or unpleasant sensations.

CRediT authorship contribution statement

Rareș Iovanov: Conceptualization, Writing – original draft. **Andreea Cornilă:** Writing – original draft, Conceptualization, Writing – review & editing. **Cătălina Bogdan:** Writing – review & editing. **Dana Hales:** Writing – review & editing. **Ioan Tomuță:** Writing – review & editing. **Marcela Achim:** Writing – review & editing. **Andrada Tăut:** Investigation. **Nela Iman:** Investigation. **Tibor Casian:** Formal analysis, Data curation, Conceptualization, Writing – original draft. **Sonia Iurian:** Conceptualization, Funding acquisition, Project administration, Supervision, Writing – original draft, Writing – review & editing.

Data availability

Data will be made available on request.

Acknowledgements

This work was supported by a grant of the Romanian Ministry of Research, Innovation and Digitization, CCCDI - UEFISCDI, project number PN-III-P2-2.1-PED-2021-4198, within PNCDI III.

Supplementary materials

Supplementary material associated with this article can be found, in the online version, at doi:10.1016/j.ejps.2024.106801.

References

Abay, F., Ugurlu, T., 2015. Orally disintegrating tablets: a short review. J. Pharm. Drug Dev. 3, 1. https://doi.org/10.15744/2348-9782.3.303.

Abd Elbary, A., Ali, A.A., Aboud, H.M., 2012. Enhanced dissolution of meloxicam from orodispersible tablets prepared by different methods. Bull. Faculty Pharm. Cairo Univ. 50, 89–97. https://doi.org/10.1016/j.bfopcu.2012.07.001.

Abd Elbary, A., Makky, A.M.A., Tadros, M.I., Alaa-Eldin, A.A., 2016. Laminated sponges as challenging solid hydrophilic matrices for the buccal delivery of carvedilol microemulsion systems: development and proof of concept via mucoadhesion and pharmacokinetic assessments in healthy human volunteers. Eur. J. Pharm. Sci. 82, 31–44. https://doi.org/10.1016/j.ejps.2015.11.006.

Abd Elbary, G., Eouani, C., Prinderre, P., Joachim, J., Reynier, J., Piccerelle, P., 2005. Determination of the *in vitro* disintegration profile of rapidly disintegrating tablets and correlation with oral disintegration. Int. J. Pharm. 292, 29–41. https://doi.org/10.1016/J.IJPHARM.2004.08.019.

Ahmed, T.A., 2021. Study the pharmacokinetics, pharmacodynamics and hepatoprotective activity of rosuvastatin from drug loaded lyophilized orodispersible tablets containing transfersomes nanoparticles. J. Drug Deliv. Sci. Technol. 63, 102489 https://doi.org/10.1016/j.jddst.2021.102489.

Al-Sharabi, M., Markl, D., Mudley, T., Bawuah, P., Karttunen, A.P., Ridgway, C., Gane, P., Ketolainen, J., Peiponen, K.E., Rades, T., Zeitler, J.A., 2020. Simultaneous investigation of the liquid transport and swelling performance during tablet disintegration. Int. J. Pharm. 584, 119380 https://doi.org/10.1016/J.IJPHARM.2020.119380.

Asiri, A., Hofmanová, J., Batchelor, H., 2021. A review of *in vitro* and *in vivo* methods and their correlations to assess mouthfeel of solid oral dosage forms. Drug Discov. Today 26, 740–753. https://doi.org/10.1016/j.drudis.2020.12.015.

Augsburger, L.L., Zellhofer, M.J., 2007. Tablet formulation. In: Swarbick, J. (Ed.), Encyclopedia of Pharmaceutical Technology. Informa Healthcare, New York, NY, pp. 3641–3652.

Bashir, S., Fitaihi, R., Abdelhakim, H.E., 2023. Advances in formulation and manufacturing strategies for the delivery of therapeutic proteins and peptides in orally disintegrating dosage forms. Eur. J. Pharm. Sci. 182, 106374 https://doi.org/10.1016/J.EJPS.2023.106374.

Basim, P., Haware, R.V., Dave, R.H., 2019. Tablet capping predictions of model materials using multivariate approach. Int. J. Pharm. 569, 118548 https://doi.org/10.1016/j.ijpharm.2019.118548.

Berardi, A., Bisharat, L., Quodbach, J., Abdel Rahim, S., Perinelli, D.R., Cespi, M., 2021. Advancing the understanding of the tablet disintegration phenomenon – An update on recent studies. Int. J. Pharm. 598, 120390 https://doi.org/10.1016/J.IJPHARM.2021.120390.

Casian, T., Bogdan, C., Tarta, D., Moldovan, M., Tomuta, I., Iurian, S., 2018a. Assessment of oral formulation-dependent characteristics of orodispersible tablets using texture profiles and multivariate data analysis. J. Pharm. Biomed. Anal. 152, 47–56. https://doi.org/10.1016/j.jpba.2018.01.040.

Casian, T., Gavan, A., Iurian, S., Porfire, A., Toma, V., Stiufiuc, R., Tomuta, I., 2021. Testing the limits of a portable NIR spectrometer: content uniformity of complex powder mixtures followed by calibration transfer for in-line blend monitoring. Molecules 26, 1129. https://doi.org/10.3390/MOLECULES26041129.

Casian, T., Iurian, S., Gavan, A., Revnic, C., Porav, S., Porfire, A., Vlase, L., Tomuță, I., 2018b. Near Infra-Red spectroscopy for content uniformity of powder blends – Focus on calibration set development, orthogonality transfer and robustness testing. Talanta 188, 404–416. https://doi.org/10.1016/J.TALANTA.2018.05.101.

Chauhan, K., Solanki, R., Sharma, S., 2018. A review on fast dissolving tablet. Int. J. Applied Pharm. 10, 1–7. https://doi.org/10.22159/IJAP.2018V10I6.28134.

Dor, P.J.M., Fix, J.A., 2000. *In vitro* determination of disintegration time of quick-dissolve tablets using a new method. Pharm. Dev. Technol. 5, 575–577. https://doi.org/10.1081/PDT-100102041.

Eiliazadeh, B., Briscoe, B.J., Sheng, Y., Pitt, K., 2003. Investigating density distributions for tablets of different geometry during the compaction of pharmaceuticals. Particul. Sci. Technol. 21, 303–316. https://doi.org/10.1080/716100572.

El-Arini, S.K., Clas, S.D., 2002. Evaluation of disintegration testing of different fast dissolving tablets using the texture analyzer. Pharm. Dev. Technol. 7, 361–371. https://doi.org/10.1081/PDT-120005732.

European Directorate for the Quality of Medicines, n.d. 2.9.5. Uniformity of mass of single-dose preparations - European Pharmacopoeia 11.0 [WWW Document]. URL https://pheur.edqm.eu/app/11-0/content/11-0/20905E.htm (accessed 7.25.23).

Guidance for Industry Orally Disintegrating Tablets, 2008.

Hackl, E.V., Ermolina, I., 2016. Using texture analysis technique to assess the freeze-dried cakes in vials. J. Pharm. Sci. 105, 2073–2085. https://doi.org/10.1016/j.xphs.2016.05.016.

Haraguchi, T., Yoshida, M., Kojima, H., Uchida, T., 2016. Usefulness and limitations of taste sensors in the evaluation of palatability and taste-masking in oral dosage forms. Asian J. Pharm. Sci. 11, 479–485. https://doi.org/10.1016/j.ajps.2016.03.001.

Hooper, P., Lasher, J., Alexander, K.S., Baki, G., 2016. A new modified wetting test and an alternative disintegration test for orally disintegrating tablets. J. Pharm. Biomed. Anal. 120, 391–396. https://doi.org/10.1016/j.jpba.2015.12.046.

Iurian, S., Tomuta, I., Leucuta, S.E., 2014. Formulation of orodispersible tablets containing meloxicam and their *in vitro* and *in vivo* characterization. Farmacia 62, 1097–1108.

Kokott, M., Lura, A., Breitkreutz, J., Wiedey, R., 2021. Evaluation of two novel co-processed excipients for direct compression of orodispersible tablets and mini-tablets. Eur. J. Pharm.d Biopharm. 168, 122–130. https://doi.org/10.1016/j.ejpb.2021.08.016.

Kumar Gupta, D., Maurya, A., Mohan Varshney, M., 2020. Orodispersible tablets: an overview of formulation and technology. World J. Pharm. Pharm. Sci. 9, 1406–1418. https://doi.org/10.20959/wjpps202010-17481.

Laity, P.R., Han, L., Elliott, J., Cameron, R.E., 2010. Variations in compaction behaviour for tablets of different size and shape, revealed by small-angle X-ray scattering. J. Pharm. Sci. 99, 4380–4389. https://doi.org/10.1002/jps.22144.

Lura, A., Tardy, G., Kleinebudde, P., Breitkreutz, J., 2020. Tableting of mini-tablets in comparison with conventionally sized tablets: a comparison of tableting properties and tablet dimensions. Int. J. Pharm. X. 2 https://doi.org/10.1016/j.ijpx.2020.100061.

Lura, A., Breitkreutz, J., 2022. Manufacturing of mini-tablets. Focus and impact of the tooling systems. J. Drug Deliv. Sci. Technol. 72, 103357 https://doi.org/10.1016/j.jddst.2022.103357.

Mazel, V., Diarra, H., Malvestio, J., Tchoreloff, P., 2018. Lamination of biconvex tablets: numerical and experimental study. Int. J. Pharm. 542, 66–71. https://doi.org/10.1016/j.ijpharm.2018.03.012.

Mistry, P., Batchelor, H., 2017. Evidence of acceptability of oral paediatric medicines: a review. J. Pharm. Pharmacol. 69, 361–376. https://doi.org/10.1111/jphp.12610.

Nguyen, T.T.H., Si, J., Kang, C., Chung, B., Chung, D., Kim, D., 2017. Facile preparation of water soluble curcuminoids extracted from turmeric (Curcuma longa L.) powder by using steviol glucosides. Food Chem. 214, 366–373. https://doi.org/10.1016/J.FOODCHEM.2016.07.102.

Pabari, R.M., Ramtoola, Z., 2012. Application of face centred central composite design to optimise compression force and tablet diameter for the formulation of mechanically strong and fast disintegrating orodispersible tablets. Int. J. Pharm. 430, 18–25. https://doi.org/10.1016/j.ijpharm.2012.03.021.

Rameesa, C.K., Drisya, M.K., 2015. ORODISPERSIBLE TABLET: a Patient friendly dosage form (a review). Bali Med. J. 4, 17. https://doi.org/10.15562/bmj.v4i1.101.

Suryawanshi, D., Wavhule, P., Shinde, U., Kamble, M., Amin, P., 2021. Development, optimization and in-vivo evaluation of cyanocobalamin loaded orodispersible films using hot-melt extrusion technology: a quality by design (QbD) approach. J. Drug Deliv. Sci. Technol. 63, 102559 https://doi.org/10.1016/j.jddst.2021.102559.

Szakonyi, G., Zelkó, R., 2013. Prediction of oral disintegration time of fast disintegrating tablets using texture analyzer and computational optimization. Int. J. Pharm. 448, 346–353. https://doi.org/10.1016/j.ijpharm.2013.03.047.

Wang, C., Hu, S., Sun, C.C., 2017. Expedited development of a high dose orally disintegrating metformin tablet enabled by sweet salt formation with acesulfame. Int. J. Pharm. 532, 435–443. https://doi.org/10.1016/j.ijpharm.2017.08.100.

Wang, C., Sun, C.C., 2020. The efficient development of a sildenafil orally disintegrating tablet using a material sparing and expedited approach. Int. J. Pharm. 589, 119816 https://doi.org/10.1016/j.ijpharm.2020.119816.

Zarmpi, P., Flanagan, T., Meehan, E., Mann, J., Fotaki, N., 2017. Biopharmaceutical aspects and implications of excipient variability in drug product performance. Eur. J. Pharm. Biopharm. 111, 1–15. https://doi.org/10.1016/J.EJPB.2016.11.004.

pharmaceuticals

MDPI

Article

Exploring Vacuum Compression Molding as a Preparation Method for Flexible-Dose Pediatric Orodispersible Films

Dana Hales [1], Cătălina Bogdan [2,*], Lucia Ruxandra Tefas [1], Andreea Cornilă [1], Maria-Andreea Chiver [1], Ioan Tomuță [1], Tibor Casian [1], Rareș Iovanov [1], Gábor Katona [3], Rita Ambrus [3,†] and Sonia Iurian [1,†]

[1] Department of Pharmaceutical Technology and Biopharmacy, Iuliu Hatieganu University of Medicine and Pharmacy, 41 Victor Babeș St, 400002 Cluj-Napoca, Romania; dudas.dana@umfcluj.ro (D.H.); tefas.lucia@umfcluj.ro (L.R.T.); ioana.an.cornila@elearn.umfcluj.ro (A.C.); maria.andr.chiver@elearn.umfcluj.ro (M.-A.C.); tomutaioan@umfcluj.ro (I.T.); casian.tibor@umfcluj.ro (T.C.); riovanov@umfcluj.ro (R.I.); sonia.iurian@umfcluj.ro (S.I.)

[2] Department of Dermopharmacy and Cosmetology, Iuliu Hatieganu University of Medicine and Pharmacy, 12 Ion Creangă St, 400002 Cluj-Napoca, Romania

[3] Institute of Pharmaceutical Technology and Regulatory Affairs, University of Szeged, Eotvos u. 6, 6720 Szeged, Hungary; katona.gabor@szte.hu (G.K.); ambrus.rita@szte.hu (R.A.)

* Correspondence: catalina.bogdan@umfcluj.ro

† These authors contributed equally to this work.

Abstract: In recent years, solid dosage forms have gained interest in pediatric therapy because they can provide valuable benefits in terms of dose accuracy and stability. Particularly for orodispersible films (ODFs), the literature evidences increased acceptability and dose flexibility. Among the various available technologies for obtaining ODFs, such as solvent casting, hot-melt extrusion, and ink printing technologies, the solvent-free preparation methods exhibit significant advantages. This study investigated Vacuum Compression Molding (VCM) as a solvent-free manufacturing method for the preparation of flexible-dose pediatric orodispersible films. The experimental approach focused on selecting the appropriate plasticizer and ratios of the active pharmaceutical ingredient, diclofenac sodium, followed by the study of their impacts on the mechanical properties, disintegration time, and drug release profile of the ODFs. Additional investigations were performed to obtain insights regarding the solid-state properties. The ODFs obtained by VCM displayed adequate quality in terms of their critical characteristics. Therefore, this proof-of-concept study shows how VCM could be utilized as a standalone method for the production of small-scale ODFs, enabling the customization of doses to meet the individual needs of pediatric patients.

Keywords: vacuum compression molding; orodispersible films; diclofenac sodium; pediatric formulations

Citation: Hales, D.; Bogdan, C.; Tefas, L.R.; Cornilă, A.; Chiver, M.-A.; Tomuță, I.; Casian, T.; Iovanov, R.; Katona, G.; Ambrus, R.; et al. Exploring Vacuum Compression Molding as a Preparation Method for Flexible-Dose Pediatric Orodispersible Films. *Pharmaceuticals* **2024**, *17*, 934. https://doi.org/10.3390/ph17070934

Academic Editor: Nitesh K. Kunda

Received: 17 June 2024
Revised: 7 July 2024
Accepted: 9 July 2024
Published: 12 July 2024

1. Introduction

The recent initiatives of the regulatory authorities provide a dynamic landscape for pediatric medicines, encouraging the development of high-quality and innovative formulations at affordable costs. The importance of research on novel delivery systems and formulation approaches for pediatric medicines is therefore emphasized [1,2]. Yet, these objectives pose financial challenges for the pharmaceutical industry due to the necessity to develop formulations with distinct characteristics for specific age groups, such as neonates, infants, children, or adolescents [3]. Moreover, the scarcity of data on patient preferences and acceptability for emerging dosage forms within the highly diverse pediatric population poses the challenge of choosing between different formulation approaches. Therefore, given the limited availability of tailored pediatric medicines, the adjustment of products manufactured by the pharmaceutical industry for the personalization of medication in the case of specific groups of patients, such as children, as well as extemporaneous compounding, have become routine practices [4]. Unfortunately, the intervention of the pharmacist

in the pharmaceutical forms prepared for adults in order to transform them into pediatric pharmaceutical forms with specific API doses, or with certain shapes or sizes, may lead to a high risk of dosing errors. Nevertheless, extemporaneous compounding is regarded as a convenient option to obtain acceptable dosage forms customized for a limited number of pediatric patients or during drug shortages. Compounded pediatric medicines are regularly available as liquid dosage forms or as powders intended for reconstitution. However, these dosage forms often have inherent limitations concerning their stability and taste.

Recently, the trend has been shifting towards replacing liquid dosage forms with solid ones due to several benefits, such as more accurate dosing, better stability, lower costs, and increasing evidence supporting better acceptability [5]. Through the collaborative efforts of the authorities and different research groups, significant progress has been made in developing age-appropriate solid formulations. In recent years, numerous innovative technologies and delivery systems with additional benefits have been proposed, but significant gaps still exist. Among them, orodispersible films (ODFs) are versatile dosage forms offering significant benefits in terms of dosing flexibility and acceptability [6]. They can be administered without water, and despite being a relatively new technology platform, several commercial products are available.

ODF manufacturing methods include solvent casting, hot-melt extrusion (HME), electrospinning, and ink printing technologies [3]. HME is a promising solvent-free technology, generally employed for APIs that display water sensitivity [7]. Moreover, an important application of HME is the preparation of amorphous solid dispersions (ASDs) from API–polymer mixtures. Their use is typically associated with improved solubility and the bioavailability of poorly soluble APIs, resulting in a faster onset of action [8]. With a better understanding of HME and amorphous systems, new technologies are continuously being explored to match individual patient needs, such as 3D printing and ODF extrusion. However, the implementation of HME involves several complex stages, and successful development requires experimental work, trained personnel [9], and significant quantities of raw materials [10,11]. Moreover, these new technologies raise concerns about the costs related to their manufacturing, as well as regulatory challenges [12]. Regarding the regulatory aspects, while some believe that a clear implementation of good manufacturing practice (GMP) and the International Organization for Standardization (ISO) is needed in order to obtain products of high and consistent quality [12], others consider that the regulatory and quality assurance for these products is comparable to that of standard magistral products [13]. Regarding the costs, it seems that personalized medicines have the potential to be cost-effective, due to the possibility of manufacturing small and versatile batches, even if they may vary widely depending on the equipment used and the country [14,15].

First applied as a sample preparation technique, Vacuum Compression Molding (VCM) is a fusion-based method used to obtain compact, HME-like samples from powders. Applying vacuum and heat, the API is melted or solubilized into a polymer, resulting in an ASD. Samples obtained via VCM are transparent discs or bars containing the amorphous form of an API incorporated in the polymeric matrix [3]. VCM was developed as a preformulation tool for quick and cost-effective ASD development, enabling the easy preparation of samples for further stability and performance testing [10]. Lately, it has been applied as a lossless processing technique to obtain small-scale formulations [10]. So far, the technique has been employed in different applications, such as the preparation of polymeric microneedles for transdermal drug delivery [16], the study of the efavirenz solubility limits in different matrix polymers [17], as a protein-stabilizing method for potential HME processing [18], or for the preparation of subcutaneous implants [19].

In pediatric therapy, there is a constant need for new preparation methods with simple working principles that deliver customized pharmaceutical products; thus, this proof-of-principle study explores the use of VCM in ODF production. The tested hy-

pothesis is that VCM could act as a method of preparing small-scale pediatric products that is accessible to community or hospital pharmacies. The data currently available show that there is increasing interest in the introduction of personalized medicines in therapy, with one of the recurring applications being the use of this technique in clinical studies [20]. A 2021 study investigated how 3D printing technologies can be implemented in the European pharmaceutical system (i.e., the Netherlands). Of the five scenarios investigated to assess issues that could affect the implementation, industry and the patient's homes were associated with the most challenges, while hospital pharmacies and compounding facilities were associated with the fewest [21]. Although the prospects are encouraging for manufacturing personalized medicines in hospital pharmacies and compounding facilities, there are still no international policies or guidelines to provide a framework in this respect [22]. For now, the personalized products are manufactured in accordance with the standard compounding regulations and are subject to quality, safety, and stability control to prove that they are suitable for patient administration [20].

In this study, the experimental approach focused on the plasticizer selection and API (diclofenac sodium) loading with varying ratios to yield the appropriate mechanical characteristics, disintegration, and drug release profile for the ODFs. Further investigations were performed to assess the solid-state properties. To the best of our knowledge, so far, there are no reports on VCM employed for the production of small-scale ODFs.

2. Results and Discussion

In this study, VCM technology was used to prepare ODFs for pediatric use. The careful selection of ingredients is a prerequisite to ensuring the product performance and acceptability.

Maltodextrin (MD) was chosen for its well-known functionality as an orodispersible-film-forming agent, which is true, especially for the sorts with dextrose equivalents between 6 and 12 [23,24]. Further, the plasticizers were chosen based on information gathered from the literature, such as the non-miscibility of MD with PEG 400 and citric acid esters [25]. Cilurzo et al. showed that MD was compatible with glycerol and propylene glycol, which acted as efficient plasticizers [25]. However, propylene glycol imparted an unpleasant taste to the films, according to data collected from volunteers [26]. Regarding glycerol, during the screening stage of the present study, there were attempts to introduce this plasticizing agent into the formulations, but it was not possible to obtain appropriate films. Other frequently used plasticizers for improving the ductility of maltodextrin ODFs are sorbitol and xylitol; therefore, they were included in the study [26]. Given the bitter taste of diclofenac sodium, the addition of plasticizers with sweetener properties increased the acceptability of the formulation [27]. Mannitol is not a first-choice plasticizer for ODF preparation, but due to the similar structure to that of sorbitol and xylitol, it was also considered a worthy option to investigate, considering that mannitol may influence the mechanical properties of the ODFs [6].

Based on the data collected in the preliminary stage, loaded ODFs were prepared with increasing diclofenac sodium concentrations, maltodextrin as a film-forming agent, xylitol as a plasticizer, and croscarmellose as a superdisintegrant.

2.1. Appearance and Size

The vacuum-molding process resulted in round-shaped, completely translucent films, slightly yellow in color, at increasing diclofenac sodium doses (as shown in Table 1 for formulations N5–N8), with a diameter of 20 mm. When compared to commercial ODFs, they are slightly smaller in size, thicker, and more transparent.

Table 1. Physical characteristics of the ODFs.

	Appearance	Thickness (µm)	Weight Yield (%)		Appearance	Thickness (µm)	Weight Yield (%)
N1		320 ± 46.4	85.12 ± 9.07	**N5**		313.3 ± 21.6	94.83 ± 2.53
N2		241.6 ± 27.8	66.33 ± 12.38	**N6**		316.6 ± 10.3	92.65 ± 5.34
N3		270 ± 27.3	79.87 ± 9.52	**N7**		306.6 ± 19.6	92.24 ± 5.94
N4		313.3 ± 26.4	94.22 ± 5.82	**N8**		308.3 ± 19.6	88.66 ± 7.47

2.2. Mechanical Characterization

Puncture tests are the most frequently cited in the literature for evaluating the mechanical properties of orodispersible films. These tests rely on fixing the sample between two plates and measuring the load needed for a probe to puncture the sample through a central orifice [28]. As mentioned by other authors [29], the gap is usually similar in size or larger compared to those of commercial film samples. As the ODFs prepared in this study were smaller than most commercial ODFs, a customized accessory with a smaller gap diameter was used. Moreover, considering the means of unpacking and manipulating the ODFs prior to administration, their mechanical properties were also assessed through tensile tests [30]. Although the two tests can lead to similar mechanical parameters, many authors consider that they can complement each other in explaining the mechanical behavior of ODFs [31]. Table 2 presents the ODF parameters obtained from the mechanical tests.

Table 2. Mechanical characterization results for the VCM ODFs.

	Puncture Test					Tensile Test		
	Load at Puncture (g)	Deformation at Puncture (mm)	Fracturability (g)	Puncture Strength (N/mm^2)	Breaking Factor (N/mm)	Tensile Strength (MPa)	Elongation at Peak Load (%)	Young's Modulus (MPa)
N1	300.30 ± 109.80	0.88 ± 0.37	97.50 ± 20.10	0.92 ± 0.35	9.2 ± 3.49	1.80 ± 0.49	111.33 ± 7.29	41.34 ± 1.04
N2	94.50 ± 9.00	0.33 ± 0.25	70.80 ± 26.00	0.37 ± 0.08	3.73 ± 0.76	2.76 ± 0.87	109.17 ± 2.25	45.33 ± 1.23
N3	160.50 ± 19.50	0.09 ± 0.04	149.20 ± 35.60	0.57 ± 0.06	5.71 ± 0.64	0.78 ± 0.29	103.5 ± 0.71	30.85 ± 12.45
N4	397.50 ± 125.30	0.80 ± 0.12	299.30 ± 196.50	1.17 ± 0.39	11.68 ± 3.91	1.86 ± 0.56	134.33 ± 7.97	29.30 ± 6.87
N5	261.50 ± 140.4	0.96 ± 0.37	218.30 ± 177.70	0.58 ± 0.10	5.77 ± 0.97	2.03 ± 0.59	135.5 ± 11.95	37.62 ± 5.61
N6	180.50 ± 5.66	0.38 ± 0.26	146.5 ± 11.80	0.49 ± 0.01	4.87 ± 0.12	2.86 ± 0.52	119.17 ± 5.97	46.14 ± 5.61
N7	145.25 ± 1.77	1.04 ± 0.42	114.50 ± 39.50	0.46 ± 0.006	4.59 ± 0.06	2.96 ± 0.12	110.83 ± 3.06	52.83 ± 11.10
N8	243.80 ± 65.80	0.83 ± 0.18	142.80 ± 68.70	0.78 ± 0.14	7.82 ± 1.39	2.32 ± 0.34	109.33 ± 0.29	49.92 ± 5.48

Formulations N1–N3 contained MD and one of three plasticizers: sorbitol, xylitol, and mannitol, respectively. Although it would have been interesting to highlight the differences in the mechanical features between the samples containing plasticizers and those made of

MD alone, the preparation and mechanical testing of the MD films were not feasible, as the MD did not melt at the VCM working temperature employed in this study.

The puncture loads obtained for the samples containing MD and the plasticizer mixtures without the disintegrant (N1–N3) ranged between 94.5 ± 9.00 g and 300.30 ± 109.80 g, which showed a promising overlap with the load values for the commercial ODF products (Figure 1). Sorbitol showed the best performance in terms of both the puncture load and flexibility, indicated by the highest puncture deformation (0.88 ± 0.37 mm). Mannitol led to the most rigid structure in terms of the intermediate load at puncture, but it allowed for a very low deformation of only 0.09 ± 0.04 mm. In the puncture test, the N2 sample containing xylitol showed the lowest puncture load and lowest fracturability (load at the first fracture), but it allowed for a higher deformation compared to that of the mannitol. Looking at the tensile test results for formulations N1–N3, using xylitol as a plasticizer led to the highest tensile strength values, meaning that the films containing xylitol needed the highest forces to be deformed by tension. This led to the selection of xylitol as a plasticizer in the further formulations (from N4 to N8).

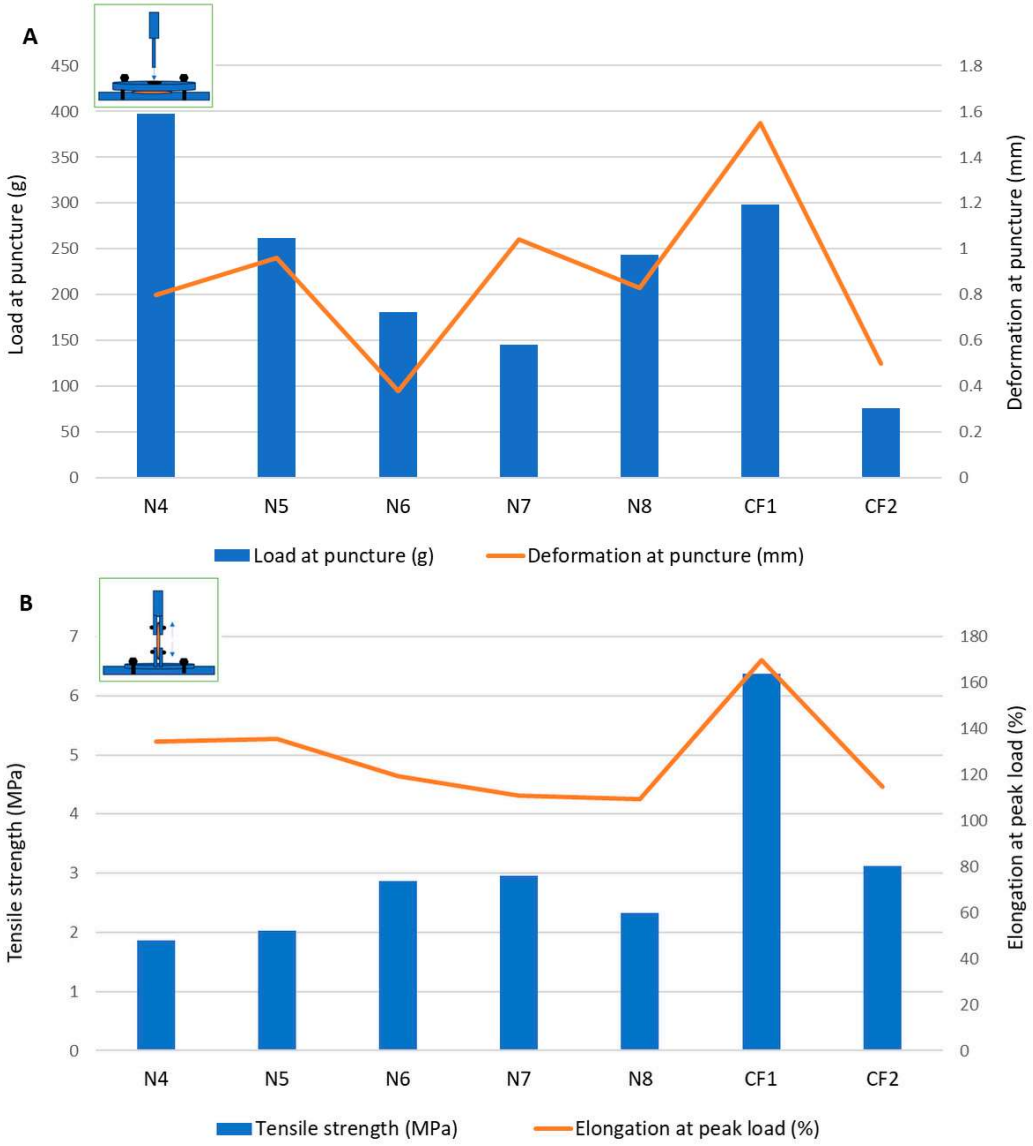

Figure 1. Mechanical characterization of films through (**A**) puncture test and (**B**) tensile test.

In formulation N4, the croscarmellose, added for its superdisintegrant properties, also positively impacted the mechanical features of the films. During the puncture test, the

puncture load increased significantly compared to formulation N2 without croscarmellose, along with the deformation at puncture and fracturability. Therefore, the croscarmellose improved the flexibility of the films, as well as their resistance to fractures. The breaking factor, which is regarded as the most appropriate parameter to consider when comparing samples with different thicknesses [29], had the highest value for N4.

The results obtained for the VCM ODFs indicate different responses according to the forces applied. For example, the ODF drug loading decreased the load needed to puncture the samples, regardless of the API dose, while it determined an increase in the tensile strength when the same samples were extended.

Additionally, the deformation obtained in the puncture test had a random variation with the lowest value corresponding to the lowest flexibility recorded for N6 (with 5 mg of API per unit) and the maximum deformation for N7 (with 10 mg of API per unit) (Figure 1). In contrast, for the tensile test, the deformation values were not influenced by lower API doses, but when the dose increased, the deformation capacity of the films decreased along with the dose. Figure 2 depicts the appearance of the ODFs submitted to the tensile tests after a constant deformation of 16.6%. The placebo sample (N4) and the low-dose diclofenac sodium formulations (N5 and N6) exhibited neck formation and elastic breaks, while brittle fractures appeared at high drug loading for N7 and N8, which also displayed higher Young's moduli. Therefore, adding the API resulted in less ductile films, which allowed for lower deformation when they were subjected to tensile stress. Our findings are in agreement with the results obtained by other researchers for maltodextrin-based, solvent-cast ODFs [23].

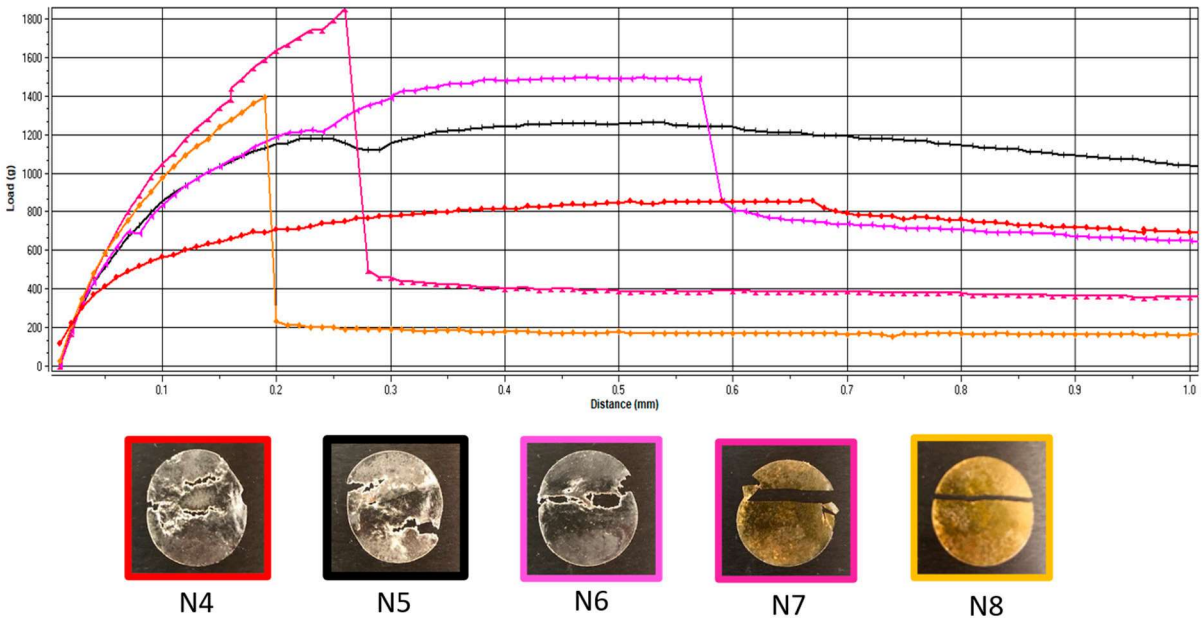

Figure 2. Representative load-versus-distance profiles of VCM ODFs and associated images of the samples at the end of the tensile test. VCM ODF formulations are represented in different colors: N4: red; N5: black; N6: pink; N7: magenta; N8: yellow.

Since there are no official limits for the mechanical parameters that describe ODFs, two authorized commercial products obtained by solvent casting were evaluated under the same conditions. The load results for the VCM ODFs were largely in the same range or higher than those for the commercial products, at all the drug loadings and regardless of the applied test. In contrast, for the deformation capacity, values lower than those of any commercial product were obtained for formulations with high drug loadings (between 10 mg and 50 mg per unit) during the tensile testing. Other researchers have attempted to establish acceptance criteria for the puncture strengths of different types of orodispersible films. The authors of [32] found values over 0.08 N/mm^2 acceptable for 3D printed films,

while the authors of [33] mentioned values over 0.06 N/mm^2 for solvent-cast films [32,33]. This indicates that VCM ODFs are well within the acceptable limits. Moreover, the authors of [25] reported values in the same ranges for their HME films containing MD and piroxicam as an API [25].

2.3. Contact Angle Measurements

Contact angle evaluation was used as a tool to predict the wettability and further disintegration of the ODFs [34]. The contact angle values for the eight formulations are noted in Table 3, expressed as the mean ± S.D. of three measurements. Figure 3 shows photographs taken during the measurements for the formulations N2, without diclofenac sodium, and N5, with 2.5 mg diclofenac sodium. Among the films containing only MD and a plasticizer, the smallest contact angle was reported for N3 (42.10 ± 4.72°), containing mannitol as the plasticizer, followed by N2 (47.39 ± 9.77°), containing xylitol as the plasticizer, and N1 (52.14 ± 2.38°), containing sorbitol. The results are consistent with the water solubilities of the three plasticizers, namely, 1:0.5 for sorbitol, 1:1.6 for xylitol, and 1:5.5 for mannitol [35]. Noticeably, the increase in the solubility of the plasticizer led to smaller values for the contact angle.

Table 3. Wettability and disintegration behavior of ODFs.

	Contact Angle (°)	Disintegration Time—Ph. Eur. Method (s)	Disintegration Time—Texture Analysis Method (s)
N1	52.14 ± 2.38	60.00 ± 0	51.42 ± 8.50
N2	47.39 ± 9.77	60.00 ± 0	50.27 ± 11.24
N3	42.10 ± 4.72	70.00 ± 0	62.13 ± 10.92
N4	47.44 ± 6.08	68.33 ± 7.64	59.57 ± 12.50
N5	64.83 ± 7.98	101.33 ± 10.26	65.33 ± 10.27
N6	58.43 ± 7.70	101.67 ± 20.21	57.93 ± 18.01
N7	48.89 ± 6.82	68.00 ± 5.20	46.53 ± 8.38
N8	47.90 ± 5.49	83.67 ± 10.12	41.00 ± 14.25

Mean ± S.D. (n = 3).

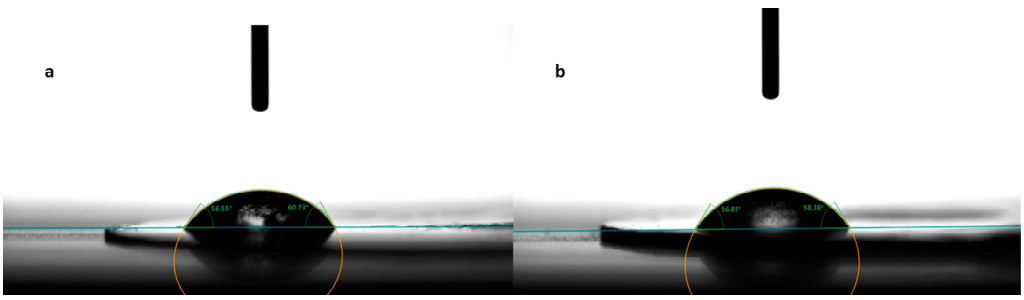

Figure 3. Contact angle measurement for formulations N2 (**a**) and N5 (**b**).

Regarding formulation N4, even though croscarmellose is insoluble in water, the addition of this disintegrant did not change the hydrophilicity of the films, and the contact angles remained almost unchanged (47.44 ± 6.08° for N4 and 47.39 ± 9.77° for N2).

The drug-loaded films showed varying values for the contact angle, as indicated in Table 3. Compared to formulation N4, which did not contain any API, the addition of diclofenac sodium imparted slight hydrophobicity to the films, evidenced by the larger values for the contact angles for formulations N5–N8. However, the contact angle decreased with the increase in the diclofenac sodium concentration. Even though diclofenac sodium is a sparingly hydrosoluble salt, at lower concentrations, it led to the highest contact angle (64.83 ± 7.98° for N5). Interestingly, as its concentration increased, it imprinted a hydrophilic character on the obtained films and, implicitly, a decrease in the contact angle (from 64.83 ± 7.98° for N5 to 47.90 ± 5.49° for N8).

The Ph. Eur.'s provisions regarding the wettability of solids are that "wettable solids should show a low contact angle and non-wettable solids show a contact angle of 90° or more" [36]. Therefore, the average contact angle of ODFs ranging between 42.10 ± 4.72° and 64.83 ± 7.98° indicates some degree of hydrophilicity [37].

2.4. Disintegration Behavior

The disintegration times of the ODFs, according to the pharmacopeial and texture analysis methods, are illustrated in Table 3. Regarding the disintegration times obtained under pharmacopeial conditions, the values ranged from 60.00 ± 0 s to 101.67 ± 20.21 s. Ph. Eur. does not have specific requirements for orodispersible films; the only information provided is that they should "disperse rapidly" after being placed on the tongue [38]. Therefore, the results were compared with the Ph. Eur. requirements for orodispersible tablets, namely, disintegration "within 3 min, using water as the liquid medium" [39], and the results show that, without a doubt, all the formulations complied with these exigencies. The films containing only MD and a plasticizer (N1–N3) had the shortest disintegration times of about 60–70 s. The addition of the disintegrant, croscarmellose, did not increase the disintegration time significantly, but the subsequent addition of diclofenac sodium led to an increase of approximately 40 s for the formulations containing low drug concentrations (N5 and N6). However, further increasing the diclofenac sodium concentration (N7 and N8) resulted in shortening the disintegration times down to values similar to those of drug-free films.

When the conditions in the oral cavity were simulated in the texture analysis method, as expected, the disintegration times were shorter than those measured according to the pharmacopeial method. Similar results were obtained by the authors of [30], who reported that less was time needed when using the non-pharmacopeial method by better mimicking the disintegration process in the human mouth (i.e., using simulated salivary fluid in a reduced volume) [30]. These findings might suggest that the pressure applied to the product and the characteristics of the medium used (pH, composition) are more important than its volume. In our study, the disintegration times fell between 41 ± 14.25 s and 65.33 ± 10.27 s. Although no significant differences were obtained between the formulations, a decreasing trend in the disintegration times was observed with the increase in the concentration of diclofenac sodium. This can be explained by the increased hydrophilicity and better wetting capacity, also reflected by the contact angle measurements. Thus, the results obtained using texture analysis are in accordance with the previously mentioned results obtained using the pharmacopeial method. The disintegration times of the VCM ODFs are well within the pharmacopeial limit of 180 s and seem robust concerning the API dose changes, which is beneficial for the preparation of small-scale personalized products.

The authors of [25] obtained similar results, with a slower disintegration of approximately 1 min for the HME films (containing piroxicam and MD) compared to the solvent-cast films with a disintegration of a few seconds [25]. The authors of [24] also obtained an average disintegration time of about 1 min for diclofenac-loaded maltodextrin orodispersible films [40].

2.5. In Vitro Dissolution Studies

For predicting the in vivo dissolution behavior of the ODFs, an in vitro test was performed using the pharmacopeial method for immediate-release tablets, since there are no official compendial methodologies for ODF dissolution studies. All formulations released more than 85% of the API within 5 min (Figure 4), which accounts for very rapidly dissolving products [41,42]. The concentration of diclofenac sodium released was influenced by the concentration of the drug in the formulation. Thus, the formulations with lower concentrations of diclofenac sodium released lower concentrations of the drug after 5 min (88.56 ± 0.30% for N5 and 85.11 ± 0.01% for N6), while for the last two formulations with higher diclofenac sodium contents, higher percentages of drug release were noticed after 5 min (97.83 ± 1.92% for N7 and 100.22 ± 0.15% for N8). These results are also valid

for the total amount of diclofenac sodium released from the formulations and are correlated with the disintegration time and the contact angle: increasing the concentration of the API increased the hydrophilicity of the films, allowing for a better wetting of the film with the dissolution medium (decrease in the contact angle) and rapid disintegration (decrease in the disintegration time), and ensuring the increased release of the diclofenac sodium.

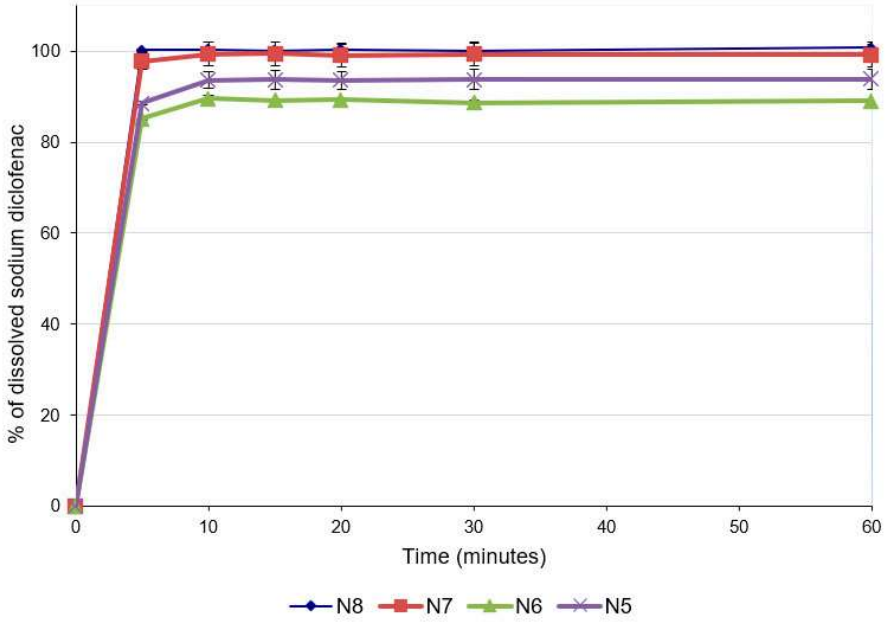

Figure 4. Dissolution profiles of ODFs with diclofenac sodium.

The ability of maltodextrins to improve the dissolution rates of the active ingredients included in ODFs has been previously demonstrated [41]. Regarding the influence of the API on dissolution, a study in which the characteristics of diclofenac sodium-loaded, maltodextrin-based films were evaluated reported that the presence of diclofenac did not affect the dissolution rate of the API [23]. However, the study did not pursue variation in the diclofenac sodium concentration, and the information provided suggests that this API does not hinder the disintegration of the films and the subsequent dissolution.

Regarding the ODF preparation method, the authors of [25] found that the dissolution rate of piroxicam was clearly higher in the case of films prepared by solvent casting compared to films prepared by the HME method. However, it seems that not only the method led to these results but also the excipient in the formulation, namely, microcrystalline cellulose, which induced a slower disintegration of the films and, subsequently, a decrease in the piroxicam dissolution rate by two different mechanisms, swelling and delaying maltodextrin dissolution, thereby reducing its solubilizing effect [25]. The results obtained in our study are very promising, the API's dissolution rate being comparable not only to those observed for films obtained by solvent casting but also to those observed in other experiments that studied ODFs prepared by HME [34,40,41,43].

2.6. Solid-State Analysis

2.6.1. DSC Studies

As described in the Materials and Methods Section, the VCM process involves sample melting and thus thermal stress is applied. Thermal analysis was of paramount importance, first to select the melting temperature used during the VCM, and further to understand the changes that occur during the preparation process.

Figures 5 and 6 display the thermograms corresponding to the pure ODF components, followed by the physical mixtures and the VCM ODF samples.

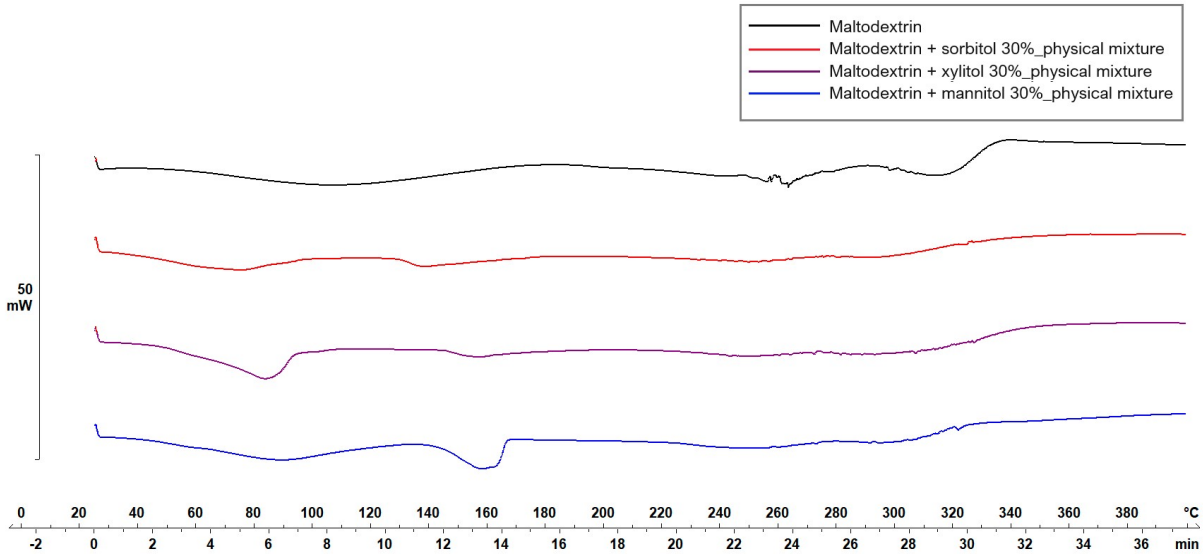

Figure 5. Thermal behavior evaluation for plasticizer selection.

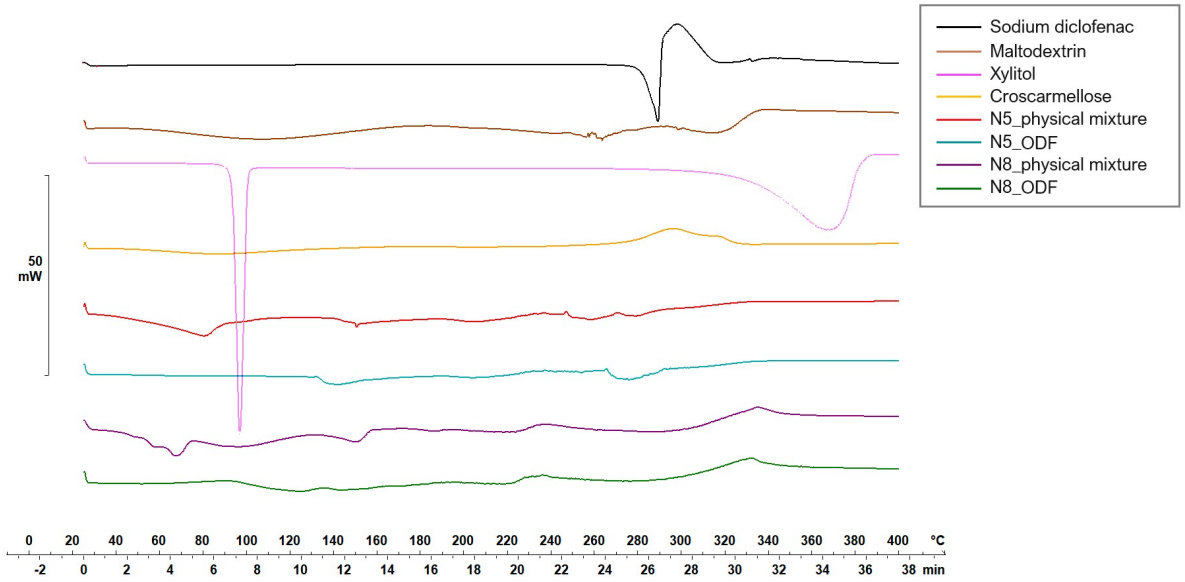

Figure 6. Thermal behaviors of the individual components of the ODFs and of the N5 and N8 physical mixtures and ODFs.

The MD displayed a large endothermic event between 38.7 and 178.06 °C, with the peak at 106.63 °C, which could be attributed to dehydration, although other authors have found the glass transition of MD at about the same temperature: 102.6 ± 2 °C [44]. Another endothermic peak was detected at 242.45 °C that could be associated with the melting phenomenon. Regarding the plasticizers, xylitol presented a sharp endothermic peak at about 94.42 °C, attributed to its melting [45,46]. The high melting enthalpy (1639.63 mJ) of xylitol is related to the cooling sensation it offers when dissolved in the oral cavity and is present only if xylitol maintains its crystalline form [45]. Sorbitol presented the endothermic peak at 100.71 °C, and mannitol at 166.04 °C (data not included). When MD was mixed with the plasticizers, namely, with xylitol, the endothermic peak that indicated the melting of the mixture appeared at about 160 °C (Figure 5). Therefore, the working conditions for the VCM ODF preparation were set at a temperature of 170 °C.

Diclofenac sodium presented a sharp endothermic peak at 298.59 °C, corresponding to its crystalline melting, followed by an exothermal phenomenon associated with the decomposition, all in agreement with other authors' findings [47,48].

The physical mixtures displayed an initial narrow peak at 91 °C, corresponding to the melting of xylitol, followed by a broader peak at 152.65 °C, attributed to crystalline diclofenac sodium melting, and then a succession of endo-/exothermal phenomena associated mainly with decomposition. For both crystalline substances (i.e., xylitol and diclofenac sodium), a melting shift to a lower temperature was noticed, which can be attributed to the dilution effect or the partial dissolution of diclofenac sodium into MD. The VCM ODF thermograms displayed no crystalline peaks but rather a succession of broad endothermal and exothermal events with decomposition after about 180 °C, which could suggest the partially amorphous state of the components, including the initially crystalline xylitol and diclofenac sodium.

2.6.2. XRD Studies

XRD was used to assess the crystalline state of the API in the physical mixtures, as well as in the VCM ODFs. As Figure 7 shows, the pure diclofenac sodium displayed many distinct peaks, among which those with the highest intensities were at 6.63°, 8.5°, and 15.2°. The amorphous maltodextrin and croscarmellose showed no distinct peaks. The physical mixtures containing all the components of the ODFs preserved the characteristic peaks of the API, but at a lower intensity due to the dilution phenomenon. Furthermore, the peaks corresponding to xylitol were visible. The diffractograms corresponding to the VCM ODFs presented no visible peaks, usually indicating amorphous contents and sustaining the previously discussed DSC evidence. Interestingly, the same appearance of the diffractogram was obtained for all the API doses, which showed that, even at high diclofenac sodium loading, MD can dissolve and turn it amorphous.

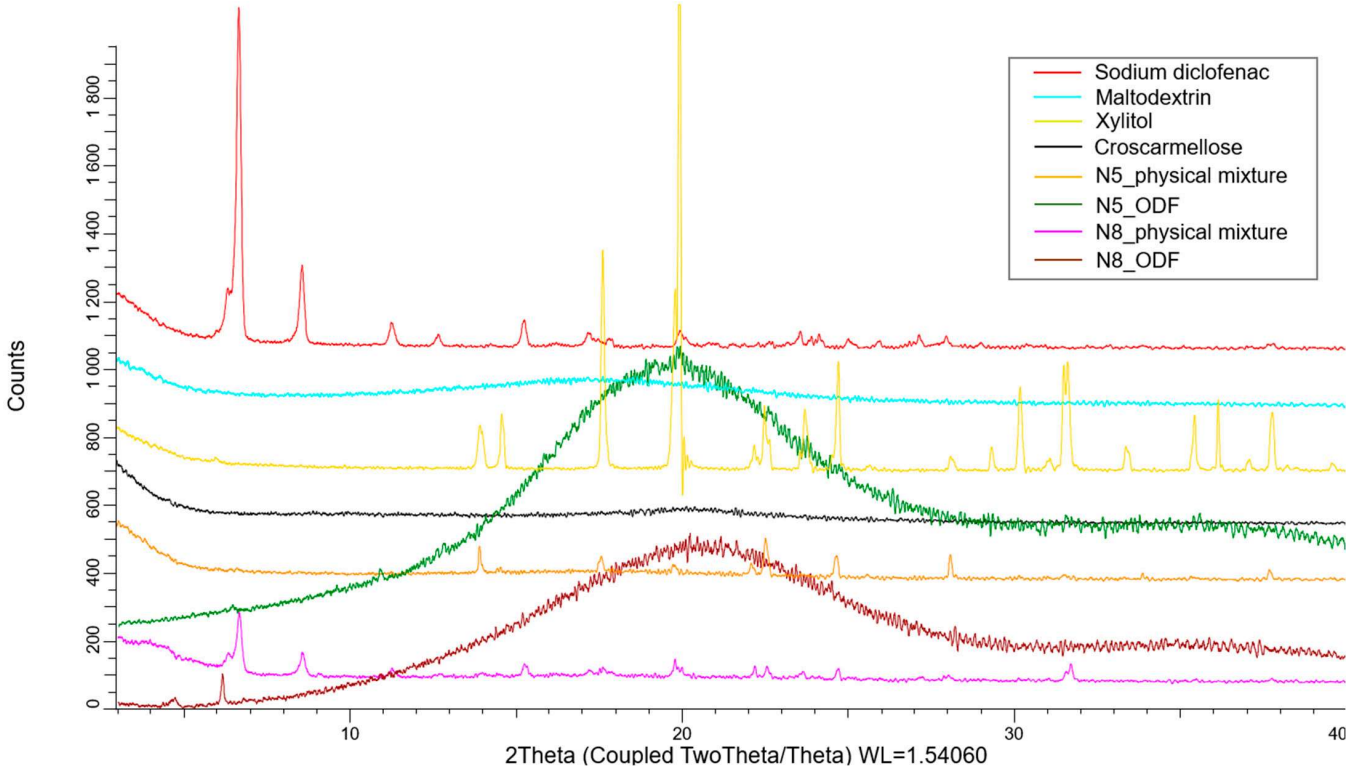

Figure 7. The X-ray diffractograms of the individual components of the ODFs and of the N5 and N8 physical mixtures and ODFs.

2.6.3. FT-IR Studies

The interactions between the ODF components were assessed by FT-IR experiments, and the resulting spectra are displayed in Figure 8. The pure diclofenac sodium showed bands representative of the symmetrical and asymmetrical stretching vibrations of the

carboxylate groups at 1454 and 1580 cm^{-1}. At 747 cm^{-1}, the C-Cl stretching peak was visible [48], while at 3375 cm^{-1}, a vibration band appeared for the secondary amino group [47]. FT-IR spectra showed the specific maltodextrin pattern with the two peaks at 992 cm^{-1} and 1012 cm^{-1}, corresponding to the C-O stretching vibration. Meanwhile, for xylitol, its spectrum showed high-intensity vibrations at 3368 cm^{-1} and 3168 cm^{-1}, which were attributed to O-H bonds [45]. Characteristic peaks corresponding to diclofenac sodium and xylitol were preserved in both VCM ODF spectra and were more evident in sample N8, due to the higher API loading.

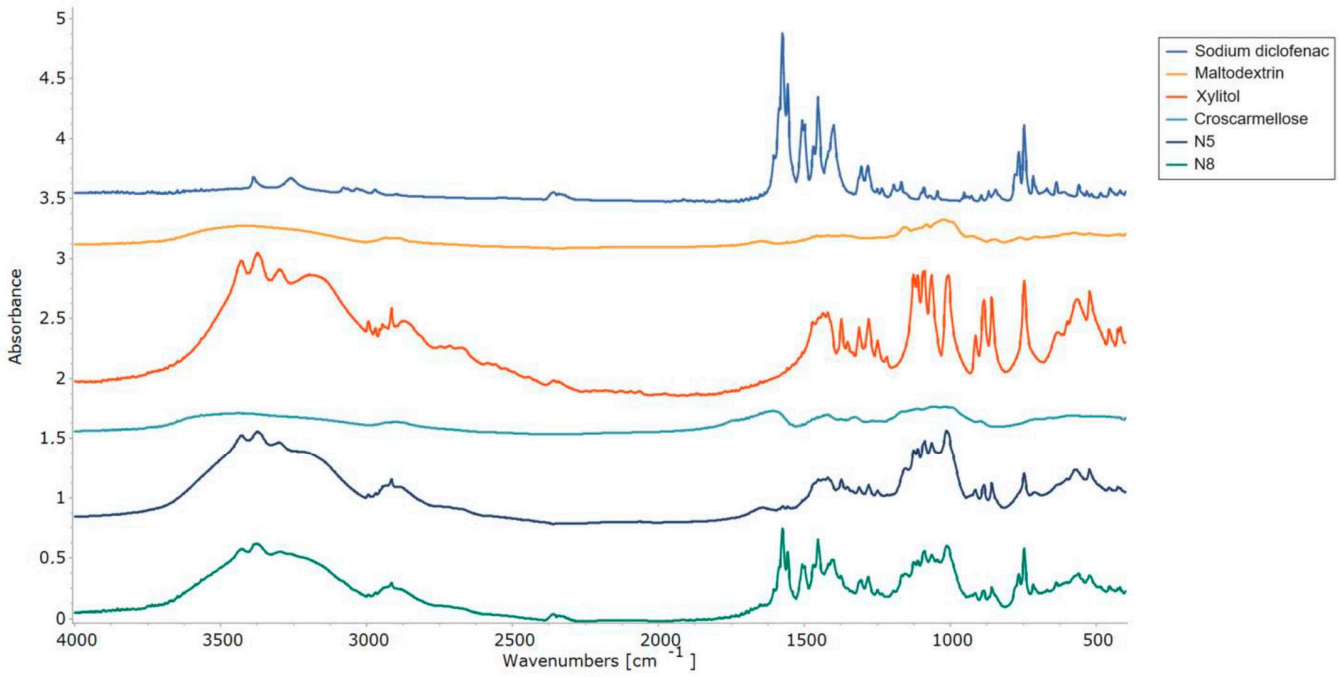

Figure 8. FT-IR patterns of the individual components of the ODFs and of the N5 and N8 ODFs.

2.6.4. SEM Studies

The SEM images (Figure 9) revealed flat, smooth, non-porous surfaces, with slight irregularities. When the scanning electron micrographs were examined for samples N4 (without diclofenac sodium), N5 (with 2.5 mg diclofenac sodium), and N8 (with 50 mg diclofenac sodium), their aspects were rather different. Sample N4 displayed small fractures that were not visible to the naked eye and could have appeared during manipulation. However, the observed fractures did not seem to harm the mechanical properties, as formulation N4 showed the highest peak loads in the puncture test. Sample N5 showed smooth surfaces with partial erosions that were also attributed to the manipulation and extraction from the VCM tool. Although sample N8 had the highest content of diclofenac sodium, no sign of recrystallization was noticed, only smooth plain surfaces.

2.6.5. Raman Microscopy

The distribution of diclofenac sodium in the VCM ODF samples was determined using Raman mapping. For the investigation, the chemical structures of the pure drug and different ODF formulations were compared to find a unique spectral region in the Raman spectra, characteristic of the drug, to be further used as a reference for its localization in the ODF samples. For the diclofenac sodium profiling, the Raman peak at 1575 cm^{-1} assigned to the COO^- asymmetric stretching vibration and the band at 1603 cm^{-1} attributed to the dichlorophenyl and phenylacetate ring stretching vibrations were applied, according to [49] (Figure 10). For each ODF sample, three randomly selected surfaces with an area of 100 × 100 μm were examined (Figure 11).

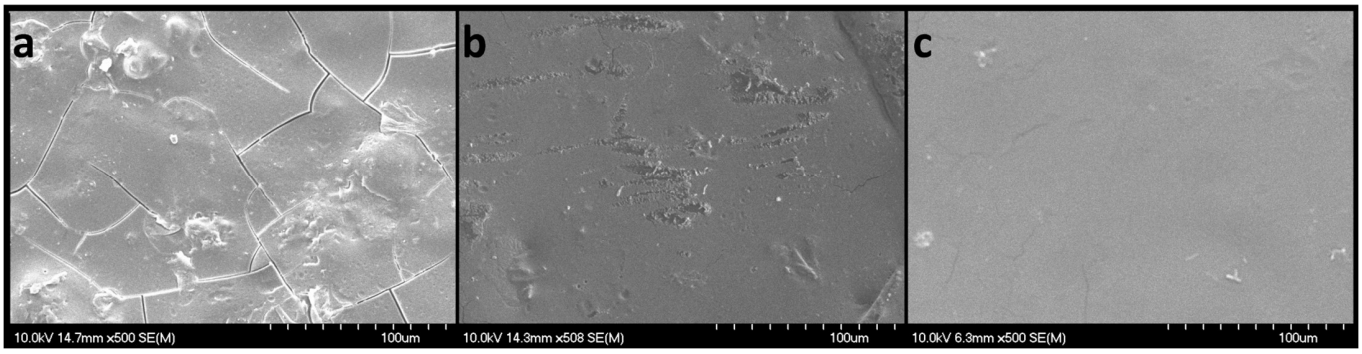

Figure 9. SEM micrographs of VCM ODFs: N4 (**a**), N5 (**b**), and N8 (**c**), captured with a magnification of 500×; scales represent 100 μm.

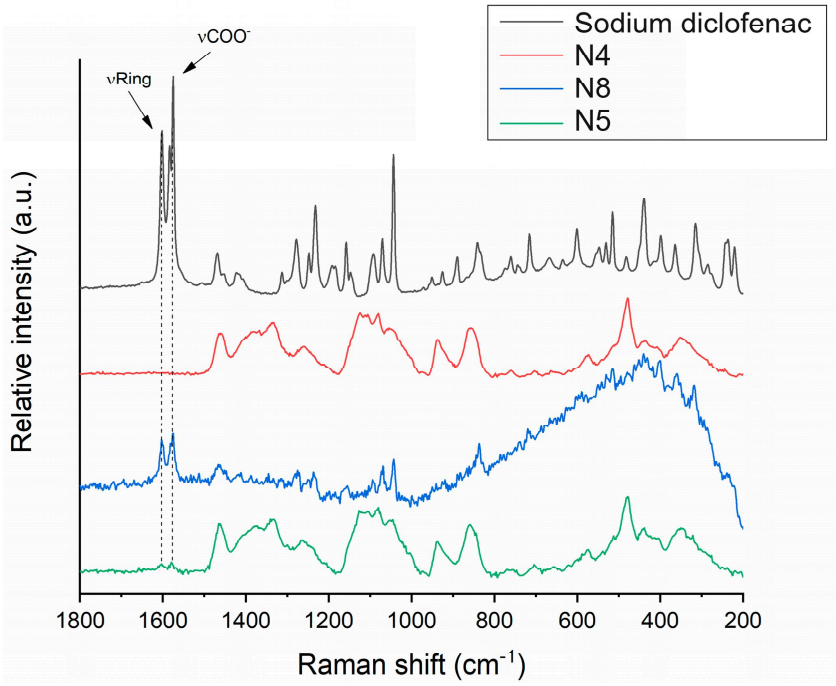

Figure 10. Raman spectra of diclofenac sodium in comparison to investigated ODF samples: diclofenac-free N4 reference, as well as diclofenac-loaded N8 and N5.

After the structural examination of the initial components, Raman mapping was performed to investigate the distribution of the diclofenac sodium in the ODF samples. For the localization, the previously mentioned spectral regions were used as a reference, the frequencies of occurrence of which are shown on the chemical maps, representing the statistical distribution of the drug (Figure 11). The different colors of the chemical map indicate the relative intensity changes of the diclofenac sodium in the investigated ODFs. The red-colored areas indicate its strong presence, the green areas show a mixture of the API with other components, and the blue color marks those regions of the map with spectral resolutions containing different spectra, characteristic of another excipient. As a reference, a diclofenac sodium-free sample (N4) was investigated, as shown in Figure 11a. In this case, no specific drug characteristics were found, indicated by the blue and slightly green colors of the chemical map. For the diclofenac sodium-containing ODFs (N8 and N5), the distribution of diclofenac was homogenous, as shown by the well-defined patches of the yellow-red color (Figure 11b,c). Moreover, the intensity of the diclofenac sodium markers was remarkably higher in the case of sample N8 in comparison to that of N5, corresponding to the higher drug content in the former.

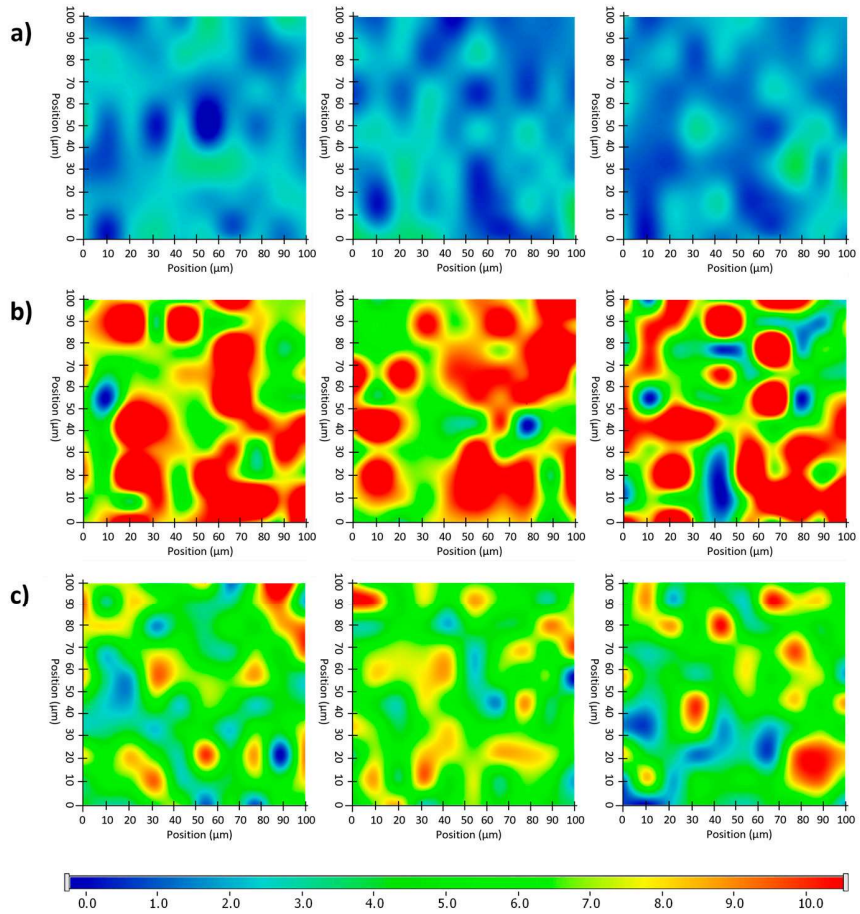

Figure 11. Randomly recorded Raman chemical maps of various ODF samples indicating the distribution and relative occurrence of diclofenac sodium: diclofenac sodium-free N4 reference (**a**), as well as diclofenac sodium-loaded N8 (**b**) and N5 (**c**).

2.7. Practical Implications and Future Applications

VCM was initially applied in 2014 as a new technology designed for sample preparation to ease the development burden of ASDs. In more recent studies, it has been applied in different pharmaceutical products, particularly for solid dosage forms.

In the formulation of ODFs, VCM can be potentially employed individually or in conjunction with other techniques to address specific formulation challenges. During preformulation studies for ODF development, VCM can assist in the selection of excipients as a screening tool. As a small-scale preparation method, VCM is convenient due to its solvent-free nature, eliminating concerns about residual solvents and providing a faster alternative to solvent-casting methods. Additionally, its cost-effectiveness in terms of equipment costs compared to HME and the small amounts of APIs and excipients needed with reduced material loss make it affordable for small production units, like pharmacies and low-income areas. As shown in the current study, this method is able to deliver personalized dosage forms tailored to individual patient needs, from a minimum of three excipients. However, the main limitations of the ODF preparation process using VCM include its restriction to thermally stable APIs and raw materials, and its suitability only for small-batch production. Future research should focus on testing various APIs and excipients, improving the working procedure to enhance the reproducibility in the weight yield, as well as on increasing the productivity.

3. Materials and Methods

3.1. Materials

The chemicals used for the preparation of the ODFs were as follows: diclofenac sodium (pharmaceutical-grade), kindly donated by Aarti Drugs Ltd. (Mumbai, India); maltodextrin with a dextrose equivalent of a maximum of 19% (Glucidex® Premium IT 19, Roquette, Lestrem, France) as a film-forming agent; sorbitol (D-Sorbitol ≥ 98%, Sigma-Aldrich, St Louis, MO, USA), xylitol (Xylisorb® 300, Roquette, Lestrem, France), and mannitol (Parteck M200, Merck, Germany) as plasticizers; and croscarmellose (Dislocel®, Mingtai Chemical Co, Ltd., Taoyuan, Taiwan) as a superdisintegrant. Commercial ODFs were purchased from community pharmacies: Melatonin Pura Fast (ESI s.p.a., Euronet Growth Milan, Italy) (Commercial Film 1, CF1) and Vitamin D3 2000 NE (IBSA Farmaceutici, Lodi, Italy) (Commercial Film 2, CF2). All other chemicals were analytical-grade.

3.2. Sample Preparation

An amount of 10 g of each powder blend, with the compositions shown in Table 4, were prepared by manually grinding and mixing the materials for 3 min in a mortar. For the VCM ODF preparation, 150 mg of mixture was loaded into the circular chamber (VCM disc tool with 20 mm diameter) of the Vacuum Compression Molding equipment (MeltPrep, Graz, Austria). Vacuum was applied, and then the insert was placed onto the heating plate for 5 min and kept at 170 °C. Afterwards, the sample was moved onto the cooling plate coupled with a source of compressed air for 8 min at room temperature. The schematic representation of the ODF preparation process is given in Figure 12. The resulting ODFs were then extracted and kept in the desiccator until further use. A total of 20 samples were prepared for each formulation. The medium weight of each ODF sample was 150 mg. The diclofenac sodium doses for samples N5–N8 were 2.5 mg, 5 mg, 10 mg, and 50 mg, respectively.

Table 4. ODF composition.

	N1	N2	N3	N4	N5	N6	N7	N8
Maltodextrin (%)	70	70	70	65	63.34	61.67	58.34	31.67
Sorbitol (%)	30							
Xylitol (%)		30		30	30	30	30	30
Mannitol (%)			30					
Croscarmellose sodium (%)				5	5	5	5	5
Diclofenac sodium (%)					1.66	3.33	6.66	33.33

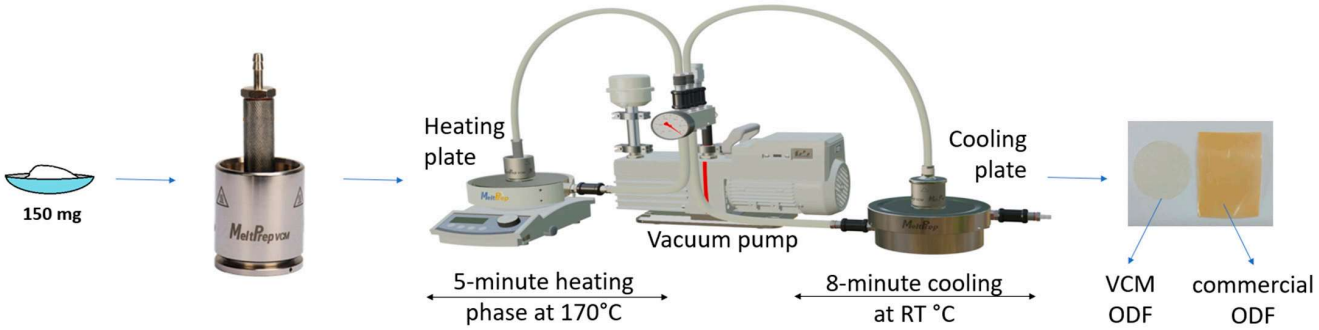

Figure 12. Graphical representation of the VCM ODF preparation steps.

3.3. Mechanical Characterization

Two tests were applied for the mechanical characterization of the films using a CT3 texture analyzer (Brookfield Ametek, Middleboro, MA 02346, USA), equipped with a 4.5 kg load cell.

Firstly, a puncture test was applied using a film fixture with a 10 mm diameter orifice (TA-RT-KIT) and a cylinder rig (2 mm diameter) (TA3/100) that descended through the sample at a speed of 0.10 mm/s after a trigger load of 5 g was attained.

Secondly, a tensile test was performed using a dual-grip rig (TA-DGF) that ascended at a speed of 0.10 mm/s and a trigger load of 1 g up to a target distance of 3 mm. The thickness was measured before the texture analysis using a digital caliper for each sample. All tests were performed in triplicate, and the load-versus-distance profiles were plotted. Texture Pro CT software (Brookfield Ametek, Middleboro, MA, USA) was used to calculate the following mechanical parameters: the load at puncture/at target, deformation at puncture/at target, and fracturability. Furthermore, the puncture strength and breaking factor were calculated from the profiles revealed by the puncture tests, according to literature-reported equations [28,29]. The tensile test enabled the calculation of the tensile strength, elongation at peak load, and Young's Modulus [28].

3.4. Contact Angle Measurement

The water contact angle was used as an instrument to evaluate the wettability of the ODF samples. The measurements were carried out with the drop-shape analyzer OCA 25 (Dataphysics Instruments, Stuttgart, Germany), using distilled water drops of 2.5 µL. Three drops were placed on each film in different places, and the software of the drop analyzer automatically calculated the angle for each measurement. The contact angle was measured at 0.05 ± 0.01 s after the drop landing.

3.5. Disintegration Testing

Many research groups use the pharmacopeial disintegration test to determine whether ODFs disintegrate within the prescribed time: 3 min [41]. Therefore, the disintegration test of the ODFs was carried out according to the specifications of the monograph "2.9.1. Disintegration of tablets and capsules" reported in the Ph. Eur., using the Erweka ZT 120 disintegration tester (Erweka GmbH, Langen, Germany). Randomly selected films of each formulation were analyzed in distilled water maintained at 37 ± 0.5 °C. The disintegration time was recorded when no residue remained in the mesh of the basket-rack assembly.

To simulate the oral conditions (e.g., a low saliva volume available for disintegration, mechanical stress applied by the tongue), the disintegration time was also evaluated through texture analysis, as shown in Figure 13. The method was adapted after [50] and involved the use of a puncture test fixture with a 10 mm orifice [50]. The VCM ODFs were placed in the sample holder and fixed with a 20 mm diameter ring. Each sample was wetted with 200 µL artificial saliva, and after a lag time of 5 s, an 8 mm round-ended cylindrical probe descended through the sample at a speed of 0.1 mm/s, down to a target distance of 10 mm. The load-versus-time profiles were recorded, and the disintegration times were calculated as the difference between the time when the probe reached the minimal sample resistance (disintegration endpoint) and the time of the peak load (marking the beginning of the disintegration) [50]. The disintegration test for both methods was performed in triplicate for each formulation, and the results were expressed as mean ± S.D.

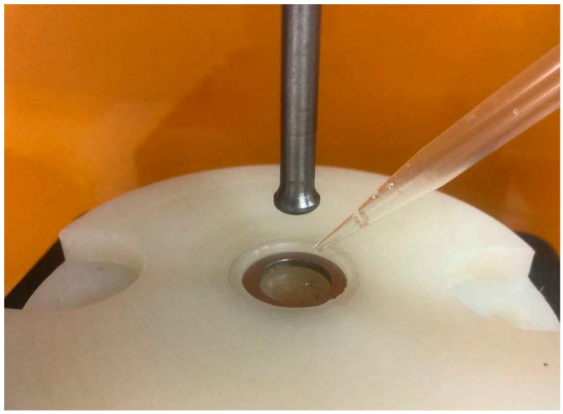

Figure 13. Experimental setup of the disintegration test performed by texture analysis.

3.6. Dissolution Studies

The dissolution studies were performed according to the Ph. Eur. 11.5 Ed. using a paddle dissolution apparatus in 900 mL phosphate buffer, pH 6.8, at 37 °C and a 50 rpm rotation speed, on accurately weighed ODFs. We withdrew 5 mL samples at 5, 10, 15, 20, 30, and 60 min throughout the test and replaced them with 5 mL of fresh medium. Diclofenac sodium was assayed through a validated HPLC method on an Agilent 1100 Series HPLC system (Agilent Technologies, Santa Clara, CA, USA), using an UV detector at 278 nm and a Luna C18(2) column (5 µm, 150 × 4.6 mm, 100 Å), a mobile phase composed of phosphoric acid 0.1% and acetonitrile 25:75 (*v*/*v*), and a flow of 1 mL/min, at a retention time of 2.9 min. The dissolution test was performed in triplicate for each formulation.

3.7. Solid-State Analysis

3.7.1. Differential Scanning Calorimetry (DSC)

DSC analysis was performed with a DSC3 Star^e System (Mettler Toledo GmbH, Zurich City, Switzerland). Samples of 2–3 mg of the pure substances, their physical mixtures, and of the VCM ODFs were accurately weighed into 40 µL aluminum pans and sealed with pierced lids. Further, they were analyzed under a dynamic nitrogen atmosphere (50 mL/min) over a temperature range of 25–400 °C with a heating rate of 10 °C/min. The resulting thermograms were analyzed using STAR SW 12.10 software (Mettler Toledo GmbH, Switzerland).

3.7.2. X-ray Diffraction (XRD)

XRD analysis was performed to investigate the physical state of the diclofenac sodium in the different stages of the preparation process: on the pure substance, on the physical mixtures, and on the VCM ODFs. XRD spectra were recorded with a BRUKER D8 Advance X-ray diffractometer (Bruker AXS GmbH, Karlsruhe, Germany) system with Cu Kα1 radiation (λ = 1.5406 Å) over the range 5–40°/2°. The following experimental setup was employed: target: Cu; filter: Ni; voltage: 40 kV; current: 40 mA; time constant: 0.1 s; angular step: 0.010°.

3.7.3. Scanning Electron Microscopy (SEM)

The morphologies of the films were evaluated through SEM (Hitachi S4700, Hitachi Scientific Ltd., Tokyo, Japan) by applying a potential of 10 kV and 1.3–13.0 mPa air pressure. Before the analysis, samples were sputter-coated with gold–palladium to ensure conductivity (Bio-Rad SC 502, VG Microtech, Uckfield, UK).

3.7.4. Raman Microscopy

Raman mapping of the ODF samples was performed using a Thermo Fisher DXR dispersive Raman instrument (Thermo Fisher Scientific Inc., Waltham, MA, USA) equipped with a CCD camera and a diode laser operating at a wavelength of 780 nm. For the analysis, ODF samples were mounted on a glass slide that was covered with aluminum foil. Raman chemical maps were recorded from 100 × 100 µm surfaces of different ODFs with a 10 µm step size, while applying a laser power of 24 mW at a 50 µm slit aperture size. The spectrum of the chemical map was recorded with an exposure time of 2 s and an acquisition time of 6 s, for a total of 16 scans per spectrum in the spectral range 3300–200 cm^{-1}, with cosmic ray and fluorescence corrections. Each Raman map was normalized in order to eliminate the intensity deviation between the measured areas.

4. Conclusions

This study was a proof-of-concept study to demonstrate the feasibility of using VCM as an ODF preparation method. This technology enables the preparation of thermoplastic dosage forms with personalized dosing, a feature that is especially useful for pediatric patients but that is not limited only to them.

Briefly, diclofenac sodium-loaded ODFs for pediatric use were successfully formulated and prepared by the VCM technique, using maltodextrin as the film-forming polymer. The study's objectives were to perform an initial selection of the plasticizer, to add an appropriate amount of disintegrant, and, finally, to add different concentrations of the API (2.5 mg, 5 mg, 10 mg, and 50 mg of diclofenac sodium) in order to evaluate the influence of each formulation factor on the quality of the ODFs, and to demonstrate that VCM is suitable for personalized medicine preparation. The mechanical characterization of the ODFs revealed that xylitol was the best plasticizer, contributing to the formation of flexible ODFs. Regarding the disintegrant, the mechanical tests showed a further improvement in terms of the flexibility and resistance to fractures. While it is true that adding the API resulted in less ductile films, their mechanical properties are comparable to those of authorized commercial products and the data in the literature. All the characterization methods applied demonstrated the obtention of high-quality, wettable films with smooth surfaces, good distributions of the API in the ODFs, good disintegration capacities, and the release of more than 85% of the API within 5 min, regardless of the API loading dose. Therefore, VCM shows great potential in functioning as a method of preparing small-scale, personalized dosage forms.

Some of the advantages are presented in Section 2.7; however it must be added that this method could find application both in community and hospital pharmacies as a cost-effective technique, providing flexibility in dosing based on the individual patient characteristics and medical conditions. Additionally, tailoring doses to individual needs has the potential to reduce the risk of adverse effects.

Author Contributions: Conceptualization, S.I. and I.T.; methodology, S.I. and R.A.; software, T.C.; validation, S.I. and T.C.; formal analysis, D.H., C.B., L.R.T., I.T., T.C., R.I., G.K., R.A. and S.I.; investigation, D.H., C.B., L.R.T., A.C., M.-A.C., I.T., T.C., R.I., G.K., R.A. and S.I.; resources, S.I. and R.A.; data curation, S.I.; writing—original draft preparation, D.H., C.B., L.R.T., A.C., R.I., G.K., R.A. and S.I.; writing—review and editing, D.H., C.B., L.R.T., A.C., M.-A.C., I.T., T.C., R.I., G.K., R.A. and S.I.; supervision, S.I.; project administration, S.I.; funding acquisition, S.I. All authors have read and agreed to the published version of the manuscript.

Funding: This work was supported by a grant of the Romanian Ministry of Research, Innovation and Digitization, CCCDI-UEFISCDI, project number PN-III-P2-2.1-PED-2021-4198, within PNCDI III.

Data Availability Statement: The raw data supporting the conclusions of this article will be made available by the authors upon request.

Acknowledgments: This work was supported by a grant of the Romanian Ministry of Research, Innovation and Digitization, CCCDI-UEFISCDI, project number PN-III-P2-2.1-PED-2021-4198, within PNCDI III.

Conflicts of Interest: The authors declare no conflicts of interest. The funders had no role in the design of the study; in the collection, analyses, or interpretation of the data; in the writing of the manuscript; or in the decision to publish the results.

References

1. Global Accelerator for Paediatric Formulations Network (GAP-f). Available online: https://www.who.int/initiatives/gap-f (accessed on 4 June 2024).
2. European Medicines Agency. Paediatric Medicines: Overview. Available online: https://www.ema.europa.eu/en/human-regulatory-overview/paediatric-medicines-overview (accessed on 4 June 2024).
3. World Health Organization. *Innovative Delivery Systems for Paediatric Medicines: Technology Landscape*; World Health Organization: Geneva, Switzerland, 2020; ISBN 978-92-4-000818-2.
4. Lopez, F.L.; Ernest, T.B.; Tuleu, C.; Gul, M.O. Formulation Approaches to Pediatric Oral Drug Delivery: Benefits and Limitations of Current Platforms. *Expert Opin. Drug Deliv.* **2015**, *12*, 1727–1740. [CrossRef]
5. Klingmann, V.; Spomer, N.; Lerch, C.; Stoltenberg, I.; Frömke, C.; Bosse, H.M.; Breitkreutz, J.; Meissner, T. Favorable Acceptance of Mini-Tablets Compared with Syrup: A Randomized Controlled Trial in Infants and Preschool Children. *J. Pediatr.* **2013**, *163*, 1728–1732.e1. [CrossRef]
6. Turković, E.; Vasiljević, I.; Drašković, M.; Parojčić, J. Orodispersible Films—Pharmaceutical Development for Improved Performance: A Review. *J. Drug Deliv. Sci. Technol.* **2022**, *75*, 103708. [CrossRef]

7. Gupta, M.S.; Kumar, T.P.; Gowda, D.V.; Rosenholm, J.M. Orodispersible Films: Conception to Quality by Design. *Adv. Drug Deliv. Rev.* **2021**, *178*, 113983. [CrossRef] [PubMed]
8. Bellantone, R.A. Fundamentals of Amorphous Systems: Thermodynamic Aspects. In *Amorphous Solid Dispersions. Advances in Delivery Science and Technology*; Shah, N., Sandhu, H., Choi, D., Chokshi, H., Malick, A., Eds.; Springer: New York, NY, USA, 2014; pp. 3–34. ISBN 978-1-4939-1598-9.
9. Jani, R.; Patel, D. Hot Melt Extrusion: An Industrially Feasible Approach for Casting Orodispersible Film. *Asian J. Pharm. Sci.* **2015**, *10*, 292–305. [CrossRef]
10. Shadambikar, G.; Kipping, T.; Di-Gallo, N.; Elia, A.G.; Knüttel, A.N.; Treffer, D.; Repka, M.A. Vacuum Compression Molding as a Screening Tool to Investigate Carrier Suitability for Hot-Melt Extrusion Formulations. *Pharmaceutics* **2020**, *12*, 1019. [CrossRef] [PubMed]
11. Sandhu, H.; Shah, N.; Chokshi, H.; Malick, A.W. Overview of Amorphous Solid Dispersion Technologies. In *Amorphous Solid Dispersions. Advances in Delivery Science and Technology*; Shah, N., Sandhu, H., Choi, D., Chokshi, H., Malick, A., Eds.; Springer: New York, USA, USA, 2014; pp. 91–122. [CrossRef]
12. Goh, O.; Goh, W.J.; Lim, S.H.; Hoo, G.S.; Liew, R.; Ng, T.M. Preferences of Healthcare Professionals on 3D-Printed Tablets: A Pilot Study. *Pharmaceutics* **2022**, *14*, 1521. [CrossRef]
13. Beer, N.; Kaae, S.; Genina, N.; Sporrong, S.K.; Alves, T.L.; Hoebert, J.; De Bruin, M.L.; Hegger, I. Magistral Compounding with 3D Printing: A Promising Way to Achieve Personalized Medicine. *Ther. Innov. Regul. Sci.* **2023**, *57*, 26–36. [CrossRef]
14. Dong, C.; Petrovic, M.; Davies, I.J. Applications of 3D Printing in Medicine: A Review. *Ann. 3D Print. Med.* **2024**, *14*, 100149. [CrossRef]
15. Patil, H.; Tiwari, R.V.; Repka, M.A. Hot-Melt Extrusion: From Theory to Application in Pharmaceutical Formulation. *AAPS PharmSciTech* **2016**, *17*, 20–42. [CrossRef]
16. Kshirsagar, S.M.; Kipping, T.; Banga, A.K. Fabrication of Polymeric Microneedles Using Novel Vacuum Compression Molding Technique for Transdermal Drug Delivery. *Pharm. Res.* **2022**, *39*, 3301–3315. [CrossRef]
17. Jørgensen, J.R.; Mohr, W.; Rischer, M.; Sauer, A.; Mistry, S.; Müllertz, A.; Rades, T. Stability and Intrinsic Dissolution of Vacuum Compression Molded Amorphous Solid Dispersions of Efavirenz. *Int. J. Pharm.* **2023**, *632*, 122564. [CrossRef]
18. Dauer, K.; Wagner, K.G. Micro-Scale Vacuum Compression Molding as a Predictive Screening Tool of Protein Integrity for Potential Hot-Melt Extrusion Processes. *Pharmaceutics* **2023**, *15*, 723. [CrossRef]
19. Bērziņš, K.; Czyrski, G.S.; Aljabbari, A.; Heinz, A.; Boyd, B.J. In Situ Imaging of Subcutaneous Drug Delivery Systems Using Microspatially Offset Low-Frequency Raman Spectroscopy. *Anal. Chem.* **2024**, *96*, 6408–6416. [CrossRef]
20. Denis, L.; Kirstine Jørgensen, A.; Fleury, T.; Daguet, E.; Vaz-Luis, I.; Pistilli, B.; Rieutord, A.; Basit, A.W.; Goyanes, A.; Annereau, M. Developing an Innovative 3D Printing Platform for Production of Personalised Medicines in a Hospital for the OPERA Clinical Trial. *Int. J. Pharm.* **2024**, 124306, *in press*. [CrossRef]
21. Beer, N.; Hegger, I.; Kaae, S.; De Bruin, M.L.; Genina, N.; Alves, T.L.; Hoebert, J.; Kälvemark Sporrong, S. Scenarios for 3D Printing of Personalized Medicines—A Case Study. *Explor. Res. Clin. Soc. Pharm.* **2021**, *4*, 100073. [CrossRef]
22. Englezos, K.; Wang, L.; Tan, E.C.K.; Kang, L. 3D Printing for Personalised Medicines: Implications for Policy and Practice. *Int. J. Pharm.* **2023**, *635*, 122785. [CrossRef]
23. Cilurzo, F.; Cupone, I.E.; Minghetti, P.; Buratti, S.; Gennari, C.G.M.; Montanari, L. Diclofenac Fast-Dissolving Film: Suppression of Bitterness by a Taste-Sensing System. *Drug Dev. Ind. Pharm.* **2011**, *37*, 252–259. [CrossRef]
24. Selmin, F.; Khalid, G.M.; Musazzi, U.M.; Demartin, F.; Minghetti, P.; Cilurzo, F. Relevance of Production Method on the Physical Stability and in Vitro Biopharmaceutical Performances of Olanzapine Orodispersible Film. *Int. J. Pharm.* **2021**, *603*, 120697. [CrossRef]
25. Cilurzo, F.; Cupone, I.E.; Minghetti, P.; Selmin, F.; Montanari, L. Fast Dissolving Films Made of Maltodextrins. *Eur. J. Pharm. Biopharm.* **2008**, *70*, 895–900. [CrossRef]
26. Pacheco, M.S.; Barbieri, D.; da Silva, C.F.; de Moraes, M.A. A Review on Orally Disintegrating Films (ODFs) Made from Natural Polymers Such as Pullulan, Maltodextrin, Starch, and Others. *Int. J. Biol. Macromol.* **2021**, *178*, 504–513. [CrossRef] [PubMed]
27. Cornilă, A.; Iurian, S.; Tomuță, I.; Porfire, A. Orally Dispersible Dosage Forms for Paediatric Use: Current Knowledge and Development of Nanostructure-Based Formulations. *Pharmaceutics* **2022**, *14*, 1621. [CrossRef] [PubMed]
28. Bogdan, C.; Hales, D.; Cornilă, A.; Casian, T.; Iovanov, R.; Tomuță, I.; Iurian, S. Texture Analysis—A Versatile Tool for Pharmaceutical Evaluation of Solid Oral Dosage Forms. *Int. J. Pharm.* **2023**, *638*, 122916. [CrossRef] [PubMed]
29. Preis, M.; Knop, K.; Breitkreutz, J. Mechanical Strength Test for Orodispersible and Buccal Films. *Int. J. Pharm.* **2014**, *461*, 22–29. [CrossRef] [PubMed]
30. Brniak, W.; Maślak, E.; Jachowicz, R. Orodispersible Films and Tablets with Prednisolone Microparticles. *Eur. J. Pharm. Sci.* **2015**, *75*, 81–90. [CrossRef] [PubMed]
31. Walicová, V.; Gajdziok, J.; Pavloková, S.; Vetchý, D. Design and Evaluation of Mucoadhesive Oral Films Containing Sodium Hyaluronate Using Multivariate Data Analysis. *Pharm. Dev. Technol.* **2016**, *22*, 229–236. [CrossRef] [PubMed]
32. Lee, J.H.; Park, C.; Song, I.O.; Lee, B.J.; Kang, C.Y.; Park, J.B. Investigation of Patient-Centric 3D-Printed Orodispersible Films Containing Amorphous Aripiprazole. *Pharmaceuticals* **2022**, *15*, 895. [CrossRef] [PubMed]
33. Preis, M.; Gronkowsky, D.; Grytzan, D.; Breitkreutz, J. Comparative Study on Novel Test Systems to Determine Disintegration Time of Orodispersible Films. *J. Pharm. Pharmacol.* **2014**, *66*, 1102–1111. [CrossRef]

34. Suryawanshi, D.; Wavhule, P.; Shinde, U.; Kamble, M.; Amin, P. Development, Optimization and in-Vivo Evaluation of Cyanocobalamin Loaded Orodispersible Films Using Hot-Melt Extrusion Technology: A Quality by Design (QbD) Approach. *J. Drug Deliv. Sci. Technol.* **2021**, *63*, 102559. [CrossRef]
35. Rowe, R.C.; Sheskey, P.; Quinn, M. *Handbook of Pharmaceutical Excipients*, 6th ed.; Sheskey, P.J., Quinn, M.E., Rowe, R.C., Eds.; Pharmaceutical Press/American Pharmacists Association: London, UK; Washington, DC, USA, 2009.
36. Wettability of Porous Solids Including Powders—European Pharmacopoeia 11.5. Available online: https://pheur.edqm.eu/app/11-5/content/11-5/20945E.htm?highlight=on&terms=wettability (accessed on 4 June 2024).
37. Cen-Puc, M.; Schander, A.; Vargasgleason, M.G.; Lang, W. An Assessment of Surface Treatments for Adhesion of Polyimide Thin Films. *Polymers* **2021**, *13*, 1955. [CrossRef]
38. Oromucosal Preparations—European Pharmacopoeia 11.5. Available online: https://pheur.edqm.eu/app/11-5/content/11-5/1807E.htm?highlight=on&terms=films&terms=films&terms=films&terms=films&terms=films&terms=films&terms=films&terms=films (accessed on 4 June 2024).
39. Tablets—European Pharmacopoeia 11.5. Available online: https://pheur.edqm.eu/app/11-5/content/11-5/0478E.htm?highlight=on&terms=tablets&terms=tablets;%20%E2%80%93orodispersible%20tablets&terms=orodispersible%20tablets&terms=tablets.%20tablets (accessed on 4 June 2024).
40. Khalid, G.M.; Musazzi, U.M.; Selmin, F.; Franzè, S.; Minghetti, P.; Cilurzo, F. Extemporaneous Printing of Diclofenac Orodispersible Films for Pediatrics. *Drug Dev. Ind. Pharm.* **2021**, *47*, 636–644. [CrossRef] [PubMed]
41. Musazzi, U.M.; Selmin, F.; Ortenzi, M.A.; Mohammed, G.K.; Franzé, S.; Minghetti, P.; Cilurzo, F. Personalized Orodispersible Films by Hot Melt Ram Extrusion 3D Printing. *Int. J. Pharm.* **2018**, *551*, 52–59. [CrossRef] [PubMed]
42. Food and Drug Administration. M9 Biopharmaceutics Classification System-Based Biowaivers: Guidance for Industry. Available online: https://www.fda.gov/vaccines-blood-biologics/guidance-compliance-regulatory-information-biologics/biologics-guidances (accessed on 4 June 2024).
43. Pimparade, M.B.; Vo, A.; Maurya, A.S.; Bae, J.; Morott, J.T.; Feng, X.; Kim, D.W.; Kulkarni, V.I.; Tiwari, R.; Vanaja, K.; et al. Development and Evaluation of an Oral Fast Disintegrating Anti-Allergic Film Using Hot-Melt Extrusion Technology. *Eur. J. Pharm. Biopharm.* **2017**, *119*, 81–90. [CrossRef] [PubMed]
44. Selmin, F.; Franceschini, I.; Cupone, I.E.; Minghetti, P.; Cilurzo, F. Aminoacids as Non-Traditional Plasticizers of Maltodextrins Fast-Dissolving Films. *Carbohydr. Polym.* **2015**, *115*, 613–616. [CrossRef] [PubMed]
45. Santos, M.G.; Carpinteiro, D.A.; Thomazini, M.; Rocha-Selmi, G.A.; da Cruz, A.G.; Rodrigues, C.E.C.; Favaro-Trindade, C.S. Coencapsulation of Xylitol and Menthol by Double Emulsion Followed by Complex Coacervation and Microcapsule Application in Chewing Gum. *Food Res. Int.* **2014**, *66*, 454–462. [CrossRef]
46. Tan, Z.; Shi, Q.; Liu, X.; Tan, Z.; Shi, Q.; Liu, X. Thermodynamic Properties of the Polyols as Phase Change Materials for Thermal Energy Storage. In *Phase Change Materials and Their Applications*; Mhadhbi, M., Ed.; IntechOpen: London, UK, 2018; pp. 83–102. ISBN 978-1-78923-531-9.
47. Barzegar-Jalali, M.; Alaei-Beirami, M.; Javadzadeh, Y.; Mohammadi, G.; Hamidi, A.; Andalib, S.; Adibkia, K. Comparison of Physicochemical Characteristics and Drug Release of Diclofenac Sodium–Eudragit® RS100 Nanoparticles and Solid Dispersions. *Powder Technol.* **2012**, *219*, 211–216. [CrossRef]
48. Crișan, A.G.; Iurian, S.; Porfire, A.; Rus, L.M.; Bogdan, C.; Casian, T.; Lucacel, R.C.; Turza, A.; Porav, S.; Tomuță, I. QbD Guided Development of Immediate Release FDM-3D Printed Tablets with Customizable API Doses. *Int. J. Pharm.* **2022**, *613*, 121411. [CrossRef] [PubMed]
49. Iliescu, T.; Baia, M.; Miclauş, V. A Raman Spectroscopic Study of the Diclofenac Sodium–β-Cyclodextrin Interaction. *Eur. J. Pharm. Sci.* **2004**, *22*, 487–495. [CrossRef]
50. Alopaeus, J.F.; Hellfritzsch, M.; Gutowski, T.; Scherließ, R.; Almeida, A.; Sarmento, B.; Škalko-Basnet, N.; Tho, I. Mucoadhesive Buccal Films Based on a Graft Co-Polymer—A Mucin-Retentive Hydrogel Scaffold. *Eur. J. Pharm. Sci.* **2020**, *142*, 105142. [CrossRef]

European Journal of Pharmaceutics and Biopharmaceutics 202 (2024) 114383

Contents lists available at ScienceDirect

European Journal of Pharmaceutics and Biopharmaceutics

journal homepage: www.elsevier.com/locate/ejpb

Acceptability of compounded preparations – A Romanian pediatric hospital perspective

Corina Briciu [a,1], Daniel Leucuța [b,1], Adina Popa [a,*], Ana Latiș [c], Tudor Lucian Pop [c,d], Ioan Tomuță [e], Sorin Claudiu Man [c,f], Călin Lazăr [c,g], Simona Voștinaru [c], Sonia Iurian [e]

[a] "Iuliu Hațieganu" University of Medicine and Pharmacy, Faculty of Pharmacy, Department of Clinical Pharmacy, Cluj-Napoca, Romania
[b] "Iuliu Hațieganu" University of Medicine and Pharmacy, Faculty of Medicine, Department of Medical Informatics and Biostatistics, Cluj-Napoca, Romania
[c] Emergency Clinical Hospital for Children, Cluj-Napoca, Romania
[d] "Iuliu Hațieganu" University of Medicine and Pharmacy, Faculty of Medicine, Second Pediatric Discipline, Mother and Child Department, Cluj-Napoca, Romania
[e] "Iuliu Hațieganu" University of Medicine and Pharmacy, Faculty of Pharmacy, Department of Pharmaceutical Technology and Biopharmacy, Cluj-Napoca, Romania
[f] "Iuliu Hațieganu" University of Medicine and Pharmacy, Faculty of Medicine, Third Pediatric Discipline, Mother and Child Department, Cluj-Napoca, Romania
[g] "Iuliu Hațieganu" University of Medicine and Pharmacy, Faculty of Medicine, First Pediatric Discipline, Mother and Child Department, Cluj-Napoca, Romania

ARTICLE INFO

Keywords:
Acceptability
Pediatric patients
Compounded medications
Hospital setting
Oral
Oromucosal and Cutaneous dosage forms

ABSTRACT

Compounded medicines are widely used, especially for pediatric patients. The aim of this study was to evaluate children's acceptability of compounded preparations and to provide information regarding compounding practices' characteristics in a Romanian hospital setting. An observational, cross-sectional, and retrospective study was conducted in three Clinical Pediatric Departments (Emergency Clinical Hospital for Children, Cluj-Napoca). The study population comprised patients under 18 years old taking at least one compounded medication. Study data was collected mainly through an interviewer-administered questionnaire and medicine acceptability was assessed based on the children's first reaction to the preparations using a 3-point facial hedonic scale. A total of 162 compounded medications were evaluated. A positive/negative reaction was reported for 20.83%/58.33%, 20.63%/49.21%, and 66.67%/7.41% of oral, oromucosal and cutaneous dosage forms. Although patient disapproval was recorded for various reasons, medication administration was successful in over 75% of cases. Factors such as fewer steps required for intake of a dose, capsule dosage form, no additional food/drink immediately after drug intake, medication perceived as "easy/very easy" to swallow, were correlated with a better acceptability of oral preparations. This study highlights the importance of identifying factors that can improve the acceptability of compounded preparations and, subsequently, treatment outcomes in pediatric patients.

1. Introduction

Pediatric patients have specific needs that require age-appropriate formulations, including personalized strengths, child-friendly dosage forms, and adequate palatability [1]. The formulation of pediatric medicines can be challenging since it is necessary to consider the diversity of this patient population in terms of age alongside compliance challenges and potential safety concerns associated with excipients [2].

In Europe, more than 70 % of marketed drugs do not include a pediatric authorization and have not been adequately tested on children [3]. For this reason, The European Pediatric Regulation that came into force on 26th January 2007 aimed to stimulate the research and development of medicines for children. Several key regulatory changes were introduced to achieve this objective, and several rewards and

Abbreviations: API, Active Pharmaceutical Ingredient; EMA, European Medicines Agency; EP, European Pharmacopoeia; EU, European Union; FDA, Food and Drug Administration; FIP, The International Pharmaceutical Federation; GDPR, General Data Protection Regulation; IQR, Interquartile Range; OTC, Over-the-Counter; PFFG, Pediatric Formulations Focus Group; PIP, Pediatric Investigational Plan; PUMA, Pediatric Use Marketing Authorization; SmPC, Summaries of Product Characteristic; UK, United Kingdom; WHO, World Health Organization.

* Corresponding author at: "Iuliu Hațieganu" University of Medicine and Pharmacy, Faculty of Pharmacy, Department of Clinical Pharmacy, I. Creanga Street, 12, 400010 Cluj-Napoca, Romania.
E-mail address: apopa@umfcluj.ro (A. Popa).
[1] Authors with equal contribution.

https://doi.org/10.1016/j.ejpb.2024.114383
Received 6 February 2024; Received in revised form 20 June 2024; Accepted 24 June 2024
Available online 25 June 2024

incentives were offered to the industry. For example, an application for marketing authorization requires a Pediatric Investigational Plan (PIP) to ensure that the necessary data are obtained through studies in children and the Pediatric Use Marketing Authorization (PUMA) was introduced for medicines developed exclusively for use in the pediatric population [3]. As reported by Petkova V et al. (2023), ten years after The Pediatric Regulation was introduced, a total of 273 new medicines and 43 additional pharmaceutical forms appropriate for use in children were authorized in the European Union (EU). Although this is a step forward, it must be acknowledged that not all medications that are needed to treat the pediatric population were developed after 2007 and benefited from those incentives [4]. In addition, when it comes to older drugs, Summaries of Product Characteristics (SmPC) are based on studies conducted at the time of drug development, and most of them are not updated based on current clinical practice [5]. Therefore, pediatric labeling and dosage forms are still not available for many medicines [1,6]. Consequently, healthcare professionals often have no choice but to treat children with off-label or compounded drugs to fill this gap [7–9].

According to the European Pharmacopoeia (EP), pharmaceutical preparations may be licensed by the competent authority or unlicensed and compounded to meet patients' specific needs. The latter category includes extemporaneous preparations (i.e., pharmaceutical preparations individually prepared for a specific patient or patient group, supplied after preparation) and stock preparations (i.e., pharmaceutical preparations prepared in advance and stored until a request for a supply is received) [10]. The technical guidelines developed by The International Pharmaceutical Federation (FIP) – World Health Organization (WHO) in 2016 define compounding as "preparation under the supervision of a pharmacist following national legislation of an unlicensed medicine to meet the specific needs of a patient when no suitable authorized dosage form is available; this may involve preparation from the authorized dosage form or the active pharmaceutical ingredient (API) and usually requires addition of excipients to produce an acceptable product" [11].

Currently, there is an increased interest in documenting pediatric compounding practices all over the world. For example, in 2022, The FIP Pediatric Formulations Focus Group (PFFG) undertook a global survey to identify current oral extemporaneous preparation practices, challenges and needs in different geographic regions across the globe [12]. Compounded formulations for pediatric patients can provide tailored and effective medication options, but questions surrounding their acceptability and safety persist [13]. Acceptability, which is defined by the European Medicines Agency (EMA) as the "overall ability and willingness of the patient to use and its caregiver to administer the medicine as intended", is a key factor in drug administration in children [14]. Acceptability may significantly affect adherence and efficacy and safety secondarily [14–16]. Evolving regulatory guidelines recommend routine assessment of the acceptability of pediatric medicines throughout clinical development processes [2,14,15].

As to the authors' best knowledge, up to date, there are no published papers that cover compounding practices in Eastern European countries, and very few papers address the acceptability of compounded pediatric medicines. Therefore, we aimed to explore the acceptability of different compounded preparations in pediatric patients and to gain insights into the practice of compounding medications in a Romanian hospital setting.

2. Methods

2.1. Study design and setting

This multicenter, cross-sectional, retrospective and observational study was conducted in three Clinical Pediatric Departments of the Emergency Clinical Hospital for Children (Cluj-Napoca, Romania), between March and July 2022. The study was performed in agreement with the ethical principles stated in the Declaration of Helsinki and according to the Romanian legislation. The study protocol was reviewed and approved by the Ethics Committee of "Iuliu Hatieganu" University of Medicine and Pharmacy (Approval no. 241/30.06.2021) and by the Quality Assurance in Clinical Trials Committee of Emergency Clinical Hospital for Children (Approval no. 85 SC/04.02.2022).

2.2. Patients

All pediatric patients with ages below 18 years old who received at least one compounded preparation during their hospital stay were eligible to be included in the study. Participation in the research was voluntary. Written informed consent from the parent or legal guardian of all pediatric subjects was obtained after the research was explained to them and before any study procedures were started. Where possible, in terms of age, the patient's assent was also obtained.

2.3. Data collection

The person responsible for collecting data was a clinical pharmacy resident. Demographic and clinical information were gathered from hospital and pharmacy records for all children included in the study: date of birth, age, sex, body weight, day of admission, medical history, and current diagnoses. Furthermore, medication use data was thoroughly documented, especially information regarding the compounded preparations administered during the children's hospital stay (composition, preparation method, dosage form, frequency of administration, number of days/doses since first drug intake). All patient data were collected and managed in agreement with the European Union's General Data Protection Regulation (GDPR) and the data security legislation of Romania.

The compounded pharmaceutical products were prepared in compliance with the "Procedure models for the application of regulations for good pharmacy practice in a hospital pharmacy" published by the College of Pharmacists of Romania [17].

For each pediatric compounded preparation dispensed by the hospital pharmacy during the study period, the clinical pharmacy resident identified the pediatric patient and at least one person present during the administration process who was able and willing to offer information regarding drug administration and acceptability.

Data were mainly collected through an interviewer-administered questionnaire. A paper-based data collection form was completed for each compounded medication. This document consisted of five sections (Fig. 1) that included a list of pre-planned questions, and for most of them, respondents were asked to choose an answer from a predetermined list of answer options. Firstly, basic information about the respondents was obtained, including the caregivers' education level [18]. Secondly, information about the children's general preferences regarding pharmaceutical dosage forms (selection form a pre-defined list) and flavors (open-ended question; 3 preferred flavors, if possible) was requested. Lastly, the main three sections were focused on gathering specific information regarding the oral, oromucosal or cutaneous compounded products prescribed by the doctor and prepared in the hospital pharmacy, such as the identity of the person responsible for the administration of each preparation, drug acceptability and the respondents' opinions about treatment outcomes (perceived level of satisfaction, effectiveness). Taking into account that oral drug delivery in pediatric patients can be more complex, additional data were collected for compounded oral dosage forms to accurately describe the administration procedure, including all the steps taken to ease/achieve administration.

In this study, pediatric medicine acceptability was determined by assessing the children's first reaction to the compounded preparations, with the help of a 3-point facial hedonic scale (Fig. 2.).

In addition, the pharmacy resident was trained to offer verbal cues during the interview in order to facilitate the sensory evaluation (e.g.,

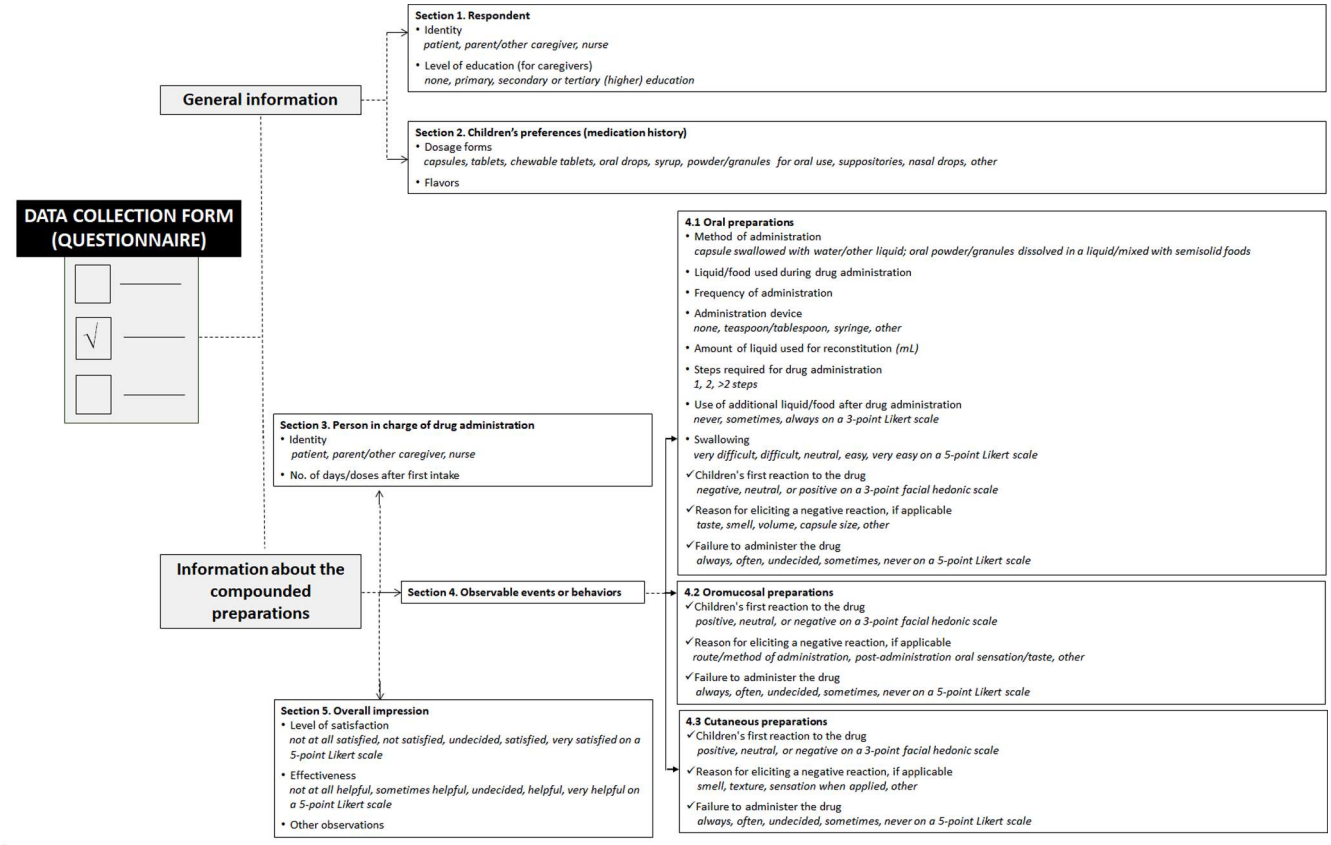

Fig. 1. Key information gathered during the data collection process.

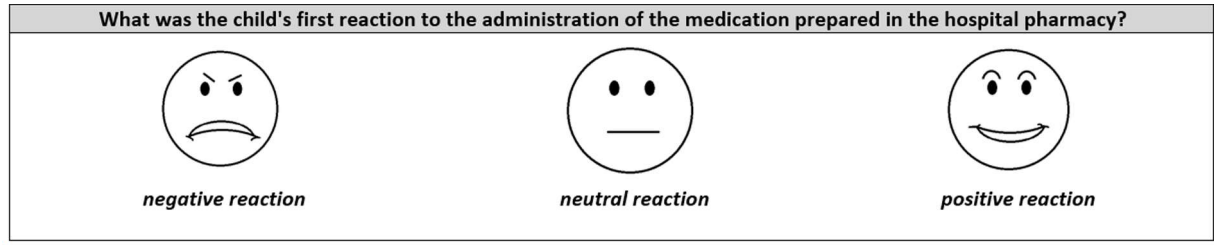

Fig. 2. The instrument used to evaluate the acceptability of all compounded preparations.

negative reaction – if facial expressions observed during administrations included eyes squeezed shut or towards shut, frown, nose wrinkle, pursed lips and/or behaviors observed during or immediately after administration such as the child cries/screams, vomits, spits out medicine, refuses medicine, voices displeasure due to factors such as unpleasant taste, smell, sensation when applied, etc.) [19].

2.4. Statistical analysis

The presentation of categorical data included counts and percentages. Quantitative data were reported as medians and interquartile ranges (IQR, first and third quartiles) when they did not fit a normal distribution. When low predicted frequencies were present, associations between categorical variables were evaluated using the Fisher exact test; otherwise, the chi-square test was employed. The Wilcoxon rank-sum test and the Kruskal-Wallis test were used to compare two or more groups of quantitative data that did not match the normal distribution. Several linear regression models were fitted to predict the acceptance of compounded oral preparations in young patients. The acceptability measured as the children's first reaction after drug administration was our dependent variable (= 1, = 2 and = 3). Clinical judgment was used to choose the independent variables for the models. The confounding effects of age and difficulty swallowing were adjusted for. To reduce the chance of overfitting, the models' variable counts were maintained to a minimum. Quantile-quantile and scale-location plots were used for the linear models to evaluate the residuals' normality and heterogeneity, respectively. Correlations and variance inflation factors were used to determine the presence of multicollinearity. Model coefficients, 95 % confidence intervals, and p-values are displayed for the regressions. All statistical tests employed bilateral p-values and a significance threshold of 0.05. All analyses were carried out in R environment for statistical computing and graphics (R Foundation for Statistical Computing, Vienna, Austria), version 4.2.1 [20].

3. Results

3.1. Patients and medicines

A total of 162 questionnaires were completed during the study

period. It usually took between 5 and 10 min for a questionnaire to be finalized. Approximately 59 % of questionnaires were completed no later than 72 h after first exposure to the compounded medication during the hospital stay.

Most respondents were the children's parents or other caregivers (78.40 %), followed by the nurses (9.88 %). There were also situations in which data was collected from two agreeing sources: child and parent/caregiver together (5.56 %) and nurse and parent/caregiver together (3.70 %). In four cases (2.47 %), information was obtained exclusively from children at least 15 years old who had the capacity to understand the research in question. As for the caregivers, they were primarily individuals with upper secondary education (30.99 %) or higher education (33.80 %).

Based on their previous experiences with medications in general, liquid dosage forms, specifically syrups, oral suspensions, or solutions, were the favorite formulations for most younger (0–6 years, 68.22 %) and older children (>6 years, 38.89 %) (Fig. 3). In terms of specific flavors, although only 59.20 % of respondents offered information regarding this aspect, in 37.84 % of cases, children had no predilection for a particular flavor. However, when specific preferences were reported, strawberries (28.38 %), oranges (22.97 %), citrus fruits (8.11 %), bananas (6.76 %), apricots (5.41 %), chocolate (5.41 %), raspberry (4.05 %), peaches (2.70 %) and pineapple (1.35 %) were cited.

The 162 compounded preparations included in this research were prescribed to 125 hospitalized children, 44 % of whom were girls. The median age of the research subjects was 21 months (IQR range 7–45 months), and the median weight was 11 kg (IQR range = 7.02–14.20 kg). Most children had multiple diagnoses and were receiving treatment for acute and/or chronic conditions. Approximately 81 % of the children received a single compounded medication during their hospital stay, while the rest were administered between 2 and 5 medications. A majority of preparations were administered by oral route (44.44 %), while the rest were given by oromucosal (38.89 %) and cutaneous route (16.67 %). Most preparations had a validity period of 30 days, but were administered in a shorter time, during hospitalization. Between 0 and 20 medications were coadministered with the compounded preparations during the children's hospital stay. Table 1 summarizes the characteristics of the pediatric population and compounded medicines prescribed and administered during hospitalization.

Most medications (83.33 %) included 1 or 2 APIs. The active ingredients most frequently used in the compounding of drug products are displayed in Table 2. In addition, a table with all the APIs contained in the compounding preparations that were administered to our study population is available in the Supplementary materials section. This also includes examples of diseases for which the APIs were indicated (Table S1).

The primary reasons for resorting to compounded preparations instead of commercial products are presented in Fig. 4.

Table 1
Compounded preparations included in the study, stratified by route of administration.

Characteristics	Compounded preparations for		
	Oral administration N = 72	*Oromucosal administration* N = 63	*Cutaneous administration* N = 27
Patient demographics			
Sex			
female	35 (48.61)	26 (41.27)	9 (33.33)
male	37 (51.39)	37 (58.73)	18 (66.67)
Age group			
<= 1 year	20 (27.78)	28 (44.44)	15 (55.56)
1–3 years	24 (33.33)	17 (26.98)	8 (29.63)
3–6 years	18 (25.00)	6 (9.52)	3 (11.11)
>6 years	10 (13.89)	12 (19.05)	1 (3.70)
Medicines			
Person in charge of drug administration			
patient	4 (5.56)	3 (4.76)	0 (0)
parent/other caregiver	53 (73.61)	49 (77.78)	22 (81.48)
nurse	15 (20.83)	8 (12.70)	4 (14.81)
Pharmaceutical dosage form			
capsule	7 (9.72)	0 (0)	0 (0)
powder/ granules	65 (90.28)	0 (0)	0 (0)
solution	0 (0)	7 (11.11)	0 (0)
suspension	0 (0)	56 (88.89)	0 (0)
lipophilic base	0 (0)	0 (0)	9 (33.33)
emulsion base	0 (0)	0 (0)	18 (66.67)
No. of APIs			
Min–Max	1–2	1–3	1–7

Min–Max, minimum–maximum; N (%), N is the number of compounded preparations and the corresponding percentages are enclosed in round brackets; No. of APIs, number of active pharmaceutical ingredients.

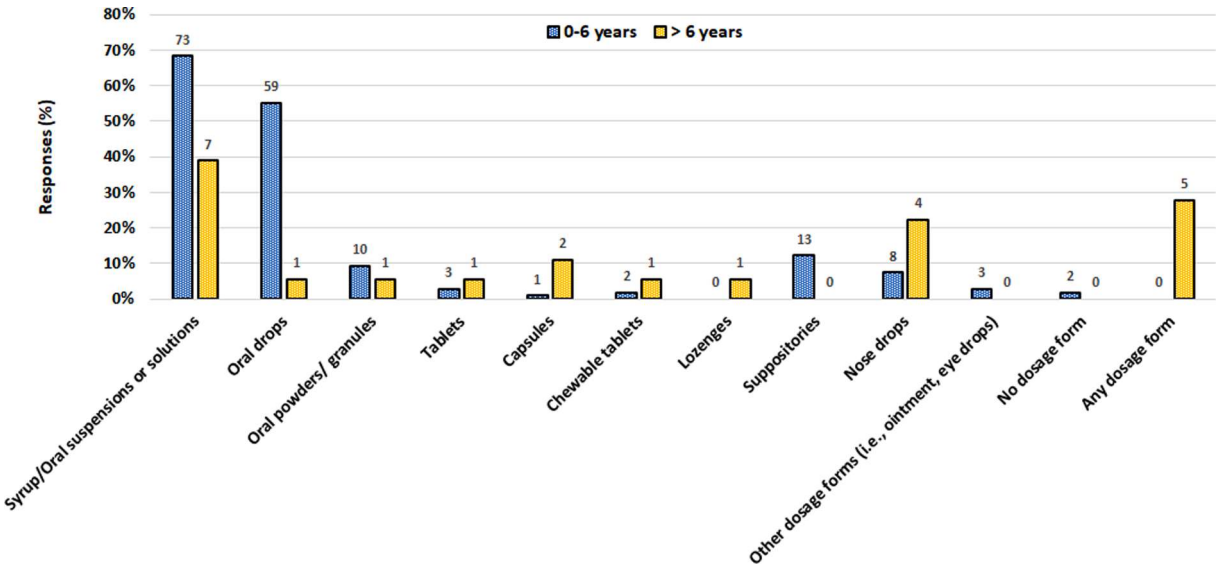

Fig. 3. Children's preferred dosage forms (0–6 years, n = 107; > 6 years, n = 18). The Y-axis displays the percentages, while the actual numbers are on top of each category.

Table 2
Top 5 Active Pharmaceutical Ingredients (APIs) or combinations of APIs used in the compounding of pediatric dosage forms, stratified by route of administration.

Oral administration
Ursodeoxycholic acid
Acyclovir
Acetylsalicylic acid
Propranolol
Prednisone
Oromucosal administration
Benzocaine, nystatin
Sodium borate, nystatin
Sodium borate, benzocaine, nystatin
Sodium borate
Nystatin
Cutaneous administration
Talc, zinc oxide, boric acid, nystatin, erythromycin, triamcinolone acetonide, neomycin sulfate
Salicylic acid
Peru balsam, sodium borate, zinc oxyde, talc
Menthol, talc, zinc oxyde
Benzyl benzoate

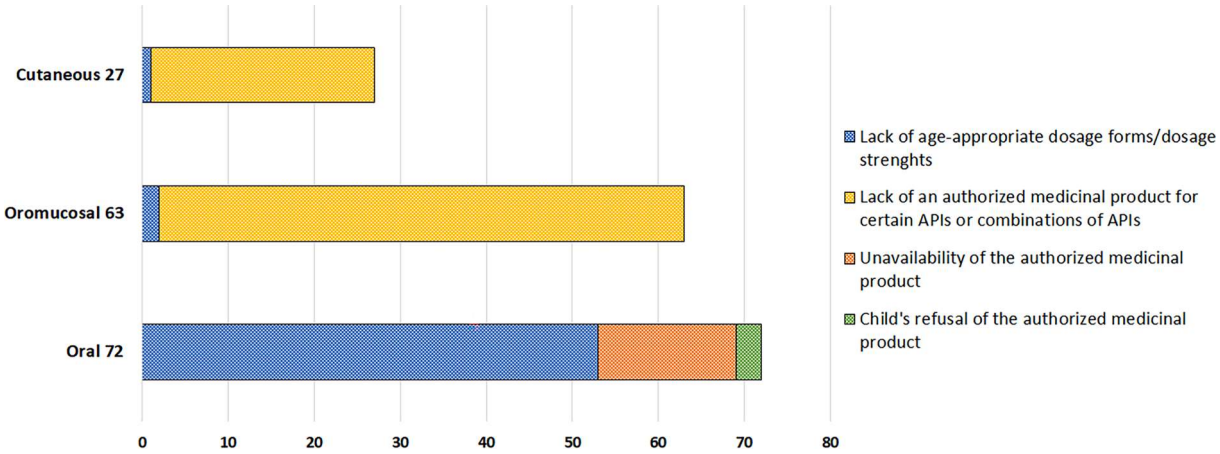

Fig. 4. Rationale behind compounded product use in the pediatric study population.

3.2. Acceptability of compounded oral dosage forms

The hospital pharmacy supplied the compounded oral preparations as finely milled, individually weighed powders or granules that were either wrapped and packaged in small paper bags in this form or filled into hard gelatine capsules with a volume of 0.7 mL. In 90.28 % of cases, the medication required reconstitution consisting of dissolution or dispersion in liquids/semisolid foods before administration. The liquids most frequently utilized to obtain child-friendly dosage forms (oral solutions/suspensions) were water (43.08 %), milk (20.00 %), and tea (16.92 %). With respect to semisolid foods, products such as yogurt, chocolate cream, banana, and semolina pudding were used only in 3 cases. In 55.38 % of situations, the volume employed for reconstitution was less or equal to 5 mL. The rest of the oral preparations included in the study (9.72 %) were administered in the capsule dosage form (formulation that does not need an administration device), and their ingestion was facilitated by drinking some water. Glucose was the excipient used as a diluent and sweetening agent for most compounded oral medications. In terms of administration devices, several types were used to facilitate the administration: syringe (52.78 %), teaspoon or tablespoon (23.61 %), or other devices such as a cup or a baby bottle (12.50 %). Half of the oral preparations required only one step for the intake of the whole dose. The swallowability was rated as "easy" or "very easy" only for 55.55 % of the compounded preparations. For 38.89 % of medications, it was reported that additional food or drink was "always" or "sometimes" consumed immediately after drug administration.

The acceptability evaluation of oral drug formulations revealed that in most cases (58.33 %), children reacted negatively toward the medication when first administered. The reason for eliciting a negative reaction was mainly unspecified, but an unpleasant taste was explicitly mentioned in 13 cases (30.95 %) and an inappropriate volume in 7 cases (14.29 %). Despite the acceptability results, for 77.78 % of oral dosage forms, there were no reported instances in which the administration was unsuccessful. In 18.06 % of cases, the respondents disclosed that the children's refusal sometimes hampered drug administration (Fig. 5).

The impact of factors such as age, type of dosage forms, and characteristics of the administration process on children's acceptability of compounded oral preparations is presented in Table 3. A statistically significant relationship was found between acceptability and several variables (i.e., age, dosage form, administration method, administration frequency, steps required for drug intake, additional food/drink after drug administration, and swallowing difficulty).

After performing univariate analyses between different predictors and the acceptability of oral preparations, all the variables significantly associated with the latter were evaluated using multivariate linear regressions, adjusted for swallowing difficulty and age (Table 4). Several predictors remained significantly related to the acceptability of oral dosage forms in the multivariate models. Capsules were better accepted compared to fine powders/granules. Furthermore, the use of additional

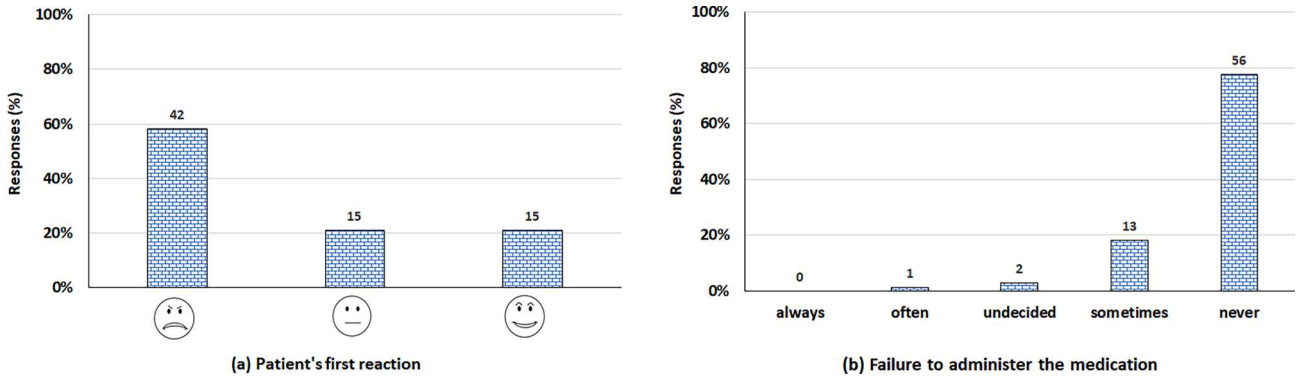

Fig. 5. Acceptability of compounded oral medications (a) versus failure to administer the medications (b) in a pediatric population. The Y-axis displays the percentages, while the actual numbers are on top of each category.

food/drink besides the measures taken to prepare the compounded oral preparations was not well received by the pediatric patients. Finally, the preparations perceived as "easy/very easy" to swallow maintained a superior acceptability compared to those that were "difficult/very difficult" to swallow in all these models.

3.3. Acceptability of compounded oromucosal dosage forms

Almost all compounded oromucosal preparations recommended to the study population were suspensions (88.89 %), while the rest were solutions. Glycerol was the vehicle used in all cases. Usually, the preparations were administered two or three times a day.

Acceptability testing of pediatric medicines revealed that, in this research, the immediate first reactions of the children were positive for 20.63 % and negative for almost 50 % of preparations. Although the reason for low acceptability was not always stated, in 35.49 % of cases, this was attributed to the method or route of administration and, in 19.35 % of cases, to the taste of the medication. Nonetheless, administration of oromucosal medications was accomplished in most instances (80.95 %) (Fig. 6).

Some potential predictors of the acceptability of oromucosal dosage forms in the pediatric population were also assessed. According to the results shown in Table 5, none of the variables collected in this study had a statistically significant impact on the acceptance of compounded oromucosal medications.

3.4. Acceptability of compounded cutaneous dosage forms

The compounded semisolid dosage forms (e.g., ointments, creams) prepared by the hospital pharmacy were mainly water-in-oil (w/o) emulsion-type products (59.26 %), but there were also 9 (33.33 %) that had a lipophilic base. Excipients such as lanolin (wool fat), white Vaseline (white petroleum jelly, white petrolatum) and distilled water were used to prepare these preparations. Regarding the frequency of administration, most medications were applied to the skin surface once or twice a day.

As reported in Fig. 7, 66.67 % of cutaneous preparations triggered a positive reaction when first administered. A negative response was reported in only 2 cases (7.41 %), although no specific reason for this was offered. Except for one product, in 96.30 % of cases, there were no reports of administration failure.

The influence of several variables on the acceptability of cutaneous preparations in pediatric patients was evaluated in Table 5. Age was the only factor that had a statistically significant impact on acceptability in this case.

3.5. Comparative acceptability and respondents' overall impression

The analysis of the children's overall acceptability of compounded dosage forms, stratified by route of administration, revealed that cutaneous preparations were better accepted ($p < 0.001$) than oromucosal or oral medications (Fig. 8.).

Table 6 summarizes the respondents' opinions regarding treatment outcomes. Irrespective of the difficulties experienced by the pediatric patients in accepting the medications, most compounded preparations (87.65 %) were characterized as "helpful or very helpful" in treating the children's health problems. Furthermore, most respondents were "satisfied" or "very satisfied" with the medications.

4. Discussion

To the best of the authors' knowledge, up to date, the use of pediatric compounded preparations in Eastern European countries did not receive much attention. Our study focused on the evaluation of medicine acceptability within a pediatric population, as well as on documenting the pediatric compounding practices in a clinical setting in Romania. While many studies describe the acceptability of different industrial preparations in various age groups [21,22], information regarding the acceptability of compounded formulations is scarce. However, such data could contribute to the significant improvement of preparation and administration practices in clinical settings.

Acceptability, a key quality attribute of pediatric medicines, relies on many formulation-dependent (palatability, swallowability, appearance, mode of administration, administration device, etc.) and patient-dependent factors (age, behavior, health problems, disabilities, background, etc.) [14,23]. As this is a multi-faceted concept, it is possible that the use of a hedonic scale as an assessment tool cannot encompass pediatric acceptability as a whole. However, according to Ranmal SR et al. (2018), there is no consensus with regards to the methodology for acceptability assessment of pharmaceutical products [23], and facial hedonic scales, with the number of faces varying from 2 to 10, were previously used as measurement tools for assessing the acceptability of oral pediatric medicines. Even though several scales have been developed until now, there is no consensus on whether any of them is superior in terms of validity, reliability, feasibility, and preference [24,25]. Some of the advantages of using a facial hedonic scale as an assessment tool include the following: it is better understood by children as this tool is adapted to the child's cognitive and language skills, it eliminates the need for the child to quantitate their experience numerically, it is more child-friendly considering that children tend to prefer cartoon-like faces and it can be suitable even for very young participants [19,25,26]. In a study that aimed to compare methodologies used to assess the acceptability of taste of liquid medicines in a large United Kingdom (UK)-based pediatric population aged 2–16 years, it was acknowledged that the

Table 3
Factors influencing the acceptability of compounded oral dosage forms in a pediatric population.

Variable	Median (IQR)	Statistical test *p-value*
Age group		*0.043*
≤1 year (n = 20)	1 (1–2)	
1–3 years (n = 24)	1.5 (1–2)	
3–6 years (n = 18)	1 (1–1)	
>6 years (n = 10)	2.5 (1.25–3)	
Pharmaceutical dosage forms		*0.016*
Capsules (n = 7)	3 (2–3)	
Powders/granules (n = 65)	1 (1–2)	
Method of administration		*0.039*
Capsule administered with water or other liquid (n = 7)	3 (2–3)	
Powder/granules dissolved in a liquid (n = 62)	1 (1–2)	
Powder/granules mixed with semisolid foods (n = 3)	1 (1–2)	
Frequency of administration (daily)		*0.046*
1 (n = 17)	2 (1–3)	
≥2 (n = 55)	1 (1–2)	
Administration device		*0.083*
None (n = 7)	3 (2–3)	
Teaspoon/tablespoon (n = 17)	1 (1–2)	
Syringe (n = 38)	1 (1–2)	
Other (n = 9)	1 (1–2)	
Amount of liquid/semisolid food used for reconstitution (mL)		0.514
1–5 (n = 36)	1 (1–2)	
>5 (n = 28)	1 (1–2)	
Steps required for drug administration of a dose		*0.031*
1 (n = 36)	2 (1–3)	
2 (n = 8)	1.5 (1–2)	
>2 (n = 13)	1 (1–1)	
Unknown (n = 15)	1 (1–1)	
Additional food/drink after drug administration		*0.01*
Never (n = 18)	2.5 (1–3)	
Sometimes (n = 8)	1.5 (1–2)	
Always (n = 20)	1 (1–1.25)	
Swallowing		*<0.001*
Difficult/very difficult (n = 16)	1 (1–1)	
Easy/very easy (n = 40)	2 (1–3)	
Undecided (n = 11)	1 (1–1)	

IQR, interquartile range.

Table 4
Multiple regression models predicting the acceptability (first reaction) of compounded oral preparations in pediatric patients, adjusted for swallowing difficulty and age.

Variables	B	(95 % CI)	*p-value*
Model 1			
Pharmaceutical dosage forms			
capsules vs. powders/granules[a]	0.58	(0.02–1.13)	*0.042*
Swallowing			
undecided vs. difficult/very difficult[a]	0.01	(−0.48–0.5)	0.976
easy/very easy vs. difficult/very difficult[a]	1	(0.63–1.38)	*< 0.001*
Age group (years)			
>3 vs. ≤1[a]	−0.15	(−0.55–0.25)	0.462
1–3 vs. ≤1[a]	0.14	(−0.26–0.53)	0.49
Model 2			
Additional food/drink after drug administration			
no vs. yes[b]	0.51	(0.1–0.93)	*0.016*
unknown vs. yes[b]	0	(−0.39–0.39)	0.989
sometimes vs. yes[b]	0.04	(−0.5–0.58)	0.879
Model 3			
Administration device			
teaspoon/tablespoon vs. other[b*]	0.27	(−0.31–0.85)	0.353
none vs. other[b*]	0.75	(0.04–1.47)	*0.038*
syringe vs. other[b*]	0.19	(−0.39–0.76)	0.516

*B, coefficient; CI, confidence interval; [a]the variables were all in the same model; [b]in multivariate models adjusted for swallowing difficulty and age, confounders that are not shown in this table; *cup or baby bottle*;* The acceptability measured as the children's first reaction after drug administration was our dependent variable ( = 1,  = 2 and  = 3).

hedonic scale was understood across the widest age range [19]. Ruiz et al. (2017) used a mapping process that took into consideration several variables for acceptability evaluation, such as the child's reaction, the result of the intake, manipulation-administration time, and methods used to achieve administration (divided dose, food/drink, reward, restraint) [27]. However, our study included compounded medications administered by different routes of administration, so the criteria mentioned above did not apply to all products. Therefore, only one variable was considered an acceptability indicator (i.e., the child's reaction at the initial administration) so that it could be applied to all dosage forms.

Considering that information about the children's first reaction to the medication was largely provided by the parents/other caregivers, we acknowledge that this was a proxy reporting. Generally patient themselves could provide more accurate data, but in our study, most were younger than six years old and could not provide valid responses. Although observational measures are generally preferred over proxy instruments, in pediatric research, a proxy assessment method could be useful as the parents' perspective can be very insightful when it comes to their children [28].

The specific reasons for choosing compounded preparations as suitable treatment options for the pediatric inpatients included in this study were analyzed with the help of the hospital pharmacists. Regarding oral medications, most compounded formulations were needed due to the lack of age-appropriate dosage forms/dosage strengths. This was previously cited by other research groups worldwide [29,30], but has not yet been documented in Romania. In many cases, the APIs considered adequate therapeutic choices were only available as solid dosage forms, tablets or capsules. These conventional formulations are limited by their rigid dose content and the ability of the child to swallow the medicines [8]. According to the compounding procedure described by the hospital pharmacists, adult pharmaceutical products such as tablets (e.g., furosemide 40 mg tablets, acyclovir 200 mg tablets, propranolol 40 mg tablets) and capsules (e.g., ursodeoxycholic acid 250 mg capsules or oseltamivir 30 mg capsules) were manipulated through crushing and opening to obtain pediatric extemporaneous oral preparations. Subsequently, the resulting powders or granules were mixed with glucose or lactose as diluents, and the final composition was mostly filled into capsules using a manual capsule filler to obtain the prescribed dose and capsule filling volume. Out of the available authorized adult pharmaceutical products, immediate-release dosage forms were selected as raw materials to minimize the impact on the APIs' release kinetics [31]. While from the point of view of the quality of the final product, the purchase and use of pure APIs would be preferable, the wide variety of pharmaceutical entities prescribed with an unpredictable frequency and the associated cost-benefit analysis led to the reformulation of adult dosage forms. In other instances, the National Agency for Medicines and

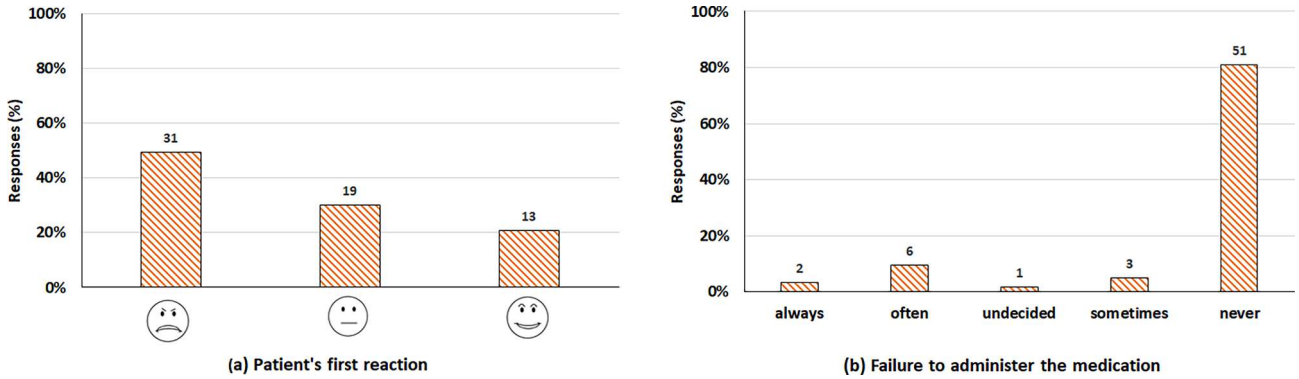

Fig. 6. Acceptability of compounded oromucosal medications (a) versus failure to administer the medications (b) in a pediatric population. The Y-axis displays the percentages, while the actual numbers are on top of each category.

Table 5
Factors influencing the acceptability of compounded oromucosal and cutaneous dosage forms in a pediatric population.

Variable	Median (IQR)	Statistical test *p-value*
Oromucosal		
Age group		0.234
≤1 year (n = 28)	2 (1–2.25)	
1–3 years (n = 17)	1 (1–2)	
3–6 years (n = 6)	1 (1–1)	
>6 years (n = 12)	2 (1–2.25)	
Pharmaceutical dosage forms		0.15
Solutions (n = 7)	2 (1.5–3)	
Suspensions (n = 56)	1 (1–2)	
Frequency of administration (daily)		0.412
2, 3 (n = 55)	2 (1–2)	
>3 (n = 8)	1 (1–2)	
Cutaneous		
Age group		*0.028*
≤1 year (n = 15)	3 (3–3)	
1–3 years (n = 8)	2.5 (1.75–3)	
>3 years (n = 4)	2 (2–2.25)	
Semisolid base type		0.088
emulsion (n = 18)	3 (2–3)	
lipophilic (n = 9)	3 (3–3)	
Frequency of administration (daily)		0.256
1, 2 (n = 14)	3 (3–3)	
>2 (n = 11)	3 (2–3)	

IQR, interquartile range.

Medical Devices of Romania granted age-appropriate products a marketing authorization. Nonetheless, they were unavailable in the hospital pharmacy for various reasons. In general, the availability of pharmaceutical products in clinical settings can be limited by supply chain issues, import difficulties, cost, and reimbursement policies, or even cultural and informational barriers [32,33]. For example, in the case of ursodeoxycholic acid, a hydrophilic bile acid that has been used for decades for intra-hepatic and extra-hepatic cholestatic diseases in childhood [34], several research groups were interested in developing oral customized extemporaneous formulations over the years due to the absence of commercial liquid formulations suitable for infants and children [35,36]. Currently, an age-appropriate dosage form is registered in the Index of Medicinal Products for Human Use of Romania, Ursofalk® 250 mg/5 ml, oral suspension (Dr. Falk Pharma). Still, the product was absent from the market during the study period [37]. On the other hand, propranolol, a beta-adrenergic receptor antagonist proved to be safe and effective in the pediatric population when used as a treatment for several conditions such as infantile hemangioma or supraventricular tachyarrhythmias [38], is available on the market as an oral solution (Hemangiol® 3.75 mg/ml, oral solution, Pierre Fabre). However, due to its prohibitive cost [39] the hospital pharmacy could not supply this pediatric-friendly formulation. Apparently, the costs associated with manufacturing an extemporaneous formulation of propranolol by manipulating the commercially available solid oral dosage form (tablet) are much lower than those corresponding to the purchase of the authorized product. Finally, in a few situations, low acceptability of suitable oral dosage forms for children was reported, such as in the case of a 6-year-old patient who refused prednisone in tablet form because of a "bad" taste perceived during initial drug intake, feedback that prompted the pharmacist to change the formulation from a tablet to a capsule dosage form.

In the present research, the first administration of almost 60 % of compounded oral preparations was accompanied by a negative response. Although most of the children were too young to explain the negative reaction, when an answer was obtained, many pointed out taste as the main reason, a result strongly supported by scientific evidence [16]. When analyzing these findings, we should take into consideration that certain diseases could also influence taste perception and subsequently, medicine acceptability. However, our study found that oseltamivir, acyclovir and prednisone were most frequently cited as having an unpalatable taste, which is in agreement with other literature reports [40–42]. Unpleasant taste is known to be one of the major barriers to drug administration to children, and thus, the subject of many research studies and formulation work to reach taste-masked formulations [43,44]. Still, the issue remains open as Medeiros et al. (2016) have shown that sometimes flavored drug preparations display lower acceptability than neutral-tasting medicines and that some bad-tasting APIs are easier to mask than others [45]. The volume of the reconstituted medication was also mentioned as a cause for low acceptability. In addition, one child reported an itching sensation on the tongue while administering acetylsalicylic acid. Interestingly, although the children's first reaction was negative for more than half of the oral preparations, the administration of these medications was successful in almost 80 % of instances. This may be attributed to some adjuvant strategies applied by caregivers, such as splitting the dose and mixing it with liquids or food. Although this was not consistently documented, some respondents anecdotally mentioned using rewards such as a pretzel, some honey, a lollypop, chocolate cream, or even restraint methods.

Based on the results of the univariate analysis (Table 3), the acceptability of oral preparations was significantly related to the patient's age. The highest acceptability was displayed by children over six years old, followed by those between one and three years of age, while the lowest scores were encountered in children under one and between

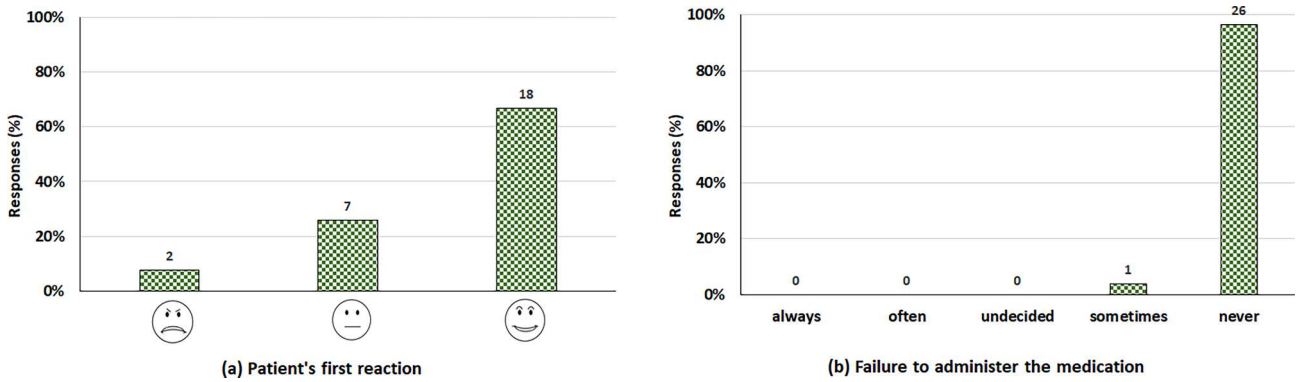

Fig. 7. Acceptability of compounded cutaneous medications (a) versus failure to administer the medications (b) in a pediatric population. The Y-axis displays the percentages, while the actual numbers are on top of each category.

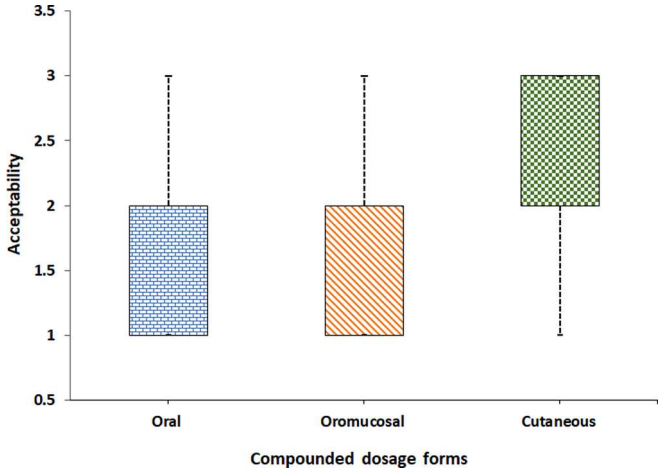

Fig. 8. Boxplot with the median acceptability scores for oral, oromucosal, and cutaneous dosage forms. Minimum, maximum, and interquartile range (IQR) are also shown.

Table 6
Perceived treatment satisfaction and effectiveness among respondents with reference to compounded medications.

Overall assessment (respondents' point of view)	Compounded preparations for		
	Oral administration N = 72 (%)	*Oromucosal administration* N = 63 (%)	*Cutaneous administration* N = 27 (%)
Perceived satisfaction			
Not at all satisfied	0 (0)	0 (0)	0 (0)
Not satisfied	1 (1.39)	2 (3.17)	0 (0)
Undecided	6 (8.33)	3 (4.76)	0 (0)
Satisfied	16 (22.22)	12 (19.05)	3 (11.11)
Very satisfied	48 (66.67)	45 (71.43)	24 (88.89)
Perceived effectiveness			
Not at all helpful	0 (0)	1 (1.59)	0 (0)
Sometimes helpful	2 (2.78)	4 (6.35)	0 (0)
Undecided	7 (9.72)	3 (4.76)	1 (3.70)
Helpful	20 (27.78)	22 (34.92)	5 (18.52)
Very helpful	42 (58.33)	32 (50.79)	21 (77.78)

N (%), N is the number of compounded preparations and the corresponding percentages are enclosed in round brackets.

three and six years old ($p = 0.043$). Older children gave better acceptability ratings, which could be connected to their previous experiences with medicine intake and to preexisting chronic conditions that require medication use over extended periods. Unfortunately, we have not collected data in the study regarding previous exposure to medications, but we acknowledge its potential impact on acceptability. For example, Bracken L et al. (2020) showed that a repeated administration of tablets improved the children's ability to swallow this type of dosage forms, an outcome that was attributed to the learning effect [46]. With regard to the clinical data, three of the children that were taking compounded oral solid dosage forms had chronic health problems (e.g., mucoviscidosis, heart failure, hypertrophic cardiomyopathy), which means that their drug administration history could have been more extensive. In terms of dosage forms, unaltered solid compounded oral dosage forms (capsules) were better accepted than those requiring some type of intervention to achieve a successful administration (powder/granules) ($p = 0.016$), such as dissolution in a liquid or incorporation into soft foods. Most patients who swallowed the whole capsules were around or over 6 years of age, with one exception. One patient was 43 months (3 years and 7 months), significantly below the average age and the recommended age for swallowing solid oral dosage forms. Vallet et al. (2020) reported good acceptability of tablets in children over six years of age and the manipulation of tablets for 95 % of children below six years old [30]. The same tendency, respectively better acceptability for whole tablets than crushed tablets, was reported by Haslund-Krog et al. (2022) [47]. Although direct intake of tablets and capsules is possible and recommended beyond six years of age [48], capsule opening and reconstituted powder/granules administration were prevalent in the present research, even for children older than six years old. This administration behavior could be connected to their preferences, their caregivers' prior medication experiences, and information received from the medical personnel. However, as higher acceptability was reported for capsules compared to powders/granules, most probably due to reduced taste perception, perhaps caregivers would accept changes in administration practices if healthcare professionals advised them.

Our study findings also showed that compounded oral medicines that were difficult/very difficult to swallow were not well accepted when compared to those that were easy/very easy to ingest ($p < 0.001$). In our research, compounded oral preparations were considered to be difficult or very difficult to swallow in 16 cases. This observation was made when various reconstituted oral solutions or suspensions (e.g., methylprednisolone, acyclovir, erythromycin, oseltamivir, acetylsalicylic acid, ursodeoxycholic acid) were administered to children aging between 1 month and 7 years and 5 months, respectively. When exploring if the volume administered could be considered a potential reason, we took into consideration that Mistry et al. (2017) proposed volumes under 0.5 ml for neonates, under 2.5 ml for children under 6 years, and less than 10 ml for children between 6 and 12 years of age in order to ensure

acceptability [48]. Our analysis revealed that in 81.25 % of cases the volume was not age-appropriate. In order to have a complete picture we also have to acknowledge patient factors that could have been involved as well, such as diseases (e.g., upper respiratory infections, stomatitis) that could make swallowing medications more difficult. The acceptability was perceived as low not only when mixing the powder/granules with food or drinks was necessary, but also when additional food/drink immediately after drug intake was needed. Also, the preparations that were swallowed all at once and administered once daily were better rated than those taken in multiple steps and requiring more frequent dosing ($p = 0.031$). Similar associations between the acceptability rating and the administration behavior were shown by Ruiz et al. (2017): poorly accepted medicines were those that triggered a negative first reaction, those administered in multiple steps, and those that required mixing with food or drinks [27]. Mainly, these study results point to lower acceptability of oral formulations with increased contact with the oral mucosa (either by split doses or high volumes). Other authors have reported the relationship between compliance decrease and dosage form manipulation, regarded as a burden by the patients or their caregivers [49]. In our case, the patient or caregiver/nurse manipulated most of the products for acceptability enhancement by mixing them with acceptable fluids. The request for additional food or drink after drug administration could be regarded as a sign of inability to swallow, unpleasant taste, or aftertaste. Regarding the dosing regimen, our observations agree with previous studies that showed that an increase in dosing frequency can lead to a decrease in adherence, likely because it involves repeating an unpleasant administration process [50]. Patients and/or caregivers used an administration device for the reconstituted preparations, which was most often a syringe, in agreement with other published papers that showed the prevalence of syringes as administration devices for pediatric liquid medicines [51]. Although previous literature reports stated that some children find syringes scary or difficult to use for the correct dosage [52], our results showed that the type of administration device had no significant association with acceptability, and they were ranked the same as the household spoon or any other device.

The purpose of the multivariate model was to evaluate whether the initial statistically significant associations remained robust after accounting for the effects of age and difficulty of swallowing. If the associations persisted, it indicated an independent effect. Otherwise, the effect might have been explained by age or the difficulty of swallowing, and not by the assessed variable. In the multivariate analysis (Table 4), four variables were confirmed as main predictors of high acceptability for oral preparations: capsule dosage form, no swallowing difficulty, no additional food/drink after drug intake, and no need for an administration device. These statistical results together with the previous ones discussed above, provide some important suggestions for enhancing the acceptability of compounded oral medications in children.

The oromucosal preparations assessed in this study were viscous solutions or suspensions containing one or more APIs, applied topically (with cotton buds or sterile compresses) on the affected area of the oral mucosa to treat specific conditions [53]. In contrast to oral preparations, pure substances were usually used for the oromucosal and cutaneous dosage forms, due to lower diversity in terms of APIs, which enabled the purchase of large amounts at once. The main reason for requiring these types of preparations was the lack of authorized pharmaceutical products comprising certain APIs/combinations of APIs on the market. In this context, compounding offered the option to associate several APIs in variable doses and granted prescribers the often-needed therapeutic flexibility. Nystatin, the oldest polyene antifungal drug that exhibits a broad antifungal spectrum and is considered a proficient candidate for the treatment of several fungal infections [54], alone or in association with other drugs (i.e., sodium borate, benzocaine), was the most cited API used for the preparation of various oromucosal glycerol suspensions. These substances were preferred for their topical effect, which leads to less systemic exposure with consequent fewer side effects and drug interactions (i.e., antifungals) [55,56]. Moreover, an immediate local effect was targeted when benzocaine, a local anesthetic that reduces or relieves painful stimuli, was used. However, benzocaine is known for the risk of producing life threatening adverse reactions like methemoglobinemia even when applied topically. Consequently, Food and Drug Administration (FDA) recommended stopping administration to children under 2 years of age and warning the public through appropriate labeling [57,58]. Sodium borate, a chemical known as borax, has antiseptic, antimicrobial, and antifungal properties [59]. Similar to our case, colleagues from Hungary have detailed the preparation process of an oromucosal glycerol preparation that includes this substance and is mainly used for its antimycotic effect to treat conditions such as infant thrush [60]. As for the cutaneous route of administration, the most frequent combination of APIs prescribed during the study period included substances with different therapeutic properties, such as antibacterial, anti-inflammatory, and antifungal activities. The hospital pharmacists also prepared topically applied salicylic acid medications during the study period. Salicylic acid is keratolytic in 3–6 % concentrations and is widely used in dermatologic therapy [61].

Similar to oral medications, the patients' initial reaction to the compounded oromucosal preparations was mostly negative. When reasons were inquired, some patients simply disliked the administration route or method. Some children also reported an unpleasant taste, as nystatin [56,62] and benzocaine [63] are known for their bitterness, while the Romanian Pharmacopoeia describes sodium borate as salty, alkaline, lye-like tasting, therefore presumably disagreeable [64]. A sensation of nausea was reported, probably because of the administration procedure, as oromucosal solutions/suspensions were applied locally within the oral mucosal cavity by using a finger wrapped in sterile compresses. In addition, one child reportedly got scared because of the tongue numbness he felt when using a preparation with benzocaine. Even if a large proportion of children initially had a negative response to the oromucosal preparations, the medications were administered successfully in over 80 % of cases. This may again suggest that some mitigation methods were employed to achieve administration. The univariate analysis (Table 5) showed that age, dosage form, and frequency of administration had no impact on children's acceptability of oromucosal preparations.

The cutaneous dosage forms were the only ones whose acceptability scores were in line with administration completion, meaning that their administration was both well accepted and ended with a successful application for most medications. A higher acceptability was associated with children below one year of age than older children (Table 5, $p = 0.028$). These results were in agreement with other reports that showed school-aged children avoided the administration of creams and ointments because of their greasy or sticky nature [65,66]. Although negative first reactions were scarce, a child mentioned that the application produced discomfort, while two respondents reported that the greasy texture made the cutaneous preparation difficult to remove from the skin once applied.

A comparative analysis revealed that the cutaneous products emerged as the most acceptable, with no significant differences between the oral and oromucosal preparations (Fig. 8). However, the route of administration is usually selected based on age, disease, and disease severity and topical administration is used only for the treatment of dermatologic conditions [67,68]. Nonetheless, knowing the comparative acceptability of different dosage forms can be useful in clinical practice, primarily to guide the selection of the appropriate type of preparation when an API can be administered by several routes (e.g., nystatin, antibiotics, corticosteroids).

Overall, most respondents declared themselves to be "very satisfied" with the pediatric compounded preparations and appreciated these products' effectiveness in managing certain clinical conditions (Table 6). These results encourage further use of compounded drugs when custom-tailored medication is not approved commercially or available. However, even though these types of medications respond in a timely manner to certain pediatric therapeutic needs encountered

during clinical practice, potential risks and challenges of compounding practices such as calculation error, microbial contamination, dose uniformity, improper excipients, patient acceptance, stability and incompatibility of extemporaneous preparations, lack of competence among compounding staff, and the absence of national guidelines for compounding practices, should be acknowledged [69]. Many papers have been published that discuss the preparation and characterization of extemporaneous preparations [70–73], reflecting the need to standardize compounding formulations for product quality assurance.

4.1. Implications for practice

Acceptability-related data in children can be used to optimize compounding practices and help medical staff and caregivers with some evidence-based strategies needed to surpass administration barriers and ensure medication adherence. Although the authors recognize the relatively small number of respondents as a limitation for this study, some important details that could improve pediatric pharmacotherapy could emerge from the results, in particular with regard to compounded oral preparations. More specifically, the choice of oral dosage forms (available for preparation in the current hospital pharmacy) could be guided in the future by a step-based strategy like the one pictured in Fig. 9. This approach will consider the children's general preferences regarding medication dosage forms and flavors, and the results of the acceptability evaluation for compounded oral extemporaneous products.

In our study, respondents pointed out liquid formulations as the most readily accepted while the solid oral dosage forms gathered a low

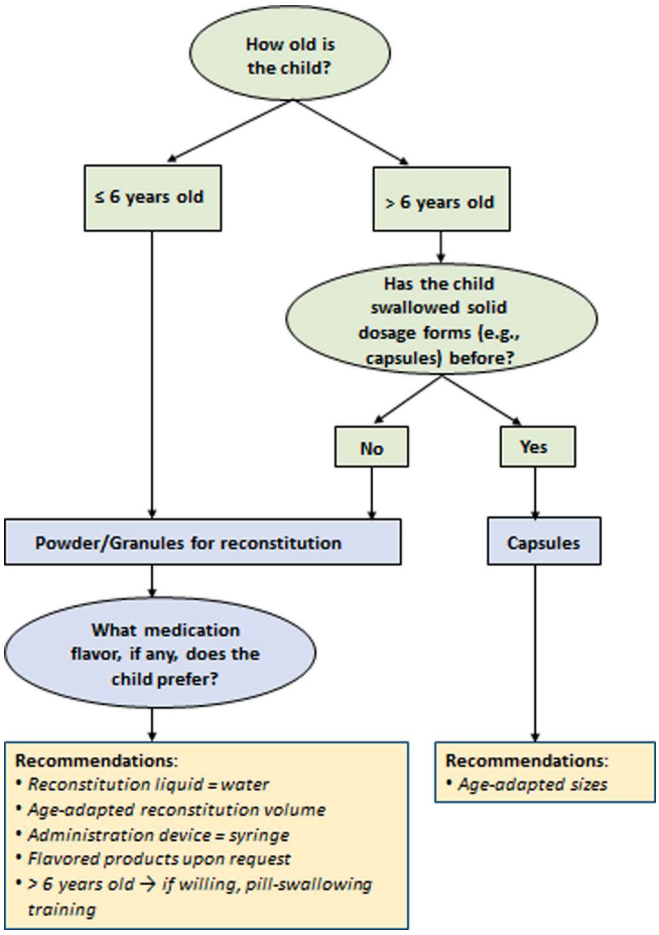

Fig. 9. Strategy to improve children's acceptability of compounded oral extemporaneous preparations.

percentage of the votes. These results are consistent with the findings from a previous study. Alessandrini et al. (2021) reported that liquid was the preferred dosage form for children younger than 12 years old and the majority chose their favorite formulation based on their current and past experience [74]. However, our study findings showed that factors such as a capsule dosage form, a more straightforward administration process, and easily swallowable products were associated with superior acceptability in children. Taking into account this information, capsules of adapted sizes could be provided for children beyond six years of age. Currently, the hospital pharmacy uses size 0 capsules with a corresponding volume of 0.7 ml and 21.5 mm long, as they accommodate a large dose range. Still, when capsules are to be swallowed whole, sizes play an important role in their acceptability. Ranmal et al. (2016) showed that when school children were allowed to choose, 43.9 % chose size 3 (15.7 mm), 28.8 % chose size 1 (19.4 mm), and only 7.1 % chose size 0 as the largest they would accept to swallow [75]. Based on a literature review, Mistry et al. (2017) proposed tablets of less than 7 mm as acceptable for children aged between 6 and 12 years [48], while Ternik et al. (2018) mentioned that oral dosage forms approved for the same ages ranged between 7 mm (for round tablets) up to 16.5 mm (for oblong tablets) [76]. However, as the current infrastructure of the hospital pharmacy does not allow tablet preparation and capsule sizes start from 11.10 mm [77], an option could be to provide the powders/granules in the smallest dose-adapted capsule size possible. As a downside, implementing this solution would require the purchase of other manual capsule fillers and, therefore, higher costs. Furthermore, doctors/clinical pharmacists/nurses could provide the caregivers with information on how to improve administration practices, especially for children beyond six years of age who could be taught to swallow solid oral dosage forms for better acceptability. The way other researchers managed to improve oral drug acceptability could lead to a strategy consisting of demonstration and training on solid oral dosage form swallowing and informative leaflets for the caregiver regarding the safe practices of drug administration in children [78,79].

If the most appropriate dosage forms are powders or granules that require reconstitution into oral solutions/suspensions, for children aged below six years or for those that do not agree to swallow capsules, a semisolid food, or a well-accepted drink in a low specified volume should be advised to aim for a minimum number of administration steps. The dose volume should be adjusted according to the patient's age to avoid multiple administration steps associated with low acceptability. As most powders contain glucose as a filler, which has a sweetening capacity of about 60–70 % of that of sucrose, suspending the capsule content in water could be appropriate to ensure an acceptable taste [80]. The simple syrup could be an alternative as it also grants the physical stability of the suspension, but the preparation time would be longer. The results of the multivariate analysis suggest that the lack of any administration device could improve acceptability, but this situation can be encountered only for solid oral dosage forms. Administration of oral liquid dosage forms warrants the use of a drug delivery device to facilitate an appropriate drug intake, and in this case, syringes would be recommended as the first choice due to the high dose accuracy and uniformity. However, they should have the capacity to measure small volumes, and the volume corresponding to the correct dose should be clearly marked [81]. Interestingly, when a preferred flavor was requested in our study, many respondents declared that pediatric patients had no preferences, which could indicate that a neutral taste would be acceptable in some cases, and this would comply with the authorities' recommendations related to the minimum number of excipients [82]. Still, a predilection for certain flavors was acknowledged in most cases, especially for strawberries and oranges. These flavors are well known by children as a commonly prescribed pediatric over-the-counter (OTC) product comes in these two flavors [83]. Thus, the use of flavors can be taken into consideration to improve or mask the taste of certain medications if this can increase children's adherence to treatment.

4.2. Limitations

The authors recognize as a main limitation of the study the relatively small sample size and the unequal distribution country-wise, which restrict the generalizing ability of the results. A larger sample size with forms collected in more pediatric hospitals in Romania would allow a broader view of the compounding practices and the acceptability of the resulting medicines and will be pursued in further studies.

For various reasons (the first administration did not take place during their working hours, the child was sleeping or was away for medical investigations or the parent was absent), the pharmacy resident could not always apply the questionnaire immediately after the first administration. However, knowing that the acceptability can change with the increase in the number of doses, the pharmacy resident was trained to explain to the respondents that our main objective was to evaluate the first reaction to the administration of the medicine. For this reason, the parents' reports were considered more accurate than the children's and we recognize that another limitation of this study is the retrospective design that makes the respondents prone to recall bias and some missing data.

Despite the limitations mentioned above, this study revealed some important points regarding the acceptability of pediatric compounded medications and will lead to a documented intervention followed by acceptability reassessment. Positive changes in terms of compounded medication acceptability would enable the transfer of the new practices in other Romanian hospitals for better pediatric care.

5. Conclusion

Compounded pharmaceutical products are often necessary due to the inappropriateness or unavailability of pediatric dosage forms. The study findings provide valuable information regarding the compounding practices of pediatric extemporaneous preparations in a Romanian hospital setting. The most valuable insights we obtained in this study were related to compounded oral preparations. Based on our study results, we encourage the use of size-appropriate solid dosage forms for children over 6 years of age, whenever possible. When it comes to younger children, the mitigation of characteristics such as unpleasant taste and age-inappropriate volume must always be considered in order to increase acceptability of compounded liquid preparations. Overall, this study highlights the importance of collecting and analyzing data available through routine clinical practice to assess children's acceptability of compounded medications and identify the challenges that need to be overcome to ensure medication adherence and optimized treatment outcomes. Considering the complexity of this topic, additional studies are needed as gaps need to be filled regarding acceptability of pediatric compounded medicines.

6. Consent to participate

Written informed consent was obtained from the parent or legal guardian. If appropriate in terms of age, the children's assent was also sought before involving them in the present research.

Ethics approval

The study was performed in agreement with the ethical principles stated in the Declaration of Helsinki and according to the Romanian legislation. Approval was granted by the Ethics Committee of "Iuliu Hatieganu" University of Medicine and Pharmacy (Reference no. 241/30.06.2021), as well as by the Quality Assurance in Clinical Trials Committee of Emergency Clinical Hospital for Children (Approval no. 85 SC/04.02.2022).

Funding

This research did not receive any specific grant from funding agencies in the public, commercial, or not-for profit sectors.

CRediT authorship contribution statement

Corina Briciu: Writing – review & editing, Writing – original draft, Visualization, Methodology, Formal analysis, Conceptualization. **Daniel Leucuța:** Writing – review & editing, Writing – original draft, Visualization, Resources, Methodology, Formal analysis. **Adina Popa:** Writing – original draft, Supervision, Methodology, Conceptualization. **Ana Latiș:** Writing – review & editing, Investigation. **Tudor Lucian Pop:** Writing – review & editing, Supervision, Resources. **Ioan Tomuță:** Writing – review & editing, Supervision. **Sorin Claudiu Man:** Writing – review & editing, Supervision, Resources. **Călin Lazăr:** Writing – review & editing, Supervision, Resources. **Simona Voștinaru:** Supervision, Resources. **Sonia Iurian:** Writing – review & editing, Writing – original draft, Visualization, Supervision, Project administration, Methodology, Formal analysis, Conceptualization.

Declaration of competing interest

The authors declare that they have no known competing financial interests or personal relationships that could have appeared to influence the work reported in this paper.

Data availability

The GDPR legislation requires us to protect the health data of participants, and for this reason the raw data cannot be publicly shared. However, the dataset collected and/or analyzed during the current study can be available from the corresponding author on reasonable request.

Appendix A. Supplementary material

Supplementary data to this article can be found online at https://doi.org/10.1016/j.ejpb.2024.114383.

References

[1] The International Pharmaceutical Federation (FIP), FIP Guidelines - Pharmaceutical Research in Paediatric Patients, 2014. <https://www.fip.org/file/1533> (Accessed 3 October 2023).
[2] S. Salunke, F. Liu, H. Batchelor, J. Walsh, R. Turner, T.R. Ju, C. Tuleu, European paediatric formulation initiative (EuPFI - formulating ideas for better medicines for children), AAPS PharmSciTech. 18 (2) (2017) 257–262, https://doi.org/10.1208/s12249-016-0584-1.
[3] M. Toma, M. Felisi, D. Bonifazi, F. Bonifazi, V. Giannuzzi, G. Reggiardo, S. de Wildt, A. Ceci, TEDDY european network of excellence for paediatric research. paediatric medicines in europe: the paediatric regulation - is it time for reform? Front. Med (Lausanne). 8 (2021) 593281 https://doi.org/10.3389/fmed.2021.593281.
[4] V. Petkova, D. Georgieva, M. Dimitrov, I. Nikolova, Off-label prescribing in pediatric population-literature review for 2012–2022, Pharmaceutics. 15 (12) (2023) 2652, https://doi.org/10.3390/pharmaceutics15122652.
[5] J. Corny, D. Lebel, B. Bailey, J.F. Bussières, Unlicensed and off-label drug use in children before and after pediatric governmental initiatives, J. Pediatr. Pharmacol. Ther. 20 (4) (2015) 316–328, https://doi.org/10.5863/1551-6776-20.4.316.
[6] The European Agency for the Evaluation of Medicinal Products (EMEA) - Human medicines evaluation unit, Report on the experts' round table on the difficulties related to the use of new medicinal products in children held on 18 December 1997, 1998. <https://www.ema.europa.eu/en/documents/report/report-experts-round-table-difficulties-related-use-new-medicinal-products-children-held-18-december_en.pdf> (Accessed 3 October 2023).
[7] D.A. Frattarelli, J.L. Galinkin, T.P. Green, T.D. Johnson, K.A. Neville, I.M. Paul, J. N. Van Den Anker, American academy of pediatrics committee on drugs, off-label use of drugs in children, Pediatrics. 133 (3) (2014) 563–567, https://doi.org/10.1542/peds.2013-4060.
[8] H.K. Batchelor, J.F. Marriott, Formulations for children: problems and solutions, Br. J. Clin. Pharmacol. 79 (3) (2015) 405–418, https://doi.org/10.1111/bcp.12268.

[9] A.J. Nunn, Making medicines that children can take, Arch. Dis. Child. 88 (5) (2003) 369–371, https://doi.org/10.1136/adc.88.5.369.

[10] M. Carvalho, I.F. Almeida, The role of pharmaceutical compounding in promoting medication adherence, Pharmaceuticals (Basel). 15 (9) (2022) 1091, https://doi.org/10.3390/ph15091091.

[11] The International Pharmaceutical Federation (FIP). Annex 2. FIP-WHO technical guidelines: points to consider in the provision by health-care professionals of children-specific preparations that are not available as authorized products. WHO Technical Report Series No. 996, 2016. <https://www.fip.org/file/1556> (Accessed 3 October 2023).

[12] H. Fadda, M. Carvalho, Y.Z. Lee, Paediatric Oral Extemporaneous Preparations and Practices: FIP Pediatric Formulation Focus Group (PFFG) Global Survey (poster), 2022. <https://www.fip.org/files/fip/BPS/PFFG_compunding_survey_results.pdf> (Accessed 4 October 2023).

[13] T. Heitman, A.J. Day, A.S. Bassani, Pediatric Compounding Pharmacy: taking on the responsibility of providing quality customized prescriptions, Children (Basel). 6 (5) (2019) 66, https://doi.org/10.3390/children6050066.

[14] European Medicines Agency - Committee for Medicinal Products for Human Use (CHMP). Paediatric Committee (PDCO), Guideline on pharmaceutical development of medicines for paediatric use - EMA/CHMP/QWP/805880/2012 Rev. 2, 2013. <https://www.ema.europa.eu/en/documents/scientific-guideline/guideline-pharmaceutical-development-medicines-paediatric-use_en.pdf> (Accessed 4 October 2023).

[15] World Health Organization (WHO), Module 5: Acceptability, 2018. <https://media.tghn.org/medialibrary/2018/07/WHO_Research_Toolkit_Module_5.pdf> (Accessed 4 October 2023).

[16] R. Venables, H. Batchelor, J. Hodson, H. Stirling, J. Marriott, Determination of formulation factors that affect oral medicines acceptability in a domiciliary paediatric population, Int. J. Pharm. 480 (1–2) (2015) 55–62, https://doi.org/10.1016/j.ijpharm.2015.01.02.

[17] College of Pharmacists of Romania, Procedure models for the application of regulations for good pharmacy practice in a hospital pharmacy, 2011. https://www.cfbucuresti.ro/wp-content/uploads/2022/10/Manual-RBPF-circuit-inchis-2011.pdf (accessed 19 June 2024).

[18] European Commission - Eurydice Network, National Education Systems - Romania, 2023. <https://eurydice.eacea.ec.europa.eu/national-education-systems/romania/overview> (Accessed 19 July 2023).

[19] P. Mistry, H. Stirling, C. Callens, J. Hodson, H. Batchelor, SPaeDD-UK project. Evaluation of patient-reported outcome measurements as a reliable tool to measure acceptability of the taste of paediatric medicines in an inpatient paediatric population, BMJ Open. 8 (2018) e021961.

[20] R Core Team. R: A Language and Environment for Statistical Computing, R Foundation for Statistical Computing (version 4.2.1), Vienna, Austria, 2022. <>.

[21] V. Klingmann, T. Vallet, J. Münch, R. Stegemann, L. Wolters, H.M. Bosse, F. Ruiz, Dosage forms suitability in pediatrics: acceptability of analgesics and antipyretics in a German hospital, Pharmaceutics. 14 (2) (2022) 337, https://doi.org/10.3390/pharmaceutics14020337.

[22] L.M. Angwa, C. Ouma, P. Okoth, R. Nyamai, N.G. Kamau, K. Mutai, M.A. Onono, Acceptability, adherence, and clinical outcomes, of amoxicillin dispersible tablets versus oral suspension in treatment of children aged 2–59 Months with pneumonia, Kenya: a cluster randomized controlled trial, Heliyon. 6 (4) (2020) e03786.

[23] S.R. Ranmal, F. O'Brien, F. Lopez, F. Ruiz, M. Orlu, C. Tuleu, J. Walsh, F. Liu, Methodologies for assessing the acceptability of oral formulations among children and older adults: a systematic review, Drug Discov. Today. 23 (4) (2018) 830–847, https://doi.org/10.1016/j.drudis.2018.01.038.

[24] E.H. Davies, C. Tuleu, Medicines for children: a matter of taste, J. Pediatr. 153 (5) (2008) 599–604.e2, https://doi.org/10.1016/j.jpeds.2008.06.030.

[25] P. Mistry, H. Batchelor, on behalf of SPaeDD-UK project, methodology used to assess acceptability of oral pediatric medicines: a systematic literature search and narrative review, Paediatr. Drugs. 19 (3) (2017) 223–233, https://doi.org/10.1007/s40272-017-0223-7.

[26] J.A. Wagner, G. Pabon, D. Terrill, S.M. Abdel-Rahman, Examining a new scale for evaluating Taste in Children (TASTY), J Pediatr Pharmacol Ther. 25 (2) (2020) 131–138, https://doi.org/10.5863/1551-6776-25.2.131.

[27] F. Ruiz, T. Vallet, A.-M. Pensé-Lhéritier, A. Aoussat, Standardized method to assess medicines' acceptability: focus on paediatric population, J. Pharm. Pharmacol. 69 (4) (2017) 406–416, https://doi.org/10.1111/jphp.12547.

[28] L.S. Matza, D.L. Patrick, A.W. Riley, J.J. Alexander, L. Rajmil, A.M. Pleil, M. Bullinger, Pediatric patient-reported outcome instruments for research to support medical product labeling: report of the ISPOR PRO good research practices for the assessment of children and adolescents task force, Value Health. 16 (4) (2013) 461–479, https://doi.org/10.1016/j.jval.2013.04.004.

[29] J. Saito, M. Akabane, Y. Ishikawa, K. Iwahashi, H. Nakamura, A. Yamatani, Retrospective survey of compounded medications for children in Japan, Eur. J. Pharm. Biopharm. 155 (2020) 122–127, https://doi.org/10.1016/j.ejpb.2020.08.016.

[30] T. Vallet, O. Elhamdaoui, A. Berraho, L.O. Cherkaoui, Y. Kriouile, C. Mahraoui, N. Mouane, A.-M. Pense-Lheritier, F. Ruiz, Y. Bensouda, Medicines acceptability in hospitalized children: an ongoing need for age-appropriate formulations, Pharmaceutics. 12 (8) (2020) 766, https://doi.org/10.3390/pharmaceutics12080766.

[31] K. Saygisever-Faikoglu, G. Faikoglu, F.O. Ozcan, T. Uskur, D.O. Yillar, B. Berk, P. K. Ugur, The pharmacological perspective on tablet splitting or crushing, Pharm. Pharmacol. Int. J. 10 (1) (2022) 22–27, https://doi.org/10.15406/ppij.2022.10.00359.

[32] G. Huss, S. Barak, L. Reali, C. Magendie, A. Carrasco-Sanz, E. Somekh, R. Cohen, C. Levy, L. Namazova-Baranova, M. Vural, M. Pettoello-Mantovani, Drug shortages in pediatrics in Europe: the position of the European pediatric societies, J. Pediatr. 261 (2023) 113472, https://doi.org/10.1016/j.jpeds.2023.113472.

[33] S. Shukar, F. Zahoor, K. Hayat, A. Saeed, A.H. Gillani, S. Omer, S. Hu, Z.U. Babar, Y. Fang, C. Yang, Drug shortage: causes, impact, and mitigation strategies, Front. Pharmacol. 12 (2021) 693426, https://doi.org/10.3389/fphar.2021.693426.

[34] A. Kriegermeier, R. Green, Pediatric cholestatic liver disease: review of bile acid metabolism and discussion of current and emerging therapies, Front. Med. (Lausanne). 7 (2020) 149, https://doi.org/10.3389/fmed.2020.00149.

[35] A. Santovena, E. Sanchez-Negrin, L. Charola, M. Llabres, J.B. Farina, Study of quality and stability of ursodeoxycholic acid formulations for oral pediatric administration, Int. J. Pharm. 477 (1–2) (2014) 32–38, https://doi.org/10.1016/j.ijpharm.2014.10.011.

[36] O. Boscolo, L. Salvo, C. Dobrecky, E.N. Fissore, F. Buontempo, V. Tripodi, S. E. Lucangioli, Pharmaceutical suspensions of ursodeoxycholic acid for pediatric patients: *in vitro* and *in vivo* studies, Pharm. Dev. Technol. 26 (5) (2021) 599–609, https://doi.org/10.1080/10837450.2021.1905662.

[37] National Agency for Medicines and Medical Devices of Romania, Notifications about drug discontinuations. <https://www.anm.ro/medicamente-de-uz-uman/autorizare-medicamente/notificari-discontinuitate-medicamente/> (Accessed 20 June 2024).

[38] A.V. Srinivasan, Propranolol: a 50-year historical perspective, Ann. Indian Acad. 22 (1) (2019) 21–26, https://doi.org/10.4103/aian.AIAN_201_18.

[39] Ministry of Health (Romania), National Public Catalogue of Maximum Prices for Medicinal Products for Human Use, 2024. <https://ms.ro/ro/minister/organizare/directia-politica-medicamentului-si-a-dispozitivelor-medicale/preturi-medicamente/catalogul-public-national-al-preturilor-maximale-ale-medicamentelor-de-uz-uman/> (Accessed June 20 2024).

[40] A. Kalra, P. Bhat, I.P. Kaur, Deciphering molecular mechanics in the taste masking ability of maltodextrin: developing pediatric formulation of oseltamivir for viral pandemia, Carbohydr. Polym. 260 (2021) 117703, https://doi.org/10.1016/j.carbpol.2021.117703.

[41] Drug reactions and interactions, A better understanding of drug-induced taste disturbances may improve management of the condition, Drugs Ther. Perspect. 24 (2008) 22–24, https://doi.org/10.2165/0042310-200824120-00007.

[42] S. Bai, N. Dormer, C. Shoults, A. Meyer, C.D. Pierce, K.A. Neville, G.L. Kearns, Palatability of a novel oral formulation of prednisone in healthy young adults, J. Pharm. Pharmacol. 69 (4) (2017) 489–496, https://doi.org/10.1111/jphp.12710.

[43] J.K. Hofmanova, J. Mason, H.K. Batchelor, Sensory aspects of acceptability of bitter-flavoured 7.5 mm film-coated tablets in adults, preschool and school children, Int. J. Pharm. 585 (2020) 119511, https://doi.org/10.1016/j.ijpharm.2020.119511.

[44] K. Al-Japairai, S.H. Almurisi, A.A. Doolaanea, S. Mahmood, F. Alheibshy, A. Alobaida, N. Abdul-Halim, B. Chatterjee, A review on taste masked multiparticulate dosage forms for paediatric, Int. J. Pharm. 632 (2023) 122571, https://doi.org/10.1016/j.ijpharm.2022.122571.

[45] M.D.S.G. Medeiros, D.D.S. Garruti, L.A.A. Batista, S.G.D. Cruz Fonseca, F. P. Fernandes, H.L. Luna Coelho, Taste acceptance of captopril and furosemide extemporaneous oral pediatric formulations among hospitalized children, J. Pharma. Care Health Sys. 3 (2016) 156, https://doi.org/10.4172/2376-0419.1000156.

[46] L. Bracken, E. McDonough, S. Ashleigh, F. Wilson, J. Shakeshaft, U. Ohia, P. Mistry, H. Jones, N. Kanji, F. Liu, M. Peak, Can children swallow tablets? Outcome data from a feasibility study to assess the acceptability of different-sized placebo tablets in children (creating acceptable tablets (CAT)), BMJ Open. 10 (10) (2020) e036508.

[47] S.S. Haslund-Krog, I.M. Jorgensen, K. Dalhoff, H. Holst, Acceptability of prednisolone in an open-label randomised cross-over study—focus on formulation in children, Children. 9 (8) (2022) 1236, https://doi.org/10.3390/children9081236.

[48] P. Mistry, H. Batchelor, on behalf of SPaeDD-UK project, evidence of acceptability of oral paediatric medicines: a review, J. Pharm. Pharmacol. 69 (4) (2017) 361–376, https://doi.org/10.1111/jphp.12610.

[49] R.H. Richey, C. Hughes, J.V. Craig, U.U. Shah, J.L. Ford, C.E. Barker, M. Peak, A. J. Nunn, M.A. Turner, A systematic review of the use of dosage form manipulation to obtain required doses to inform use of manipulation in paediatric practice, Int. J. Pharm. 518 (1–2) (2017) 155–166, https://doi.org/10.1016/j.ijpharm.2016.12.032.

[50] D. Khan, D. Kirby, S. Bryson, M. Shah, A. Rahman Mohammed, Paediatric specific dosage forms: patient and formulation considerations, Int. J. Pharm. 616 (2022) 121501, https://doi.org/10.1016/j.ijpharm.2022.121501.

[51] J. Walsh, D. van Riet-Nales, E. Hermans, R. de Vries, G. Hilton, P. Blowers, S. Salunke, European Paediatric Formulation Initiative workshop report: Improving the administration of oral liquid medicines in paediatrics using dosing syringes and enteral accessories, Eur. J. Pharm. Biopharm. 151 (2020) 91–97, https://doi.org/10.1016/j.ejpb.2020.04.007.

[52] E. Alessandrini, J. Walsh, S. Salunke, Usability of administration devices for oral and respiratory medicines: Views from a UK primary school, Eur. J. Pharm. Biopharm. 178 (2022) 150–158, https://doi.org/10.1016/j.ejpb.2022.08.006.

[53] European Pharmacopoeia (Ph. Eur.) - 11th edition, Oromucosal Preparations, 2023. <https://pheur.edqm.eu/home> (Accessed 13 June 2024).

[54] F. Sousa, C. Nascimento, D. Ferreira, S. Reis, P. Costa, Reviving the interest in the versatile drug nystatin: a multitude of strategies to increase its potential as an

effective and safe antifungal agent, Adv. Drug Deliv. Rev. 199 (2023) 114969, https://doi.org/10.1016/j.addr.2023.114969.
[55] X. Lyu, C. Zhao, Z.M. Yan, H. Hua, Efficacy of nystatin for the treatment of oral candidiasis: a systematic review and meta-analysis, Drug Des. Devel. Ther. 10 (2016) 1161–1171, https://doi.org/10.2147/DDDT.S100795.
[56] Z. Sklenar, V. Scigel, K. Horackova, O. Slanar, Compounded preparations with nystatin for oral and oromucosal administration, Accessed 3 October 2023, Acta Pol. Pharm. 70 (4) (2013) 759–762, https://pubmed.ncbi.nlm.nih.gov/23923400/.
[57] R. Singh, Y. Al Khalili, Benzocaine, in: StatPearls, Treasure Island (FL), StatPearls Publishing, 2023. <https://www.ncbi.nlm.nih.gov/books/NBK541053/> (Accessed 3 July 2023).
[58] US Food & Drug Administration, Safety Information on Benzocaine-Containing Products, 2018. <https://www.fda.gov/drugs/postmarket-drug-safety-information-patients-and-providers/safety-information-benzocaine-containing-products> (Accessed 20 June 2024).
[59] S.S.F. dos Santos, D.F.A. Pereira, C.A.P. Martins, M.S.A.C. Zöllner, A.O.C. Jorge, C. Y. Koga Ito, Antifungal activity of borax-based formula on Candida spp, Accessed 3 October 2023, Rev. Odontol. UNESP. 40 (2) (2011) 91–95, https://www.revodontolunesp.com.br/article/588018d17f8c9d0a098b4e31/pdf/rou-40-2-91.pdf.
[60] M. Vecsernyés, I. Bácskay, F. Fenyvesi, J. Váradi, P. Fehér, Practicals in Pharmaceutical Technology-Prescription Pharmacy, Department of Pharmaceutical Technology, Medical and Science Center, University of Debrecen (Hungary), 2011. (Accessed 3 July 2023).
[61] D.B. Robertson, H.I. Maibach, Chapter 61: Dermatologic Pharmacology, in: B.G. Katzung, T.W. Vanderah (Eds.), Basic & Clinical Pharmacology, 15e, McGraw Hill, 2021. <https://accesspharmacy.mhmedical.com/content.aspx?bookid=2988&sectionid=250604644> (Accessed 4 October 2023).
[62] S.M. Bojorquez-Cuevas, E. Armenta-Rojas, A. Serrano-Medina, A. Olivas-Sarabia, L. J. Villarreal-Gómez, L.A. Hurtado-Ayala, J.M. Cornejo-Bravo, Improved mucoadhesivity of polyelectrolyte complexes films by electrospinning for the release of nystatin in the oral cavity, J. Drug Deliv. Sci. Technol. 92 (2024) 105385, https://doi.org/10.1016/j.jddst.2024.105385.
[63] M.A. Al-Melh, L. Andersson, Comparison of topical anesthetics (EMLA/Oraqix vs. benzocaine) on pain experienced during palatal needle injection, Oral. Surg. Oral Med. Oral Pathol. Oral. Radiol. Endod. 103 (5) (2007) e16-20. doi: 10.1016/j.tripleo.2006.11.033.
[64] Romanian Pharmacopoeia, 10th ed., Medical Publishing House, Bucharest, 1993.
[65] R. Venables, H. Batchelor, H. Stirling, J. Marriott, Barriers to administering non-oral formulations in a paediatric population: a semi-structured interview study, Int. J. Pharm. 497 (1–2) (2016) 12–17, https://doi.org/10.1016/j.ijpharm.2015.11.010.
[66] M. Santer, H. Burgess, L. Yardley, S. Ersser, S. Lewis-Jones, I. Muller, C. Hugh, P. Little, Managing childhood eczema: qualitative study exploring carers' experiences of barriers and facilitators to treatment adherence, J. Adv. Nurs. 69 (11) (2013) 2493–2501, https://doi.org/10.1111/jan.12133.
[67] H. Phan, V.B. Pai, M.C. Nahata, Chapter 2: pediatrics pharmacotherapy, in: M. A. Chisholm-Burns, T.L. Schwinghammer, P.M. Malone, J.M. Koleesar, K.C. Lee, P. B. Bookstaver (Eds.), Pharmacotherapy Principles & Practice, McGraw Hill, 2022 accessed 4 October 2023, 6e.
[68] A. Rabindranathnambi, M. Abid, Topical treatments in dermatology, Br. J. Hosp. Med. 82 (8) (2021) 1–9, https://doi.org/10.12968/hmed.2020.0567.
[69] S.H. Yuliani, D.C.A. Putri, D.M. Virginia, M.R. Gani, F.D.O. Riswanto, Prevalence, risk, and challenges of extemporaneous preparation for pediatric patients in developing nations: a review, Pharmaceutics. 15 (3) (2023) 840, https://doi.org/10.3390/pharmaceutics15030840.
[70] D. Nguyen, P.-H. Secretan, S. Auvity, F. Vidal, M. Postaire, S. Cisternino, J. Schlatter, Assessment of practices for suspended oral drugs by tablet crushing in pediatric units, Eur. J. Pharm. Biopharm. 157 (2020) 175–182, https://doi.org/10.1016/j.ejpb.2020.10.013.
[71] M.C. Nahata, L.V. Allen Jr, Extemporaneous Drug Formulations, Clin. Ther. 30 (11) (2008) 2112–2119, https://doi.org/10.1016/j.clinthera.2008.11.020.
[72] F. Brion, A.J. Nunn, A. Rieutord, Extemporaneous (magistral) preparation of oral medicines for children in European hospitals, Acta Paediatr. 92 (4) (2003) 486–490, https://doi.org/10.1111/j.1651-2227.2003.tb00583.x.
[73] H. Alarie, V.G. Gaelle Roullin, G. Leclair, Development of a safe and versatile suspension vehicle for pediatric use: formulation development, Int. J. Pharm. 569 (2019) 118552, https://doi.org/10.1016/j.ijpharm.2019.118552.
[74] E. Alessandrini, F. Brako, M. Scarpa, M. Lupo, D. Bonifazi, V. Pignataro, M. Cavallo, O. Cullufe, C. Enache, B. Nafria, J. Claverol, L. De Taeye, E. Vermeulen, J. Preston, C. Tuleu, Children's preferences for oral dosage forms and their involvement in formulation research via EPTRI (European Paediatric Translational Research Infrastructure), Pharmaceutics. 13 (5) (2021) 730, https://doi.org/10.3390/pharmaceutics13050730.
[75] S.R. Ranmal, A. Cram, C. Tuleu, Age-appropriate and acceptable paediatric dosage forms: Insights into end-user perceptions, preferences, and practices from the Children's Acceptability of Oral Formulations (CALF) Study, Int. J. Pharm. 514 (1) (2016) 296–307, https://doi.org/10.1016/j.ijpharm.2016.07.054.
[76] R. Ternik, F. Liu, J.A. Bartlett, Y.M. Khong, D.C. Thiam Tan, T. Dixit, S. Wang, E.A. Gallela, Z. Gao, S. Klein, Assessment of swallowability and palatability of oral dosage forms in children: Report from an M-CERSI pediatric formulation workshop, Int. J. Pharm. 536 (2) (2018) 570-581. doi: 10.1016/j.ijpharm.2017.08.088.
[77] PureCapsUSA®, Capsule Size Chart, 2024. <https://capsulesupplies.com/pages/capsule-size-chart> (Accessed 5 February 2024).
[78] E.O. Meltzer, M.J. Welch, N.K. Ostrom, Pill swallowing ability and training in children 6 to 11 years of age, Clin. Pediatr. 45 (8) (2006) 725–733, https://doi.org/10.1177/0009922806292786.
[79] A. Patel, L. Jacobsen, R. Jhaveri, K.K. Bradford, Effectiveness of pediatric pill swallowing interventions: a systematic review, Pediatrics. 135 (5) (2015) 883–889, https://doi.org/10.1542/peds.2014-2114.
[80] G. Eggleston, B. Legendre, M.A. Godshall, Sugar and other sweeteners, in: J. A. Kent, T.V. Bommaraju, S.D. Barnicki (Eds.), Handbook of Industrial Chemistry and Biotechnology, Springer International Publishing, USA, 2017, pp. 933–978, https://doi.org/10.1007/978-3-319-52287-6_15.
[81] J. Walsh, M.-C. Math, J. Breitkreutz, T. Zerback, H. Wachtel, European Paediatric Formulation Initiative (EuPFI), devices for oral and respiratory paediatric medicines: what do healthcare professionals think? Int. J. Pharm. 492 (1–2) (2015) 304–315, https://doi.org/10.1016/j.ijpharm.2015.05.041.
[82] A. Belayneh, E. Tadese, F. Molla, Safety and biopharmaceutical challenges of excipients in off-label pediatric formulations, Int. J. Gen. Med. 13 (2020) 1051–1066, https://doi.org/10.2147/IJGM.S280330.
[83] Reckitt Benckiser Ireland LTD, Nurofen®, 2021. <https://www.nurofen.ie/products/children/> (Accessed 3 October 2023).